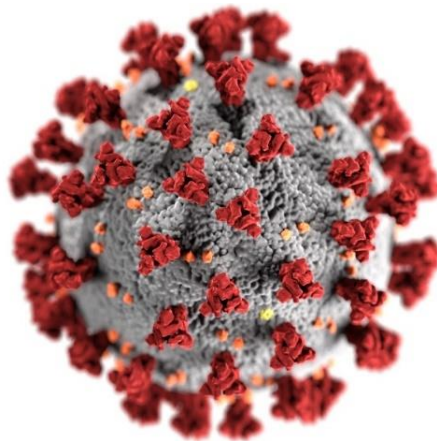


# **Development of diagnostics methods for new emerging viruses**

Alexis Claude Raymond Hoste

Submitted in accordance with the requirements for  
the degree of Doctor of Philosophy



The University of Leeds  
Faculty of Biological Sciences  
School of Molecular and Cellular Biology

February 2021

The present thesis was supported by the EU Marie Skłodowska-Curie  
Actions Innovative Training Network

Project: Host switching pathogens, infectious outbreaks and zoonosis,  
HONOURS

GRANT AGREEMENT NUMBER 721367

Under the supervision of:

Dr Patricia Sastre (Eurofins-Ingenasa)

Dr John N. Barr (The University of Leeds)

# **Intellectual property and publication statement**

The candidate confirms that the work submitted is his own, and that appropriate credit has been given where reference has been made to the work of others.

This copy has been supplied on the understanding that it is copyright material and that no quotation from the thesis may be published without proper acknowledgement.

© 2021 Eurofins-Ingenasa, The University of Leeds and Alexis C. R. Hoste

*Health is not everything, but without health, everything is nothing.*

*Arthur Schopenhauer*

# Acknowledgments

Chapter 3: Paco and Dr. Miguel Ángel Jiménez Clavero for welcoming me at INIA-CISA and helping me in the BSL-3 to test CCHFV positive sera.

Chapter 4: Dr Christian Tiede for the guidance on the production of Affimers anti-RVFPV N protein.

Chapter 5: Tamara Ruiz produced the recombinant MPB83 used in the five-plex assay.

Chapter 6: Dr Ángel Venteo for his supervision and guidance of my work on the development of the double recognition ELISA and the LFA department of Eurofins-Ingenasa, Dr Alba Fresco-Taboada, Istar Tapia and Alejandro Monedero, for training me in the LFA technology.

First and foremost, I would like to thank my two supervisors, John and Patricia, for their help and their guidance during this PhD. It was not always easy to have a PhD done at two different places, but your support made it easier.

Many thanks to the EU Marie Skłodowska-Curie Actions Innovative Training Network for the funding of this PhD, to everybody involved in the HONOURs network, especially Lia and the ESRs for all the courses, trips and all the amazing times spent together mixing science and beer.

A huge thanks to everybody in John's lab and at Eurofins-Ingenasa that made my stay in both Leeds and Madrid special moments. This PhD was a wonderful experience because I felt so welcomed at the two labs.

A special thanks to Istar, our discussions, meals and your rooftop made the last year in Spain so much better. Muchas gracias!

So many thanks to my sister, my brother, my mom, and my dad for their support during these three years and a half, putting up with my scientific talk and trying to understand what I was doing during all these years. Special thanks to my dad who was so interested in my work that he read the whole thesis almost faster than I did!

Finally, Amélie, I would like to thank you for everything, the weekends spent together in so many different places after so many days far from each other, listening to my complains and the amazing support during the whole thesis but especially the last month of writing with the huge help for moving to a new place with you.

# Abstract

The impact of new emerging viruses on human and animal health, as well as on the economy, has recently increased due to environmental and socio-economic changes such as global warming, land development, and ease of travel. These changes have led to the emergence or re-emergence of viruses that can cross the species barrier and infect humans. Thus, some zoonotic viruses such as the Crimean-Congo haemorrhagic fever virus (CCHFV) and Rift Valley fever virus (RVFV) have the potential to become major public health threats. Indeed, CCHFV and RVFV are considered by the World Health Organization to have epidemic potential and for which the necessary countermeasures do not currently exist.

Thus, this thesis, as part of the work package “advanced diagnostics” within the EU-financed Marie Skłodowska-Curie Action (MSCA) training network ‘HONOURS’, aimed to develop new diagnostic tools, both for pathogen detection and serology studies, of emerging viruses in case of an outbreak or in cases of the discovery of new viruses that could emerge unexpectedly during the course of this project. In this last scenario, the technologies and resources would be adapted to the new isolates, as it happened at the end of 2019 with the discovery of severe acute respiratory syndrome coronavirus 2 (SARS-CoV-2).

As a first approach for test development, CCHFV and RVFV, both belonging to the *Bunyvirales* order, were the initial focus of this work with the aim of addressing the gaps identified in their diagnosis. For this purpose, some of the most immunogenic viral antigens identified for each virus were expressed in different expression systems and were used to produce detection molecules: monoclonal antibodies by hybridoma technology and non-antibody molecules (Affimers) by phage display. These tools were further used to develop several serological assays detecting antibodies against CCHFV and RVFV or antigens of these viruses. For the differential diagnosis of CCHFV, RVFV and other related pathogens affecting ruminants, a multiplex assay for antibody detection was developed. Finally, the discovery of SARS-CoV-2 at the end of 2019 created a high demand for diagnostic tools. After identification and production of immunogenic targets of this virus, new serological diagnostic assays were developed.

The new diagnostic tools described in this thesis could be used in surveillance programs and in epidemiological studies, to provide a better understanding of the immune response to these viruses and to help in preventing the spread of some of these viruses, such as CCHFV or RVFV, to countries that are currently free of these pathogens. Moreover, the knowledge acquired during the present work could be applied and adapted to future situations, in cases of infectious outbreaks in animals and humans that can emerge unexpectedly, or caused by a yet undiscovered pathogen, as it has been illustrated by the recent outbreak of SARS-CoV-2.

# Table of Contents

Acknowledgments .....	iv
Abstract.....	v
Abbreviations .....	xx
Chapter 1 Introduction .....	1
1.1. Emerging zoonotic viruses.....	1
1.2. Bunyaviruses.....	4
1.2.1. Crimean-Congo haemorrhagic fever virus .....	11
1.2.2. Rift Valley fever virus .....	14
1.3. Severe acute respiratory syndrome coronavirus 2 .....	18
1.4. Immune response to viral infection.....	24
1.5. Diagnostics tools for detection of viral infection.....	29
1.5.1. Direct methods.....	31
1.5.2. Indirect methods (serological assays).....	38
1.5.3. Multiplex assays .....	41
1.6. Recombinant proteins .....	44
1.6.1. Bacterial expression system.....	46
1.6.2. Yeast expression system.....	51
1.6.3. Insect cells / Baculovirus expression system.....	52
1.6.4. Mammalian expression system.....	55
1.6.5. Recombinant protein purification.....	56
1.7. Detection molecules.....	59
1.7.1. Production of monoclonal antibodies .....	59
1.7.2. Non-antibody molecules: Affimers .....	62
1.8. Aim of this project .....	65
Chapter 2 Materials and Methods .....	66
2.1. Materials .....	66
2.1.1. Synthetic genes .....	66
2.1.2. Primers.....	67
2.1.3. Plasmids.....	68
2.1.4. Cells.....	69
2.1.5. Baculovirus.....	70



2.1.6.	Laboratory mice.....	71
2.1.7.	Antibodies.....	71
2.1.8.	Samples.....	75
2.1.9.	Dilution buffers for the immunoassays .....	78
2.2.	Methods .....	79
2.2.1.	Classical molecular cloning by restriction enzyme digestion .....	79
2.2.2.	Gateway system for molecular cloning .....	82
2.3.	Expression and purification of recombinant proteins .....	82
2.3.1.	Expression of recombinant proteins in <i>E. coli</i> .....	83
2.3.2.	Expression of recombinant proteins in insect cells using the baculovirus expression system.....	88
2.4.	Protein analysis techniques .....	95
2.4.1.	Sodium dodecyl sulphate–polyacrylamide gel electrophoresis.....	95
2.4.2.	Coomassie staining .....	95
2.4.3.	Western blotting .....	95
2.5.	Production of monoclonal antibodies and non-antibody binding proteins to the target antigens and their characterization .....	96
2.5.1.	Monoclonal antibodies .....	96
2.5.2.	Anti-RVSV N protein Affimers .....	102
2.5.3.	Characterization of the detection molecules by pull-down assay.....	108
2.6.	Development of diagnostic tests for detection of the immune response to different emerging viruses .....	109
2.6.1.	ELISA.....	109
2.6.2.	LFA.....	112
2.7.	Development of diagnostic tests for direct detection of different emerging viruses .....	114
2.7.1.	Double antibody sandwich ELISA .....	114
2.7.2.	Double antibody sandwich LFA.....	115
2.8.	Multiplex assays using the Luminex technology.....	117
2.8.1.	Coating of the beads with the target antigens.....	117
2.8.2.	Confirmation assay .....	118
2.8.3.	Multiplex assays .....	118
2.9.	Statistical analysis.....	120
Chapter 3	Development of diagnostic tools for CCHFV .....	122

3.1.	Chapter introduction .....	122
3.2.	Production and purification of CCHFV N protein.....	127
3.2.1.	Expression of the CCHFV N protein.....	127
3.2.2.	Purification of the CCHFV N protein .....	128
3.3.	Production and purification of CCHFV G <sub>NE</sub> and GP38 .....	132
3.3.1.	Expression of CCHFV G <sub>NE</sub> and GP38 .....	132
3.3.2.	Purification of CCHFV G <sub>NE</sub> and GP38 .....	139
3.4.	Production, purification and characterization of monoclonal antibodies against CCHFV N protein.....	141
3.4.1.	Production of the monoclonal antibodies against CCHFV N protein ....	141
3.4.2.	Purification of the monoclonal antibodies.....	150
3.4.3.	Characterization of the monoclonal antibodies .....	151
3.5.	Development of a double recognition ELISA to detect antibodies against CCHFV .....	157
3.5.1.	Labelling of CCHFV N protein.....	157
3.5.2.	Serum samples.....	159
3.5.3.	Optimization of the double recognition ELISA .....	159
3.5.4.	Validation of the double recognition ELISA.....	162
3.6.	Development of a double antibody sandwich ELISA to detect CCHFV N protein .....	164
3.6.1.	Selection of the best pair of mAbs.....	165
3.6.2.	Optimization of the double antibody sandwich ELISA conditions.....	167
3.6.3.	Spiking assay .....	168
3.7.	Development of a CCHFV triplex assay to detect antibodies against three CCHFV antigens.....	170
3.7.1.	Serum samples.....	170
3.7.2.	Immunogenicity of the CCHFV recombinant proteins .....	170
3.7.3.	Optimal serum dilution.....	171
3.7.4.	CCHFV triplex assay.....	173
3.8.	Chapter summary and discussion .....	175
Chapter 4	Development of diagnostic tools for RVFV .....	181
4.1.	Chapter introduction .....	181
4.2.	Production and purification of RVFV N protein .....	184
4.2.1.	Expression of RVFV N protein .....	184

4.2.2.	Purification of RVFV N protein .....	185
4.3.	Production and purification of RVFV G <sub>Ne</sub> .....	190
4.3.1.	Expression of RVFV G <sub>Ne</sub> .....	190
4.3.2.	Purification of RVFV G <sub>Ne</sub> .....	193
4.4.	Production, purification and characterization of detection molecules against RVFV N protein .....	194
4.4.1.	Monoclonal antibodies against RVFV N protein .....	194
4.4.2.	Affimers against RVFV N protein .....	208
4.4.3.	Characterization of the detection molecules by pull-down assay .....	214
4.5.	Development of a double recognition ELISA to detect antibodies against RVFV .....	216
4.5.1.	Labelling of the RVFV N protein .....	217
4.5.2.	Serum samples .....	218
4.5.3.	Optimization of the double recognition ELISA .....	219
4.5.4.	Validation of the double recognition ELISA .....	220
4.6.	Development of a double antibody sandwich ELISA to detect RVFV N protein .....	222
4.6.1.	Serum samples .....	223
4.6.2.	Selection of the best pair of anti-RVFV N protein mAbs/Affimers .....	223
4.6.3.	Double antibody sandwich ELISA with spiked sera .....	227
4.6.4.	Validation of the assay with sheep-infected plasma .....	228
4.7.	Transfer of the double antibody sandwich ELISA to a LFA format for the detection of RVFV N protein at the POC .....	230
4.7.1.	Optimization of the assay .....	230
4.7.2.	Validation of the assay with negative sheep sera and RVFV-infected sheep plasma .....	232
4.8.	Development of a RVFV duplex assay to detect antibodies against two RVFV antigens .....	233
4.8.1.	Serum samples .....	233
4.8.2.	Optimization of the duplex assay .....	234
4.8.3.	Validation of the duplex assay .....	235
4.9.	Chapter summary and discussion .....	238
Chapter 5	Development of a multiplex assay for serological diagnosis of related pathogens affecting ruminants .....	246
5.1.	Chapter introduction .....	246

5.2.	Production and purification of the target proteins .....	248
5.3.	Development of a multiplex assay for antibody detection in serum against pathogens affecting ruminants .....	250
5.3.1.	Development and optimization of the multiplex assay .....	250
5.3.2.	Screening of serum samples .....	252
5.3.3.	Multiplex assay validation using experimental and field serum samples .... .....	254
5.4.	Chapter summary and discussion .....	257
Chapter 6	Development of tools for the diagnosis of COVID-19.....	260
6.1.	Chapter introduction .....	260
6.2.	Production of SARS-CoV-2 N protein .....	264
6.2.1.	Expression of SARS-CoV-2 N protein.....	264
6.2.2.	Purification of SARS-CoV-2 N protein .....	265
6.3.	Development of two serological approaches for detection of antibodies to SARS-CoV-2 in different scenarios: a screening tool and a point-of-care test .....	266
6.3.1.	Development of the double recognition ELISA .....	266
6.3.2.	Development of the double recognition LFA.....	269
6.3.3.	Validation of the newly developed tools: double recognition ELISA and double recognition LFA with samples from positive patients to COVID-19 and healthy donors .....	271
6.3.4.	Cross-reactivity by antibodies directed to common-cold <i>Alpha-</i> and <i>Betacoronavirus</i> and other respiratory pathogens.....	274
6.4.	Development of an indirect ELISA to detect human IgG and IgM against SARS-CoV-2 .....	275
6.4.1.	Optimization of the assay .....	275
6.4.2.	Validation of the indirect anti-human IgG and IgM ELISA .....	277
6.4.3.	Indirect ELISA with positive sera at different time points.....	281
6.5.	Development of a double antibody sandwich LFA to detect SARS-CoV-2 S antigens .....	284
6.5.1.	Optimization of the double antibody sandwich LFA .....	284
6.5.2.	Validation of the double antibody sandwich LFA with spiked samples .....	289
6.5.3.	Validation of the double antibody sandwich LFA with human samples..... .....	291
6.6.	Development of a SARS-CoV-2 triplex assay to study the immune response to three SARS-CoV-2 proteins .....	292

6.6.1. Serum samples .....	292
6.6.2. Optimal serum dilution .....	292
6.6.3. SARS-CoV-2 triplex assay .....	295
6.7. Chapter summary and discussion .....	300
Chapter 7 Concluding remarks .....	308
References .....	311

# List of Figures

<i>Figure 1.1 Map of newly and reemerging viral disease.</i>	2
<i>Figure 1.2 The One Health approach developed by the WHO.</i>	3
<i>Figure 1.3 Bunyavirales virion structure.</i>	5
<i>Figure 1.4 Representation of the replication cycle of Nairoviruses (Bunyavirales).</i>	8
<i>Figure 1.5 Representation of CCHFV GPC domains with their processing and the resulting proteins.</i>	9
<i>Figure 1.6 Representation of RVFV GPC domains with their processing and the resulting proteins.</i>	10
<i>Figure 1.7 Geographic distribution of Crimean-Congo haemorrhagic fever and its vector (Hyalomma ticks).</i>	12
<i>Figure 1.8 Life cycle of Hyalomma ticks (blue arrows) and the transmission of CCHFV to animals and humans (red arrows).</i>	13
<i>Figure 1.9 Geographic distribution of Rift Valley fever.</i>	15
<i>Figure 1.10 Aedes/Culex mosquitos' life cycle and the transmission of RVFV to animals and humans.</i>	16
<i>Figure 1.11 Coronavirus virion structure.</i>	20
<i>Figure 1.12 Representation of the replication cycle of SARS-CoV-2.</i>	23
<i>Figure 1.13 Structure and function of immunoglobulin G.</i>	25
<i>Figure 1.14 Structure of immunoglobulin M.</i>	26
<i>Figure 1.15 Diagram of the virus' and immunoglobulin's (IgM and IgG) levels after a viral infection.</i>	28
<i>Figure 1.16 Diagram of the different targets of diagnostic methods to detect a viral infection.</i>	29
<i>Figure 1.17 Steps involved in a double antibody sandwich ELISA.</i>	34
<i>Figure 1.18 Composition of a LFA strip.</i>	36
<i>Figure 1.19 Technical basis of a double antibody sandwich LFA.</i>	37
<i>Figure 1.20 Steps involved in an indirect ELISA.</i>	39
<i>Figure 1.21 Steps involved in a double recognition ELISA.</i>	40
<i>Figure 1.22 xMAP microspheres.</i>	43
<i>Figure 1.23 Indirect format used in the multiplex assay.</i>	43
<i>Figure 1.24 Advantages and disadvantages of the main recombinant expression systems.</i>	46
<i>Figure 1.25 Regulation system involved in the pET vectors under the control of the lac operon and the T7 promoter.</i>	48
<i>Figure 1.26 Representation of the Gateway system.</i>	50
<i>Figure 1.27 Generation of recombinant baculovirus by homologous recombination.</i>	54
<i>Figure 1.28 Representation of immobilized metal affinity chromatography.</i>	57
<i>Figure 1.29 Size Exclusion Chromatography.</i>	59
<i>Figure 1.30 Schematic representation of the most common antibody fragments.</i>	62
<i>Figure 1.31 Crystal structure of an Affimer against the protein p300.</i>	63

<i>Figure 1.32 Schematic representation of Affimer screening process using phage display.</i>	64
<i>Figure 2.1 Workflow of the production of baculovirus stock.</i>	90
<i>Figure 2.2 Scale of the intensity of the signal obtained for the LFA test line.</i>	114
<i>Figure 3.1 Expression of the CCHFV N protein and its purification by Ni<sup>2+</sup>-NTA affinity chromatography.</i>	129
<i>Figure 3.2 CCHFV N protein purification by size exclusion chromatography.</i>	130
<i>Figure 3.3 Chromatogram of final purification step of the CCHFV N protein sample by size exclusion chromatography after two Ni<sup>2+</sup>-NTA affinity chromatography purifications.</i>	131
<i>Figure 3.4 Observation under the microscope of infected Sf9 after the co-transfection.</i>	132
<i>Figure 3.5 Co-transfections of Sf9 with the triple-cut baculovirus DNA and the transfer vector to obtain recombinant baculoviruses expressing the target protein.</i>	133
<i>Figure 3.6 Infection of Sf9 cells with plaques corresponding to different recombinant baculoviruses.</i>	135
<i>Figure 3.7 Kinetic analysis of the expression of CCHFV G<sub>NE</sub>-GST (MW = 46 kDa) by Sf900 cells infected with two MOI (0.1 and 2) of BacPAK6 CCHFV G<sub>NE</sub>.</i>	137
<i>Figure 3.8 Kinetic analysis of the expression of CCHFV GP38-GST (MW = 58 kDa) by Sf900 cells infected with two MOI (0.1 and 2) of BacPAK6 CCHFV GP38.</i>	138
<i>Figure 3.9 CCHFV G<sub>NE</sub>-GST protein purification by affinity chromatography.</i>	140
<i>Figure 3.10 CCHFV GP38-GST protein purification by affinity chromatography.</i>	141
<i>Figure 3.11 Antibody titration by indirect ELISA with 6xHis-SUMO-CCHFV N protein of the mouse sera after three immunizations with 6xHis-SUMO-CCHFV N protein.</i>	142
<i>Figure 3.12 Antibody titration by indirect ELISA of the mouse sera after ten immunizations with 6xHis-SUMO-CCHFV N protein.</i>	143
<i>Figure 3.13 First screening of the three plates containing the hybridoma clones by indirect ELISA.</i>	145
<i>Figure 3.14 Indirect ELISA screening of the hybridoma clones 3G7 (A) and 1G4 (B) at 50 cells per well with CCHFV N protein and 6xHis-SUMO-RVFPV N protein.</i>	146
<i>Figure 3.15 Indirect ELISA screening of the hybridoma clones 3G7 (A) and 1G4 (B) at 20 cells per well with CCHFV N protein.</i>	148
<i>Figure 3.16 Indirect ELISA screening of the hybridoma clone 3G7 at 2 cells per well with CCHFV N protein.</i>	149
<i>Figure 3.17 Anti-CCHFV N protein mAbs purification by affinity chromatography.</i>	151
<i>Figure 3.18 Determination of the isotype of the anti-CCHFV N protein mAbs produced.</i>	152
<i>Figure 3.19 Analysis of the specificity of the three anti-CCHFV N protein mAbs in denaturing and reducing conditions.</i>	153
<i>Figure 3.20 Titration of the anti-CCHFV N protein mAbs.</i>	154
<i>Figure 3.21 Titration of the HRP-labelled anti-CCHFV N protein mAbs.</i>	155
<i>Figure 3.22 Determination of the mapping of anti-CCHFV N protein mAbs for the same epitopes.</i>	156
<i>Figure 3.23 Confirmation of the labelling of CCHFV N protein with HRP.</i>	158

<i>Figure 3.24 Titration of the CCHFV positive field serum in double recognition ELISA.</i>	160
<i>Figure 3.25 Serum dilutions tested in the double recognition ELISA.</i>	162
<i>Figure 3.26 Dot plot diagram between the double recognition ELISA CCHFV N protein and the reference technique where each dot represents an individual sample.</i>	163
<i>Figure 3.27 Receiver operating characteristic curve analysis of the double recognition ELISA CCHFV N protein.</i>	164
<i>Figure 3.28 Selection of the best pair of anti-CCHFV N protein mAbs for the double antibody sandwich ELISA.</i>	166
<i>Figure 3.29 Selection of the best conditions of the double antibody sandwich ELISA.</i>	167
<i>Figure 3.30 Optimization of the double antibody sandwich ELISA conditions.</i>	168
<i>Figure 3.31 Spiking assay with the double antibody sandwich ELISA.</i>	169
<i>Figure 3.32 Confirmation of the immunogenicity of the CCHFV recombinant proteins (N protein, G<sub>NE</sub> and GP38).</i>	171
<i>Figure 3.33 Determination of the screening conditions for the triplex assay.</i>	172
<i>Figure 3.34 Screening of the positive and negative field sera for antibodies against CCHFV GP38 (A), CCHFV G<sub>NE</sub> (B) and CCHFV N protein (C) in the CCHFV triplex assay.</i>	174
<i>Figure 4.1 Expression of the RVFV N protein and its purification by Ni<sup>2+</sup>-NTA affinity chromatography.</i>	185
<i>Figure 4.2 RVFV N protein purification by a second Ni<sup>2+</sup>-NTA affinity chromatography step after SUMO cleavage and dialysis.</i>	187
<i>Figure 4.3 Chromatogram of the final purification step of the RVFV N protein sample by size exclusion chromatography after two Ni<sup>2+</sup>-NTA affinity chromatography purification steps.</i>	188
<i>Figure 4.4 RVFV N protein purification by size exclusion chromatography.</i>	189
<i>Figure 4.5 Confirmation of the presence of RVFV N protein in the fraction F35.</i>	189
<i>Figure 4.6 Infection of Sf9 cells with plaques corresponding to recombinant baculoviruses expressing RVFV G<sub>NE</sub>-GST (MW = 73 kDa).</i>	191
<i>Figure 4.7 Kinetic analysis of the expression of RVFV G<sub>NE</sub>-GST (MW = 73 kDa) in insect cells at different time points and two MOI.</i>	192
<i>Figure 4.8 RVFV G<sub>NE</sub>-GST protein purified by affinity chromatography analysed by SDS-PAGE followed by Coomassie staining (A) and Western blot (B).</i>	193
<i>Figure 4.9 Antibody titration by indirect ELISA of the mouse sera after eight immunizations with RVFV N protein.</i>	195
<i>Figure 4.10 First screening of the three plates containing the hybridoma clones anti RVFV N protein by indirect ELISA.</i>	197
<i>Figure 4.11 Screening of the hybridoma clones selected by indirect ELISA with the RVFV N protein and the 6xHis-SUMO-CCHFV N protein.</i>	198
<i>Figure 4.12 Indirect ELISA screening of the hybridoma clones at 2 cells per well with RVFV N protein and the 6xHis-SUMO-CCHFV N protein.</i>	200
<i>Figure 4.13 Anti-RVFV N protein mAbs purification by affinity chromatography.</i>	202



<i>Figure 4.14 Determination of the isotype of the anti-RVFPV N protein mAbs produced.</i>	203
<i>Figure 4.15 Analysis of the specificity of the three anti-RVFPV N protein mAbs in denaturing and reducing conditions.</i>	204
<i>Figure 4.16 Titration of the mAbs anti-RVFPV N protein.</i>	205
<i>Figure 4.17 Titration of the HRP-labelled anti-RVFPV N protein mAbs.</i>	206
<i>Figure 4.18 Determination of the mapping of anti-RVFPV N protein mAbs for the same epitopes.</i>	207
<i>Figure 4.19 Confirmation of the biotinylation of the two RVFPV N proteins fractions F20 and F35.</i>	209
<i>Figure 4.20 Phage ELISA with the Affimers selected against the RVFPV N protein F20.</i>	210
<i>Figure 4.21 Phage ELISA with the Affimers selected against the RVFPV N protein F35.</i>	211
<i>Figure 4.22 Alignment of the amino acid sequences of the fifteen unique Affimers selected against the RVFPV N protein F20 and subcloned into pET-11a vector.</i>	212
<i>Figure 4.23 Alignment of the amino acid sequences of the eight unique Affimers selected against the RVFPV N protein F35 and subcloned into pET-11a vector.</i>	213
<i>Figure 4.24 Affimer P1 production and purification by Ni<sup>2+</sup>-NTA affinity chromatography.</i>	214
<i>Figure 4.25 Confirmation of the biotinylation of the anti-RVFPV N protein Affimers.</i>	215
<i>Figure 4.26 Pull-down assay with the Affimers and anti-RVFPV N protein mAbs.</i>	216
<i>Figure 4.27 Confirmation of the labelling of RVFPV N protein with HRP.</i>	217
<i>Figure 4.28 Titration of RVFPV positive experimental sera and negative field sera in double recognition ELISA.</i>	219
<i>Figure 4.29 Dot plot diagram between the double recognition ELISA RVFPV N protein and the reference technique where each dot represents an individual sample.</i>	221
<i>Figure 4.30 Receiver operating characteristic curve analysis of the double recognition ELISA RVFPV N protein.</i>	222
<i>Figure 4.31 Titration of RVFPV N protein with the Affimers and mAbs anti-RVFPV N protein to select the best capture Affimers.</i>	224
<i>Figure 4.32 Selection of the best combinations of capture and detection molecules to detect RVFPV N protein in a double antibody sandwich ELISA.</i>	226
<i>Figure 4.33 Titration of RVFPV N protein with the best combinations of anti-RVFPV N protein capture/detection molecules.</i>	227
<i>Figure 4.34 Spiking assay with the double antibody sandwich ELISA to detect RVFPV N protein.</i>	228
<i>Figure 4.35 Validation of the double antibody sandwich ELISA RVFPV N protein with experimental sheep plasma.</i>	229
<i>Figure 4.36 Titration of RVFPV N protein with the double antibody sandwich LFA Test 1 and Test 2.</i>	231
<i>Figure 4.37 Double antibody sandwich LFA 1E9/1F8 with the experimental sheep plasma.</i>	232

<i>Figure 4.38 Determination of the screening conditions for the duplex assay.</i>	235
<i>Figure 4.39 Screening of the positive experimental and negative field sera for antibodies against RVFV N protein (A) and RVFV G<sub>NE</sub> (B) in the RVFV duplex assay.</i>	237
<i>Figure 5.1 SDS-PAGE analysis followed by Coomassie staining of the five purified proteins used in the multiplex assay.</i>	250
<i>Figure 5.2 Determination of the screening conditions for the bead-based assay.</i>	252
<i>Figure 5.3 Validation of the five-plex bead-based assay.</i>	255
<i>Figure 6.1 Different diagnostic assays commercialized and in development for COVID-19 diagnosis at the beginning of 2021.</i>	263
<i>Figure 6.2 Production of the SARS-CoV-2 N protein.</i>	264
<i>Figure 6.3 Purification of the SARS-CoV-2 N protein by affinity chromatography.</i>	265
<i>Figure 6.4 Confirmation of the labelling of SARS-CoV-2 N protein with HRP.</i>	267
<i>Figure 6.5 Selection of the best SARS-CoV-2 N protein-HRP dilution buffer.</i>	268
<i>Figure 6.6 Determination of the optimal SARS-CoV-2 N protein-HRP dilution.</i>	269
<i>Figure 6.7 Double recognition LFA Test 7 and 16 tested with 10 positive serum samples.</i>	271
<i>Figure 6.8 Validation of the double recognition ELISA and double recognition LFA.</i>	273
<i>Figure 6.9 Detection of IgG and IgM by indirect ELISA, using negative and positive serum samples to COVID-19.</i>	276
<i>Figure 6.10 Validation of the indirect anti-human IgG ELISA for the detection of IgG against SARS-CoV-2.</i>	278
<i>Figure 6.11 Validation of the indirect anti-human IgM ELISA for the detection of IgM against SARS-CoV-2.</i>	280
<i>Figure 6.12 Indirect ELISA for the detection of IgG against SARS-CoV-2 with the sera of two positive patients collected at different time-points.</i>	283
<i>Figure 6.13 Optimization of the double antibody sandwich LFA for detection of SARS-CoV-2 S protein.</i>	286
<i>Figure 6.14 Additional different double antibody sandwich LFA combinations tested with SARS-CoV-2 S.</i>	287
<i>Figure 6.15 Titration of SARS-CoV-2 S protein with the 17 best combinations of double antibody sandwich LFA.</i>	288
<i>Figure 6.16 Determination of the screening conditions for the SARS-CoV-2 triplex assay detecting IgG.</i>	294
<i>Figure 6.17 Determination of the screening conditions for the SARS-CoV-2 triplex assay detecting IgM.</i>	295
<i>Figure 6.18 Detection of IgG against SARS-CoV-2 N protein (A), SARS-CoV-2 S protein (B) and SARS-CoV-2 RBD (C) in a triplex assay.</i>	297
<i>Figure 6.19 Detection of IgM against SARS-CoV-2 N protein (A), SARS-CoV-2 S protein (B) and SARS-CoV-2 RBD (C) in a triplex assay.</i>	298

# List of Tables

<i>Table 1.1 Summary of the main information about the different immunoglobulin classes.</i>	27
<i>Table 1.2 Summary of the different diagnostic tools for the detection of viral infections and their primary use.</i>	30
<i>Table 2.1 Synthetic genes.</i>	66
<i>Table 2.2 Oligonucleotides used for cloning.</i>	67
<i>Table 2.3 Oligonucleotides used for sequencing.</i>	68
<i>Table 2.4 Plasmids.</i>	69
<i>Table 2.5 Recombinant baculoviruses produced.</i>	71
<i>Table 2.6 Commercial and in-house antibodies used in WB, ELISA, LFA and Luminex.</i>	72
<i>Table 2.7 Monoclonal antibodies produced.</i>	74
<i>Table 2.8 Animal serum samples.</i>	75
<i>Table 2.9 Human serum classification by real-time RT-PCR and serological assays.</i>	77
<i>Table 2.10 Classification of the oropharyngeal and nasopharyngeal samples.</i>	77
<i>Table 2.11 Dilution buffers (DB) used in ELISAs.</i>	78
<i>Table 2.12 Dilution buffers used in LFAs (LDB).</i>	78
<i>Table 2.13 Plasmid constructs used to produce recombinant proteins in E. coli.</i>	83
<i>Table 2.14 Specific steps and conditions of the double recognition ELISA developed in this project.</i>	111
<i>Table 2.15 Pair of mAbs and Affimers used in the double antibody sandwich ELISA RVFV N protein.</i>	115
<i>Table 2.16 Luminex bead regions, the corresponding coupled protein and mAbs used for the confirmation assay.</i>	118
<i>Table 3.1 Commercial serological assays available for CCHFV antigen and antibody detection.</i>	123
<i>Table 3.2 Minimal and optimal performances defined by the WHO R&amp;D Blueprint: Priority Diagnostics for CCHF for ELISA and LFA.</i>	126
<i>Table 3.3 Summary of the characteristics of the anti-CCHFV N protein mAbs obtained.</i>	157
<i>Table 3.4 Classification of the serum samples used to develop the double recognition ELISA to detect antibodies against CCHFV.</i>	159
<i>Table 4.1 Commercial serological assays available for RVFV antigen and antibody detection.</i>	183
<i>Table 4.2 Summary of the characteristics of the anti-RVFV N protein mAbs obtained.</i>	208
<i>Table 4.3 Classification of the serum samples used to develop the double recognition ELISA to detect antibodies against RVFV.</i>	218
<i>Table 4.4 Summary of the results of the double antibody sandwich ELISA to detect RVFV N protein with the different combinations of anti-RVFV N protein capture Affimer and detection mAb.</i>	225

<i>Table 4.5 Best combinations of capture and detection molecules in the double antibody sandwich ELISA to detect RVFV N protein.</i> .....	226
<i>Table 5.1 Summary of the antigens used in the multiplex assay.</i> .....	249
<i>Table 5.2 Serum classification with the ELISAs used as reference techniques for the different antigens.</i> .....	253
<i>Table 5.3 Correlation between the bead-based assay and the ELISAs used as reference for the different antigens.</i> .....	256
<i>Table 5.4 Cross-reactivity between the positive experimental and field sera with the four other bead regions.</i> .....	256
<i>Table 6.1 First double recognition LFA prototypes by combination of different concentration of SARS-CoV-2 N protein on the membrane and as conjugate.</i> .....	270
<i>Table 6.2 Comparison between the samples tested in the double recognition LFA and the double recognition ELISA.</i> .....	274
<i>Table 6.3 Cross-reactivity of the double recognition ELISA and LFA with other respiratory pathogens.</i> .....	275
<i>Table 6.4 Serum samples classification by real-time RT-PCR and serological assay.</i> .....	277
<i>Table 6.5 Comparison between the indirect ELISAs and the double recognition ELISA.</i> .....	281
<i>Table 6.6 Combinations possible with the 10 monoclonal antibodies used to conjugate red latex beads and immobilized on the membrane.</i> .....	285
<i>Table 6.7 Titration of SARS-CoV-2 S protein with test 8.6.</i> .....	289
<i>Table 6.8 Spiking assay of SARS-CoV-2 S protein in viral transport medium with test 8.6.</i> .....	290
<i>Table 6.9 Spiking assay of SARS-CoV-2 virus with double antibody sandwich LFA test 8.6.</i> .....	291
<i>Table 6.10 Double antibody sandwich LFA test 8.6 tested with positive and negative oropharyngeal and nasopharyngeal samples.</i> .....	291
<i>Table 6.11 Comparison of the results obtained for the bead region #12 SARS-CoV-2 N protein and the reference assay (INgezim COVID 19 double recognition ELISA).</i> .....	299
<i>Table 6.12 Comparison of the results obtained for the bead region #20 SARS-CoV-2 S protein and the reference assay (INgezim COVID 19 double recognition ELISA).</i> .....	299
<i>Table 6.13 Comparison of the results obtained for the bead region #25 SARS-CoV-2 RBD and the reference assay (INgezim COVID 19 double recognition ELISA).</i> .....	299
<i>Table 6.14 Sequence identity between the SARS-CoV-2 N protein and the N protein of other human coronaviruses.</i> .....	301

# Abbreviations

6xHis: polyhistidine

A: absorbance

Ab: antibody

ABTS: 2,2'-azino-bis(3-ethylbenzothiazoline-6-sulfonic acid)

AcMNPV: *Autographa californica* multicapsid nucleopolyhedrovirus

ADCC: antibody-dependent cellular cytotoxicity

Ag: antigen

AIDS: acquired immunodeficiency syndrome

APC: antigen-presenting cell

APS: ammonium persulfate

ASe: analytical sensitivity

AUC: area under the curve

BES: baculovirus expression system

BSA: bovine serum albumin

BSL: biosafety level

BTV: Bluetongue virus

C+: positive control

C-: negative control

CCHF: Crimean-Congo haemorrhagic fever

CCHFV: Crimean-Congo haemorrhagic fever virus

cDNA: complementary DNA

C<sub>H</sub>: constant region of the immunoglobulin's heavy chain

C<sub>L</sub>: constant region of the immunoglobulin's light chain

CLIA: chemiluminescence immunoassay

CM: convoluted membrane

COVID-19: coronavirus disease 2019

CPE: cytopathic effect

Ct: cycle threshold

DB: dilution buffers

DC: dendritic cell

DIVA: differentiating infected from vaccinated animals

DMEM: Dulbecco's modified eagle medium

DMS: double-membrane spherule

DMV: double-membrane vesicle

DPI: days post-infection

DSe: diagnostic sensitivity

D<sub>Sp</sub>: diagnostic specificity  
E protein: envelope protein  
EDC: 1-Ethyl-3-(3-dimethylaminopropyl)carbodiimide  
ELISA: enzyme-linked immunosorbent assay  
ER: endoplasmic reticulum  
ERGIC: ER-to-Golgi intermediate compartment  
EUA: emergency use authorization  
Fab: antigen-binding fragment  
FBS: foetal bovine serum  
Fc: fragment crystallizable region  
FDA: American Food and Drug Administration  
G<sub>C</sub>: C-terminal glycoprotein  
G<sub>N</sub>: N-terminal glycoprotein  
G<sub>NE</sub>: G<sub>N</sub> ectodomain  
GPC: glycoprotein precursor  
GST: glutathione S-transferase  
H: heavy chain  
hACE2: human angiotensin-converting enzyme 2  
HAT: hypoxanthine-aminopterin-thymidine  
HCoV: human coronavirus  
HGPR: hypoxanthine-guanine phosphoribosyl transferase  
His: Histidine  
HIV: human immunodeficiency virus  
HRP: horseradish peroxidase  
hRSV: human respiratory syncytial virus  
IFA: immunofluorescence assay  
Ig: immunoglobulins  
IHC: immunohistochemistry  
IMAC: immobilized metal affinity chromatography  
IPTG: isopropyl β-d-1-thiogalactopyranoside  
ITN: Innovative Training Network  
IU: Ingenasa Unit  
J chain: joining chain  
L segment: large segment  
L: light chain  
lac: lactose  
LAMP: loop-mediated amplification method  
LB: lysogeny broth  
LDB: dilution buffer used in lateral flow assay

LFA: lateral flow assay  
LOD: limit of detection  
M protein: membrane protein  
M segment: medium segment  
mAb: monoclonal antibody  
MERS-CoV: Middle East respiratory syndrome coronavirus  
MFI: median fluorescence intensity  
MLD: mucin-like domain  
MOI: multiplicity of infection  
mRNA: messenger RNA  
MSCA: Marie Skłodowska-Curie Action  
MW: molecular weight  
MWCO: molecular weight cut-off  
N protein: nucleocapsid protein  
nAb: neutralizing antibodies  
NGS: next-generation sequencing  
NHS: N-Hydroxysuccinimide  
NP: N protein  
NS<sub>M</sub>: non-structural protein encoded by the M segment  
nsp: non-structural proteins  
NS<sub>S</sub>: non-structural protein encoded by the S segment  
NTA: nitrilotriacetic acid  
OD: optical density  
OIE: Office International des Epizooties (World Organization for Animal Health)  
ON: overnight  
ORF: open reading frame  
pAb: polyclonal antibody  
PCR: polymerase chain reaction  
PI: post-infection  
POC: point-of-care  
PreG<sub>C</sub>: G<sub>C</sub> precursor  
PreG<sub>N</sub>: G<sub>N</sub> precursor  
PTM: post-translational modifications  
R2: Rosetta 2  
R<sub>0</sub>: reproductive number  
RBC: red blood cell  
RBD: receptor binding domain  
RdRp: RNA-dependent RNA polymerase  
RNP: ribonucleoprotein

ROC: receiver operating characteristic  
RT: room temperature  
RTase: reverse transcriptase  
RTC: replication and transcription complex  
RT-LAMP: reverse transcription loop-mediated amplification method  
RT-RPA: real-time recombinase polymerase amplification  
RT-PCR: reverse transcription polymerase chain reaction  
RVF: Rift Valley fever  
S protein: spike protein  
S segment: small segment  
S/P: sample to positive control  
SARS: severe acute respiratory syndrome  
SARS-CoV-2: severe acute respiratory syndrome 2  
SDS-PAGE: sodium dodecyl sulphate–polyacrylamide gel electrophoresis  
SEC: size exclusion chromatography  
sg mRNA: subgenomic mRNA  
SKI-1/S1P: subtilisin kexin isozyme-1/site-1 protease  
Strep-PE: streptavidin-phycoerythrin  
SUMO: small ubiquitin-like modifier  
TB: tuberculosis  
TBE: Tris/Borate/EDTA buffer  
TEMED: tetramethylethylenediamine  
TGN: trans-Golgi network  
TMB: 3,3',5,5'-Tetramethylbenzidine  
TMPRSS2: transmembrane protease serine 2  
Ulp1: SUMO ubiquitin-like specific protease 1  
V<sub>H</sub>: variable region of the immunoglobulin's heavy chain  
V<sub>L</sub>: variable region of the immunoglobulin's light chain  
VLP: virus like particles  
VNT: virus neutralization test  
vRNA: viral RNA  
VTM: viral transport medium  
WB: western blotting  
WHO: World Health Organization  
xMAP: multi-analyte profiling



# Chapter 1 Introduction

## 1.1. Emerging zoonotic viruses

The existence of a disease agent smaller than bacteria was proven in 1892 by Dimitri Ivanovsky with the description of the first virus, the tobacco mosaic virus, later confirmed by Martinus Beijerinck in 1898 (1,2). Viruses are obligate intracellular parasites that require a host for their replication with the potential to cause infectious diseases.

Nowadays, about 25% of the 57 million annual human deaths worldwide can be attributed to infectious diseases (3). Over the last century, newly emerging pathogens have become more and more frequent with an impact on both human and animal health, as well as on the economy (4). “Emerging or reemerging diseases” were formally defined by Joshua Lederberg, Robert B. Shope, and Mary Wilson in 1987 as diseases that have been discovered for the first time or diseases that had previously existed but have had an increasing incidence or an increasing geographical distribution range (5). Two surveys listed over 1,400 human pathogens (6,7) with around 60% of these defined as zoonotic, meaning that they are spread between animals and humans (such as influenza, rabies and smallpox viruses), and 177 pathogens as emerging or reemerging diseases. More precisely, out of those human pathogens, only around 15% are viruses; however, disproportionally, among the emerging or reemerging pathogens 43.5% are viruses and most of them are RNA viruses (37% of all emerging or reemerging pathogens) (7). Some examples of emerging zoonotic viruses are, Zika virus which caused a large outbreak in Brazil in 2014/2015 (8), Crimean-Congo haemorrhagic fever virus (CCHFV) which is expanding to Europe, following the expansion of its vector (9), or the recent emergence of the severe acute respiratory syndrome coronavirus 2 (SARS-CoV-2), which has been declared as a pandemic by the World Health Organization (WHO) in March 2020 (10).

Environmental and socio-economic changes such as global warming, host migration and globalization, have influenced the distribution of some infectious diseases (Figure 1.1). Human factors such as urbanization (4,11), deforestation, globalization and international trade of animals and products of animal origin, greatly influences the emergence of viruses (12–14). Deforestation has increased exponentially since the 20<sup>th</sup> century, which

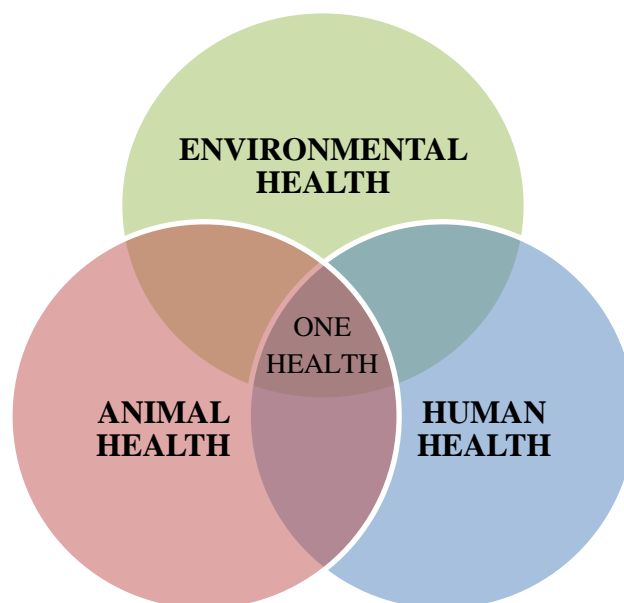
raises the contacts between wild animals and humans (15). The ease of travelling and especially air travelling, with over 100 million passenger per year, has led to the rapid spread of numerous diseases with as an example the rapid spread of SARS-CoV-2 in 2020 (16). Ecological factors such as climate change modifies the life cycle and increases the geographical range of vectors, thus impacting the distribution of vector-borne diseases (17). For example, a longer adult activity season was observed in the United Kingdom for *Culicoides* biting midges (vector of the Bluetongue virus, BTV) due to climate change (18), the *Hyalomma marginatum* tick (vector of CCHFV) is now found in Southwestern Europe (19) and the first case of a locally acquired CCHFV case was recently found in Spain in 2016 (20). A final factor is evolution, as RNA viruses, which constitute most of the emerging or reemerging viruses, have a high mutation rate (21). Some groups of RNA viruses, such as the *Bunyavirales* order, have a segmented genome, which can lead to reassortment events when a cell is infected with two distinct viruses. Furthermore, genetic recombination events have been shown to play an important role for some RNA viruses such as Coronaviruses (22). All these factors lead to the emergence or re-emergence of viruses that can cross the species barrier and infect humans.



**Figure 1.1** Map of newly and reemerging viral disease.

Figure adapted from Marston et. al. *Emerging Viral Diseases: Confronting Threats with New Technologies*. *Science Translational Medicine*. 2014;6(253).

For these reasons, the WHO has been developing the One Health approach (23), a multisectoral approach to achieve the optimal health between people, animals, plants, and their shared environment (Figure 1.2). This approach has been focused on food safety, zoonosis and antibiotic resistance as they not only concern one sector but need a multisectoral approach between specialized agencies of the United Nations (such as the WHO, World Organization for Animal Health (*Office International des Epizooties* (OIE)) and Food and Agriculture Organization), experts, government officials and workers from different sectors at local and global levels to tackle the risks at the human-animal-ecosystem interface and promote a global response.



**Figure 1.2** *The One Health approach developed by the WHO.*

*It is a multisectoral approach to achieve the optimal health between people, animals, plants, and their shared environment.*

In addition to the One Health approach, as the total number of potential pathogens is high and R&D resources are limited, the WHO has established a list of pathogens likely to be responsible of severe outbreaks in the future and for which a deeper knowledge and countermeasures are needed. By developing this list, the overall aim is to ensure that the R&D response to a pandemic of public health concern is faster and more effective in order to accelerate the R&D results and adapt to the scientific, logistical and social challenges

specific to epidemics (24). This list, detailed below, includes the diseases that will be relevant for this thesis and other pathogens:

- Crimean-Congo haemorrhagic fever virus
- Rift Valley fever virus (RVFV)
- Highly pathogenic emerging coronaviruses relevant to humans (Middle East respiratory syndrome-related coronavirus (MERS-CoV) and severe acute respiratory syndrome (SARS))
- Other pathogens such as:
  - Filoviruses (i.e. Zaire ebolavirus and Marburg virus)
  - Lassa virus
  - Nipah virus
  - Zika virus
  - Disease X, a pathogen currently unknown which has the potential to cause a serious international epidemic

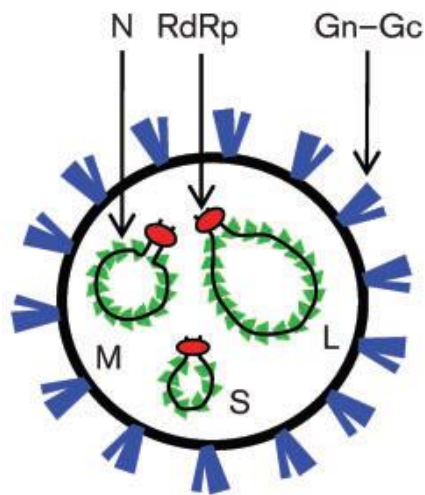
This altogether makes zoonotic emerging viruses a challenge to protect human and animal health, and their consequences on the economy, as we have seen recently with the outbreak of a previously unknown disease, SARS-CoV-2, which was declared a pandemic less than 4 months from its discovery. More research needs to be done on emerging viruses to avoid this kind of situations in the future.

## 1.2. Bunyaviruses

The *Bunyavirales* order constitutes over 380 segmented negative stranded enveloped RNA viruses divided into twelve families (25), namely *Arenaviridae*, *Hantaviridae*, *Nairoviridae*, *Peribunyaviridae*, *Phenuiviridae*, *Cruliviridae*, *Fimoviridae*, *Leishbunyaviridae*, *Myxoviridae*, *Phasmaviridae*, *Tospoviridae* and *Wupedeviridae*, with only the first five of these families containing human- and animal-infecting viruses. All bunyavirales members share the following characteristics: spherical virus particles of 80-120 nm in diameter, which are enveloped by a lipid bilayer with glycoprotein surface spikes; a negative-sense or ambisense single-stranded RNA genome, in the form of pseudo-circular ribonucleoprotein (RNP), RNA-nucleocapsid protein (N protein) complexes that are associated with a virus-encoded polymerase. For the human- and

animal-infecting bunyavirales members classified within *Hantaviridae*, *Nairoviridae*, *Peribunyaviridae* and *Phenuiviridae* families, the genome is divided into three segments known as Small (S), Medium (M) and Large (L) (Figure 1.3), whereas members of the *Arenaviridae* family possess just 2 segments (S and L).

The S segment of all *Bunyavirales* encodes the N protein that encapsidates the viral RNA to form RNP complexes (26). The S segment can also encode a non-structural protein called NS<sub>S</sub>, whose primary role is to modulate the host-cell antiviral response through diverse innate-immunity pathways (27). The M segment encodes a polyprotein precursor that is processed into two structural glycoproteins, G<sub>N</sub> and G<sub>C</sub>, and in some cases a non-structural protein (NS<sub>M</sub>). The G<sub>N</sub>-G<sub>C</sub> moieties form a heterodimer that performs critical roles in mediating virus assembly, formation of the virus particle and attachment to new target cells (driven by G<sub>N</sub>) and fusion (driven by G<sub>C</sub>) (27). The L segment encodes the RNA-dependent RNA polymerase (RdRp) (28) that is responsible for all viral RNA synthetic events. The N protein and G<sub>N</sub>-G<sub>C</sub> are thought to be the main immunogenic proteins of these viruses as the N protein is highly expressed in infected cells and G<sub>N</sub>-G<sub>C</sub> by decorating the surface of the virions are exposed to the immune system and antibodies have been detected in infected animals and humans against these proteins (29–31).



**Figure 1.3** *Bunyavirales* virion structure.

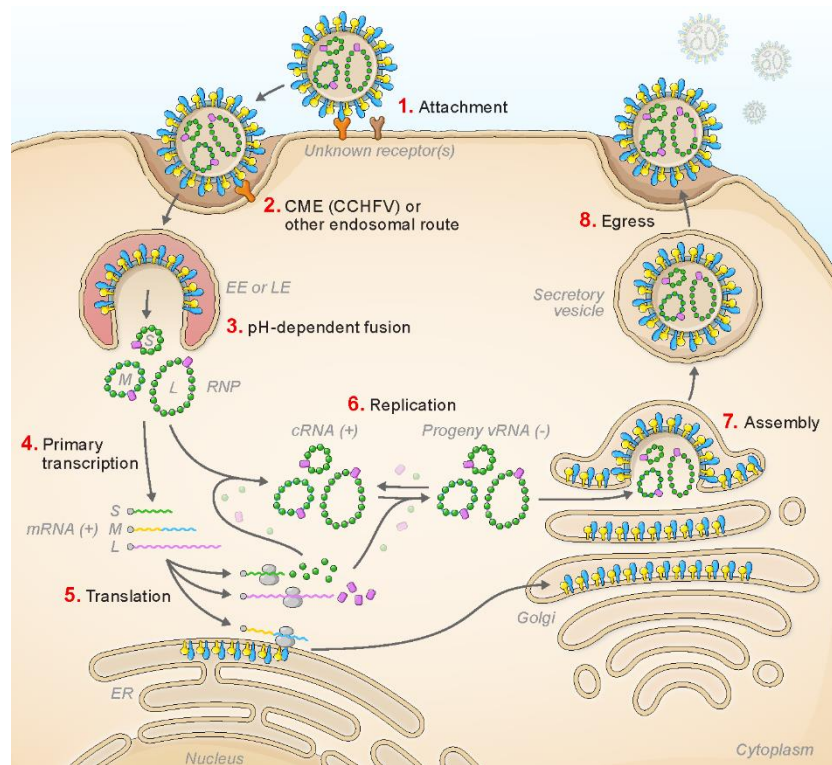
*Bunyavirus* particles are enveloped and generally spherical, with spikes comprising Gn–Gc heterodimers arranged in genus specific arrays on the membrane exterior. The bunyavirales genome comprises three RNA segments (S, M and L) wrapped in the viral nucleocapsid (N) protein in a circular conformation. Figure adapted from Walter CT, Barr JN. Recent advances in the molecular and cellular biology of bunyaviruses. *J Gen Virol.* 2011;92(11):2467–84.

Members of the *Bunyavirales* order follow the same general replication cycle stages (see Figure 1.4). For most bunyaviruses the receptors involved in the virus entry remain unidentified. For viruses of the *Phlebovirus* genus (such as RVFV) it has been shown that DC-SIGN, a C-type lectin expressed on the surface of dermal dendritic cells (DCs), can be used to infect dermal DCs (32). However, phleboviruses likely use other receptors as they can infect cell lines not expressing DC-SIGN. Regarding CCHFV, the cell receptor has not been identified yet, but a plausible CCHFV receptor has been suggested by Xiao *et al.* which have found a functional interaction between CCHFV G<sub>C</sub> and human cell surface nucleolin (33). Other bunyaviruses such as New World hantaviruses including Andes virus and Sin Nombre virus recognize the outermost extracellular repeat domain of protocadherin-1 for their entry in endothelial cells (34). Bunyaviruses enter the cell by endocytosis. For RVFV it has been shown that caveola-mediated endocytosis is the primary endocytic pathway for a strain of RVFV (RVFV MP-12) in mammalian cell lines and that ribonuclease kappa is required for RVFV uptake in mammalian cell lines (35,36). CCHFV is endocytosed through a clathrin-mediated endocytosis mechanism and is dependent on pH and cholesterol (37). After endocytosis, the endosomal membrane fuses with the viral membrane.

Following the fusion event, the RNPs associated with the viral polymerase are released into the cytoplasm where primary transcription is initiated yielding viral mRNAs. This primary transcription is primer-dependent, using host-cell derived capped primers cleaved by the endonuclease domain located in the L protein, using a process called ‘cap-snatching’ (28). Shortly after the onset of primary mRNA transcription, the viral polymerase initiates RNA replication, which is a primer-independent process resulting in the synthesis of a full-length positive sense complementary copy of the input negative sense RNA, which is co-transcriptionally encapsidated with N protein forming an RNP. This copy is known as the anti-genome and is used as a template from which to copy further negative sense viral RNAs (vRNAs). These vRNAs are subsequently used for further transcription (secondary transcription) or are assembled into virions, destined for release. It is thought that bunyaviruses establish “virus factories”, as shown for Bunyamwera virus by Fontana *et al.* by recruiting cell organelles around the Golgi complex to build “viral tubes” where the viral replication and morphogenesis takes place (38,39).

The maturation of CCHFV glycoprotein precursor (GPC) is complex and different than of other bunyaviruses. The maturation of CCHFV GPC produces the structural proteins  $G_N$  and  $G_C$ , several secreted non-structural glycoproteins (GP38, GP85 and GP160) and the non-structural M protein ( $NS_M$ ) (Figure 1.5) (40,41). The GPC has an N-terminal signal peptide to direct its synthesis to the secretory pathway before cleavage of this signal peptide (42). The GPC is synthesized in the endoplasmic reticulum (ER) where N-glycosylation occurs and the signal peptide is removed. The GPC is thought to be co-translationally cleaved by signal peptidase and intramembrane cleaving protease leading to generation of the  $G_N$  precursor (Pre $G_N$ ) formed by the mucin-like domain (MLD), GP38 and  $G_N$ , the  $G_C$  precursor (Pre $G_C$ ), and the  $NS_M$ . (41). Then, Pre $G_N$  and Pre $G_C$  are transported to the Golgi complex where the MLD is extensively O-glycosylated, Pre $G_N$  is cleaved by subtilisin kexin isozyme-1/site-1 protease (SKI-1/S1P) protease at the RRLI motif which results in  $G_N$  and the N-terminal products GP85/GP160 formed by the MLD and GP38 (40,43). These N-terminal products GP85/GP160 are further cleaved by a furin-like protease in the *trans*-Golgi network (TGN) at a conserved RSKR motif releasing MLD and the glycoprotein GP38 (40). The role these non-structural proteins, has not yet been elucidated, but it was shown that GP38 is highly secreted by infected cells and a monoclonal antibody (mAb) targeting this protein could protect mice from a lethal challenge and its crystal structure has recently been solved, providing a 3D template for exploration of GP38 function (31,44). Pre $G_C$  is cleaved at a RKPL motif potentially recognized by a SKI/S1P-like protease, however the exact protease responsible for the cleavage event is still unknown.

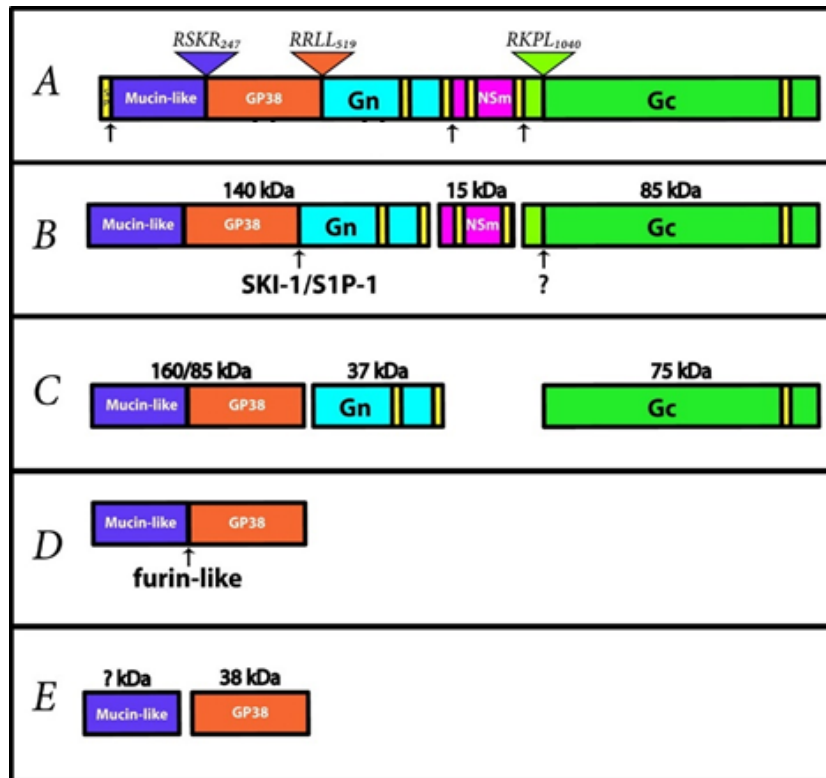
The RVFV M segment possesses 5 in-frame methionine codons near the beginning of the open reading frame (ORF) (45). The maturation of RVFV GPC produces the structural proteins  $G_N$  and  $G_C$  and two non-structural proteins of 78 kDa ( $NS_{M1}$ ) and of 14 kDa ( $NS_{M2}$ ) (46,47). The glycoproteins produced depend on the methionine used for the translation (Figure 1.6). When translation starts from the first methionine,  $NS_{M1}$  (containing the  $G_N$  precursor and  $G_N$ ) and  $G_C$  are produced (48). Translation initiating at the second methionine yields  $NS_{M2}$ ,  $G_N$  and  $G_C$  (48). A glycoprotein precursor that is co-translationally cleaved into  $G_N$  and  $G_C$  is produced when the translation initiates at the fourth and fifth methionine (49).  $G_N$  contains a Golgi localization signal and  $G_N$  and  $G_C$  transit from the ER to the Golgi (50).



**Figure 1.4 Representation of the replication cycle of Nairoviruses (Bunyavirales).**

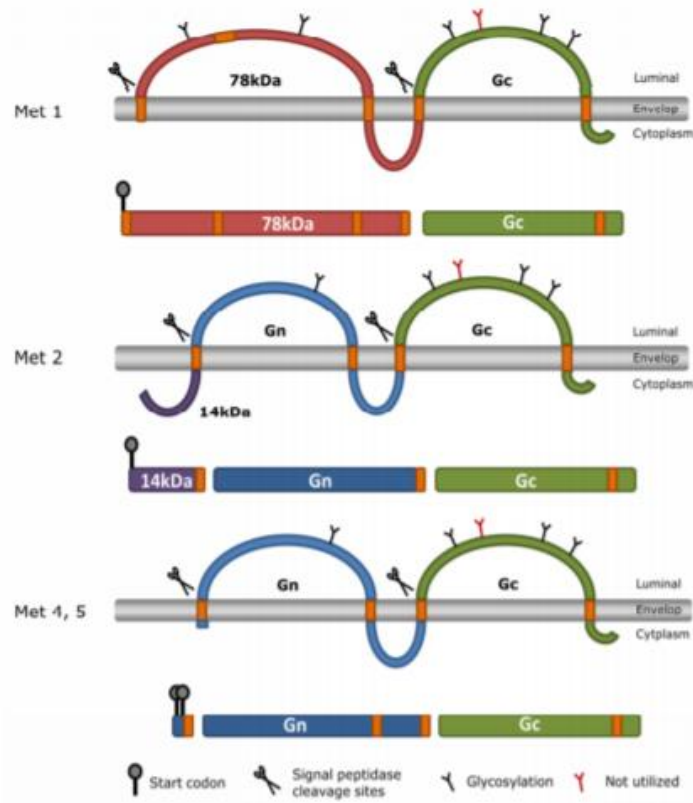
(1) Viral attachment; (2) endocytosis-mediated entry of the virion; (3) cell membrane fusion with the virion; (4) primary transcription; (5) translation; (6) replication; (7) viral assembly; (8) budding and egress. Figure adapted from ICTV ([https://talk.ictvonline.org/ictv-reports/ictv\\_online\\_report/negative-sense-rna-viruses/w/nairoviridae](https://talk.ictvonline.org/ictv-reports/ictv_online_report/negative-sense-rna-viruses/w/nairoviridae)).





**Figure 1.5** Representation of CCHFV GPC domains with their processing and the resulting proteins.

(A) Signal peptide (first domain in yellow), mucin-like (purple), GP38 (orange), Gn (turquoise), NSm (pink), and Gc (green) domains are represented. Potential transmembrane domains (yellow) and signal peptidase cleavage sites are indicated by black arrows. Defined furin-like, SKI-1/S1P and SKI-1/S1P-like cleavage sites are illustrated by inverted triangles. (B) The first proteolytic products after the synthesis of the GPC results in PreGn (140 kDa), NSm (15 kDa) and PreGc (85 kDa). SKI-1/S1P and PreGc convertase (?) will then cleave (indicated by arrows) PreGn and PreGc. (C) The activity of SKI-1/S1P and the PreGc convertase generates a non-structural mucin-like GP38 protein of either 160 or 85 kDa, and the structural glycoproteins Gn (37 kDa) and Gc (75 kDa). (D) The mucin-like GP38 is further cleaved (arrow) by a furin-like protease. (E) Furin-like enzyme cleavage results in production of a GP38 glycoprotein (38 kDa) and a mucin-like protein of unknown mass (? kDa). Figure adapted from Bergeron E et al. *Creean-Congo hemorrhagic fever virus glycoprotein processing by the endoprotease SKI-1/S1P is critical for virus infectivity. J Virol.* 2007;81(23):13271-13276.



**Figure 1.6 Representation of RSV GPC domains with their processing and the resulting proteins.**

The translation products are shown starting from the different methionine (1, 2 and 4/5). The different predicted glycosylation sites are shown by the “Y” symbols (with the red one known not to be utilized). The three protein products NS<sub>M</sub>1, NS<sub>M</sub>2, Gn and Gc are represented in red, purple, blue and green, respectively. The domains in orange show the predicted transmembrane domains. Figure adapted from de Boer, S. M. (2013). Rift Valley fever virus Glycoproteins, Key to Entry and Control.

The virus assembly is driven by the accumulation of G<sub>N</sub>-G<sub>C</sub> heterodimers in the Golgi with the tails of the heterodimers interacting with the N proteins of the RNPs, bringing in one location the major structural proteins of the virus particle (27). Most bunyaviruses bud into the Golgi apparatus (38), however, RSV buds from the plasma membrane in primary liver cells, meaning that the assembly could be cell-type dependent (27). Infectious particles are finally released from the infected cell by exocytosis.

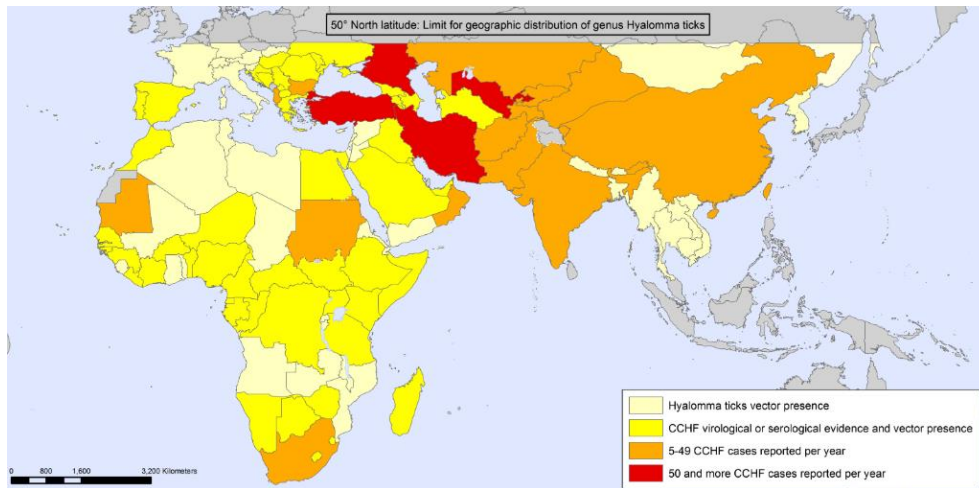
Viruses of the *Bunyavirales* order infect a wide range of animals as well as humans, sometimes causing serious diseases. Infection in these mammalian hosts is mediated by vectors, and for members of the *Nairoviridae*, *Peribunyaviridae* and *Phenuiviridae* families, these vectors are exclusively biting arthropods. In contrast, members of the *Arenaviridae* and *Hantaviridae* families are spread by rodents and possibly by non-rodent insectivores.

Recently, there has been a growing interest in several viruses of the *Bunyavirales* order, which can cause in humans and animals non-specific febrile illness, encephalitis, and haemorrhagic fever, and many species are teratogenic in infected gestating livestock (51). Moreover, some of these viruses have a growing importance because of the ongoing spread of their vectors, notably CCHFV, which is transmitted by the *Hyalomma* species of hard-bodied tick, and the *Aedes*, *Culex* and *Anopheles* species of mosquitoes, which are important vectors for RVFV. The habitats of all these vectors are changing with time, and are encroaching upon more Northerly regions of Europe, possibly due to changes in global climate (9). CCHFV and RVFV viruses are zoonotic viruses and thus they are a real threat that must not be neglected as the consequences of the associated diseases Crimean-Congo haemorrhagic fever (CCHF) and Rift Valley fever (RVF) are dramatic, both for human and animal health. Finally, to emphasize even more their relevance, both CCHF and RVF are included in the OIE list of notifiable terrestrial and aquatic animal diseases (52).

### **1.2.1. Crimean-Congo haemorrhagic fever virus**

The CCHF is a tick-borne zoonotic disease caused by CCHFV, belonging to the *Orthonairovirus* genus in the *Nairoviridae* family.

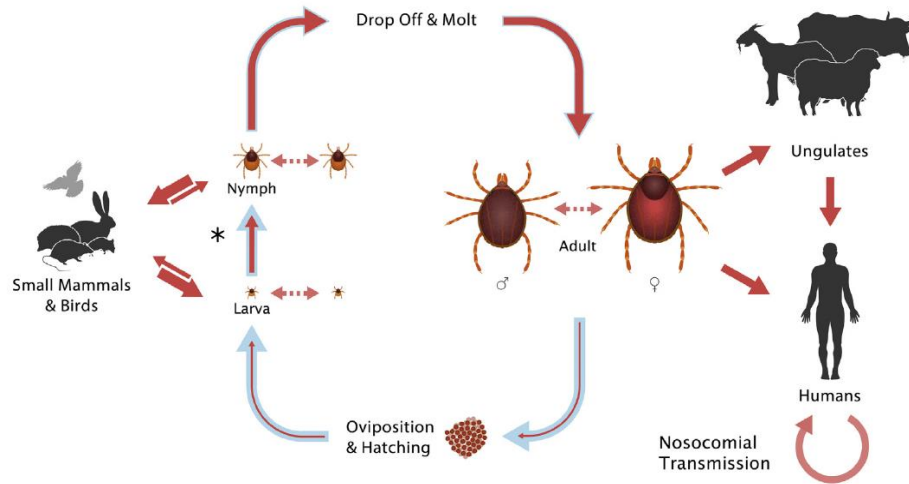
The disease was discovered in the Crimean peninsula where it caused an outbreak in 1944 in Soviet troops, with 200 soldiers infected, around 10% of which died (53). This virus was then found to be serologically identical to a virus discovered in the Belgian Congo in 1956 and called the Congo virus (54). CCHF is the most important and widespread tick-borne viral disease of humans (Figure 1.7) and is the most widespread arboviral pathogen after the dengue virus (55).



**Figure 1.7 Geographic distribution of Crimean-Congo haemorrhagic fever and its vector (*Hyalomma* ticks).**

Figure adapted from the World Health Organization (<https://www.who.int/health-topics/crimean-congo-haemorrhagic-fever/>).

CCHFV is the most genetically diverse of the arboviruses, with nucleotide sequence differences among isolates ranging from 20% for the viral S segment to 31% for the M segment (53). It causes sporadic cases or outbreaks of severe illness across a huge geographic area based on the distribution of *Hyalomma* ticks, the predominant vector of the virus (56). Its range covers a huge geographic area from western China to the Middle East and South-Eastern Europe and throughout most of Africa and more recently was found in Spain (53,57). CCHFV is maintained through trans-stadial, transovarial and venereal transmission in several species of ixodid (hard) ticks (53), as shown in Figure 1.8.



**Figure 1.8** Life cycle of *Hyalomma* ticks (blue arrows) and the transmission of CCHFV to animals and humans (red arrows).

After hatching, larvae feed on small mammals or birds for their first blood meal (hematophagy), followed by molting (asterix). The nymphs continue to feed on small animals and drop off their host and molt into adults. Adults feed on large mammals and mate. Engorged females drop off and find a suitable location for ovipositing. Virus transmission between ticks through co-feeding is represented by dashed arrows and, between ticks and animals, by solid red arrows. Figure adapted from Bente DA et al. *Creean-Congo hemorrhagic fever: History, epidemiology, pathogenesis, clinical syndrome and genetic diversity*. *Antiviral Res.* 2013;100(1):159–89.

*Hyalomma* ticks infest a wide spectrum of different wildlife species (e.g. deer and hares) and free-ranging livestock animals (e.g. goat, cattle, and sheep). Hard ticks are the natural reservoir of CCHFV and they remain infected throughout their lifetime. Humans are only “dead-end” hosts for the virus (53), meaning further natural spread either does not occur or is unlikely. In addition to tick exposure, CCHF can also result from contact with the body fluid of infected animals or humans, and nosocomial human-to-human transmission is often associated with outbreaks, resulting in the infection of health care workers (58). Finally, there are some concerns that climate change and warmer climates in central and northern Europe might permit the expansion of the geographic range of infected ticks by migratory birds or the international livestock trade, and thus expansion of the CCHFV geographic distribution (53).

The disease is asymptomatic in infected animals but can develop into severe illness in humans, with case-fatality rates ranging between 10-40% (59).

The susceptibility to CCHFV is often species-dependent, but CCHFV can infect a broad range of mammals including sheep, lambs, goats, cattle, calves, horses, dogs and camels. Birds are not susceptible to CCHFV infection, with an exception for ostriches which can

be infected by CCHFV (60). It has been shown that CCHFV occurs most frequently in larger mammals than smaller mammals, because these are the preferred hosts of adult *Hyalomma* ticks (61). As animals do not develop clinical signs, CCHFV infections have no effect on the economic burden regarding livestock animal production.

However, for humans, infection outcome is different; the incubation period is typically 3–7 days, with sudden onset of myalgia, headache, and fever that can develop into a severe haemorrhagic syndrome (53). In severe cases of CCHF in humans, there is a deregulation and an excessive release of cytokines that are combined with endothelial activation. This cascade leads to an increase in the vascular permeability, vasodilatation, multiple organ failure, shock and death. It has been shown that this virus can also impair the innate immune system and delay the adaptive immune response leading to an uncontrolled viral replication and spread of the virus throughout the body (62). Until recently, the only animal model to manifest the disease was the newborn mouse (63), but more recently some knock-out mice models (64,65) and a non-human primate model (cynomolgus macaque model) have been used (66).

Due to the lack of animal models, neither effective treatment nor vaccine has been discovered against CCHFV. Ribavirin, a guanosine analog, is usually used to treat patients infected with CCHFV with mixed results (67). More recently, another antiviral drug, favipiravir, has been used *in vitro* and *in vivo* with promising results (68).

### **1.2.2. Rift Valley fever virus**

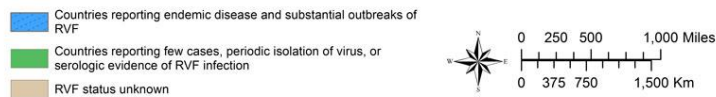
The RVF is a mosquito-borne disease caused by the RVFV, which belongs to the *Phlebovirus* genus included in the *Phenuiviridae* family. The virus was first discovered in 1930, as the causative agent of an enzootic hepatitis in the Rift Valley of Kenya (69). RVF is a zoonotic disease infecting both humans and livestock with a mortality rate of 1–3% among humans (70). There is only one serotype recognized for this virus, but strains exist of variable virulence (71).

RVFV is endemic in tropical regions of Southern and Eastern Africa but the geographic range of the virus has grown significantly since its discovery (Figure 1.9). Its geographic range now includes most of the countries in Africa and Madagascar and it emerged for the first time outside Africa in the Arabian Peninsula in 2000–2001 (72), where it caused

a large outbreak in livestock and humans. In recent years it has been detected for the first time in the Comoros and on the French Island of Mayotte (73).



**Rift Valley Fever Distribution Map**

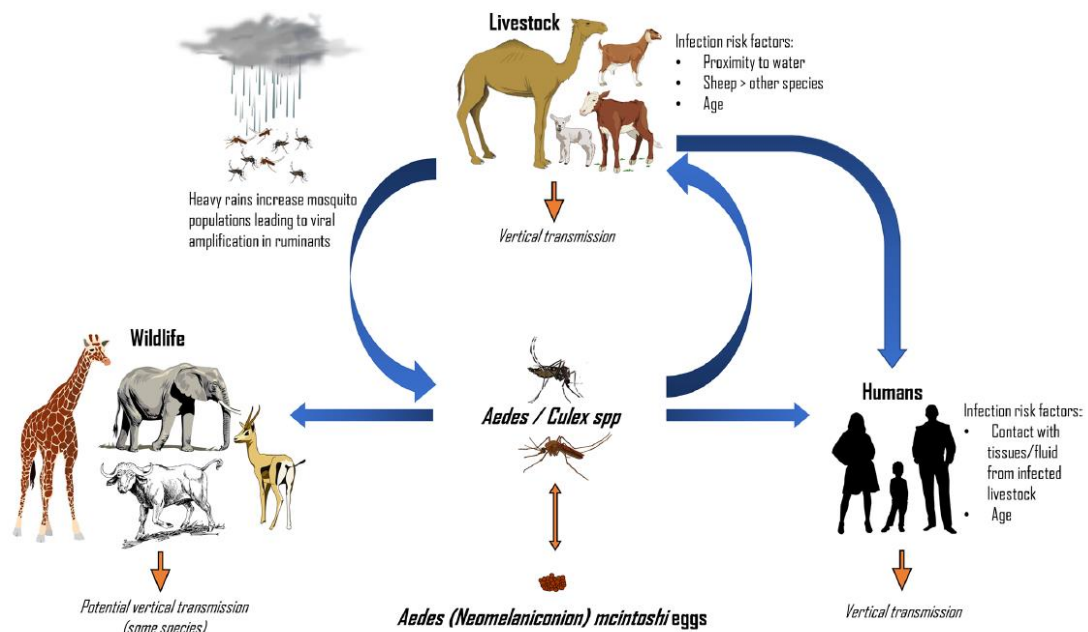


**Figure 1.9 Geographic distribution of Rift Valley fever.**

Figure adapted from Centers for Disease Control and Prevention (<https://www.cdc.gov/vhf/rvf/outbreaks/distribution-map.html>).

The main vectors of RVPV are mosquitoes (*Aedes*, *Anopheles*, *Culex*, *Eretmapodites*, *Mansonia*, etc.) but RVPV can infect a large array of vectors including ticks, midges and sand flies (14). The members of the *Culex* and *Aedes* genera are considered the main vectors with the latter being the reservoir for this virus, as its transovarially infected eggs withstand desiccation and larvae hatch when in contact with water. Moreover, once this vector is infected with RVPV, it is infectious for the rest of its life. According to the OIE, the transmission of the virus to animals can occur through wild fauna and various vectors (Figure 1.10). Transmission to humans, occur either through contact with bodily fluids of infected animals, mosquito bites or infected meat and also by aerosols (contamination

through droplets containing RVFV occurred in laboratory settings) and possibly by consumption of raw milk (74). Finally, there is an increasing risk of dissemination of RVFV to RVF-free countries, such as in Europe and in the USA, due to the broad range of vectors present in RVF-free regions, the international trade of live animals and the influence of climate change on the vector habitat (75,76).



**Figure 1.10** *Aedes/Culex* mosquitoes' life cycle and the transmission of RVFV to animals and humans.

RVFV is maintained in *Aedes* eggs through transovarial transmission. Heavy rains increase mosquito populations, which leads to viral amplification in ruminants and can then cause outbreaks in both animal and human populations. Figure adapted from Wright D et al. Rift Valley Fever: Biology and Epidemiology. *Journal of General Virology*. 2019;100(8):1187–1199.

Infection of RVFV causes high rates of abortions in pregnant domestic ruminants, and high mortality rates among newborns, causing devastating socioeconomic impact (77). In addition, numerous outbreaks have been reported in humans especially in Africa and Middle Eastern countries (78–80). RVFV infection in humans primarily causes a self-limiting febrile illness; however, in some patients, infection results in blindness, encephalitis or haemorrhagic fever with a generally fatal outcome (81). The signs of disease are non-specific, but an influenza-like disease in humans and a high number of abortions and deaths in young animals is indicative of RVF.



According to the OIE, the severity of the disease varies according to the species. Some species such as equids, dogs, cats and pigs exhibit low or invisible signs of infection. In contrast, other species are moderately susceptible to RVF including cattle, goats and humans, with mortalities below 10%. Other species such as sheep and calves are highly susceptible with a mortality rate ranging between 20% and 70%. Finally, young animals (lambs, puppies, kittens and human children) are extremely susceptible with a mortality rate between 70% and 100% (74).

Currently, there are no commercial human vaccines to protect against RVFV, but some vaccines have been developed and are commercially available for ruminants. The two historic vaccines used in animals are based on the Smithburn RVFV strain. This strain is a derivative of the Entebbe strain isolated in 1944 from a mosquito in Uganda, which was passed in suckling mice (82). This strain was further passed in mice and chicken eggs before being used as a vaccine. This vaccine has a relatively low cost, induces a long lasting immunity after one immunization, but as it is a live attenuated vaccine, it was shown to lead to abortion or teratology of pregnant animals and has potential for reversion, thus should not be used in RVFV-free countries (83–85)). A formalin-inactivated derivative of the Smithburn RVFV strain is also commercially available for veterinary use. This vaccine is more expensive and needs regular boosts to maintain immunity, which makes it less attractive in developing countries. Another vaccine, named Clone 13 is licensed in South Africa for veterinary use. This clone is a naturally attenuated mutant obtained from a plaque-derived clone that was isolated in the Central African Republic from a patient infected with RVFV (86). This vaccine appears to be very immunogenic and safe in sheep and cattle, and is starting to be widely used in Africa to control RVFV (85). Finally, a human inactivated vaccine, TSI-GSD-200 was used in the USA to protect laboratory and military staff, but it is not licensed and is not commercially available (87). Many vaccines are being developed for humans and/or animals and in the coming years new safe and efficient vaccines should be available (88).

Just as for CCHFV, there are no effective treatments and the strategy to treat severe cases with RVF is focused on supportive care. Ribavirin which is used to treat a range of haemorrhagic fevers and favipiravir which is used to treat a wide range of RNA viruses have been tested using animal models, with contrasted results (89).

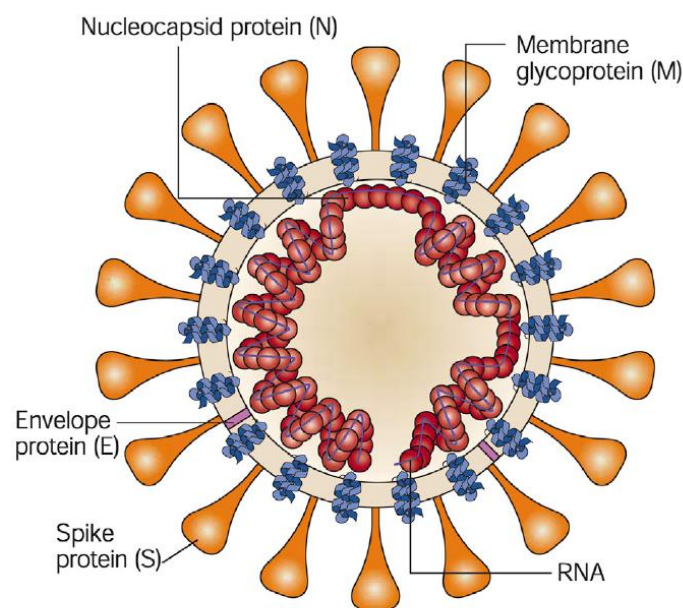
### 1.3. Severe acute respiratory syndrome coronavirus 2

In December 2019, a novel coronavirus of animal origin, SARS-CoV-2, emerged in the city of Wuhan, in China, with the ability for human-to-human transmission (10). SARS-CoV-2 (at first named 2019-nCoV) is a member of the *Coronaviridae* family and has a 89% nucleotide similarity with the coronavirus responsible for the SARS outbreak (90). A group of coronavirus related to SARS were isolated from bats in China (91) and these coronaviruses are part of the genus *Betacoronavirus*, one of the four genera (with *Alphacoronavirus*, *Deltacoronavirus* and *Gammacoronavirus*) of the *Orthocoronavirinae* subfamily. The *Alphacoronavirus* and *Betacoronavirus* genera regroup the seven human coronavirus (HCoV), which, before the outbreak of SARS-CoV in China in 2002/2003 (92), were thought to only cause mild disease, in humans. Before this outbreak, only HCoV-229E (*Alphacoronavirus*, (93)) and HCoV-OC43 (*Betacoronavirus*, (94)) were known as human pathogens, however, after the outbreak of SARS-CoV, more research was done on coronaviruses leading to the discovery of HCoV-NL63 (*Alphacoronavirus*, (95)) and HCoV-HKU1 (*Betacoronavirus*, (96)). However, the other three HCoV cause severe disease and had higher impacts in the last two decades by provoking outbreaks: SARS-CoV in China in 2002/2003, MERS-CoV in the Middle East in 2012 and SARS-CoV-2 causing a pandemic in 2020. SARS-CoV-2 is highly similar to a bat coronavirus (BatCoV RaTG13) with an overall genome sequence identity of 96% (97) and to pangolin coronavirus with an overall genome sequence identity of ~90% and nearly identical receptor binding domains (RBD) (98,99). This hints that SARS-CoV-2 probably originated in one of these animal hosts before being transmitted to humans directly or through transmission to an intermediate host. However, a 96 and 90% identity between SARS-CoV-2 and a bat coronavirus or a pangolin coronavirus is not as high as observed for SARS-CoV and MERS-CoV that had an animal origin and their intermediate host. Indeed, SARS-CoV and MERS-CoV had a genome identity of 99.8% and 99.5% with the one found in their likely intermediate host, palm civets (100) and dromedary camels (101), respectively. These results have highlighted the potential involvement of an intermediate host in the transmission of SARS-CoV-2 to humans, however this intermediate host has not been identified yet, also increasing the risks of transmission of other potential SARS-CoV-2-like viruses to humans.

The associated disease, named COVID-19 (for coronavirus disease 2019), spread rapidly all over the world, and was declared a pandemic by the WHO on March 11th, 2020. Infection due to SARS-CoV-2 induces high rates of morbidity and mortality as described by the WHO (102). Most symptoms of COVID-19 are flu-like symptoms with symptoms ranging from fever, associated with respiratory symptoms (such as cough, breathing difficulties, chest distress), fatigue, myalgia, digestive symptoms, anosmia and ageusia (103,104,105). However, in some cases, for the elderly, or patients presenting comorbidities (such hypertension, cardiovascular disease, obesity, diabetes,...) (106) it can develop into a severe disease such as acute respiratory distress syndrome and require intensive care unit admission and can result in death (107). The case fatality rate and the basic reproductive number ( $R_0$ ) of SARS-CoV-2 are difficult to estimate due to the ongoing pandemic and the lack of data on the total number of people infected by SARS-CoV-2. Despite that, some studies have tried to predict these numbers and found a case fatality rate around 0.5-1% and a  $R_0 \sim 2.5$  (108,109). One of the problems to control the rapid spread of the virus is the number of asymptomatic or pre-symptomatic carriers of the virus that can unknowingly spread the virus (110,111). Thus, to control the spread of the virus, the main preventive methods are hygiene measures together with social distancing. Moreover, to reduce the spread of the virus, countries have decreed travel restrictions and partial or complete lockdown (such as in China, France (108,112,113) or had an approach with massive testing and isolation of confirmed cases and their contacts (such as in South Korea (114) or even without or with late measures (such as Brazil and the USA (115)). Since the beginning of the pandemic, several drugs or biological products have been approved by agencies such as the American Food and Drug Administration (FDA, granting Emergency Use Authorization, EUA) to treat COVID-19, including using plasma from COVID-19 convalescent patients, drugs such as casirivimab and imdevimab, remdesivir, and bamlanivimab (116). However, these treatments have shown mixed clinical efficacy as a recent study by the WHO has shown that several drugs including remdesivir, hydroxychloroquine, lopinavir, and interferon regimens had little or no effect (117). Moreover, early results from the Randomised, Embedded, Multi-factorial, Adaptive Platform Trial for Community-Acquired Pneumonia has shown that administration of convalescent plasma was unlikely to be beneficial (118), when another recent study has shown that administration of convalescent plasma reduced the progression of COVID-19 in mildly ill patients (119). In addition to treatments, vaccines have been rapidly developed, recently authorized by regulatory agencies and vaccination

campaigns have now started worldwide. Two of the three vaccines that are now authorized (Moderna COVID-19 Vaccine and Pfizer-BioNTech COVID-19 Vaccine) are RNA vaccines that have conferred over 94% protection against COVID-19 (120,121). The last vaccine authorized (Oxford-AstraZeneca COVID-19 Vaccine) is a replication-deficient chimpanzee adenoviral vector ChAdOx1 containing the SARS-CoV-2 S protein that showed between 60 and 90% protection against COVID-19 (122). All these solutions to fight the COVID-19 pandemic could change the pattern of SARS-CoV-2, which could become a seasonal coronavirus (123).

Members of the *Coronaviridae* family are enveloped, single stranded RNA viruses, with large genomes of around ~30 kb. Their genome encodes four major structural proteins: the spike (S) glycoprotein, the membrane (M) glycoprotein, the envelope (E) protein and the nucleocapsid (N) protein, as represented in Figure 1.11.



**Figure 1.11 Coronavirus virion structure.**

*Coronavirus particles are enveloped and generally spherical, with spike (S) trimers on the viral envelope. The membrane is formed of the membrane glycoprotein (M) and envelope protein (E). The coronavirus genome is wrapped in the viral nucleocapsid (N) protein in a beads-on-a-string type conformation. Figure adapted from Burrell CJ et al. Coronaviruses. In: Fenner and White's Medical Virology. Fifth edition. p. 437–46.*

The S protein of SARS-CoV-2 is a large class I fusion glycoprotein (~140 kDa), which forms trimers that are inserted within the viral envelope, and which give the coronaviruses their characteristic appearance. Each monomer has 22 glycosylation sites, which make the trimer a highly glycosylated protein (124). This trimer recognizes as cellular receptor the human angiotensin-converting enzyme 2 (hACE2), which is expressed on the surface of cells of the lungs, heart, kidneys, and intestines as well as other tissues such as nasal and olfactory mucosa and is involved in the cell entry of the virus (125). The wide location of hACE2 can explain the broad SARS-CoV-2 virus tropism and the replication of SARS-CoV-2 was demonstrated to take place in tissues of the upper respiratory tract (126). hACE2 is the same cellular receptor as recognized by SARS-CoV to mediate cell entry (127), although different to that used by MERS-CoV (128). The SARS-CoV-2 S protein contains the RBD, the region (~20 kDa) specifically involved in the binding to hACE2, which had a stronger affinity for hACE2 in than SARS-CoV (129).

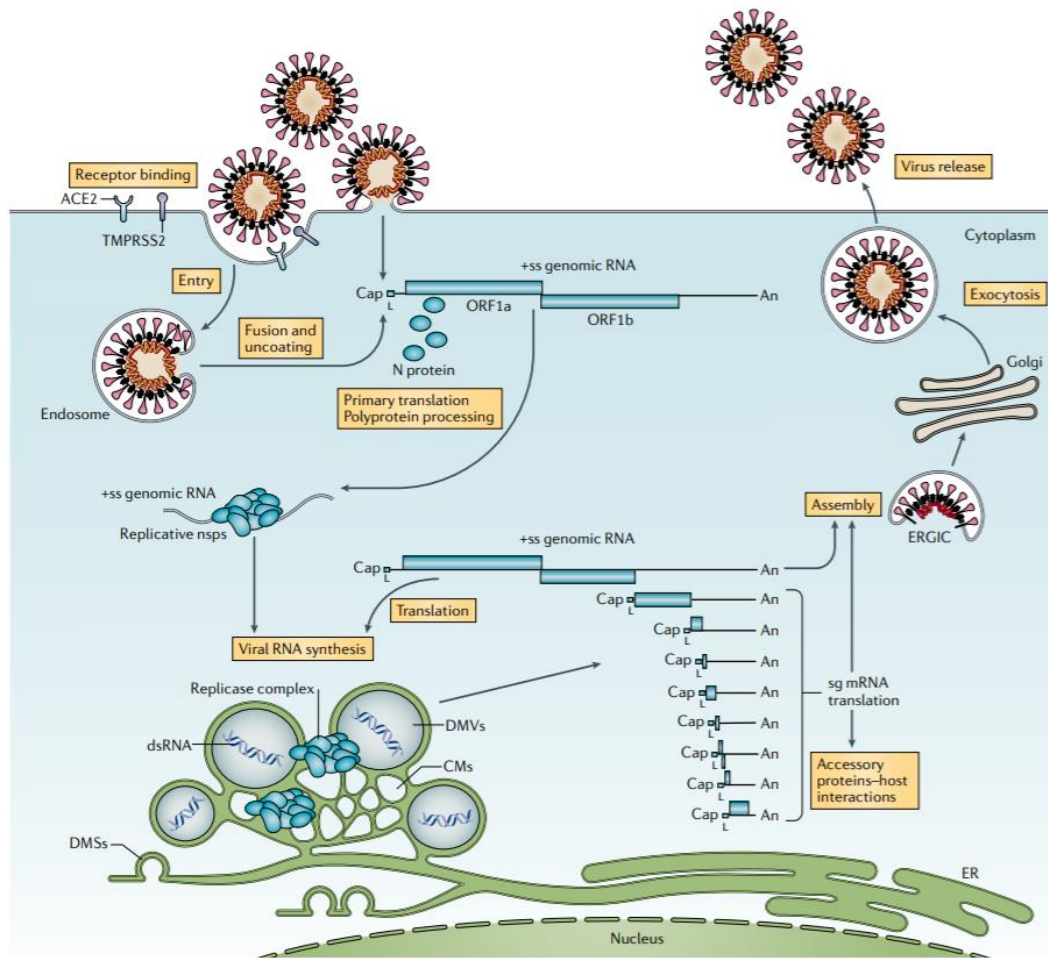
The M protein is a short transmembrane glycoprotein with three transmembrane domains, which is the most abundant glycoprotein in the virion (130). It is involved in the curvature of the cellular membrane that becomes the virion envelope and promotes virus assembly (131).

The E protein is a short integral membrane protein that is found in low quantities in the virion (132). The role of the E protein has not been fully elucidated but it has been demonstrated that it is involved in virus assembly, membrane curvature and budding process, but also has an anti-apoptotic function (demonstrated in SARS-CoV) and inflammatory response (130,132).

The N protein (~45 kDa) is the protein involved in the binding of the viral RNA in a beads-on-a-string type conformation, in the package of encapsidated genome into viral particles and in virus particle release (133,134). It contains an N-terminal domain and a C-terminal domain, both involved in the binding of the viral RNA (134).

As stated above, the attachment of SARS-CoV-2 to the target cell is mediated by the binding of the RBD in the S1 region of the S protein to the hACE2. SARS-CoV-2 uses the transmembrane protease serine 2 (TMPRSS2) for the S protein priming, which causes cleavage of the S protein at two sites (between the S1 and S2 regions and at a second site on the S2 region), and these conformational rearrangements allow S2 to drive the fusion of the viral and cellular membranes (135). Following the fusion event, SARS-CoV-2

genome is released in the host cell cytoplasm. Two polyproteins (pp1a and pp1ab) are produced from the translation of ORF1a and ORF1b of the genomic RNA, which, after proteolytic cleavage by Papain-like protease and 3C-like protease, produces 16 non-structural proteins (nsp1-16) (136). At the same time, SARS-CoV-2 has been shown to modify ER membranes to form viral replication organelles including double-membrane vesicles, double-membrane spherules and convoluted membranes, to create a protective space for viral RNA synthesis (137,138). Nsp1 has been shown to bind to the 40S ribosomal subunit and stop host mRNA translation (139,140), when nsp2-16 form the viral replication and transcription complex (RTC). The synthesis of viral RNA is done by the nsp12 RdRp with cofactors nsp7 and nsp8 (141) and nsp14 contains a 3'-to-5' exoribonuclease domain which is thought to have a proofreading activity during genome replication (142). Genomic replication starts with the synthesis of copies of negative-sense genomic RNA, which can then be used as templates to produce positive-sense genomic RNA. During the transcription of negative-sense RNA, the RTC stops the transcription when finding transcription regulatory sequences, creating a set of subgenomic negative-sense RNAs, which can then be transcribed into subgenomic mRNAs (136). The ORFs encoding the structural proteins (S, M, E and N proteins) are translated and S, M and E proteins translocate into the ER membranes and transit through the ER-to-Golgi intermediate compartment (ERGIC) (136). Accessory proteins are also expressed from ORFs encoding accessory genes. The N protein, which encapsidates the genomic RNA, forming RNPs, bud to the ERGIC to interact with the other structural proteins for virus assembly, creating virions. Finally, it has been shown that SARS-CoV-2 uses lysosomal trafficking for egress (143). These steps are summarized in Figure 1.12.



**Figure 1.12 Representation of the replication cycle of SARS-CoV-2.**

SARS-CoV-2 binds to human angiotensin-converting enzyme 2 (hACE2) and uses transmembrane protease serine 2 (TMPRSS2) for spike priming and promote viral uptake and fusion at the cellular membrane. Following entry, the genomic RNA is released and ORF1a and ORF1b are translated into two polyproteins pp1a and pp1ab. These are co-translationally and post-translationally processed into the individual non-structural proteins (nsps) that form the viral replication and transcription complex. Creation of viral replication organelles (double-membrane vesicles (DMVs), double-membrane spherules (DMSs) and convoluted membranes (CMs)) create a protective microenvironment for viral genomic RNA replication and transcription of subgenomic mRNAs (sg mRNAs) comprising the characteristic nested set of coronavirus mRNAs. Translated structural proteins translocate into endoplasmic reticulum (ER) membranes and transit through the ER-to-Golgi intermediate compartment (ERGIC), where interaction with N-encapsidated genomic RNA results in budding into the lumen of secretory vesicular compartments. Finally, virions use lysosomal trafficking for egress. An, 3' polyA sequence; cap, 5' cap structure; dsRNA, double-stranded RNA; L, leader sequence; RdRP, RNA-dependent RNA polymerase. Figure adapted from V'kovski P et al. Coronavirus biology and replication: implications for SARS-CoV-2. *Nat Rev Microbiol.* 2020

## 1.4. Immune response to viral infection

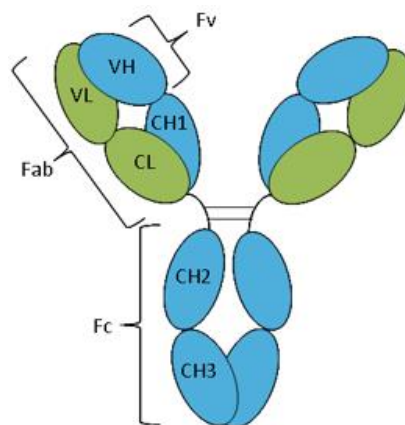
To prevent the entry of a virus, humans have many defences, the first of which are mechanical barriers such as the skin and mucous membranes and chemical barriers such as the low pH of the digestive tract.

Innate immunity is the first response and aims to block or inhibit the initial infection, to protect cells from infection or to eliminate virus-infected cells and then initiate the adaptive immunity (144). Adaptive immunity takes longer to develop and can be divided into two main responses: the cellular immune response and the humoral immune response. The cellular immune response (or T-cell mediated) is dependent on antigen-presenting cells (APCs) for their activation. T cells (or T lymphocytes) are divided into two subsets: CD8<sup>+</sup> T cells that kill the infected cell by a receptor-induced apoptotic signal and by releasing perforins and granzymes, and CD4<sup>+</sup> T cells that activate the antibody response through the secretion of different cytokines and interaction with membrane molecules (145). The humoral immune response (or antibody-mediated) is driven by B cells by recognition of a soluble antigen or antigen presented by APCs. The B cells then, with the help of CD4<sup>+</sup> T cells, differentiate into plasma cells (antibody-producing cells) or memory B cells. In case they do not receive help from the CD4<sup>+</sup> T cells, they differentiate into plasmablasts (short-lived antibody-producing cells) (146).

Antibodies (Ab), also called immunoglobulins (Ig) are glycoproteins used by the immune system to bind and neutralize pathogens such as viruses and bacteria, blocking their entry into new cells. Antigens (Ag) are defined as “any molecule recognized by the antigen-binding domain of an antibody” (147). The site at which the antibody binds on the antigen is called “epitope” and the region on the antibody where the antigen binds is called “paratope”. The binding between the antigen and the antibody is non-covalent and is driven by hydrogen bonds, ionic bonds, hydrophobic interactions and van der Waals forces (148,149). Igs all have a Y-like shape unit, which can be divided into two identical light polypeptide chains and two identical heavy polypeptide chains. This Y-like shape has two main effector regions, the antigen-binding fragment (Fab) where the antibody binds to the antigen and the fragment crystallizable region (Fc) which interacts with the Fc receptors on some cell surfaces. The heavy chain determines the five classes in which the Igs are divided, IgG, IgM, IgA, IgE and IgD and their subclasses. The two main classes of Igs involved in the immune response to a viral infection are IgG and IgM.



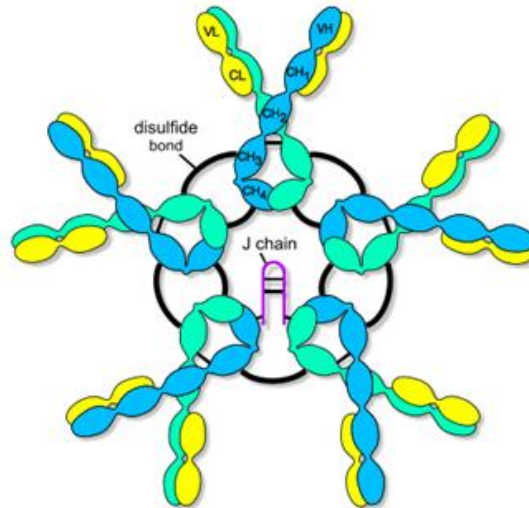
IgG are the most abundant class of antibodies present in the sera, making about 10-20% of the plasma proteins and up to 75 % of the total humans' antibodies (150). They are produced by plasma cells during the adaptive immune response to bind to pathogens and facilitate their removal. IgG typically appear around 14 days after an infection and remain in the bloodstream for months, even years. Thus, providing long-lasting immunity against pathogens, by the formation of memory B cells which will enable a rapid production of specific antibodies when a pathogen reinfects the host. IgG possess two heavy chains (50 kDa each) and two light chains (25 kDa each). IgG has a classic antibody structure with two light chains that have a constant ( $C_L$ ) and variable region ( $V_L$ ) and two heavy chains with one variable region ( $V_H$ ) and three constant regions ( $C_{H1}$ ,  $C_{H2}$  and  $C_{H3}$ ) as shown on Figure 1.13. IgG can further be divided into four subclasses (IgG1, IgG2, IgG3 and IgG4) depending on their amino acid sequence, with the main differences being found at the hinge region and constant region domains (151). As these domains are implicated in the binding of Fc receptors and complement proteins, these subclasses have different effector functions to trigger antibody-dependent cellular cytotoxicity (ADCC) and activating the complement cascade. Finally, the subclasses are usually induced by different antigens with IgG1 and IgG3 being induced by protein antigens and IgG2 and IgG4 by polysaccharide antigens (151).



**Figure 1.13 Structure and function of immunoglobulin G.**

The heavy chains (H) are represented in blue and the light chains (L) in green. V: variable region. C: constant region. Figure adapted from Absolute Antibody (<https://absoluteantibody.com/antibody-resources/antibody-overview/antibody-isotypes-subtypes/>).

IgM make up 10 % of the serum's antibodies (150). IgM are the first antibodies expressed by naïve B cells and are responsible for the primary immune response to pathogens, thus, they are indirect indicators of early stages of an infection. They have a pentameric structure (rarely hexameric) with five Y-like shape units linked together by disulfide bonds at the constant region and association with a joining chain (Figure 1.14).



**Figure 1.14 Structure of immunoglobulin M.**

*The five Y-like shape units are linked together by disulfide bonds at the constant region and associated with a joining chain (J chain). The heavy chains (H) are represented in blue or green and the light chains (L) in yellow. V: variable region. C: constant region. Figure adapted from <https://microbenotes.com/immunoglobulin-m-igm-structure-and-functions>.*


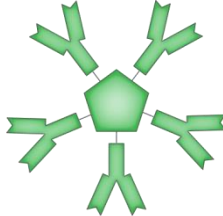
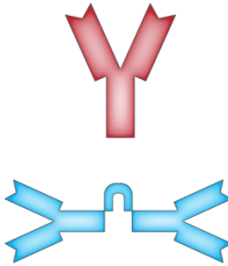


There are other classes of Igs produced and their role and characteristics are summarized in Table 1.1.

IgA are present on mucosal surfaces and in secretions (such as saliva, respiratory tract) and their role is to protect mucosal surfaces from pathogens by direct neutralization or binding to the pathogen to prevent its binding to mucosal surfaces (152). This type of Ig is produced mainly as a response to respiratory infections.

IgD are mostly present on the surface of B cells and are thought to recruit physiologically autoreactive B cells (153).

IgE are involved in the defence against parasitic worms, but are also involved in hypersensitivity and allergic reactions (154).

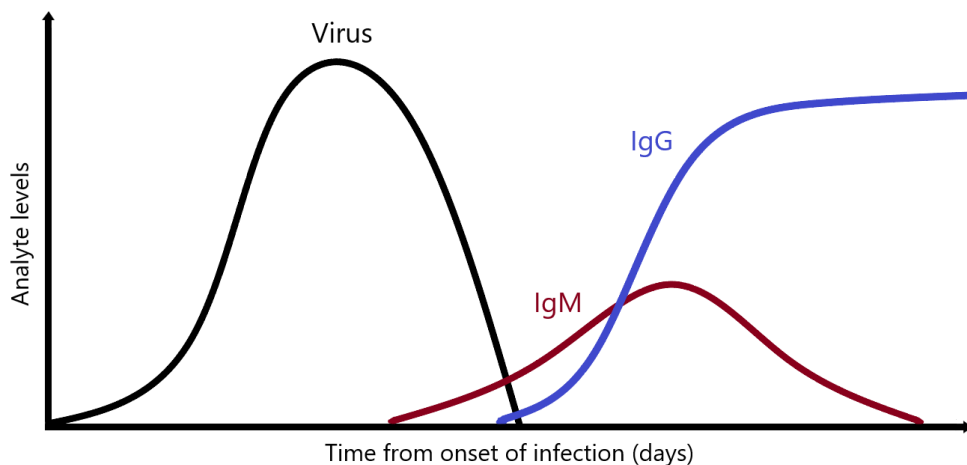
**Table 1.1 Summary of the main information about the different immunoglobulin classes.**

	Immunoglobulin class				
	IgG	IgM	IgA	IgD	IgE
Heavy chain	$\gamma$	$\mu$	$\alpha$	$\delta$	$\epsilon$
Molecular weight	146 kDa	970 kDa	160 kDa (monomeric) 385 kDa (dimeric)	184 kDa	188 kDa
Structure <sup>a</sup>					
Valency	2	10	2 or 4	2	2
Serum concentration	8-16 mg/mL	0.5-2 mg/mL	1-4 mg/mL	0-0.4 mg/mL	10-400 ng/mL
Half-life (days)	21	10	6	3	2
Function	Secondary response to pathogens	Primary response to pathogens	Protection of mucosal surfaces	Recruitment of autoreactive B cells	Protection against worm parasites

<sup>a</sup>Figures adapted from Martin Brändli

Antibodies can also lead to viral lysis by activation of the complement, opsonization or by ADCC. The complement system, which is part of the innate immune system, can be activated in the classical pathway by IgG or IgM bound to an antigen and leads to opsonization and phagocytosis, chemotaxis and lysis. (155). IgG coated to the cell surfaces of infected cells are recognized by natural killer cells which kill the target infected cell in a process called ADCC (156).

When the immune system reacts to a pathogen such as a virus, the virus will compete with the innate immune system and potentially proliferate. If the virus is able to proliferate and infect cells, the cytotoxic T lymphocytes will be activated and proliferate to stop the infection. Naïve B cells produce IgM isotype as the primary Ab-mediated immune response to the viral infection, usually 3 to 5 days post-infection (DPI) (Figure 1.15). Then, B cells are activated, proliferate and produce IgG specific to the virus (7 to 10 DPI), to work with the T cells to eliminate the viral infection. Memory T and B cells are also generated during this infection and these are critical in a secondary encounter with the pathogen to produce a rapid and specific secondary response (157).



**Figure 1.15 Diagram of the virus' and immunoglobulin's (IgM and IgG) levels after a viral infection.**

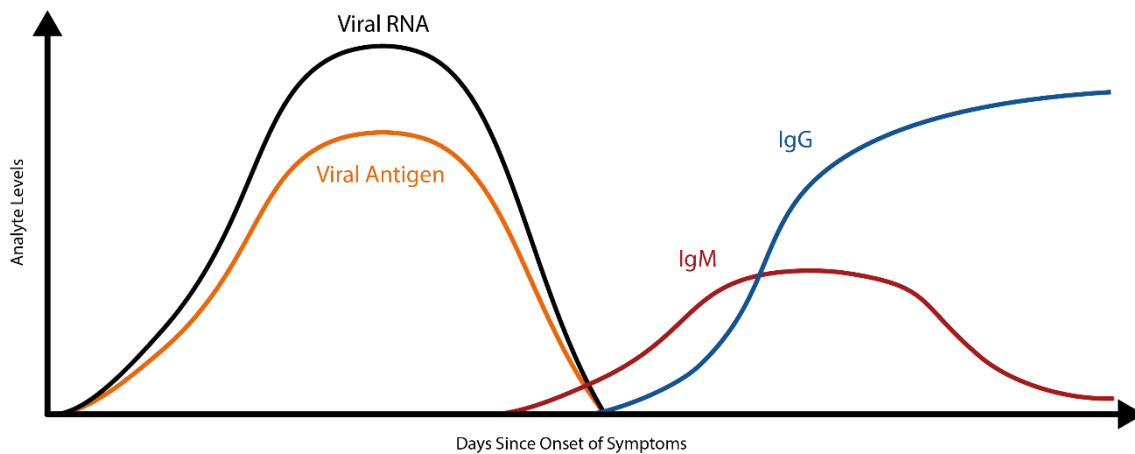
*Viremia begins 2-3 days post-infection reaching a peak at day 5 after infection. IgM seroconversion occurs 3-5 days post-infection, remain in serum for 10 days and then drop, while the IgG appear 7-10 days post-infection and remain in the bloodstream for months, even years, depending on the virus.*

This combination of innate immune response and adaptive immune response usually destroys all the virus and virus-infected cells and leads to the recovery of the infected host. However, most viruses have developed a broad variety of strategies to resist or escape these immune responses, with most viruses expressing at least one protein product with immune regulatory activities. Some viruses are so successful at immune evasion that they can cause chronic infections and persist for the lifetime of the host, such as human immunodeficiency virus (HIV) (158).

## 1.5. Diagnostics tools for detection of viral infection

The rapid and specific detection of a viral infection in a suspected host is crucial for the identification of the pathogen for further treatment and implementation of control measures to prevent the spread of the infectious agent. Some viruses cause distinctive clinical signs and symptoms and can clearly be identified, however most cause a wide range of clinical signs and symptoms which are often non-specific, thus diagnostic tools are of utmost importance to identify the etiologic agent.

The diagnostic methods to detect a viral infection can be divided into two categories: direct methods, which directly detects the presence of virus particles, virus antigen or viral nucleic acid in a given sample early days after the onset of symptoms, or indirect methods, which will detect the antibody response to a viral infection later in the course of infection (Figure 1.16). Multiplex assays are also useful diagnostic tools, to identify several pathogens or antibody response to different pathogens simultaneously. These methods are summarized in Table 1.2 below.



**Figure 1.16** Diagram of the different targets of diagnostic methods to detect a viral infection. Direct methods detect the presence of viral RNA or antigens when indirect methods detect the antibody response to the viral infection later in the course of infection.

**Table 1.2 Summary of the different diagnostic tools for the detection of viral infections and their primary use.**

Method	Target	Detection	Tool	Primary use
Direct	Virus	Whole virus	Virus isolation	Virus discovery Outbreak confirmation
		Nucleic acid detection	PCR	Suspicious case Surveillance Individual and group testing
			NGS	Virus discovery Outbreak management Surveillance Metagenomics
		Antigen	ELISA (double antibody sandwich)	Screening Acute testing
			LFA (double antibody sandwich)	POC Suspicious case Acute testing
			WB	Protein mixture
			HA	Hemagglutinin-expressing viruses
			IHC	Confirmatory test
		Indirect	Immune response	Antibody
LFA (Indirect, Competition, double recognition)	POC			
Neutralizing Antibody	VNT			Confirmatory test Detection nAbs
Multiplex	Virus	Antigen	ELISA (double antibody sandwich)	Differentiation Suspicious case Screening
	Immune response	Antibody	ELISA (Indirect)	Differentiation Surveillance Screening DIVA

*PCR: polymerase chain reaction; NGS: next-generation sequencing; ELISA: enzyme-linked immunosorbent assay; LFA: lateral flow assay; WB: western blotting; HA: haemagglutination assay; IHC: immunohistochemistry; VNT: virus neutralization test; POC: point-of-care; nAb: neutralizing antibodies; DIVA: differentiating infected from vaccinated animals.*

## **1.5.1. Direct methods**

### **1.5.1.1. Virus isolation**

Virus isolation involves the amplification of infectious virus from appropriate clinical specimens in living cells, which can be laboratory animals, embryonated chicken eggs or cultured cells (159). Virus isolation is a simple, reliable and widely used method for the diagnosis of viral infection but requires days or weeks to obtain a result and can only be completed in specialized laboratory settings with skilled technicians. Besides, the specimen used for direct detection and virus isolation is very important as a positive result from the site of disease is of much greater diagnostic significance than those from other sites.

Cultures are inoculated with the specimen and incubated until the appearance of cytopathic effects (CPE), which can take from 24 hrs for viruses such as herpes simplex virus, but usually take 5 to 10 days of incubation (160). The CPE can be observed under the light microscope and many viruses can be identified through the characteristic CPE they provoke in a susceptible cell line. As some viruses do not induce CPE, in order to confirm the identification of the causative virus, immunostaining can be performed. The cell culture is then fixed and stained by antibodies against viral antigens labelled with horseradish peroxidase (HRP) or fluorescein isothiocyanate (159).

Virus isolation in cell culture has been considered the “gold standard” in clinical virology for decades, but is now replaced by molecular diagnostics or serological assays. Virus isolation is no longer appropriate for routine daily diagnosis as it is slow, time-consuming, requires technical expertise and the difficulty to maintain cell cultures, despite being more sensitive than rapid antigen detection tests and its ability to detect a broader spectrum of viruses (159). Virus isolation is now mainly used for virus discovery, detection of variants of well-recognized viruses that might be missed by molecular methods or confirmation of an outbreak (161). The proliferation of a virus also differentiates between viable or non-viable virus, which usually cannot be done by antigen detection or molecular assays (160).

### 1.5.1.2. Nucleic acid detection

Methods based on the detection of the viral genome, commonly known as molecular methods, are widely used for diagnosis of viral infections. The first step to detect viral nucleic acid is to extract genetic material from the sample.

Polymerase chain reaction (PCR) consists of a rapid, sensitive and specific amplification of DNA *in vitro* using a thermostable DNA polymerase, deoxynucleotides of each base, alongside a pair of short oligonucleotides that exhibit complementarity to separate strands of a target double-stranded DNA template (162). The PCR involves repeated cycling of the sample through three incubation temperatures that allow steps of denaturation, annealing and DNA synthesis (or elongation). Between 30 and 50 cycles allow the exponential increase in the quantity of the target DNA (163), allowing the amplification and thus detection of initially very small quantities of DNA. Generally, the analysis of the PCR products will be done by gel electrophoresis and then visualization by staining with DNA dyes.

PCR has become the workhorse of molecular diagnosis as it can amplify minute quantities of DNA to make it detectable. Thus other methods have been derived from it such as the nested PCR (164) which uses two sets of primers to increase the sensitivity and the specificity of the PCR or real-time PCR (or quantitative PCR) in which the DNA is amplified and there is a simultaneous quantification of this amplification by emission of a fluorescence signal (165). Finally, the discovery in retroviruses of reverse transcriptase (RTase), an enzyme which uses RNA as a template to make complementary DNA (cDNA), opened new fields of application of PCR (166) as the genomes of RNA viruses can be analysed by using RTase to reverse transcribe the RNA into cDNA, followed by subsequent amplification by conventional PCR methods (called RT-PCR). All these variations of the PCR method are widely used in diagnosis but this technology is expensive and requires specific equipment and skilled personnel (167). That is why new methods are being developed to amplify nucleic acid, such as PCR variants without heat denaturation, transcription-based amplification methods, loop-mediated amplification method (LAMP) and strand displacement amplification (168). However, assays detecting the viral genome are impacted by the genetic variation between different strains of a virus.



Techniques have also been developed to determine a nucleic acid sequence such as next-generation sequencing (NGS), which allows the simultaneous sequencing of millions of DNA fragments. DNA fragments are amplified with microbeads by emulsion PCR (Roche 454, Life Technologies' SOLiD, and Ion Torrent) or by solid-phase PCR using primers attached to a solid surface (Illumina's HiSeq/MiSeq platforms) with nucleotide incorporation detected by luminescence signals or changes in electrical charge during the sequencing (169). NGS is used in diagnosis to directly sequence the DNA of a pathogen in a single run. NGS is also used in clinical microbiology for virus discovery, outbreak management, characterization and surveillance of pathogens, molecular case finding, metagenomics approaches on clinical samples, and the determination of the transmission of zoonotic micro-organisms from animals to humans (170).

### **1.5.1.3. Antigen detection**

The most commonly used technique to detect antigen in a sample is the enzyme-linked immunosorbent assay (ELISA). This technique allows to have the result available within a few hours. Additionally, lateral flow assays (LFA) can be used as a point-of-care (POC), rapid tests for Ag detection. In both cases, the quality of the specimen obtained is of utmost importance in order for the test to work properly and the sample should be obtained during the acute phase of the viral infection, as the utility of these techniques depends on the presence of short-lived viral antigens with an abundance above a specific limit of detection. Many specimens can be applied to these assays such as serum, plasma, whole blood, urine, saliva and other body fluids.

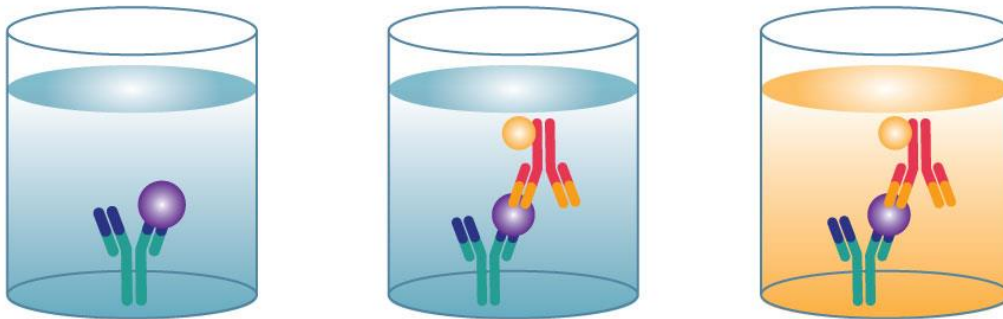
#### **1.5.1.3.1. Double antibody sandwich ELISA**

The ELISA is a solid phase-based assay that detects and/or quantifies a target antigen in a heterogeneous mixture, by utilizing enzyme-linked antibodies and a chromogenic reaction. There are several types of ELISA, depending on the target analyte and the one used for antigen detection is the sandwich ELISA or double antibody sandwich ELISA.

In a sandwich ELISA, the target antigen is captured by a pair of antibodies (Figure 1.17). The capture Ab is immobilized by adsorption on the solid phase (typically 96-well plates).

Then, the sample containing the target antigen is added, followed by the detection of the antigen by the detection antibody that is either enzyme-linked (direct format) or unlabelled, in which case a labelled secondary anti-species antibody will be needed (indirect format).

The main advantage of this type of ELISA is high specificity since signal detection requires the binding of two antibodies and thus a crude sample can be used as the target antigen-antibody complex is immobilized to the plate, allowing for the unbound material to be washed off.



**Figure 1.17 Steps involved in a double antibody sandwich ELISA.**

*Left: the antigen is captured by the coated Ab. Middle: the enzyme-linked detection Ab is added and recognizes the antigen. Right: the specific substrate is added which will develop a colour. The reaction is then stopped and read by a spectrophotometer. Figure adapted from R&D Systems (<https://www.rndsystems.com/resources/what-is-an-elisa-and-elisa-types>).*

The sandwich ELISA is more sensitive and specific than direct or indirect ELISAs as a pair of antibodies are used, but is limited by the characteristics of the set of antibodies. Moreover, the target antigen needs to have at least two epitopes for the two antibodies to bind. However, the same antibody can be used as both capture and detection antibody if there is no competition for the corresponding epitope, such as when multiple identical epitopes are available. Otherwise, the detection and capture antibody need to be different. Finally, these assays need extensive antibody optimization to find the best pair of antibodies to detect an antigen.

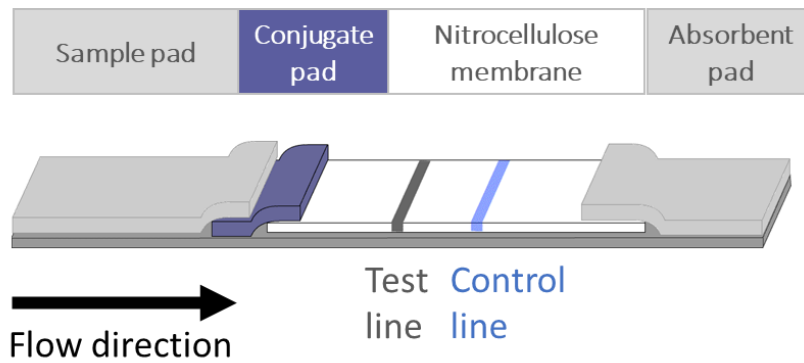
#### **1.5.1.3.2. LFA for antigen detection**

The principle of LFA is that the analyte of interest, in a liquid phase (by nature, or extracted from a solid sample), moves by capillary action through a strip of polymeric material where it can interact with previously attached detection molecules that provide an unambiguous chromogenic readout (171).

LFAs are POC tools that can be used for antigen detection, having the additional advantages in comparison with ELISA: it is a low-cost, fast, simple assay that can be used for the immediate diagnosis of a disease at the point of care. Furthermore, they are versatile and have a prolonged shelf life without refrigeration. Thus, they are very useful as a cheap POC test when there are no or few laboratory settings; for example, they are very well adapted to developing countries as the test does not require any skilled personnel to be performed, do not need to be refrigerated and gives the results in a few minutes. The main drawbacks of these assays are that they are only qualitative or semi-quantitative with some sensitivity limits compared to other immunoassays such as ELISAs. Moreover, the matrix used can be challenging and the sample needs a pre-treatment if it is not a fluid. LFAs are mainly used for primary screening at the POC and the results need to be confirmed using an independent method.

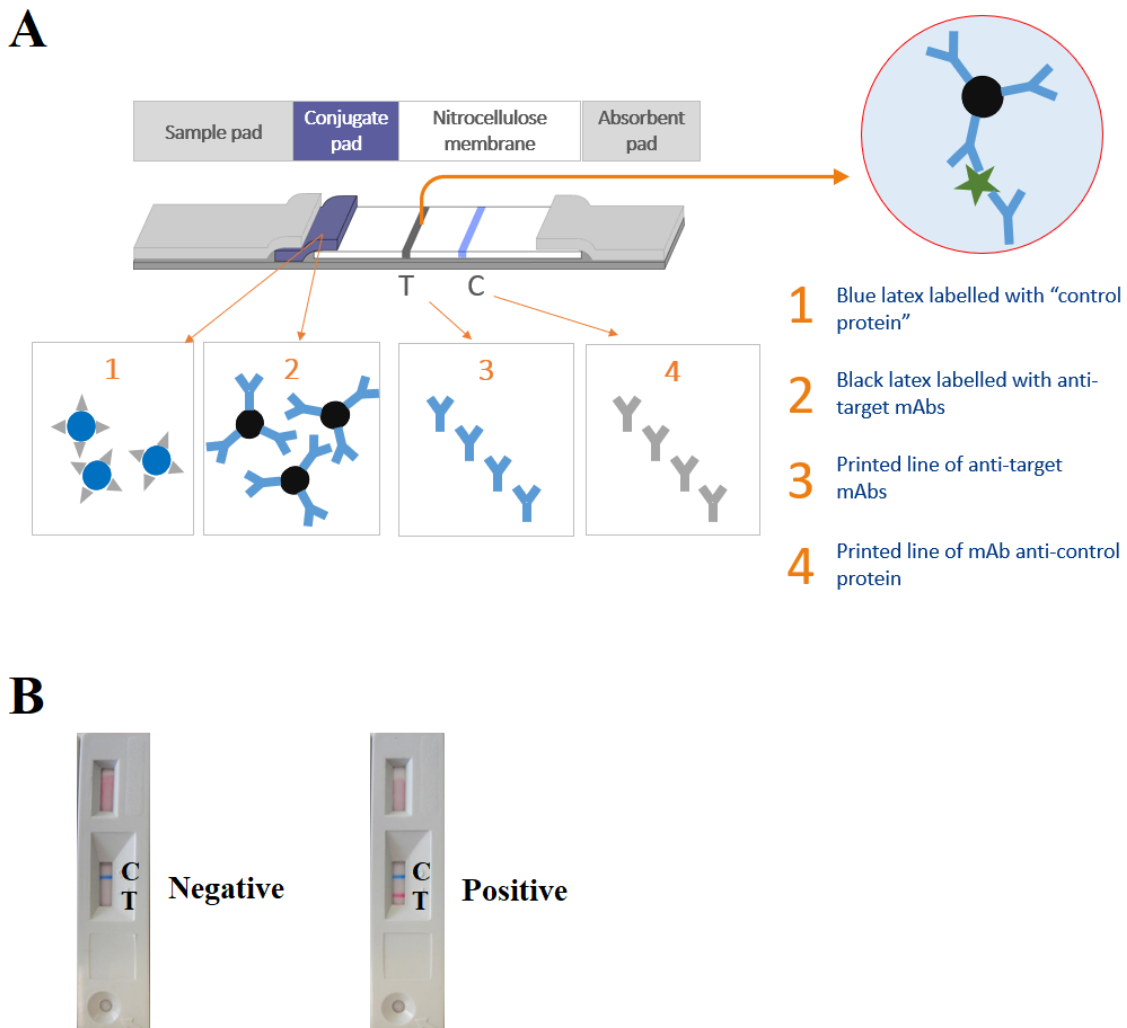
As shown on Figure 1.18, a LFA consists of over-lapping membranes and pads attached on a card for better handling (172). The sample is applied to the sample pad which can absorb the sample and release it at a steady rate into the conjugate release pad. It can contain some salt buffers and surfactants or act as a filter (e.g. to remove RBCs) to make the sample suitable for the LFA detection system. The sample passes through the conjugate release pad, which contains the recognition element conjugated to fluorescent or coloured nanoparticles (most commonly latex microspheres or colloidal gold). The conjugated recognition element is dried onto the pad and when the sample flows through it, specific interactions will happen between the sample and the recognition element and will migrate along the strip to the membrane and the detection zone. The membrane is porous with at least two immobilized lines of specific recognition elements. The first line is the test line which is composed of antibodies or antigens. Their role is to capture the analyte of interest in the sample, previously bound to the conjugated recognition element in the conjugate release pad. The second line is the control line which confirms the proper flow of the sample through the strip in order to validate the assay. The result is read as a

line that appears with different intensities and that can be measured by eye or by a reader. An absorbent pad is attached at the end of the strip to maintain the capillary force by wicking the liquid at the end of the strip to maintain the flow and avoid backflow of the liquid.



**Figure 1.18** Composition of a LFA strip.

As for the ELISA, different LFA formats exist depending on the analyte to detect and on the detection elements used. When antibodies are used as detection elements, the assay is called a lateral flow immunoassay. For antigen detection, a double antibody sandwich assay is performed in which the Ag to detect is captured by two complementary antibodies, one conjugated to microspheres and the other immobilized at the test line (Figure 1.19A). In that case, a positive result will be read by the presence of a test line (Figure 1.19B).



**Figure 1.19** Technical basis of a double antibody sandwich LFA.

(A) Representation of a LFA and its mechanism. The sample containing the analyte is added to the sample pad. Then, the sample migrates towards the conjugate and the conjugated antibodies bind the target and migrate to the test line. Finally, the bound target is captured at the test line by the immobilized antibodies. (B) Examples of negative and positive results obtained with a double antibody sandwich LFA. C: control line; T: test line.

Another technique that can detect antigens is immunoblotting (or western blotting, WB), which uses antibodies for the detection of target proteins in a protein mixture in reducing or non-reducing conditions (173). Immunoblotting is advantageous as it allows the separation of a protein mix and the detection of different targets, but it is a laboratory-based, time-consuming method and is usually less sensitive than other serological techniques.

Haemagglutination assay is an assay used for the diagnosis of some enveloped viruses expressing hemagglutinin (such as influenza virus) which can absorb red blood cells (RBCs) and lead to the formation of a lattice instead of precipitation of RBCs.

Immunohistochemistry (IHC) uses antibodies to recognize antigens in a tissue section by colorimetry (chromogenic IHC) or fluorochrome (immunofluorescence assay, IFA) (174). This technique allows analysis of infected whole cells in a tissue sample without destructing the tissue architecture, and biopsies, preserved in formaldehyde, can be transported without cold chain and preserved for years.

### **1.5.2. Indirect methods (serological assays)**

Serology is applied for surveillance purposes and is a valuable tool for further epidemiological investigations, for example, for determining the time point of agent introduction into a certain population. Antibodies appear soon after an infection and persist for up to several months or even years. For most viral infections, the antibody response is driven by IgM and IgG, with IgM appearing a few days after the infection (usually 3-5 days post infection with a rapid decline) and IgG appearing a few days later (usually 7-10 days post infection, persisting for months or years). Thus, indirect methods can be used to diagnose a current or recent infection by detecting IgM, and a past infection, by detecting IgG.

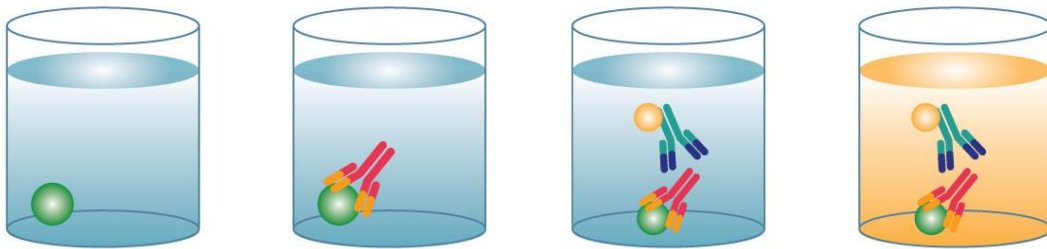
#### **1.5.2.1. ELISA for antibody detection**

Here, the different formats of ELISA used in this thesis for the detection of antibodies are described:

- Indirect ELISA

In an indirect ELISA, the target antibodies recognize an antigen or sample coated on the solid phase and this primary antibody is detected by a conjugated anti-species antibody (secondary antibody). The chromogenic signal, corresponding to the binding of the target antibody, is detected by a spectrophotometer after the addition of a chromogenic substrate (Figure 1.20).

Indirect ELISA is mainly used in diagnosis for the screening of large numbers of samples from the same species, to detect an immune response to a pathogen. The main advantages of indirect ELISA are their sensitivity as a secondary antibody is used to amplify the signal and their flexibility as different primary antibodies can be used with a single labelled anti-species secondary antibody. However, the use of a secondary antibody can cause potential cross-reactivity.



**Figure 1.20 Steps involved in an indirect ELISA.**

*Left: the antigen or sample is immobilized onto the solid phase. Middle left: the target antibody is added and binds to the antigen. Middle right: the primary antibody is recognized by a conjugated anti-species antibody. Right: the specific substrate is added which will develop a colour. The reaction is then stopped and read by a spectrophotometer. Figure adapted from R&D Systems (<https://www.rndsystems.com/resources/what-is-an-elisa-and-elisa-types>).*

#### - Competition ELISA

Competition ELISA, also known as inhibition or blocking ELISA is an assay in which the quantification of the antigen or the antibody is through its interference with an expected signal. All the formats of the previous described assays can be adapted to antigen or antibody competition, depending on the target to quantify. An inhibition assay refers to a competition assay where the sample is previously mixed with the antigen or the antibody used in the assay before being added to the coated wells. Competition ELISAs are useful for the detection of small antigens and their advantages and limitations depend on the format used.

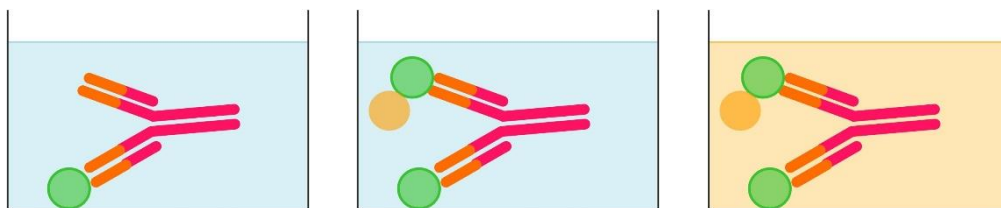
Competition ELISA is mostly used when only one antibody is available for the targeted antigen or if the antigen does not have multiple epitopes in order to perform a sandwich ELISA. Competition assays are also suitable in an indirect ELISA format to detect

antibodies against an antigen in different species. The main drawback of these assays is the need for a reference assay to be developed before developing the competition assay.

- Double recognition ELISA

In a double recognition ELISA, also called double antigen sandwich ELISA, the target antibody is captured between two antigens. In this assay, the same antigen is used as the capture and detection molecule, using the principle that antibodies possess multiple antigen binding regions (two for IgG, four for IgA and ten for IgM), allowing their binding twice to the target antigen. The capture antigen is coated onto the solid phase, then the sample containing the target antibody is added, followed by the detection of the antibody by the detection antigen that is enzyme-linked. The addition of the chromogenic substrate will develop a colour that can be read by a spectrophotometer. These steps are represented in Figure 1.21.

The main advantage of the double recognition ELISA is that it can detect antibodies from different species, as no secondary anti-species antibody is used. Additionally, it is useful when there is no need to distinguish between the different subtypes of immunoglobulins, and furthermore the absence of a secondary antibody reduces the risks of cross-reactivity.



**Figure 1.21** Steps involved in a double recognition ELISA.

*Left: the antibody recognizes the immobilized antigen. Middle: the conjugated antigen binds to the antibody. Right: the specific substrate is added, which will develop a colour. The reaction is then stopped and read by a spectrophotometer.*

### 1.5.2.2. LFA for antibody detection

In order to detect antibodies in a sample, two formats of LFA can be used: a double recognition assay or an indirect assay, but only the first has been used here. Just as in the double recognition ELISA, in the double recognition LFA, the antigen is used as the



capture and detection molecule, as conjugated to the microspheres and immobilized at the test line. The antibodies in the sample will capture the microsphere-conjugated antigen and then bind to the immobilized antigen at the test line. This will indicate the presence of antibodies in the sample regardless of the antibody class (IgA, IgE, IgG or IgM).

Other techniques to detect antibodies are virus neutralization test (VNT), which is used to quantify the neutralizing antibodies from a sample for a specific virus. It consists in incubating a cell culture with the serum sample to be tested and check for inhibition of viral replication. VNT does not detect all antibodies but only the ones blocking the viral replication, named neutralizing antibodies. VNT is very sensitive and specific method, considered the “gold standard” for many viral infectious diseases, although is a time-consuming method.

### **1.5.3. Multiplex assays**

The primary described use of microarrays was for sequencing, as DNA-based microarrays for NGS. Nevertheless, protein microarrays have also a huge potential for serological diagnosis as they can generate high quantities of diagnostically relevant information simultaneously, from a single sample, in a few hours.

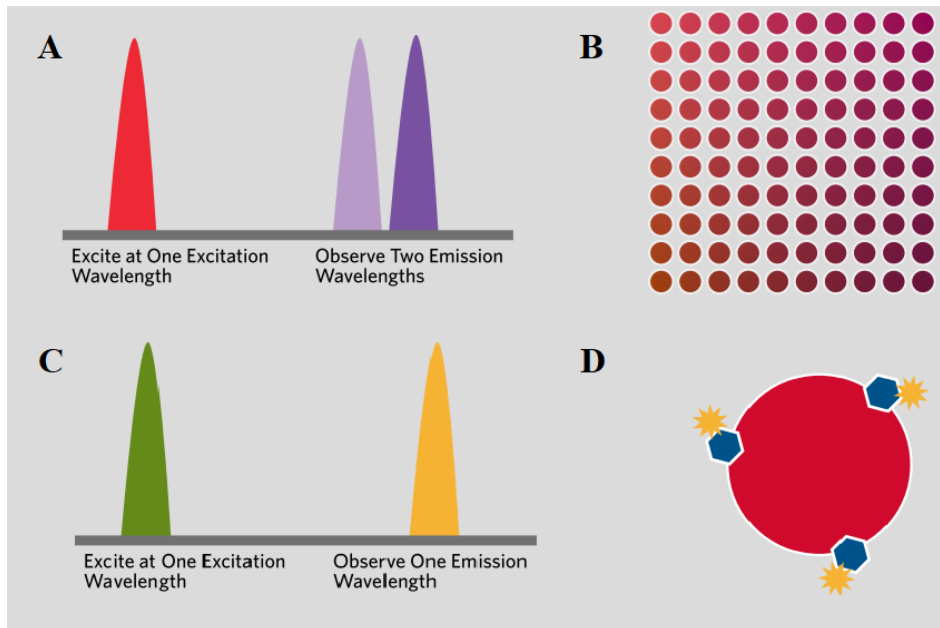
In 1990, R. Ekins theorized that highly sensitive assays could be developed using microspots of antibodies which could measure simultaneously, a large number of different substances in a small volume of sample (175). However, one of the first descriptions of the feasibility of such assay was in 1998, by Silzel *et al.* (176).

The first formats of protein microarray to be developed were planar microarrays, which use a planar solid phase, to immobilize microspots of different capture molecules (e.g. antibodies). These microarrays have the ability to measure multiple analytes in a given sample simultaneously; this was called multiplexing. The planar analytical microarrays are high-throughput, highly sensitive, have the possibility to be automated and require less sample and reagent volumes compared to other serological assays such as ELISAs and LFAs. However, they have limitations such as their slow solid-phase kinetics, the instability of the immobilized capture molecule and poor reproducibility which may limit its application. Thus, another format of this technology was developed, the suspension microarrays, where the solid phase are nanoparticles.

Suspension microarrays use microspheres as their solid phase to immobilize capture molecules. These assays are also called bead-based microarrays as the microspheres are in suspension in a liquid phase. The assay is usually performed in microtiter plates, which are used to transport the beads in suspension. These beads are divided into recognizable sets, which allow the immobilization of distinct capture molecules. Thus, multiplexing is performed by mixing different sets of beads in a single well. The bead-based microarrays are analysed by a flow cytometry instrument or similar instruments, which will, one-by-one, recognize individual beads (e.g. through fluorescence, light scattering) and detect the binding of the target molecule to the bead. Different systems have been developed to perform bead-based microarrays, as reviewed by Hsu *et al.* (177). The description here will focus on the xMAP (Multi-Analyte Profiling) Luminex technology, which is the most established bead-based microarray technology.

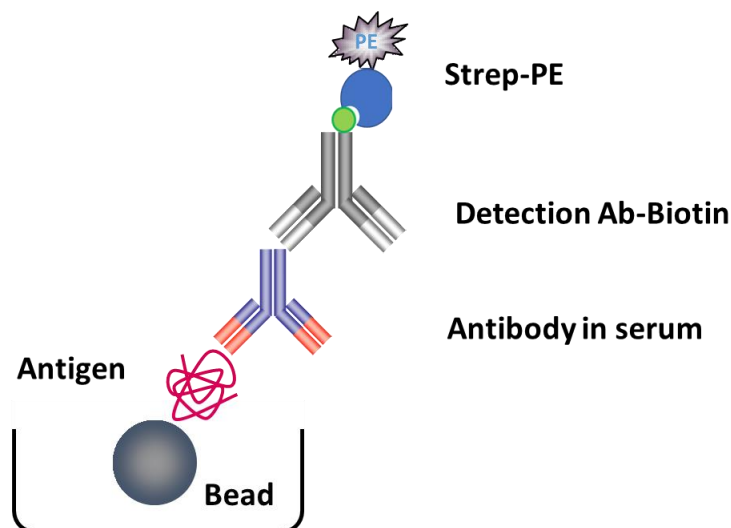
The set of Luminex beads are internally labelled with different concentrations of two or three fluorescent dyes and this combination of two or three dyes encodes 100 to 500 different sets of beads (Figure 1.22A and Figure 1.22B). The coupling of the proteins to the beads is done through carbodiimide chemistry to covalently bind the microspheres through their carboxyl groups, previously activated with 1-Ethyl-3-(3-dimethylaminopropyl)carbodiimide (EDC) and N-Hydroxysuccinimide (NHS), to the amine of the coupling molecule (178). Depending on the capture molecule immobilized on the microspheres, different assay formats can be performed:

- If antibodies are immobilized, sandwich assays (direct or indirect) or competition assays can be performed to detect antigens or target molecules.
- If antigens are immobilized, indirect assays can be performed to detect antibodies (Figure 1.23).



**Figure 1.22** *xMAP microspheres.*

The microspheres include two internal dyes where (A) a first excitation wavelength allows the identification of each microsphere from (B) 100 unique microsphere sets if the beads have two dyes (or 500 unique microspheres sets if they have three dyes). (C): A second excitation wavelength allows the observation of a separate fluorescent reporter molecule, allowing the detection (D) of the analyte captured on the surface of the microsphere. Figures adapted from Angeloni S et al. *xMAP Cookbook*. 3rd ed. Luminex Corporation, editor. Luminex Corporation. 2016. p. 148.



**Figure 1.23** *Indirect format used in the multiplex assay.*

The microspheres are coated with specific antigens that are recognized by the target antibodies in the serum. A secondary antibody (Ab) biotin-conjugated recognized the primary antibody. After addition of streptavidin-phycoerythrin (Strep-PE), the binding can be detected by a reader.

Nowadays, magnetic beads are more frequently used than non-magnetic beads. They are easily washed by using a magnetic separator and their handling is easier, only requiring the use of 96-well microtiter plates. In contrast, non-magnetic beads required washing by the use of spinning or filter plates.

The antigen-antibody interaction that occurs on the surface of the coated beads is similar to that of an ELISA and because of the microscopic size and low density of these beads, assay reactions exhibit virtually solution-phase kinetics (178).

For indirect assays, which were used in this thesis, the sample to be tested binds to the antigens coupled to the beads. Then, an anti-species antibody labelled with biotin recognizes the primary antibodies and finally, Strep-PE is added which will be detected by the reader. Using the MAGPIX® System, each well is analysed similarly to a flow cytometer: a wavelength excites the internal bead dyes to identify each microsphere and another wavelength excites the reporter molecules captured by the bead (Figure 1.22C and Figure 1.22D) (178). Using this method allows the detection of many different target analytes from a single sample.

Compared to the planar microarrays, the bead-based microarrays have larger surface areas than the planar microarrays, are more reproducible, more flexible and more robust (177). Moreover, the microspheres can be produced in large-scale, can be stored after coating with a molecule and are very flexible and customizable as bead mixes can be prepared depending on the needs of the client (179). As they have many advantages, the bead-based microarrays' use is expanding and is now used in infectious disease management to detect the immune response or directly detect the pathogen (180), in immunology to detect cytokines (181), but also in food industry to detect many allergens simultaneously (182) and many commercial kits are now available for all these usages. However, the use of Luminex assays is limited by the necessity of a reader.

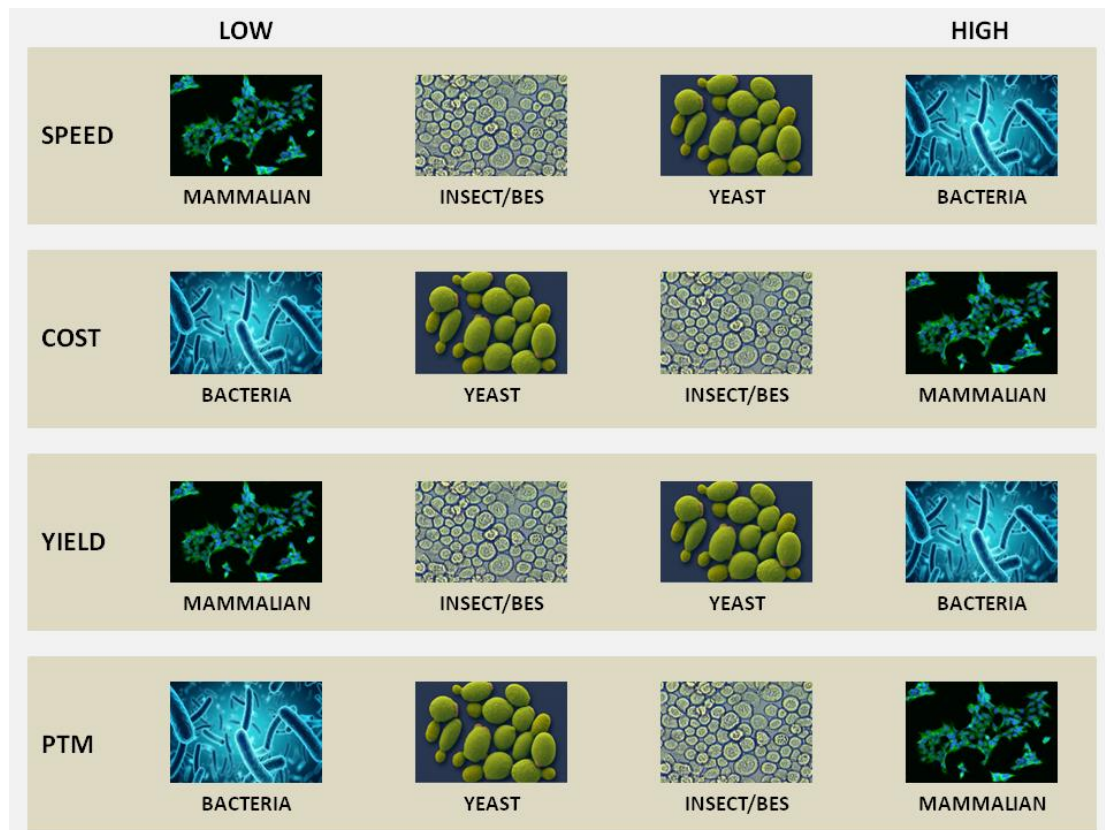
### **1.6. Recombinant proteins**

To develop the diagnostics methods described above, two kinds of reagents are needed: antigens of the targeted viruses and capture molecules such as antibodies and other molecules to recognize these antigens.

Virus propagation and purification has commonly been the main way to obtain viral antigens in order to develop serological assays (183). Nonetheless, this method is limited due to the fact that many clinically-relevant viruses cannot be cultured which hinders the production of sufficient viruses for subsequent protein purification. In addition, such approaches are also limited by the difficulty of purifying un-tagged proteins and the risk of cultivating large quantities of hazardous viruses (184). Thus, being able to produce any antigen of a virus, without viral cultures, in order to use it in diagnostic assays was of paramount importance.

This was achieved by Cohen *et al.* in 1973, with the *in vitro* construction of DNA plasmids (185), leading to the production of the first recombinant protein in 1978 by Goeddel *et al.* in *Escherichia coli* using recombinant DNA technology (186). Recombinant DNA technology revolutionized the field of microbiology, as using simple tools such as enzymes, vectors and hosts, a gene of interest can be cloned and introduced into a host. The host will then transcribe and translate the gene of interest into the corresponding protein using its cellular machinery. Since the production of recombinant insulin in *E. coli*, the recombinant protein industry rapidly grew and over 170 recombinant proteins from hormones to growth factors and interleukins are now available worldwide for clinical use to treat diseases of primary importance (187). Recombinant proteins are not only used for clinical purposes but also for structural, *in vitro* and *in vivo* studies, development of diagnostics and production of mAbs.

Nowadays, four major expression systems are used in research and industry for the production of recombinant proteins with different advantages and disadvantages depending on the nature of the protein to be expressed (188). The factors to be considered when electing an expression system are summarized in Figure 1.24 such as the intended use of the recombinant protein, post-translational modifications (PTM), the presence of disulfide bonds, the yield and costs.



**Figure 1.24 Advantages and disadvantages of the main recombinant expression systems.** These depend on: the speed and cost of production, the potential yield of recombinant protein and the post-translational modifications (PTM) that can be carry out.

The basic steps for recombinant protein expression are: identification of gene of interest, clone it in an expression vector, transform it into the chosen host, induce the expression, purify the protein and characterize it.

### 1.6.1. Bacterial expression system

Bacterial expression systems were the first to be used for production of recombinant proteins and are still one of the major systems used. The species *E. coli* is one of the most commonly used hosts for recombinant protein expression for the following reasons: it is non-pathogenic, they replicate extremely fast under the right condition at a low cost, while the expression level is high, which makes it an efficient and economical way for large scale production. Its genome has been entirely sequenced and the genetic backgrounds

and metabolic pathways are well known. Additionally, bacteria are easily transformed. These desirable characteristics make the expression procedure easy and quick.

However, this high-level of protein expression can lead to the expression of partially or misfolded proteins, which will interact with each other and form insoluble aggregated proteins called inclusion bodies (189). These inclusion bodies require high concentration of denaturant to be solubilized, which can impact the recombinant protein, and then need to be refolded in its native state (190). However, these inclusion bodies can also protect the recombinant protein from proteases and mainly contain the recombinant protein which eases its purification. Moreover, the prokaryotic system has additional limitations, such as the lack of many PTM that can be found in eukaryotes and the difficult formation of disulfide bonds in *E. coli*. Depending on the vector used, the recombinant proteins are usually expressed in the cytoplasm, but can be targeted to the periplasm and even secreted (191).

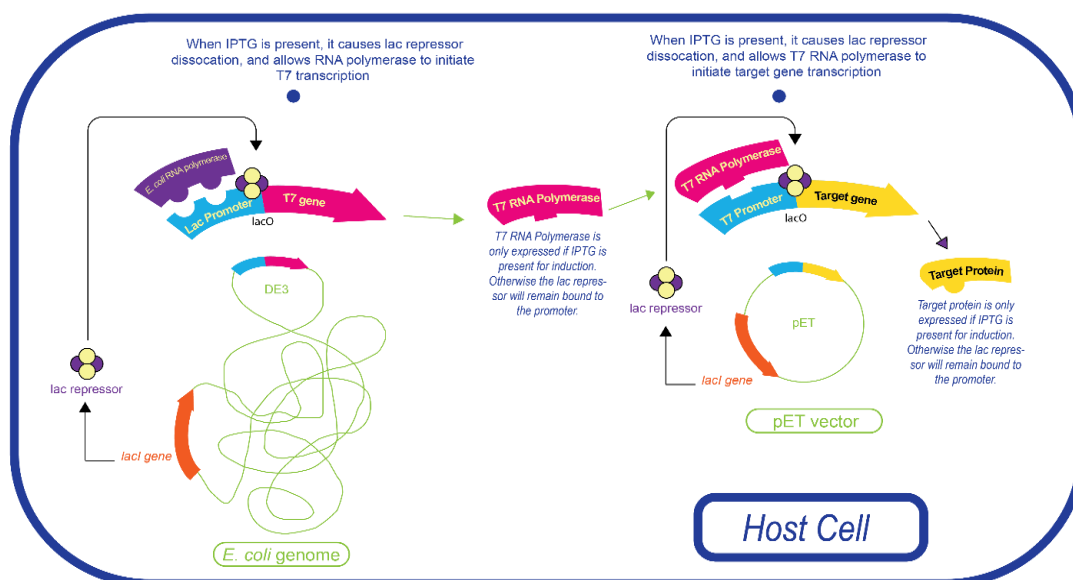
When selecting this system, the main factors to take into consideration are the plasmids and the bacterial strain. There is a broad variety of plasmids that are used and they have different combinations of replicons, promoters, selection markers, multiple cloning sites and fusion proteins, and their selection depends on the recombinant protein to express.

### 1.6.1.1. pET expression system

Here, the pET expression system was adopted for expression of several N proteins. This system is powerful, capable of expressing recombinant proteins at levels of up to 50% of the total cell protein. The pET vectors carry the pBR322 *ori*, which leads to a number of copies of the plasmid between 15 and 20. To avoid plasmid loss and the growth of untransformed bacteria, pET vectors contain a selection marker conferring an antibiotic resistance (ampicillin or kanamycin).

The promoter used in the pET expression vectors is based on the lactose (*lac*) promoter, which is part of the *lac* operon, an inducible promoter and the T7 RNA polymerase promoter (192). Expression of the gene of interest is regulated by the T7 RNA polymerase promoter, which represents the binding site for T7 RNA polymerase, and a *lac* operator. The polymerase is provided by the host (in another plasmid or in its genome such as for the BL21(DE3) *E. coli* strains) and its expression is controlled by the *lacUV5* promoter.

In the absence of lactose, the *lac* repressor (encoded by *lac I* gene included in the *E. coli* genome and the pET vector) blocks the RNA polymerase by binding to the *lac* operator present before the T7 RNA polymerase gene and the target gene. However, in the presence of the inducer allolactose (lactose isomer) or isopropyl  $\beta$ -d-1-thiogalactopyranoside (IPTG), the inducer binds to the *lac* repressor, preventing its binding to the operator and allowing the transcription by the RNA polymerase. However, in presence of other carbon sources (e.g. glucose) there is a catabolite repression which prevents efficient transcription from the *lac* operon. The *lacUV5*, used in the pET vectors, has a higher transcription of target genes than the *lac* promoter and has a reduced sensitivity to catabolite regulation (193). Figure 1.25 summarizes the expression system used with the pET vectors and BL21(DE3) *E. coli* strains.



**Figure 1.25 Regulation system involved in the pET vectors under the control of the *lac* operon and the T7 promoter.**

Figure adapted from Gold Biotechnology, Inc. (<https://www.goldbio.com/articles/article/a-deep-dive-into-iptg-induction>).

In order to increase the solubility, facilitate the purification or follow the production and purification of the recombinant protein, amino acids can be added at the N- or C-terminal ends of the protein. They are called tags and can be purification tags if their role is to enable a rapid and efficient purification of the recombinant protein, or solubilization tags



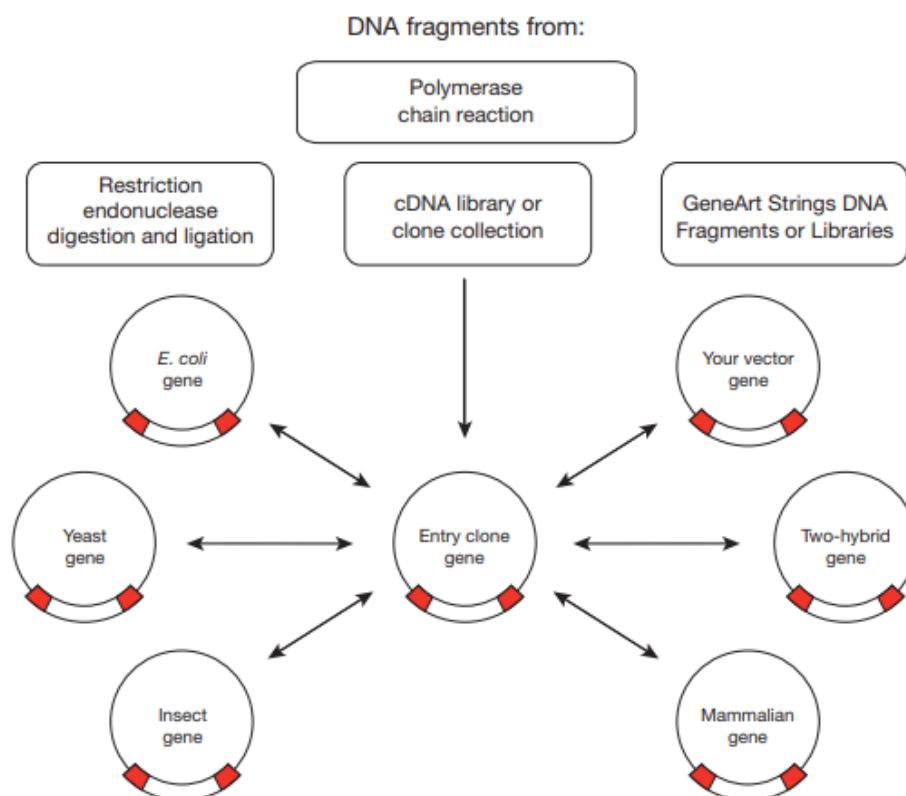
if their role is to increase the solubility and proper folding of the recombinant protein or both. Sequences can be added between the tags and the recombinant protein to subsequently eliminate the tag by enzymatic or chemical cleavage. The tags are often removed because they potentially can impact the recombinant protein folding, structure and activity.

The pET28a-SUMO vector used in experiments described in this thesis has an N-terminal yeast small ubiquitin-like modifier (SUMO) tag (smt3 from *Saccharomyces cerevisiae*) to act as a fusion partner to the expressed protein of interest to increase its solubility and stability. Furthermore, there is a polyhistidine (6xHis) tag at the N-terminal of the SUMO tag to allow the purification of the fusion protein by affinity chromatography. These tags can be cleaved by SUMO ubiquitin-like specific protease 1 (Ulp1) to separate the tags and the target protein.

### **1.6.1.2. Gateway system**

To avoid the restriction enzyme cleavage strategies for each target and vector, used for the cloning into the pET vectors, different methods were developed to allow the easy transfer of the gene of interest into different vectors and different systems. These methods include the ligation-independent cloning (194) and site-specific recombination methods such as Gateway® Technology (195).

The Gateway® Technology is based on the site-specific recombination properties of bacteriophage lambda (196). This method allows the transfer of DNA sequences into various vectors and system for protein expression once it has been cloned into an entry vector (197,198) (Figure 1.26).



**Figure 1.26 Representation of the Gateway system.**

This system allows the easy cloning of a gene in different systems once it has been cloned into an entry vector via site-specific recombination. Figure adapted from Invitrogen. pCR<sup>TM</sup>8/GW/TOPO<sup>®</sup> TA Cloning<sup>®</sup> Kit. 2012. 1–34.

The entry vector pCR<sup>TM</sup>8/GW/TOPO<sup>®</sup> is linearized with single 3'-thymidine overhangs for TA Cloning and topoisomerase I is covalently bound to the vector (199). These allow an efficient ligation of the PCR product to the entry vector as the *Taq* polymerase used in the PCR adds a single deoxyadenosine (A) to the 3' ends of PCR products due to a non-template-dependant terminal transferase activity. Moreover, topoisomerase I from vaccinia virus has a specific binding site on double stranded DNA and does so by cleaving the phosphodiester backbone in one strand forming a covalent bond between the DNA and the enzyme. This bond is reversible when attacked by the 5' hydroxyl of the PCR product, releasing the topoisomerase I and efficiently cloning the PCR product (199).

The lambda integration into the *E. coli* chromosome occurs by recombination mediated by lambda and host enzymes. This recombination occurs through site-specific attachment sites (*att*) catalysed by bacteriophage lambda integrase and excisionase proteins and *E.*

*coli* integration host factor (200). This system is used to transfer the gene of interest in the entry vector (flanked by *attL* sites) to destination vectors (flanked by *attR* sites) for the expression of recombinant proteins.

Here, the SARS-CoV-2 N protein ORF was cloned into the Gateway entry vector for expression of the protein in *E. coli*. The gene was then transferred into the pDEST17 expression vector which contains an N-terminal 6xHis tag. In this system, the gene of interest is regulated by the T7 RNA polymerase promoter and the *E. coli* strain (BL21-AI™ *E. coli* strain) used for the expression of the SARS-CoV-2 N protein contains the gene encoding T7 RNA polymerase under the control of the *araBAD* promoter (201). This *araBAD* promoter is positively and negatively regulated by the product of the *araC* gene (202). In the absence of L-arabinose, *araC* product forms a DNA loop before the *araBAD* promoter, inhibiting the transcription of the T7 RNA polymerase (203). In the presence of L-arabinose, *araC* product forms a complex with L-arabinose, allowing the transcription of the T7 RNA polymerase. In presence of other carbon sources (such as glucose) there is a catabolite repression which prevents efficient transcription from the *araBAD* promoter.

### **1.6.2. Yeast expression system**

The yeast expression system is another traditional expression system used for the expression of recombinant proteins. Yeasts exhibit advantages of bacteria such as a short doubling time, high density cultures, ease to handle and ease to genetically manipulate and advantages of eukaryotes such as better folding and PTM. Regarding the recombinant protein expression, yeasts can be divided in two groups: non-methylotrophic and methylotrophic hosts (204). The first yeast that was used for recombinant protein expression in the 1980s was *S. cerevisiae*, a non-methylotrophic yeast. *S. cerevisiae* was the first eukaryote genome to be completely sequenced in 1996 (205). A wide range of protein produced in *S. cerevisiae* are available on the market such as insulin, hepatitis B surface antigen, urate oxidase, glucagons, granulocyte macrophage colony stimulating factor, hirudin, and platelet-derived growth factor (206). However, the production of recombinant proteins in *S. cerevisiae* is limited by its low yield, plasmid instability and hyper-glycosylation of the recombinant protein (207). This hyper-glycosylation is of high mannose type, which is different from human glycosylation, which can lead to lower

activity and higher immunogenicity (208,209). This led to the development of alternative hosts, such as other non-methylotrophic yeasts (e.g. *Kluyveromyces lactis* or *Yarrowia lipolytica*) or methylotrophic yeasts (e.g. *Pichia pastoris* or *Hansenula polymorpha*) (210). Methylotrophic yeasts are yeast that can use methanol as its only carbon source and which were developed more recently in 1985 by Cregg *et al.* (211). Methylotrophic yeasts are advantageous as they have the ability to grow at high cell densities and possess very strong and tightly regulated promoters for the expression of methanol oxidizing enzymes (e.g. alcohol oxidase) (204). In these yeasts, for recombinant protein expression, most of the promoters use the methanol utilization pathway promoters.

### **1.6.3. Insect cells / Baculovirus expression system**

Insect cells offer high levels of protein expression with PTM approaching that of mammalian cells, ease of scale-up, and simplified cell growth that can be readily adapted to high-density suspension culture for large-scale expression (212). Most of the PTM pathways present in mammalian systems also occur in insect cells, resulting in a recombinant protein that is antigenically, immunogenically, and functionally similar to the native one. The baculovirus expression system (BES) is a powerful and versatile delivery and expression system for producing high levels of recombinant protein in insect cells. The *Baculoviridae* is a family of large, double-stranded, circular DNA viruses which infect insects. The best known baculovirus used for recombinant protein expression is *Autographa californica* multicapsid nucleopolyhedrovirus (AcMNPV). The high level of expression reached using this system is due to the native characteristics of baculovirus gene expression, and generally exploits one of two strong promoters involved in very late gene transcription, namely *polh* and *p10* (213–217).

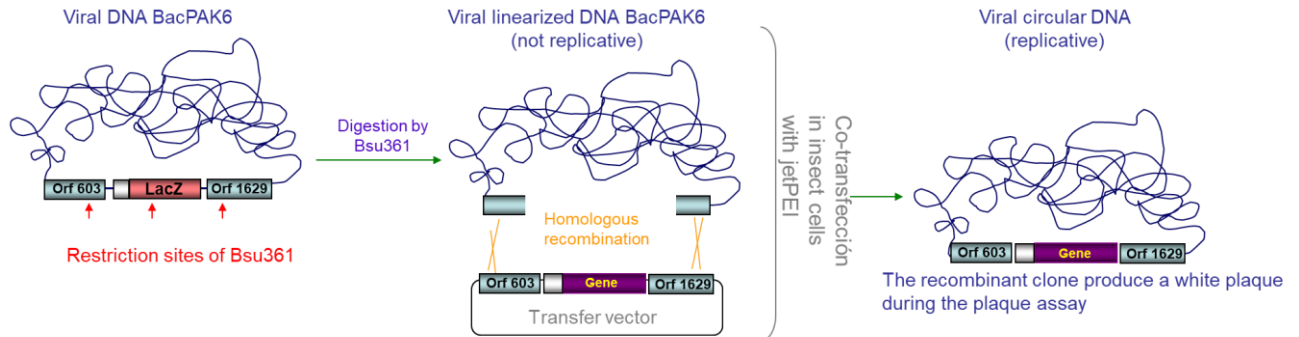
AcMNPV is used to infect insect cells lines derived from the fall armyworm *Spodoptera frugiperda* such as *Sf9* or *Sf21* or from the cabbage looper *Trichoplusia ni* such as High-Five (188). Moreover, the baculoviruses have a limited host range, thus are safe for vertebrates, and insect cells are fairly easy to grow and to scale-up, can grow in serum-free media and are safe to use (free of human pathogens) (218). Finally, this expression system is very efficient to produce multiple proteins simultaneously in a single infection and thus expressing virus like particles (VLPs) which have been used for vaccine production (219).

In contrast to the N proteins, the G<sub>N</sub> ectodomain (G<sub>NE</sub>) of CCHFV and RVFV and CCHFV GP38 are post-translationally modified by glycosylation, and as bacterial expression systems are unable to perform such processing, they are unsuitable for glycoprotein over-expression. Instead, insect cells paired with a baculovirus expression vector are often the system of choice for heterologous glycoprotein expression, such as the BES expression system used here, for which the production of recombinant proteins is faster and often in higher yields than in mammalian cells.

Due to the large size of AcMNPV genome (around 134 kbp), the main challenge to produce recombinant proteins in insect cells has been the insertion of the gene of interest in AcMNPV. The first way of making recombinant baculoviruses was through homologous recombination (214). However, due to the low frequency of homologous recombination, this method was highly inefficient, with less than 0.1% of recombinant baculovirus generated, and time-consuming due to sequential plaque purification to separate the recombinant baculoviruses from parental baculoviruses (220). This technique was improved by using baculovirus DNA containing a unique *Bsu36I* site in the polyhedrin locus and thus the DNA could be linearized (221). As linearized parental baculoviruses theoretically could not replicate, this method greatly improved the efficiency of recombinant baculovirus generation to 10-20%.

Finally, Kitts and Possee developed BacPAK6, a recombinant baculovirus DNA which can achieve over 95% efficiency of recombinant baculovirus generation (222). This BacPAK6 viral DNA was used in this thesis to produce recombinant proteins in insect cells as it is a very convenient and efficient way to produce recombinant baculoviruses. This technique is based on the linearized baculovirus DNA but in this baculovirus DNA two additional *Bsu36I* sites have been introduced and the polyhedrin gene has been replaced by the *lacZ* gene (Figure 1.27). These two sites are situated in the *lacZ* gene and in the *orf1629* gene. *Orf1629* encodes P78/83, a viral Wiskott-Aldrich syndrome protein-like protein involved in nuclear actin assembly, essential for progeny production (223). The lack of a functional *orf1629* in parental baculovirus DNA decreases the generation of parental baculovirus, as, even if the digested parental DNA re-ligates, it cannot initiate virus production. Homologous recombination with the transfer plasmids restores *orf1629* and the recombinant baculoviruses can be selected from parental baculoviruses by blue-white screening, due to the presence of the *lacZ* gene in the parental DNA. This technique results in recombination efficiencies of close to 100% (224). The triple digested

BacPAK6 and the transfer vector pAcSecG2T used have been modified at Eurofins-Ingenasa to be adapted to the Gateway system.



**Figure 1.27 Generation of recombinant baculovirus by homologous recombination.**

Recombinant baculovirus are generated by homologous recombination between the linearized triple-digested BacPAK6 viral DNA and the transfer vector containing the gene of interest. The recombination yields a replicative recombinant baculovirus by restoring *orf1629* essential for progeny production that can be selected by blue–white screening. The polyhedrin promoter is represented as a grey domain.

Once the recombinant baculovirus is generated, it can be used to infect insect cells for the production of the target recombinant protein. The gene expression of baculoviruses is divided into three successive phases (217). The first phase is the early phase, in which the genes which have host-like promoters are transcribed by the host RNA polymerase II. The genes expressed during this early phase are required for the late phase. The late phase genes are transcribed from 6 to 24 hours post infection (PI), after the onset of viral DNA replication, by the virus-encoded transcriptional machinery (216). Finally, the very late genes are transcribed, 18 to 72 hours PI, under the control of two strong promoters *polh* and *p10*, encoding two major proteins (the polyhedron and the 10 kDa protein (P10)) non-essential for viral replication in insect cell cultures (213,215) that are transcribed at very high levels (216). The BacPAK6 baculovirus DNA uses the promoter *polh* for the expression of the gene of interest.

#### 1.6.4. Mammalian expression system

The mammalian expression system has an ability for proper folding and PTM compared to the systems previously described. If the main driver of the production of a recombinant protein is a protein with near-native glycosylation, active and well folded (e.g. for therapeutic use), then it should be expressed in mammalian cells (225). However, this expression of recombinant proteins is timely and costly, which is the main drawbacks of this system. There is also the potential for contamination of the mammalian cells with mammalian viruses.

The two techniques that have been developed to produce recombinant proteins in mammalian cells are through the generation of a stable cell line expressing the recombinant protein or through a transient expression. The generation of a stable cell line expressing the recombinant protein of interest, consists in designing plasmids with the gene of interest and a selection marker. After linearization of the plasmids and transfection of mammalian cells, the plasmids are ligated and a small number integrate the host cell genome by non-homologous recombination (226). This is a very timely method as it can take minimum 6-12 months to produce the recombinant protein. The other technique is faster as it is based on transient expression. With this technique, the plasmid DNA are only used to transfect mammalian cells and the recombinant DNA is not integrated to the host cell genome (227). This technique is faster than the stable cell line expression, as a recombinant protein can usually be produced in 2 weeks (228). However, the non-integration of the recombinant DNA into the host genome leads to loss during cellular division or degradation, thus stopping or reducing the recombinant protein production. The advantages of the stable gene expression over the transient gene expression, is that the first not require as much plasmid DNA as the second, it is easier to scale up and once a cell line has been established it can be frozen for further use (229). Moreover, the production from a stable cell line can reach up to ~90 pg/cell/day (226), when it only reaches up to 10 pg/cell/day when using a transient expression (230). However, the gap between the timelines of the two methods is tremendous.

Finally, the integration can also be done using the CRISPR/Cas9 genome editing system, as recently Lee *et al.* were able to target the gene integration into site-specific loci in CHO cells (231).

### **1.6.5. Recombinant protein purification**

The purification of recombinant proteins is an essential step to obtain a pure recombinant protein, separated from the unwanted host-derived proteins, while also allowing the protein to be exchanged into the desired buffer. Among other techniques, chromatography is a very efficient technique for the purification of proteins. Proteins can be separated based on their physicochemical properties such as size and shape, total charge, hydrophobic groups present on the surface, and binding capacity with the stationary phase (232). In chromatography, the mobile (liquid) phase, a fluid carrying the protein mixture, interacts with different affinities with a stationary (solid) phase. Depending on these interactions, the molecules will travel at different velocities in the mobile phase, allowing the separation of the molecules of the mixture at the end of the system. Chromatography methods include those based on the state of the mobile phase (liquid or gas chromatography), ion-exchange chromatography, size-exclusion chromatography and affinity chromatography. Affinity chromatography and size exclusion chromatography (SEC) have been used to purify the recombinant proteins produced, and thus are described here in some detail.

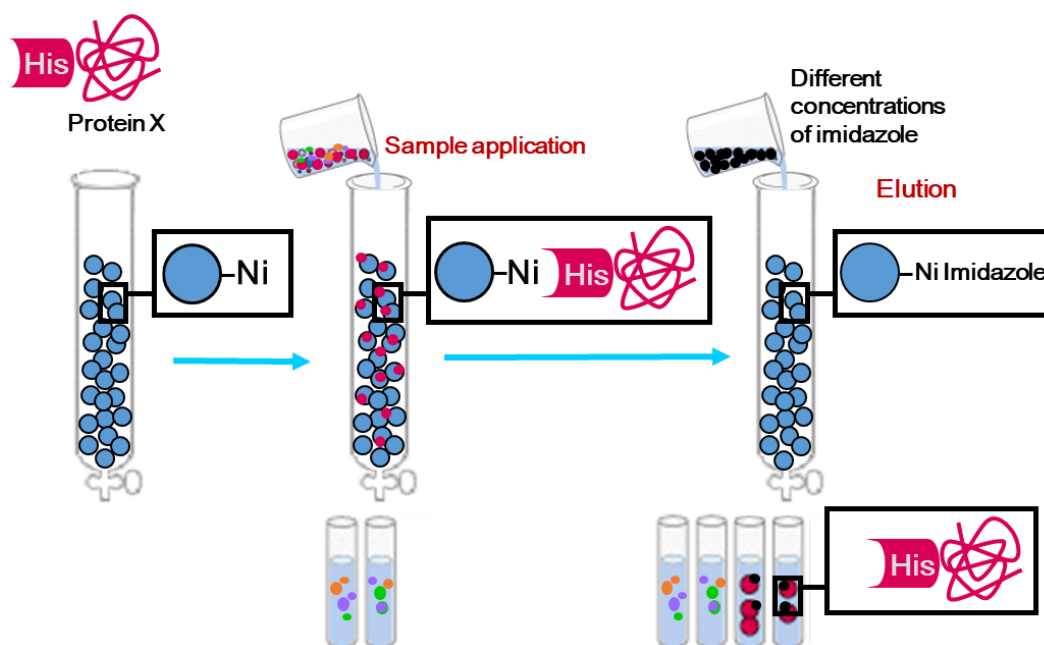
#### **1.6.5.1. Affinity chromatography**

Affinity chromatography use the principle of specific binding interactions between the analyte and a ligand. The ligand is usually covalently bound to a solid matrix. The analyte specifically interacts with the ligand when the other contaminants can be collected as the non-binding material.

Immobilized Metal Affinity Chromatography is based on the affinity of metal ions (such as  $Zn^{2+}$ ,  $Cu^{2+}$ ,  $Ni^{2+}$ , and  $Co^{2+}$ ) for the lone pair electrons of nitrogen-containing amino side chains (such as in Histidine). The stationary phase consists in a chelating ligand covalently attached to a support (most commonly agarose beads). Iminodiacetic acid or nitrilotriacetic acid (NTA) can be used as chelating ligand and they entrap metal ions via coordinate binding.



Electron donor groups on the Histidine imidazole ring form coordination bonds with the immobilized metal ions. Using this principle, Histidine-tagged (His-tagged) proteins (usually a polyhistidine tag of 6 or 8 Histidine, called 6xHis or 8xHis) can be purified from unwanted material as the Histidine-tagged proteins will be retained by the metal ions when the unwanted material can be washed away (Figure 1.28). The metal ions affinity for Histidine tags from stronger to weaker is  $\text{Cu}^{2+}$ ,  $\text{Ni}^{2+}$ ,  $\text{Zn}^{2+}$  and  $\text{Co}^{2+}$ . The His-tagged proteins can be eluted from the transition metal by decreasing the pH of the liquid phase, causing the protonation of Histidines, disrupting their binding with the metal. His-tagged proteins can also be eluted from the metal by addition of free imidazole to the buffer which acts as a competitive binder for the metal ions. This technique has many advantages as the tag is small and can easily be added to the N- or C-terminal of the recombinant protein, the proteins are eluted under mild conditions and yields purified proteins with purities up to 95% (233).



*Figure 1.28 Representation of immobilized metal affinity chromatography.*

Immunoaffinity chromatography is based on the specific binding of antibodies for their given target to purify the target from unwanted material. The stationary phase consists of antibodies covalently attached or adsorbed on different supports such as carbohydrate-related supports (e.g. agarose and cellulose) or synthetic organic supports (e.g. acrylamide

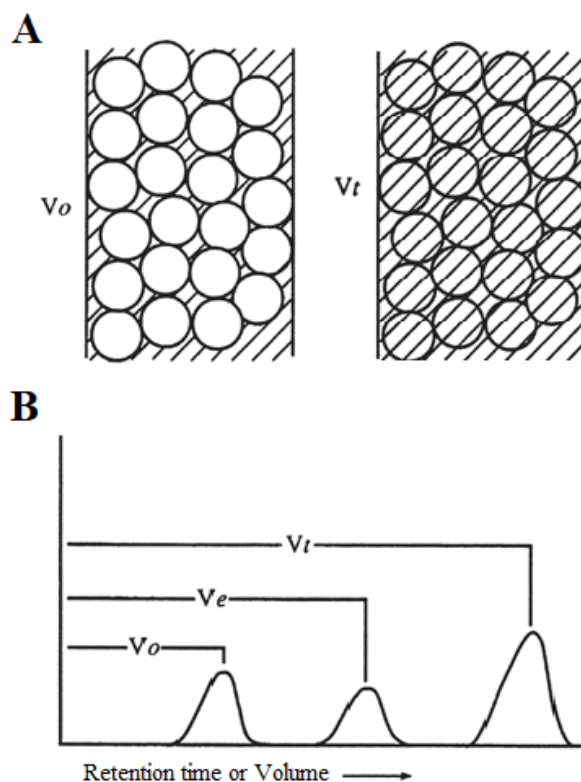
polymers and copolymers). Specific interactions between the target protein in the liquid phase and the antibodies bound to the solid phase allow the separation of target protein from unwanted material. To elute the target proteins, the strength of the antibody-antigen interaction must be lowered (234). Lowering the pH of the liquid phase inhibits the antibody-antigen reaction thus liberating the target antigen. This interaction can also be lowered by addition of chaotropic agent to the liquid phase as they are effective in dissociating high-affinity antibody-antigen complexes. Immunoaffinity chromatography has a high specificity and affinity for a target antigen, however it is also the main disadvantage of this technique as to elute the antigen harsh conditions are usually needed (235).

#### **1.6.5.2. Size-Exclusion Chromatography (SEC)**

SEC is a chromatography method separating molecules based on their hydrodynamic volume. The solid phase consists in spherical beads containing pores, and the separation is due to the interaction of the molecules with this porous solid phase. Smaller molecules can enter the beads' pores, thus their flow through the column is retarded compared to bigger molecules that cannot enter the pores and instead flow rapidly through the column.

Molecules too large to enter the pores stay in the interparticle volume and are eluted first from the column, this interparticle volume is called the void volume. The elution volume corresponds to the volume between the injection of the sample and the elution of a protein. The solvent volume corresponds to the volume inside the pores of the beads and the total volume corresponds to the void volume plus the solvent volume (Figure 1.29).

SEC is mostly applied for fractionation, to separate molecules with different sizes and for buffer exchange as the molecule of interest will be found in the void volume when the smaller molecules are retained in the column.



**Figure 1.29** Size Exclusion Chromatography.

A: schematic representation of the Size Exclusion Chromatography with the void volume ( $V_o$ ) and the total volume ( $V_t$ ). B: schematic representation of a chromatogram with the high molecular weight proteins being eluted in the  $V_o$ , the medium molecular weight proteins being eluted in the elution volume ( $V_e$ ) and the low molecular weight proteins being eluted in the  $V_t$ . Figure adapted from Cutler P. (2008) *Size-Exclusion Chromatography*. In: Walker J.M., Rapley R. (eds) *Molecular Biomethods Handbook*. Springer Protocols Handbooks. Humana Press.

## 1.7. Detection molecules

### 1.7.1. Production of monoclonal antibodies

Antibodies can be very useful in various fields of medicine where they can be used in disease therapy, but also in research and in diagnosis. mAbs are identical antibodies produced by a unique clonal population derived from a single B cell. The fact that these antibodies are identical presents several advantages compared to a pool of antibodies (referred to polyclonal antibodies, pAbs) with the main feature being a unique specificity. The mAbs are produced by hybridomas, which are immortal cells, leading to a virtual unlimited source of antibody and a high reproducibility in their production.

The field of antibodies was revolutionized in 1975 by G. Köhler and C. Milstein when they were able to generate mAbs by culture of fused cells, which is currently known as hybridoma technology (236). Hybridoma technology involves immunizing an animal, usually mice or rats, to elicit a strong immune response against an antigen (237). The antigen can be injected by many different routes of administration and is usually injected with a strong adjuvant. Adjuvants non-specifically stimulate the immune response and can be oil-based (such as Freund's adjuvants) or water-based. Adjuvants have two roles, the first is to prevent the rapid catabolism of the antigen and the second is to non-specifically stimulate the immune system (238). The B cells from an immunized animal are fused with myeloma cells, which are derived from tumours, are immortal and have been adapted to grow *in vitro*. The fusion generates heterokaryons (multinucleate cell with distinct nuclei) and unfused cells. The B cells cannot grow *in vitro* and will subsequently die; however, the myeloma cells are immortal and need to be removed. In order to select the hybridomas resulting of the correct fusion of a myeloma and a B cell, there is a drug selection step. The myelomas used for the fusion lack hypoxanthine-guanine phosphoribosyl transferase (HGPRT). If the main synthesis pathway for purine and pyrimidine nucleotides is blocked, cells can survive using the salvage pathway requiring HGPRT. After the fusion, the cells are grown in a hypoxanthine-aminopterin-thymidine (HAT) medium, first described in 1962 (239), which will block this main synthesis pathway. HGPRT-deficient myelomas are not able to use the salvage pathway, thus will die. Only the hybridomas that have obtained HGPRT from the B cells will be able to proliferate. This technique was developed by Littlefield in 1964 (240). Finally, the hybridomas are screened, usually by indirect ELISA, to select the most specific and sensitive mAb produced against the antigen and this mAb is purified.

This technique efficiently produces mAbs from animals, however it has some drawbacks; it is time consuming (minimum of 6 months between the first immunization of an animal and the purification of the mAbs), the process is expensive and the cultures can be contaminated. For these reasons, the production of pAbs is often an attractive option as their production is faster, less expensive and could lead to a higher affinity reagent as the population of different antibodies can recognize different epitopes. These attributes must be balanced alongside the drawbacks of pAbs, which are that their supply is less reproducible, and they often exhibit higher cross-reactivity due to the different epitopes recognized.

Since some countries such as the Netherlands, the United Kingdom and Germany started to ban the production of mAbs in animals, new techniques have been developed to produce recombinant antibodies using a recombinant expression system or using phage display (described below), creating a bacteriophage library, which can then be used to recognize an antigen *in vitro* and then produce part or whole IgG recombinantly (241,242). The main advantages of these techniques are that they do not require the use of animals, they reduce the production time (from 6 months to around 2 months) and have a better reproducibility than mAbs produced with the hybridoma technology.

Finally, by proteolytic cleavage or genetic engineering, antibody fragments can be obtained when some functions of the full-length antibody are not required (243). Indeed, in some cases the Fc-mediated effects such as long serum half-life and activation of Fc receptor expressing cells are not needed or unwanted (244). Although the high affinity and specificity of the antibodies to recognize antigens is required for most applications. This led to the development of antibodies fragments, small molecules derived from full-length antibodies, keeping the binding properties of the full-length antibody with more efficient tissue penetration. Some examples of antibody fragments are represented in Figure 1.30. The digestion of an IgG by papain results in two Fab fragments and one Fc fragment. A Fab fragment consists of one light chain and one heavy chain linked by a disulfide bond, thus is monovalent. The digestion of an IgG by pepsin results in a  $F(ab')_2$  fragment and a Fc fragment with the  $F(ab')_2$  being divalent as it contains two Fab fragments joined at the hinge by disulfide bonds. This  $F(ab')_2$  fragment can be reduced to obtain two monovalent  $F(ab')$  fragments containing a free sulfhydryl group. Finally, smaller molecules can be obtained by genetic engineering such as the single chain variable fragments, which consists of the variable regions of heavy and light chains joined together by a flexible peptide linker (245). Single domain antibody is a single monomeric variable antibody domain that can be engineered from heavy chain antibodies found in camelids or sharks (246).



**Figure 1.30 Schematic representation of the most common antibody fragments.**

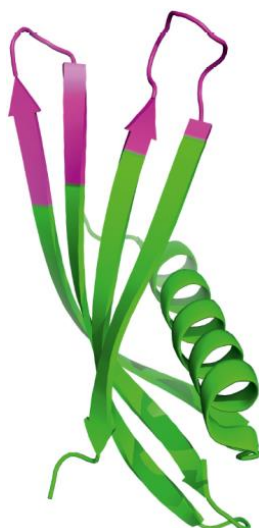
The heavy chain is represented in dark blue and the light chain in light blue. Figure adapted from Biologics International Corp at <https://www.biologicscorp.com/fab-fragment-antibody/>

### 1.7.2. Non-antibody molecules: Affimers

Many non-antibody molecules have been developed and have been thoroughly reviewed in Škrlec *et al.*, Vazquez-Lombardi *et al.* and Simeon and Chen (247–249). New protein scaffolds are continuously being discovered or designed, with some of them already being used in humans or under clinical trials (248). These molecules have some common characteristics to address the drawbacks of mAbs, such as their small size, the lack of PTM and of disulfide bonds. Among others, these include Adnectin (250), Affibody (251), Anticalin (252), DARPin (253), Kunitz Domain (254) or Affimers.

Affimer molecules (or adhirons) are small proteins, 12 – 14 kDa, that bind specifically to a target molecule with two variable loops. The scaffold is derived from a synthetic cystatin consensus sequence or engineered from human stefin A, which are both sequence-related (255). The scaffold has a high thermal stability ( $T_m=101^\circ\text{C}$ ) and can be expressed in *E. coli* as it does not have any PTM (256). The two variable loops are formed by nine random amino acids, which form a very extensive library of Affimers. The example of the crystal structure of an Affimer can be found in Figure 1.31.

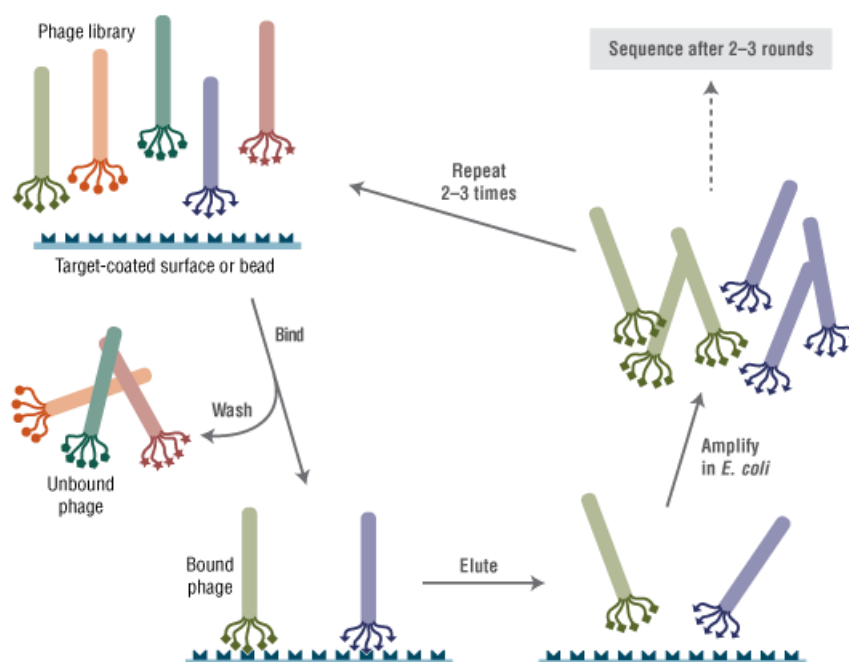
Affimers have many advantages over antibodies as they are faster to develop (around 7 weeks), are smaller meaning that they can be selected against smaller compounds, do not use animals and have high batch reproducibility.



**Figure 1.31** Crystal structure of an Affimer against the protein p300.

The two variable loops are shown in pink. Figure adapted from Tiede C et al. Affimer proteins are versatile and renewable affinity reagents. *Elife*. 2017;6:e24903.

The selection of the Affimers against a target protein is done through phage display technology. Phage display is a technique invented by G. Smith in 1985 to present polypeptides on the surface of a filamentous bacteriophage (257). This technique uses the fact that the genotype and the phenotype of the filamentous bacteriophage are physically linked as the peptide displayed on the phage's surface is encoded by a gene contained in the virion (258). The selection of Affimers is done through phage display with a library of high complexity with over  $1.3 \times 10^{10}$  different Affimer clones with unique variable loops (256). In this process, the Affimers are cloned into a phagemid vector, based on the bacteriophage M13, which will express an Affimer/truncated-pIII fusion protein on the coat of the bacteriophage (256). The target protein is used to pan the library to find the best Affimers to bind to the target protein. The phages are then eluted and *E. coli* cells are electroporated with the phagemid vectors and infected with a helper phage containing the complete M13 genome encoding all the phage proteins required for capsid production, phage assembly, chromosome replication and budding (259). The enriched phage mixture obtained is used for two other panning cycles to enrich the mixture with the best binding Affimers to the target protein, as represented in Figure 1.32. These phages are sequenced to obtain the sequences of the two variable loops which are then cloned in an *E. coli* expression vector. The Affimers are then expressed and purified.



**Figure 1.32 Schematic representation of Affimer screening process using phage display.**

Phage-expressing Affimers bind to the target protein. Unbound phages are washed off and the bound phages are eluted and amplified in *E. coli*. These panning rounds are repeated twice to obtain individual phages displaying target-binding Affimers. The binders are then tested in ELISA and the phages are sent to sequencing. Figure adapted from <https://international.neb.com/tools-and-resources/feature-articles/applications-of-the-phd-phage-display-peptide-libraries>

Affimers have been used in diagnostics such as ELISAs (255), sandwich chemiluminescence immunoassay (CLIA) (260), biosensors (261,262), histochemistry (255) and for western blotting (WB) (256). They could also be used as therapeutics as their high stability, small size, which could mean higher tissue penetration, and human origin confer them many advantages (263,264). However, in some cases, for diagnosis, a combination of Affimer and mAb has shown better results than a pair of Affimers or mAbs, maybe exhibiting a synergetic action of these two detection molecules (260).



## 1.8. Aim of this project

This work is part of HONOURs, a Marie Skłodowska-Curie Action (MSCA) Innovative Training Network (ITN) comprising 15 Early Stage Researchers in all aspects of infectious outbreaks to become preparedness-experts on host switching pathogens, infectious outbreaks and zoonosis (265). More specifically, this work is part of the work package “advanced diagnostics”, aiming to prepare the rapid development of serological diagnostic tools in case of an outbreak scenario or the discovery of a new virus.

Concretely, the aim of this thesis was to develop new diagnostic tools for the detection of newly emerging viruses such as RVFV and CCHFV, as, according to the WHO and OIE, there are still some gaps in their diagnosis, especially in animals and these tools will help in the prevention of the spreading of these viruses and also in surveillance programs. Finally, as mentioned above, the discovery of new viruses that could emerge unexpectedly during the course of this project may force the change of the targets described above. In this case, the technologies and resources will be adapted to the new isolates, which happened at the end of 2019 with the discovery of SARS-CoV-2.

Four main objectives were defined:

1. Expression and purification of recombinant CCHFV N protein and glycoproteins and production of monoclonal antibodies against the N protein. Development and validation of serological assays for diagnosis of CCHFV.
2. Expression and purification of recombinant RVFV N protein and glycoprotein. Production of monoclonal antibodies and non-antibody binding molecules (Affimers) against the RVFV N protein. Development and validation of serological assays for diagnosis of RVFV.
3. Development of a multiplex assay for differential diagnosis of CCHFV, RVFV and other relevant related pathogens such as Schmallenberg virus (SBV), BTV and *Mycobacterium bovis*.
4. Production of the SARS-CoV-2 N protein and development of several diagnostic assays to identify the virus or the immune response towards it. Development of a multiplex serological assay targeting different proteins of SARS-CoV-2.

## Chapter 2 Materials and Methods

### 2.1. Materials

#### 2.1.1. Synthetic genes

A cDNA to express the full-length N protein of RVFV, strain ZH-548 M12 (Genbank accession No. X53771.1), optimized for bacterial expression and flanked with *Bam*HI and *Xho*I restriction sites, was generated synthetically (Genewiz) in the donor plasmid pUC57-Kan.

The cDNAs of RVFV G<sub>N</sub> ectodomain (G<sub>NE</sub>) (strain ZH-548 M12, GenBank accession No. M25276.1, nucleotides 480:1766), CCHFV GP38 (strain Nigeria/IbAr10200/1970, GenBank accession No. AF467768.2, nucleotides 834:1649) and CCHFV G<sub>N</sub> (strain Nigeria/IbAr10200/1970, GenBank accession No. AF467768.2 nucleotides 1650:2618) optimized for expression in *S. frugiperda* were synthetically produced by IDT.

The cDNA encoding for the full-length nucleocapsid protein of SARS-CoV-2, isolate Wuhan-Hu-1 (GenBank accession NC\_045512, nucleotides 28274:29533), was kindly provided by Dr. Volker Thiel (Institute of Virology and Immunology, Switzerland).

On arrival, the synthetic genes were resuspended in nuclease-free H<sub>2</sub>O and stored at -20°C.

The synthetic genes used during this project are summarized in Table 2.1.

*Table 2.1 Synthetic genes.*

Gene	Strain	Genbank	Plasmid	Optimized	Origin
RVFV N protein	ZH-548 M12	X53771.1	pUC57	<i>Escherichia coli</i>	Genewiz
RVFV G <sub>NE</sub>	ZH-548 M12	M25276.1	/	<i>Spodoptera frugiperda</i>	IDT
CCHFV G <sub>N</sub>	Nigeria/IbAr 10200/1970	AF467768.2	/	<i>Spodoptera frugiperda</i>	IDT
CCHFV GP38	Nigeria/IbAr 10200/1970	AF467768.2	/	<i>Spodoptera frugiperda</i>	IDT
SARS-CoV-2 N protein	Isolate Wuhan-Hu-1	NC_045512	pUC57	/	Dr. Volker Thiel

### 2.1.2. Primers

The oligonucleotides were produced by Thermo Fisher Scientific and Eurofins Genomics for use in sequencing and PCR. On arrival, each was resuspended in nuclease-free H<sub>2</sub>O and stored at -20°C.

The primers used to amplify the genes mentioned above are listed in Table 2.2.

*Table 2.2 Oligonucleotides used for cloning.*

Target	Primer name	Primer sequence
RVFV N protein	Forward RVFV N protein	5'-ATG GAC AAT TAT CAA GAA CTG CGT G-3'
	Reverse RVFV N protein	5'-TTA TGC TGC GGT TTT ATA TGC CTG-3'
RVFV G <sub>Ne</sub>	Forward RVFV G <sub>Ne</sub>	5'-ATG GAA GAT CCC CAC CTG AGG AAC C-3'
	Reverse RVFV G <sub>Ne</sub>	5'-TTA AGC GGT GTG GCA CTG GTA GTT G -3'
CCHFV G <sub>Ne</sub>	Forward CCHFV G <sub>Ne</sub>	5'-ATG TCC GAG GAA CCT TCC G-3'
	Reverse CCHFV G <sub>Ne</sub>	5'-TTA CAG GAA GGC CAT AGT AGT CTT AGG-3'
CCHFV GP38	Forward CCHFV GP38	5'-ATG AAC CTG AAG ATG GAA ATC ATC C-3'
	Reverse CCHFV GP38	5'-TTA CAG CAG ACG ACG AGA ACC-3'
SBV N protein	Forward SBV N protein	5'-CGC GGA TCC ATG TCA AGC CAA TTC ATT TTT GAA G-3'
	Reverse SBV N protein	5'-CCG CTC GAG TTA GAT GTT GAT ACC GAA TTG CTG-3'
SARS-CoV-2 N protein	Forward SARS-CoV-2 N protein	5'-ATG TCT GAT AAT GGA CCC CAA AAT C-3'
	Reverse SARS-CoV-2 N protein	5'-TTA GGC CTG AGT TGA GTC AGC-3'
Affimers	Forward	5'-ATG GCT AGC AAC TCC CTG GAA ATC GAA G-3'
	Reverse Cys	5'-TTA CTA ATG CGG CCG CAC AAG CGT CAC CAA CCG GTT TG-3'

Moreover, for sequencing, the following oligonucleotides were also used (Table 2.3):

**Table 2.3 Oligonucleotides used for sequencing.**

<b>Name</b>	<b>Primer sequence</b>
GW1	5'-GTT GCA ACA AAT TGA TGA GCA ATG C-3'
GW2	5'- GTT GCA ACA AAT TGA TGA GCA ATT A- 3'
T7 forward	5'- TAA TAC GAC TCA CTA TAG GG-3'
T7 reverse	5'-GCT AGT TAT TGC TCA GCG G-3'
GST 621+	5'-GCC ACG TTT GGT GGT GGC GAC-3'
Bac Rev	5'-CGC ACA GAA TCT AGC GCT TAA-3'

### **2.1.3. Plasmids**

The expression plasmid pET28a-SUMO was used as backbone to produce the target proteins (CCHFV N, RVFV N and SBV N proteins) in *E. coli*, with the various ORFs inserted such that the resulting expressed protein was N-terminally appended by SUMO and 6xHis tags.

For the Gateway technology (Thermo Fisher Scientific), the pCR<sup>TM</sup>8/GW/TOPO® vector was used as entry vector and the expression vector pDEST17 was used for production of recombinant proteins in *E. coli* (SARS-CoV-2 N protein) and pAcSecG2T for production of recombinant proteins in insect cells (CCHFV GP38, CCHFV G<sub>NE</sub> and RVFV G<sub>NE</sub>).

The pAcYM1 vector containing the full-length cDNA of the VP7 of BTV serotype 10 (GenBank accession No. YP\_052967) was used to produce a recombinant baculovirus expressing the VP7 protein (this material was already available in Eurofins-Ingensasa).

The vectors used are detailed in Table 2.4.

**Table 2.4 Plasmids.**

Plasmid	Antibiotic resistance	Promoter	System	Tags	Application
pET28a-SUMO	Kanamycin	T7	<i>Escherichia coli</i>	6xHis-SUMO (N-terminal)	Expression of CCHFV, RVFV and SBV N proteins
pET11a	Ampicillin	T7	<i>Escherichia coli</i>	8xHis (C-terminal)	Expression of Affimers
pCR™8/GW/TOPO	Spectinomycin	T7	<i>Escherichia coli</i>		Entry vector (Gateway)
pDEST17	Ampicillin	T7	<i>Escherichia coli</i>	6xHis (N-terminal)	Expression of SARS-CoV-2 N protein (Gateway)
pAcSecG2T*	Ampicillin	Polyhedrin	Insect cells/BES	GST (N-terminal)	Expression of CCHFV GP38, G <sub>NE</sub> and RVFV G <sub>NE</sub> (Gateway)
pAcYM1		Polyhedrin	Insect cells/BES		Expression of BTB VP7

\*Plasmid modified at Eurofins-Ingensa for its use in the Gateway system.

## 2.1.4. Cells

### 2.1.4.1. Bacterial strains

For most cloning steps, competent *E. coli* NZY5 $\alpha$  cells (NZYTech, genotype: fhuA2 $\Delta$ (argF-lacZ)U169 phoA glnV44  $\Phi$ 80  $\Delta$ (lacZ)M15 gyrA96 recA1 relA1 endA1 thi-1 hsdR17) were used for transformation.

The ORFs of the CCHFV N, RVFV N and SBV N proteins were expressed using the *E. coli* BL21 derivative Rosetta™ 2 (DE3) Singles™ Competent Cells (Novagen, genotype: F- ompT hsdSB(rB- mB-) gal dcm (DE3) pRARE2 (CamR)).

After performing the TOPO® Cloning reaction, the pCR™8/GW/TOPO® constructs were transformed into One Shot® Mach1™-T1<sup>R</sup> chemically competent *E. coli* (Thermo Fisher Scientific, genotype: F-  $\phi$ 80(lacZ) $\Delta$ M15  $\Delta$ lacX74 hsdR(rK-mK+)  $\Delta$ recA1398 endA1 tonA). The ORF of the SARS-CoV-2 N was expressed using the BL21-AI™ *E. coli* strain (Invitrogen, genotype: F- ompT hsdSB(rB - mB - ) gal dcm araB::T7RNAP-tetA).

For phage display to select Affimers, the *E. coli* strain K12 ER2738 was used (New England Biolabs, Inc., genotype: F'proA+B+ lacIq  $\Delta$ (lacZ)M15 zzzf::Tn10(TetR)/ fhuA2 glnV  $\Delta$ (lac-proAB) thi-1  $\Delta$ (hsdS-mcrB)5).

#### **2.1.4.2. Insect cell lines**

Sf9 insect cells (ATCC<sup>®</sup> CRL-1711<sup>™</sup>), derived from ovarian tissue of *Spodoptera frugiperda*, were used for the production of recombinant baculoviruses, baculovirus stocks and intracellular expression. Sf900 cells, variant of Sf9 adapted for growth without serum, were used for extracellular protein expression.

#### **2.1.4.3. Mammalian cell lines**

The mouse myeloma cell lines P3X63Ag8.653 and SP2/0-Ag14 were used for the fusion with the B cells of immunized mice and the production of monoclonal antibodies.

### **2.1.5. Baculovirus**

#### **2.1.5.1. Parental baculovirus**

BacPAK6 linear DNA from *Autographa californica* nucleopolyhedrovirus genome with *lacZ* inserted instead of the native polyhedrin gene coding region was used to produce recombinant baculoviruses.

#### **2.1.5.2. Recombinant baculovirus**

The recombinant baculoviruses produced during this project are summarized in Table 2.5.

**Table 2.5 Recombinant baculoviruses produced.**

<b>Name</b>	<b>Gene of interest</b>	<b>Tag</b>	<b>Expression</b>
BacPAK6 pAcSecG2T CCHFV G <sub>Ne</sub> #1	CCHFV G <sub>Ne</sub>	GST	Insoluble Soluble Secreted
BacPAK6 pAcSecG2T CCHFV GP38 #2	CCHFV GP38	GST	Insoluble Soluble Secreted
BacPAK6 pAcSecG2T RVFV G <sub>Ne</sub> #5	RVFV G <sub>Ne</sub>	GST	Insoluble Soluble
BacPAK6 pAcYM1 BTB VP7	BTB VP7		Insoluble Soluble

### 2.1.6. Laboratory mice

Female BALB/c mice aged from 9 to 12 weeks, with a weight range between 20 g to 40 g were housed in temperature-controlled, pathogen-free rooms with access to pelleted food and water *ad libitum*. Originally, the mice were commercially obtained from Harlan Interfauna Ibérica (Spain) and were bred and maintained under standard animal housing conditions by the Animal Department of Eurofins-Ingenasa (Eurofins-Ingenasa, Community of Madrid registration number ES280790000095). The animal research was approved by the Consejería de Medio Ambiente, Administración Local y Ordenación del Territorio (Department of Environment, Local Administration and Territorial Planning) from the Comunidad de Madrid (Community of Madrid, Spain) reference PROEX n°024/18.

### 2.1.7. Antibodies

The primary and secondary antibodies used in WB, ELISAs, LFA, Luminex and affinity chromatography are summarized in Table 2.6. The commercial lyophilized antibodies were dissolved in the corresponding volume of dH<sub>2</sub>O as instructed by the manufacturer, mixed in an equal volume of 99.9% glycerol and stored at -20°C.

**Table 2.6 Commercial and in-house antibodies used in WB, ELISA, LFA and Luminex.**

Antibody	Target	Label	Type/ Isotype	Species of production	Applica- tion	Dilution (v/v) or $\mu\text{g/mL}$	Source	mAb / pAb
6x-His Tag Monoclonal Antibody	6X His tag	/	IgG2b	Mouse	WB	1:2,000	Thermo Fisher Scientific (MA1- 21315)	mAb
3C11	SUMO tag	/	IgG2b	Mouse	WB	0.5 $\mu\text{g/mL}$	Eurofins- Ingenasa	mAb
3H11	GST tag	HRP	IgG1	Mouse	WB	1:150,000	Eurofins- Ingenasa	mAb
		/			Luminex	From 5 $\mu\text{g/mL}$		
		/			Affinity chromato- graphy	/		
EG5	Ruminants IgG	HRP	IgG1	Mouse	WB	1:150,000	Eurofins- Ingenasa	mAb
		Biotin			Luminex	0.5 $\mu\text{g/mL}$		
F1D11	RVFV N protein	/	IgG	Mouse	WB	10 $\mu\text{g/mL}$	A. Brún (INIA- CISA)	mAb
Goat anti- Mouse IgG (H+L) Secondary Antibody, HRP conjugate	Mouse IgG (H+L)	HRP	IgG	Goat	ELISA	1:2,000	Invitrogen (31430)	pAb
Goat anti Mouse IgG	Mouse IgG ( $\gamma$ -chain specific)	HRP	IgG	Goat	ELISA	1:5,000	Accurate Chemical & Scientific Corporati on (SBA103 001)	pAb
Anti-Mouse IgG1 ( $\gamma$ - chain specific)- Peroxidase	Mouse IgG1 ( $\gamma$ - chain specific)	HRP	IgG	Rabbit	ELISA	1:2,000	Sigma- Aldrich (SAB370 1171)	pAb
Anti-Mouse IgG2a ( $\gamma$ - chain specific)- Peroxidase	Mouse IgG2a	HRP	IgG	Rabbit	ELISA	1:2,000	Sigma- Aldrich (SAB370 1178)	pAb
Anti-Mouse IgG2b ( $\gamma$ - chain	Mouse IgG2b	HRP	IgG	Rabbit	ELISA	1:2,000	Sigma- Aldrich	pAb



specific)- Peroxidase							(SAB370 1185)	
Anti-Mouse IgG3 ( $\gamma$ - chain specific)- Peroxidase	Mouse IgG3	HRP	IgG	Rabbit	ELISA	1:2,000	Sigma- Aldrich (SAB370 1192)	pAb
Anti-Mouse IgA ( $\alpha$ -chain specific)-Per oxidase	Mouse IgA	HRP	IgG	Goat	ELISA	1:2,000	Sigma- Aldrich (A4789)	pAb
Anti-Mouse IgM ( $\mu$ -chain specific)- Peroxidase	Mouse IgM	HRP	IgG	Goat	ELISA	1:2,000	Sigma- Aldrich (A8786)	pAb
Peroxidase AffiniPure Goat Anti- Human IgG, Fc $\gamma$ fragment specific	Human IgG	HRP	IgG	Goat	ELISA	1:50,000	Jackson ImmunoR esearch (109-035- 008)	pAb
Peroxidase AffiniPure Goat Anti- Human IgM, Fc $\mu$ fragment specific	Human IgM	HRP	IgG	Goat	ELISA	1:15,000	Jackson ImmunoR esearch (109-035- 129)	pAb
COVA2-29	SARS- CoV-2 RBD		IgG	Human	LFA	1 mg/mL	M.J. van Gils (AUMC)	mAb
					Luminex	From 5 $\mu$ g/mL		
COVA2-03	SARS- CoV-2 S		IgG	Human	LFA	1 mg/m <sup>2</sup>	M.J. van Gils	mAb
1D5D12	SBV N protein		IgG2a	Mouse	Luminex	From 5 $\mu$ g/mL	Eurofins- Ingenasa	mAb
2D7	BTV VP7		IgG1	Mouse	Luminex	From 5 $\mu$ g/mL	Eurofins- Ingenasa	mAb
					Affinity chromato graphy			
83CA3	MPB83		IgG1	Mouse	Luminex	From 5 $\mu$ g/mL	Eurofins- Ingenasa	mAb
14E11	SARS- CoV-2 N protein		IgG2a	Mouse	Luminex	From 5 $\mu$ g/mL	Eurofins- Ingenasa	mAb
14E4	SARS- CoV-2 RBD		IgG1	Mouse	Competiti on	1:10,000	Eurofins- Ingenasa	mAb
Biotin-SP (long spacer) AffiniPure Goat Anti- Human IgG,	Human IgG	Biotin	IgG	Goat	Luminex	0.35 $\mu$ g/mL	Jackson ImmunoR esearch (109-065- 008)	pAb

Fcγ fragment specific								
Biotin-SP (long spacer) AffiniPure Goat Anti-Human IgM, Fc5μ fragment specific	Human IgM	Biotin	IgG	Goat	Luminex	0.4 μg/mL	Jackson ImmunoResearch (109-065-129)	pAb

The mAbs produced in this project are summarized in Table 2.7.

*Table 2.7 Monoclonal antibodies produced.*

Antibody	Target	Label	Type/ Isotype	Species of production	Application	Dilution (v/v) or μg/mL	Clonality
1E9	RVFV N protein		IgG1	Mouse	WB	10 μg/mL	mAb
					Double antibody sandwich ELISA	5 μg/mL	
1F8			IgG1	Mouse	WB	10 μg/mL	mAb
					Double antibody sandwich ELISA	5 μg/mL	
		Biotin			Double antibody sandwich ELISA	2 μg/mL	
HRP		Double antibody sandwich ELISA			1:30,000		
2D10			IgG1	Mouse	WB	10 μg/mL	mAb
1D6			IgG1	Mouse	WB	10 μg/mL	mAb
2G10	CCHFV N protein		IgG1	Mouse	WB	10 μg/mL	mAb
					Double antibody sandwich ELISA	1:4,000	
HRP							
3G7			IgG1	Mouse	WB	10 μg/mL	mAb
					Double antibody sandwich ELISA	5 μg/mL	

## 2.1.8. Samples

### 2.1.8.1. Animal serum samples

A total of 910 serum samples from different animal species were used in this project (detailed in Table 2.8). For the detection of antibodies to RVFV, 68 serum samples from sheep experimentally inoculated with RVFV were kindly provided by Dr A. Brún from Centro de Investigación en Sanidad Animal-Instituto Nacional de Investigación y Tecnología Agraria y Alimentaria ((INIA-CISA), Madrid, Spain), some of them previously characterized (266,267). For detection of antibodies to SBV, 33 serum samples from calves and 41 serum samples from lambs experimentally infected with SBV were available at Eurofins-Ingenasa, from a previous internal project. For the detection of antibodies to *M. bovis*, 29 serum samples from cattle vaccinated intramuscularly with *M. bovis* were available at Eurofins-Ingenasa, from the European project WildTBVac (Call Identifier: FP7-KBBE-2013-7; Grant agreement nº 613799). For detection of antibodies to CCHFV, 31 field serum samples from cattle, 33 from sheep, 5 from horses and 3 from goats naturally infected by CCHFV were provided by the Faculty of Veterinary Medicine in Skopje (USCM, North Macedonia). For the detection of antibodies to BTV, 73 serum samples from cattle experimentally infected with BTV were available at Eurofins-Ingenasa, obtained from previous projects (PROFIT, Ref. CIT-010000-2005-81 and Comunidad de Madrid, Ref. 27/2007) and 15 serum samples from SBV infected animals, also positive to BTV.

Finally, a collection of 579 negative field samples (208 from cattle, 184 from goats, 185 from sheep and 2 from horses) from Spanish farms were evaluated in the different assays developed.

**Table 2.8 Animal serum samples.**

	Field or experimental serum samples positive to					Negative	Total
	RVFV	SBV	<i>Mycobacterium bovis</i>	CCHFV	BTV		
Number of samples	68	74	29	72	88	579	910

### 2.1.8.2. Human serum samples

A total of 1,065 human serum samples were used in this project. Eighty-seven serum samples were provided by the Hospital General Universitario Gregorio Marañón in Madrid (Spain), 140 serum samples by the Instituto de Salud Carlos III (Madrid, Spain), 665 serum samples from the “Program of Surveillance and Early Detection Program of COVID-19 in essential services personnel of the city of Madrid” given by the Institute of Public Health of the Madrid City Council (Spain), 109 serum samples by the Amsterdam University Medical Center in Amsterdam (the Netherlands), and 64 serum samples already available in the lab from a previous European project, RespViruses (EU-FP6-2005-LIFESCHEALTH-7). The samples were classified as follows: 163 serum samples of patients positive to COVID-19 by PCR (all the PCRs described in this study were real-time RT-PCRs done in respiratory material) and confirmed by a commercial assay (NovaLisa® SARS-CoV-2 IgG and IgM ELISAs (Novatec) or 2019-nCoV IgG/IgM Rapid Test (T&D Diagnostics Canada)), 43 serum samples of patients positive to COVID-19 by PCR but negative in the serological assays, 174 serum samples of patients negative to COVID-19 by PCR but positive in a commercial serological assay, 452 serum samples of patients negative to COVID-19 both by PCR and serological assay, and 233 negative sera collected before 2019. A summary of these data is shown in Table 2.9. A collection of sera positive to other infectious diseases which can provoke pneumonia (5 sera positive to *Chlamydia trachomatis*, 17 to *Mycoplasma pneumoniae*, and 21 to *Legionella pneumophila*) was tested and classified by the Department of Serology of the Spanish National Center of Microbiology and was included in the study. The 64 samples from the RespViruses project were collected from blood donors and people requesting serological tests and other virological investigations at the University Hospital Bonn, and 62 were found positive to human respiratory syncytial virus (hRSV) in different assays (268). Finally, the collection provided by the Amsterdam University Medical Center included a total of 20 serum samples from the Amsterdam Cohort Studies on HIV infection and acquired immunodeficiency syndrome (AIDS) (269). The sera were obtained shortly (within 6 months) after infection by a seasonal *Alphacoronavirus* (HCoV-NL63 or HCoV-229E) or a seasonal *Betacoronavirus* (HCoV-HKU1 or HCoV-OC43) and contained high concentrations of antibodies to these common-cold coronaviruses. For all the human serum samples collected, the participation was voluntary

and without incentive. Formal agreements with the institutions providing the serum samples or written informed consent of each participant at enrolment were obtained.

*Table 2.9 Human serum classification by real-time RT-PCR and serological assays.*

	Serum samples
<b>Real-time RT-PCR + / Antibody +</b>	163
<b>Real-time RT-PCR + / Antibody -</b>	43
<b>Real-time RT-PCR - / Antibody +</b>	174
<b>Real-time RT-PCR - / Antibody -</b>	452
<b>Samples prior 2019</b>	233
<b>Total</b>	1065

### 2.1.8.3. Respiratory samples

Six oropharyngeal samples and five nasopharyngeal samples were available at Eurofins-Ingenasa. The samples were classified as positive or negative to COVID-19 by real-time RT-PCR. The classification of the samples is described in Table 2.10.

*Table 2.10 Classification of the oropharyngeal and nasopharyngeal samples.*

Specimen	Sample	Real-time RT-PCR result (Ct values)	Positive or negative to COVID-19
Oropharyngeal samples	1	24.5	Positive
	2	26	Positive
	3	28.5	Positive
	4	29	Positive
	5		Negative
	6		Negative
Nasopharyngeal samples	7	28	Positive
	8		Negative
	9		Negative
	10		Negative
	11		Negative

### 2.1.9. Dilution buffers for the immunoassays

The following dilution buffers were used in ELISAs (Table 2.11):

*Table 2.11 Dilution buffers (DB) used in ELISAs.*

Name	Composition
DB1	0.35 M NaCl, 0.05% (v/v) Tween 20, 0.05% (v/v) Kathon CG (Escuder)
DB2	250 mM Tris-HCl, 1 M NaCl, 1% (v/v) Tween 20, 1% (w/v) bovine serum albumin (BSA), 0.095% (v/v) NaN <sub>3</sub> , pH 7.2
DB3	1X PBS, 0.05% (v/v) Tween 20, 2.5% (v/v) foetal bovine serum (FBS, Gibco™)
DB4	StabilZyme® SELECT stabilizer (Surmodics) supplemented with 0.5 M NaCl

The following dilution buffers were used in LFA (LDB) (Table 2.12):

*Table 2.12 Dilution buffers used in LFAs (LDB).*

Name	Composition
LDB1	250 mM Tris-HCl, 150 mM NaCl, 1% (w/v) casein, 0.095% (v/v) NaN <sub>3</sub> , pH 7.5
LDB2	250 mM Tris-HCl, 1 M NaCl, 1% (w/v) BSA, 1% (v/v) Tween 20, 0.095% (v/v) NaN <sub>3</sub> , pH 7.2
LDB3	250 mM Tris-HCl, 150 mM NaCl, 1% (w/v) casein, 0.5% (v/v) Tween 20, 0.095% (v/v) NaN <sub>3</sub> , pH 7.5
LDB4	250 mM Tris-HCl, 0.75 M NaCl, 1% (w/v) casein, 0.095% (v/v) NaN <sub>3</sub> , pH 7.5
LDB5	250 mM Tris-HCl, 1 M NaCl, 1% (w/v) casein, 0.095% (v/v) NaN <sub>3</sub> , pH 7.5

## **2.2. Methods**

### **2.2.1. Classical molecular cloning by restriction enzyme digestion**

#### **2.2.1.1. Polymerase chain reaction**

Polymerase chain reactions were completed in a total volume of 50  $\mu\text{L}$  using the FastStart™ *Taq* DNA polymerase (Roche). The reaction was set up with 5  $\mu\text{L}$  of PCR reaction buffer with 20 mM  $\text{MgCl}_2$  10X concentrated, 100 ng of DNA template, 200 ng of each forward and reverse primers, 12 mM of deoxyribose nucleotide triphosphate, 1  $\mu\text{L}$  of FastStart™ *Taq* DNA Polymerase (5U) and up to 50  $\mu\text{L}$  with nuclease-free  $\text{H}_2\text{O}$ . The PCR was performed in an Applied Biosystems™ 2720 thermal cycler (Thermo Fisher Scientific) according to the manufacturer's instruction depending on the melting temperature of the primers and the length of the product to amplify. The number of amplifying cycles was between 25 and 30. The products were analysed by agarose gel electrophoresis and visualized by transillumination.

#### **2.2.1.2. DNA digestion**

Restriction enzymes and buffers were obtained from Thermo Scientific. Restriction enzyme digestion was performed on PCR products and plasmid DNA for subcloning of the RVFV N protein gene and SBV N protein gene into the pET28a-SUMO expression vector. A sequential digestion was performed with the reaction components and conditions described by the manufacturer. The digested products were analysed by agarose gel electrophoresis.

#### **2.2.1.3. Agarose gel electrophoresis**

To check the size and purity of the PCR products, products of restriction enzyme digestion and plasmid DNA were separated using 0.8-1% (w/v) agarose gels in 0.5X Tris/Borate/EDTA (TBE) buffer, supplemented with 1:10,000 of GelRed® nucleic acid gel stain (Biotum). The samples were prepared by adding 1/6<sup>th</sup> of DNA loading buffer (0.25% (w/v) bromophenol blue, 40% (w/v) sucrose). Samples were run on gels at 100 V in 0.5X TBE buffer for a predetermined time depending on the products to observe. The

gels were observed and photographed in a UV transilluminator using Gel Logic 2200 Digital Imaging System (Kodak) and were visualized using Kodak Molecular Imaging Software.

If the DNA products were to be extracted from the gel and purified, 0.8-1% (w/v) low melting temperature agarose gels were made and observed using an UV transilluminator.

#### **2.2.1.4. DNA gel extraction and purification**

The digested plasmid DNA was loaded onto a 0.8% (w/v) low melting temperature agarose and electrophoresed as described above. Plasmid DNA was excised from the gel using a sterile scalpel and extracted from the agarose gel using NZYGelpure (NZYTech) following the manufacturer's instructions. Digested PCR products were purified using the same kit for PCR products. The purified digested plasmid DNA and PCR products were quantified by spectrophotometry using a NanoDrop™ 1000 spectrophotometer (Thermo Scientific).

#### **2.2.1.5. Ligation**

Ligations were performed using the rapid DNA ligation kit (Roche). The reaction contained 50 ng of digested plasmid DNA, 1:1 molecular ration of insert:plasmid DNA, up to 10  $\mu$ L 1X DNA dilution buffer, 10  $\mu$ L of 2X T4 DNA ligation buffer and 1  $\mu$ L T4 DNA ligase (5U). The reaction was incubated for 15 min at room temperature (RT). This ligation product was used to transform *E. coli* competent cells.

#### **2.2.1.6. Bacterial transformation**

The *E. coli* strains described in section 2.1.4.1 were transformed with the corresponding plasmids for plasmid amplification or recombinant protein expression. Cells were thawed on ice and 10 ng of plasmid DNA, 2  $\mu$ L of the TOPO® cloning reaction or 2  $\mu$ L of ligation product were added. This mix was incubated on ice for 30 minutes, then heat-shocked for 30-40 seconds at 42°C and the tubes were transferred on ice for 2 min. A 250  $\mu$ L volume of S.O.C. medium (Invitrogen™) was added to the mix and the tube was incubated at



37°C for 1 hr with shaking at 220 rpm (incubator CERTOMAT® IS (Sartorius)). Finally, the mix (transformed *E. coli*) was spread on a lysogeny broth (LB) agar plate containing the appropriate antibiotic for the selection and the plates were incubated overnight (ON) at 37°C.

#### **2.2.1.7. Plasmid DNA amplification and isolation**

A single colony from a transformed *E. coli* LB agar plate or a glycerol stock was used to inoculate 20 mL of LB medium containing the appropriate antibiotic for selection. The inoculated medium was incubated ON at 37°C, 220 rpm. The plasmid DNA isolation was done with NZYMiniprep kits (NZYTech) following the manufacturer's instruction. Purified plasmid DNAs were eluted in nuclease-free H<sub>2</sub>O and quantified by spectrophotometry using a NanoDrop™ 1000.

#### **2.2.1.8. Glycerol stocks**

Bacterial cultures were grown ON at 37°C, with shaking at 220 rpm in LB medium containing the appropriate antibiotic for selection. The cultures were mixed with 99% glycerol to a final concentration of 15% (v/v) and the glycerol stocks were stored at -80°C.

#### **2.2.1.9. Sequencing**

The constructs were sent to the Servicio de Secuenciación Automática de ADN (Automatic DNA Sequencing Service) of the Centro de Investigaciones Biológicas (Center for Biological Research, Madrid) for sequencing by the Sanger method. The chromatograms obtained were analysed using Chromas Lite 2.1 and the sequences were analysed using DS Gene 1.5.

## **2.2.2. Gateway system for molecular cloning**

### **2.2.2.1. TOPO cloning reaction**

The ligations between the gene of interest and the Gateway entry vector were performed with 40 ng of PCR product and 1  $\mu\text{L}$  of TOPO<sup>®</sup> vector according to the manufacturer's instructions. The reaction was incubated for 5 min at RT. 2  $\mu\text{L}$  of the TOPO cloning reaction was used to transform One Shot<sup>®</sup> Mach1<sup>™</sup>-T1<sup>®</sup>.

With the transformed colonies, a colony PCR was performed to check the presence of the insert in the entry vector, with suitable colonies selected for plasmid DNA amplification and subsequent sequence analysis.

### **2.2.2.2. LR recombination**

The LR recombination was performed between the entry vector and the destination vectors following the manufacturer's instructions using 150 ng of entry vector, 150 ng of destination vector, 2  $\mu\text{L}$  of LR Clonase<sup>™</sup> and up to 10  $\mu\text{L}$  of TE buffer. The reaction was incubated for 1 hr at 25°C. Then, 1  $\mu\text{L}$  of proteinase K was added to the reaction and incubated for 10 min at 37°C. Finally, 1  $\mu\text{L}$  of the LR recombination was used to transform NZY5 $\alpha$  cells.

A colony PCR screen was performed on the transformed colonies with suitable colonies selected for plasmid DNA amplification and subsequent sequence analysis.

## **2.3. Expression and purification of recombinant proteins**

The recombinant proteins used in this project were produced in two different expression systems, the N proteins were produced in bacteria and the glycoproteins were produced in insect cells.

### 2.3.1. Expression of recombinant proteins in *E. coli*

The N protein of CCHFV, RVFV and SBV were expressed in *E. coli* using a derivative of the pET28a-SUMO vector, whereas the N protein of SARS-CoV-2 was expressed in *E. coli* using the Gateway system. The final constructs of the plasmids used to express the recombinant proteins in *E. coli* are summarized in Table 2.13.

**Table 2.13 Plasmid constructs used to produce recombinant proteins in *E. coli*.**

Name	Plasmid	Gene expressed	Tag	Promoter	Antibiotic resistance	Amplification strain	Expression strain	Induction
pET28a-SUMO CCHFV N protein	pET28a-SUMO	CCHFV N protein	6xHis-SUMO (N-terminal)	T7	Kanamycin	NZY5 $\alpha$ Competent Cells	BL21 (DE3) Rosetta2	Isopropyl- $\beta$ -thio-galactoside
pET28a-SUMO RVFV N protein	pET28a-SUMO	RVFV N protein						
pET28a-SUMO SBV N protein	pET28a-SUMO	SBV N protein						
pDEST17 SARS-CoV-2 N protein	pDEST17	SARS-CoV-2 N protein	6xHis (N-terminal)	T7	Ampicillin	One Shot <sup>®</sup> Mach1 <sup>™</sup> -T1 <sup>R</sup> Chemically Competent <i>E. coli</i>	BL21-AI <sup>™</sup> One Shot <sup>™</sup>	Arabinose

#### 2.3.1.1. Expression of the nucleocapsid proteins of CCHFV, RVFV and SBV using the pET28a-SUMO vector

##### 2.3.1.1.1. Cloning of CCHFV, RVFV and SBV nucleocapsid proteins

cDNA designed to express the full-length N protein of CCHFV Baghdad 12 strain (GenBank accession CAD61342.1, but with conservative substitutions T111I, R195H and H445D) optimized for bacterial expression was cloned into the pET28a-SUMO plasmid and provided by Dr. Emma Punch. cDNA sequence of the SBV N protein (GenBank

accession No. KC108844.1) was available at Eurofins-Ingenasa cloned into the pCR™8/GW/TOPO® vector.

The cDNA of the CCHFV N protein, RVFV N protein and SBV N protein were cloned into the pET28a-SUMO plasmid for bacterial expression of corresponding fusion proteins with the SUMO and 6xHis tag and used to transform *E. coli* BL21 (DE3) strain Rosetta2 (R2) following the methods described in section 2.2.1.6.

#### **2.3.1.1.2. Expression of CCHFV, RVFV and SBV nucleocapsid proteins**

The transformed R2 cells were grown ON in LB medium supplemented with kanamycin (50 µg/mL), at 37°C and with shaking at 180 rpm in an Infors HT Multitron incubator. Glycerol stocks of the ON cultures were generated and stored at -80°C and 2 mL of the ON cultures were used to inoculate each 1 L of LB medium supplemented with kanamycin (50 µg/mL) until an optical density (OD) at 600nm between 0.6 and 0.8 was reached. The expression of CCHFV, RVFV and SBV N protein in R2 cells was then induced by addition of 500 µM IPTG to the culture medium. After the induction, the temperature of incubation was decreased to reach 18°C and the bacterial cultures were incubated for 16 hrs at 18°C, with shaking at 180 rpm.

#### **2.3.1.1.3. Purification of CCHFV, RVFV and SBV nucleocapsid proteins**

The cells were harvested by centrifugation at 3,000 x g for 45 minutes at 4°C using an SLC-6000 rotor (Sorvall). The cell pellets were resuspended in 15 mL of lysis buffer per litre of cell culture (500 mM NaCl, 20 mM Tris-HCl pH 7.4, 20 mM imidazole, 1 mM MgCl<sub>2</sub>, 1 mg/mL lysozyme from chicken egg white (Sigma Aldrich), 0.1% (v/v) Triton X-100, 1 complete protease inhibitor cocktail tablet EDTA-free (Roche), Benzonase® nuclease (Millipore)) at pH 7.4, 8.2 and 8, for CCHFV N protein, RVFV N protein and SBV N protein respectively, and incubated on ice for 30 minutes. The cell lysates were then sonicated on ice for 25 rounds of 10 seconds on, 50 seconds off at 10 mA using a Soniprep 150 (MSE). The soluble fractions were then separated from the insoluble

fractions by centrifugation at 30,000 x g for 45 minutes at 4°C using a SS-34 rotor (Thermo Fisher Scientific). The N proteins were further purified sequentially by immobilized metal affinity chromatography (IMAC) and SEC.

### **Purification by immobilized metal affinity chromatography with Ni<sup>2+</sup>**

The CCHFV N protein, RVFV N protein and SBV N protein were then purified from the soluble fractions using high-density metal free agarose beads (ABT). The resins were first washed with dH<sub>2</sub>O to remove the preservative, then 0.1 M NiSO<sub>4</sub> was applied to the resin to complete the metal adsorption. The resins were washed with dH<sub>2</sub>O to remove the non-retained metal and the resins were equilibrated with binding buffer (500 mM NaCl, 20 mM imidazole, 20 mM Tris-HCl pH 7.4, 8.2 and 8, for CCHFV N protein, RVFV N protein and SBV N protein respectively). The soluble fractions were filtrated with 0.45 µm filters and were then applied to the resins previously equilibrated and incubated ON at 4°C with gentle agitation. The non-binding materials were collected and the resins were washed with binding buffer with increasing concentrations of imidazole. The 6xHis-SUMO-CCHFV N protein was eluted with the first elution buffer (500 mM NaCl, 20 mM Tris-HCl pH 7.4, 100 mM imidazole) and the second elution buffer (500 mM NaCl, 20 mM Tris-HCl pH 7.4, 500 mM imidazole). The 6xHis-SUMO-RVFV N protein was eluted with the same elution buffers at pH 8.2. The 6xHis-SUMO-SBV N protein was eluted with the first elution buffer (500 mM NaCl, 20 mM Tris-HCl pH 8, 300 mM imidazole) and the second elution buffer (500 mM NaCl, 20 mM Tris-HCl pH 8, 500 mM imidazole). Samples were analysed by SDS-PAGE (sodium dodecyl sulphate–polyacrylamide gel electrophoresis) followed by Coomassie staining and the fractions containing the 6xHis-SUMO-CCHFV N, 6xHis-SUMO-RVFV N and 6xHis-SUMO-SBV N proteins were dialysed separately ON at 4°C with a magnetic stirrer. The dialysis of the elution fractions against dialysis buffer (500mM NaCl, 20mM Tris-HCl pH 7.4, 8.2 and 8, for CCHFV N protein, RVFV N protein and SBV N protein respectively) was done to increase the SUMO protease efficiency to cleave the 6xHis-SUMO from the CCHFV N, RVFV N and SBV N proteins. The SUMO protease Ulp1 was produced in-house at the University of Leeds (cleavage efficiency: 100 mg of protein cleaved by 1 mg of SUMO protease) and 1 mg of SUMO protease was added in the dialysis bag (molecular weight cut-off (MWCO), 10 kDa).

The cleaved CCHFV N, RVFV N and SBV N proteins were further purified by repeating the Ni<sup>2+</sup>-NTA affinity chromatography in order to remove the cleaved 6xHis and SUMO tags from the N proteins. The non-binding materials, containing the N proteins, were concentrated to 5 mL by centrifugation using an Amicon Ultra 15 Ultracel 10K regenerated cellulose concentrator (Millipore).

### **Purification by size exclusion chromatography**

As a final step of purification, SEC was performed injecting the concentrated N proteins to an equilibrated HiLoad® 26/600 Superdex® 75 pg (GE Healthcare) (binding buffer: 500 mM NaCl, 20 mM Tris-HCl pH 7.4, 8.2 and 8, for CCHFV N protein, RVFV N protein and SBV N protein respectively; filtered and de-gassed) using an ÄKTA prime at a flow rate of 0.5 mL/min, at 4°C. The purified N proteins were collected in 3 mL fractions after the void volume. The purity of the N proteins was analysed by SDS-PAGE followed by Coomassie staining and by WB. The fractions containing the pure CCHFV N, RVFV N and SBV N proteins were pooled and concentrated. Finally, glycerol was added to the pure N proteins to a final volume of 5% (v/v) and the aliquots were stored at -80°C. The purified proteins were quantified by spectrophotometry using a NanoDrop™ 1000 spectrophotometer.

#### **2.3.1.2. Expression of the nucleocapsid protein of SARS-CoV-2 using the Gateway system**

##### **2.3.1.2.1. Cloning of SARS-CoV-2 N protein**

The N protein of SARS-CoV-2 was cloned in the pCR™8/GW/TOPO™ and subsequently in the pDEST17 vector, carrying a polyhistidine tag, according to section 2.2.2. Resulting plasmid was verified by sequence analysis and used to transform BL21-AI™ One Shot™.

#### **2.3.1.2.2. Expression of the SARS-CoV-2 N protein**

The transformed BL21-AI™ One Shot™ cells were grown ON in LB medium supplemented with ampicillin (100 µg/mL), at 37°C and shaking at 220 rpm in an CERTOMAT® IS (Sartorius) incubator. Three millilitres of the ON culture were used to inoculate each 1 L of LB medium supplemented with ampicillin (100 µg/mL) until an OD<sub>600nm</sub> between 0.6 and 0.8 was reached. Glycerol stocks of the ON culture were generated and stored at -80°C. The expression of SARS-CoV-2 N protein was induced by addition of L-arabinose to a final concentration of 0.2% (v/v) to the culture medium. After the induction, the temperature of incubation was decreased to reach 18°C and the bacterial culture was incubated for 16 hrs at 18°C, with shaking at 220 rpm.

#### **2.3.1.2.3. Purification of the SARS-CoV-2 N protein**

The cells were harvested by centrifugation as described above. The cell pellet was resuspended in 30 mL of lysis buffer per litre of cell culture (300 mM NaCl, 20 mM Tris-HCl, pH 7.4, 20 mM imidazole, 1 mM MgCl<sub>2</sub>, 0.1% (v/v) Triton X-100, 1 mg/mL lysozyme, 1 tablet cComplete™, EDTA-free protease inhibitor cocktail) at pH 7.4 and incubated on ice for 30 minutes. The cell lysates were then sonicated and centrifuged to separate the soluble fraction from the insoluble fraction as described above.

The SARS-CoV-2 N protein was purified from the soluble fraction using Ni<sup>2+</sup>-NTA affinity chromatography as described above. The resin was equilibrated with binding buffer (300 mM NaCl, 20 mM Tris-HCl pH 7.4, 20 mM imidazole). The soluble fraction was passed through a 0.45 µm filter and then applied ON at 4°C to the resin previously equilibrated. The non-binding material was collected and the resin was washed with binding buffer with increasing concentrations of imidazole. The 6xHis-SARS-CoV-2 N protein was eluted with the elution buffer (300 mM NaCl, 20 mM Tris-HCl pH 7.4, 500 mM imidazole). The purity of the N protein was analysed by SDS-PAGE followed by Coomassie staining and by WB and the fractions containing the 6xHis-SARS-CoV-2 N protein were dialysed in 1X PBS ON at 4°C on a magnetic stirrer.

### **2.3.2. Expression of recombinant proteins in insect cells using the baculovirus expression system**

The recombinant glycoproteins used in this project were expressed in insect cells using the BES.

#### **2.3.2.1. Growth and maintenance of insect cells**

Sf9 insect cells were cultured in complete Grace's medium (Grace's medium (Life Technologies) supplemented with 8% (v/v) inactivated FBS (Gibco™, Thermo Fisher Scientific, incubated at 56°C for 30 min), 0.2% (v/v) Kolliphor® P 188 (Sigma-Aldrich) and 50 µg/mL of gentamycin). Sf900 were cultured in Sf-900™ II SFM (Thermo Fisher Scientific) supplemented with 0.2% (v/v) Kolliphor® P 188 and 50 µg/mL of gentamycin. Both cell lines were cultured attached in plates at 27°C or in suspension at 27°C and with stirring at 125 rpm in an Infors HT Multitron incubator until reaching a maximum cell density of  $4 \times 10^6$  cells/mL.

#### **2.3.2.2. Expression and purification of CCHFV G<sub>NE</sub>, CCHFV GP38 and RVFV G<sub>NE</sub>**

The expression and purification of the glycoproteins of CCHFV and RVFV followed the same method.

##### **2.3.2.2.1. Cloning of CCHFV G<sub>NE</sub>, CCHFV GP38 and RVFV G<sub>NE</sub>**

The cDNA of CCHFV G<sub>NE</sub>, CCHFV GP38 and RVFV G<sub>NE</sub> were subcloned into the pAcSecG2T vector following the methods described in section 2.2.2 for their subsequent expression in insect cells following the formation of recombinant baculoviruses.



**2.3.2.2.2. Generation of recombinant baculoviruses expressing CCHFV G<sub>NE</sub>, CCHFV GP38 and RVFV G<sub>NE</sub>**

To generate recombinant baculoviruses expressing CCHFV G<sub>NE</sub>, CCHFV GP38 or RVFV G<sub>NE</sub>, Sf9 insect cells were co-transfected with triple-cut baculovirus DNA and the vectors pAcSecG2T-CCHFV G<sub>NE</sub>, pAcSecG2T-CCHFV GP38 or pAcSecG2T-RVFV G<sub>NE</sub>, using JetPEI<sup>®</sup> (Polyplus Transfection) as a transfection agent. The reaction was set up by mixing 100 µL of 150 mM sterile NaCl (Polyplus Transfection) and 6 µL JetPEI<sup>®</sup> over a mix of 100 µL of 150 mM NaCl, 200 ng of triple-cut Bsu36I baculovirus DNA and 2 µg plasmid DNA. These mixes were incubated for 20 min at RT. A total of 2 x 10<sup>6</sup> Sf9 cells were added to 25 cm<sup>2</sup> rectangular cell culture flask (Corning) and incubated for 30 min at 27°C to let the cells attach. The medium was removed and replaced with 1 mL of fresh complete Grace's medium and the transfection mixes were added. The flasks were incubated for 5 hrs at 27°C and gently shaken every 15-20 min. The transfection mixes were replaced by 5 mL of fresh media and the Sf9 were incubated at 27°C for 5 days. Confirmation of infection by appearance of CPE within the infected Sf9 cells was observed using an optical microscope (Eclipse Ts2R, Nikon).

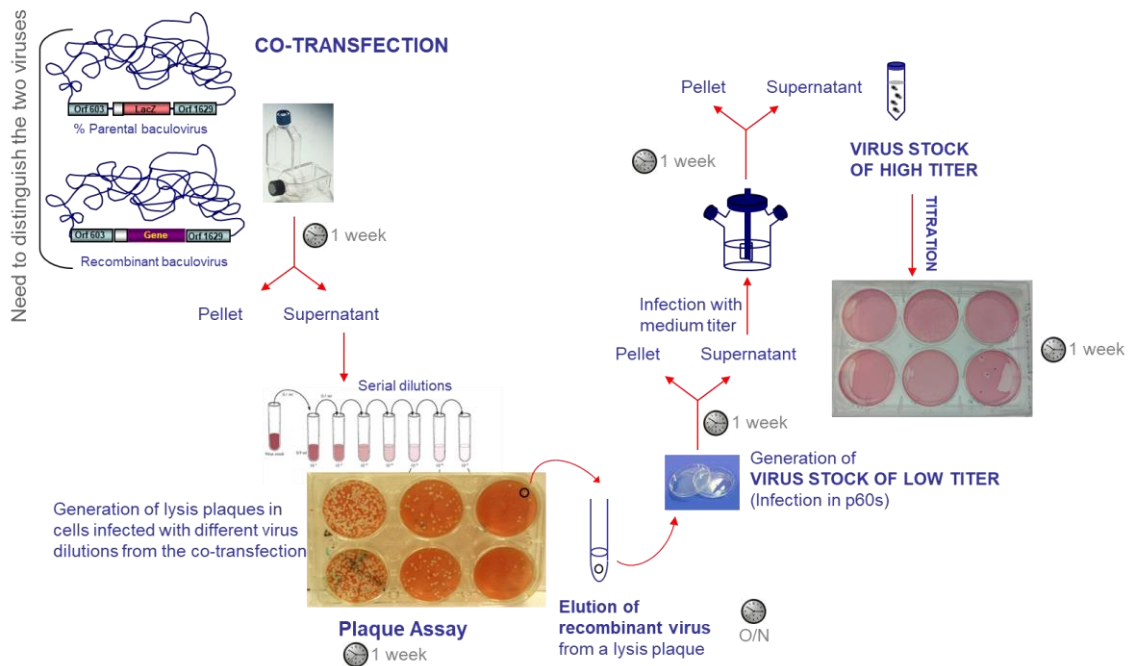
When CPE could be observed, the cells were harvested by centrifugation (1,590 x g for 10 min at 4°C) and lysed in 25 mM sterile sodium bicarbonate buffer (1 mL/ 2 x 10<sup>7</sup> cells) and the total extracts were analysed by WB. Plaque assays were completed with the supernatant of the transfection reactions to differentiate and select the recombinant baculoviruses by blue-white selection. Briefly, 1.5 x 10<sup>6</sup> Sf9 cells per well were added in a 6-well plate (Corning). The plates were incubated for 30 min at 27°C. The cells were detached from the co-transfection plates, transferred to 50 mL centrifuge tubes (Corning) and centrifuged at 1,590 x g for 10 min at 4°C. With the supernatant, serial dilutions were prepared from 10<sup>-3</sup> to 10<sup>-7</sup> in complete Grace's medium. The media was removed from the 6-well plates and 250 µL of the viral dilutions from 10<sup>-3</sup> to 10<sup>-7</sup> were added over the cell monolayer. A volume of 250 µL of medium was added to one well for negative control. The plates were incubated between 1 hr and 1 hr 30 min at 27°C, with gentle shaking of the plates every 15 min. The viral dilutions were removed from the cell monolayer without disturbing the cells and 2 mL of overlay media (3% (w/v) low melting point agarose in sterile water, boiled, to which an equal volume of complete Grace's medium was added) was added per well. The plates were incubated for 10 min at RT and 1 mL of complete Grace's medium was added per well. The plates were incubated at 27°C

for 5 days. The media was removed from the wells and 1.5 mL of staining solution (per plate: 10 mL 1X PBS, 400 µL 0.33% neutral red solution (Sigma), 100 µL 2% (w/v) X-gal (in dimethylformamide)) was added per well. The plates were incubated at 27°C for 4 hrs. Finally, the staining solution was removed and the plates were incubated upside down ON at 4°C in the dark.

The titre of the virus could be determined by the number of white plaques:

$$\text{Titer (pfu/mL)} = \frac{n^{\circ} \text{ of lysis plaques in a well}}{\text{corresponding dilution} \times \text{volume dilution added}}$$

The following day white plaques (recombinant baculoviruses) were picked and dissolved ON at 4°C in 500 µL complete Grace’s medium. Figure 2.1 represents the workflow from the co-transfection until obtaining the baculovirus stock of high titre.



**Figure 2.1** Workflow of the production of baculovirus stock.

**2.3.2.2.3. Preparation of recombinant viral stocks expressing CCHFV G<sub>Ne</sub>, CCHFV GP38 and RVFV G<sub>Ne</sub>**

The recombinant baculoviruses were used to infect  $2 \times 10^6$  Sf9 cells in 60 mm dishes (Corning) to produce a low titre virus stock. The plates were incubated 30 min at 27°C. The medium was removed and each plate was infected with 200 µL of dissolved recombinant plaques and 300 µL of complete Grace's medium. The dishes were incubated for 1 hr at RT. Then, 4.5 mL of complete Grace's medium was added and the dishes were incubated at 27°C for 5 to 6 days, until CPE could be observed under the microscope. Once the CPE were observed, the recombinant baculoviruses were harvested by centrifugation of the resuspended cells at 1,590 x g for 10 min at 4°C.

A 100 µL volume of this low titre baculovirus stock was used to infect Sf9 cells maintained in suspension ( $1 \times 10^8$  Sf9 cells in 100 mL of complete Grace's medium), which were incubated at 27°C for 5 to 6 days, until CPE was evident, in order to produce a high titre virus stock. This high titre baculovirus stock was harvested by centrifugation at 1,590 x g for 10 min at 4°C and was titrated by plaque assay, as described previously.

To confirm the production of the glycoproteins in insect cells, the recombinant baculoviruses stocks were used to infect Sf9 cells grown in serum-free medium at a multiplicity of infection (MOI) of 0.1 and 2. Infected cells were incubated at 27°C, with stirring at 125 rpm and were harvested at 24, 48, 72, 96 and 120 hrs post-infection (PI) by centrifugation at 1,590 x g for 10 min at 4°C. Cells were lysed in 25 mM sterile sodium bicarbonate buffer (1 mL/  $2 \times 10^7$  cells) and the insoluble fraction was separated from the soluble fraction by centrifugation at 11,000 x g for 10 min at 4°C using a SS-34 rotor. The insoluble fraction was resuspended in 1X PBS in the same volume of sodium bicarbonate buffer previously used. The samples were analysed by SDS-PAGE followed by Coomassie staining and WB using a monoclonal antibody anti-glutathione S-transferase (GST)-PO, produced "in-house" at Eurofins-Ingenasa, to determine the best production conditions for each protein.

#### **2.3.2.2.4. Expression of CCHFV G<sub>NE</sub>, CCHFV GP38 and RVFV G<sub>NE</sub> in insect cells**

For the production of CCHFV G<sub>NE</sub>, CCHFV GP38 and RVFV G<sub>NE</sub> using the pAcSecG2T vector, Sf900 cells were infected at MOI = 2, MOI = 0.1 and MOI = 0.1 for CCHFV G<sub>NE</sub>, CCHFV GP38 and RVFV G<sub>NE</sub>, respectively. The cells were incubated at 27°C, with shaking at 125 rpm for 120 hrs, 96 hrs and 96 hrs for CCHFV G<sub>NE</sub>, CCHFV GP38 and RVFV G<sub>NE</sub> respectively.

#### **2.3.2.2.5. Purification of CCHFV G<sub>NE</sub>, CCHFV GP38 and RVFV G<sub>NE</sub>**

The cells were harvested by centrifugation at 1,590 x g for 10 min at 4°C and the supernatant was kept. The cells were lysed with 1 mL/ 2 x 10<sup>7</sup> cells of 25 mM sterile sodium bicarbonate buffer and incubated on ice for 4°C. The soluble fraction was separated from the insoluble fraction by centrifugation at 11,000 x g for 10 min at 4°C using a SS-34 rotor. The CCHFV G<sub>NE</sub> and CCHFV GP38 were purified from the culture supernatant and the RVFV G<sub>NE</sub> was purified from the soluble fraction.

For purification of expressed proteins, supernatants were filtered using a 5 µm filter (Millex-SV; 5,0 µm, PVDF, 25 mm, Merck). An affinity column was prepared as described in section 2.3.2.3.2 using an anti-GST mAb (3H11). The column was regenerated by passing 5 bed volumes of basic buffer (0.1 M Tris-HCl pH 8.5), then 5 bed volumes of acidic buffer (0.1 M sodium acetate, 0.5 M NaCl, pH 4) and finally 5 bed volumes of basic buffer. The column was washed with 20 bed volumes of 1X PBS. The filtered supernatant was incubated with the affinity column ON at 4°C with gentle agitation. The non-binding material was collected and the resin was rinsed with 40 bed volumes of 1X PBS and the absorbance (A) at 280 nm of the washing buffer was checked by spectrophotometry to be equal to zero. The elution was performed using 0.1 M glycine hydrochloride pH 2.6 and the elution fractions were neutralized by addition of 3 M Tris-HCl, pH 10 until the pH reached 7 using pH strips 0-14 (Ahlstrom Munksjö). The elution fractions were dialysed ON in 1X PBS at 4°C.

Regarding the purification from the soluble fraction, the same protocol than above was used but the non-filtered soluble fraction was applied to the affinity column anti-GST.

The purity of the proteins was analysed by SDS-PAGE followed by Coomassie staining and by WB.

### **2.3.2.3. Expression and purification of BTV VP7**

#### **2.3.2.3.1. Expression of BTV VP7**

The VP7 of BTV was produced in insect cells from a recombinant baculovirus that was already available in Eurofins-Ingenasa. Briefly, Sf9 insect cells, cultured in complete Grace's medium, were pumped into a WAVE bioreactor bag at  $0.5 \times 10^6$  cells/mL in a total volume of one litre. Cells were grown at 27°C, 0.5 litre per minute mix out, DO 35, 22 rpm and angle 9° until they reached a cell density of  $1 \times 10^6$  cells/mL. The cells were then infected at MOI 2 with the recombinant baculovirus expressing the BTV VP7. The infection was incubated for 72 hrs using the same settings.

#### **2.3.2.3.2. Purification of anti-VP7 BTV mAb (2D7) and coupling to sepharose beads**

The anti-VP7 BTV mAb (named 2D7) was purified from ascites liquid from mice immunized with hybridoma producing 2D7. The ascites liquid was first filtered with glass wool and then using a 0.45 µm filter. One volume of ascites liquid was mixed with two volumes of 50 mM acetate buffer at pH 4 and stirred for 30 min at RT. Then 1.1 mL of caprylic acid was added drop by drop to 100 mL of solution and stirred for 30 min at RT. The solution was then centrifuged at 11,000 x g for 30 min at 4°C using a SS-34 rotor. The supernatant was filtered with a 2 µm glass filter and the filtrate was dialysed ON in 1X PBS at 4°C.

The purity of the mAb 2D7 was assessed by SDS-PAGE followed by Coomassie staining.

The purified mAb 2D7 was coupled to NHS-activated Sepharose 4 fast flow (GE Healthcare) beads according to the manufacturer's instructions. Briefly, mAb 2D7 was dialysed ON in coupling buffer (0.2 M NaHCO<sub>3</sub>, 0.5 M NaCl, pH 8.3) and then diluted to a final volume of 10 mL in coupling buffer. A 12 mL volume of NHS-activated Sepharose 4 fast flow was centrifuged for 3 min at 2,500 x g at 4°C and the supernatant

was discarded. To wash the resin, it was resuspended in 10 mL of washing buffer (1 mM HCl) and centrifuged at 2,500 x g for 3 min at 4°C. This step was repeated 3 times. The resin was then resuspended in 10 mL of coupling buffer and gently agitated for 1 min before centrifugation at 2,500 x g for 3 min at 4°C. The 2D7 solution in coupling buffer was added to the resin and agitated gently for 30 min at RT. Finally, 10 mL of coupling buffer was added to the mix and it was incubated ON at 4°C with gentle agitation.

The supernatant was discarded after centrifugation and the resin was resuspended in 10 mL of basic washing buffer (0.1 M Tris-HCl, pH 8.5) and incubated for 2 hrs at RT with gentle agitation. The resin was centrifuged, the supernatant discarded and resuspended in 10 mL of acidic washing buffer (0.1 M acetate buffer, 0.5 M NaCl, pH 4). This mix was agitated for 1 min at RT and then centrifuged. The washing steps with basic and acidic washing buffers were repeated 6 times. The resin was then resuspended in 10 mL of 1X PBS, agitated for 1 min and centrifuged. This step was repeated 5 times. The resin was then stored at 4°C in coupling buffer supplemented with 20% (v/v) ethanol until needed.

#### **2.3.2.3.3. Purification of BTV VP7 by affinity chromatography**

The cells were centrifuged at 2,500 x g for 25 min at 4°C. The pellet was resuspended in 1 mL of 25 mM sodium bicarbonate buffer per  $2 \times 10^7$  cells and incubated 30 min on ice. The soluble fraction was separated from the insoluble fraction by centrifugation at 11,000 x g for 10 min at 4°C. The resin with the anti-VP7 BTV mAb 2D7 coupled to the NHS-activated Sepharose 4 fast flow was reactivated by washing it with the basic and acidic washing buffers and the resin was then rinsed with 1X PBS as described above. The soluble fraction was added to the resin and the mix was incubated ON at 4°C with gentle agitation. The mix was poured in a column and the non-binding material was collected. The resin was washed 6 times with 50 mL of 1X PBS. The VP7 BTV was eluted by adding 4 x 5 mL of 0.1 M glycine-HCl, pH 2.6 and then 4 x 5 mL of 0.1 M acetic acid. The elution fractions were neutralized with 3 M Tris-HCl, pH 10 until the pH was neutral. The elution fractions were dialyzed ON at 4°C in 1X PBS. The purification of the VP7 BTV and the purity of the elution fractions were assessed by SDS-PAGE followed by Coomassie staining and by WB.

## **2.4. Protein analysis techniques**

### **2.4.1. Sodium dodecyl sulphate–polyacrylamide gel electrophoresis**

SDS-PAGE gels with resolving gel acrylamide concentrations ranging between 11 to 15% were made, with acrylamide concentration chosen depending on the intended application. As an example, a 12% SDS-PAGE gel was made with 12% (v/v) resolving gel (2.03 mL acrylamide-solution (PanReac AppliChem), 1.31 mL 4X ProtoGel<sup>®</sup> resolving buffer (National Diagnostics), 1.65 mL dH<sub>2</sub>O, 50 µL 10% (w/v) ammonium persulfate (APS) and 5 µL tetramethylethylenediamine (TEMED, Sigma-Aldrich)) and a 4% stacking gel (195 µL acrylamide-solution, 375 µL ProtoGel<sup>®</sup> stacking buffer (National Diagnostics), 915 µL dH<sub>2</sub>O, 7.5 µL 10% APS and 2 µL TEMED). The protein samples were mixed with 5X SDS sample buffer (80 mM Tris-HCl (pH 6,8), 5% (v/v) β-mercaptoethanol, 2% (w/v) SDS, 10% (v/v) glycerol, 0.01% (w/v) bromophenol blue) and then denatured by heating 5 min at 100°C. Samples were loaded beside 4 µL of Precision Plus Protein<sup>™</sup> dual color standards (BIO-RAD) and the electrophoresis was conducted at 200 V for 45 min in electrophoresis running buffer (25 mM Tris, 192 mM glycine, 0.1% (w/v) SDS).

### **2.4.2. Coomassie staining**

To observe the proteins separated by SDS-PAGE, the gels were stained with Coomassie staining solution (0.25 g of PhastGel<sup>™</sup> Bleu R dissolved in 45 mL methanol, 45 mL H<sub>2</sub>O and 10 mL acetic acid) for 15 min at RT. The gels were destained by addition of destaining solution (20% (v/v) methanol, 8% (v/v) acetic acid, 72% (v/v) H<sub>2</sub>O) ON at RT. Gels were then washed with dH<sub>2</sub>O.

### **2.4.3. Western blotting**

To transfer the proteins from SDS-PAGE to a nitrocellulose membrane, the gel, chromatography paper (Whatman) and the nitrocellulose membrane (0.2 µm, BIO-RAD) were incubated for 10 min in transfer solution (0.25 M Tris, 1.92 M glycine). The semi-

dry transfer was done using Trans-Blot Turbo Transfer System (BIO-RAD) at 25 V, 2.5 A for 10 min. After the transfer, the membrane was blocked in 3% (w/v) milk in 1X PBS, for 1 hr at RT or ON at 4°C while shaking. The membrane was then rinsed with dH<sub>2</sub>O and incubated for 1 hr at RT with a primary Ab while shaking. The membrane was washed three times with 1X PBS with 0.05% (v/v) Tween 20 (PBS-T) for 5 min and was then developed with precipitating 3,3',5,5'-Tetramethylbenzidine (TMB) (ep(HS)TMB-mA, SDT-Reagents) if the primary Ab was conjugated with HRP or was incubated with a secondary Ab for 1 hr at RT while shaking. The membrane was washed with PBS-T as described above and developed with either precipitating TMB or alkaline phosphatase substrate by mixing 10 mL of a buffer containing 100 mM NaCl, 5 mM MgCl<sub>2</sub>, 100 mM Tris-HCl, pH 9.5 with 66 µL of 5% (w/v) nitro blue tetrazolium chloride in 70% (v/v) dimethylformamide and 33 µL of 5% (w/v) 5-Bromo-4-chloro-3-indolyl phosphate in dimethylformamide depending on the conjugated enzyme. After development of the colorimetric signal, the membranes were washed with dH<sub>2</sub>O to stop the reaction. The antibodies used for WB are described in Table 2.6.

## **2.5. Production of monoclonal antibodies and non-antibody binding proteins to the target antigens and their characterization**

### **2.5.1. Monoclonal antibodies**

mAbs against the N protein of SBV (1D5D12), the VP7 of BTV (2D7), the MPB83 of *M. bovis*, ruminant IgG (EG5), SUMO tag (3C11) and GST tag (3H11) were already available in Eurofins-Ingenasa. New mAbs were produced against the N proteins of CCHFV and RVFV using the protocol below.

#### **2.5.1.1. Maintenance of mammalian cell lines**

The mouse myeloma cell lines P3X63Ag8.653 and SP2/0-Ag14 used for the fusion were cultured attached in 100 mm dishes (Corning) in Dulbecco's modified Eagle's medium (DMEM), high glucose, pyruvate (Gibco™), supplemented with 15% (v/v) inactivated FBS and antibiotic cocktail (penicillin and streptomycin). They were cultured at 37°C in a controlled atmosphere with 5 % (v/v) CO<sub>2</sub>.



### **2.5.1.2. Immunization of BALB/c mice**

The mice (four per group, plus one negative control) were injected intraperitoneally with the purified RVFV N protein and 6xHis-SUMO-CCHFV N protein produced in *E. coli*. For the first immunization, 25 µg of antigen emulsified by sonication in complete Freund's adjuvant (Sigma-Aldrich) was used. For the following four immunizations (once every two weeks), the same quantity of antigen was emulsified in incomplete Freund's adjuvant (Sigma-Aldrich). Additionally, three immunizations were performed using the same adjuvant with an increased concentration of antigen: 50 µg/mouse for 6xHis-SUMO-CCHFV N protein and 43 µg/mouse for RVFV N protein. As a control, one mouse was immunized with sterile 1X PBS instead of antigen.

Mice were bled from the tail 7 days after the first three immunizations and 7 days after each subsequent immunization. Mice sera were obtained by allowing the blood to coagulate for 30 min at RT and further centrifugation at 1,500 x g for 10 min at 4°C.

### **2.5.1.3. Titration of mouse sera by indirect ELISA**

The antibody titre was checked by indirect ELISA. 96-well high-binding microplate (Corning) were coated at 1 µg/mL, 100 µL/well with 6xHis-SUMO-CCHFV and RVFV N proteins in carbonate buffer (15 mM CO<sub>3</sub>Na<sub>2</sub>, 35 mM CO<sub>3</sub>HNa, pH 9,6) ON at 4°C. After washing the plates three times with 300 µL/well of PBS-T, they were blocked with 150 µL/well of StabilZyme<sup>®</sup> SELECT stabilizer for 1 hr at RT to prevent unspecific binding of the sample. The blocking buffer was removed and the plates were incubated with serial dilutions of the mouse sera starting from 1:100 with a 1:3 dilution fraction in DB1 for 1 hr at RT. The plates were washed as described above and incubated for 1 hr at RT with Goat anti-mouse IgG (H+L) secondary antibody, HRP conjugate (Invitrogen) at 1:2,000 in DB1. The plates were washed as previously described. The plates were incubated 10 min with 100 µL/well 2,2'-azino-bis(3-ethylbenzothiazoline-6-sulfonic acid) (ABTS) and then 100 µL/w of 2% (w/v) SDS was added. Finally, the A<sub>405nm</sub> was measured with a SpectraMax M5 (Molecular Devices) plate reader.

#### 2.5.1.4. Fusion

After reaching the desired antibody titre (Absorbance at 450 nm,  $A_{450\text{nm}} > 1$  for a serum dilution of 1:60,000), the mice were immunized on three consecutive days with 50  $\mu\text{g}$  of the corresponding protein in sterile 1X PBS. This antibody titre of  $A_{450\text{nm}} > 1$  for a serum dilution of 1:60,000 determined by indirect ELISA (as described in section 2.5.1.3) is the minimal threshold defined at Eurofins-Ingenasa to perform the fusion with the tested mouse. Experimentally, mice reaching this antibody titre are likely to yield a sufficient number of B cells necessary for the fusion. For each fusion, two mice with the higher titre were sacrificed. The mice were euthanized by inhalation of  $\text{CO}_2$  and the spleens were collected. To obtain hybridomas producing specific mAbs, fusions were done with spleen cells from the mice and P3X63Ag8.653 or SP2/0-Ag14 mouse myeloma cells following a published protocol with some modifications (270).

After the spleens were harvested and cleaned, they were grinded in a 100 mm dish containing 10 mL of DMEM without serum. This mixture was filtered and transferred into a 50 mL centrifuge tube with 20 mL of DMEM without serum. The tube was centrifuged at 485 x g for 5 min at 4°C. The pellet was resuspended in 2 mL of lysis buffer (red blood cell lysing buffer Hybri-Max™, Sigma-Aldrich) and incubated 1 min on ice. 28 mL of DMEM with serum was added to the tube and it was centrifuged at 485 x g for 5 min at 4°C. The pellet was resuspended in 30 mL of DMEM with serum and centrifuged as described above. This washing step was repeated and, in the meantime, the cultured myeloma cells were harvested and centrifuged. The spleen cells and myeloma cells were resuspended in 30 mL of DMEM without serum and centrifuged. They were resuspended in 20 mL of DMEM without serum and counted using a Neubauer chamber. For the fusion reaction, a 4:1 ratio is needed between the spleen cells and the myeloma cells. The myeloma cells were added to the spleen cells and the mix was centrifuged. The supernatant was discarded and the pellet was resuspended drop by drop in the fusion buffer (polyethylene glycol and DMEM without serum at a 1:1 ratio) at 1 mL per  $1.6 \times 10^8$  spleen cells. DMEM with sera was then added in a sequential order: 1 volume (equal to the volume of fusion buffer added) in 1 min, 1 volume in 1 min, 8 volumes in 2 min and finally filled up to 40 mL. This mix was incubated for 5 min and centrifuged as described above. The pellet was resuspended in hybridoma-SFM (Gibco™) supplemented with 8% (v/v) inactivated FBS and antibiotics at 10 mL per  $5 \times 10^7$  spleen cells. This was aliquoted at 100  $\mu\text{L}$ /well into 96-well plates. The plates were incubated at

37°C with 5% (v/v) CO<sub>2</sub>. The following day, 2X HAT medium (hybridoma-SFM with HAT supplement 50X Gibco™) was added at 100 µL/well. Five days later, the medium was replaced by 1X HAT and the medium was replaced every 48 hrs until the screening.

#### **2.5.1.5. Screening and selection**

To reach a unique clonal population derived from a single B cell producing a mAb, the cloning procedure at Eurofins-Ingenasa was to dilute the hybridoma clones from the fusion step to 50 cells per well, then to 20 cells per well, 10 cells per well and finally to 2 or 1 cell per well.

Two weeks after the fusion, the supernatants of hybridoma clones were screened by indirect ELISA for the production of antibodies with the corresponding N protein and a negative antigen (the 6xHis-SUMO-N protein of CCHFV for the hybridomas producing mAbs against the RVFV N protein and 6xHis-SUMO-RVFV N protein for the hybridomas producing mAbs against the 6xHis-SUMO-CCHFV N protein). The positive control (C+) corresponded to the sera collected from the corresponding euthanized mice and the negative control (C-) to mouse sera against a non-related antigen. The wells giving a positive signal ( $A_{405nm} > 0.2$ ) and no background in the negative control plate ( $A_{405nm} < 0.1$ ), were resuspended in growth medium, their concentration was determined using Neubauer chambers and they were aliquoted at 50 cells/well in a 96-well plate. The leftovers of resuspended cells were added to a 24-well plate (Corning) and kept in case of contamination of the subcloned plates. The medium was replaced when necessary. The screening by ELISA was done every two weeks and the cell concentration per well was reduced by successive cloning until obtaining clones of hybridomas at 1 cell/well positive to the target antigen and negative to the negative control.

#### **2.5.1.6. Purification**

Once the hybridomas were cloned at 1 cell/well, they were grown into 6-well plates, then to 100 mm<sup>2</sup> plates and finally to 75 cm<sup>2</sup> flasks. Some plates were used to produce stock vials by centrifugation of the cells, and resuspending the pellets in freezing solution (9:1 ratio between FBS sera and DMSO) and storing the vials at -80°C.

The other plates were grown until the cells died and the supernatants of these hybridoma cultures were collected and clarified by centrifugation (485 x g, 5 min, 4°C). The supernatants were then filtered with a Chromafil Xtra 1.0 µm (Macherey-Nagel) and purified using protein A/protein G GraviTrap columns (GE Healthcare) following the manufacturer's instructions. The purified mAbs were dialyzed ON in 1X PBS. SDS-PAGE followed by Coomassie staining was used to assess the purity of each monoclonal antibody. The protein concentration of monoclonal antibodies obtained were quantified by spectrophotometry using a NanoDrop™ 1000 spectrophotometer.

#### **2.5.1.7. Labelling with horseradish peroxidase**

The mAbs were labelled with HRP according to a modified method described by Nakane and Kawaoi for their further characterization (271).

Briefly, the mAbs were dialyzed ON at 4°C in 0.1 M sodium bicarbonate, pH 9.2 (pH adjusted by addition of sodium carbonate anhydrous). The peroxidase (Roche) was activated by dissolution in 0.1 M sodium bicarbonate, pH 9.2 and then in the same volume of 10 mM sodium periodate (100 µL of each per mg of peroxidase). The reaction was incubated for 2 hrs at RT protected from light. The activated peroxidase was added at a 1:1 ration (1 mg of peroxidase to 1 mg of mAb). By centrifugation rounds 3,000 x g for 5 min with Vivaspin® 500 10 kDa MWCO concentrator (Sartorius), the reaction was concentrated to reach 10 mg/mL and was incubated for 3 hrs at RT protected from light. The reaction was stopped by addition of a solution of sodium cyanoborohydride (10 mg dissolved in 0.1 M NaOH) at a volume of 1/10<sup>th</sup> of the total volume. This was incubated for 30 min at RT and 30 min at 4°C and dialyzed in 1X PBS ON at 4°C. Glycerol was added at a 1:1 ratio to the conjugated mAbs and they were stored at -20°C.

### 2.5.1.8. Characterization of the mAbs

Different assays were performed to determine some of the characteristics of the mAbs produced:

1. **Monoclonal antibody isotyping.** To determine the isotype of the mAbs produced, an ELISA was done with the supernatant of the mAb-producing hybridomas. The supernatants of the selected hybridomas were diluted 1:100 in carbonate buffer, pH 9.6, added to a 96-well plate and incubated for 1 hr at 37°C. The wells were washed three times with 300 µL/well of PBS-T and blocked for 15 min at RT with 150 µL of blocking solution. The blocking solution was discarded and the anti-isotype antibodies were diluted 1:2,000 in blocking buffer and incubated 1 hr at 37°C in the wells. The wells were washed four times as described above and 100 µL of TMB was added in the wells. The reaction was incubated 10 min at RT in the dark, stopped by addition of sulfuric acid at 0.5 M and the absorbance was measured at 450 nm using a spectrophotometer.
2. The antibodies were further characterized to determine their potential use in **WB**.
3. **Indirect** and **direct ELISA** were performed to titre the mAbs.
4. **Competition ELISA** between the different mAbs was performed to determine whether the mAbs towards a given antigen, recognised the same or different epitopes of the protein. Briefly, the N proteins were coated, washed and blocked as described in section 2.5.1.3. Serial dilutions of unlabelled mAbs from 10 µg/mL with a factor 10 in DB1 were added to the wells, with addition of conjugated mAbs depending on the titre obtained in the direct ELISA. The plate was incubated for 1 hr at RT, washed three times as described with PBS-T and ABTS was aliquoted at 100 µL/w and allowed to develop for 10 min in the dark. The reaction was stopped by addition of 2% (w/v) SDS and the plates were read at 405 nm using a spectrophotometer.

## 2.5.2. Anti-RVSV N protein Affimers

The protocols used to select anti-RVSV N protein Affimers were adapted from Tang *et al.* (272).

### 2.5.2.1. Phage display

The purified RVSV N protein was dialysed in 1X PBS with 5% (v/v) glycerol ON at 4°C. The biotinylation reaction was set up by mixing 50 µg of dialysed RVSV N protein with 12 µL of 0.34 mg/mL of NHS-SS-Biotin in DMSO in 100 µL of 1X PBS. The mix was incubated for 10 minutes at RT. To remove the remaining biotin, the mix was desalted using desalting columns, 7K MWCO (Thermo Scientific) according to the manufacturer's instructions. The desalted biotinylated RVSV N protein was mixed with an equal volume of 80% (v/v) glycerol and stored at -20°C.

An ELISA was done to check the biotinylation of the RVSV N proteins. Briefly, 1 µL of the biotinylated RVSV N protein was incubated in 50 µL of 1X PBS in Nunc-Immuno™ MaxiSorp™ strips (Thermo Scientific), ON at 4°C. The wells were washed three times with 300 µL of PBS-T per well on a plate washer (TECAN HydroFlex). 10X blocking buffer (Sigma) was added at 250 µL per well and incubated at 37°C for 3 hrs. The wells were then washed as mentioned previously. High sensitivity Streptavidin-HRP (Thermo Scientific) diluted 1:1,000 in 2X blocking buffer was added at 50 µL per well and incubated for 1 hr at RT on a vibrating platform shaker (Heidolph VIBRAMAX 100; speed setting 3). The wells were washed three times with 300 µL of PBS-T per well on a plate washer. TMB (Seramun) was aliquoted at 50 µL per well and allowed to develop for 5 min. The resulting colour change was measured using a spectrophotometer at 620 nm.

A colony of ER2738 *E. coli* was grown in 5 mL of 2TY media supplemented with 12 µg/mL tetracycline and incubated ON at 37°C, 230 rpm. Three strips of Streptavidin coated 8-well strips (Thermo Scientific) were blocked with 300 µL per well of 2X blocking buffer and incubated ON at 37°C.

The strips were washed three times with 300 µL per well of PBS-T on the plate washer. Then, 2X blocking buffer was added at 100 µL per well. The phage library was pre-

panned by adding 10  $\mu\text{L}$  of phage library (a mix between the one loop and two loops phage libraries) to the first well supplemented with 10  $\mu\text{g}$  of SUMO tag (kindly provided by T. Passchier, University of Leeds, UK) and 10  $\mu\text{g}$  of SUMO protease and incubated on a vibrating platform shaker for 1 hr. Biotinylated RVFV N protein was added (20  $\mu\text{L}$  each) to a well, used for panning and incubated for 3 hrs at RT on the vibrating platform shaker. The wells containing the targets were washed six times with 200  $\mu\text{L}$  of PBS-T per well. The phage library was transferred from the pre-panning well to the target well and incubated for 2 hrs at RT on the vibrating platform shaker. A fresh culture of ER2738 *E. coli* was set up by diluting the ON culture 1:15 in 2TY media and incubating it until the  $\text{OD}_{600\text{nm}}$  reached 0.6 at 37°C, with shaking at 230 rpm. The panning wells were washed 6 times with 300  $\mu\text{L}$  per well of PBS-T using the plate washer. The phages were eluted by addition of 100  $\mu\text{L}$  of 0.2 M glycine, pH 2.2 per well and incubated for 10 min at RT on a vibrating platform shaker. The eluted phages were neutralized by addition of 15  $\mu\text{L}$  of 1 M Tris-HCl, pH 9.1 and transferred into 5 mL of the fresh ER2738 *E. coli* culture. The remaining phages were eluted by addition of 100  $\mu\text{L}$  of 1.4% (v/v) triethylamine in PBS and incubated for 6 minutes at RT on the vibrating platform shaker. The eluted phages were neutralized by addition of 50  $\mu\text{L}$  1 M Tris-HCl, pH 7 and they were transferred to the ER2738 *E. coli* culture. The cells were incubated for 1 hr at 37°C at 90 rpm. One microliter of the phage-infected ER2738 cells were spread onto LB carbenicillin plates (LB agar plates supplemented with 100  $\mu\text{g}/\text{mL}$  carbenicillin) and the plates were incubated ON at 37°C. The remaining phage-infected ER2738 cells were centrifuged at 3,000  $\times$  g for 5 minutes, resuspended in 100  $\mu\text{L}$  of LB medium, plated onto LB carbenicillin plates, which were incubated ON at 37°C.

To harvest the colonies, 5 mL of 2YT supplemented with 100  $\mu\text{g}/\text{mL}$  carbenicillin were added to each plate and after scraping the colonies, the cells were diluted to reach  $\text{OD}_{600\text{nm}} = 0.2$  and incubated at 37°C, 230 rpm for 1 hr. The M13K07 helper phage (titre at  $10^{14}/\text{mL}$ ) was added at 0.32  $\mu\text{L}$  per tube and incubated at 37°C, 90 rpm for 30 min. 16  $\mu\text{L}$  of kanamycin at 25 mg/mL was added per tube and the mix was incubated ON at 25°C, 170 rpm.

Dynabeads™ MyOne™ Streptavidin T1 (Invitrogen) were blocked ON in 2X blocking buffer (20  $\mu\text{L}$  per target) on a Stuart SB2 fixed speed rotator at 20 rpm. The pre-blocked streptavidin beads were centrifuged at 800  $\times$  g for 1 min, then immobilized on a magnet and the supernatant was replaced with 2X blocking buffer (100  $\mu\text{L}$  per 20  $\mu\text{L}$  of beads).

---

The phage-infected cultures were centrifuged at 3,500 x g for 10 minutes. The second pre-panning of the phages was done by mixing 100  $\mu$ L of streptavidin beads in 2X blocking buffer, removing the 2X blocking buffer, and adding 300  $\mu$ L of phage supernatant and 60  $\mu$ L of 10X blocking buffer in protein LoBind tubes (Eppendorf). The target was bound to the beads by adding 5  $\mu$ L of biotinylated target to 100  $\mu$ L of pre-blocked streptavidin beads. The tubes were incubated for 3 hrs at RT on the rotator at 20 rpm. The tubes were then centrifuged for 1 min at 800 x g and the beads bound to the biotinylated targets were washed three times with 500  $\mu$ L of 2X blocking buffer. The supernatant containing the pre-panned phages was transferred to the beads bound to the target and the mix was incubated 1 hr at RT on the rotator. The beads were washed ten times with 900  $\mu$ L of PBS-T. The beads were resuspended into 500  $\mu$ L of 1X PBS with addition of 50  $\mu$ g of SUMO protease and 50  $\mu$ g of SUMO tag and incubated for 24 hrs at RT on the rotator. An ON culture of ER2738 *E. coli* was done by growing one colony in 5 mL of 2YT media supplemented with 12  $\mu$ g/mL of tetracycline ON at 37°C, with shaking at 230 rpm.

The tubes were centrifuged at 800 x g for 1 min, placed on a magnetic rack and the beads were washed six times with 500  $\mu$ L of 2X blocking buffer. The phages were eluted from the beads and neutralized as described above. To the eluted phages, 5 mL of fresh ER2738 *E. coli* culture was added and the mix was incubated for 1 hr at 37°C, 90 rpm. A 10  $\mu$ L volume of the phage-infected ER2738 cells were spread onto LB carbenicillin plates and the plates were incubated ON at 37°C. The colonies were harvested, the helper phage was added and the phage-infected *E. coli* were grown ON as described above.

A third panning round was done using NeutrAvidin coated 8-well strips (Thermo Scientific), blocked as described above. The culture was centrifuged at 3,500 x g for 10 min at 4°C. Four wells were used to pre-pan the phages with 200  $\mu$ L of culture supernatant, 15  $\mu$ g of SUMO protease and 15  $\mu$ g of SUMO tag. After 1 hr incubating at RT on a vibrating platform, the content of the first pre-panning well was transferred to the second well containing 200  $\mu$ L of 2X blocking buffer and incubated for 1 hr at RT on a vibrating platform. This step was repeated for the third and fourth pre-panning wells. The biotinylated target was bound to the panning well by adding 1  $\mu$ L of biotinylated target in 200  $\mu$ L 2X blocking buffer and incubating this mix in the panning well for 1 hr at RT on a vibrating platform. The well containing the target was washed three times with PBS-T. Half of the pre-panned phages were added to the well containing the target and



the other half to a blank well for negative control. The stripes were incubated onto a vibrating platform for 30 min at RT. The wells were washed twenty-seven times with 300  $\mu$ L of PBS-T. Two-hundred microliters of a mix containing 120  $\mu$ L (PBS with 20% (v/v) glycerol), 40  $\mu$ L 10X blocking buffer, 20  $\mu$ L SUMO protease (1 mg/mL) and 20  $\mu$ L SUMO tag (1 mg/mL) were added to each well. The plate was incubated for 24 hrs at RT on the vibrating platform.

The panning wells were washed twenty-seven times with 300  $\mu$ L PBS-T and the phages were eluted following the same elution protocol as described above. To the eluted phages, 5 mL of ER2738 *E. coli* was added and incubated at 37°C for 1 hr. After this incubation, 10  $\mu$ L, 1  $\mu$ L and 0.1  $\mu$ L volumes of the phage-infected ER2738 cells were spread onto LB carbenicillin plates and they were incubated ON at 37°C.

#### **2.5.2.2. Phage ELISA**

In a 96-deep well plate (Greiner Bio-One), 200  $\mu$ L of 2TY carbenicillin was added per well. Individual colonies from the third panning round of the phage display were picked and used to inoculate each well. The plate was then incubated for 6 hrs at 37°C, 1,200 rpm in an incubating microplate shaker Titramax 1000 (Heidolph). The helper phage M13K07 was diluted at 1:1,000 in 2YT carbenicillin and 10  $\mu$ L was added per well. The plate was incubated for 30 min at RT in the incubating microplate shaker, with shaking at 600 rpm. A solution of 2YT supplemented with 1.25 mg/mL of kanamycin was added at 10  $\mu$ L per well and the plate was incubated ON at RT in the incubating microplate shaker, with shaking at 750 rpm. A streptavidin coated 96 well microplate was prepared by aliquoting 50  $\mu$ L per well of 2.5  $\mu$ g/mL streptavidin (Life Technologies) to a 96 well plate (Thermo Scientific) and incubating the plate for 6 hrs at 37°C. A solution of 2X blocking buffer was added at 150  $\mu$ L per well to the streptavidin coated plate and it was incubated ON at 37°C.

The streptavidin coated plate was washed with 300  $\mu$ L/well of PBS-T. The biotinylated target and the negative control were diluted at 1:1,000 in 2X blocking buffer and added at 50  $\mu$ L/well. The plate was incubated for 1 hr at RT on the vibrating platform shaker, speed setting 3. The plate was washed once as described above and 10  $\mu$ L of 10X blocking buffer was aliquoted per well. The phage-containing culture plate was centrifuged at

3,500 x g for 10 min and 40  $\mu$ L of the supernatant was added to the test well and to the negative control well. The plate was incubated for 1 hr at RT on the vibrating platform shaker. The plate was washed once as described above. The anti-Fd-Bacteriophage-HRP (Seramun Diagnostica GmbH) was diluted 1:1,000 in 2X blocking buffer, added at 50  $\mu$ L per well and the plate was incubated for 1 hr at RT on the vibrating platform shaker. The plate was washed twelve times with 300  $\mu$ L per well of 1X PBS. A 50  $\mu$ L volume of TMB was added per well, developed for 3 min and the absorbance was read at 620 nm. The positive clones in the phage ELISA were grown ON and sent to sequencing.

### 2.5.2.3. Cloning of the Affimer cDNAs into the expression vector

The expression vector pET11a plasmid was digested by mixing 20  $\mu$ g of pET11a plasmid with 50  $\mu$ L CutSmart™ Buffer (NEB), 10  $\mu$ L *NheI*-HF™ (NEB), 10  $\mu$ L *NotI*-HF™ (NEB) and bringing the volume to 500  $\mu$ L with sterile deionised water. This mix was incubated for 6 hrs at 37°C. To the mix, 2  $\mu$ L of Alkaline Phosphatase, Calf Intestinal (NEB) was added and incubated for 1 hr at 37°C. The digested vector was extracted from a 0.8% (w/v) agarose gel using the Monarch® DNA gel extraction kit (NEB).

A PCR was done with the forward (shortened form) and reverse primers (addition of a C-terminal Cysteine). The PCR products were then *DpnI* digested by adding 0.5  $\mu$ L of *DpnI* (NEB) per PCR product and incubating the mixes at 37°C for 1 hr. The amplified DNA was purified using QIAquick PCR purification kit (Qiagen), following the manufacturer's instructions. The PCR products were checked by agarose gel electrophoresis and they were digested ON with *NheI*-HF™ and *NotI*-HF™. The digested PCR products were purified using QIAquick PCR purification kit as described above.

The ligation mixes were set up by adding 2  $\mu$ L of 10X T4 DNA ligase buffer (NEB), 75 ng of digested vector DNA, 25 ng of digested PCR products, T4 DNA ligase (NEB) and sterile water up to 20  $\mu$ L. They were mixed and incubated ON at RT.

The ligation mixes were used to transform NZY5 $\alpha$  cells as described in section 2.2.1.6.

Two colonies were picked per plates and incubated ON in 5 mL of LB carbenicillin at 37°C, 230 rpm. The plasmid DNA was purified and verified by sequencing with T7 reverse primer.

#### 2.5.2.4. Production and purification

The pET11a vector containing the Affimers anti RVFV N protein were used to transform R2 cells according to the transformation protocol.

From the transformation plates, a colony was picked and grown ON in 5 mL LB supplemented with 100 µg/mL carbenicillin at 37°C, with shaking at 230 rpm. A 15 mL volume of LB supplemented with 100 µg/mL carbenicillin were inoculated with 300 µL of ON culture and incubated at 37°C, with shaking at 230 rpm, until the OD<sub>600nm</sub> reached 0.8. The cultures were induced by addition of IPTG to a final concentration of 0.1 mM and incubated for 6 hrs at 25°C, with shaking at 180 rpm.

The cells were harvested by centrifugation at 4,300 x g for 20 min. The cells were resuspended in 300 µL of lysis buffer (300mM NaCl, 50 mM NaH<sub>2</sub>PO<sub>4</sub> pH 7.4, 20 mM imidazole, 0.1 mg/mL lysozyme, 10% (v/v) glycerol, 1X Halt™ Protease Inhibitor Cocktail, EDTA free (Thermo Scientific)) and incubated for 20 min at RT on a rotator. The lysates were then incubated at 50°C for 20 min and centrifuged at 4,850 x g for 20 min at 4°C. The soluble fraction was transferred to 200 µL of Ni-NTA slurry (Ni-NTA resin, Expedeon) previously washed with 1 mL of lysis buffer. The resin was incubated for 2 hrs with the soluble fraction at RT on a rotator. The tubes were centrifuged at 1,000 x g for 1 min to remove the supernatant and the resin was washed by four rounds of wash/resuspension of the resin with 1 mL of wash buffer (500mM NaCl, 50 mM NaH<sub>2</sub>PO<sub>4</sub>, 20 mM imidazole, pH 7.4) and centrifugation at 1,000 x g for 1 min to remove the wash buffer. The absorbance of the final wash buffer was checked at 280 nm to be lower than 0.09 using a spectrophotometer. The 8xHis-Affimers were eluted by resuspending the resin in 350 µL of elution buffer (500mM NaCl, 50 mM NaH<sub>2</sub>PO<sub>4</sub>, 300 mM imidazole, 10% (v/v) glycerol, pH 7.4), incubating the mix 10 min at RT on a rotator, centrifuging the tube at 1,000 x g for 1 min and collecting the supernatant. This elution step was repeated three times with 150 µL of elution buffer. The purity of the Affimers were analysed by SDS-PAGE followed by Coomassie staining.

#### **2.5.2.5. Biotinylation of the Affimers and the mAbs anti-RVFV N protein**

The immobilized TCEP disulfide reducing gel (Thermo Scientific) was prepared by washing 150  $\mu\text{L}$  of the gel stock three times with 300  $\mu\text{L}$  of 1X PBS containing 1 mM EDTA, mixing, centrifugation at 100 x g for 1 min and removing the supernatant. To the washed gel, was added 4  $\mu\text{L}$  of 1X PBS containing 50 mM EDTA and 75  $\mu\text{g}$  of the Affimers to label and the mixes were incubated for 1 hr at RT on a rotator. The tubes were centrifuged at 100 x g for 1 min and the supernatant was carefully collected. To the supernatant, 6  $\mu\text{L}$  of 2 mM biotin-maleimide (Sigma-Aldrich) was added and after mixing, the solution was incubated for 2 hrs at RT. The solution was then desalted using desalting columns according to the manufacturer's instructions. Glycerol was added to the labelled Affimers to give a final concentration of 5% (v/v) and their concentration was measured using a spectrophotometer.

The anti-RVFV N protein mAbs produced in this project were labelled following the same protocol.

The biotinylation of the Affimers and mAbs was checked by ELISA.

#### **2.5.3. Characterization of the detection molecules by pull-down assay**

A 30  $\mu\text{L}$  volume of Dynabeads™ MyOne™ Streptavidin T1 was prepared, for each Affimer or mAb, by mixing the beads with 1 mL of PBS-T, removing the supernatant with a magnetic rack and blocking the beads by addition of 1 mL of 10X blocking buffer and incubating ON at RT on a rotator at 20 rpm. The beads were washed with 200  $\mu\text{L}$  of 2X blocking buffer diluted in PBS-T per 30  $\mu\text{L}$  of beads. The Affimers and mAbs were immobilized onto the beads by adding 10  $\mu\text{g}$  of each biotinylated Affimer and mAb to each 30  $\mu\text{L}$  of bead slurry and the mixes were incubated for 1 hr at RT on a rotator. Using a magnetic rack, the supernatant was removed and the beads were washed three times with 1 mL of PBS-T. A 200  $\mu\text{L}$  volume of 2X blocking buffer containing 25  $\mu\text{g}/\text{mL}$  RVFV N protein was added to each tube and the mixes were transferred into a KingFisher™ Flex 96 deep-well plate (Thermo Fisher Scientific). The plate was loaded to a KingFisher™ Flex and the program consisted in four washes with 2X blocking buffer

in PBS-T and elution of beads in 40  $\mu$ L of sample buffer. The elutions were boiled 5 min at 95°C and centrifuged at 1,000 x g for 1 min and the supernatant was collected and analysed by WB using the anti RVFV N protein mAb (F1D11) at 10  $\mu$ g/mL.

## **2.6. Development of diagnostic tests for detection of the immune response to different emerging viruses**

### **2.6.1. ELISA**

#### **2.6.1.1. Double recognition ELISA**

##### **2.6.1.1.1. Labelling of the N proteins with HRP**

The N proteins of CCHFV, RVFV and SARS-CoV-2 were labelled with HRP, following the same protocol as in section 2.5.1.7 with some modifications. The ratio between the molecular weight of the protein to be labelled and HRP (44 kDa) determines the quantity of HRP used for the labelling. To stop the reaction, the sodium cyanoborohydride solution was added at a volume corresponding to 1/20<sup>th</sup> of the total volume and incubated for 30 min at RT. Then, the sodium cyanoborohydride solution was added at a volume of 1/10<sup>th</sup> of the total volume and incubated for 1 hr at 4°C.

##### **2.6.1.1.2. Steps of the double recognition ELISA**

A double recognition ELISA was developed as previously described by Venteo *et al.* (273). Briefly, 96-well plates (Corning) were coated at 50  $\mu$ L/well with the recombinant antigen in carbonate buffer and incubated ON at 4°C. After washing the wells three times with 300  $\mu$ L/well of PBS-T, a blocking step was performed by incubating the plates with 150  $\mu$ L/well of StabilZyme® SELECT stabilizer for 1 hr at RT. The plates were then dried ON at RT and stored at 4°C in sealed bags.

Serum samples were diluted in a specific dilution buffer and incubated at RT. Duplicates of positive and negative controls were included in each plate. The wells were washed three times as described above and incubated with the HRP-conjugated antigen diluted in dilution buffer and incubated at RT. Finally, after three washing steps, the plate was

incubated with TMB in the dark, and the reaction was stopped by addition of 0.5 M sulfuric acid. The absorbance was measured at 450 nm using a SpectraMax M5 plate reader (Molecular Devices, LLC).

**2.6.1.1.3. Double recognition ELISA to detect antibodies against CCHFV, RVFV and SARS-CoV-2**

The conditions of each double recognition ELISA for antibody detection against each specific virus are detailed in Table 2.14

**Table 2.14** Specific steps and conditions of the double recognition ELISA developed in this project.

Test	Coating	Controls	Serum sample dilution	Sample dilution buffer	Time of incubation	Detection molecule	HRP-antigen dilution	Dilution buffer	Time of incubation	Time of incubation of the substrate
Double recognition ELISA CCHFV	CCHFV NP (0.7 $\mu\text{g/mL}$ ) + BSA (20 $\mu\text{g/mL}$ )	C+: mouse pAb to CCHFV NP C-: FBS	1:2	DB2	1 hour	CCHFV N protein-HRP	1:10,000	DB4	1 hour	15 min
Double recognition ELISA RVFV	RVFV NP (2 $\mu\text{g/mL}$ )	C+: mouse mAb to RVFV NP C-: FBS	1:10	DB2	1 hour	RVFV N protein-HRP	1:10,000	DB4	1 hour	10 min
Double recognition ELISA SARS-CoV-2	SARS-CoV-2 NP (2 $\mu\text{g/mL}$ )	C+: rabbit pAb to SARS-CoV-2 NP C-: dilution buffer	1:5	DB3	30 min	SARS-CoV-2 N protein HRP	1:10,000	DB4	30 min	15 min

*NP: nucleocapsid protein*

### **2.6.1.2. Indirect ELISA SARS-CoV-2**

Two indirect ELISAs were developed to detect human IgG and IgM against SARS-CoV-2 N protein. Briefly, 96-well plates were coated with the N protein at 2 µg/mL in carbonate buffer, pH 9.6 and incubated ON at 4°C. After washing the wells three times with PBS-T, a blocking step was performed for 1 hr at RT. The plates were dried and stored as described above until needed.

The plate was incubated with serum samples diluted 1:100 in DB3 for 1 hr at RT. Two positive, two cut-off and two negative controls were added to each plate. For human-IgG detection, the wells were washed four times and incubated with anti-human IgG HRP conjugated diluted 1:50,000 in DB4 for 1 hr at RT. Finally, after a washing step, the plate was incubated for 15 min with TMB and the reaction was stopped by addition of 0.5 M sulfuric acid. The absorbance was measured at 450 nm using a plate reader. To detect human-IgM, the same protocol was followed, but the secondary antibody used was an anti-human IgM HRP conjugated at a 1:15,000 dilution.

## **2.6.2. LFA**

### **2.6.2.1. Double recognition LFA SARS-CoV-2**

#### **2.6.2.1.1. Covalent binding of SARS-CoV-2 N protein to latex microspheres**

Black latex microspheres (Merck-Millipore) were washed in 10 mM MES pH 6, centrifuged at 10,400 x g for 15 min and sonicated at 15% amplitude using a SFX250 digital sonifier (Branson). The size of the microspheres was measured by dynamic light scattering (DLS) using a Zetasizer Nano S system (Malvern).

The beads were activated with EDC and NHS for 45 min at RT. Then the beads were centrifuged as described above and resuspended in 10 mM MES pH 6. After sonication and measurement of the size of the particles, the SARS-CoV-2 N protein was covalently conjugated to the beads at a surface concentration of 1.25 mg/m<sup>2</sup> for 2 hrs at RT. The beads were then blocked by addition of imidazole and incubated for 15 min at RT. Conjugated latex particles were diluted in 10 mM Tris-HCl, pH 8.2 at a concentration of 1% (v/v).



The conjugate solution was prepared by diluting the N-latex and control-latex (biotin-BSA) particles diluted at a concentration of 0.15% (v/v) each, in a 25 mM Tris-HCl, pH 9.5 buffer containing humidity preservatives and blocking agents. The mixture was dispensed onto the conjugate pad (rayon conjugate pad 25 mm (Operon)) using a Matrix 1600 dispensing module (Kinematic Automation, Inc.), dried for 30 min at 45°C and stored at RT under dry conditions.

#### **2.6.2.1.2. Capture reagents**

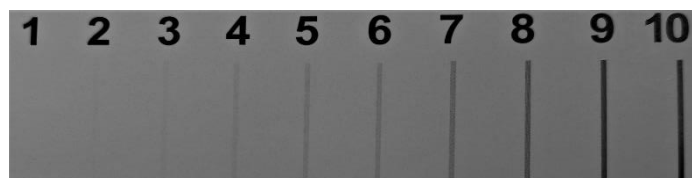
The SARS-CoV-2 N protein was diluted at 0.2 mg/mL in 20 mM Tris-HCl, pH 8.5 containing 5.0% (w/v) sucrose and 0.095% (w/v) sodium azide as preservative to be used as the test line capture reagent. As control line capture reagent, an anti-control protein IgG monoclonal antibody at 1 mg/mL was used. Both reagents were dispensed in two parallel lines on HiFlow Plus nitrocellulose membrane (HF120, Millipore). After drying for 5 min at 45°C, the membranes were sealed and stored at RT under dry conditions.

#### **2.6.2.1.3. Preparation of chromatographic strips**

To assemble the 30 cm master card, nitrocellulose membrane, conjugate pad, sample pad (Cytosep 1662, Ahlstrom-Munksjö), and wicking pad were pasted on a plastic backing card with adhesive and covered with a protector film. The master card was then cut into strips of 4.2 mm width using a Matrix 2360 machine (Kinematic Automation).

#### **2.6.2.1.4. Test procedure**

The LFA was designed to be used with serum, plasma, and blood samples. A 20 µL volume of blood or 10 µL of serum/plasma was applied to the sample pad followed by 110 µL of LDB1. Results were interpreted 10 min after running buffer addition. A scale of the intensity of the signal of the test line from 1 to 10 was used in order to give a semi-quantitative value for statistical purposes (Figure 2.2).



*Figure 2.2 Scale of the intensity of the signal obtained for the LFA test line.*

## **2.7. Development of diagnostic tests for direct detection of different emerging viruses**

### **2.7.1. Double antibody sandwich ELISA**

In order to detect an acute viral infection, double antibody sandwich ELISAs have been developed, based on the capture of the target viral antigen using a pair of monoclonal antibodies in a sandwich format.

#### **2.7.1.1. Double antibody sandwich ELISA CCHFV N protein**

The mAb 3G7 anti-CCHFV N protein was used to coat 96-well plates at 50  $\mu\text{L}/\text{well}$  at 5  $\mu\text{g}/\text{mL}$  in carbonate buffer ON at 4°C. The wells were washed, blocked, dried ON and stored at 4°C in sealed bags.

The serum samples were diluted 1:2 in DB2 and incubated for 1 hr at RT. The wells were washed three times with PSB-T, after which the detection HRP-labelled antibody anti-CCHFV N protein (2G10) was added diluted 1:4,000 in DB4 and incubated for 1 hr at RT. The wells were washed three times with PBS-T and the reaction was developed by adding TMB (50  $\mu\text{L}/\text{well}$ ). After 10 min incubation at RT in the dark, the reaction was stopped by addition of 0.5 M  $\text{H}_2\text{SO}_4$ . The results were read at absorbance 450 nm using a plate reader.

#### **2.7.1.2. Double antibody sandwich ELISA RVFV N protein**

The double antibody sandwich ELISA for detection of RVFV N protein follows the same steps as the double antibody sandwich ELISA CCHFV N protein, but using biotin as the

label molecule. For this assay the mAbs anti-RVSV N protein (1E9 or 1F8) were coated at 5 µg/mL in carbonate buffer ON at 4°C. After the washing, blocking, drying steps, the serum or plasma samples were diluted 1:2 in DB2 and incubated for 1 hr at RT. After a washing step, the biotin-labelled anti-RVSV N protein mAb (1F8) or Affimer (P20) were added at 2 µg/mL in DB4, depending on the pair used, as described in Table 2.15, and incubated 1 hr at RT. After a washing step, streptavidin-HRP (Sigma) was added at 1:40,000 in DB4 and incubated 1 hr at RT. After a washing step, TMB was added and incubated 10 min at RT, then the reaction was stopped by addition of sulphuric acid and the results were read at 450 nm using a plate reader.

The mAb 1F8-HRP was also used instead of its biotinylated form at 1:30,000, using the same conditions as the assay described above.

*Table 2.15 Pair of mAbs and Affimers used in the double antibody sandwich ELISA RVSV N protein.*

<b>mAb/Affimer for capture (coated)</b>	<b>mAb/Affimer for detection (labelled)</b>
mAb 1E9	mAb 1F8
mAb 1F8	Affimer P20
Affimer P20	mAb 1F8
Affimer P28	mAb 1F8

## **2.7.2. Double antibody sandwich LFA**

### **2.7.2.1. Double antibody sandwich LFA RVSV N protein**

The steps to develop the LFA detecting SARS-CoV-2 S protein are similar to the ones detailed in section 2.6.2. The same protocol was followed, with a few modifications described below.

First, the anti-RVSV N protein mAb 1F8 was covalently coupled to red carboxyl-modified latex microspheres (IKERLAT polymers). Following the method in section 2.6.2.1.1, the mAb was coupled to the microspheres at a surface concentration of 1 mg/m<sup>2</sup>.

The conjugate solution was prepared by diluting the mAb-latex and control-latex (biotin-BSA) particles diluted at a concentration of 0.15% (v/v), in a 25 mM Tris-HCl, pH 9.5 buffer containing humidity preservatives and blocking agents.

The anti-RVSV N protein mAb 1E9 was diluted at 0.5 mg/mL to be used as the test line capture reagent.

The test was assembled as described in section 2.6.2.1.3.

The LFA was designed to be used with plasma. 10 microliters of plasma were applied to the sample pad followed by 110  $\mu$ L of running buffer (LDB2). Results were interpreted 15 min after running buffer addition. A scale of the intensity of the signal of the test line from 1 to 10 was used in order to give a semi-quantitative value for statistical purposes (Figure 2.2).

#### **2.7.2.2. Double antibody sandwich LFA SARS-CoV-2 S**

The steps to develop the LFA detecting SARS-CoV-2 S protein are similar to the ones detailed in section 2.6.2. The same protocol was followed, with a few modifications described below.

First, the anti-SARS-CoV-2 S mAb (COVA2-03) was covalently coupled to red carboxyl-modified latex microspheres (IKERLAT polymers). Following the method in section 2.6.2.1.1, the mAb was coupled to the microspheres at a surface concentration of 1 mg/m<sup>2</sup>.

The conjugate solution was prepared by diluting the mAb-latex and control-latex (biotin-BSA) particles diluted at a concentration of 0.2% (v/v) and 0.15% (v/v) respectively, in a 25 mM Tris-HCl, pH 9.5 buffer containing humidity preservatives and blocking agents.

The anti-SARS-CoV-2 RBD mAb (COVA2-29) was diluted at 1 mg/mL to be used as the test line capture reagent.

No sample pad was used as these tests were not to be used with blood samples.

The LFA was designed to be used with nasopharyngeal and oropharyngeal samples. 20 microliters of sample were applied to the sample pad followed by 100  $\mu$ L of running buffer (LDB3). Results were interpreted 15 min after running buffer addition. A scale of

the intensity of the signal of the test line from 1 to 10 was used in order to give a semi-quantitative value for statistical purposes (Figure 2.2).

## **2.8. Multiplex assays using the Luminex technology**

### **2.8.1. Coating of the beads with the target antigens**

The target proteins were covalently coupled to different regions of carboxylated magnetic microspheres (Luminex) using the xMAP® Cookbook by Angeloni *et al.* (178). Two similar protocols were followed, however one had an extra blocking step to avoid high background due the proteins used.

Briefly,  $1 \times 10^6$  microspheres, identified individually by a unique fluorescence ratio, were activated by addition of NHS and EDC, which is based on a two-step carbodiimide reaction (274). Once activated, the beads were incubated with different amounts of the corresponding protein ranging from 12.5  $\mu\text{g}$  to 75  $\mu\text{g}$  per  $10^6$  beads in a final incubation volume of 500  $\mu\text{L}$ , and incubated for 2 hrs with rotation protected from light. After washing, if needed, the beads were blocked with 1X PBS, 10 mM imidazole as an extra step. Finally, the beads were resuspended in 1 mL of storage buffer (1X PBS with 1% (w/v) BSA and 0.05% (v/v) azide) and were kept in the dark at 4°C. Beads concentration was determined by counting on a Neubauer plate.

The list of the bead regions used, and the corresponding coupled proteins, is described in Table 2.16.

**Table 2.16** *Luminex bead regions, the corresponding coupled protein and mAbs used for the confirmation assay.*

<b>Bead region</b>	<b>Coupled protein</b>	<b>mAbs used for confirmation</b>
#12	RVFV N protein	1F8 anti-RVFV N protein
#18	SBV N protein	1D5D12 anti-SBV N protein
#21	MPB83	83CA3 anti-MPB83
#25	CCHFV N protein	2G10 anti-CCHFV N protein
#30	BTV VP7	2D7 anti-BTV VP7
#15	CCHFV GP38	3H11 anti-GST
#20	CCHFV G <sub>Ne</sub>	3H11 anti-GST
#30	RVFV G <sub>Ne</sub>	3H11 anti-GST
#12	SARS-CoV-2 N protein	14E11 anti-SARS-CoV-2 N protein
#20	SARS-CoV-2 S	COVA2-29 anti-SARS-CoV-2 RBD
#25	SARS-CoV-2 RBD	COVA2-29 anti-SARS-CoV-2 RBD

## 2.8.2. Confirmation assay

Serial dilutions of monoclonal antibodies specific to each protein or its tag were used to perform a confirmation assay, in order to assess the coupling efficiency. All the mAbs used for the confirmation assay can be found in Table 2.16.

## 2.8.3. Multiplex assays

### 2.8.3.1. Five-plex to detect antibodies to pathogens affecting ruminants

The five-plex assay to detect antibodies against different pathogens affecting ruminants was performed with bead #12 RVFV N protein, bead #18 SBV N protein, bead #21 MPB83, bead #25 CCHFV N protein and bead #30 BTV VP7.

As the beads are light-sensitive, they were protected from the light at all time. The five respective antigen-coupled microspheres were resuspended by vortex and sonication in order to perform the five-plex assay. A mix of beads was prepared mixing the five bead regions in assay buffer (1X PBS with 1% (w/v) BSA) to a final concentration of 25 beads/ $\mu$ L for each bead region. 96-well plates (Stripwell™ microplate medium binding polystyrene, Costar) previously blocked for 30 min with StabilZyme® SELECT

stabilizer, were used for the assay. To 50  $\mu\text{L}$  of individual ruminants' serum samples, diluted at 1:100 in assay buffer, was added 50  $\mu\text{L}$  of the bead mixture. This mix was incubated for 1 hr at RT and 650 rpm in a mini-shaker PSU-2T (Biosan). After every incubation step, a magnetic plate separator (Luminex) was used to wash the plate twice with washing buffer (1X PBS with 1% (w/v) BSA and 0.05% (v/v) Tween 20). Then, 50  $\mu\text{L}$  of the monoclonal anti-ruminant antibody EG5 labelled with biotin (Eurofins-Ingenasa) was added to each well, at a final concentration of 0.5  $\mu\text{g}/\text{mL}$  in assay buffer, for 1 hr at RT and 650 rpm. Next, 50  $\mu\text{L}$  of Streptavidin R-phycoerythrin (Life Technologies) at 2  $\mu\text{g}/\text{mL}$  in assay buffer were added per well and incubated for 30 min at RT and 650 rpm. Finally, the beads were washed twice with washing buffer and resuspended in 100  $\mu\text{L}/\text{well}$  of washing buffer. The results were read out using MAGPIX® reader (Luminex). To be measured the median fluorescence intensity (MFI) had to count a minimum of 50 events of each bead region.

One well per assay was incubated with FBS as background signal. ELISA confirmed positive sera to each antigen, used as positive controls for the targeted bead region and negative controls for the other beads, were included in every plate to assess the performance of the test.

### **2.8.3.2. Triplex CCHFV**

The triplex assay to detect antibodies against different proteins of CCHFV was performed with the bead #15 CCHFV GP38, bead #20 CCHFV G<sub>NE</sub> and bead #25 CCHFV N protein.

The assay conditions are similar to the ones found above in section 2.8.3.1 with some modifications to reduce the background of the assay. Briefly, the three antigen-coupled microspheres were resuspended by vortex and sonication and the bead mixture was prepared in assay buffer (1X PBS with 5% (w/v) milk and 0.3% (v/v) Tween 20) to a final concentration of 25 beads/ $\mu\text{L}$  for each bead region. The ruminants' serum samples were diluted at 1:50 in assay buffer, 50  $\mu\text{L}$  of the diluted serum samples were added to 96-well plates previously blocked for 30 min (as described above) and 50  $\mu\text{L}$  of the bead mixture was added per well. The plate was incubated for 30 min at RT, with shaking at 650 rpm in a mini-shaker. After every incubation step, the plate was washed three times with washing buffer (1X PBS with 0.3% (v/v) Tween 20) with the magnetic plate

separator. Then, 50  $\mu\text{L}$  of the monoclonal anti-ruminant antibody EG5 labelled with biotin was added to each well, at a final concentration of 0.5  $\mu\text{g}/\text{mL}$  in assay buffer, for 30 min at RT and with shaking at 650 rpm. The plate was washed three times as described above. Streptavidin R-phycoerythrin at 2  $\mu\text{g}/\text{mL}$  in assay buffer was added to each well and incubated for 30 min at RT and with shaking at 650 rpm. Finally, after the last three washes, the beads were resuspended in 100  $\mu\text{L}/\text{well}$  of washing buffer. The results were read as described in section 2.8.3.1.

### **2.8.3.3. Duplex RVFV**

The duplex assay to detect antibodies against different proteins of RVFV was performed with the bead #12 RVFV N protein and bead #30 RVFV G<sub>NE</sub>. The conditions of this assay followed the ones of the triplex CCHFV (section 2.8.3.2).

### **2.8.3.4. Triplex SARS-CoV-2**

The triplex assay to detect antibodies against different proteins of SARS-CoV-2 was performed with the bead #12 SARS-CoV-2 N protein, bead #20 SARS-CoV-2 S and bead #25 SARS-CoV-2 RBD.

The conditions of this assay are similar to the ones of the triplex CCHFV described in section 2.8.3.2. However, to detect human antibodies, the anti-species antibodies used in this assay were the Biotin-SP (long spacer) AffiniPure Goat Anti-Human IgG, Fc $\gamma$  fragment specific and the Biotin-SP (long spacer) AffiniPure Goat Anti-Human IgM, Fc $\delta$  fragment specific at 0.35 and 0.4  $\mu\text{g}/\text{mL}$  respectively.

## **2.9. Statistical analysis**

In this thesis, some of the performance characteristics of the assays were determined such as the analytical sensitivity and specificity, the cut-off values and the diagnostic sensitivity and specificity. The analytical sensitivity (ASe) can be measured by the limit of detection (LOD) of an assay. The diagnostic sensitivity (DSe) and diagnostic specificity (DSp) can be calculated as follow:



$$DSe = \frac{\textit{True positive}}{\textit{True positive} + \textit{False negative}}$$

$$DSp = \frac{\textit{True negative}}{\textit{True negative} + \textit{False positive}}$$

The data obtained in the assays were statistically analysed using the MedCalc® 10 software. Receiver operating characteristic (ROC) curves analysis and dot plot diagrams were made to establish the optimal cut-off value for each assay. The 95% confidence intervals were also determined using this software.

For the double recognition ELISAs developed, using the MedCalc® 10 software, McNemar test was performed to examine the relation between the results obtained in the double recognition ELISAs and in the reference ELISAs. For the five-plex assay and the SARS-CoV-2 triplex assay, to measure the inter-rater reliability between the reference ELISAs and the bead-based assay, Cohen's kappa coefficient was calculated using the MedCalc® 10 software. Finally, using the same software, the statistical dependence between the two assays developed double recognition ELISA SARS-CoV-2 and the double recognition LFA SARS-CoV-2 was determined by performing Fisher's exact test.

# Chapter 3 Development of diagnostic tools for CCHFV

## 3.1. Chapter introduction

Currently, there are several techniques available for CCHFV diagnosis, such as virus isolation, nucleic acid detection, viral antigen detection and serological diagnosis. Most of them have been designed for the human diagnosis market, and, so far, methods are lacking for the veterinary sector.

CCHF can be diagnosed by isolating the virus from blood, plasma or tissues during the five first days of infection, when the viremia is high, as cell cultures can only detect high concentrations of the virus (275). As this virus is poorly cytopathic, infectivity is measured by immunofluorescence within infected cells or by RT-PCR. The viral culture can be set up using cell lines from chickens, hamsters or monkeys, which takes 1 to 6 days, although virus propagation can also be performed using intracerebral inoculation of mice, which is 10 to 100-fold more sensitive but takes between 5 to 10 days (276). This technique is advantageous as it can detect a wide range of CCHFV strains, but is time-consuming and requires a biosafety level (BSL)-4 laboratory.

With regard to molecular techniques, many nucleic acid amplification tests have been developed. A recent review described all the nucleic acid test available (277), but few of them are commercially available. RT-PCR is usually used for the diagnosis of CCHF during the first days of the viremia (before the production of antibodies) in whole blood, plasma, serum, cerebrospinal fluid, urine, saliva, biopsy, and necropsy samples (275). Other molecular assays such as reverse transcription LAMP (RT-LAMP), which can be used without any lab resources as a POC test, has been recently described (278). Molecular diagnostic assays are faster than virus culture and they serve as the front-line tool in the diagnosis of CCHF but their sensitivity is impacted by the high genetic diversity between the CCHFV strains (277). Moreover, most of the molecular techniques also need to be carried out in a BSL-4 laboratory.

Viral antigen detection has been described by Shepherd *et al.* (279) using ELISA and reverse passive hemagglutination assay. These tests were found to be most effective during the first few days of the illness, before the development of antibodies. More recently, an antigen-capture ELISA has been developed using a monoclonal antibody to the recombinant CCHFV N protein (280). This assay detected N protein in acute sera of CCHF patients, with a lower sensitivity compared to RT-PCR, and its sensitivity decreased after the appearance of antibodies in the sera. These assays could be useful for the detection of acute infections and especially in fatal cases, but overall their sensitivity is lower than the one of virus isolation and RT-PCR.

Finally, there are serological assays to detect antibodies to CCHFV. There are a few commercial ELISA for IgG and IgM detection as well as IFA based on recombinant antigens (recombinant N protein) for the detection of CCHFV specific antibodies, as summarized in Table 3.1.

**Table 3.1 Commercial serological assays available for CCHFV antigen and antibody detection.**

<b>Assay</b>	<b>Species</b>	<b>Producer</b>
ELISA IgM	Human	Vector-Best, Russia
ELISA IgG		Vector-Best, Russia
Double recognition ELISA	Multi-species	IDVet, France
IFA IgM	Human	Euroimmun, Germany
IFA IgG		Euroimmun, Germany
Antigen capture ELISA	Human	Vector-Best, Russia

Usually, IgM and IgG antibodies are detectable after the 5th day and 7th day of CCHF illness, but in severe and fatal cases, this production can be delayed or lower/absent (275). Commercial and in-house ELISAs and IFA have been developed for diagnosis in humans, but they still lack sensitivity (281). More recently, some multispecies ELISAs have been developed to detect antibodies to CCHFV. A competition assay has been developed by Schuster *et al.* (282), which was tested with serum samples from 12 different animal species and humans. It was able to detect positive antibodies in four different species with

a sensitivity of 95% and was tested with negative sera from 12 species with a specificity of 99%. Another type of ELISA has been recently developed by Sas *et al.* (283), based on a double recognition ELISA, which can detect total antibodies to CCHFV in a wide range of species (monkeys, camels, rats, ferrets, raccoon dogs, raccoons, foxes, hares, pigs and humans were tested). This ELISA exhibited a high sensitivity (100%) and specificity (99.9%) and is now commercially available (ID Screen® CCHF Double Antigen Multi-species, IDVet, France). Finally, an indirect ELISA has been developed based on the recombinant N protein to detect IgG to CCHFV with a sensitivity of 79.4% and specificity of 100% (284). Virus neutralization tests have also been used to detect neutralizing antibodies against CCHFV in the serum of a variety of species, but these tests can only be performed with live virus and are not recommended for use outside endemic areas and in laboratories without appropriate biosecurity facilities. Nevertheless, a recent in-house CCHF VLP-based neutralizing test has been developed allowing the diagnostic of CCHFV under non-BSL-4 conditions (285).

Regarding the serological assays, as summarized in Table 3.1, only a few ELISAs are commercially available and all of these but one (the multi-species double recognition ELISA developed in 2018) are designed for human samples. Moreover, there is only one commercial ELISA detecting viral antigens and no commercial LFAs have been developed so far to detect antibodies or antigens. Thus, there is an unmet need for sensitive, rapid, reliable, simple-to-use and easily accessible diagnostics for humans but more specifically for animals.

DISCONTOOLS is a database created as part of an EU project, with the aim to identify the gaps in knowledge to speed up the development of new DISEase CONtrol TOOLS (diagnostics, vaccines and pharmaceuticals) and reduce the burden of animal diseases. Their section concerning CCHFV has last being updated at the end of 2016 (286), but already identified some important gaps regarding CCHFV diagnostics. Firstly, at this time no commercial diagnostic kits were available for animals, thus there was a need for the development of diagnostic tests for monitoring CCHFV seroprevalence in reservoir animals. Secondly, commercial serological tests for humans and animals with increased sensitivity and specificity were needed.

Finally, these needs were also underlined by the WHO under the WHO R&D Blueprint: Priority Diagnostics for CCHF and the Roadmap for Research and Product Development

against CCHFV, published in 2019 and 2018 respectively. The goal of the CCHF Roadmap is “to be able to reduce death and morbidity from CCHF through safe and affordable effective treatments informed by rapid, reliable, simple-to-use and easily accessible diagnostics by 2023” (287). According to these, the first step is to develop affordable and qualified molecular and serological tests for use in CCHF-affected countries by 2020 and then develop some POC tests by 2023. The Roadmap (288) underlines some essential points, among others:

- Anti-CCHFV antibodies should be produced and characterized for their use in antigen detection assays and these antibodies could include mAbs developed for therapeutic purposes.
- The tests to be developed should cover a range of CCHFV antigenic targets to be used as differentiating infected from vaccinated animals (DIVA) assays or confirmatory diagnostic tests needed for vaccine evaluation.
- Commercial serological assays detecting IgM and IgG against CCHFV should be developed and tested to be used as supplementary diagnostic tests, for epidemiology and surveillance during outbreaks, and for evaluation of vaccine immunogenicity and durability.
- Commercial multi-species ELISA should be developed to detect anti-CCHF antibodies for monitoring CCHFV in animals.

Thus, according to the WHO, the development and validation of in vitro diagnostic assays for CCHF is a priority. Finally, depending on the diagnostic assay to develop, the WHO has detailed performance specifications, detailed here in Table 3.2 for ELISAs and LFAs.

**Table 3.2 Minimal and optimal performances defined by the WHO R&D Blueprint: Priority Diagnostics for CCHF for ELISA and LFA.**

Assay	ELISA		LFA	
	Minimal performance	Optimal performance	Minimal performance	Optimal performance
Intended use	ELISA for detection of CCHFV-specific human IgM <u>or</u> CCHFV Ag in humans for evidence of active CCHFV infection	ELISA for detection of CCHFV-specific human IgM <u>and</u> CCHFV Ag in humans for evidence of active CCHFV infection	Rapid lateral flow immunoassay for detection of CCHFV-specific human IgM <u>or</u> CCHFV Ag in human specimens for evidence of active CCHFV infection	Rapid lateral flow immunoassay for detection of CCHFV-specific human IgM <u>and</u> CCHFV Ag in human specimens for evidence of active CCHFV infection
Analytes	IgM or Ag detection, validated for Eurasian clades IV-VII	IgM and Ag detection, validated for Eurasian and African clades I-VII	IgM or Ag detection, validated for Eurasian clades IV-VII	IgM and Ag detection, validated for Eurasian and African clades I-VII
Time to result	≤6 hours for one 96-well plate	≤6 hours for three 96-well plate	≤30 minutes	≤10 minutes
Specimen type	Plasma, serum	Plasma, serum, whole blood, saliva, breast milk	Plasma, serum (venepuncture)	Plasma, serum, whole blood (venepuncture and fingerstick)
Sample input	≤5 mL venepuncture	≤200 µL	≤100 µL of specimen	≤30 µL of specimen
Sample preparation	Centrifugation and dilution of specimen for use in BSL-3/4	Inactivation protocol for use in BSL-2 sample preparation	Serum or plasma separation	None
Test output	Qualitative (positive, negative) result as defined by signal relative to an empirical cut-off established for each assay run	Semi-Quantitative (sample to cut-off value, S/CO) for calibrator dilution series	Qualitative: detected/not detected visual readout compared to full process control line	
Limit of detection	Empirical cut-off for each assay run using positive and negative controls	Reference (statistical) methods to define an assay cut-off	Empirical cut-off established for each assay run using positive control	Signal detected over background at clinically relevant minimum
Clinical sensitivity	>85%	>90%	>80% IgM, Ag	>90% IgM, Ag
Clinical specificity	>85%	>95%	>90% IgM, Ag	>95% IgM, Ag

Cross-reactivity	Minimal but characterized cross-reactivity with other endemic or syndromic pathogens			
Interfering Substances	No interference for individual or mixtures of analytes, endogenous/exogenous substances			
Assay process controls and calibration (to international standard when available)	Each run includes positive and negative controls – not supplied with kit	Each run includes positive and negative controls - lyophilized controls included in kit	Full process internal control, external positive/negative controls (not supplied with kit)	Full process internal control, external positive/negative controls (lyophilized, included in kit)
Third-party instrumentation	Manual ELISA plate washer and reader, calibrated pipettes	Automated ELISA plate washer and reader	Timer, materials required for venepuncture or fingerstick	
Opened kit stability	Diluents stable at 2-8°C until expired; reagent dilutions stable at RT for 1 working day		Stable at 18-30°C for 1 working day	Stable at 18-40°C for 1 working day
Unopened kit storage and shelf life	-20°C (or dry ice) for transport and up to 6 months storage	Kit reagent stability 2-8°C for transport and up to 12 months storage	Kit reagent stability 2-30°C for transport and up to 6 months storage	Kit reagent stability 2-30°C for transport and up to 12 months storage
Price of single test	≤\$15 USD at volume production	≤\$10 USD at volume production	≤\$15 USD at volume production	≤\$10 USD at volume production

This chapter describes the recombinant expression and purification of three CCHFV structural proteins, namely N, the G<sub>N</sub> ectodomain and GP38, and their subsequent use for both antibody production, and development of diagnostic assays to detect the incidence of previous CCHFV infection in animals. These assays aim to respond to the gaps in CCHFV diagnostics.

## 3.2. Production and purification of CCHFV N protein

### 3.2.1. Expression of the CCHFV N protein

In order to develop new diagnostic tests against CCHFV, the first step was the production of the CCHFV N protein. The pET28a-SUMO plasmid containing the CCHFV N gene was used to transform into *E. coli* BL21 (DE3) R2. The expression of CCHFV N protein was induced by addition of IPTG (Figure 3.1). After the ON induction, the cells were harvested and lysed. The soluble and insoluble fractions of the cell lysate were separated by centrifugation and analysed by SDS-PAGE followed by Coomassie staining (Figure

3.1). A band at the expected molecular size of the 6xHis-SUMO-CCHFV N protein (molecular weight, MW= 67.5 kDa) was detected after induction and in the insoluble and soluble fractions. As the CCHFV N protein was abundantly present in the soluble fraction, this was used for further purification of the CCHFV N protein.

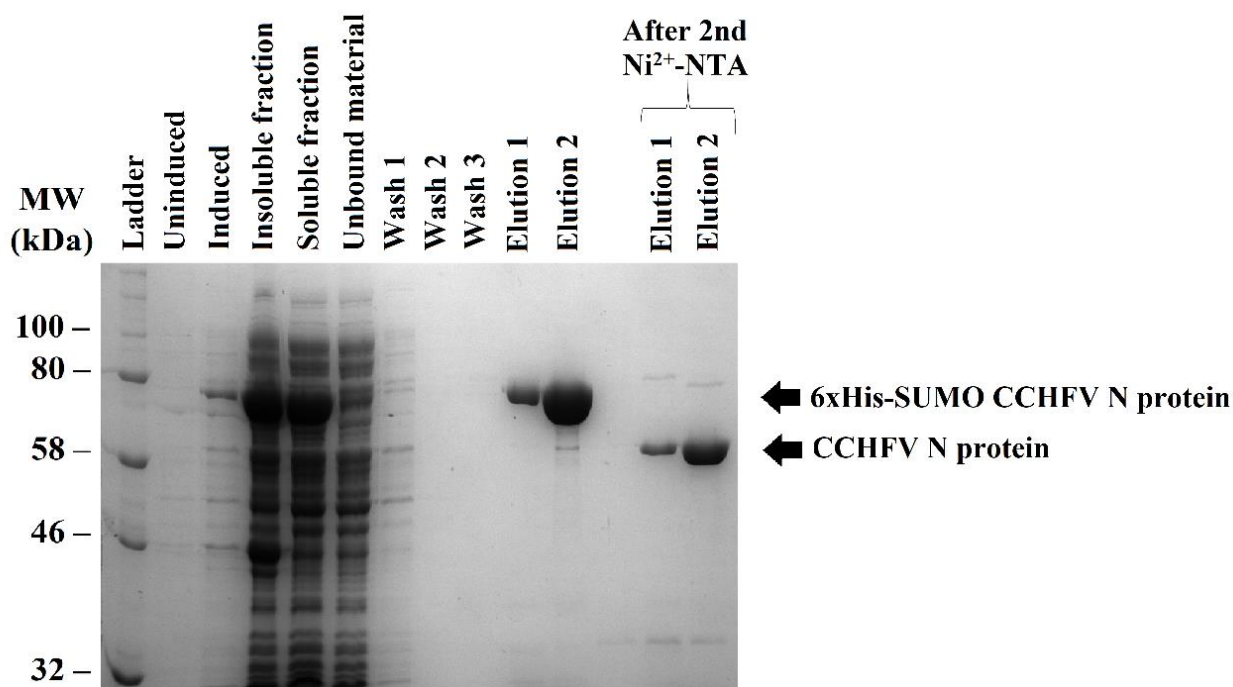
### **3.2.2. Purification of the CCHFV N protein**

The soluble fraction was first purified by IMAC using a Ni<sup>2+</sup>-NTA affinity chromatography column to separate the 6xHis-SUMO-CCHFV N protein from the other proteins contained in the soluble fraction, with full details of the experimental procedure described in section 2.3.1.1.

The soluble fraction was applied to the Ni<sup>2+</sup>-NTA matrix and incubated ON at 4°C. The resin was then washed to remove the unbound proteins and the elution of the 6xHis-SUMO-CCHFV N protein was performed with elution buffers containing 100 mM (elution 1) and 500 mM imidazole (elution 2). The elution fractions were observed by SDS-PAGE followed by Coomassie staining and the 6xHis-SUMO-CCHFV N protein was present in the two elution fractions but at higher quantities in the 500 mM fraction (see Elution 1 and 2 in Figure 3.1).

The elution fractions were then dialyzed ON with the addition of the SUMO protease Ulp1 to cleave the 6xHis-SUMO tag from the CCHFV N protein and after dialysis, loaded on a SDS-PAGE followed by Coomassie staining (Figure 3.1). The cleavage of the 6xHis-SUMO tag from the CCHFV N protein could be observed with the appearance of a band corresponding to the MW of the native CCHFV N protein (MW= 54 kDa). Additionally, a faint band around 80 kDa was detected, most likely corresponding to the uncleaved 6xHis-SUMO-CCHFV N protein, as well as a band around 35 kDa corresponding to an unknown protein.

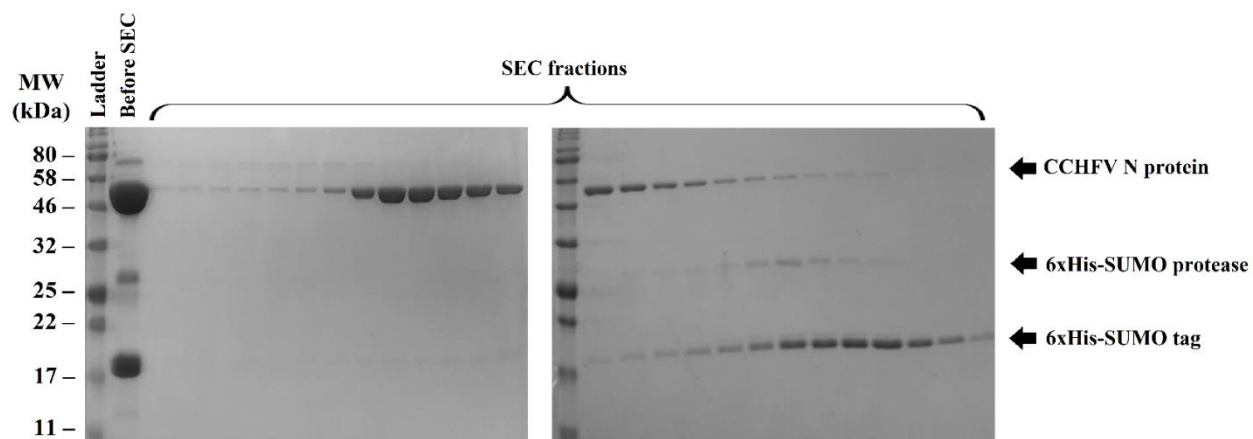




**Figure 3.1** Expression of the CCHFV N protein and its purification by Ni<sup>2+</sup>-NTA affinity chromatography.

SDS-PAGE followed by Coomassie staining of samples taken at different steps of the expression and purification of the 6xHis-SUMO CCHFV N protein. After its purification from the soluble fraction by a first Ni<sup>2+</sup>-NTA affinity chromatography and elution with elution buffers containing 100 mM (elution 1) and 500 mM imidazole (elution 2), the 6xHis-SUMO CCHFV N protein was dialysed and cleaved with SUMO protease Ulp1 and the CCHFV N protein was further purified by a second Ni<sup>2+</sup>-NTA affinity chromatography. Arrows indicate the bands corresponding to the specified proteins.

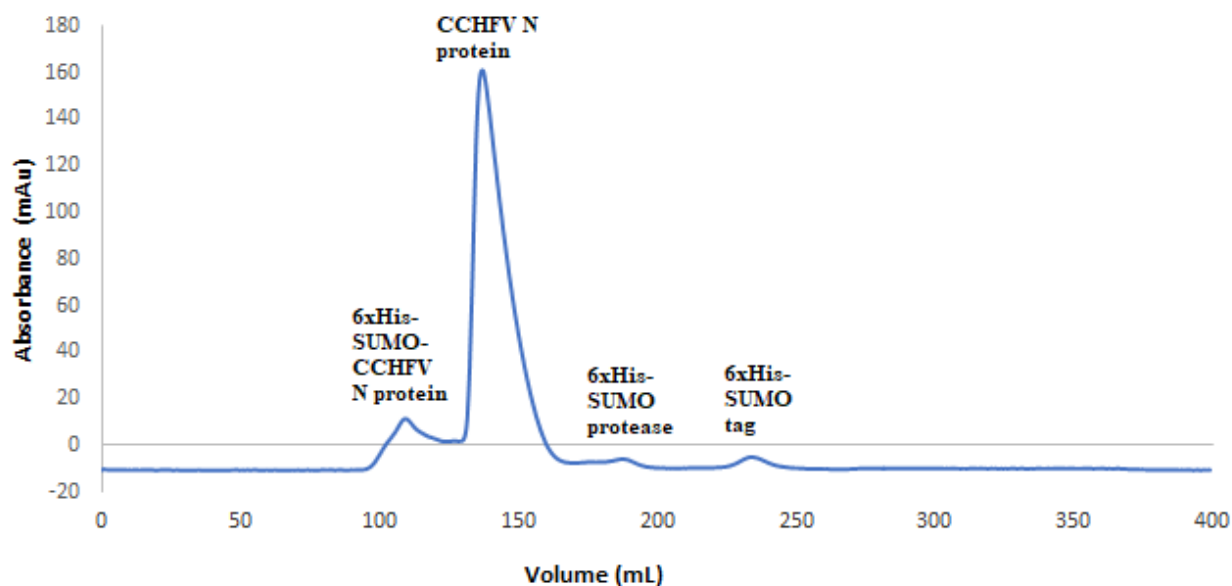
The samples collected from the dialysis were applied to a second Ni<sup>2+</sup>-NTA column, to separate the CCHFV N protein from the uncleaved proteins; the 6xHis-SUMO tag and the 6xHis-SUMO protease Ulp1. The CCHFV N protein was collected in the unbound material and the bound material was eluted by addition of elution buffer containing 500 mM imidazole. The samples were analysed by SDS-PAGE followed by Coomassie staining (corresponding to the ‘before SEC’ lane in Figure 3.2). The unbound material mostly contained the CCHFV N protein, however some faint bands around 80 kDa, 25 kDa and 17 kDa, were observed, probably corresponding to the uncleaved 6xHis-SUMO-CCHFV N protein (74.5 kDa), 6xHis-SUMO protease Ulp1 (27 kDa) and the 6xHis-SUMO tag (13 kDa).



**Figure 3.2 CCHFV N protein purification by size exclusion chromatography.**

SDS-PAGE analysis followed by Coomassie staining of the different fractions collected after the size exclusion chromatography. After the  $\text{Ni}^{2+}$ -NTA affinity chromatography, the CCHFV N protein was purified from proteins by size exclusion chromatography to separate them according to their molecular weight. Arrows indicate the bands corresponding to the specified proteins. SEC: size exclusion chromatography.

The final purification step was to use SEC to separate the proteins according to their molecular weight using a HiLoad<sup>®</sup> 26/600 Superdex<sup>®</sup> 75 pg mounted on an ÄKTA prime pump and controller. Four different peaks could be observed on the chromatogram obtained (Figure 3.3). The first peak corresponded to the void volume (110 mL) containing the 6xHis-SUMO-CCHFV N protein (74.5 kDa), the second to the CCHFV N protein (54 kDa), the third to the 6xHis-SUMO protease (27 kDa) and the fourth to the 6xHis-SUMO tag (13 kDa).



**Figure 3.3** Chromatogram of final purification step of the CCHFV N protein sample by size exclusion chromatography after two  $\text{Ni}^{2+}$ -NTA affinity chromatography purifications. The proteins corresponding to each peak are indicated on the chromatogram.

The fractions collected by the ÄKTA prime were observed by SDS-PAGE followed by Coomassie staining (Figure 3.2). As shown by the chromatogram, the first fractions collected by the SEC contained the uncleaved 6xHis-SUMO-CCHFV N protein and the CCHFV N protein, followed by fractions only containing the CCHFV N protein. In the last SEC fractions, the CCHFV N protein was present in lower concentrations along with the 6xHis-SUMO protease (27 kDa) and the 6xHis-SUMO tag (13 kDa). The fractions containing the pure CCHFV N protein were pooled, concentrated, quantified by spectrophotometry using a NanoDrop™ 1000 Spectrophotometer and stored at  $-80^{\circ}\text{C}$  after addition of glycerol.

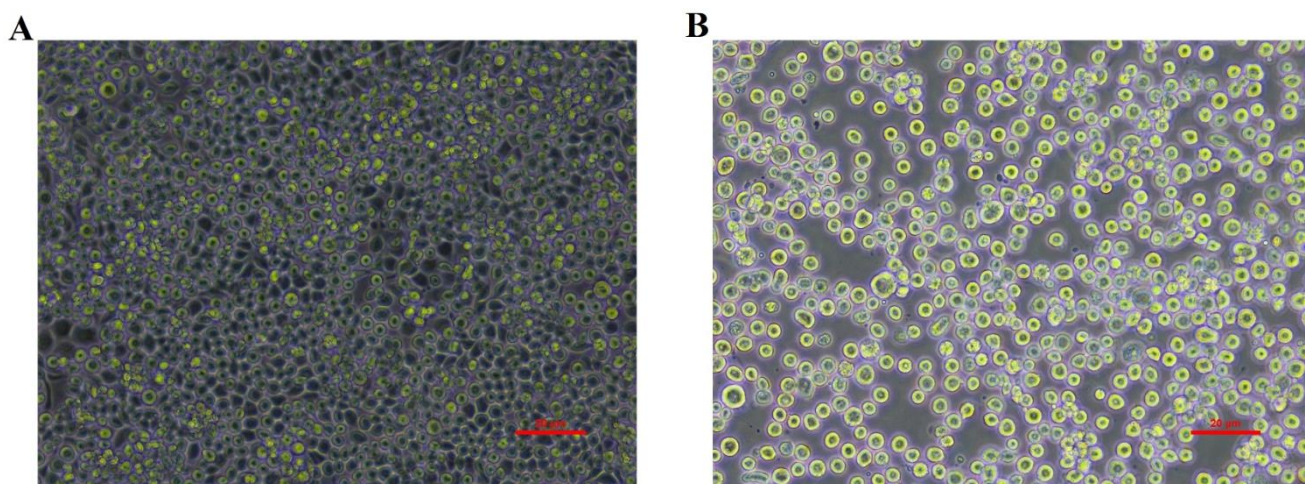
Following the same protocol, 6xHis-SUMO-CCHFV N protein was also expressed and purified by  $\text{Ni}^{2+}$ -NTA affinity chromatography without removal of the tag and without SEC.

### 3.3. Production and purification of CCHFV G<sub>NE</sub> and GP38

#### 3.3.1. Expression of CCHFV G<sub>NE</sub> and GP38

To express the CCHFV G<sub>NE</sub> and GP38 proteins in insect cells, the first step was to produce recombinant baculoviruses containing the CCHFV G<sub>NE</sub> and GP38 ORFs. The CCHFV G<sub>NE</sub> and GP38 ORFs were cloned into the Gateway system as described in Materials and Methods and a LR recombination was performed between the entry vector and the expression vector pAcSecG2T, to obtain pAcSecG2T CCHFV G<sub>NE</sub> and pAcSecG2T CCHFV GP38.

The pAcSecG2T CCHFV G<sub>NE</sub> and pAcSecG2T CCHFV GP38 were independently used to perform a co-transfection of Sf9 insect cells together with the triple-cut recombinant baculovirus DNA. After a week of incubation, clear CPE could be observed (Figure 3.4).

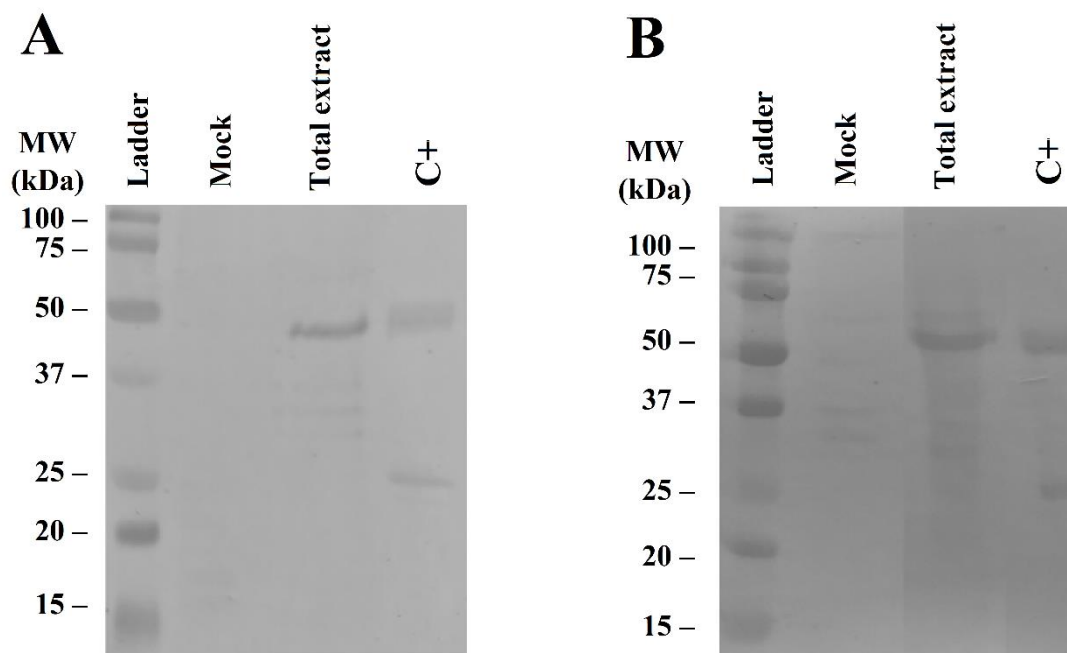


**Figure 3.4** Observation under the microscope of infected Sf9 after the co-transfection.

*A: mock uninfected Sf9 cells. B: Sf9 cells a week post-infection with clear cytopathic effects. Red scale bar represents 20  $\mu$ m.*

To confirm the co-transfection was successful, the cells were harvested by centrifugation and lysed, after which the total extracts were analysed by WB using an anti-GST mAb: a band corresponding to the molecular weight of CCHFV G<sub>NE</sub>-GST (46 kDa) was observed

(Figure 3.5A) along with one corresponding to the molecular weight of CCHFV GP38-GST (58 kDa) (Figure 3.5B).



**Figure 3.5** Co-transfections of Sf9 with the triple-cut baculovirus DNA and the transfer vector to obtain recombinant baculoviruses expressing the target protein.

A Western blot was performed with an anti-GST mAb used as primary antibody. A: Co-transfection performed with pAcSecG2T CCHFV G<sub>NE</sub> (MW of CCHFV G<sub>NE</sub>-GST = 46 kDa). B: Co-transfection performed with pAcSecG2T CCHFV GP38 (MW of CCHFV GP38-GST = 58 kDa). The positive control (C<sup>+</sup>) corresponds to a recombinant protein with a GST-tag (MPB83-GST, MW = 46.3 kDa).

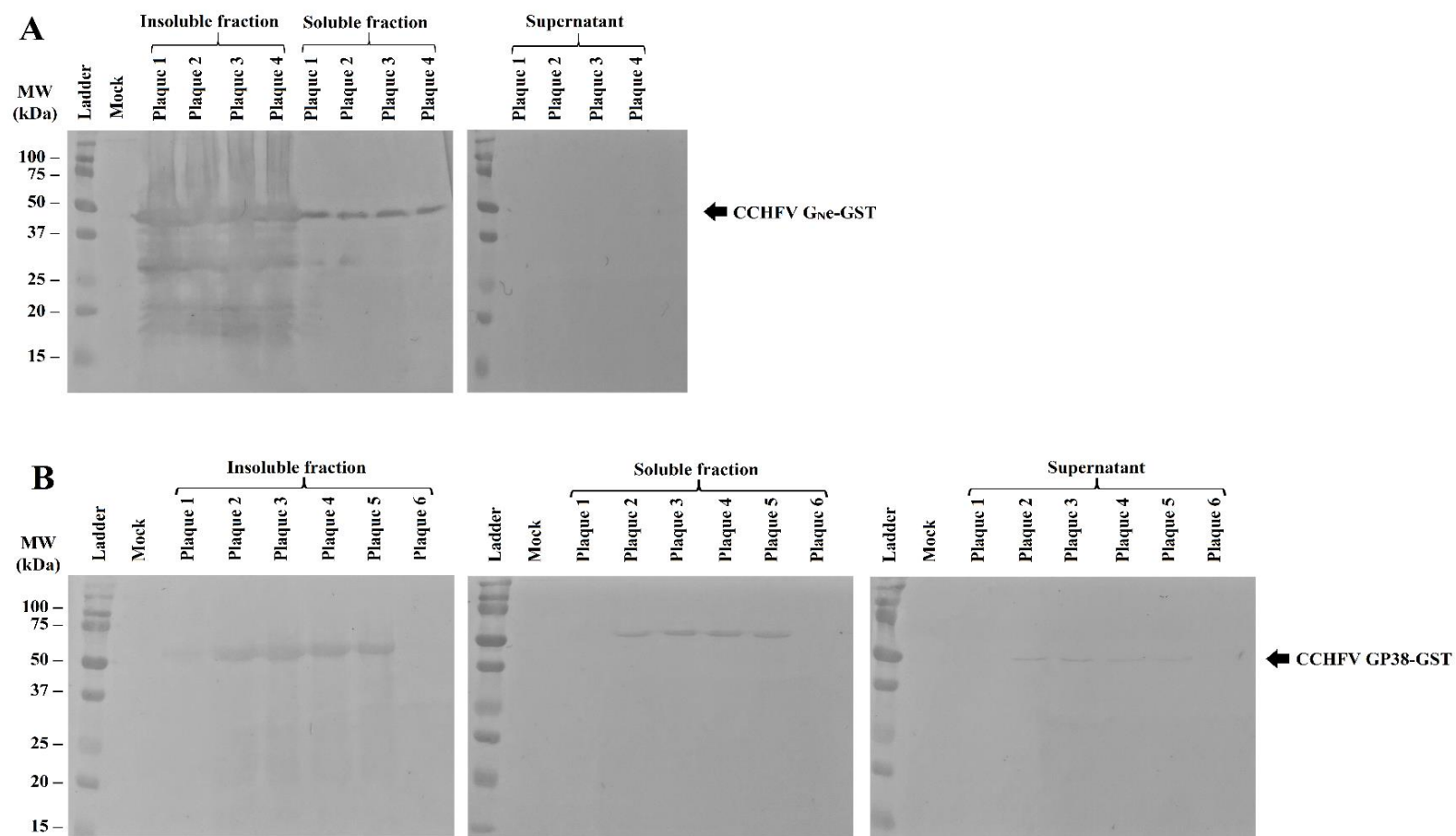
To differentiate recombinant baculoviruses from potential parental baculoviruses, a plaque assay was performed with the supernatant of the co-transfections. After staining the plaque assays for blue–white screening, all the observable plaques were white plaques, corresponding to recombinant baculoviruses.

A few plaques were selected from each plaque assay (4 for CCHFV G<sub>NE</sub> and 6 for CCHFV GP38) and, after dissolution in media, the plaques were used to infect Sf9 cells in 60 mm dishes. The dishes were incubated for five days, until when the CPE was evident. The cells were harvested by centrifugation, lysed and the soluble and insoluble

fractions were separated by centrifugation and analysed by WB with an anti-GST mAb (Figure 3.6).

Regarding CCHFV G<sub>NE</sub> (Figure 3.6A), in the insoluble fraction, a smear with an intense band corresponding to CCHFV G<sub>NE</sub>-GST was observed in the four plaques selected, but several unknown contaminants were detected as well. In the soluble fraction, a clear band was present around 45 kDa in the four plaques, corresponding to CCHFV G<sub>NE</sub>-GST, without any of the contaminants detected in the insoluble fraction. Finally, regarding the supernatant, no band was observable. All the plaques selected expressed the CCHFV G<sub>NE</sub>-GST in high quantities in the insoluble fraction and at a lower amount in the soluble fraction, without any production of secreted protein.

Regarding CCHFV GP38 (Figure 3.6B), in the insoluble fraction, a lighter smear with a clear band around 60 kDa, corresponding to the CCHFV GP38-GST, was observed in four plaques out of the six selected (plaques 2 to 5). In the soluble fraction, a band of the same size was present in the same plaques as in the insoluble fraction (2 to 5). Finally, in the supernatant, a faint band was detected in the same plaques (2 to 5). Thus, out of the six plaques selected, four expressed the CCHFV GP38-GST, mainly in the insoluble fraction, but some were produced in the soluble fraction and the protein was even secreted in the supernatant.



**Figure 3.6** Infection of Sf9 cells with plaques corresponding to different recombinant baculoviruses.

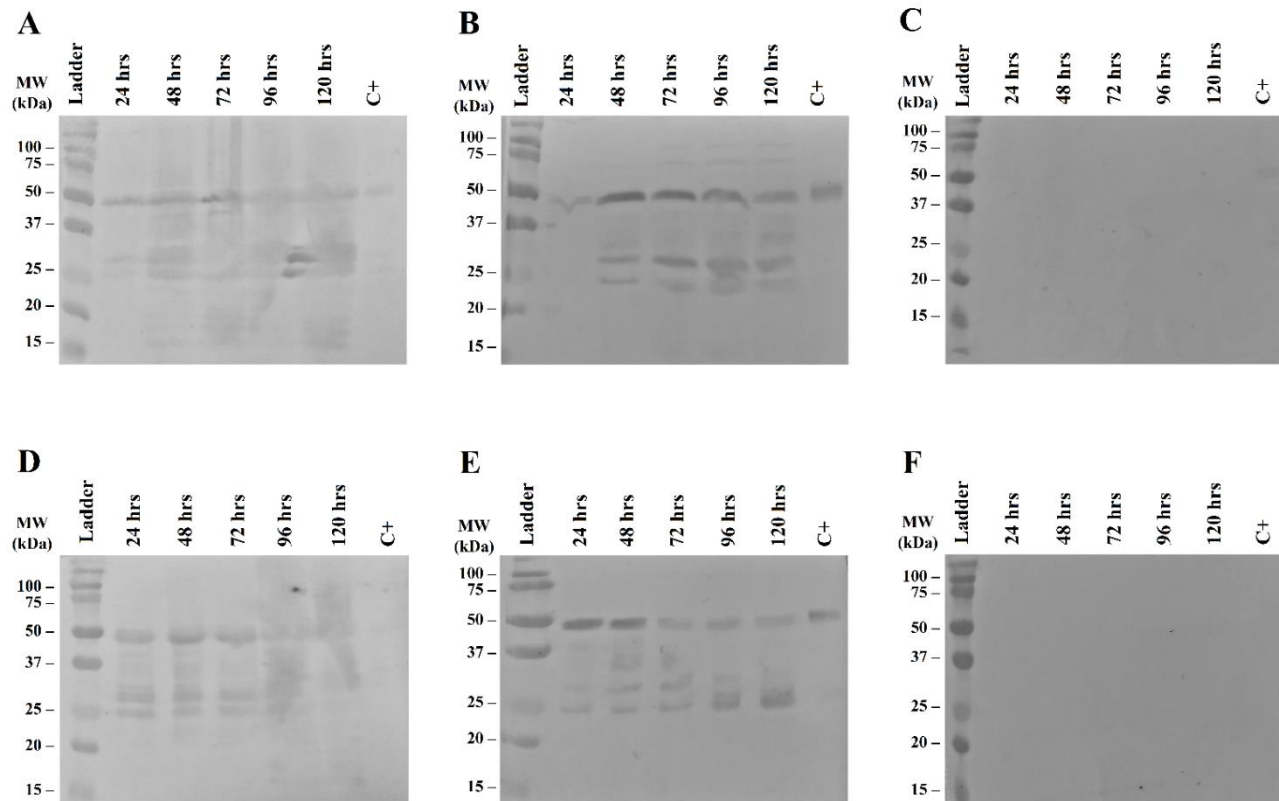
Five days post-infection, the insoluble fraction, soluble fraction and supernatant from Sf9 infected with baculoviruses from the plaque assay were analysed by Western blot with an anti-GST mAb used as primary antibody. A: four plaques were selected for CCHFV G<sub>Ne</sub>. B: six plaques were selected for CCHFV GP38. Arrows indicate the bands corresponding to the specified proteins.

A plaque corresponding to the best recombinant protein-producing plaque was selected for each protein expression (plaque 1 for CCHFV G<sub>NE</sub>-GST and plaque 2 CCHFV GP38-GST) and the corresponding supernatant was used to infect Sf9 to produce a high titre baculovirus stock. The high titre baculovirus stock was titrated by plaque assay. For the BacPAK6 CCHFV G<sub>NE</sub>, a virus titre of  $6 \times 10^8$  pfu/mL was determined and for BacPAK6 CCHFV GP38 the virus titre was  $1.8 \times 10^8$  pfu/mL.

The high titre baculovirus stock for CCHFV G<sub>NE</sub>-GST expression and for CCHFV GP38-GST expression were used to infect Sf900 cells at MOI 0.1 and MOI 2 to perform a kinetic analysis of the expression of both proteins and select the best conditions of expression of the proteins. Cells and supernatants were harvested every 24 hrs until reaching extensive CPE and the beginning of cell death (120 hrs PI for CCHFV G<sub>NE</sub>-GST and 96 hrs PI for CCHFV GP38-GST). Samples were analysed by WB with an anti-GST mAb (Figure 3.7 and Figure 3.8).

Regarding the CCHFV G<sub>NE</sub>-GST expression kinetics (Figure 3.7), a band corresponding to the CCHFV G<sub>NE</sub>-GST could be observed at both MOI in the insoluble fractions (Figure 3.7A and Figure 3.7D) and in the soluble fractions (Figure 3.7B and Figure 3.7E), however no band was observable in the supernatant at both MOI (Figure 3.7C and Figure 3.7F). The band corresponding to the CCHFV G<sub>NE</sub>-GST was overall more intense in the insoluble fraction than in the soluble fraction, showing a higher expression in the insoluble fraction. The protein production was detected as soon as 24 hrs PI. After 24 hrs, the band was more intense and visible at MOI 2 than at MOI 0.1, corresponding to a better expression at MOI 2, however in both cases, a decrease in the expression and an increase of the protein degradation could be observed 72 hrs PI. Regarding the expression in the soluble fraction, a band appeared 24 hrs PI, at higher intensity at MOI 2. However, after 48 hrs the protein seemed to be degraded at MOI 2, as the band became fainter. At MOI 0.1, the production of CCHFV G<sub>NE</sub>-GST increased until 72 hrs, before decreasing.

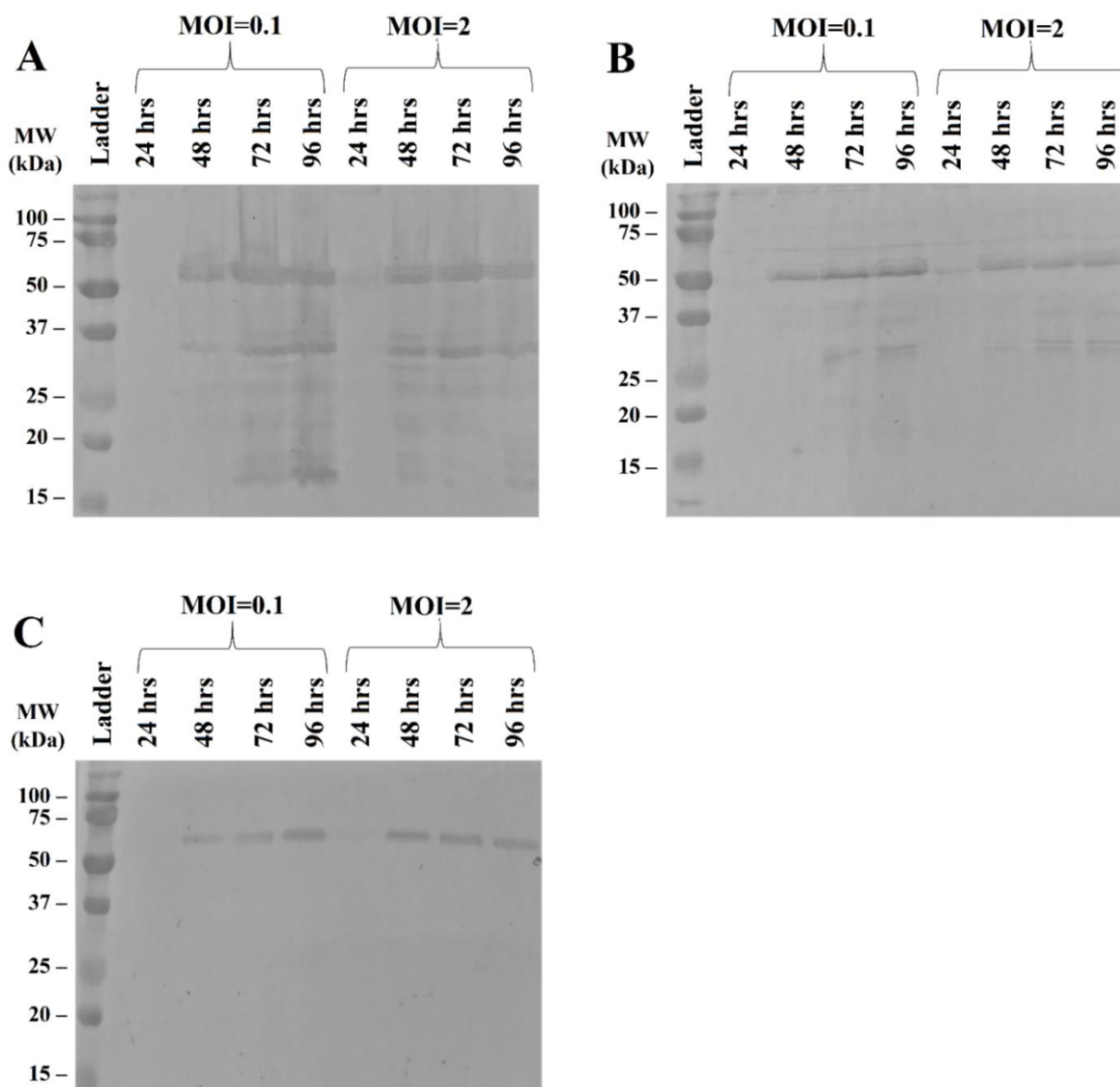




**Figure 3.7** Kinetic analysis of the expression of CCHFV  $G_{Ne}$ -GST (MW = 46 kDa) by Sf900 cells infected with two MOI (0.1 and 2) of BacPAK6 CCHFV  $G_{Ne}$ .

Samples were taken at different time points (24 hrs, 48 hrs, 72 hrs, 96 hrs and 120 hrs) and the expression in the insoluble fraction, soluble fraction and supernatant was analysed by Western blot with an anti-GST mAb used as primary antibody. A: insoluble fractions at MOI 0.1. B: soluble fractions at MOI 0.1. C: supernatant at MOI 0.1. D: insoluble fraction at MOI 2. E: soluble fraction at MOI 2. F: supernatant at MOI 2. The positive control (C+) corresponds to a recombinant protein with a GST-tag (MPB83-GST, MW = 46.3 kDa).

Regarding the CCHFV GP38-GST expression kinetics (Figure 3.8), at both MOIs and in all the fractions, a band corresponding to the GP38-GST was observable. The protein was first detected at 48 hrs PI and the expression increased until 96 hrs PI. Overall, the expression seemed higher at MOI 0.1 than at MOI 2.



**Figure 3.8 Kinetic analysis of the expression of CCHFV GP38-GST (MW = 58 kDa) by Sf900 cells infected with two MOI (0.1 and 2) of BacPAK6 CCHFV GP38.**

Samples were taken at different time points (24 hrs, 48 hrs, 72 hrs and 96 hrs) and the expression in the insoluble fraction, soluble fraction and supernatant was analysed by Western blot with an anti-GST mAb used as primary antibody. A: insoluble fractions at MOI 0.1 and 2. B: soluble fractions at MOI 0.1 and 2. C: supernatant at MOI 0.1 and 2.

The kinetic analysis showed that the best conditions for the production of CCHFV G<sub>NE</sub>-GST were to set up an infection at MOI 2 and harvest at 48 hrs PI. However, when performing a large-scale infection for the expression of CCHFV G<sub>NE</sub>-GST at MOI 2, with a harvest at 120 hrs PI, the CCHFV G<sub>NE</sub>-GST was detected in the culture supernatant. Thus, this condition was preferred for the CCHFV G<sub>NE</sub>-GST expression. The best expression condition for CCHFV GP38-GST was at MOI 0.1 for 96 hrs. Large-scale infections were done with  $6 \times 10^8$  Sf900 cells that were infected with the selected conditions.

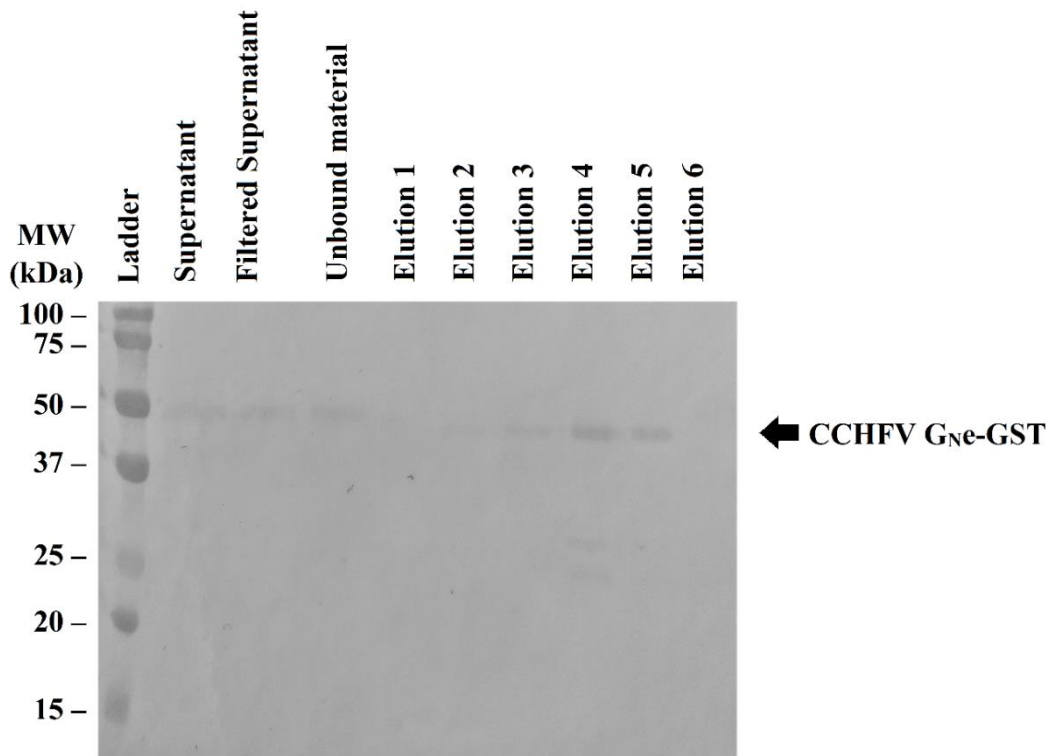
### **3.3.2. Purification of CCHFV G<sub>NE</sub> and GP38**

The supernatants of the insect cell infections were harvested by centrifugation and further filtered. The filtered supernatants were incubated with an affinity column prepared with the anti-GST mAb. The unbound material was collected, the column was washed and the bound proteins were eluted by addition of 0.1 M glycine hydrochloride, pH 2.6. The elution fractions were neutralized, dialyzed ON in PBS and analysed by SDS-PAGE followed by Coomassie staining and by WB with an anti-GST mAb.

In the WB analysis, a faint band around 50 kDa, corresponding to the molecular weight of the CCHFV G<sub>NE</sub>-GST protein (46 kDa), can be detected in the supernatant fraction (Figure 3.9). This protein was successfully purified by affinity chromatography and can be observed at a higher concentration in the elution fractions. This band was not visible in the SDS-PAGE followed by Coomassie staining.

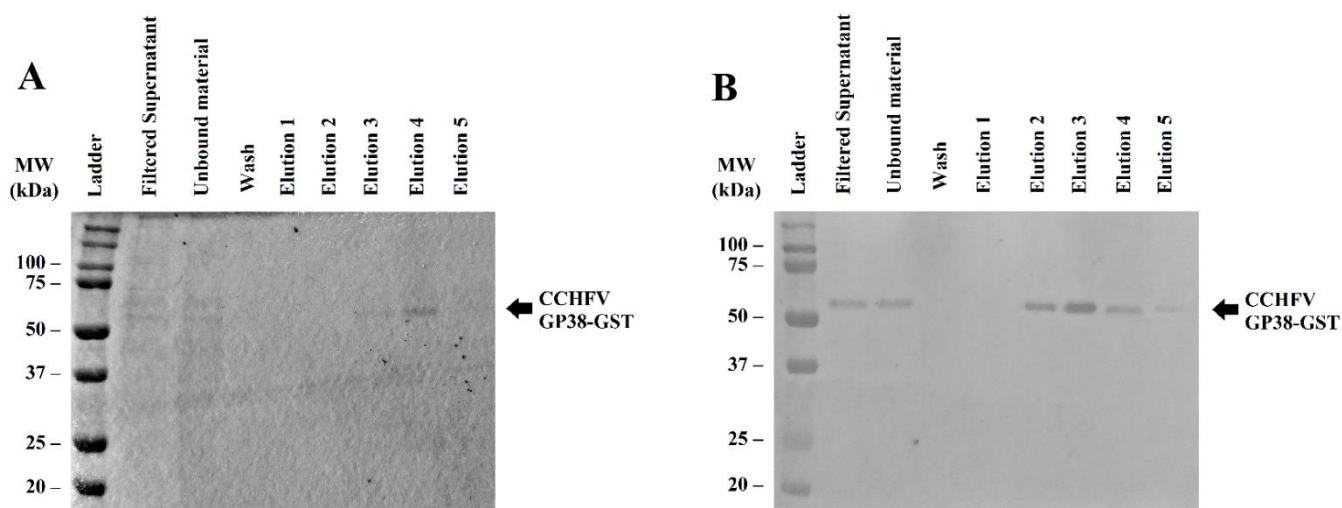
In Figure 3.10A, a band corresponding to the molecular weight of CCHFV GP38-GST was detected in the elution fractions 3 and 4 on the SDS-PAGE followed by Coomassie staining of the purification by affinity chromatography. This purification was confirmed by WB and the observable bands corresponded to CCHFV GP38-GST (Figure 3.10B).

Both recombinant proteins were concentrated after their dialysis and stored at -80°C for further use.



**Figure 3.9 CCHFV G<sub>Ne</sub>-GST protein purification by affinity chromatography.**

The CCHFV G<sub>Ne</sub>-GST (MW = 46 kDa) was purified from the supernatant of Sf900 cells infected with BacPAK6 CCHFV G<sub>Ne</sub> by affinity chromatography with an anti-GST mAb and eluted by addition of 0.1 M glycine hydrochloride, pH 2.6. The purification was analysed by Western blot with an anti-GST mAb used as primary antibody. Arrows indicate the bands corresponding to the specified proteins.



**Figure 3.10 CCHFV GP38-GST protein purification by affinity chromatography.**

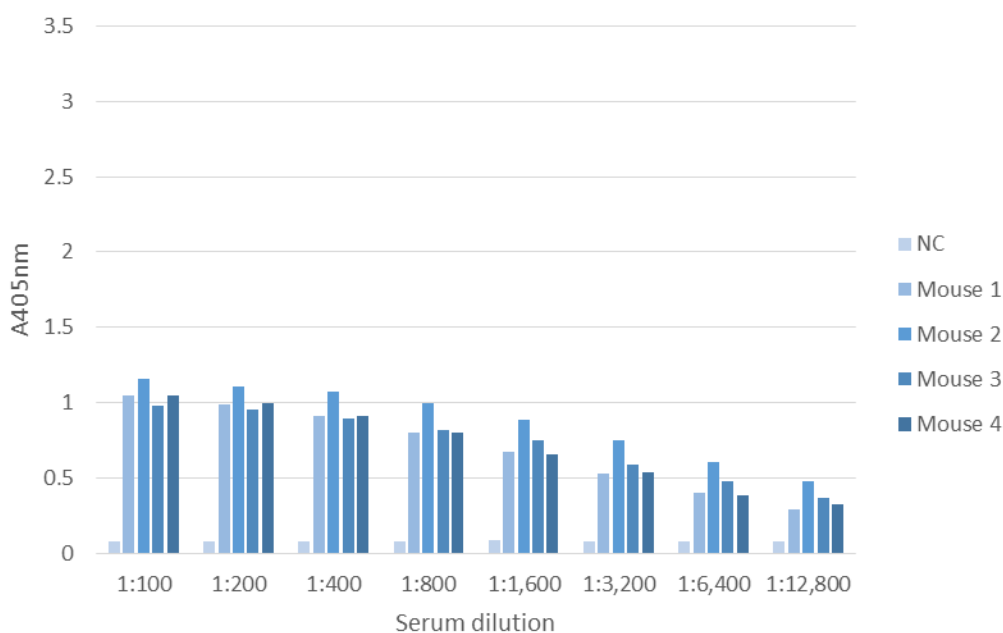
SDS-PAGE analysis followed by Coomassie staining (A) and Western blot analysis (B) of the different samples collected during the purification of CCHFV GP38-GST (MW = 58 kDa). The CCHFV GP38-GST was purified from the supernatant of Sf900 cells infected with BacPAK6 CCHFV GP38, by affinity chromatography with an anti-GST mAb and eluted by addition of 0.1 M glycine hydrochloride, pH 2.6. An anti-GST mAb was used as primary antibody for the Western blot analysis. Arrows indicate the bands corresponding to the specified proteins.

### 3.4. Production, purification and characterization of monoclonal antibodies against CCHFV N protein

#### 3.4.1. Production of the monoclonal antibodies against CCHFV N protein

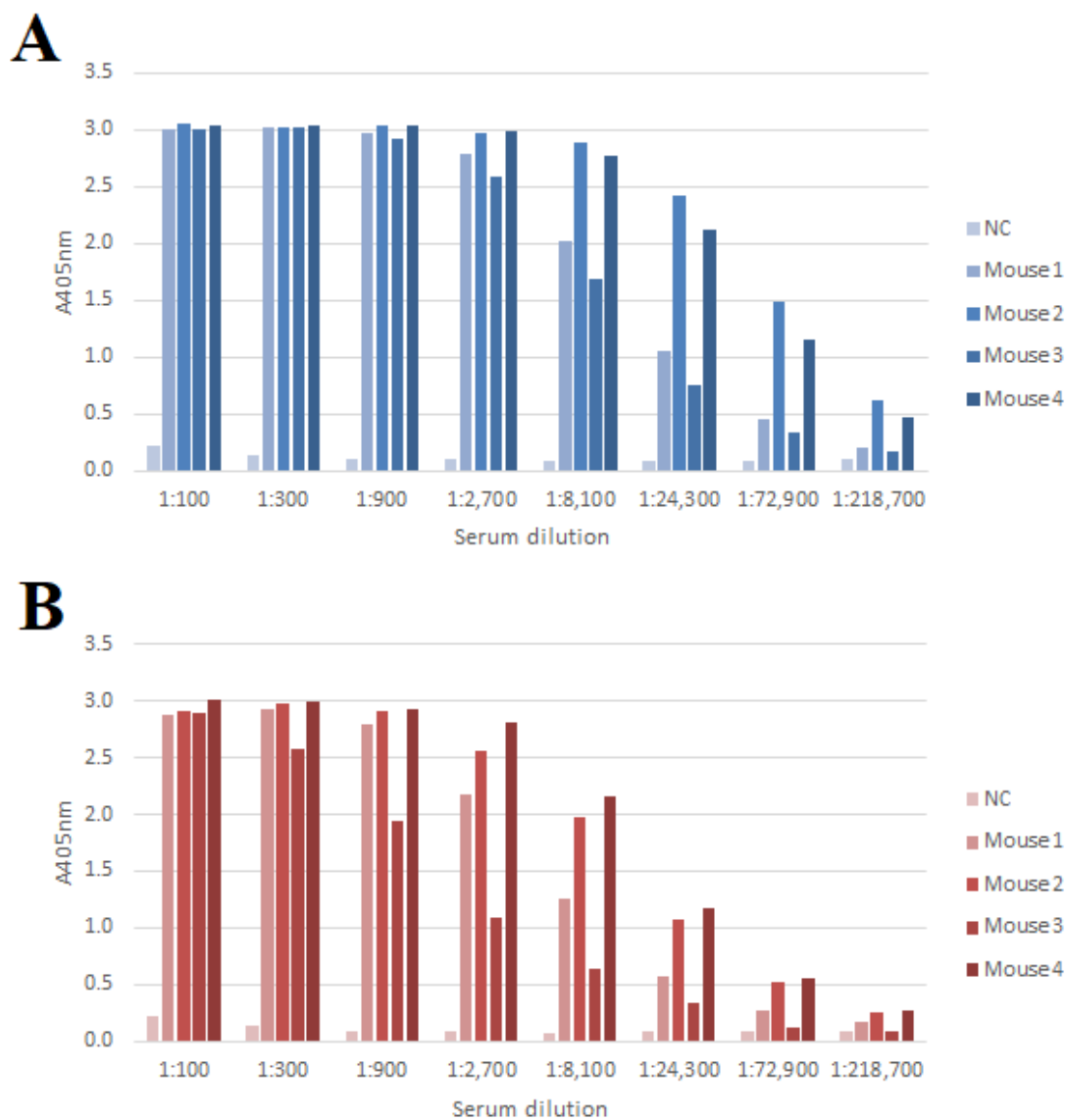
To produce monoclonal antibodies against the CCHFV N protein, a group of 4 mice was immunized with the purified 6xHis-SUMO-CCHFV N protein. A week after the third immunization, and after each subsequent immunization, the mice were bled from the tail and their antibody titre was checked by indirect ELISA coated with the 6xHis-SUMO-CCHFV N protein (Figure 3.11). At Eurofins-Ingenasa, the standard antibody titre that should be reached by indirect ELISA to perform the fusion with the tested mouse is  $A_{405nm} > 1$  at a serum dilution of 1:60,000. The antibody titre of the four mice after the first three immunizations was not high enough with an  $A_{405nm}$  lower than 1 for all the mice at a 1:800 dilution of their sera. Thus, the mice were immunized every two weeks to increase their antibody titre. After the 10<sup>th</sup> immunization, the overall titre of the mice was checked by indirect ELISA with the protein used for the immunization and a negative control protein (6xHis-SUMO-RVFPV N protein) (Figure 3.12). The titre of all the mice

substantially increased with mouse 2 and mouse 4 exhibiting an  $A_{405\text{nm}}$  between 1 and 1.5 at 1:72,900. However, the titre obtained with the 6xHis-SUMO-RVSV N protein was very high with the signal reaching 0.5 at 1:72,900 for mice 2 and 4. The same titre trend could be observed between the two ELISAs. The titre reached after the 10<sup>th</sup> immunization for mice 2 and 4 was enough to perform the fusion step ( $A_{405\text{nm}} > 1$  at a dilution of 1:60,000), however an extensive screening step with the negative control protein was required to dispose of the antibodies recognizing the 6xHis-SUMO.



**Figure 3.11 Antibody titration by indirect ELISA with 6xHis-SUMO-CCHFV N protein of the mouse sera after three immunizations with 6xHis-SUMO-CCHFV N protein.**

After three immunizations with 6xHis-SUMO-CCHFV N protein, the four mice (Mouse 1, 2, 3 and 4) were bled from the tail and serial dilutions of the sera were used to assess the antibody titre of the mice by indirect ELISA. The indirect ELISA was performed using 6xHis-SUMO-CCHFV N protein as coating antigen and an anti-mouse IgG (H+L) HRP-conjugated pAb as secondary antibody. One mouse used as negative control (NC) was immunized with sterile 1X PBS. All the samples were tested once due to sample volume constraints.



**Figure 3.12** Antibody titration by indirect ELISA of the mouse sera after ten immunizations with 6xHis-SUMO-CCHFV N protein.

After ten immunizations with 6xHis-SUMO-CCHFV N protein, the four mice (Mouse 1, 2, 3 and 4) were bled from the tail and serial dilutions of the sera were used to assess the antibody titre of the mice by indirect ELISA. The indirect ELISA was performed using 6xHis-SUMO-CCHFV N protein (A) or 6xHis-SUMO-RVSV N protein (B) as coating antigen. An anti-mouse IgG (H+L) HRP-conjugated pAb was used as secondary antibody. One mouse used as negative control (NC) was immunized with sterile 1X PBS. All the samples were tested once due to sample volume constraints.

The two mice were sacrificed, their spleens were harvested and the fusion was performed between P3X63Ag8.653 and the collected B cells. From the spleen,  $1.5 \times 10^8$  B cells were purified and to ensure a 4:1 ratio between the B cells and the myeloma cells,  $3.7 \times 10^7$

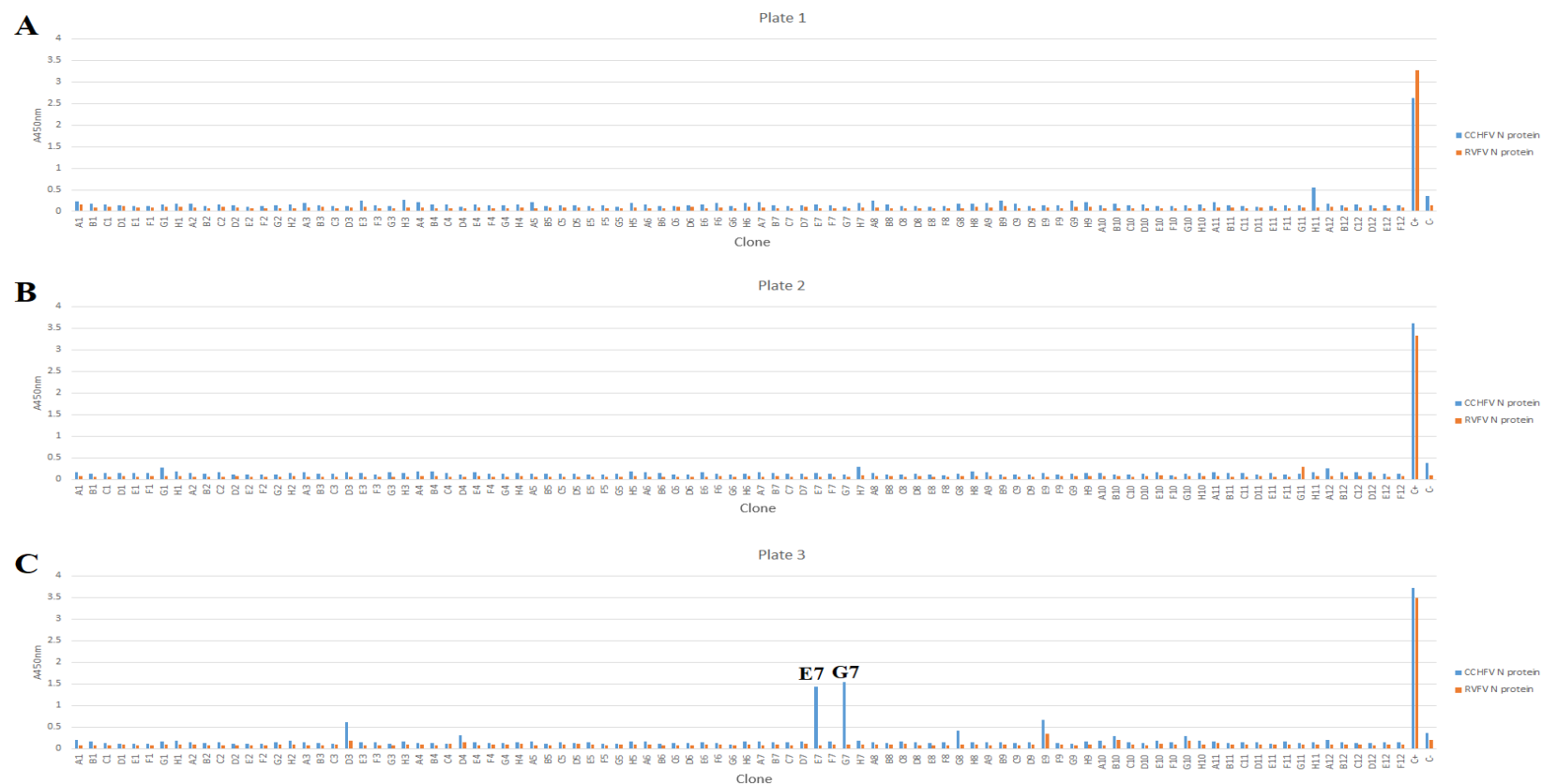
P3X63Ag8.653 were required for the fusion. The fused cells were dispensed into three 96-well plates and incubated. The following day, 2X HAT medium was added to the fused cells and this medium was replaced every 48 hrs. Eighteen days after the fusion, the fused cells were screened by indirect ELISA using purified CCHFV N protein (without tags) and 6xHis-SUMO-RVSV N protein (shorten to RVSV N protein in this part) as shown on Figure 3.13. This first screen was performed with an anti  $\gamma$ -chain specific antibody that only detects IgG and revealed with TMB.

Out of this first screening of the viable hybridomas, only two wells gave a positive signal with  $A_{450nm} > 1$  in the indirect ELISA CCHFV N protein with a low background obtained in the indirect ELISA RVSV N protein. These two wells corresponded to the wells E7 and G7 from the third plate (subsequently called 3E7 and 3G7). The cells in the wells 3E7 and 3G7 were resuspended, counted and aliquoted at 50 cells per well in new 96-well plates. As only two wells were positive during this first screening, a new indirect ELISA was done a few days later to let the hybridomas grow and check if more were positive to the CCHFV N protein.

This second screening (data not shown) was done with an antibody targeting the heavy and light chain (H+L) of IgG but can also react with other antibody classes due to shared light chains between the classes. This ELISA was also developed with TMB to increase sensitivity and revealed 5 new wells (1F1, 1E2, 1B3, 1G4 and 3A11) containing hybridomas positive to CCHFV N protein with an  $A_{450nm} > 1$ . These were also aliquoted at 50 cells per well. Twelve days later, the corresponding seven 96-well plates containing hybridomas at 50 cells/well were screened as described above. Out of the seven plates, only 3G7 and 1G4 showed some positive signals (Figure 3.14).



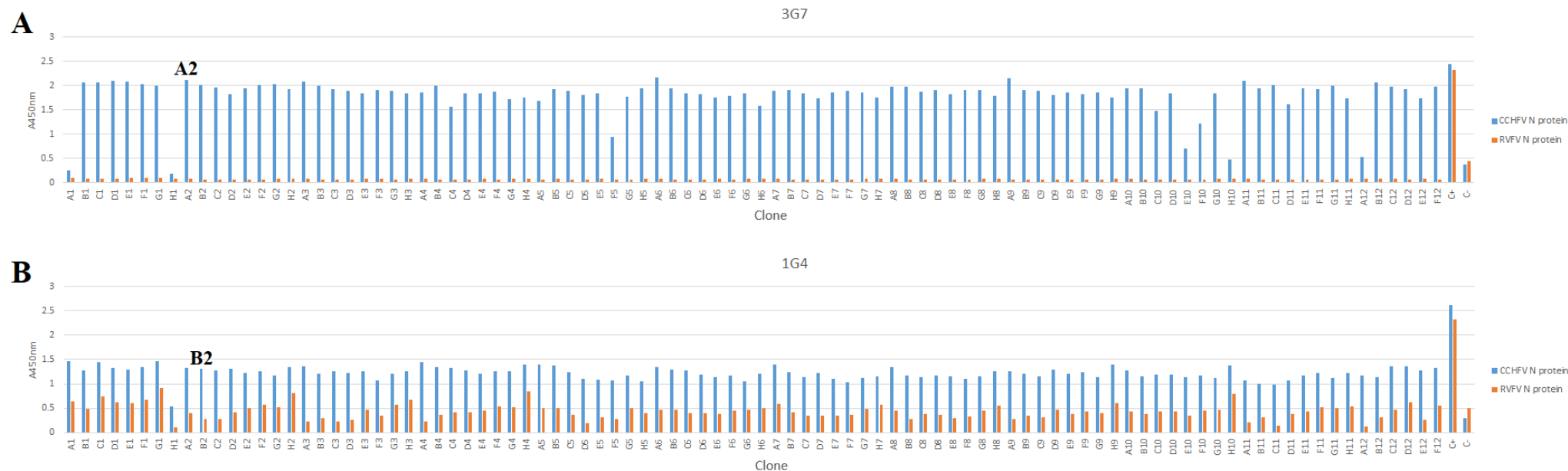
## Chapter 3 Development of diagnostic tools for CCHFV



**Figure 3.13 First screening by indirect ELISA of the three plates containing the hybridoma clones anti-CCHFV N protein.**

Eighteen days after the fusion step, indirect ELISAs with the CCHFV N protein or the 6xHis-SUMO-RVFV N protein as coating antigens and an anti  $\gamma$ -chain specific pAb were performed to select hybridomas positive to the CCHFV N protein. The two wells (E7 and G7 on plate 3) with an  $A_{450nm} > 1$  and no cross-reactivity with the 6xHis-SUMO-RVFV N protein are indicated in bold. A: plate 1; B: plate 2; C: plate 3. The positive control (C+) corresponds to the sera collected from the corresponding euthanized mice and the negative control (C-) to mouse sera against a non-related antigen. All the samples were tested once due to sample volume constraints.

### Chapter 3 Development of diagnostic tools for CCHFV

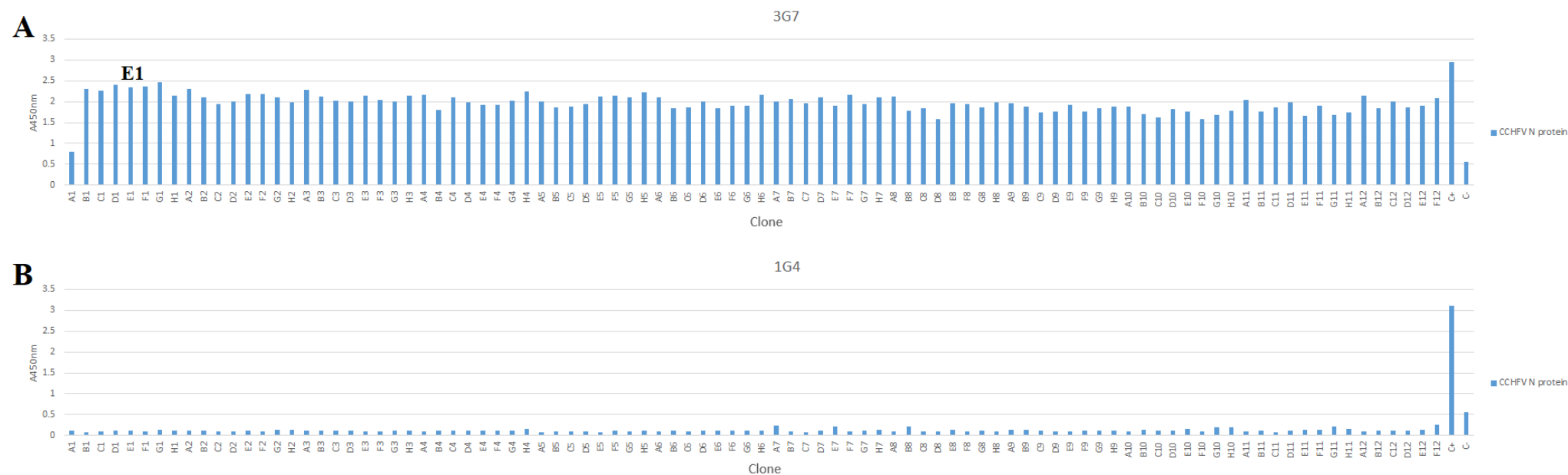


**Figure 3.14 Indirect ELISA screening of the hybridoma clones 3G7 (A) and 1G4 (B) at 50 cells per well with CCHFV N protein and 6xHis-SUMO-RVFV N protein.**

The seven hybridoma clones, selected with the first screening, at 50 cells per well were tested in indirect ELISAs with the CCHFV N protein or the 6xHis-SUMO-RVFV N protein as coating antigens and an anti-heavy and light chain antibody. Out of the seven hybridoma clones, only two (3G7 and 1G4) were positive to the CCHFV N protein. The wells selected from clone 3G7 and 1G4 for further subcloning are indicated in bold. The positive control (C+) corresponds to the sera collected from the corresponding euthanized mice and the negative control (C-) to mouse sera against a non-related antigen. All the samples were tested once due to sample volume constraints.

At 50 cells per well, most of the wells in the 3G7 plate were positive with an  $A_{450nm}$  around 2 and no visible cross-reactivity with the 6xHis-SUMO-RVSV N protein. Regarding the 1G4 plate, most of the wells were also positive with a signal around 1.5, however, some cross-reactivity could be observed with the 6xHis-SUMO-RVSV N protein. The plates 1E2, 1B3 and 1F1 were all negative and the plate 3A11 was negative to CCHFV N protein but highly positive to 6xHis-SUMO-RVSV N protein. The subcloning was continued with the plates 3G7 and 1G4, with the well giving the highest positive to negative ratio: A2 for 3G7 and B2 for 1G4. These wells were aliquoted at 20 cells per well and screened 8 days later (Figure 3.15).

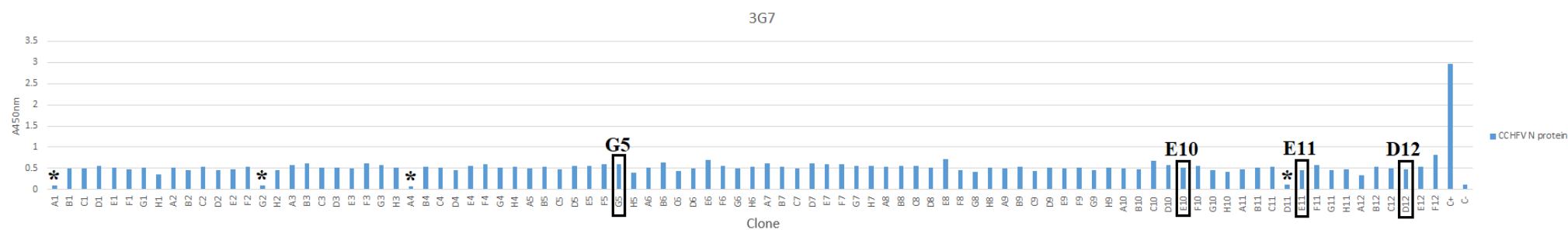
Regarding the 3G7 plate, all the wells exhibited a positive signal with an  $A_{450nm}$  around 2, when all the signals obtained for the 1G4 plate were negative. The leftovers of the subcloning of the 1G4 in the 24 well-plate were also found to be negative to CCHFV N protein. As this plate and the 24 well-plate from 1G4 were negative, this plate was discarded. The hybridomas from the 1G4 plate were probably IgM as these were recognized by an H+L antibody but not by an antibody targeting the  $\gamma$ -chain (see Figure 3.13). The well E1 from the 3G7 plate was further subcloned until reaching 2 cells per well and was then screened (Figure 3.16).



**Figure 3.15 Indirect ELISA screening of the hybridoma clones 3G7 (A) and 1G4 (B) at 20 cells per well with CCHFV N protein.**

The two hybridoma clones at 20 cells per well were tested in indirect ELISAs with the CCHFV N protein as coating antigen and an anti-heavy and light chain antibody. Out of the two hybridoma clones, only 3G7 was positive to the CCHFV N protein. The well selected from clone 3G7 for further subcloning is indicated in bold. The positive control (C+) corresponds to the sera collected from the corresponding euthanized mice and the negative control (C-) to mouse sera against a non-related antigen. All the samples were tested once due to sample volume constraints.

## Chapter 3 Development of diagnostic tools for CCHFV



**Figure 3.16 Indirect ELISA screening of the hybridoma clone 3G7 at 2 cells per well with CCHFV N protein.**

The hybridoma clone 3G7 at 2 cells per well was tested in indirect ELISAs with the CCHFV N protein as coating antigen and an anti-heavy and light chain antibody. Out of the 94 wells, 90 were positive to the CCHFV N protein and 4 were empty, checked using a light microscope (denoted by \*). The wells selected for the mAb production and purification are indicated in bold. The positive control (C+) corresponds to the sera collected from the corresponding euthanized mice and the negative control (C-) to mouse sera against a non-related antigen. All the samples were tested once due to sample volume constraints.

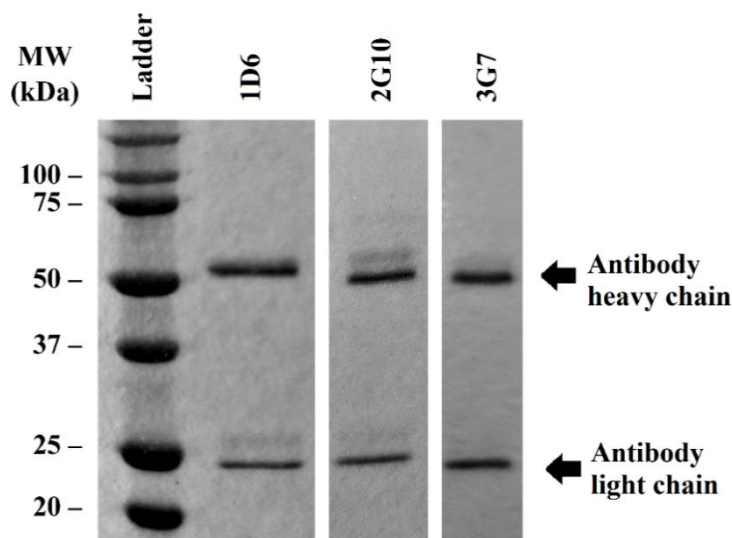
Out of the 94 wells of the 3G7 plate, 90 gave a positive signal with an  $A_{450\text{nm}}$  around 0.5 and four wells gave a negative signal (A1, G2, A4 and D11). These wells were checked using a light microscope, and found to be empty and all the other 90 positive wells contained one or two hybridoma clones, meaning that single hybridoma clones were obtained expressing the same monoclonal antibody. The wells G5, E10, E11 and D12 contained a unique hybridoma clone, which was resuspended and transferred into a 6-well plate for further growth and monoclonal antibody production.

A second fusion was done with mice immunized with purified CCHFV N protein without any tags to obtain other monoclonal antibodies. This second fusion, done with mouse myeloma cell line SP2/0-Ag14, yielded two other monoclonal antibodies: 2G10 and 1D6.

The anti-CCHFV N protein mAbs obtained were named 3G7, 2G10 and 1D6.

### **3.4.2. Purification of the monoclonal antibodies**

To obtain pure and concentrated monoclonal antibodies, the supernatant of the hybridomas had to be purified. The supernatant of the clones 3G7, 2G10 and 1D6 were centrifuged, filtered and purified by affinity chromatography using their affinity for Protein A and Protein G. After their purification and dialysis, the purity of the monoclonal antibodies was assessed by SDS-PAGE followed by Coomassie staining (Figure 3.17).



**Figure 3.17 Anti-CCHFV N protein mAbs purification by affinity chromatography.** SDS-PAGE analysis followed by Coomassie staining of the three different anti-CCHFV N protein mAbs (1D6, 2G10 and 3G7) produced by hybridoma technology. Arrows indicate the bands corresponding to the specified proteins.

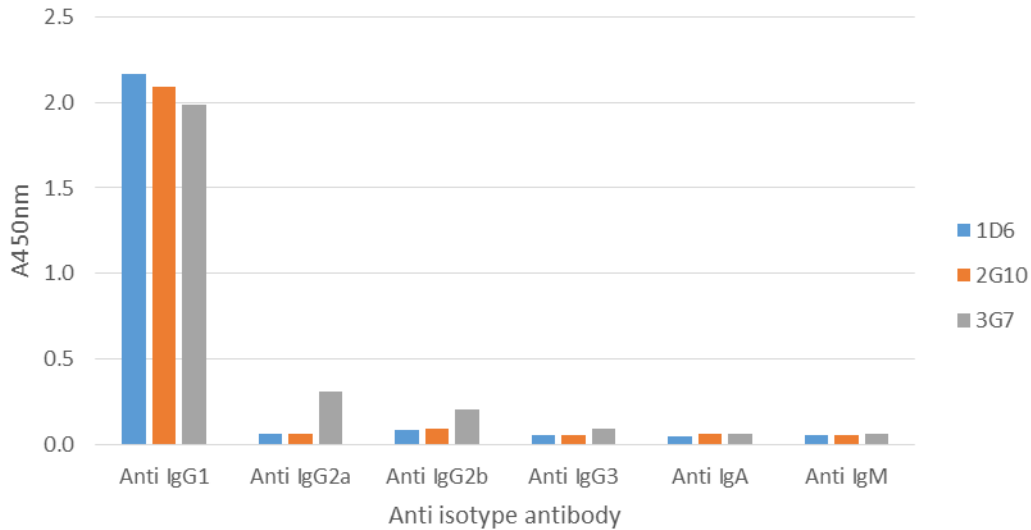
On the SDS-PAGE gel, two bands could be observed for each monoclonal antibody, one around 25 kDa and the second around 50 kDa. The lower band corresponded to the light chain of IgG (25 kDa) and the higher band corresponded to the heavy chain (50 kDa). The mAbs obtained from the hybridoma supernatants were highly pure and were then quantified by spectrophotometry.

The three mAbs were then labelled with horseradish peroxidase. Labelled and unlabelled mAbs were further characterized.

### 3.4.3. Characterization of the monoclonal antibodies

Different techniques were used to characterize the anti-CCHFV N protein mAbs produced.

First, the determination of their isotype was done by performing an ELISA using anti-isotype secondary antibodies (Figure 3.18).

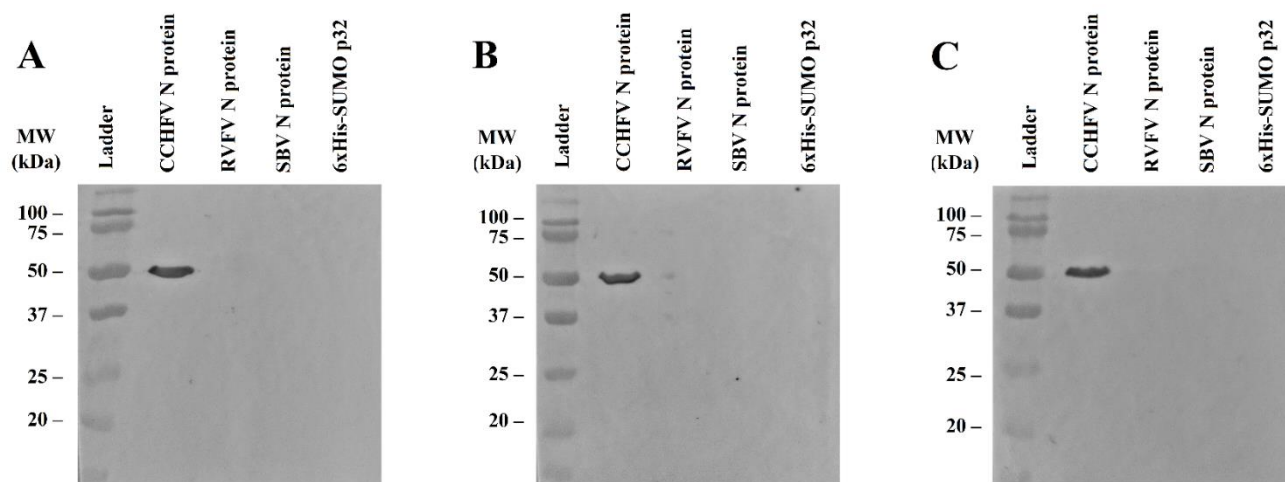


**Figure 3.18 Determination of the isotype of the anti-CCHFV N protein mAbs produced.**  
 An indirect ELISA was performed with the three anti-CCHFV N protein mAbs (1D6, 2G10 and 3G7) and secondary anti-isotypes antibodies to determine the isotypes of the mAbs. The experiment was performed once.

The three mAbs 1D6, 2G10 and 3G7 were recognized by the antibody targeting IgG1 and none of the other anti-isotype antibody reacted with the mAbs, although some cross-reactivity could be observed with mAb 3G7 for IgG2a and IgG2b. The three anti-CCHFV N protein mAbs belong to the IgG1 isotype.

A WB analysis was done with the mAbs to determine if they could recognize specifically the CCHFV N protein in reducing condition. The WBs were done with other nucleocapsid proteins of bunyaviruses produced during this thesis (RVFV N protein and SBV N protein) and a control protein with a 6xHis-SUMO tag (African swine fever virus p32, available at Eurofins-Ingenasa). The proteins were loaded at 0.5  $\mu$ g and the mAbs were used at 10  $\mu$ g/mL (Figure 3.19).



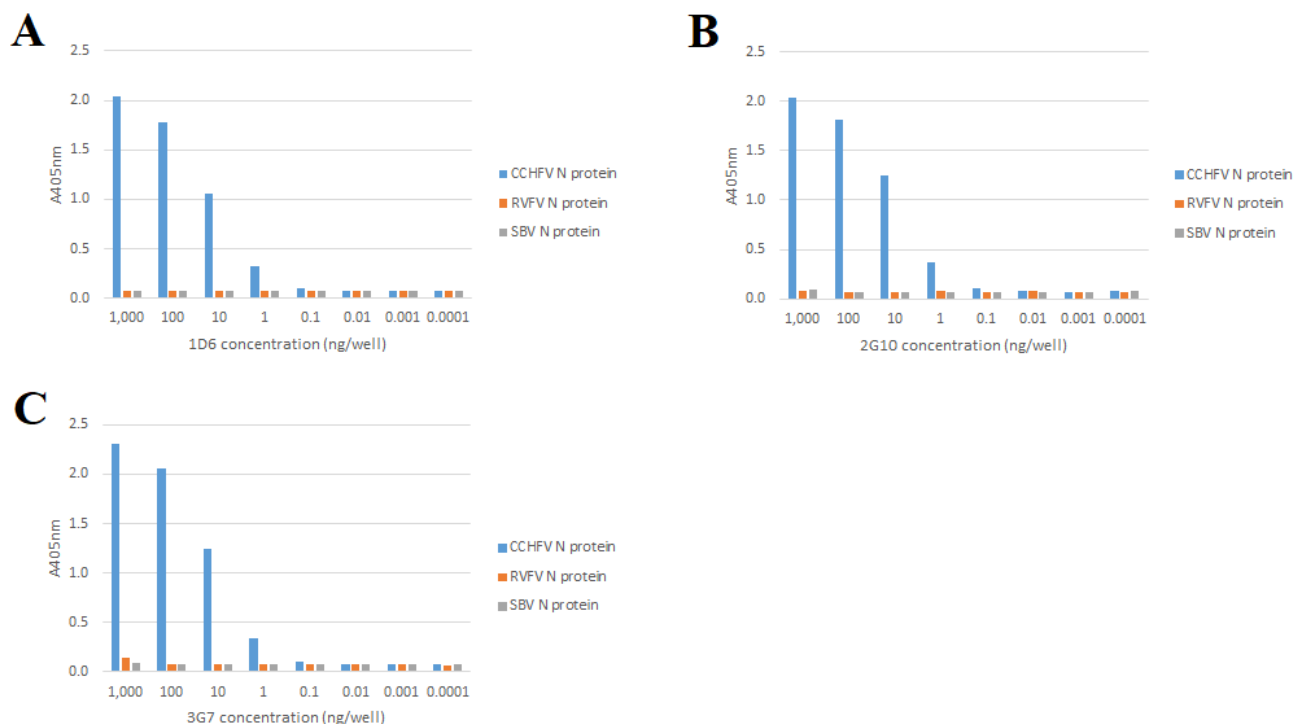


**Figure 3.19** Analysis of the specificity of the three anti-CCHFV N protein mAbs in denaturing and reducing conditions.

A Western blot analysis of different nucleocapsid proteins of bunyaviruses (CCHFV, RVFV and SBV N proteins) was performed with the three different anti-CCHFV N protein mAbs (A: mAb 1D6, B: mAb 2G10, C: mAb 3G7). The 6xHis-SUMO p32 was used as a negative control protein with the 6xHis-SUMO purification tag.

On the three WBs, a band corresponding to the size of the CCHFV N protein was observed with the three different mAbs. No cross-reactivity was detected with the N proteins of RVFV and SBV and neither with the 6xHis-SUMO p32. Thus, the mAbs were specific and could recognize the CCHFV N protein in denaturing and reducing conditions, which could hint that the anti-CCHFV N protein mAbs recognize non-conformational epitopes.

An indirect ELISA with the anti-CCHFV N protein mAbs was performed to titre the mAbs against the different proteins of bunyaviruses (CCHFV, RVFV and SBV) and to determine the LOD of these mAbs (Figure 3.20).

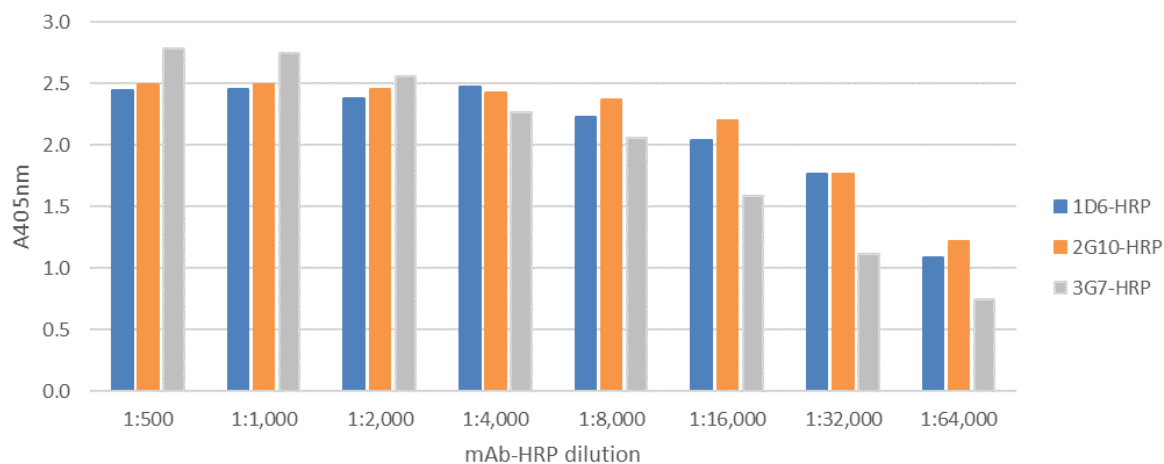


**Figure 3.20 Titration of the anti-CCHFV N protein mAbs.**

*CCHFV, RVFV and SBV N proteins were used to coat ELISA plates and indirect ELISAs were performed with serial dilutions of the anti-CCHFV N protein mAbs (A: 1D6; B: 2G10; C: 3G7) to determine their limit of detection. The experiment was performed once.*

In these indirect ELISAs, the titration of the anti-CCHFV N protein mAbs revealed a decrease of the signal of the three mAbs when their concentration per well decreased. At 1 ng/well (corresponding to a concentration of 10 ng/mL), the signal obtained with the mAbs with the CCHFV N protein could be differentiated from the one obtained with the RVFV and SBV N proteins. Moreover, as in the WB, no-cross reactivity could be detected with the RVFV and SBV N proteins. This assay confirmed the specificity of the mAbs for the CCHFV N protein in non-reducing conditions compared to the control proteins and the three mAbs can detect the CCHFV N protein until 10 ng/mL.

After this titration of the unlabelled mAbs, the same assay was performed with the HRP-conjugated mAbs by direct ELISA, to confirm the successful labelling of the mAbs and to titre them. As no-cross reactivity was present in the previous ELISA with other N proteins, this titration was only performed with the CCHFV N protein (Figure 3.21).

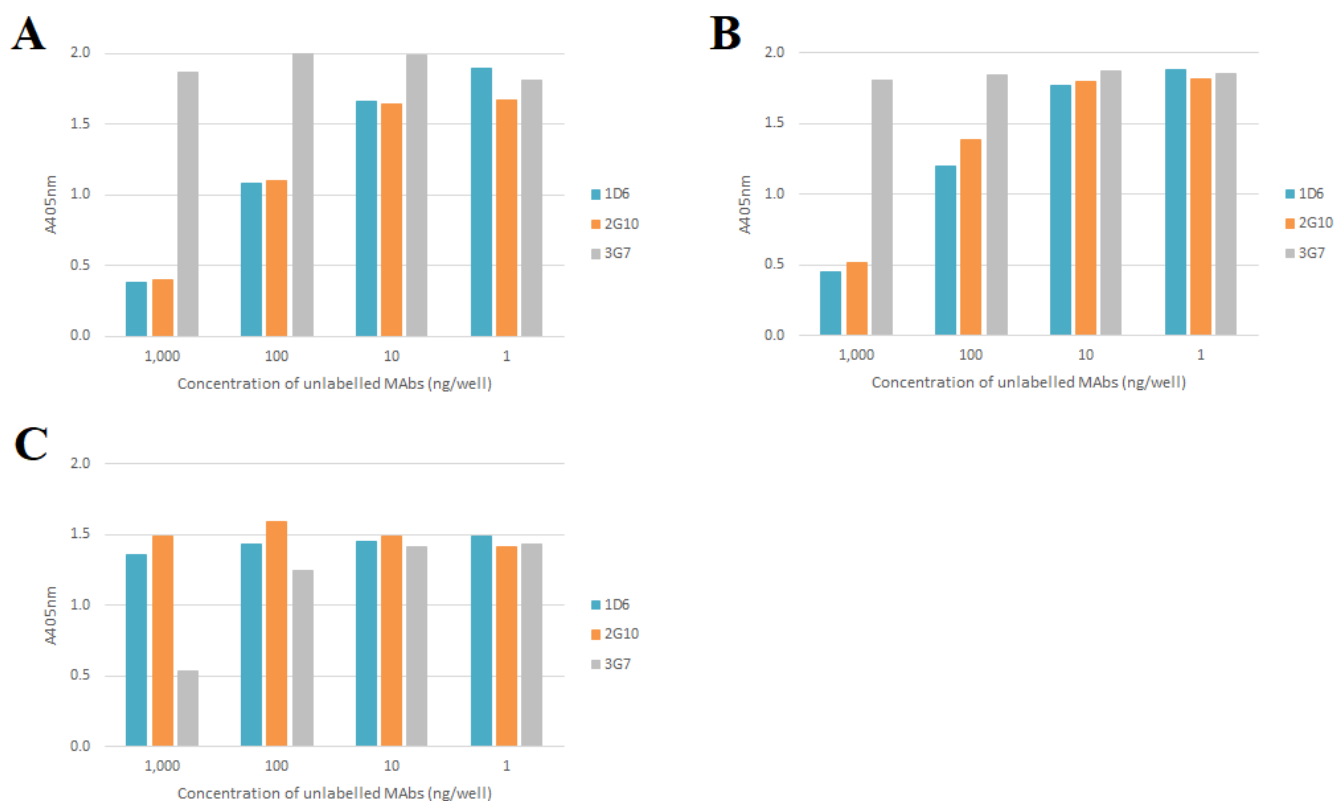


**Figure 3.21 Titration of the HRP-labelled anti-CCHFV N protein mAbs.**

Direct ELISAs were performed with the CCHFV N protein and serial dilutions of HRP-labelled anti-CCHFV N protein mAbs (1D6-HRP, 2G10-HRP and 3G7-HRP) as primary antibodies. The experiment was performed once.

The signal obtained for the three mAbs confirmed the conjugation was successful. The three mAbs showed a decrease in the signal obtained when decreasing their concentration. The mAbs 1D6 and 2G10 showed almost the same titration pattern, with a decrease in the signal obtained after 1:4,000 and an A<sub>405nm</sub> around 1 at a 1:64,000 dilution. The signal obtained with mAb 3G7 decreased at a lower dilution (after 1:1,000) and faster than the two other mAbs, with an A<sub>405nm</sub> around 1 at a 1:32,000 dilution. For the next assay, the conjugated mAbs were used at a concentration to obtain an A<sub>405nm</sub> around 2, which corresponded to a dilution of 1:16,000 for mAbs 1D6 and 2G10 and of 1:8,000 for 3G7.

In order to determine if the three anti-CCHFV N protein mAbs produced mapped in the same epitopes of the protein, a competition ELISA was performed between the unlabelled mAbs and the HRP-conjugated mAbs (Figure 3.22).



**Figure 3.22** Determination of the mapping of anti-CCHFV N protein mAbs for the same epitopes.

Competition ELISAs were performed between the unlabelled and labelled anti-CCHFV N protein mAbs to check if they competed for the same epitopes. A: Competition ELISA with mAb 1D6-HRP at 1:16,000. B: Competition ELISA with mAb 2G10-HRP at 1:16,000. C: Competition ELISA with mAb 3G7-HRP at 1:8,000. The experiment was performed once.

Regarding the competition ELISA with 1D6-HRP, the signal obtained with both 1D6 and 2G10 at 1,000 ng/well was around 0.5 and increased when the concentration of these two mAbs decreased, to reach around 1.5 at 10 and 1 ng/well. Thus, there is a signal inhibition between 1D6 and itself and between 1D6 and 2G10. The same result can be observed between 2G10 and itself and 2G10 and 1D6. Finally, regarding 3G7, no signal increase could be observed with 1D6 and 2G10, but one could be observed for 3G7. 3G7 competed with itself at a high concentration but not with the other mAbs. This competition assay showed that 1D6 and 2G10 seemed to map the same epitope of the CCHFV N protein.

Table 3.3 summarizes the mAbs obtained and some of their characteristics that were determined in this chapter.

*Table 3.3 Summary of the characteristics of the anti-CCHFV N protein mAbs obtained.*

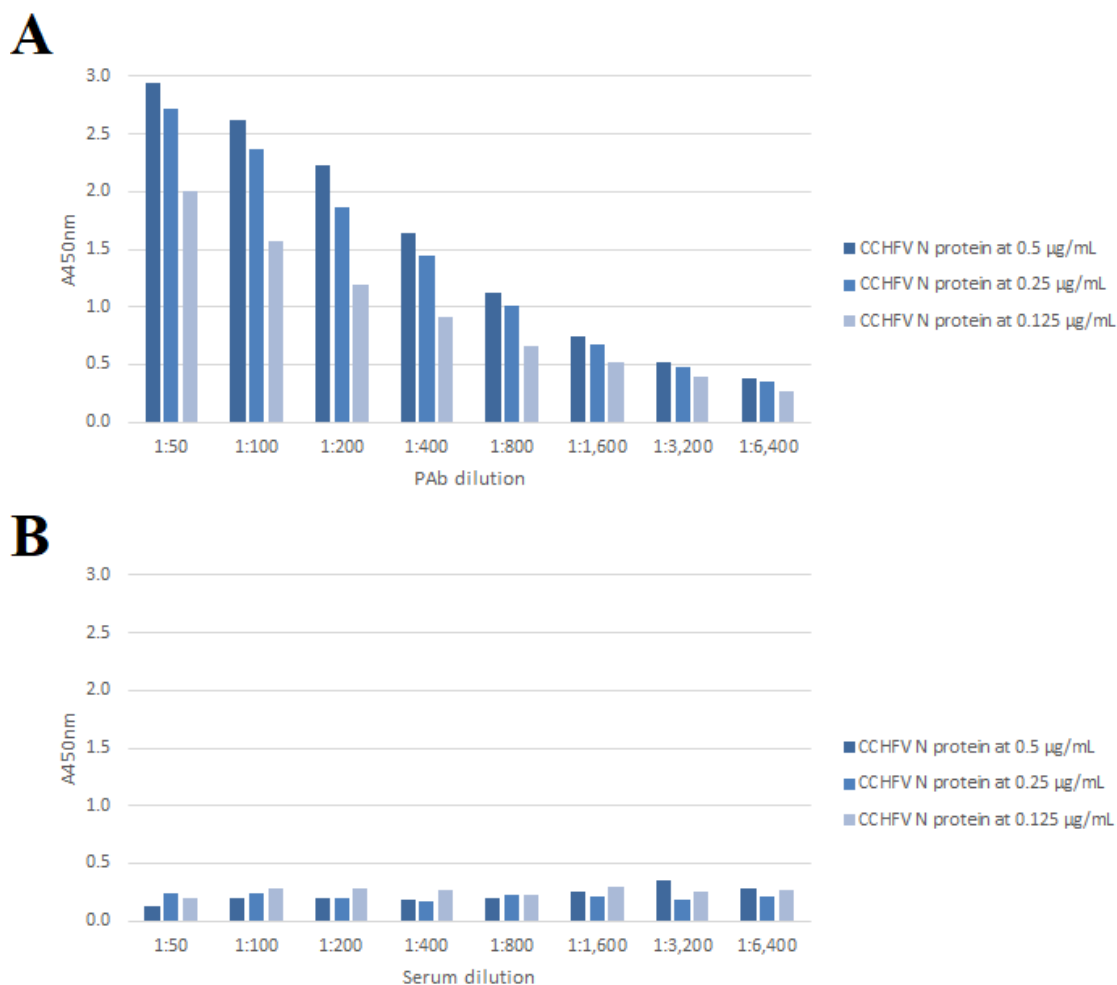
<b>mAbs anti-CCHFV N protein</b>	<b>Isotype</b>	<b>CCHFV N protein identification in reducing conditions</b>	<b>Concentration of mAb detecting CCHFV N protein in non-reducing conditions</b>	<b>Titre of HRP-mAbs to obtain an <math>A_{405nm} \approx 2</math></b>	<b>Competition for the same epitope</b>
1D6	IgG1	Yes	10 ng/mL	1:16,000	Yes, with 2G10
2G10	IgG1	Yes	10 ng/mL	1:16,000	Yes, with 1D6
3G7	IgG1	Yes	10 ng/mL	1:8,000	No

### **3.5. Development of a double recognition ELISA to detect antibodies against CCHFV**

The WHO highlighted the lack of commercial serological assays detecting human IgM and IgG against CCHFV and the lack of diagnostic assays to detect antibodies to CCHFV in different animal species. Thus, to answer these needs, a double recognition ELISA was developed using the CCHFV N protein as the target antigen. This assay is a multi-species test that can detect total antibody response (IgM and IgG) in serum. The first step of this development was the labelling of CCHFV N protein with HRP, then the optimization of the assay and finally the validation of the assay with positive and negative field samples.

#### **3.5.1. Labelling of CCHFV N protein**

As for the anti-CCHFV N protein mAbs, the CCHFV N protein was conjugated to HRP to be used as the detection molecule in this double recognition ELISA. To confirm the labelling of the HRP, a double recognition ELISA was performed with CCHFV N protein coated in the 96-well plates and a mouse pAb obtained from the blood of the mice immunized with the CCHFV N protein. This pAb was titrated and detected by the newly labelled CCHFV N protein at 1:10,000 (Figure 3.23).



**Figure 3.23 Confirmation of the labelling of CCHFV N protein with HRP.**

A double recognition ELISA was performed with different concentrations of CCHFV N protein as coating molecule and CCHFV N protein-HRP as detection molecule diluted at 1:10,000. A: serial dilutions of the sera of euthanized mice immunized with CCHFV N protein (pAb) was used as positive sera. B: serial dilutions of mouse sera against a non-related antigen was used as negative sera. The experiment was performed once.

At a 1:50 dilution of the pAb, an  $A_{450\text{nm}}$  of 3 was detected with the plates coated with CCHFV N protein at 0.5 µg/mL. This signal was lower for the plates coated with 0.25 µg/mL ( $A_{450\text{nm}} \approx 2.7$ ) and 0.125 µg/mL ( $A_{450\text{nm}} \approx 2$ ). This signal decreased when the pAb was further diluted. In comparison, when diluting negative mice serum (immunized with PBS), only background signal could be observed with the different serum dilution and the different coatings.

This assay showed the correct labelling of the CCHFV N protein with HRP, which, diluted at 1:10,000 was able to detect the pAb anti-CCHFV N protein bound to the

CCHFV N protein immobilized on the plate. Then, the optimal conditions of the double recognition ELISA had to be determined.

### 3.5.2. Serum samples

In this study, for the development of the double recognition ELISA, the panel of serum samples consisted in 72 positive field samples and 410 negative field sera. For detection of antibodies to CCHFV, 33 field serum samples from cattle, 31 from sheep, 5 from horses and 3 from goats naturally infected by CCHFV were provided by the Faculty of Veterinary Medicine in Skopje (USCM, North Macedonia) and all these sera were tested at INIA-CISA in a BSL-3 laboratory.

A collection of 410 negative field samples (208 from cattle, 146 from sheep, 54 from goats and 7 from horses) from Spanish farms were evaluated.

All these samples were assayed in the ID Screen® CCHF Double Antigen Multi-species (IDVet), used as the reference technique for the development of this assay, and were classified as positive and negative according to the results obtained. A summary of the classification is detailed in Table 3.4.

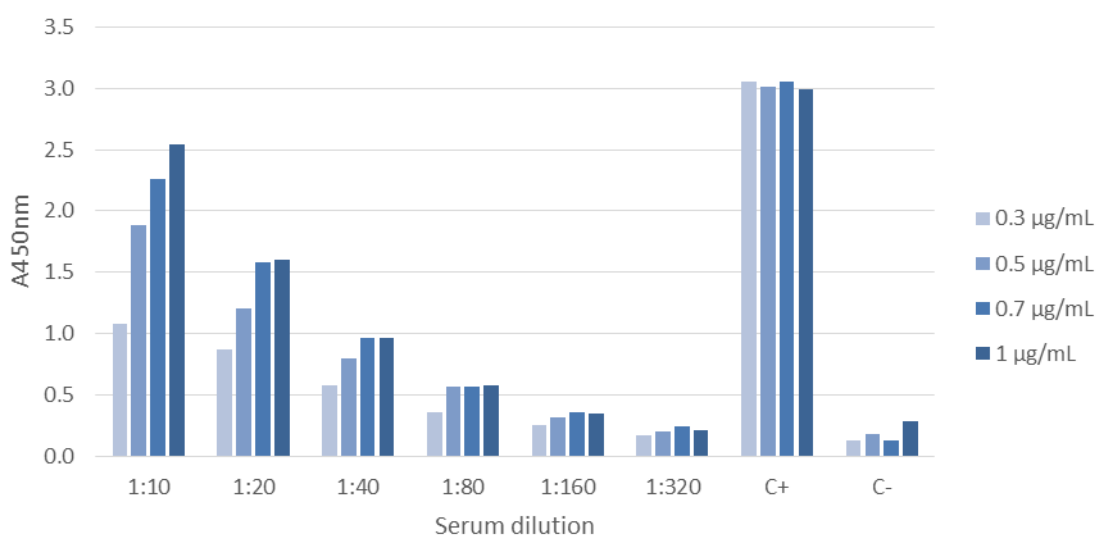
*Table 3.4 Classification of the serum samples used to develop the double recognition ELISA to detect antibodies against CCHFV.*

<b>Samples</b>	<b>Cattle</b>	<b>Sheep</b>	<b>Goat</b>	<b>Horse</b>	<b>Total</b>
Positive	33	31	3	5	72
Negative	208	146	54	2	410
Total	241	177	57	7	482

### 3.5.3. Optimization of the double recognition ELISA

The optimal conditions of the double recognition ELISA such as coating concentration, the serum dilution and its dilution buffer, the detection molecule dilution and its buffer and the times of incubation were determined.

To optimize the condition of the assay, an inactivated cow CCHFV positive serum sample was provided by INIA-CISA. This sample was confirmed to be positive by ID Screen® CCHF Double Antigen Multi-species (IDVet). First, this positive serum sample was titrated in DB1 with different concentration of CCHFV N protein coated and one concentration of CCHFV N protein-HRP (at 1:10,000 in DB4). The results of this first titration can be found in Figure 3.24. The positive control (C+) was the anti-CCHFV N protein pAb and the negative control (C-) the negative mouse serum, both diluted at a 1:200 in DB1.



**Figure 3.24 Titration of the CCHFV positive field serum in double recognition ELISA.**

*Different coating concentrations of CCHFV N protein (from 0.3 µg/mL to 1 µg/mL) have been used with serial dilutions of the CCHFV positive field serum and the CCHFV N protein-HRP at 1:10,000 as detection molecule. All the samples were tested once due to sample volume constraints.*

The signal obtained in this double recognition ELISA increased with increasing concentrations of CCHFV N protein used to coat the plates. The optimal signal obtained was at a coating concentration of 1 µg/mL. However, this signal was only higher than 0.7 µg/mL at a 1:10 dilution of the serum. When the serum was further diluted the signals between 0.7 and 1 µg/mL were equivalent. Thus, the best coating condition seemed to be using a concentration of 0.7 µg/mL of CCHFV N protein to capture the antibodies. A

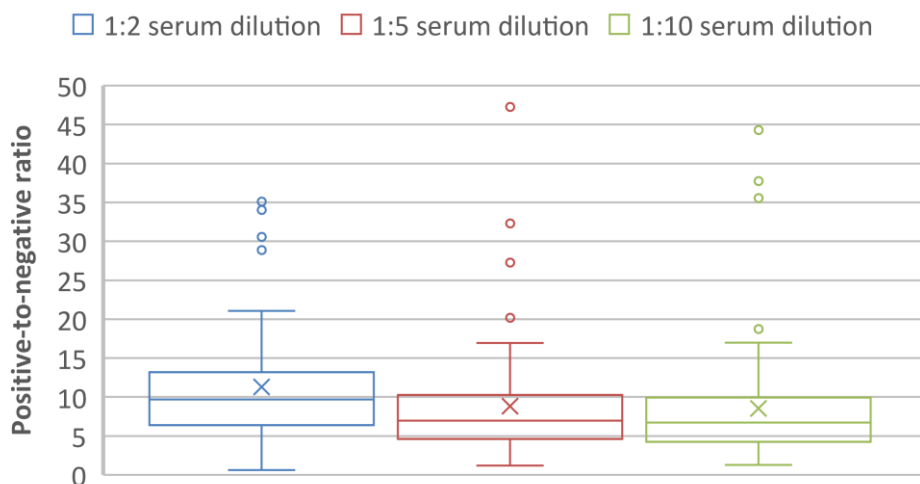


1:20 serum dilution was kept as the provisional serum dilution until the testing of negative serum to check the background at this dilution.

After the first step, establishing the coating conditions and a provisional serum dilution, negative serum samples from cow, sheep and goat were tested (data not shown). This assay showed some high background obtained from some negative serum samples. Out of the 32 cow samples tested, 1 gave some background signal and none of the 26 goat samples gave some background signal. However, the sheep sera tested (30 samples) had a higher background than the cow and goat sera with some of these sera reaching signals close to the positive field sample.

As a consequence, a new dilution buffer (DB2) was tested to dilute the serum samples, which did not affect the signal obtained with the positive sample but did reduce the background signal obtained with the negative serum samples previously tested.

Finally, an assay was done with the coating conditions previously established and the new dilution buffer with different serum dilutions to elect the best serum dilution with these conditions. Some of the negative serum samples which gave some background signal were tested, along with the positive serum sample. The serum dilutions tested were 1:2, 1:5 and 1:10 and the best positive-to-negative ratio was obtained with a 1:2 serum dilution (Figure 3.25).



**Figure 3.25 Serum dilutions tested in the double recognition ELISA.**

Box plot representing the positive-to-negative ratio in the double recognition ELISA at different serum dilution. Twenty-four field negative sera and seventy-five positive field sera were tested once at 1:2, 1:5 and 1:10 dilution and the positive-to-negative ratio was calculated. The lower (Q1) and upper quartile (Q3) represent observations outside the 9 –91 percentile range. The diagram also shows the median (cross) and mean (straight line) observation for a particular dilution. Data falling outside the Q1 – Q3 range are circles plotted outside of the box.

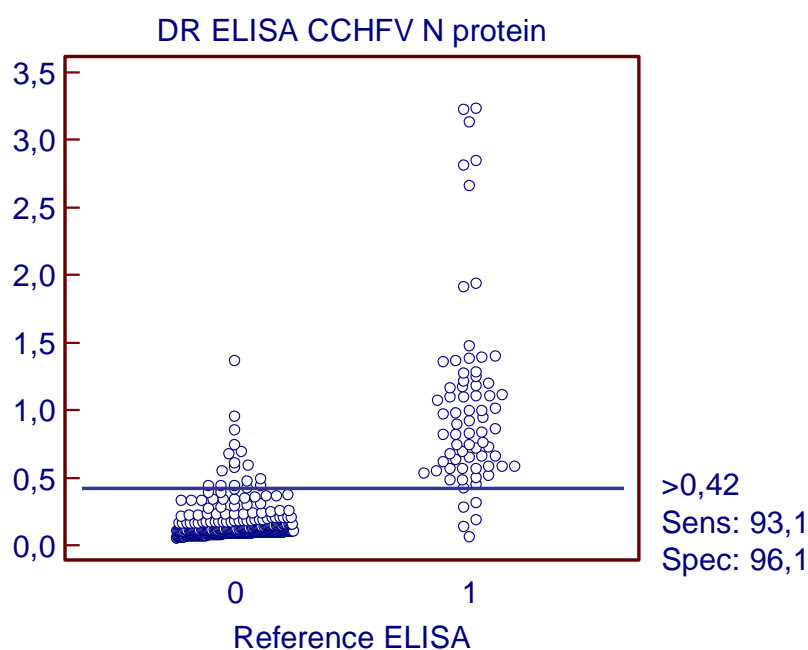
The final conditions of the double recognition ELISA were: a mix of CCHFV N protein at 0.7  $\mu\text{g/mL}$  and BSA at 20  $\mu\text{g/mL}$  in carbonate buffer to coat the ELISA plates, a serum dilution of 1:2 in DB2 and the CCHFV N protein-HRP diluted at 1:10,000 in DB4, as detection molecule.

### 3.5.4. Validation of the double recognition ELISA

Once the conditions were established, the double recognition ELISA was tested at INIA-CISA, with 72 positive field samples to CCHFV and 228 negative field samples. An additional 182 negative field serum samples were tested at Eurofins-Ingensa to increase the number of negative samples and confirm the specificity of the assay. The complete panel of 482 serum samples from different species were assayed once in the double recognition ELISA and the results were statistically analysed by comparison with the results obtained with the reference technique. A cut-off value was determined using the

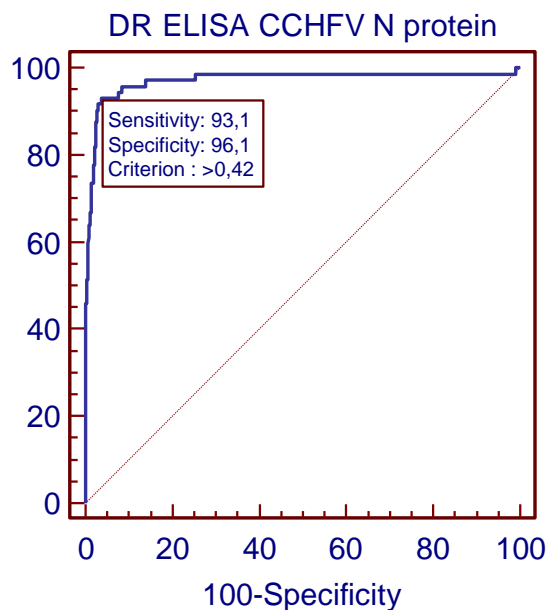
MedCalc® software and based on this cut-off, the performance characteristics of the double recognition ELISA were determined.

The optimal cut-off for the double recognition ELISA developed was  $A_{450\text{nm}}=0.42$  and with this cut-off, out of the 72 positive field samples, 5 were not detected with the double recognition ELISA, corresponding to a sensitivity of 93.1% with a 95% confidence interval between 84.5%-97.7%. Out of the 410 negative field samples tested, 18 had a signal over the cut-off, corresponding to a specificity of 96.1% with a 95% confidence interval between 93.7%-97.8%. This sensitivity could be explained by the probable higher sensitivity of the double recognition assay for IgM than for IgG, due to the assay's design and the high genetic diversity of CCHFV between the different clades. Figure 3.26 shows the dot plot corresponding to the serum tested in this assay and Figure 3.27 the corresponding ROC curve analysis.



**Figure 3.26** Dot plot diagram between the double recognition ELISA CCHFV N protein and the reference technique where each dot represents an individual sample.

The horizontal solid line corresponds to the cut-off value of the assay, according to the MedCalc® 10 software. X axis shows the positive (1) or negative (0) classification of samples according to reference ELISA and Y axis shows the absorbance at 450 nm obtained in the double recognition ELISA. All the samples were tested once due to sample volume constraints.



**Figure 3.27 Receiver operating characteristic curve analysis of the double recognition ELISA CCHFV N protein.**

The blue line shows the mean area under the curve (AUC) plot and the red dotted line corresponds to an AUC of 0.5. The sensitivity and specificity values corresponding to the cut-off are represented on the graph. All the samples were tested once due to sample volume constraints.

Using the MedCalc<sup>®</sup> 10 software, McNemar test was performed to examine the relation between the results obtained in the double recognition ELISA and in the reference assay. The calculated Chi squared equalled 6.26 with a two tailed P-value of 0.0123 which is lower than 0.05, thus there is a significant difference between the two proportions and there is a significant relationship between the 2 assays.

Using the CCHFV N protein, a double recognition ELISA detecting antibodies to CCHFV was developed. This assay exhibited a sensitivity of 93.1% with 72 positive field samples tested and a specificity of 96.1% with 410 negative field samples tested.

### **3.6. Development of a double antibody sandwich ELISA to detect CCHFV N protein**

With the three anti-CCHFV N protein mAbs produced, a double antibody sandwich ELISA was developed to detect CCHFV N protein in serum samples. This assay could

be useful to detect live virus in humans or animals. The first step of the development was the selection of the best pair of mAbs and then determining the minimum concentration of CCHFV N protein the pair could detect. As no acute samples containing CCHFV N protein could be obtained, a proof-of-concept was done by spiking serum samples with the CCHFV N protein.

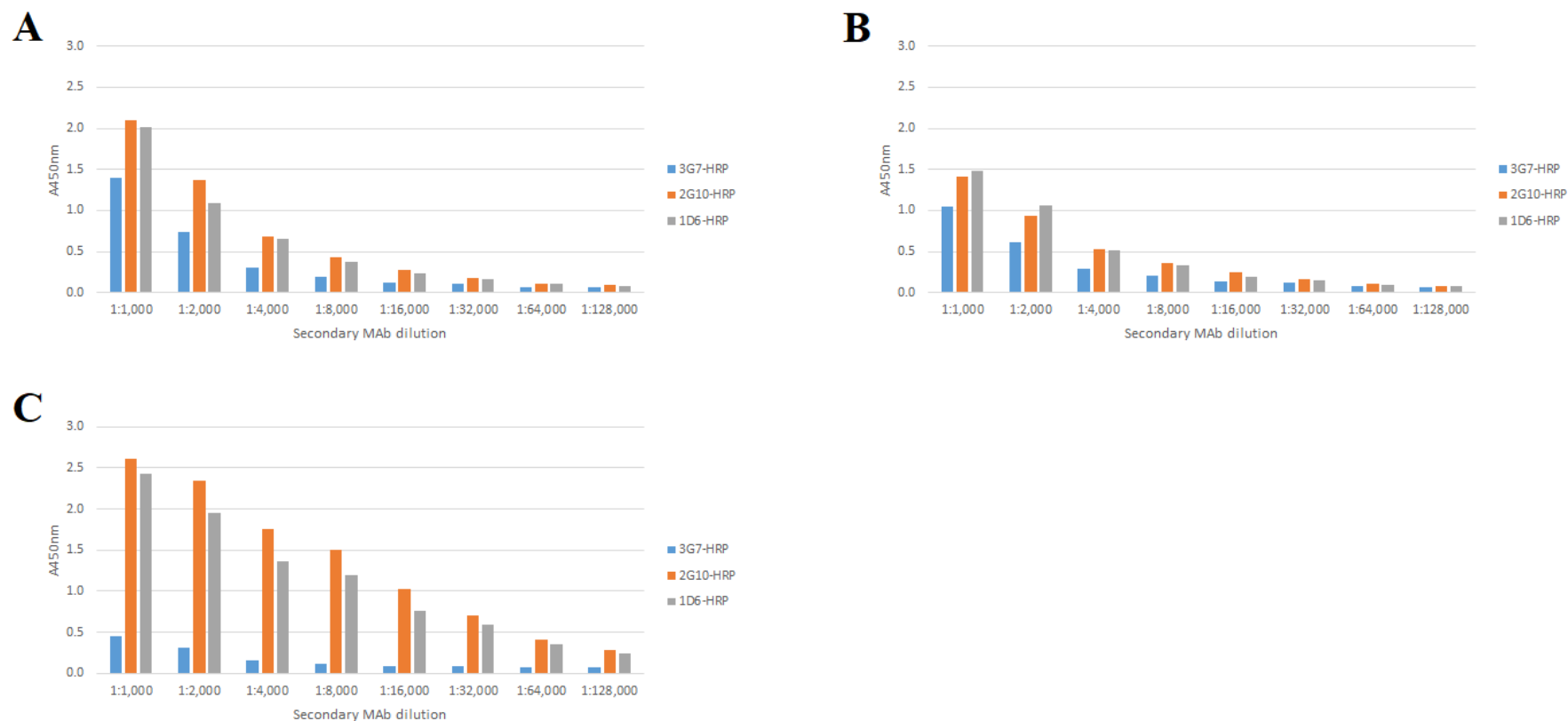
### 3.6.1. Selection of the best pair of mAbs

The aim of the first assay was to assess the different mAbs pairs and select the best couple to develop the double antibody sandwich ELISA.

Different concentrations (at 2, 5 and 10  $\mu\text{g}/\text{mL}$ ) of the three different anti-CCHFV N protein mAbs were coated on ELISA plate. Then, a high concentration of CCHFV N protein (4  $\mu\text{g}/\text{mL}$ ) was added to be captured by the immobilized mAbs. Finally, a titration of the detection mAbs was done. The results of this assay can be observed in Figure 3.28 and Figure 3.29.

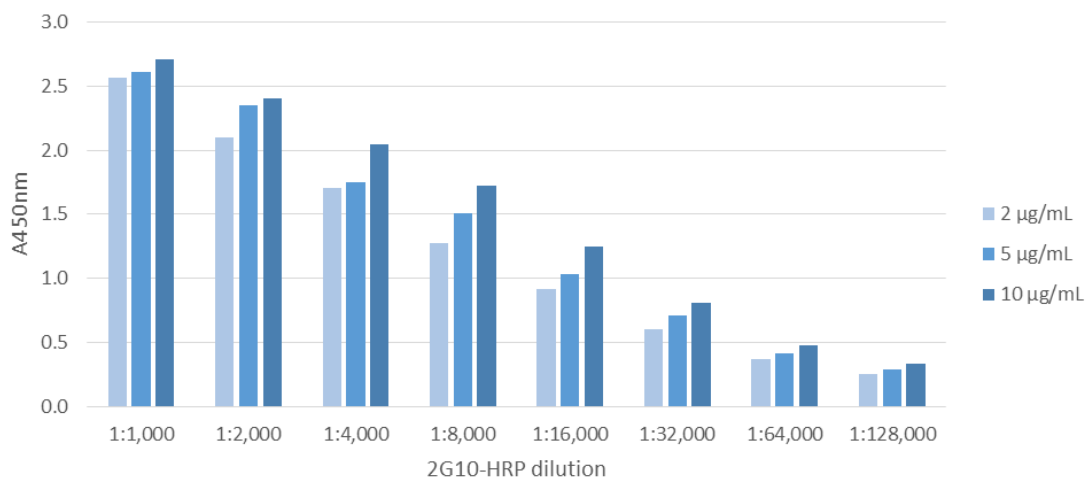
Figure 3.28 shows the nine different pairs of mAbs at a same coating concentration (a coating concentration of 5  $\mu\text{g}/\text{mL}$ ). A significant difference between these nine pairs could be observed. Indeed, at a same secondary mAb concentration, for example at 1:4,000, the two pairs formed with 3G7 as capture molecule and 2G10 and 1D6 as detection molecule had an  $A_{450\text{nm}}$  of 1.7 and 1.35 respectively (Figure 3.28C), when all the other pairs had an  $A_{450\text{nm}}$  around 0.5 or lower (Figure 3.28A, B, C). Thus, two pairs (3G7 with 2G10-HRP and 3G7 with 1D6-HRP) were significantly better than the others to detect the same concentration of CCHFV N protein at a same coating concentration and a given secondary mAb dilution. Out of these two pairs, 3G7 with 2G10-HRP was giving a higher signal than 3G7 with 1D6-HRP at all dilutions.

The results of the different coating concentrations of the best pair of mAbs are shown in Figure 3.29. An increase could be observed between 2  $\mu\text{g}/\text{mL}$ , 5  $\mu\text{g}/\text{mL}$  and 10  $\mu\text{g}/\text{mL}$  of 3G7 coated. The highest signal was observed with 10  $\mu\text{g}/\text{mL}$ , however, to avoid using a high amount of the mAb 3G7, the medium coating condition (5  $\mu\text{g}/\text{mL}$ ) could be used to perform the double antibody sandwich ELISA.



**Figure 3.28 Selection of the best pair of anti-CCHFV N protein mAbs for the double antibody sandwich ELISA.**

Titration of the HRP-labelled anti-CCHFV N protein mAbs in double antibody sandwich ELISA. The different anti-CCHFV N protein mAbs were coated at 5 µg/mL (A: mAb 1D6; B: mAb 2G10; C: mAb 3G7) and the CCHFV N protein was added at 4 µg/mL. The experiment was performed once.



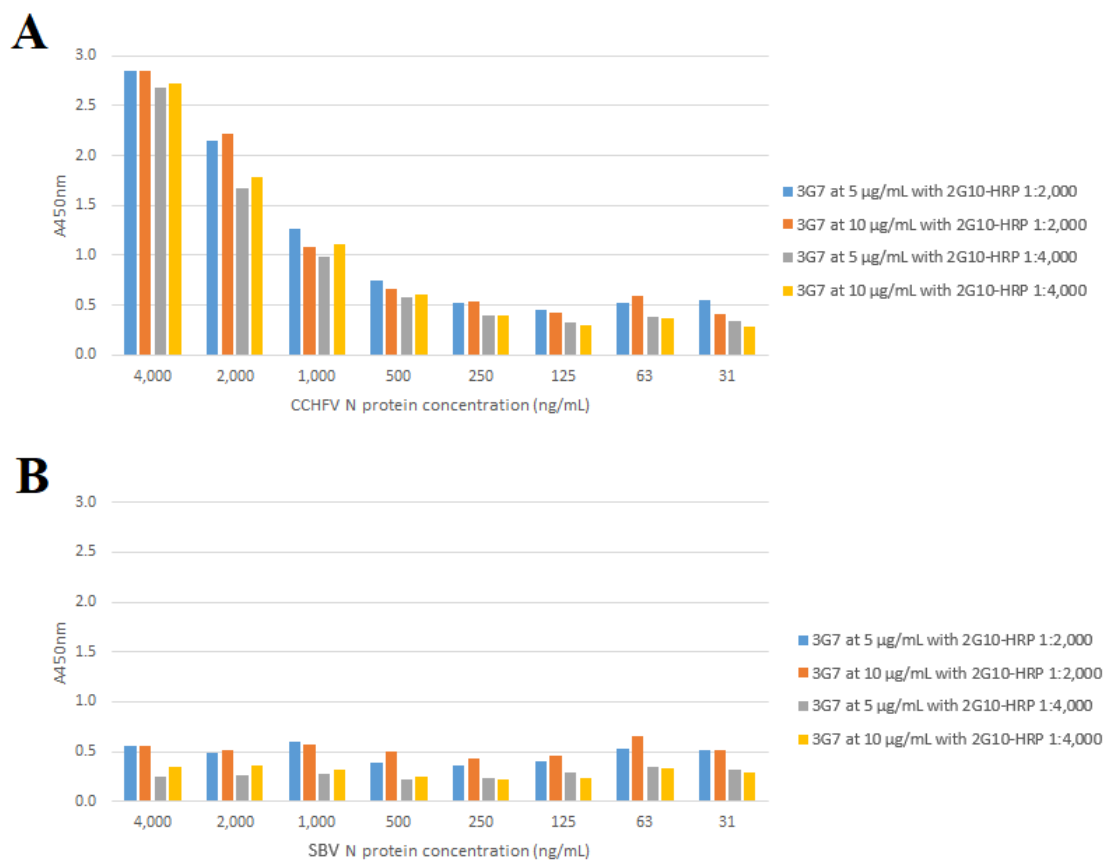
**Figure 3.29 Selection of the best conditions of the double antibody sandwich ELISA.**

The anti-CCHFV mAb 3G7 was used as capture molecule, with different coating concentrations (2, 5 and 10 µg/mL) and serial dilutions of 2G10-HRP were used. The CCHFV N protein was added at 4 µg/mL to saturate the capture antibodies. The experiment was performed once.

### 3.6.2. Optimization of the double antibody sandwich ELISA conditions

With the best mAb pair (3G7 as capture and 2G10-HRP as detector), an assay was performed to determine the best coating conditions (between 5 and 10 µg/mL) and the best detection antibody dilution (1:2,000 or 1:4,000) using serial dilutions of CCHFV and SBV N protein. The results of this assay are displayed in Figure 3.30.

The highest signal was obtained for a dilution at 1:2,000 of the detection antibody (Figure 3.30A). However, at all CCHFV N protein concentrations, the signals obtained were not significantly different. The four conditions detected the titration of the CCHFV N protein with a decrease in the signal obtained until 250 ng/mL where it reached a plateau. When using SBV N protein (Figure 3.30B), no titration of the SBV N protein was observed and only background signal was detected. The ratio between the positive signal (CCHFV N protein) and the background signal (SBV N protein) was the highest when using the mAb 3G7 at 5 µg/mL and the mAb 2G10-HRP at 1:4,000. With these conditions, the LOD of the assay was about 250 ng/mL of CCHFV N protein. These conditions were selected to perform a spiking assay.



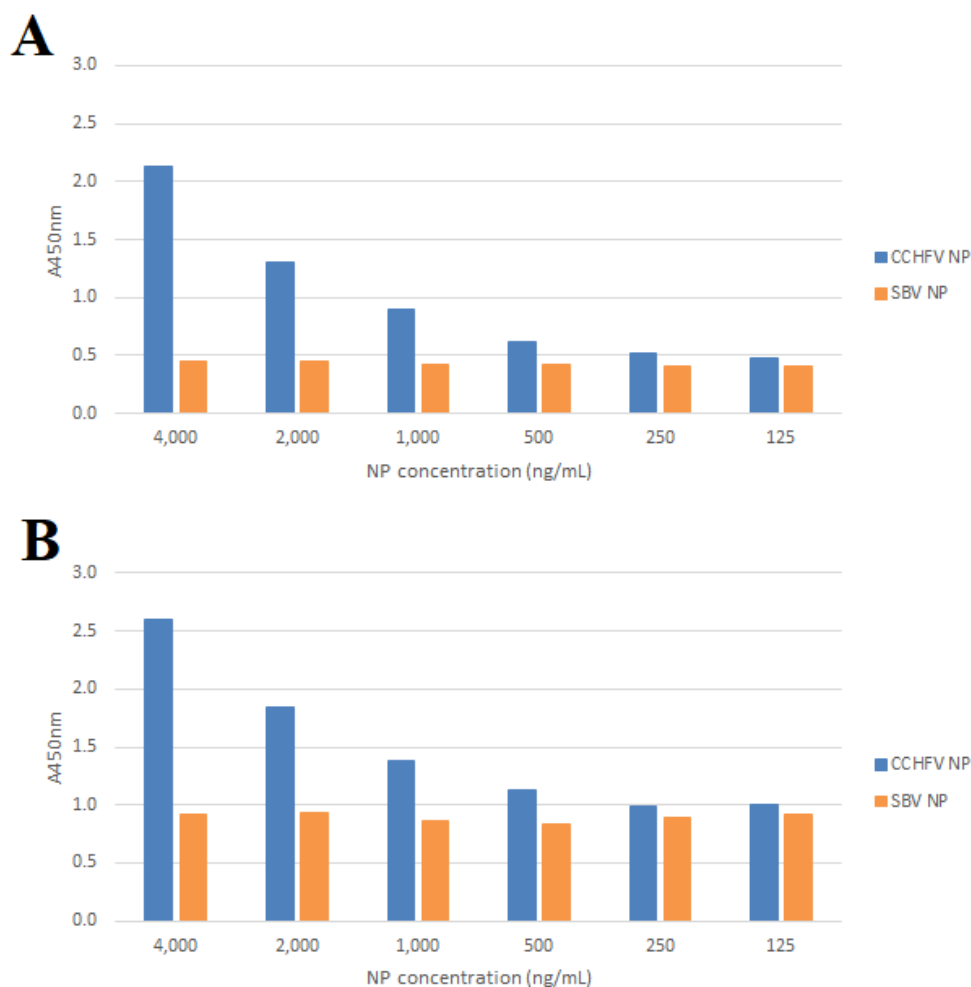
**Figure 3.30 Optimization of the double antibody sandwich ELISA conditions.**

The CCHFV N protein (A) and SBV N protein (B) were titrated using two different 3G7 coating concentrations (5 and 10 µg/mL) and two different 2G10-HRP dilutions (1:2,000 and 1:4,000). The experiment was performed once.

### 3.6.3. Spiking assay

As a proof-of-concept, negative cow and human sera were spiked with different concentrations of CCHFV N protein. The spiked serum was tested with the double antibody sandwich ELISA CCHFV N protein and the results are shown in Figure 3.31.





**Figure 3.31 Spiking assay with the double antibody sandwich ELISA.**

*Titration of the CCHFV N protein and SBV N protein spiked in cow (A) and human serum (B) in the double antibody sandwich ELISA with the anti-CCHFV N protein mAb 3G7 used as capture (coated at 5 µg/mL) and the mAb 2G10-HRP used as detection (diluted 1:4,000) molecules. The different conditions were only tested once.*

The double antibody sandwich ELISA with the spiked cow serum (Figure 3.31A) and spiked human serum (Figure 3.31B) showed a titration of the CCHFV N protein until 500 ng/mL. The serum spiked with the SBV N protein exhibited some background signal for both serum samples, with a higher background observable for the spiked human serum ( $A_{450nm} \approx 1$ ) than for the cow serum ( $A_{450nm} \approx 0.5$ ). After a concentration of 500 ng/mL, the CCHFV N protein could not be differentiated from the SBV N protein. The spiked serum seemed to interfere with the LOD of the assay, which decreased from 250 ng/mL in buffer to 500 ng/mL in cow or human serum.

### **3.7. Development of a CCHFV triplex assay to detect antibodies against three CCHFV antigens**

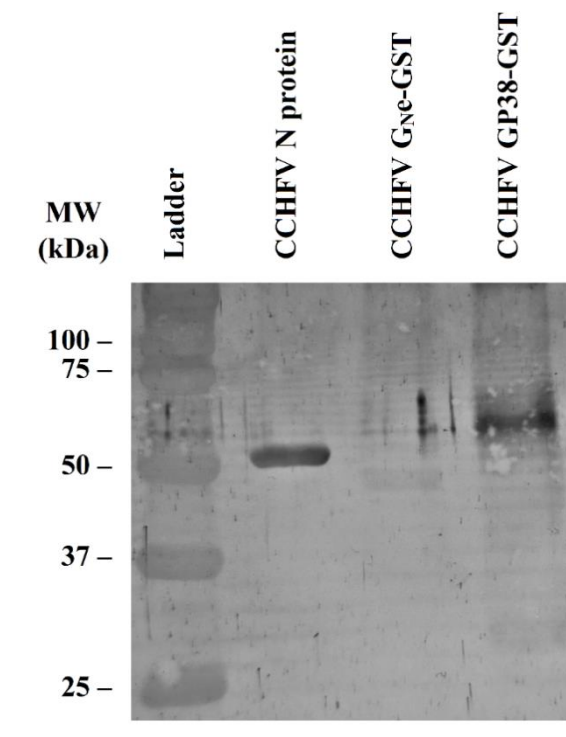
As the WHO highlighted the need of assays that could cover a range of CCHFV antigenic targets and that could potentially be used as a DIVA assay or for vaccine evaluation, a multiplex assay using the Luminex technology with the CCHFV N protein, CCHFV G<sub>NE</sub> and CCHFV GP38 as target antigens was developed. This triplex assay was used to assess the antibody response in naturally infected animals. After optimization of the triplex assay using reference sera, a collection of positive field samples from different animal species was assayed.

#### **3.7.1. Serum samples**

To develop this assay, the panel of serum samples consisted of 29 CCHFV positive field sera and 147 negative field sera. For detection of antibodies to CCHFV, 15 field serum samples from cattle, 10 from sheep and 4 from goats naturally infected by CCHFV were provided by the Faculty of Veterinary Medicine in Skopje (USCM, North Macedonia). A collection of 147 negative field samples (63 from cattle, 44 from goats and 40 from sheep) from Spanish farms were evaluated. The samples were confirmed positive or negative based on a commercial ELISA: ID Screen<sup>®</sup> CCHF Double Antigen Multi-species (IDvet) for detection of specific antibodies against CCHFV N protein. As no commercial ELISAs based on CCHFV glycoproteins are available, the above-mentioned ELISA detecting antibodies against the CCHFV N protein was used to classify the sera as positive or negative.

#### **3.7.2. Immunogenicity of the CCHFV recombinant proteins**

To confirm the immunogenicity of the CCHFV recombinant proteins, a Western blot analysis was performed using a pool of CCHFV positive field sera. A specific band for each protein was observed (Figure 3.32) with a strong band corresponding to CCHFV N protein (lane 1) and CCHFV GP38 (lane 3) and a fainter band for CCHFV G<sub>NE</sub> (lane 2).



**Figure 3.32 Confirmation of the immunogenicity of the CCHFV recombinant proteins (N protein, G<sub>Ne</sub> and GP38).**

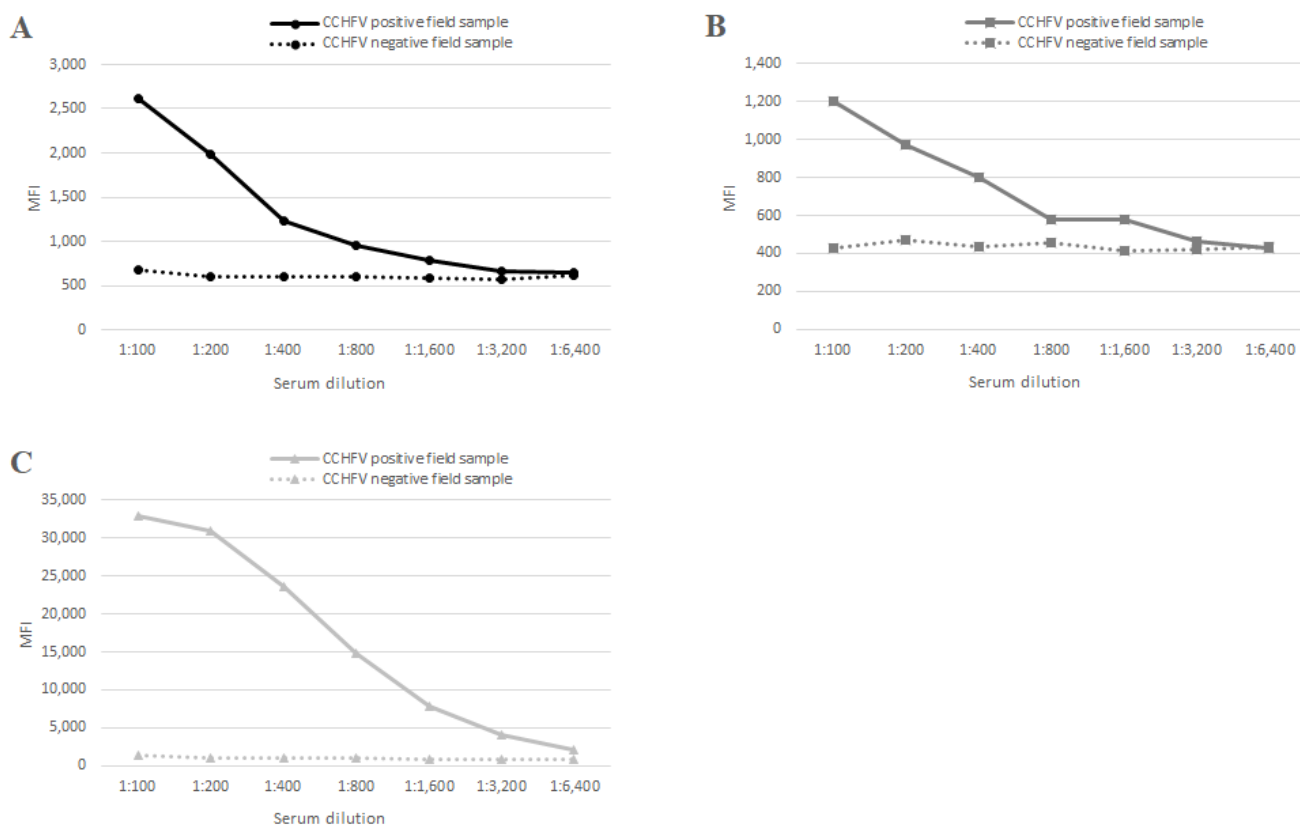
Western blot analysis of the CCHFV N protein, CCHFV G<sub>Ne</sub>-GST and CCHFV GP38-GST with a pool of CCHFV positive sera as primary antibody. 0.5 µg of each protein was loaded per well. From left to right: CCHFV N protein (MW=54 kDa), CCHFV G<sub>Ne</sub>-GST (MW=46.2 kDa) and CCHFV GP38-GST (MW=57.8 kDa).

### 3.7.3. Optimal serum dilution

The three CCHFV target proteins were used to coat different microsphere regions. Then, anti-CCHFV N protein and anti-GST mAbs were used to confirm the coupling of each individual antigen to its bead region and then to optimize the coupling concentration of each antigen. The optimal protein coupling concentration was established as the highest MFI obtained with the minimum amount of protein. The following quantities were used to coat  $1 \times 10^6$  beads for each bead region: 25 µg of CCHFV GP38-GST (region #15), 50 µg of CCHFV G<sub>Ne</sub>-GST (region #20) and 25 µg of CCHFV N protein (region #25).

Field positive and negative serum samples were used to establish the optimal assay conditions for the screening. A mix of the 3 bead regions coupled to the CCHFV target proteins was incubated with serial dilutions of these positive and negative sera, and the assay was performed as described in Materials and Methods. For the positive serum

samples, the same pattern of results was obtained for each bead region with a titration of the serum samples from the first dilution at 1:100 until 1:3,200 and the highest MFI was observed for 1:100 dilution (Figure 3.33A, B and C). The beads region also gave some background signal with the negative serum samples, but these signals were lower than the ones observed for the positive serum samples (Figure 3.33A, B and C). For screening purposes, a serum dilution of 1:100 was selected (corresponding to a sample volume of 1  $\mu$ L), since this was the dilution showing the highest positive/negative ratio for the three beads coated with the recombinant viral proteins and the highest signal with the three beads regions with the positive serum samples.

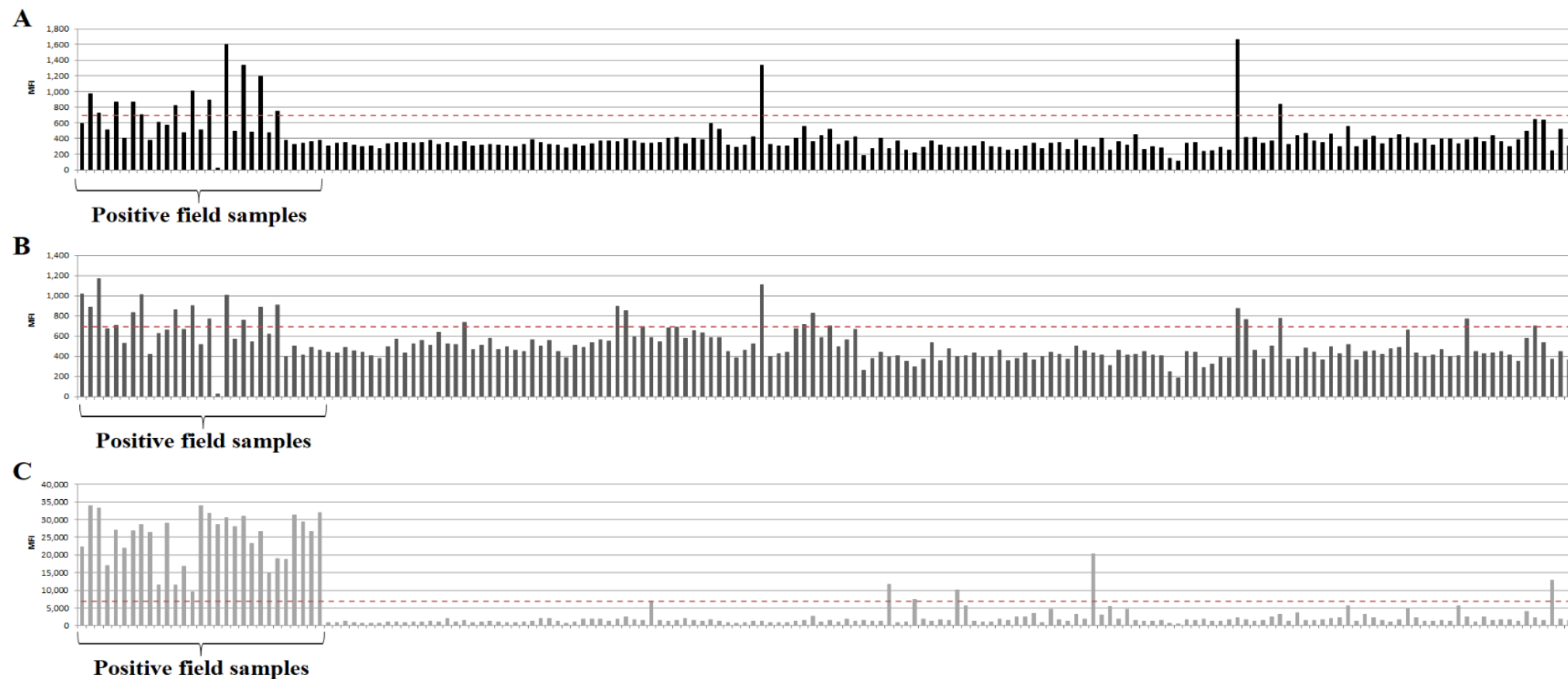


**Figure 3.33 Determination of the screening conditions for the triplex assay.**

The MFI for each bead region is given for different field serum dilutions (one positive serum sample and one negative serum sample). A: positive and negative field samples with bead #15 CCHFV GP38-GST. B: positive and negative field samples with bead #20 CCHFV G<sub>Ne</sub>-GST. C: positive and negative field samples with bead #25 CCHFV N protein. The signal was measured as MFI of at least 50 events of each bead region. MFI: median fluorescence intensity.

#### **3.7.4. CCHFV triplex assay**

The 29 positive ruminants' field sera and the 147 negative field sera were confirmed to be positive and negative, respectively, by the reference ELISA to CCHFV. These samples were then tested in the triplex assay to check for the presence of antibodies against these three CCHFV proteins (Figure 3.34). The cut-off value was established for each bead region as the mean obtained for the 147 negative field samples plus two standard deviation. Thus, cut-off values of 692.1 MFI, 757.5 MFI and 6,868.5 MFI were obtained for bead #15 CCHFV GP38-GST, bead #20 CCHFV G<sub>NE</sub>-GST and bead #25 CCHFV N protein, respectively. With these cut-off values, out of the 29 positive field sera to CCHFV N, 12 were considered positive for CCHFV GP38 and CCHFV G<sub>NE</sub> (41%) and 29 to CCHFV N protein (100%) (see Figure 3.34A, B and C, respectively). Moreover, 11 of the 12 samples positive for CCHFV GP38 were also positive for CCHFV G<sub>NE</sub>. Seven of the 12 samples positive to CCHFV GP38 and G<sub>NE</sub> come from cows and the other 5 from sheep with none of the 4 goat samples, positive to the N protein, being positive to a glycoprotein. However, with these cut-offs, out of the 147 negative field sera tested, 3 were positive for CCHFV GP38 (2%), 8 were positive for CCHFV G<sub>NE</sub> (5.4%) and 5 for CCHFV N protein (3.4%). The three negative field samples positive to CCHFV GP38 are included in the 8 positive to CCHFV G<sub>NE</sub>.



**Figure 3.34** Screening of the positive and negative field sera for antibodies against CCHFV GP38 (A), CCHFV G<sub>N</sub> (B) and CCHFV N protein (C) in the CCHFV triplex assay.

The dashed line corresponds to the cut-off values for each bead region calculated as the mean obtained for the negative field samples plus two standard deviations. The signal was measured as MFI of at least 50 events of each bead region. MFI: median fluorescence intensity.

### 3.8. Chapter summary and discussion

This chapter describes the production of three CCHFV proteins, the N protein, the G<sub>N</sub> and the GP38. The CCHFV N protein was used to produce monoclonal antibodies by hybridoma technology. Finally, these reagents were used to develop different serological assays: a double recognition ELISA detecting antibodies to CCHFV N protein in different animal species, a double antibody sandwich ELISA detecting the CCHFV N protein and a triplex assay detecting antibodies against the three CCHFV target proteins.

The CCHFV N protein has been previously expressed in bacteria using the pET SUMO system (289). This expression system yielded high quantities of pure CCHFV N protein that could be used for crystallisation assays. In this chapter, the CCHFV N protein was produced using the same system. The cell lysis buffer contained some Benzonase<sup>®</sup> nuclease to degrade DNA and RNA to avoid the potential binding of bacterial nucleic acid to the CCHFV N protein. In order to obtain a highly pure protein two Ni<sup>2+</sup>-NTA columns followed by a purification step by SEC were performed. As result, the CCHFV N protein obtained was highly pure and separated from the identified contaminants such as uncleaved 6xHis-SUMO-CCHFV N protein, the 6xHis-SUMO protease Ulp1 and the 6xHis-SUMO tag. As described previously, the peak corresponding to the CCHFV N protein on the chromatogram corresponded to a molecular weight of around 55 kDa, meaning that the CCHFV N protein produced is likely to be a CCHFV N protein monomer (289). The high purity of the CCHFV N protein was important as this protein was to be used to immunize mice in order to produce monoclonal antibodies.

The complete CCHFV G<sub>N</sub> has been previously produced in insect cells (290). Rahpeyma *et al.* showed that the recombinant CCHFV G<sub>N</sub> was immunogenic and could be recognized by CCHFV positive human sera and could elicit high titres of antigen-specific antibodies. Furthermore, another study showed that a soluble version of G<sub>N</sub> lacking its transmembrane and cytoplasmic domains was also localized to the Golgi apparatus (291). Thus, in this chapter, to increase the solubility and expression yields of the CCHFV G<sub>N</sub>, the CCHFV G<sub>N</sub> ectodomain was produced in insect cells using the BES with the GP67 signal peptide and a fusion tag (GST tag). The GP67 signal peptide forced the secretion

of the CCHFV G<sub>NE</sub> in the culture medium. The CCHFV G<sub>NE</sub> was then purified by affinity chromatography, which yielded low amounts of pure CCHFV G<sub>NE</sub>. The CCHFV G<sub>NE</sub> was also purified from the soluble fraction of the cell lysate, which yielded higher amounts of pure protein but this one exhibited a lower immunogenicity when tested in ELISA and Luminex assays with positive field sera (data not shown).

A growing interest was observed for CCHFV GP38, since its first description by Sanchez *et al.* (40). Its function is unknown, however, GP38 was shown to be highly secreted by infected cells, a monoclonal antibody targeting this protein could protect mice from a lethal challenge (31) and its crystal structure has recently been solved (44). This is the first description of the recombinant expression of CCHFV GP38 in insect cells using the BES. The CCHFV GP38 was highly expressed in the cell culture supernatant due to the GP67 signal peptide and this protein was expressed with a GST tag which allowed its purification by affinity chromatography. The CCHFV GP38 expression, yielded higher amounts of protein than for the CCHFV G<sub>NE</sub> and could be observed by SDS-PAGE followed by Coomassie staining to confirm its high purity.

In reducing conditions, the N protein, the G<sub>NE</sub> and the GP38 produced were recognized by CCHFV positive ruminant sera. However, under these conditions, the N protein and the GP38 seemed to be more immunogenic than the G<sub>NE</sub>, as shown by their higher intensity on the WB analysis. This could mean a proper folding and post-translational modifications of the recombinant GP38 expressed in insect cells compared to the G<sub>NE</sub>. To produce recombinant CCHFV glycoproteins with post-translational modifications closer to the native proteins, the CCHFV G<sub>NE</sub> and GP38 could have been produced in mammalian cells. At the time of this thesis, the mammalian expression system was not in place in the lab, thus the expression system used was the BES with production in insect cells. As described in the introduction, this system presents many advantages, however, as the PTM are not the same than in mammalian cells, this could have led to a lower immunogenicity of the glycoproteins produced.



In order to produce anti-CCHFV N protein mAbs, mice were immunized with the N protein obtained in bacteria. Two groups of mice were used for the production of mAbs anti-CCHFV N protein: the first was immunized with the 6xHis-SUMO-CCHFV N protein and the second with the CCHFV N protein. Since the 6xHis-SUMO tag seems to be highly immunogenic, a negative control produced in the same construct (6xHis-SUMO-RVSV N) was used for the screening steps of the hybridoma clones. Three mAbs were obtained, which were highly specific for the CCHFV N protein in reducing and non-reducing conditions and could detect up to 10 ng/mL of CCHFV N protein. These mAbs were used as tools to develop serological assays to detect the CCHFV N protein. Anti-CCHFV glycoprotein mAbs could not be produced in this chapter as the amount of CCHFV GP38 and G<sub>NE</sub> purified were not enough to immunize mice. Anti-CCHFV glycoproteins mAbs are interesting as these mAbs could have a virus neutralizing activity as shown by Zivcec *et al.* (292). Moreover, recently, a non-neutralizing mAb targeting the GP38 was shown to protect mice from a lethal CCHFV infection, which underlines the interest for mAbs targeting the CCHFV glycoproteins (31).

In the R&D roadmap published by the WHO in 2018 (288), experts identified some product development goals that should be met in the near future. Regarding CCHF diagnosis, axes of research and development are to: “continue to develop and test commercial serology assays for detecting IgM and IgG antibodies to CCHFV for use in supplementary diagnostic tests, for epidemiology and surveillance during outbreaks, and for evaluation of vaccine immunogenicity and durability” and to “develop one or more commercial multi-species ELISA kits to detect anti-CCHF antibodies for monitoring CCHFV in animals”. In this regard and to meet some of the gaps in CCHF diagnosis highlighted by the WHO, a double recognition ELISA was developed using the CCHFV N protein. The double recognition ELISA was tested with ruminant serum samples from cattle, sheep and goat. Compared to the reference assay, the double recognition ELISA developed had a sensitivity of 93.1% and a specificity of 96.1%. The sensitivity and specificity exhibited by the double recognition ELISA meet the requirement of the WHO about the development of new diagnostics for CCHFV shown in Table 3.2 (287). However, the sensitivity is not perfect, which could be explained by some factors. The first one, as described below, is the probable higher sensitivity of the double recognition assay for IgM compared to IgG, due to the design of the assay. In case of only a low

amount of CCHFV positive IgG, the double recognition ELISA could give a false negative result. Another factor to consider is that there is a high diversity between the CCHFV clades, with nucleotide sequence differences around 20% for the S segment (53). This diversity could impact the sensitivity of the double recognition ELISA developed as the CCHFV N protein produced recombinantly is from an Iranian strain, when the antibodies detected in cattle in North Macedonia are likely raised against a European strain. Compared to the commercial serological antibody detection tests available, the double recognition ELISA is a multi-species assay that could help to monitor the presence of CCHFV antibodies in animals as a surveillance tool and can detect total antibodies in the same assay. Moreover, as the WHO highlighted the need of diagnostics able to detect acute or early infections (detection of antigens or IgM) this double recognition ELISA could prove to be useful, as the design of the double recognition ELISA should lead to a higher sensitivity and specificity of the assay for the detection of IgM than for IgG. Indeed, the double recognition ELISA is based on the principle that antibodies possess multiple antigen binding regions (2 for IgG, 4 for IgA, and 10 for IgM), allowing their binding to both the target and detection antigens. As IgM have a higher number of antigen binding sites than IgG, they should have a better binding to the capture and detection molecule. This higher sensitivity and specificity for IgM should be confirmed by testing well characterized CCHFV positive serum samples containing only IgM or IgG to CCHFV. Moreover, this assay is a multi-species assay, thus, to increase the impact and usefulness of this assay, CCHFV positive and negative human serum samples need to be tested to characterize this assay for humans. Finally, due to sample constraints, the negative and positive field samples used to develop the double recognition ELISA were only tested once. Although the samples were only used once, a significant number of samples were used to support the results obtained.

In the WHO R&D Blueprint: Priority Diagnostics for CCHF, the WHO prioritized the diagnostic needs identified in the R&D Roadmap for acute and early case detection of CCHF (287). Thus, to answer this gap in early case detection of CCHF, the anti-CCHFV N protein mAbs produced were used to develop a double antibody sandwich ELISA. The limit of detection of the double antibody sandwich ELISA was 250 ng/mL of CCHFV N protein in buffer and 500 ng/mL in spiked sera. Indeed, an assay was performed with negative cow and human sera, spiked with the CCHFV N protein, as no acute CCHFV positive sera could be obtained. The sera seemed to interfere with the detection of the

CCHFV N protein in the spiking assay as it reduced the limit of detection of the assay. A previous study developing a double antibody sandwich ELISA with a limit of detection of 20 ng/mL of CCHFV N protein could detect native CCHFV in acute sera of CCHFV-infected patients (280). As the double antibody sandwich ELISA developed in this chapter is significantly less sensitive, this could mean that this assay is probably not sensitive enough to detect CCHFV antigen in acute samples.

Finally, in the WHO R&D roadmap for CCHFV diagnostics, a gap identified by the experts was to “ensure tests under development cover a range of CCHFV antigenic targets to enable their use in the assessment of live attenuated vaccines and/or as confirmatory diagnostic tests” (288). Indeed, most of the diagnostics developed to detect antibodies against CCHFV use the CCHFV N protein. To address this need, in this chapter, a multiplex assay has been developed with different CCHFV antigenic targets (N protein, G<sub>NE</sub> and GP38 of CCHFV) in order to detect antibodies against these three proteins in ruminant sera. One of the advantages of this assay compared to the reference assay is the volume of serum necessary to perform the triplex assay (1 µL) compared to the reference ELISA (30 µL). The triplex assay, after optimization, allowed the simultaneous detection of antibodies against these three proteins in different animal species. Out of the 29 positive sera to CCHFV, confirmed by a commercial ELISA detecting antibodies against the N protein, in all the sera the triplex assay detected antibodies against the N protein. However, only 40% of the animals positive to the N protein had antibodies against the G<sub>NE</sub> and the GP38. These results could not be confirmed by ELISAs based on these glycoproteins as none are commercially available. Some previous studies showed that the G<sub>NE</sub> and the GP38 elicited an immune response (31), however, in this assay, not all the animals having antibodies against the N protein had detectable antibodies against the G<sub>NE</sub> and the GP38. Moreover, this assay shows that the N protein of CCHFV seems to be a good candidate for serological assays as it exhibited a higher MFI than for the two glycoproteins. This hypothesis should be confirmed with human positive sera to CCHFV to check if the same immunogenic pattern can be observed in humans. Finally, to analyse the immunogenicity of all the CCHFV proteins in the same assay, other CCHFV proteins could be included in the assay such as the CCHFV G<sub>C</sub>, NS<sub>S</sub> and NS<sub>M</sub>.

The results of this chapter respond to the first aim of this project, producing the different tools to allow the development of CCHFV diagnostic tests to respond to the current gaps in CCHF diagnosis.

# Chapter 4 Development of diagnostic tools for RVFV

## 4.1. Chapter introduction

Early detection of suspected cases of RVF is vital to ensure timely control measures are implemented to reduce the disease burden. This is characterized by « abortion storms » in pregnant animals, high mortality in young animals and transmission of the disease to humans. Currently, there are several techniques available for RVF diagnosis, including histopathology, virus isolation, molecular methods and serological diagnosis.

For the histopathological examination, the liver (or other tissues) is fixed in formaldehyde which inactivates the virus, thus facilitating handling and transportation from remote areas. This analysis will reveal hepatic lesions characteristic of RVFV infection and immunostaining may allow the specific identification of viral antigen in tissue (293).

RVFV can also be diagnosed by isolating the virus from serum, plasma or blood or from organs of animals that have died or aborted fetuses. The *in vitro* isolation of RVFV is possible using mammalian cell lines with a clear CPE 12-24 hours PI (294). The virus isolation can be confirmed by RT-PCR or immunostaining. However, diagnostic techniques that rely on virus isolation or the handling of potentially infected body fluids can only be carried out in a few laboratories that are authorized to work with RVFV, since it is a hazardous pathogen and a BSL-3 laboratory is required.

Moreover, molecular methods that detect viral RNA during the acute phase of the disease are an alternative to virus isolation. The molecular assays are most effective at early days post infection (2 to 4 DPI) (295) and the viral load can be correlated to disease severity (296,297). A broad range of highly sensitive nucleic acid based molecular tests have been developed for RVFV as reviewed by Mansfield *et al.* and Petrova *et al.* (70,298). Different quantitative real-time RT-PCR have been developed (299–303), as well as nested real-time RT-PCR methods (304). Other methods include one-step multiplex reverse transcriptase PCR assay to differentiate RVFV from other related viruses, such as BTV, rinderpest virus and peste des petits ruminants virus (305), RT-LAMP targeting the

L segment (306,307) and real-time recombinase polymerase amplification (RT-RPA) (308) were also developed. Even if molecular tests are very sensitive, they present some drawbacks such as the short-lasting viremia and the necessity of lab equipment (but for the RT-LAMP and the RT-RPA) that reduces the usefulness of these methods in developing countries where there is little or no lab equipment.

An alternative to the molecular assays to detect an acute infection of RVFV is the direct detection of RVFV antigens. The detection of RVFV antigens is mainly based on ELISAs as described by Fukushi *et al.* (309), but can also be done by IFA as more recently described by Mroz *et al.* (310). In both cases, monoclonal antibodies against different proteins of the virus are used for detection. The ELISA developed by Fukushi *et al.* (309) was able to detect up to 0.8-1.6 ng/mL of recombinant N protein and between 78–313 pfu/mL of RVFV in the culture supernatant of cells infected with RVFV. Mroz *et al.* (310) developed mAbs that could detect the presence of RVFV glycoproteins (G<sub>N</sub> and G<sub>C</sub>) in infected Vero 76 cells at 2 hours PI followed by N protein and the non-structural proteins NS<sub>S</sub> and NS<sub>M</sub> at 3–4 hours PI. The same assay in mosquito cells gave similar results. Finally, a LFA was recently developed by Cêtre-Sossah *et al.* (311) to detect RVFV N protein, with good performance characteristics when compared with real-time RT-PCR. The sensitivity and specificity of antigen LFA are usually lower than the ones of molecular techniques, but they can be used as POC and in developing countries where the laboratory equipment is sometimes not adequate to use molecular techniques.

Finally, there are two main methods available for detection of antibodies anti-RVFV in a variety of animal species. VNT is the gold standard serological test as it is the prescribed test by the OIE for international trade (312). Neutralization tests are very sensitive and specific tests, but they can only be performed with live virus and are not recommended for use outside endemic areas or in laboratories without appropriate biosecurity facilities and vaccinated personnel. However, a recent in-house VNT based on an avirulent RVFV expressing the enhanced green fluorescent protein has been developed, allowing the safe use of this test outside BSL-3 or -4 (313). Still, nowadays ELISA is the most widely used technique for the detection of antibodies in both humans and animals.

Table 4.1 shows a current list of commercially available ELISAs and in-house ELISAs. Most of them are based on the recombinant RVFV N protein for the detection of corresponding antibodies, despite reports that the recombinant RVFV N protein exhibits

potential high background and cross-reactivity (314). However, many in-house indirect ELISA (315), competition ELISA (316), sandwich ELISA (317) have been described with high sensitivities and specificities. These ELISAs can detect specific IgM antibodies (which appear from 4 days after infection) or specific IgG antibodies (which appear from 8 days after infection and may persist for years) (70).

Finally, bead-based suspension microarrays have been developed for the simultaneous detection of antibodies against different RVFV proteins, which could be used as DIVA assays. F. van der Wal *et al.* (318) described the production of recombinant N and G<sub>N</sub> protein and their use in a multiplex immunoassay to detect IgG antibodies in sheep, cattle and human sera against these two proteins. The same format of assay was used by Ragan *et al.* (319) for detection of IgG and IgM antibodies against the N protein, the G<sub>N</sub> protein and the NS<sub>S</sub> and NS<sub>M</sub> proteins. In this assay, the NS<sub>S</sub> and NS<sub>M</sub> showed weaker antibody response than the N and G<sub>N</sub> proteins, highlighting the importance of immune response against the N and G<sub>N</sub> proteins. Finally, Lindahl *et al.* (320) developed a multiplex bead-based suspension assay with recombinant N, G<sub>N</sub>, NS<sub>S</sub> and NS<sub>M</sub>. NS<sub>M</sub> showed high background but the three other proteins showed high antibodies response and seemed to be promising targets to develop new assays.

**Table 4.1 Commercial serological assays available for RVFV antigen and antibody detection.**

Assay	Target	Species	Producer
Competition ELISA	IgM/IgG	Ruminants	Eurofins-Ingensa, Spain
Capture ELISA	IgM	Ruminants	Eurofins-Ingensa, Spain
Competition ELISA	IgM/IgG	Ruminants, camels, horses, dogs	IDVet, France
Capture ELISA	IgM	Ruminants	IDVet, France
IFA	IgG	Humans	EUROIMMUN, Germany
IFA	IgM	Humans	EUROIMMUN, Germany

As seen in Table 4.1, there are no commercial and validated serological POC tools detecting RVFV antigens, nor a POC molecular assay. As underlined by the WHO and some studies such as the one from Petrova *et al.* (298), there is an urgent need for the development of tools that could be used at the patient's site. Moreover, as only a few

commercial serological assays are available for the detection of RVFV antibodies, more serological assays need to be developed. Due to the broad symptoms caused by RVFV, its differential diagnosis alongside other animal- and human-related pathogens is challenging and needs to be addressed. Finally, vaccine development of DIVA-compliant vaccines leads to the need of diagnosis including different viral targets to differentiate vaccinated from naturally infected animals.

The aim of this chapter was to answer the current gaps in RVFV diagnosis. For this, novel diagnostic tools have been developed for detection of specific antibodies against RVFV and antigen of RVFV.

In order to obtain these tests, firstly, some viral target antigens were recombinantly produced in *E. coli* such as the RVFV N protein, one of the most immunogenic proteins of RVFV, and a RVFV glycoprotein, the G<sub>N</sub> ectodomain, produced recombinantly in insect cells to process its PTM. The second step was the immunization of mice in order to produce mAbs targeting the RVFV N protein using the hybridoma technology. The same protein was used to select Affimers targeting this N protein by phage display.

Once the reagents were obtained, the N protein was used to develop a double recognition ELISA to detect total antibodies of animals which have been previously infected by RVFV. After the production and characterization of the monoclonal antibodies and Affimers, they were used to develop a double antibody sandwich ELISA to detect RVFV N protein. This double antibody sandwich ELISA was transferred to LFA technology to develop a POC tool that can rapidly detect RVFV acute infections. Finally, the N protein and the G<sub>NE</sub> were used to develop a duplex assay to detect the immune response of laboratory animals infected with RVFV.

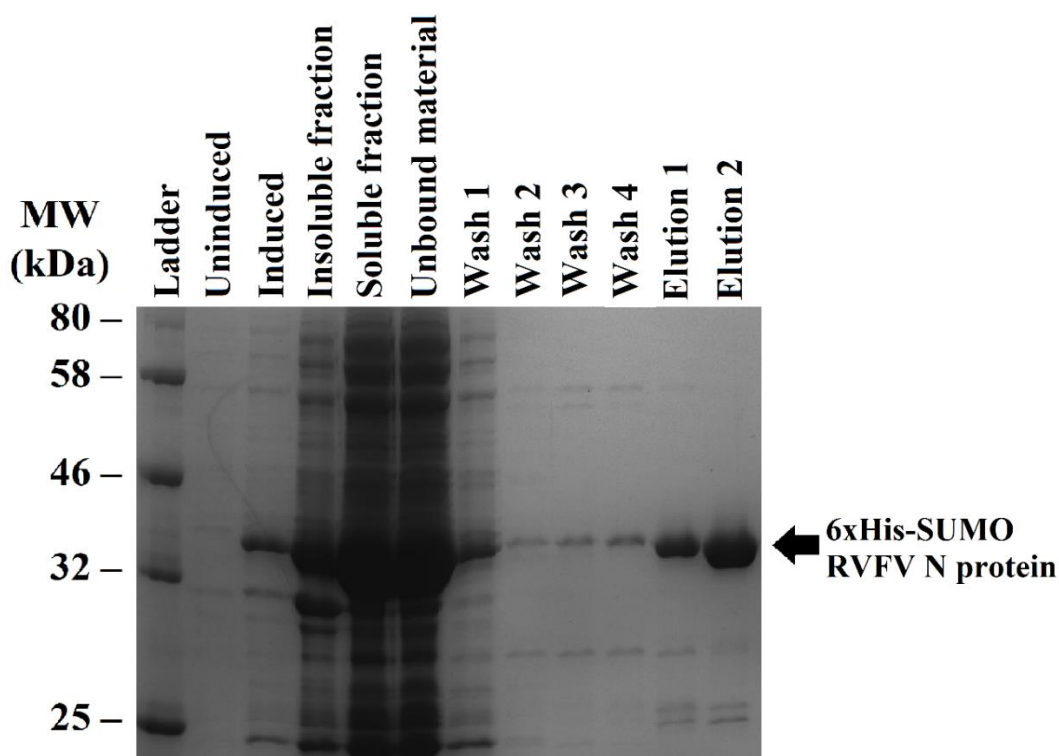
## **4.2. Production and purification of RVFV N protein**

### **4.2.1. Expression of RVFV N protein**

The ORF of the RVFV N protein was cloned into the pET28a-SUMO plasmid and used to transform *E. coli* BL21 (DE3) R2. The expression of the RVFV N protein followed the same steps than the ones of the CCHFV N protein expression. Briefly, after induction with IPTG, the cells were harvested, lysed and the soluble fraction was separated from



the insoluble fraction by centrifugation and analysed by SDS-PAGE followed by Coomassie staining (Figure 4.1). A band at the expected molecular size of the 6xHis-SUMO-RVFV N protein (MW= 38.6 kDa) was observed after induction and in the insoluble and soluble fractions.



**Figure 4.1** Expression of the RVFV N protein and its purification by  $\text{Ni}^{2+}$ -NTA affinity chromatography.

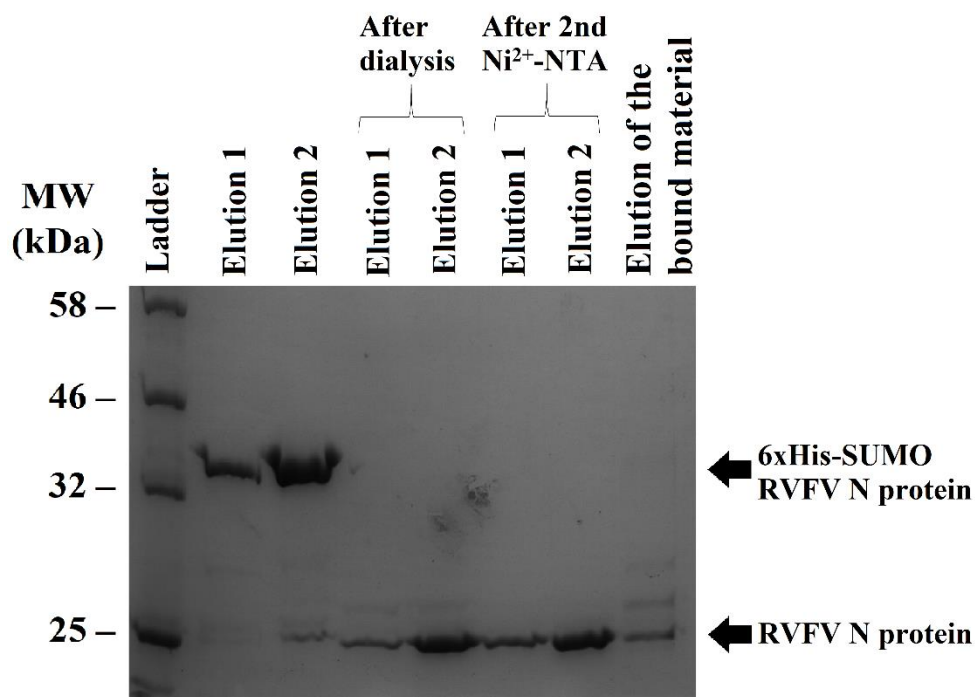
SDS-PAGE followed by Coomassie staining of samples taken at different steps of the expression and purification of the 6xHis-SUMO RVFV N protein. Purification from the soluble fraction by a first  $\text{Ni}^{2+}$ -NTA affinity chromatography and elution with elution buffers containing 100 mM (elution 1) and 500 mM imidazole (elution 2). Arrows indicate the bands corresponding to the specified proteins.

#### 4.2.2. Purification of RVFV N protein

To separate the 6xHis-SUMO-RVFV N protein from the other proteins contained in the soluble fraction, a first purification was performed by affinity chromatography using a  $\text{Ni}^{2+}$ -NTA column. As described in section 2.3.1.1, the soluble fraction was incubated ON with the  $\text{Ni}^{2+}$ -NTA matrix, the resin was washed and the elution of the 6xHis-SUMO-

RVFV N protein was performed with elution buffers containing 100 mM (elution 1) and 500 mM imidazole (elution 2). The elution fractions were observed by SDS-PAGE followed by Coomassie staining (Figure 4.1). The 6xHis-SUMO-RVFV N protein was present in the washes and at a higher concentration in the two elution fractions with most of the protein being found in the 500 mM fraction (see elution 1 and 2 in Figure 4.1).

To cleave and remove the 6xHis-SUMO tag from the RVFV N protein, the elution fractions were incubated with the SUMO protease Ulp1 and then purified by a second Ni<sup>2+</sup>-NTA affinity chromatography step. The RVFV N protein was collected in the unbound material and the bound material containing the uncleaved proteins, the 6xHis-SUMO tag and the 6xHis-SUMO protease Ulp1 were eluted by addition of imidazole. The samples were analysed by SDS-PAGE followed by Coomassie staining (Figure 4.2). The cleavage of the 6xHis-SUMO-RVFV N protein was observed after the dialysis (Figure 4.2). After the second Ni<sup>2+</sup>-NTA affinity chromatography, the unbound material contained the cleaved RVFV N protein (27.4 kDa) and the eluted material contained the RVFV N protein with another band (around 27 kDa, higher than the RVFV N protein), probably corresponding to the 6xHis-SUMO protease Ulp1 (27 kDa).



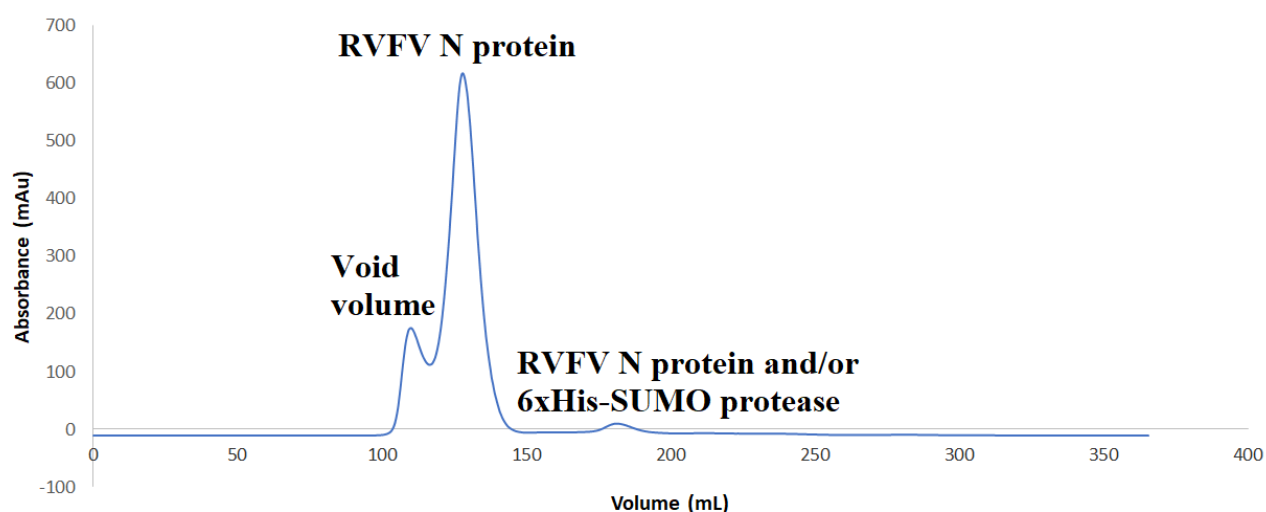
**Figure 4.2** RVFV N protein purification by a second Ni<sup>2+</sup>-NTA affinity chromatography step after SUMO cleavage and dialysis.

SDS-PAGE followed by Coomassie staining of RVFV N protein samples taken after the first Ni<sup>2+</sup>-NTA affinity chromatography, after the dialysis and cleavage by SUMO protease Ulp1 and the second Ni<sup>2+</sup>-NTA affinity chromatography. Arrows indicate the bands corresponding to the specified proteins.

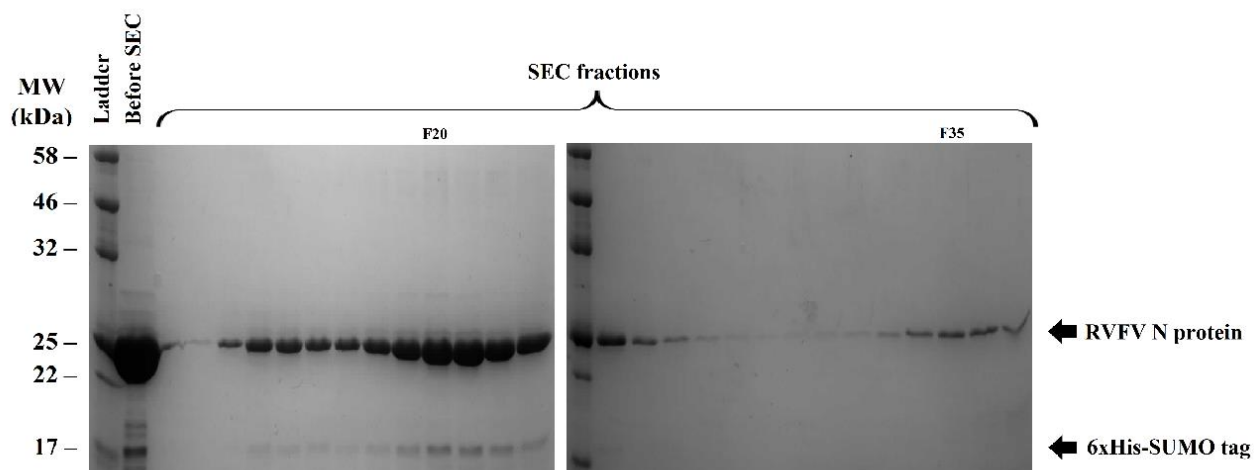
As for the CCHFV N protein, the final purification step was performed by SEC to separate the proteins according to their molecular weight. Three different peaks were observed on the chromatogram (Figure 4.3). The first peak corresponded to the void volume (110 mL), the second to polymers of the RVFV N protein (27.4 kDa) and the third to the 6xHis-SUMO protease and/or a monomeric form of RVFV N protein (both around 27 kDa). No clear peak corresponding to the 6xHis-SUMO tag (13 kDa) was detected. The RVFV N protein and the 6xHis-SUMO protease have similar molecular weights, however, they could be separated by SEC as the RVFV N protein formed polymers, which passed through the column faster than the protease. These polymers were observed by negative stain electron microscopy (data not shown).

The collected fractions were analysed by SDS-PAGE followed by Coomassie staining (Figure 4.4). Before the SEC, the sample contained the cleaved RVFV N protein as well as the 6xHis-SUMO tag. As seen on the chromatogram, the first fractions contained the

RVFV N protein, with some of the fractions still containing a small amount of 6xHis-SUMO tag. The last SEC fractions contained the 6xHis-SUMO protease (27 kDa) and/or a monomeric form of the RVFV N protein (27.4 kDa). The first fractions containing the RVFV N protein were pooled, concentrated, quantified by spectrophotometry using a spectrophotometer and stored at  $-80^{\circ}\text{C}$  after addition of glycerol. As the last fractions could correspond to a monomeric form of the RVFV N protein or to the 6xHis-SUMO protease, a WB was performed with an anti-RVFV N protein mAb (Figure 4.5). A clear band corresponding to the RVFV N protein was observed, which confirmed that the last fractions contained some RVFV N protein. Moreover, after the second  $\text{Ni}^{2+}$ -NTA purification, no other bands than the one corresponding to the RVFV N protein was present (Figure 4.2), confirming that this fraction contained some RVFV N protein.

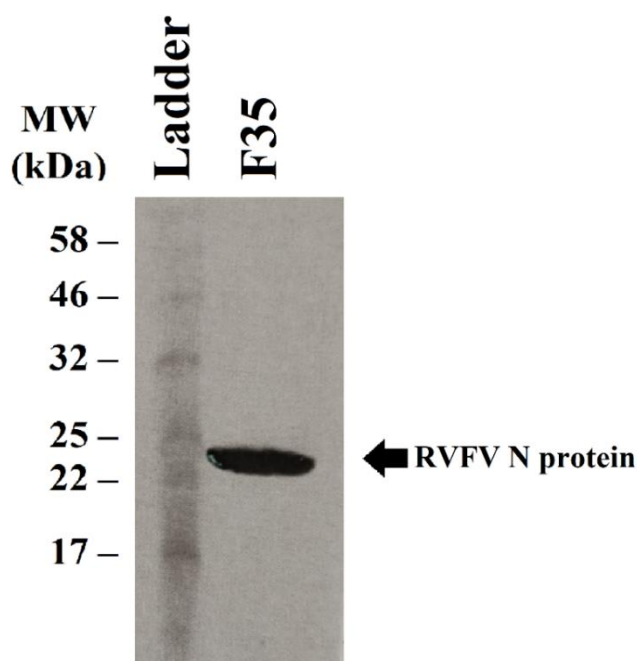


*Figure 4.3 Chromatogram of the final purification step of the RVFV N protein sample by size exclusion chromatography after two  $\text{Ni}^{2+}$ -NTA affinity chromatography purification steps. The proteins corresponding to each peak are indicated on the chromatogram.*



**Figure 4.4** RVFV N protein purification by size exclusion chromatography.

SDS-PAGE analysis followed by Coomassie staining of the different fractions collected after the size exclusion chromatography. After the  $\text{Ni}^{2+}$ -NTA affinity chromatography, the RVFV N protein was purified from contaminant proteins by size exclusion chromatography to separate them according to their molecular weight. Arrows indicate the bands corresponding to the specified proteins. F20 and F35 denote the RVFV N protein fraction 20 (polymeric) and 35 (monomeric), respectively. SEC: size exclusion chromatography.



**Figure 4.5** Confirmation of the presence of RVFV N protein in the fraction F35.

Western blot analysis with an anti-RVFV N protein mAb as primary antibody. Arrows indicate the bands corresponding to the specified proteins.

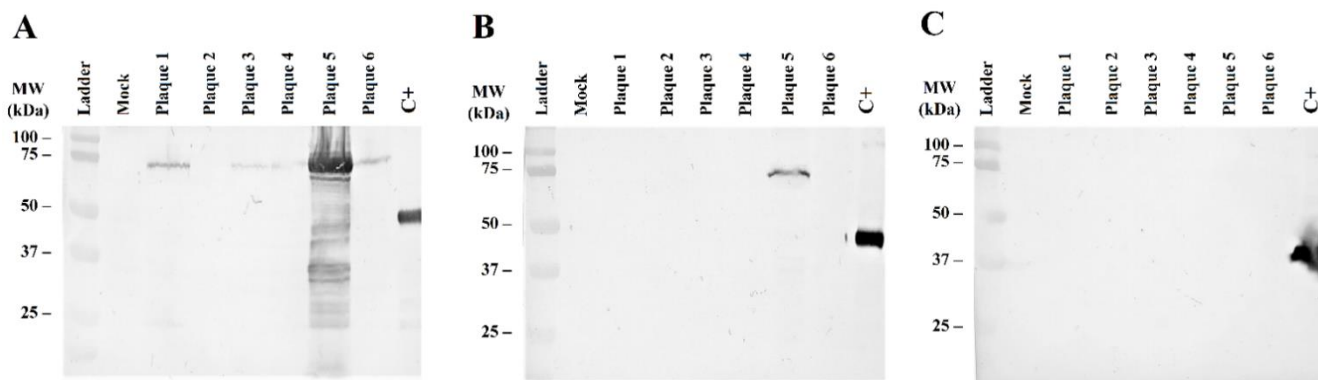
Following the same protocol, 6xHis-SUMO-RVFV N protein was also expressed and purified by Ni<sup>2+</sup>-NTA affinity chromatography without removal of the tag and without SEC.

### **4.3. Production and purification of RVFV G<sub>NE</sub>**

#### **4.3.1. Expression of RVFV G<sub>NE</sub>**

The production of RVFV G<sub>NE</sub> was done in insect cells using the BES as described for the production of the CCHFV glycoproteins in the same system (section 3.3). Briefly, the RVFV G<sub>NE</sub> ORF was cloned into the entry vector of the Gateway system as described in Materials and Methods and a LR recombination was performed to obtain pAcSecG2T RVFV G<sub>NE</sub>. This vector was used to co-transfect insect cells with the triple-cut baculovirus DNA. After a week of incubation, CPE were observed in the co-transfection flasks.

To select recombinant baculoviruses, a plaque assay with blue–white screening was performed with the supernatant of the co-transfection. After staining, six white plaques were selected and used to infect Sf9 cells in 60 mm dishes. After eight days of incubation, only one plaque showed some clear CPE (plaque 5). The cells were harvested by centrifugation, lysed and the soluble and insoluble fractions of the lysate were separated by centrifugation. The samples of the insoluble fraction, soluble fraction and supernatant were analysed by WB with an anti-GST mAb (Figure 4.6).



**Figure 4.6** Infection of Sf9 cells with plaques corresponding to recombinant baculoviruses expressing RVFV G<sub>NE</sub>-GST (MW = 73 kDa).

The insoluble fraction, soluble fraction and supernatant were analysed by Western blot 8 days post-infection of Sf9 with six recombinant baculoviruses from the plaque assay. An anti-GST mAb was used as primary antibody. A: insoluble fraction. B: soluble fraction. C: supernatant. The positive control (C+) corresponds to a recombinant protein with a GST-tag (CCHFV G<sub>NE</sub>-GST, MW = 46 kDa).

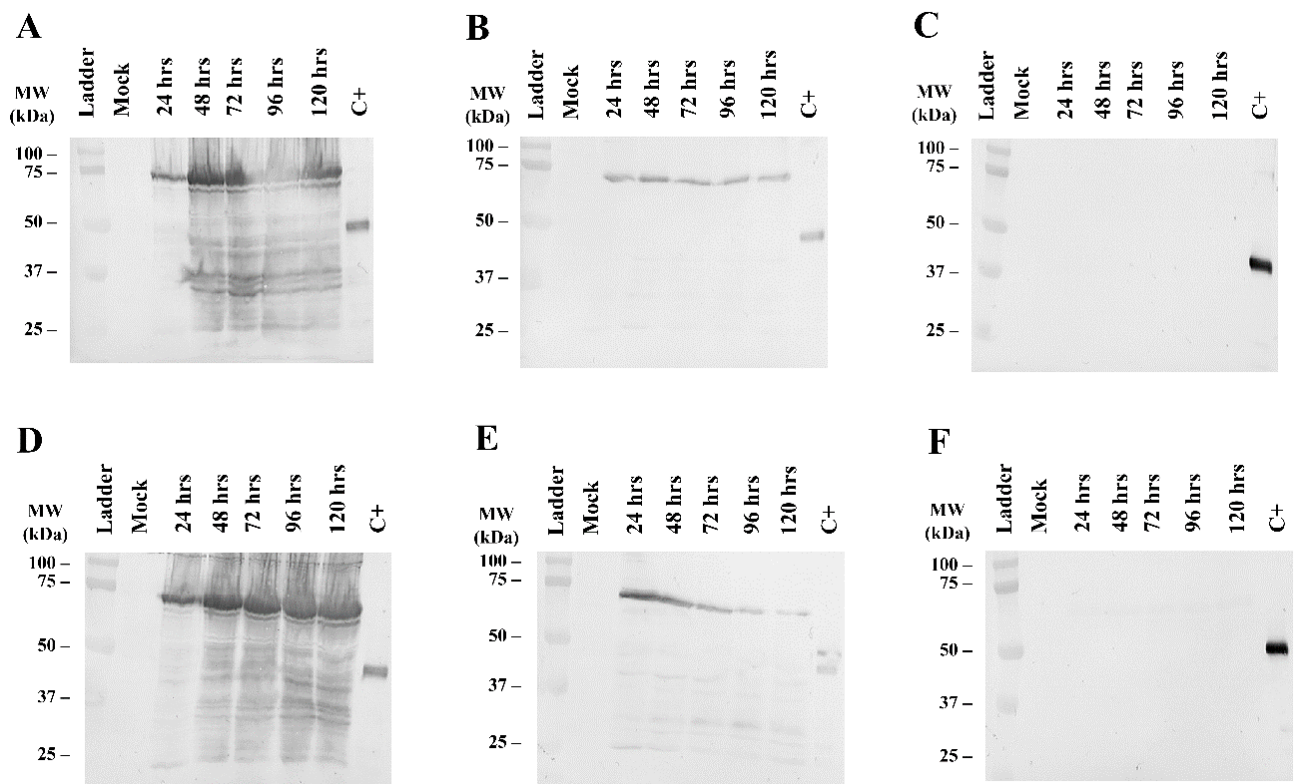
From the six plaques selected, the plaques 1, 3, 4, 5 and 6 (Figure 4.6A) presented a band around 75 kDa in the insoluble fraction, corresponding to the RVFV G<sub>NE</sub>-GST (MW: 73 kDa). The plaque 5 clearly exhibits higher G<sub>NE</sub> protein expression than the other plaques in the insoluble fraction. Regarding the expression in the soluble fraction, a band was only detected for plaque 5 (Figure 4.6B). Finally, no expression was observed in the WB analysis of the cell medium (Figure 4.6C). The plaque 5, expressing the RVFV G<sub>NE</sub>-GST in the insoluble and the soluble fraction corresponded to the only culture dish presenting some clear CPE.

The plaque 5 was selected for the protein expression and its supernatant was used to infect Sf9 to produce a high titre baculovirus stock, which was titrated by plaque assay. The virus titre obtained for BacPAK6 RVFV G<sub>NE</sub> plaque 5 was  $4 \times 10^7$  pfu/mL.

This baculovirus stock was used to infect Sf900 cells at MOI 0.1 and MOI 2 to perform a kinetic analysis of the expression of RVFV G<sub>NE</sub> and thus allow selection of the best conditions to express this protein. Cells and supernatants were harvested every 24 hrs until reaching 120 hrs PI with extensive CPE and the beginning of cell death. Samples were analysed by WB with an anti-GST mAb (Figure 4.7).

The expression of RVFV G<sub>NE</sub>-GST in the insoluble fraction (Figure 4.7A and D) was detected at both MOIs at 24 hrs PI, with the expression increasing at 48 hrs PI and staying constant after 48 hrs. The expression of RVFV G<sub>NE</sub>-GST was also observed after 24 hrs PI in the soluble fraction at both MOIs (Figure 4.7B and E). This expression seemed to decrease after 24 hrs at high MOI when it stayed equivalent after 24 hrs at low MOI. No expression of RVFV G<sub>NE</sub>-GST was detected in the supernatant of the culture (Figure 4.7C and F).

The best expression condition for RVFV G<sub>NE</sub>-GST was to set up an infection at MOI 0.1 with the time of harvest not being determinant, thus a harvest at 96 hrs pi was kept. A large-scale production was done with infection of  $6 \times 10^8$  Sf900.



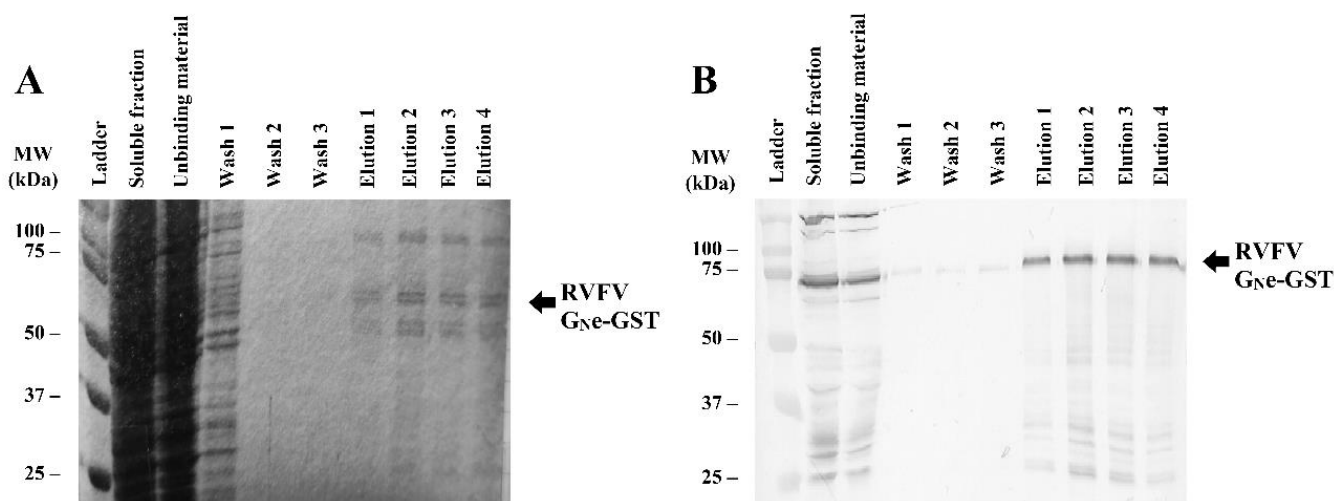
**Figure 4.7** Kinetic analysis of the expression of RVFV G<sub>NE</sub>-GST (MW = 73 kDa) in insect cells at different time points and two MOI.

Samples were taken at different time points (24 hrs, 48 hrs, 72 hrs, 96 hrs and 120 hrs) and the expression in the insoluble fraction, soluble fraction and supernatant was analysed by Western blot with a mAb anti-GST used as primary antibody. A: insoluble fractions at MOI 0.1. B: soluble fractions at MOI 0.1. C: supernatant at MOI 0.1. D: insoluble fraction at MOI 2. E: soluble fraction at MOI 2. F: supernatant at MOI 2. The positive control (C+) corresponds to a recombinant protein with a GST-tag (CCHFV G<sub>NE</sub>-GST, MW = 46 kDa).



### 4.3.2. Purification of RVFV G<sub>NE</sub>

The RVFV G<sub>NE</sub>-GST was purified from the soluble fraction of the cell lysate. The cells were harvested by centrifugation and lysed. The soluble fraction was separated from the insoluble fraction by centrifugation. The soluble fraction was then incubated with an affinity column prepared with the anti-GST mAb. The unbound material was collected, the column was washed with PBS and the bound proteins were eluted by addition of 0.1 M glycine hydrochloride, pH 2.6. The elution fractions were neutralized, dialyzed ON in PBS and analysed by SDS-PAGE followed by Coomassie staining and by WB with an anti-GST mAb (Figure 4.8).



**Figure 4.8** RVFV G<sub>NE</sub>-GST protein purified by affinity chromatography analysed by SDS-PAGE followed by Coomassie staining (A) and Western blot (B).

The RVFV G<sub>NE</sub>-GST (MW = 73 kDa) was purified from the soluble fraction of Sf900 cells infected with BacPAK6 RVFV G<sub>NE</sub> by affinity chromatography with a mAb anti-GST and eluted by addition of 0.1 M glycine hydrochloride, pH 2.6. For the Western blot analysis an anti-GST mAb was used as primary antibody. Arrows indicate the bands corresponding to the specified proteins.

A band corresponding to the RVFV G<sub>NE</sub>-GST was observed in the SDS-PAGE analysis of the elution fractions (Figure 4.8A, elutions 1 to 4). Other unknown contaminants were co-purified by the affinity chromatography (around 60 and 100 kDa). The Western blot analysis (Figure 4.8B) confirmed the protein corresponding to the size of RVFV G<sub>NE</sub>-

GST was purified, however the other bands present in the Coomassie staining were not detected.

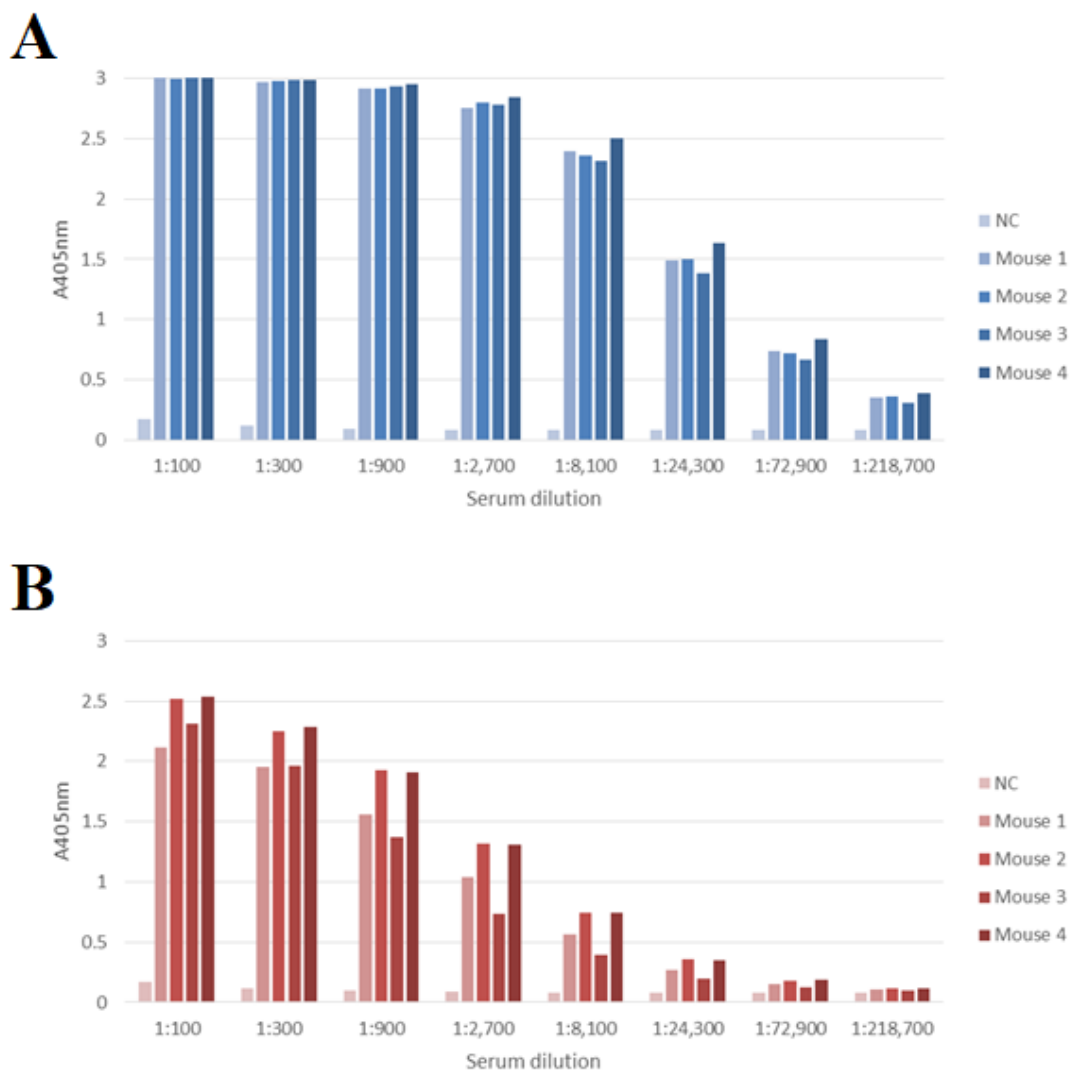
The dialysed elution fractions were concentrated after their dialysis and stored at -80°C.

#### **4.4. Production, purification and characterization of detection molecules against RVFV N protein**

##### **4.4.1. Monoclonal antibodies against RVFV N protein**

###### **4.4.1.1. Production of mAbs against RVFV N protein**

To produce monoclonal antibodies against the RVFV N protein, four mice were immunized with the purified RVFV N protein. A week after the third immunization, and after each subsequent immunization, the mice were bled and their antibody titre was checked by indirect ELISA with the RVFV N protein as the coating antigen. Since the antibody titre was not high enough to perform the fusion, the mice were immunized five more times, with their Ab titre checked by indirect ELISA one week after each immunization. The results obtained after the 8<sup>th</sup> immunization are shown in Figure 4.9.



**Figure 4.9** Antibody titration by indirect ELISA of the mouse sera after eight immunizations with RVFV N protein.

After ten immunizations with RVFV N protein, the four mice (Mouse 1, 2, 3 and 4) were bled from the tail and serial dilutions of the sera were used to assess the antibody titre of the mice by indirect ELISA. The indirect ELISA was performed using RVFV N protein (A) or 6xHis-SUMO-CCHFV N protein (B) as coating antigen. An anti-mouse IgG ( $\gamma$ -chain specific)-HRP conjugated pAb was used as secondary antibody. One mouse used as negative control (NC) was immunized with sterile 1X PBS. All the samples were tested once due to sample volume constraints.

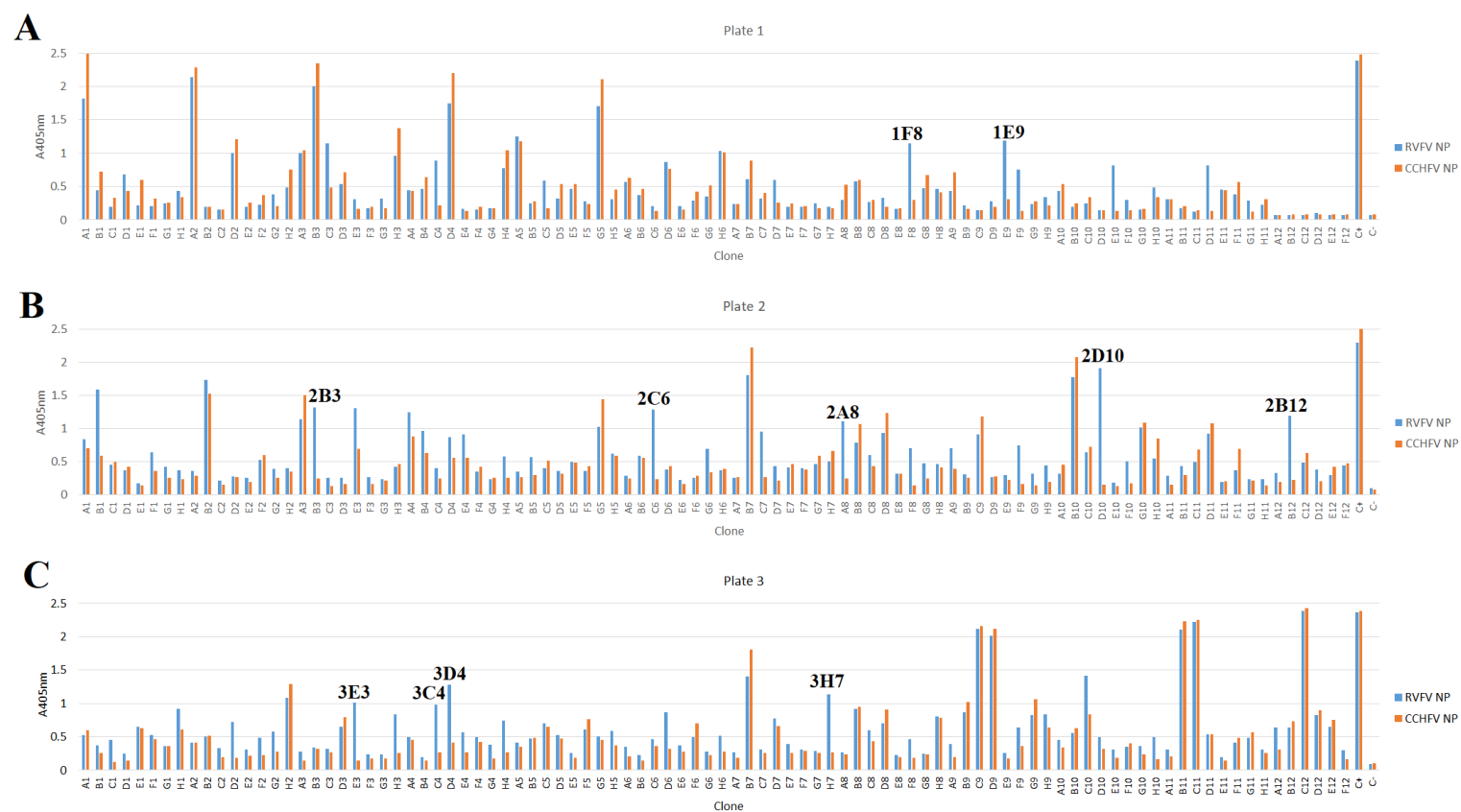
At Eurofins-Ingenssa, the standard antibody titre that should be reached by indirect ELISA to perform the fusion with the tested mouse is  $A_{405nm} > 1$  at a dilution of 1:60,000. After the 8<sup>th</sup> immunization, the Ab titre against the RVFV N protein (Figure 4.9A) was deemed high enough, with an  $A_{405nm}$  around 0.75 at 1:72,900 for all the mice, with a slightly higher titre for mouse 4. The reactivity to the negative antigen (6xHis-SUMO-

CCHFV N protein, Figure 4.9B), was high at low dilutions, however at 1:72,900 only background signal was observed ( $A_{405\text{nm}}$  around 0.16). Thus, mice 2 and 4 were selected to perform the fusion.

Briefly, the two mice were sacrificed, their spleens were harvested and the fusion was performed between P3X63Ag8.653 and the B cells from the spleen. From the spleen,  $1.44 \times 10^8$  B cells were purified and  $3.6 \times 10^7$  P3X63Ag8.653 were required for the fusion. The fused cells were dispensed into three 96-well plates and incubated. The following day, 2X HAT medium was added to the fused cells and this medium was replaced every 48 hrs.

Two weeks after the fusion, the fused cells were screened by indirect ELISA using purified RVFV N protein (without tags) and 6xHis-SUMO-CCHFV N protein (called CCHFV NP in this section) as shown on Figure 4.10. All the ELISAs performed for these screenings were performed with an anti  $\gamma$ -chain specific antibody and revealed with ABTS.

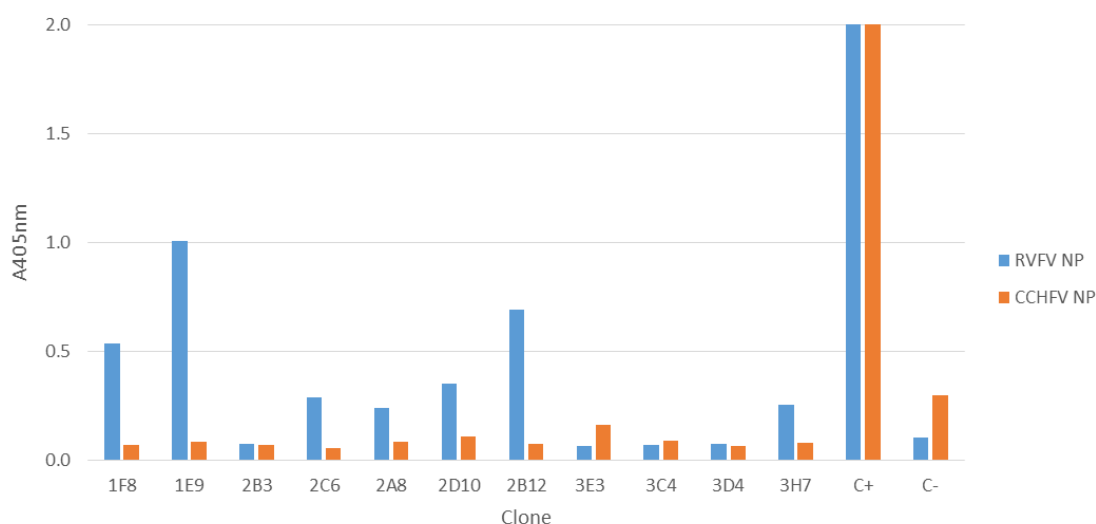
## Chapter 4 Development of diagnostic tools for RVFV



**Figure 4.10 First screening of the three plates containing the hybridoma clones anti RVFV N protein by indirect ELISA.**

Two weeks after the fusion step, indirect ELISAs with the RVFV N protein or the 6xHis-SUMO-CCHFV N protein as coating antigens and an anti  $\gamma$ -chain specific pAb were performed to select hybridomas positive to the RVFV N protein. The eleven clones with an  $A_{405nm} > 1$  to the RVFV N protein and an  $A_{405nm} < 0.5$  to the 6xHis-SUMO-CCHFV N protein are indicated in bold. A: plate 1; B: plate 2; C: plate 3. The positive control (C+) corresponds to the sera collected from the corresponding euthanized mice and the negative control (C-) to mouse sera against a non-related antigen. All the samples were tested once due to sample volume constraints.

This first screening of viable hybridomas resulted in numerous clones giving signal both for the RVFV N protein but also for the CCHFV N protein. To discriminate the clones giving a high background signal, only the clones giving a signal of  $A_{405nm} > 1$  for the RVFV N protein and a signal under 0.5 for the CCHFV N protein were considered. On the first plate (Figure 4.10A), the clones fulfilling these conditions were 1F8 and 1E9. On the second plate (Figure 4.10B) these parameters were met by clones 2B3, 2C6, 2A8, 2D10 and 2B12, whereas on the third plate (Figure 4.10C), these conditions were satisfied by clones 3E3, 3C4, 3D4 and 3H7. The cells present in each of these clones were resuspended and passed in a 24-well plate and incubated for a week. Another ELISA was performed with the supernatant of the 24-well plate to confirm the production of Ab specific to the RVFV N protein (Figure 4.11).



**Figure 4.11 Screening of the hybridoma clones selected by indirect ELISA with the RVFV N protein and the 6xHis-SUMO-CCHFV N protein.**

The eleven hybridoma clones selected with the first screening were tested by indirect ELISA with the RVFV N protein and the 6xHis-SUMO-CCHFV N protein to confirm the production of Ab specific to the RVFV N protein. The indirect ELISA was performed with an anti  $\gamma$ -chain specific pAb. Out of the eleven hybridoma clones, four (clones 1F8, 1E9, 2D10 and 2B12) were selected for subsequent subcloning at 50 cells per well. The positive control (C+) corresponds to the sera collected from the corresponding euthanized mice and the negative control (C-) to mouse sera against a non-related antigen. All the samples were tested once due to sample volume constraints.

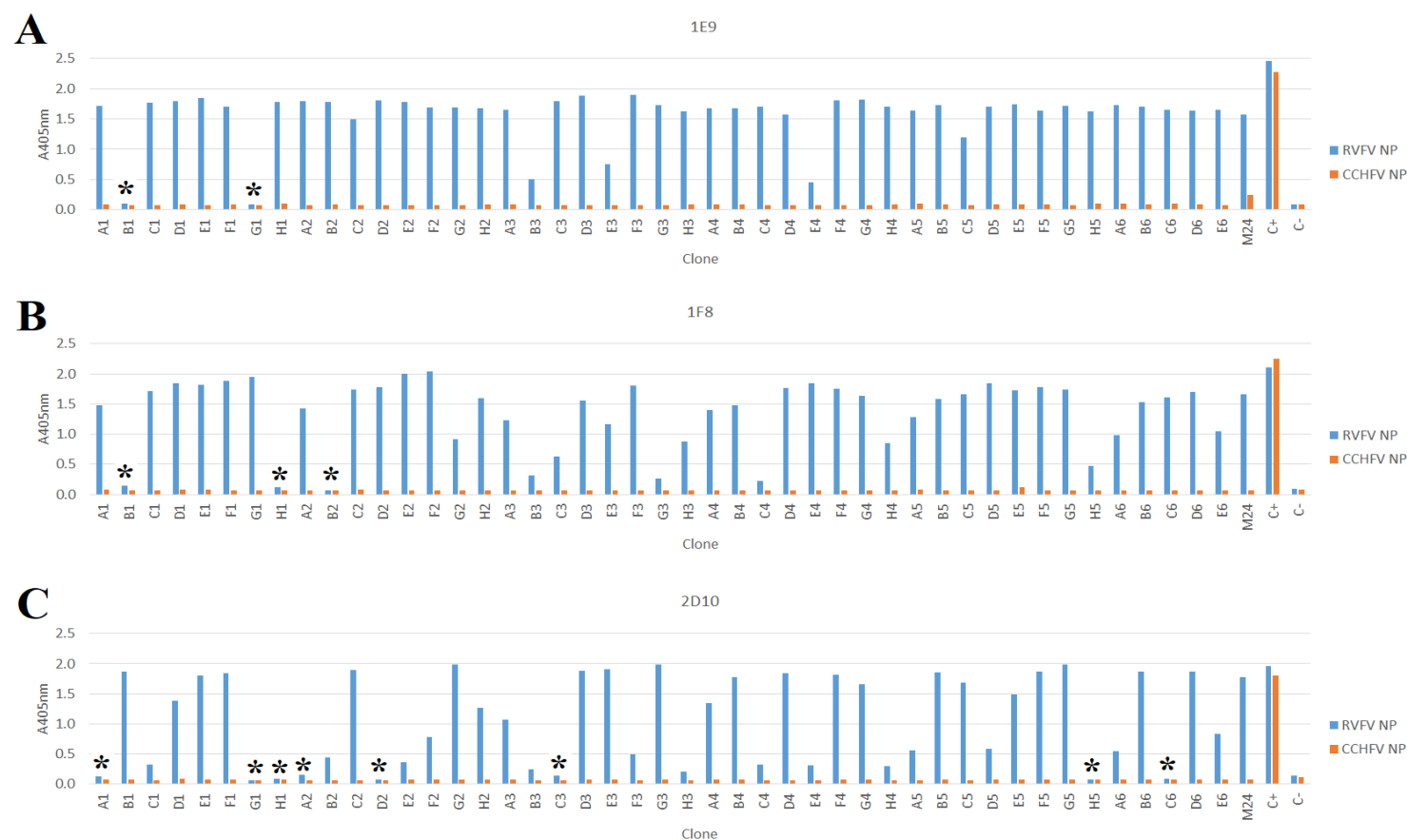
Out of the eleven clones selected, three (1F8, 1E9 and 2B12) had an  $A_{405nm} > 0.5$  for RVFV N protein. Four clones (2C6, 2A8, 2D10 and 3H7) had a lower  $A_{405nm}$  between 0.23 and

0.35. The last four had an  $A_{405nm}$  equivalent to the signal obtained for CCHFV N protein and to the negative control. The cells corresponding to the three clones with the higher signal were resuspended, counted and aliquoted at 50 cells per well in new 96-well plates. Out of the four clones giving some low positive signal, the clone 2D10 was thought to be promising as during the first screening this clone was the only one giving an  $A_{405nm}$  close to 2 with a very low background. Thus, this clone was also subcloned at 50 cells per well.

During the subsequent subcloning procedure, the clone 2B12 did not give any positive signal to RVFV N protein and so was discarded.

The screening and the subcloning of the three remaining hybridoma clones continued until reaching 2 cells per well. A final ELISA was done to check if these were successfully cloned (Figure 4.12).

## Chapter 4 Development of diagnostic tools for RVFV



**Figure 4.12 Indirect ELISA screening of the hybridoma clones at 2 cells per well with RVFV N protein and the 6xHis-SUMO-CCHFV N protein.**

The hybridoma clones 1E9, 1F8 and 2D10 at 2 cells per well were tested in indirect ELISAs with the RVFV N protein or the 6xHis-SUMO-CCHFV N protein as coating antigens and an anti  $\gamma$ -chain specific pAb. The wells were checked using a light microscope and an empty well is denoted by \*. The positive control (C+) corresponds to the sera collected from the corresponding euthanized mice and the negative control (C-) to mouse sera against a non-related antigen. A: 1E9 clone; B: 1F8 clone; C: 2D10 clone. All the samples were tested once due to sample volume constraints.



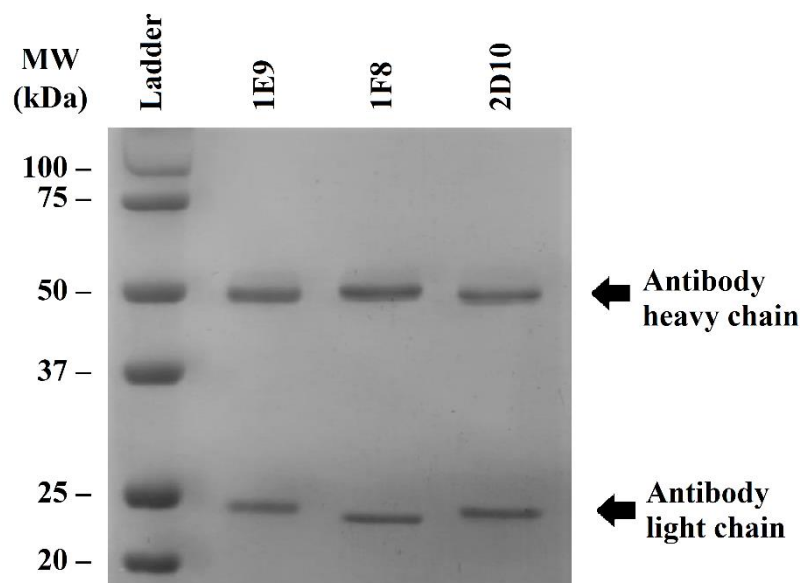
Out of the 45 clones of the 1E9 plate (Figure 4.12A), 43 gave a positive signal with an  $A_{450\text{nm}}$  over 0.45 and two wells had a negative signal (B1 and G1). These wells were checked using a bench-top light microscope and these two wells were found empty with all the other positive wells containing one or two hybridoma clones. Thus, single hybridoma clones were obtained expressing the same monoclonal antibody.

The same results were observed for the 1F8 and 2D10 plates (Figure 4.12B and C). After this step, the three plates (1E9, 1F8 and 2D10) were cloned and wells containing single hybridoma clones were selected and transferred into 6-well plates in order to produce the three monoclonal antibodies.

The anti-RVFV N protein mAbs obtained were named 1E9, 1F8 and 2D10.

#### **4.4.1.2. Purification of mAbs against the RVFV N protein**

The monoclonal antibodies were purified from the supernatant of the hybridomas. The supernatants were centrifuged, filtered and applied onto protein A and G columns for antibody purification. After dialysis, the purity of the monoclonal antibodies was assessed by SDS-PAGE followed by Coomassie staining (Figure 4.13).



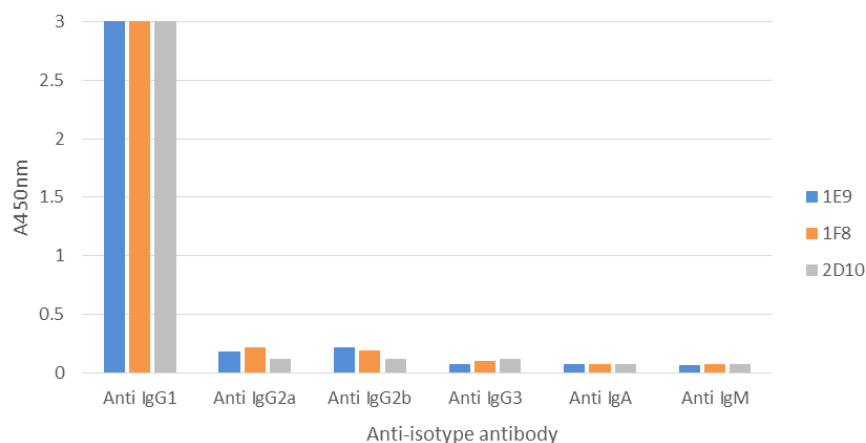
**Figure 4.13** *Anti-RVFV N protein mAbs purification by affinity chromatography.* SDS-PAGE analysis followed by Coomassie staining of the three different anti-RVFV N protein mAbs (1E9, 1F8 and 2D10) produced by hybridoma technology and purified by affinity chromatography with protein A and G columns. Arrows indicate the bands corresponding to the specified proteins.

The anti-RVFV N protein mAbs were highly pure and the two bands corresponding to the heavy and light chain of the IgG were observed for each mAb. These mAbs were quantified by spectrophotometry and further labelled with horseradish peroxidase.

#### 4.4.1.3. Characterization of the anti-RVFV N protein mAbs

Different techniques were used to characterize the anti-RVFV N protein mAbs.

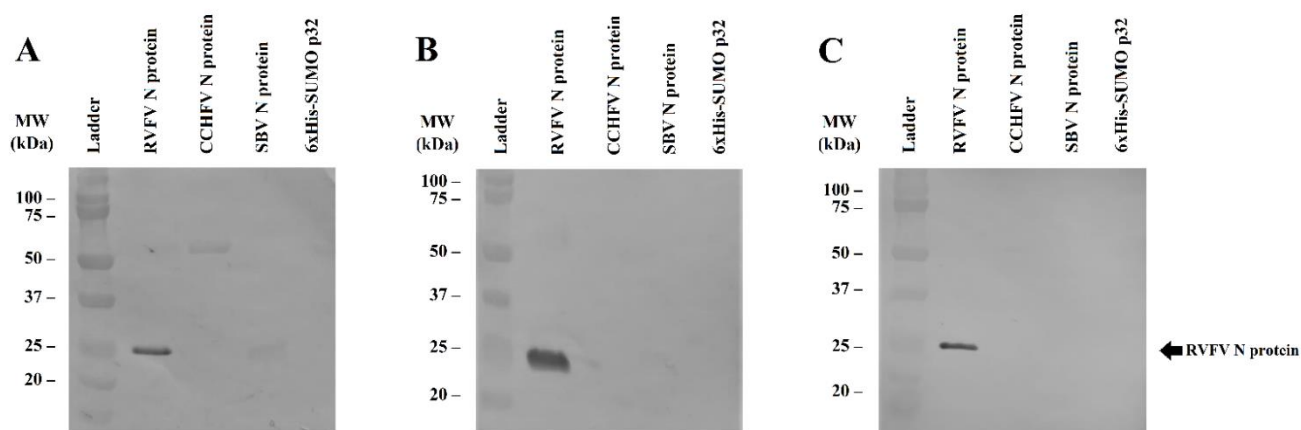
First, the determination of their isotype by performing an ELISA using anti-isotype secondary antibodies (Figure 4.14).



**Figure 4.14 Determination of the isotype of the anti-RVFV N protein mAbs produced.**  
 An indirect ELISA was performed with the three anti-RVFV N protein mAbs (1E9, 1F8 and 2D10) and secondary anti-isotypes antibodies to determine the isotypes of the mAbs. The experiment was performed once.

The signal observed was significantly higher with the secondary antibody anti-IgG1 compared to the other anti-isotype antibodies. Thus, the three anti-RVFV N protein mAbs were classified as IgG1 isotype.

To determine the capacity of the mAbs to detect the N protein in reducing conditions, a WB was performed with the mAbs (Figure 4.15).

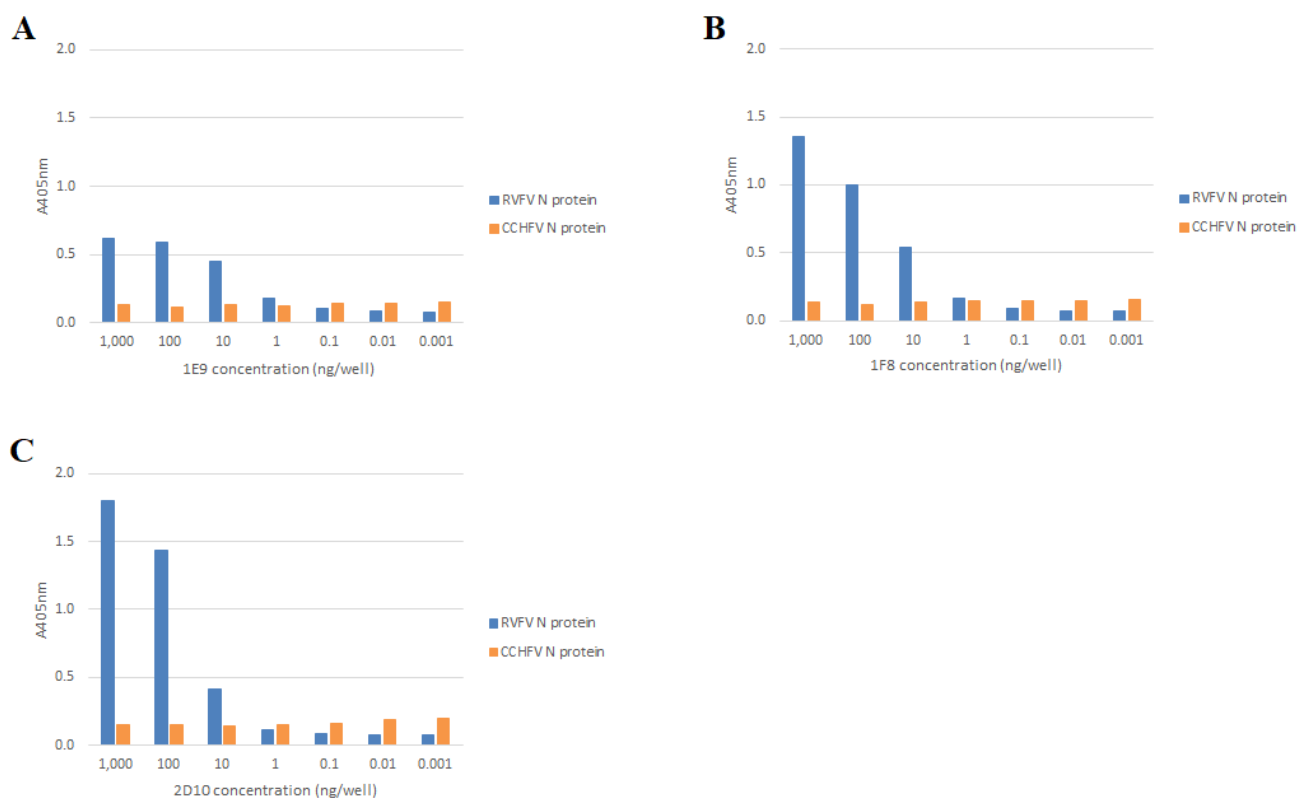


**Figure 4.15** Analysis of the specificity of the three anti-RVFV N protein mAbs in denaturing and reducing conditions.

A Western blot analysis of different nucleocapsid proteins of bunyaviruses (RVFV, CCHFV and SBV N proteins) with the three different anti-RVFV N protein mAbs (A: mAb 1E9. B: mAb 1F8. C: mAb 2D10). The 6xHis-SUMO p32 was used as a negative control protein with the 6xHis-SUMO purification tag.

On the three WBs (Figure 4.15A, B and C), a band corresponding to the size of the RVFV N protein was observed with the three different mAbs. No cross-reactivity was detected against the N proteins of CCHFV and SBV and neither with the 6xHis-SUMO p32, used as negative controls, for the mAbs 1F8 and 2D10 (Figure 4.15B and C). However, with the mAb 1E9 (Figure 4.15A), a faint band corresponding to the CCHFV N protein and a fainter band corresponding to the N protein of SBV were present. However, no band corresponding to the 6xHis-SUMO p32 was observed. Thus, the mAbs recognized the RVFV N protein in denaturing and reducing conditions, which could hint that the anti-RVFV N protein mAbs recognize non-conformational epitopes. mAbs 1F8 and 2D10 were specific for RVFV N protein and mAb 1E9 slightly cross-reacted with the N protein of other bunyaviruses.

To determine the LOD of the mAbs anti-RVFV N protein, an indirect ELISA was performed to titre these mAbs against the RVFV and CCHFV N protein (Figure 4.16).

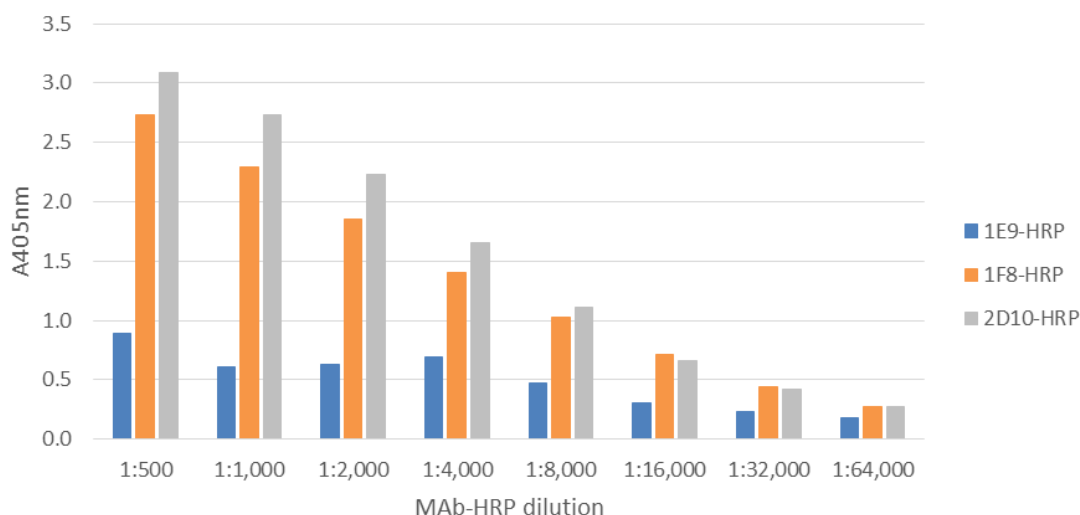


**Figure 4.16 Titration of the mAbs anti-RVFV N protein.**

RVFV and CCHFV N proteins were used to coat ELISA plates and indirect ELISAs were performed with serial dilutions of the anti-RVFV N protein mAbs (A: 1E9; B: 1F8; C: 2D10) to determine their limit of detection. The experiment was performed once.

In these indirect ELISAs, the titration of the anti-RVFV N protein mAbs can be observed with a decrease of the signal of the three mAbs as their concentration decreased (Figure 4.16A, B and C). Until 10 ng/well (corresponding to a concentration of 100 ng/mL), the signal obtained with the mAbs with the RVFV N protein could be differentiated from that for the CCHFV N protein. As observed in the WB, no-cross reactivity could be detected with the CCHFV N protein for the mAbs 1F8 and 2D10, and the mAb 1E9 did not show some cross-reactivity in this assay compared to the WB analysis. This assay confirmed the specificity of the mAbs for the RVFV N protein in non-reducing conditions compared to the control protein and the three mAbs can detect the RVFV N protein until 100 ng/mL.

Then, a direct ELISA was performed with the HRP-conjugated mAbs to confirm the successful labelling of the mAbs and to titre the conjugated mAbs (Figure 4.17).

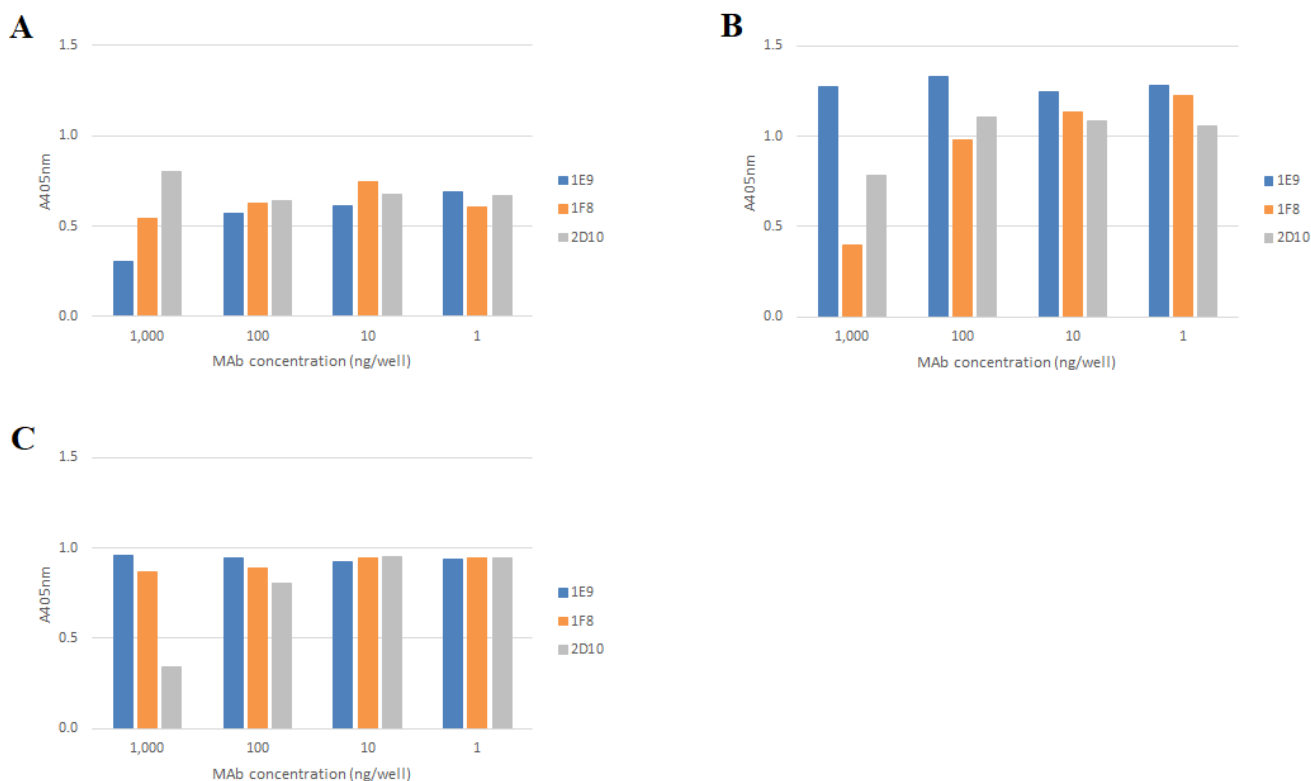


**Figure 4.17 Titration of the HRP-labelled anti-RVFV N protein mAbs.**

Direct ELISAs were performed with the RVFV N protein and serial dilutions of HRP-labelled anti-RVFV N protein mAbs (1E9-HRP, 1F8-HRP and 2D10-HRP) as primary antibodies. The experiment was performed once.

The conjugation of the three mAbs with HRP was successful. The three mAbs showed a decrease in the  $A_{405nm}$  obtained when decreasing their concentration. The mAbs 1F8-HRP and 2D10-HRP showed the same titration pattern, with a similar decrease in the signal obtained and an  $A_{405nm}$  around 1 at a 1:8,000 dilution. The mAb 1E9-HRP gave a lower  $A_{405nm}$  and to obtain an  $A_{405nm}$  around 1, a 1:500 dilution was required.

Finally, to determine if the anti-RVFV N protein mAbs mapped the same epitopes of the RVFV N protein, a competition ELISA was performed between the unlabelled mAbs and the HRP-conjugated mAbs (Figure 4.18).



**Figure 4.18 Determination of the mapping of anti-RVFV N protein mAbs for the same epitopes.** Competition ELISAs were performed between the unlabelled and labelled anti-RVFV N protein mAbs to check if they compete for the same epitopes. A: Competition ELISA with 1E9-HRP at 1:500. B: Competition ELISA with 1F8-HRP at 1:8,000. C: Competition ELISA with 2D10-HRP at 1:8,000. The experiment was performed once.

The mAb 1E9 inhibited the signal obtained with the 1E9-HRP (Figure 4.18A) at a high concentration of mAb ( $A_{405nm}=0.3$  at 1,000 ng/well compared to  $A_{405nm}>0.5$  at 1 ng/well), but the mAbs 1F8 and 2D10 did not affect the signal obtained with the 1E9-HRP ( $A_{405nm}>0.5$  at every mAb concentration). Regarding the competition with 1F8-HRP (Figure 4.18B), the  $A_{405nm}$  obtained with the mAb 1F8 at 1,000 ng/well was below 0.5, when at lower concentrations the  $A_{405nm}$  detected was around 1. A similar effect, but with a smaller difference, was observed with 2D10 at 1,000 ng/well and none with 1E9. Finally, with the 2D10-HRP (Figure 4.18C), the only difference in  $A_{405nm}$  was obtained with 2D10 at 1,000 ng/well. This assay showed that the mAbs seemed not to map in the same epitopes of the RVFV N protein.

Table 4.2 summarizes the mAbs anti-RVFV N protein obtained and some of their characteristics that were determined in this chapter.

*Table 4.2 Summary of the characteristics of the anti-RVFV N protein mAbs obtained.*

<b>Anti-RVFV N protein mAbs</b>	<b>Isotype</b>	<b>RVFV N protein identification in reducing conditions</b>	<b>Concentration of mAb detecting RVFV N protein in non-reducing conditions</b>	<b>Titre of HRP-mAbs to obtain an <math>A_{405nm} \approx 1</math></b>	<b>Competition for the same epitope</b>
1E9	IgG1	Yes, with slight cross-reactivity	100 ng/mL	1:500	No
1F8	IgG1	Yes	100 ng/mL	1:8,000	No
2D10	IgG1	Yes	100 ng/mL	1:8,000	No

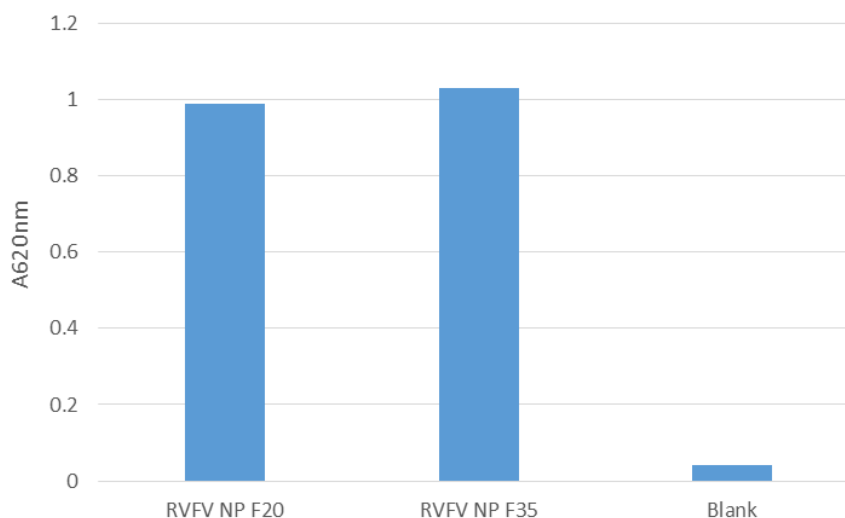
#### **4.4.2. Affimers against RVFV N protein**

##### **4.4.2.1. Selection and production of Affimers against RVFV N protein**

###### **4.4.2.1.1. Biotinylation of the RVFV N protein**

For the production of Affimers against RVFV N protein, two different RVFV N protein elution fractions (Figure 4.4, F20 and F35) were selected for the panning rounds. The two RVFV N protein fractions were biotinylated and an ELISA was done to check the successful biotinylation of the RVFV N proteins (Figure 4.19).





**Figure 4.19 Confirmation of the biotinylation of the two RVFV N proteins fractions F20 and F35.**

A direct ELISA was performed with 1  $\mu$ L of the biotinylated RVFV F20 and F35 as coating reagent and Streptavidin-HRP as detection molecule. The blank corresponds to a well coated with 1X PBS. The experiment was performed once.

The two fractions F20 and F35 were correctly biotinylated and could be used for the panning rounds to select binding Affimers.

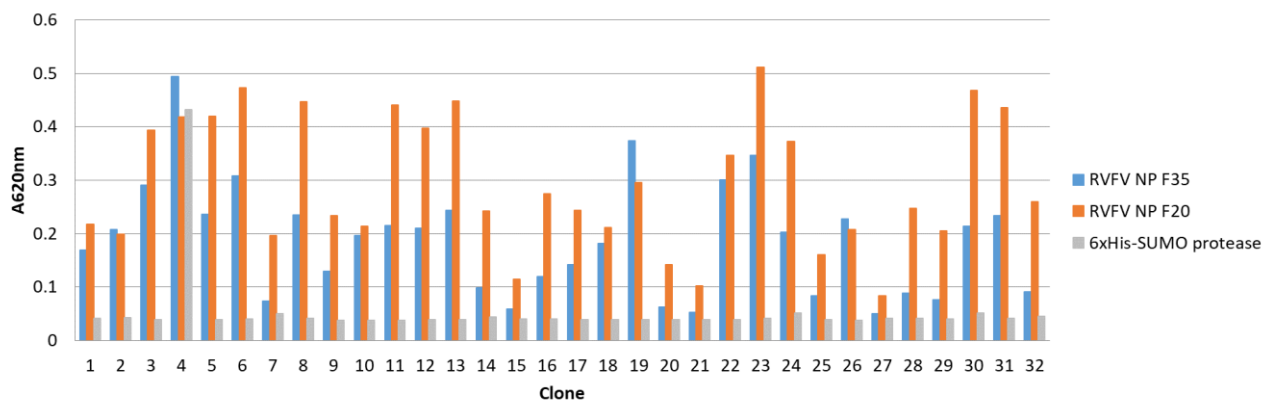
#### 4.4.2.1.2. RVFV N protein-specific Affimer selection

For the first panning round, the phage library was pre-panned with purified 6xHis-SUMO tag and 6xHis-SUMO protease to remove the binders to these contaminants that still could be present in small quantities in the purified RVFV N protein fractions F20 and F35. The first panning round was performed with 5  $\mu$ L of the biotinylated RVFV N protein F20 or F35. This first panning round yielded  $1.15 \times 10^6$  phage-infected *E. coli* colonies for RVFV N protein F20 and  $1 \times 10^6$  for RVFV N protein F35. To select the best binders from this first panning round, the second panning round was performed with the same quantities of RVFV N protein F20 and F35, but with increased quantities of 6xHis-SUMO tag and 6xHis-SUMO protease and with a longer incubation step. This second panning round yielded 22,000 phage-infected *E. coli* colonies for RVFV N protein F20 and 5,000 for RVFV N protein F35. Four pre-panning rounds with 6xHis-SUMO tag and 6xHis-SUMO protease were performed before the final panning round with 1  $\mu$ L of the biotinylated

RVFV N protein F20 or F35 and harsh washing conditions to only keep the best binders. After the final panning round,  $2.3 \times 10^6$  phage-infected *E. coli* colonies for RVFV N protein F20 and 175,000 for RVFV N protein F35 were obtained. The phage amplification was successful for binders recognizing the RVFV N protein F20 as many colonies were obtained for this protein, however, this was less successful for binders recognizing the RVFV N protein F20 as less colonies were observed.

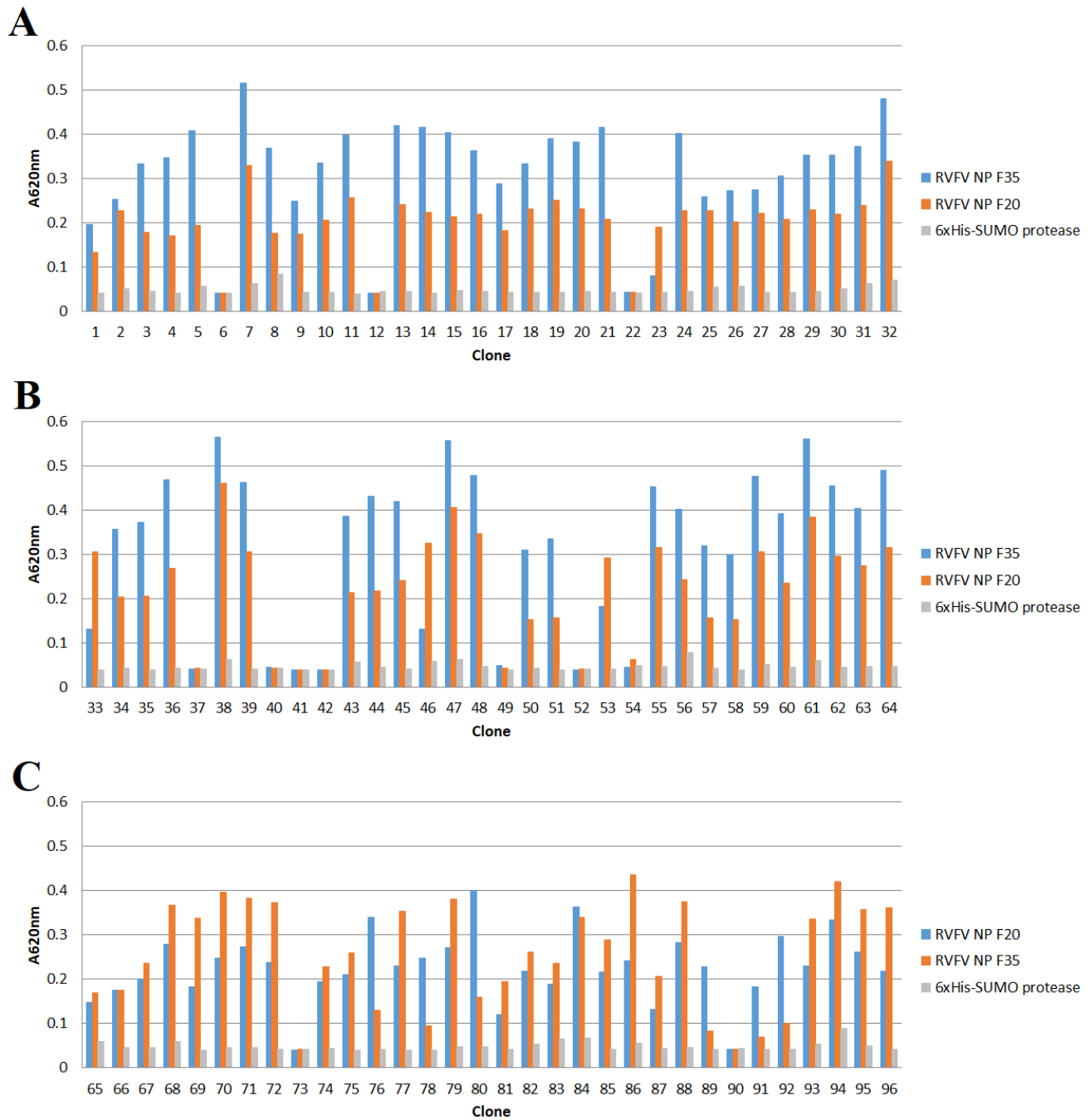
#### 4.4.2.1.3. Phage ELISA to confirm the specific binding of the Affimers

To confirm the binding of the selected Affimers, a phage ELISA was performed with the supernatant of the phage-infected cultures. For this phage ELISA, 32 colonies were selected for the Affimers binding to the RVFV N protein F20 and 96 for those binding to the RVFV N protein F35. The results of the phage ELISA are shown in Figure 4.20 and Figure 4.21.



**Figure 4.20 Phage ELISA with the Affimers selected against the RVFV N protein F20.**

An indirect ELISA was performed by incubating the biotinylated RVFV N protein F20, F35 and 6xHis-SUMO protease (used as negative control) onto a streptavidin coated plate. The supernatants of Affimer-containing culture selected against the RVFV N protein F20 were incubated with the antigens and an anti-Fd-Bacteriophage-HRP antibody was used as secondary antibody. All the samples were tested once due to sample volume constraints.



**Figure 4.21 Phage ELISA with the Affimers selected against the RVFV N protein F35.** An indirect ELISA was performed by incubating the biotinylated RVFV N protein F20, F35 and 6xHis-SUMO protease (used as negative control) onto a streptavidin coated plate. The supernatants of Affimer-containing culture selected against the RVFV N protein F35 were incubated with the antigens and an anti-Fd-Bacteriophage-HRP antibody was used as secondary antibody. A: clones 1 to 32; B: clones 33 to 64; C: clones 65 to 96. All the samples were tested once due to sample volume constraints.

Out of the 32 binders selected for the RVFV N protein F20 (Figure 4.20), only n°4 had unspecific binding and bound both to the RVFV N protein and the 6xHis-SUMO protease. All the other clones had a specific binding for RVFV N protein with most of the binders giving a higher A<sub>620nm</sub> for F20 than for F35.

Out of the 96 binders selected for the RVFV N protein F35 (Figure 4.21A, B and C), 12 clones (n°6, 12, 22, 37, 40, 41, 42, 49, 52, 54, 73 and 90) did not bind to any of the antigen and did not give any signal. All the other binders specifically bound to the RVFV N protein, with most of them giving a higher A<sub>620nm</sub> for the F35 than for the F20.

This phage ELISA confirmed the specific binding of the Affimers selected against the RVFV N protein F20 or F35. Cultures were set up with the 31 Affimers binding to RVFV N protein F20 and the 84 Affimers binding to RVFV N protein F35 and these were sent to sequencing.

#### 4.4.2.1.4. Identification of unique binders

The sequencing results (Figure 4.22) identified 15 unique binders (P1, P2, P3, P5, P7, P9, P11, P14, P15, P16, P19, P20, P25, P28 and P29) out of the 31 clones recognizing the RVFV N protein F20, with 9 binders present once and 6 binders present multiple times with binder 1 (called P1) having the most hits (6 hits). Binders with multiple hits could mean a high specificity for the target protein as they have been enriched. The sequencing results for the binders to RVFV N protein F35 (Figure 4.23) showed 8 unique binders (M1, M2, M3, M21, M23, M33, M76 and M84) with 2 binders only present once when M1 and M3 were present 21 and 38 times respectively.

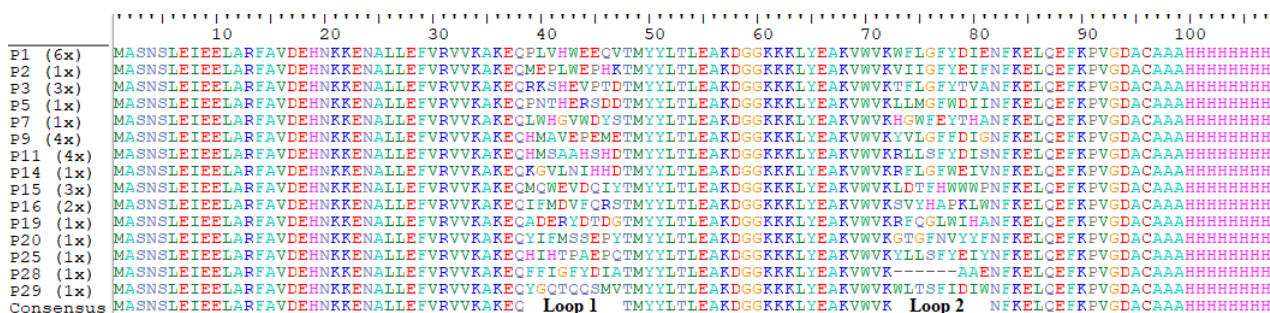


Figure 4.22 Alignment of the amino acid sequences of the fifteen unique Affimers selected against the RVFV N protein F20 and subcloned into pET-11a vector.



**Figure 4.23** Alignment of the amino acid sequences of the eight unique Affimers selected against the RVFV N protein F35 and subcloned into pET-11a vector.

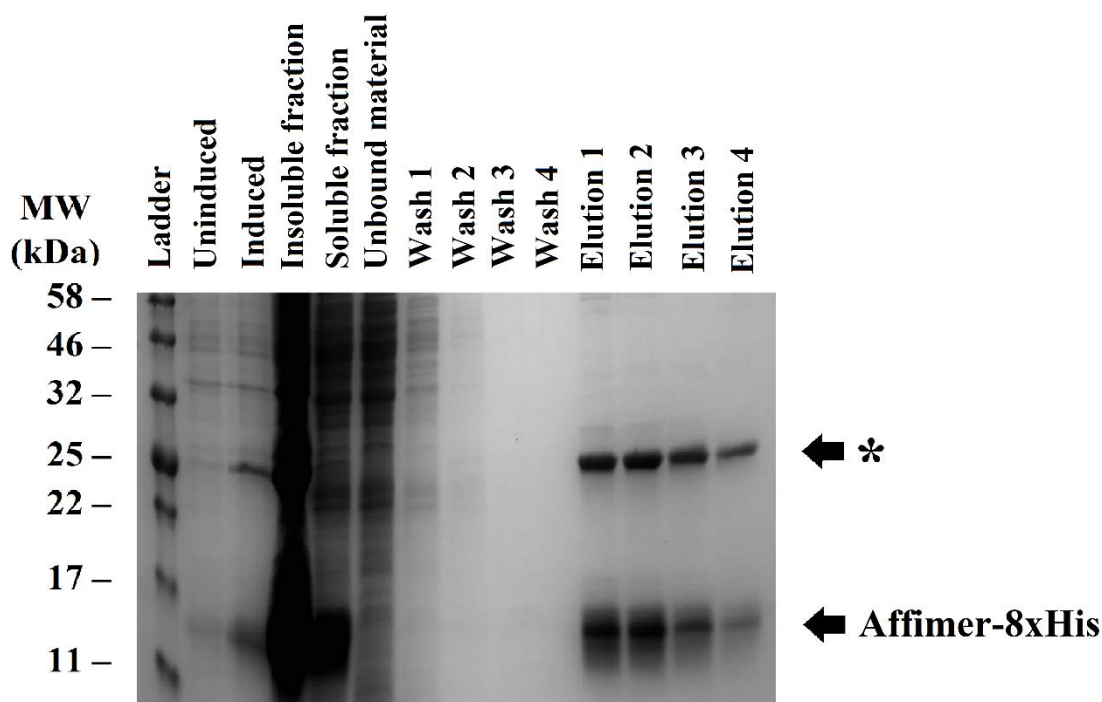
#### 4.4.2.2. Production of Affimers against RVFV N protein

The ORFs of the 23 Affimers were cloned into pET11a plasmid for their expression in *E. coli* following the steps described in 2.5.2.3. A unique cysteine was added at the C-terminal region of the Affimer sequence and the 8xHis sequence present in the pET11a plasmid will allow the purification of the produced Affimers by affinity chromatography.

The Affimer-pET11a plasmid was used to transform *E. coli* BL21 (DE3) R2. The expression of the Affimer was induced with IPTG, then the cells were harvested, lysed and the soluble fraction was separated from the insoluble fraction by centrifugation and analysed by SDS-PAGE followed by Coomassie staining (Figure 4.24). A band at the expected molecular size of the Affimers (MW= 13 kDa) was observed after induction, and in the soluble fraction.

#### 4.4.2.3. Purification of Affimers against RVFV N protein

The 8xHis-Affimers were purified from the soluble fraction by IMAC using Ni<sup>2+</sup>-NTA affinity chromatography. The soluble fraction was incubated with the Ni<sup>2+</sup>-NTA affinity chromatography, the resin was washed and the elution of the 8xHis-Affimers was performed with an elution buffer containing 300 mM imidazole. The elution fractions were analysed by SDS-PAGE followed by Coomassie staining (Figure 4.24).



**Figure 4.24** Affimer P1 production and purification by  $\text{Ni}^{2+}$ -NTA affinity chromatography.

SDS-PAGE analysis followed by Coomassie staining of samples taken at different steps of the expression and purification of Affimer P1. Affimer P1 was purified from the soluble fraction by a  $\text{Ni}^{2+}$ -NTA affinity chromatography and eluted with elution buffers containing imidazole. Arrows indicate the bands corresponding to the specified proteins and \* denotes an unknown protein.

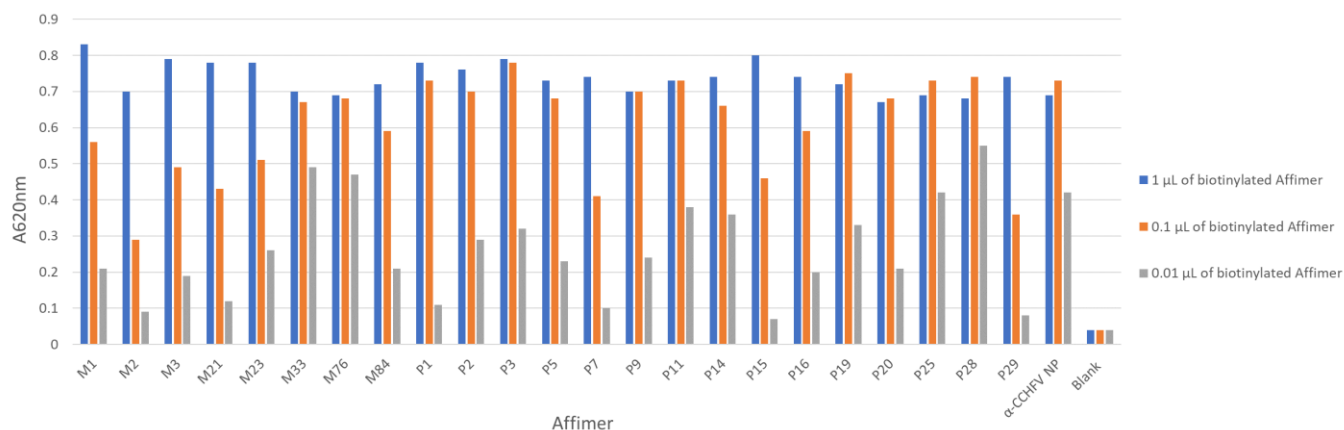
The elution fractions contained one band around 13 kDa, corresponding to the molecular weight of the Affimers. However, the elution fractions of some Affimers also contained an additional band of an unknown protein around 25 kDa (Figure 4.24, elutions 1 to 4). This band around 25 kDa suggested that some Affimers (such as Affimer P1) were forming dimers, despite the presence of reducing agents in the SDS-PAGE analysis

The fractions containing the eluted Affimers were stored at  $-20^{\circ}\text{C}$  or used to biotinylate the Affimers.

#### 4.4.3. Characterization of the detection molecules by pull-down assay

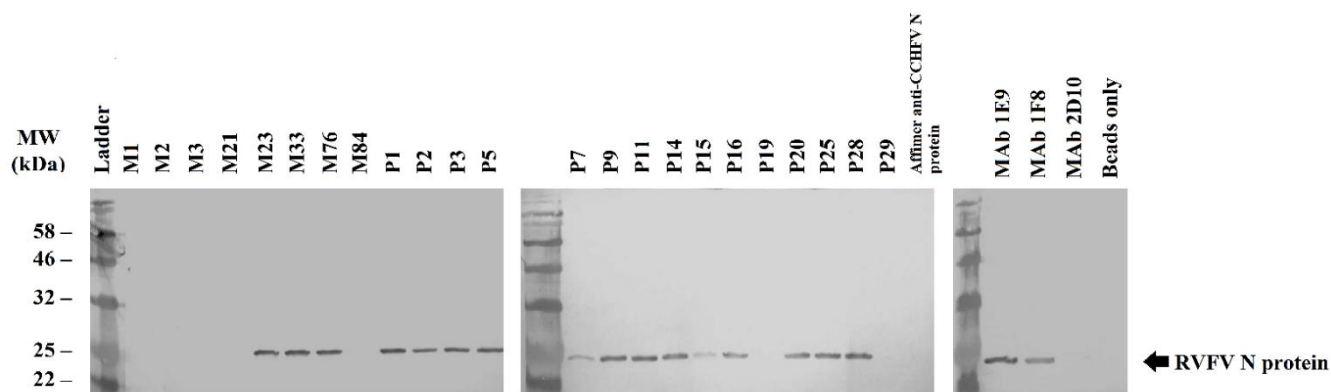
The 23 purified Affimers were biotinylated using biotin-maleimide. The maleimide groups specifically reacts with the sulfhydryl groups from the C-terminal cysteine of the

Affimers to form stable thioether bonds to link the biotin to the Affimers. The correct biotinylation of the 23 Affimers was assessed by ELISA (Figure 4.25). The 23 Affimers were all correctly biotinylated. The three anti-RVFV N protein mAbs were also biotinylated following the same protocol.



**Figure 4.25 Confirmation of the biotinylation of the anti-RVFV N protein Affimers.** Direct ELISA performed with different coating concentration of biotinylated Affimers (1 μL, 0.1 μL and 0.01 μL) and Streptavidin-HRP as detection molecule. The biotinylated anti-CCHFV NP Affimer already available in the lab was used as a positive control and the blank correspond to wells coated with 1X PBS. The experiment was performed once.

The binding capability of the Affimers and the mAbs to the RVFV N protein was assessed by pull-down assay. The biotinylated Affimers and anti-RVFV N protein mAbs were individually bound to magnetic streptavidin-conjugated beads. RVFV N protein was added to the beads, the beads were washed to remove unbound RVFV N protein and eluted in sample buffer. The eluted samples were analysed by Western blotting using a anti-RVFV N protein mAb (F1D11) (Figure 4.26).



**Figure 4.26 Pull-down assay with the Affimers and anti-RVFV N protein mAbs.**

Western blot analysis of pull-down samples using RVFV N protein as target antigen and biotinylated Affimers or mAbs immobilized onto streptavidin coated beads. The Western blot was performed with an anti-RVFV N protein mAb as primary antibody. A negative control Affimer (Affimer anti-CCHFV N protein) and a beads only control were included. Arrows indicate the bands corresponding to the specified proteins.

Out of the 23 anti-RVFV N protein Affimers tested, 17 successfully bound to the RVFV N protein, with different affinities. Eleven of them seemed to be strong binders (M23, M33, M76, P1, P2, P3, P5, P9, P11, P25 and P28), three medium binders (P14, P16 and P20), three low binders (M3, P7 and P15) and six did not bind to the RVFV N protein (M1, M2, M21, M84, P19 and P29). Finally, out of the three anti-RVFV N protein mAbs, 1E9, bound well to the RVFV N protein, when 1F8 less strongly bound to the protein and 2D10 had a low binding to the RVFV N protein. The Affimers not binding to the RVFV N protein were discarded.

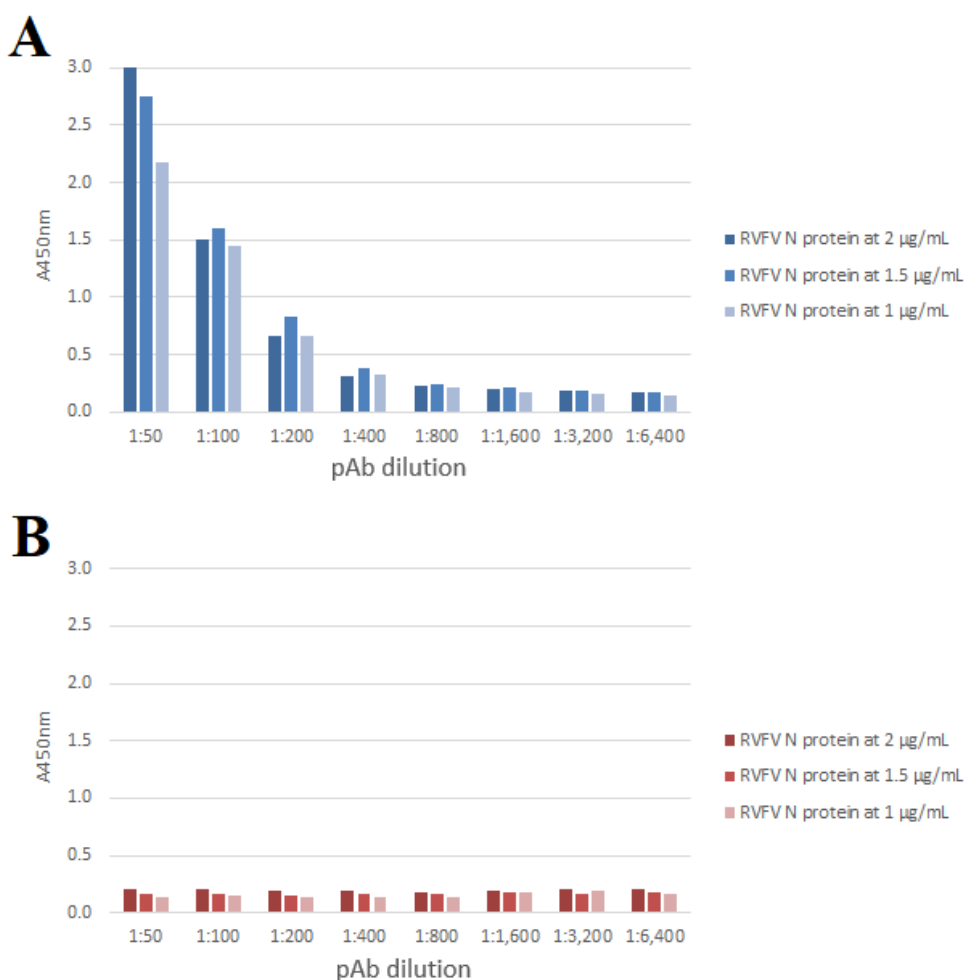
#### **4.5. Development of a double recognition ELISA to detect antibodies against RVFV**

To address the low number of commercial serological assays that are available for the detection of RVFV antibodies, a double recognition ELISA was developed using the RVFV N protein as the target antigen. This assay can detect total antibody response (IgM and IgG) in serum of different animal species. The first step of this development was the labelling of RVFV N protein with HRP, then the optimization of the assay and finally the validation of the assay with positive and negative field samples.



### 4.5.1. Labelling of the RVFV N protein

The RVFV N protein was conjugated to HRP as described in section 2.6.1.1.1, to be used as the detection molecule in this double recognition ELISA. To confirm the labelling of the HRP, a double recognition ELISA was performed with RVFV N protein coated in the 96-well plates and a mouse pAb obtained from the blood of the mice immunized with the RVFV N protein. This pAb was titrated and detected by the newly labelled RVFV N protein at 1:2,000 (Figure 4.27).



**Figure 4.27 Confirmation of the labelling of RVFV N protein with HRP.**

A double recognition ELISA was performed with different concentrations of RVFV N protein as coating molecule and RVFV N protein-HRP as detection molecule diluted 1:2,000. A: serial dilutions of the sera of euthanized mice immunized with RVFV N protein (pAb) was used as positive sera. B: serial dilutions of serum of a mouse immunized with 1X PBS was used as negative serum.

At a 1:50 dilution of the positive pAb (Figure 4.27A), an  $A_{450\text{nm}}$  of 3 was detected with RVFV N protein at 2  $\mu\text{g/mL}$ . This signal decreased with 1.5  $\mu\text{g/mL}$  ( $A_{450\text{nm}} \approx 2.7$ ) and 1  $\mu\text{g/mL}$  ( $A_{450\text{nm}} \approx 2.2$ ). This signal difference was reduced when the pAb was further diluted and the signal decreased with the dilution of the pAb. In comparison, when diluting negative mice serum (immunized with PBS, Figure 4.27B), only background signal was observed with the different serum dilution and the different coatings.

This assay showed the correct labelling of the RVFV N protein with HRP. In a second time, the optimal conditions of the double recognition ELISA had to be determined.

### 4.5.2. Serum samples

In this study, for the development of the double recognition ELISA, the panel of serum samples consisted of 68 positive experimental samples and 456 negative field sera. For detection of antibodies to RVFV, 68 sheep positive experimental samples were kindly provided by Dr. A. Brún from INIA-CISA. These samples were inactivated and tested at Eurofins-Ingenasa.

A collection of 456 negative field samples (93 from cattle, 178 from sheep and 185 from goats) from Spanish farms were evaluated.

All these samples were assayed in the ID Screen® Rift Valley Fever Competition Multi-species (IDVet) and INgezim FVR Compac (Eurofins-Ingenasa), used as the reference techniques for the development of this assay, and were classified as positive and negative according to the results obtained. A summary of the classification is detailed in Table 4.3.

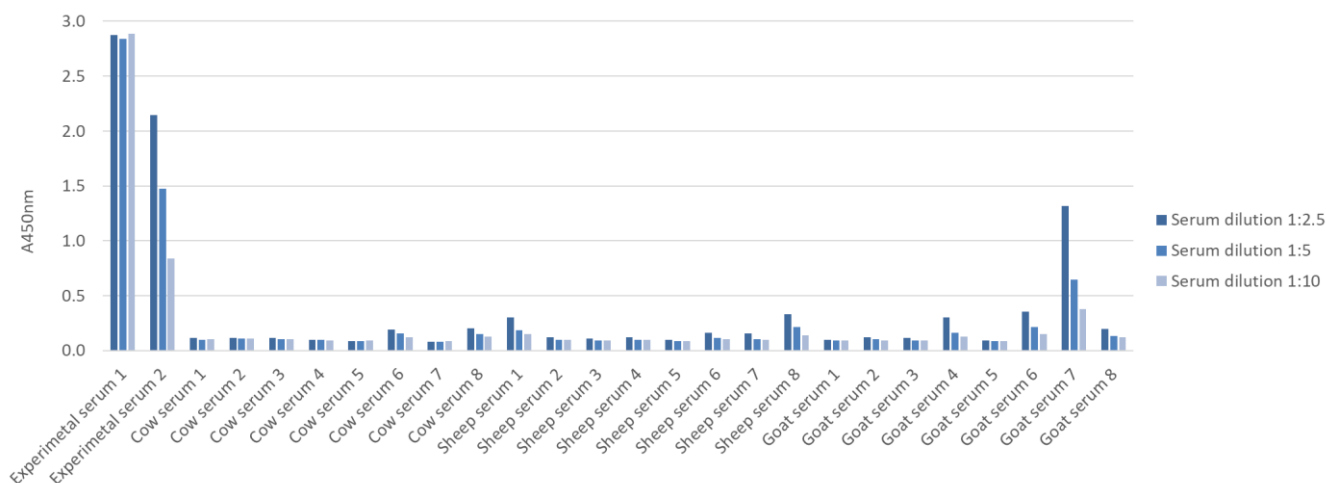
**Table 4.3 Classification of the serum samples used to develop the double recognition ELISA to detect antibodies against RVFV.**

<b>Samples</b>	<b>Cattle</b>	<b>Sheep</b>	<b>Goat</b>	<b>Total</b>
Positive	0	62	0	62
Negative	93	184	185	462
Total	93	246	185	524

### 4.5.3. Optimization of the double recognition ELISA

The optimal conditions of the double recognition ELISA were determined. This included coating concentration, serum dilution, the detection molecule dilution, dilution buffers and the times of incubation.

To ascertain these conditions, two positive experimental sera, characterized in the reference assays (one highly positive and one weakly positive), were tested at a 1:2.5, 1:5 and 1:10 serum dilution in DB2 with a few negative field sera. The RVFV N protein was coated at 2  $\mu\text{g}/\text{mL}$  and different concentrations of RVFV N protein-HRP (at 1:2,000; 1:4,000 and 1:8,000 in DB4) were tested. The results of this titration with the RVFV N protein-HRP at 1:8,000 can be found in Figure 4.28.



**Figure 4.28** Titration of RVFV positive experimental sera and negative field sera in double recognition ELISA.

A double recognition ELISA was performed with the RVFV N protein coated at 2  $\mu\text{g}/\text{mL}$  and the RVFV N protein-HRP at 1:8,000. Serial dilutions of positive experimental sera and negative field sera were used from 1:2.5 to 1:10. All the samples were tested once due to sample volume constraints.

The  $A_{450\text{nm}}$  obtained for the highly positive serum sample (experimental serum 1) was around 3 at a 1:2.5 dilution and did not decrease at a higher serum dilution. The  $A_{450\text{nm}}$  of the weakly positive serum sample was around 2 at a 1:2.5 serum dilution and decreased when the serum dilution increased, to reach  $A_{450\text{nm}}=0.8$  at a 1:10 serum dilution. The eight

cow and sheep negative field sera only gave some background signal, which was reduced when the serum dilution increased. One goat serum sample (n°7) had a high  $A_{450\text{nm}}$  at a 1:2.5 dilution ( $A_{450\text{nm}} \approx 1.5$ ), but this signal was reduced to 0.4 at a 1:10 dilution. As the experimental positive serum samples had a high signal in this assay, and to avoid the high background signal given by some of the negative field sera, the 1:10 serum dilution was chosen.

After this first step, where the coating condition and serum dilution were determined, another assay was performed with a RVFV N protein-HRP dilution at 1:5,000, with a higher number of positive experimental, and negative field sera (data not shown). This assay showed some good results for the positive experimental samples tested, however out of the 355 negative serum samples tested, 7 had a false positive signal.

A final assay was performed to reduce the background signal obtained with these problematic negative field sera by increasing the RVFV N protein conjugate dilution at 1:10,000 (data not shown). These conditions greatly reduced the background signal obtained with the problematic negative field sera.

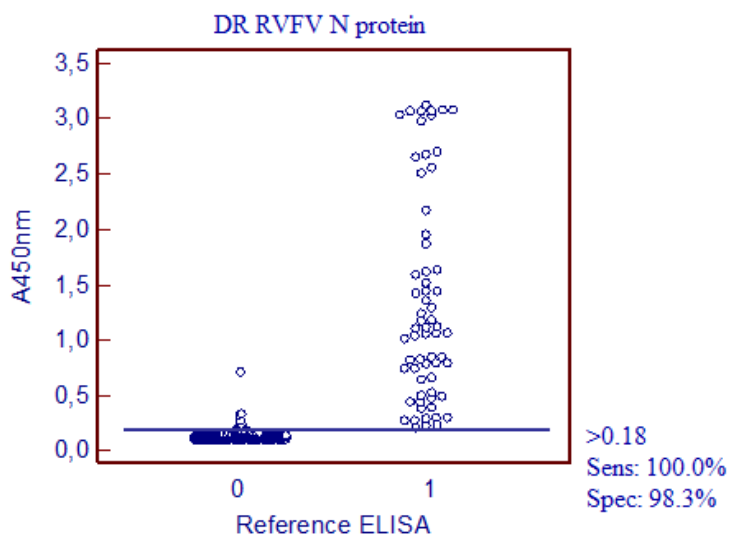
The final conditions of the double recognition ELISA were: RVFV N protein at 2  $\mu\text{g/mL}$  in carbonate buffer to coat the ELISA plates, a serum dilution of 1:10 in DB2 and the RVFV N protein-HRP diluted at 1:10,000 in DB4, as detection molecule.

#### **4.5.4. Validation of the double recognition ELISA**

Once the conditions of the double recognition ELISA were established, 62 positive experimental samples to RVFV and 462 negative field samples were tested in the assay. The results were statistically analysed by comparison with the results obtained with the reference techniques. A cut-off value was determined using the MedCalc® software and based on this cut-off, the performance characteristics of the double recognition ELISA were determined.

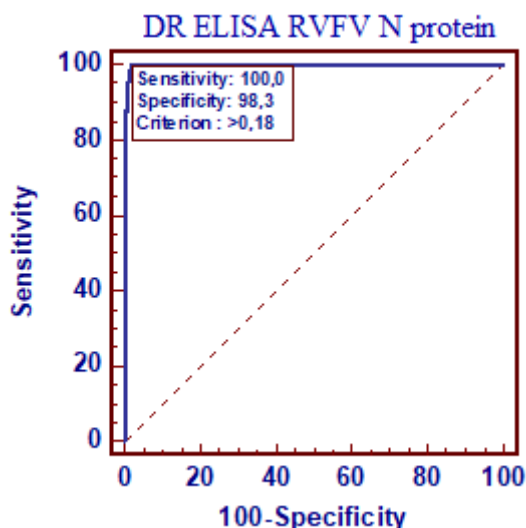
The optimal cut-off for the double recognition ELISA developed was  $A_{450\text{nm}}=0.18$  and with this cut-off, the 62 positive samples were all detected by the double recognition ELISA, corresponding to a sensitivity of 100% with a 95% confidence interval between 94.3 – 100.0%. Out of the 462 negative field samples tested, 8 had a signal superior to

the cut-off, corresponding to a specificity of 98.3% with a 95% confidence interval between 96.6 – 99.2%. Figure 4.29 shows the dot plot corresponding to the sera tested in this assay and Figure 4.30 the corresponding ROC curve analysis.



**Figure 4.29** Dot plot diagram between the double recognition ELISA RVFV N protein and the reference technique where each dot represents an individual sample.

The horizontal solid line corresponds to the cut-off value of the assay, according to the MedCalc® 10 software. X axis shows the positive (1) or negative (0) classification of samples according to reference ELISA and Y axis shows the absorbance at 450 nm obtained in the double recognition ELISA. All the samples were tested once due to sample volume constraints.



**Figure 4.30** Receiver operating characteristic curve analysis of the double recognition ELISA RVFV N protein.

The blue line shows the mean area under the curve (AUC) plot and the red dotted line corresponds to an AUC of 0.5. The sensitivity and specificity values corresponding to the cut-off are represented on the graph. All the samples were tested once due to sample volume constraints.

Using the MedCalc<sup>®</sup> 10 software, McNemar test was performed to examine the relation between the results obtained in the double recognition ELISA and in the reference assay. The calculated chi squared equalled 6.13 with a two tailed P-value of 0.0133 which is lower than 0.05, thus there is a significant difference between the two proportions and there is a significant relationship between the 2 assays.

Using the RVFV N protein, a double recognition ELISA detecting antibodies to RVFV was developed. This assay exhibited a sensitivity of 100% with 62 positive experimental samples tested and a specificity of 98.3% with 462 negative field samples tested.

#### **4.6. Development of a double antibody sandwich ELISA to detect RVFV N protein**

Using the three mAbs and the 17 Affimers produced against the RVFV N protein, a double antibody sandwich ELISA was developed to detect RVFV N protein in serum/plasma samples. This assay could be used to detect RVFV in acute samples of humans or animals. The first step of the development was the selection of the best pair of

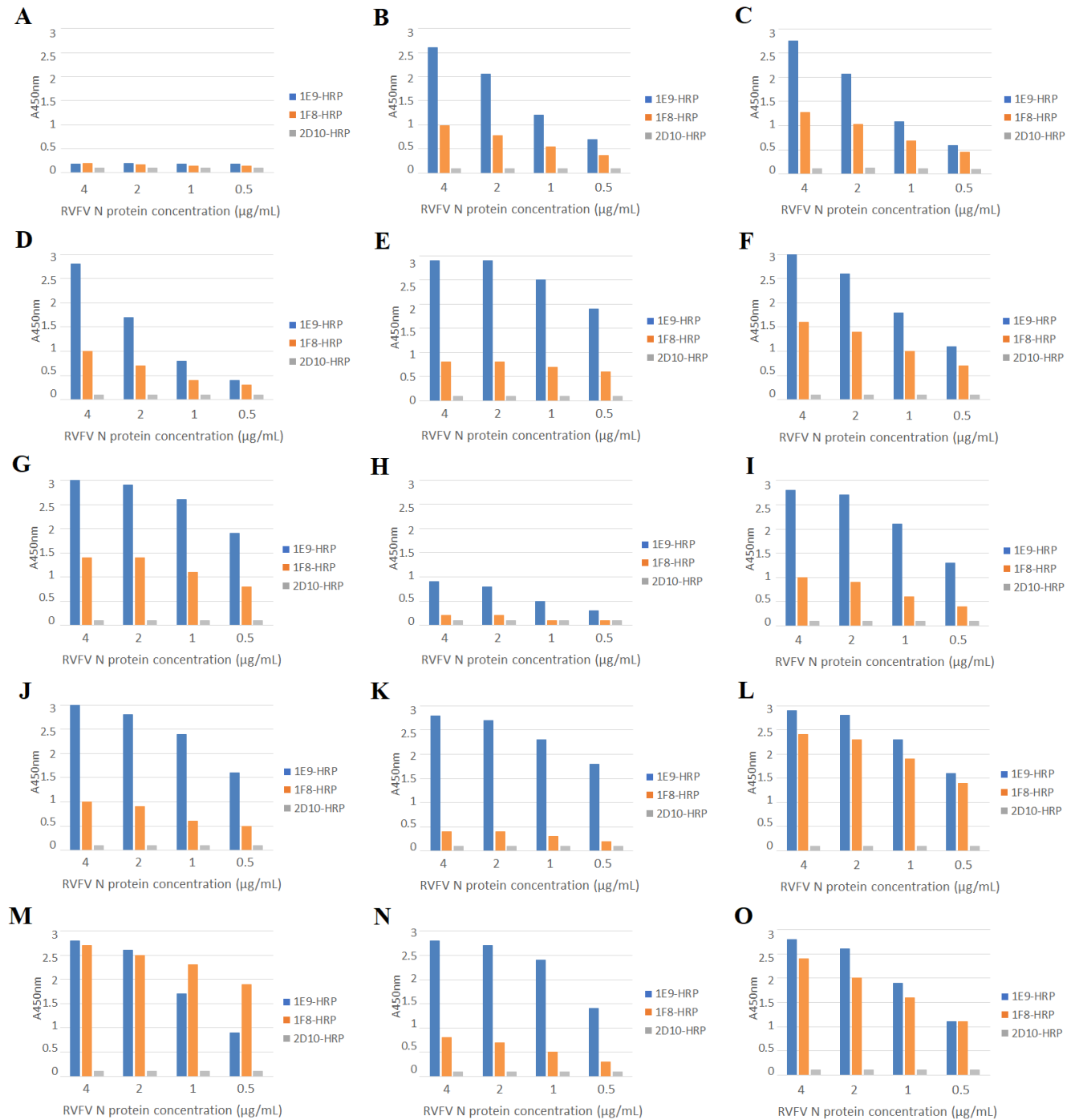
mAbs and/or Affimers. Then, the limit of detection of the assay was determined. Finally, some acute samples from RVFV-infected sheep were tested in the double antibody sandwich ELISA.

#### **4.6.1. Serum samples**

To develop this assay, we used the plasma of three sheep infected with RVFV and collected at different DPI: at 1, 2, 3, 4, 5, 7, 9 and 11 (samples kindly provided by Dr. A. Brún from INIA-CISA). For detection of RVFV antigen in the plasma samples, they were tested in the double antibody sandwich ELISA when the assay conditions were optimized.

#### **4.6.2. Selection of the best pair of anti-RVFV N protein mAbs/Affimers**

To determine the best pair of mAbs and/or Affimers that could detect the RVFV N protein, a first assay was done with the 17 Affimers that could bind the RVFV N protein in the pull-down assay. In this first assay, the Affimers were used as the capture molecule and the three anti-RVFV N protein mAbs were used as the detection molecule. The mAbs-HRP were used at a concentration to obtain an  $A_{450\text{nm}}$  around 2 and the RVFV N protein was titrated from 4  $\mu\text{g/mL}$  to 0.5  $\mu\text{g/mL}$ . The Affimers P1 and P15 could not be used as capture molecule as their purification did not yield enough protein. The SBV N protein was used as a negative control. Figure 4.31 shows the results obtained for the RVFV N protein titration with all the Affimers used as capture.



**Figure 4.31 Titration of RVFV N protein with the Affimers and mAbs anti-RVFV N protein to select the best capture Affimers.**

Double antibody sandwich ELISAs were performed with the anti-RVFV N protein Affimers used as capture molecule and the HRP-labelled anti-RVFV N protein mAbs as detection molecules. A: Affimer M3; B: Affimer M23; C: Affimer M33; D: Affimer M76; E: Affimer P2; F: Affimer P3; G: Affimer P5; H: Affimer P7; I: Affimer P9; J: Affimer P11; K: Affimer P14; L: Affimer P16; M: Affimer P20; N: Affimer P25; O: Affimer P28. The experiment was performed once.



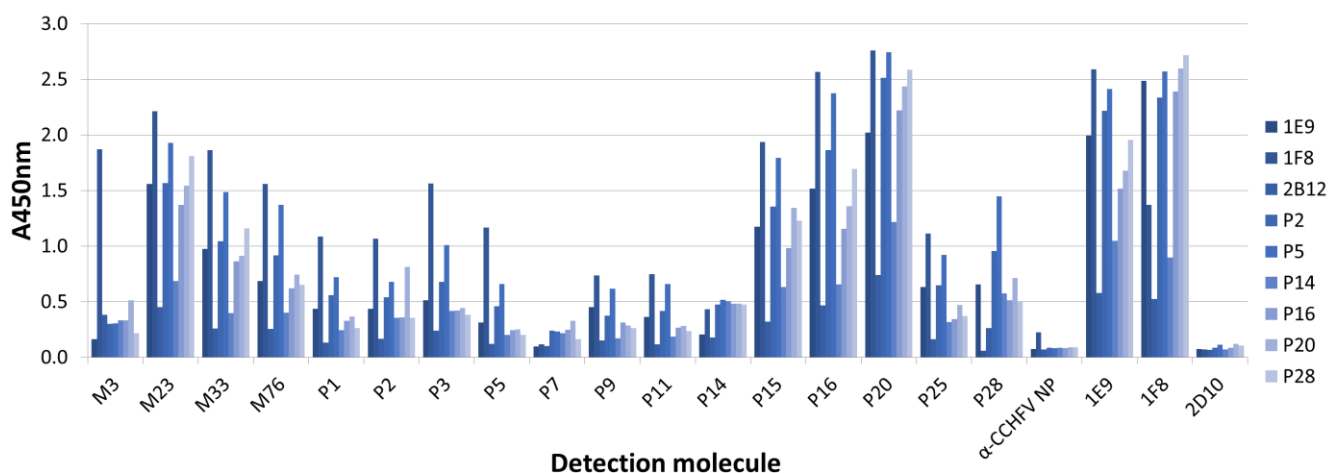
Overall, the anti-RVFV N protein Affimers worked better as capture molecules with the mAb 1E9-HRP as detector molecule. The mAb 2D10-HRP did not give any positive signal with any Affimer. No background signal was observed with the SBV N protein (data not shown). The Affimers giving the best  $A_{450\text{nm}}$  with the mAb 1E9-HRP at 0.5  $\mu\text{g/mL}$  of RVFV N protein were the Affimers P2, P5 and P14, which had an  $A_{450\text{nm}} \approx 2$  and the P11 and P16 with an  $A_{450\text{nm}} \approx 1.5$ . Regarding the mAb 1F8-HRP, the best Affimers were P16 and P20 which gave an  $A_{450\text{nm}} \approx 1.5$  at the same RVFV N protein concentration. The results are summarized in Table 4.4.

**Table 4.4 Summary of the results of the double antibody sandwich ELISA to detect RVFV N protein with the different combinations of anti-RVFV N protein capture Affimer and detection mAb.**

		Capture Affimer														
		Monomeric (M)				Polymeric (P)										
		3	23	33	76	2	3	5	7	9	11	14	16	20	25	28
Detection mAb	1E9	-	++	++	++	++	++	++	-	++	++	++	++	++	++	++
	1F8	-	+	+	+	+	++	++	-	+	+	-	++	++	+	++
	2D10	-	-	-	-	-	-	-	-	-	-	-	-	-	-	-

-: weak or no signal; +: low signal; ++: medium signal; +++: high signal; ++++: very high signal.

A second assay was done to determine the best detection molecules with the coating molecules found in the first assay. The anti-RVFV N protein mAbs 1F8 and 1E9 and the Affimers P2, P5, P14, P16, P20 and P28 were used as the capture and, alongside the 17 Affimers and the 3 biotinylated anti-RVFV N protein mAbs as detector. A unique concentration of RVFV N protein at 4  $\mu\text{g/mL}$  was used. The results of the assay are shown in Figure 4.32.



**Figure 4.32 Selection of the best combinations of capture and detection molecules to detect RVFV N protein in a double antibody sandwich ELISA.**

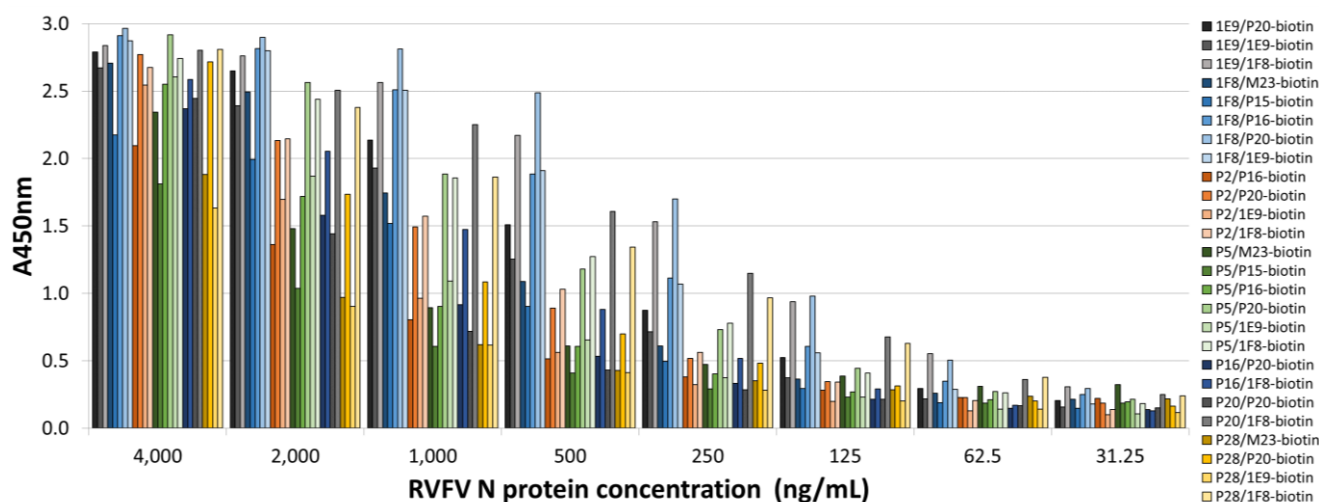
The previously selected best capture molecules (anti-RVFV N protein mAbs 1F8 and 1E9 and the Affimers P2, P5, P14, P16, P20 and P28) were used in combination with all the biotinylated detection molecules anti-RVFV N protein. Anti-CCHFV N protein Affimer was used as a negative control. The experiment was performed once.

27 combinations of pairs of anti-RVFV N protein Affimers/mAbs gave an  $A_{450nm}$  over 1.8 and these pairs are summarized in Table 4.5.

**Table 4.5 Best combinations of capture and detection molecules in the double antibody sandwich ELISA to detect RVFV N protein.**

Capture molecule	Detection molecule
1E9	P20, 1E9 and 1F8
1F8	M23, P15, P16, P20 and 1E9
P2	P16, P20, 1E9 and 1F8
P5	M23, P15, P16, P20, 1E9 and 1F8
P14	None
P16	P20 and 1F8
P20	P20 and 1F8
P28	M23, P20, 1E9 and 1F8

Finally, to obtain the best pairs detecting the RVFV N protein, the 27 combinations were tested with a titration of RVFV N protein (Figure 4.33).



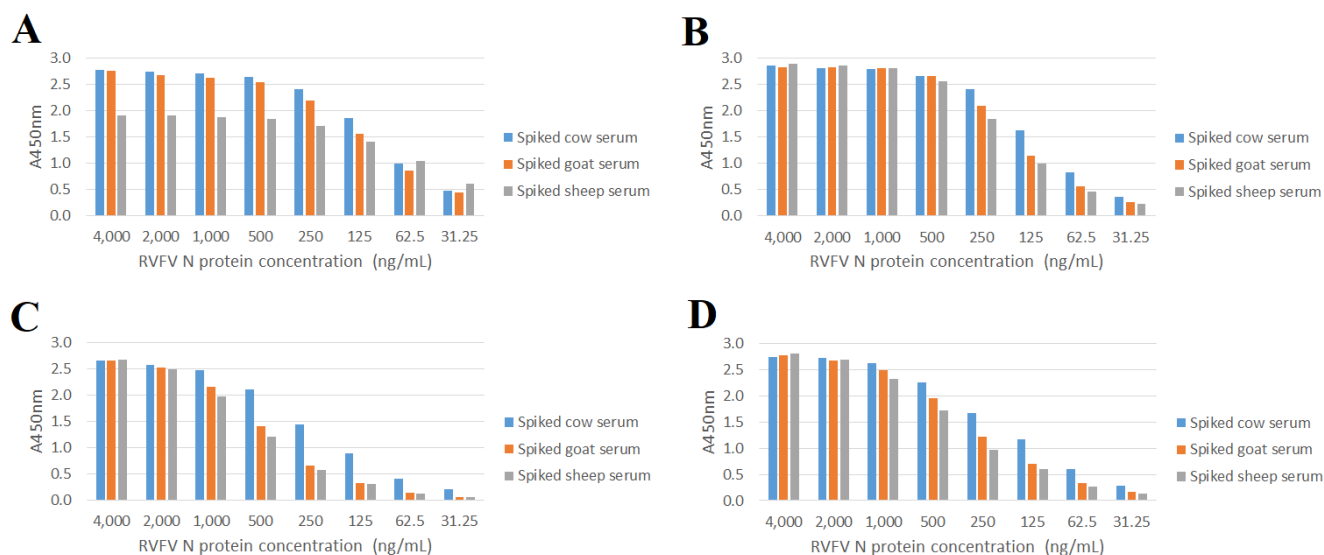
**Figure 4.33 Titration of RVFV N protein with the best combinations of anti-RVFV N protein capture/detection molecules.**

Double antibody sandwich ELISAs were performed with a titration of RVFV N protein with the best combinations of capture/detection molecules to select the best pairs for the development of the double antibody sandwich ELISA. The experiment was performed once.

The two best pairs 1E9/1F8-biotin and 1F8/P20-biotin could detect 125 ng/mL of RVFV N protein with an  $A_{450\text{nm}} \approx 1$ . Two other pairs (P20/1F8-biotin and P28/1F8-biotin) gave an  $A_{450\text{nm}} > 0.5$  when 125 ng/mL of RVFV N protein was present.

### 4.6.3. Double antibody sandwich ELISA with spiked sera

The four pairs of molecules selected previously were used to perform a titration of negative field sera taken from different animal species spiked with the RVFV N protein. The RVFV N protein was spiked in cow, goat and sheep sera from 4  $\mu\text{g/mL}$  up to 31.25 ng/mL. The SBV N protein was titrated and used as a negative control. The difference between the results obtained with the RVFV N protein and with the SBV N protein are shown in Figure 4.34.



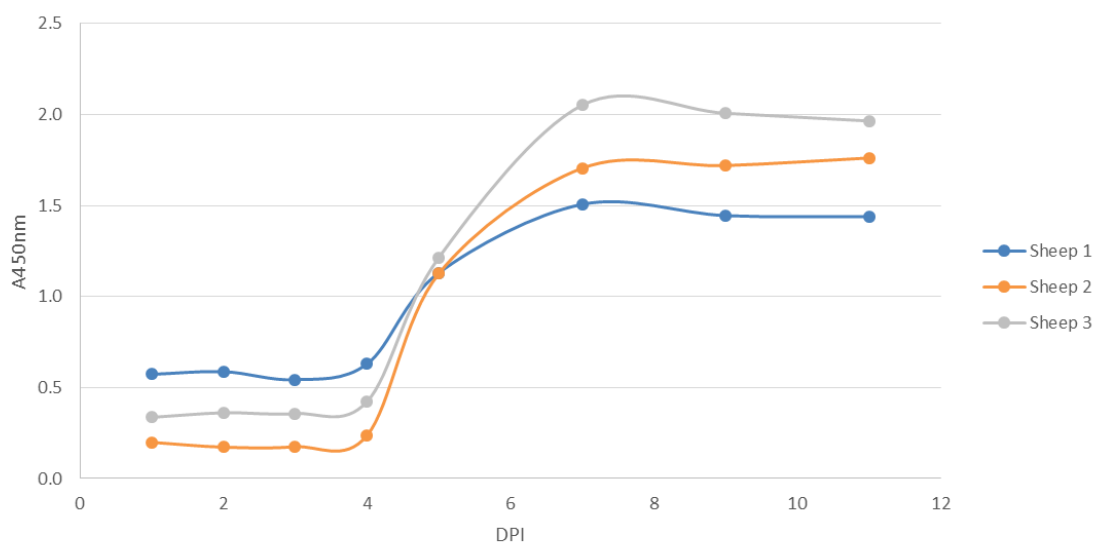
**Figure 4.34 Spiking assay with the double antibody sandwich ELISA to detect RVFV N protein.** Titration of the RVFV N protein spiked in cow, goat and sheep serum in the double antibody sandwich ELISA with four anti-RVFV N protein pairs. The SBV N protein was titrated in the same conditions and used as a negative control. The results shown are the difference between the results obtained with the RVFV N protein and with the SBV N protein. A: pair 1E9/1F8; B: pair 1F8/P20; C: pair P20/1F8; D: pair P28/1F8. The different conditions were only tested once.

For the four pairs of mAbs/Affimers, a titration of the RVFV N protein was observed. For the pair 1E9/1F8-biotin (Figure 4.34A), a higher background signal was obtained for the spiked sheep serum compared to the other sera. With this pair, a concentration of 62.5 ng/mL of RVFV N protein was detected (with an  $A_{450\text{nm}} \approx 1$ ) in all the spiked sera. The pair 1F8/P20-biotin (Figure 4.34B) detected 62.5 ng/mL of RVFV N protein in cow serum but only 125 ng/mL of RVFV N protein in goat and sheep sera (with an  $A_{450\text{nm}} \approx 1$ ). The pair P20/1F8-biotin was less sensitive (Figure 4.34C), with an  $A_{450\text{nm}} \approx 1$  reached for 125 ng/mL of RVFV N protein in cow sera and 500 ng/mL in goat and sheep sera. The last pair P28/1F8-biotin (Figure 4.34D) was able to detect 125 ng/mL of RVFV N protein in cow sera and 250 ng/mL in goat and sheep sera.

#### 4.6.4. Validation of the assay with sheep-infected plasma

The pair of molecules used in the spiked sera assay were also used for the confirmation assay performed with sheep plasma of three animals experimentally infected with RVFV. The assay was optimized for the use of plasma: the plasma was diluted 1:2 in DB2. For

the three pairs using 1F8 as the detector molecule (1E9/1F8; P20/1F8; P28/1F8), this mAb was used conjugated to HRP instead of biotin. The pair 1F8/P20 used P20 conjugated to biotin. A positive signal was present only for the 1E9/1F8-HRP pair (Figure 4.35).



**Figure 4.35** Validation of the double antibody sandwich ELISA RVFV N protein with experimental sheep plasma.

The pair 1E9/1F8 was used in the double antibody sandwich ELISA to test sheep plasma of three animals experimentally infected with RVFV and collected at different time points. All the samples were tested once due to sample volume constraints. DPI: days post-infection.

For the three sheep, the same pattern of results was observed. Some constant background signal was detected from day 1 to day 4 post infection. Then at 5 DPI the A<sub>450nm</sub> started to increase reaching an A<sub>450nm</sub> over 1, then at 7 DPI the A<sub>450nm</sub> was at its maximum and the signal remained until day 11.

These results showed that out of the four pairs selected, only the pair 1E9/1F8 could detect the presence of RVFV N protein in experimental sheep plasma. As this pair showed promising results in the double antibody sandwich ELISA, it was transferred into the LFA to develop a double antibody sandwich LFA.

## **4.7. Transfer of the double antibody sandwich ELISA to a LFA format for the detection of RVFV N protein at the POC**













One of the gaps in RVFV diagnostics is the absence of POC tests that can detect acute RVFV infections without the need of specialized equipment. As the newly developed double antibody sandwich ELISA could detect RVFV N protein in experimentally infected sheep, the same detection molecules were transferred to LFA to develop an assay that could detect the virus on site, especially in the field, at places where there is an absence of the required infrastructure, and skilled personnel.

### **4.7.1. Optimization of the assay**

The selected pair of mAbs in the double antibody sandwich ELISA were tested for the development of the double antibody sandwich LFA. Thus, anti-RVFV N protein mAbs 1E9 and 1F8 were tested as the capture reagent (immobilized at the test line) or as the detector reagent (conjugated to the latex beads).

Red latex beads were conjugated at  $1 \text{ mg/m}^2$  with 1F8 or 1E9 and nitrocellulose membranes were made by immobilizing the mAbs at the highest concentration possible: 1E9 at  $0.94 \text{ mg/mL}$  and 1F8 at  $0.65 \text{ mg/mL}$ . The LFA with 1E9 in the membrane at  $0.94 \text{ mg/mL}$  and 1F8 in the conjugate pad at  $1 \text{ mg/m}^2$  was named Test 1 and the LFA with 1F8 in the membrane at  $0.65 \text{ mg/mL}$  and 1E9 in the conjugate pad at  $1 \text{ mg/m}^2$  was named Test 2.

Test 1 and Test 2 were tested with different buffers to check for any potential background signal with the assay buffers. As none gave any background, LDB1 was selected for the first assays. A titration of the RVFV N protein was done with these two tests to determine their limit of detection (Figure 4.36).

			RVFV N protein concentration in LDB1					
			1 mg/mL	0.5 mg/mL	0.25 mg/mL	0.125 mg/mL	62.5 µg/mL	31.3 µg/mL
Test	Test 1	Intensity units	9	8	7	6	5	4
		Picture						
	Test 2	Intensity units	10	9	8	7	5	4
		Picture						

**Figure 4.36 Titration of RVFV N protein with the double antibody sandwich LFA Test 1 and Test 2.**

Serial dilutions of RVFV N protein were assayed with Test 1 and Test 2. The intensity was determined using the intensity scale shown in Figure 2.2. The experiment was performed once.

The two tests gave similar results with the RVFV N protein titration and at 31.3 µg/mL of RVFV N protein, they both gave a weak positive signal with an intensity around 4 (Figure 4.36).

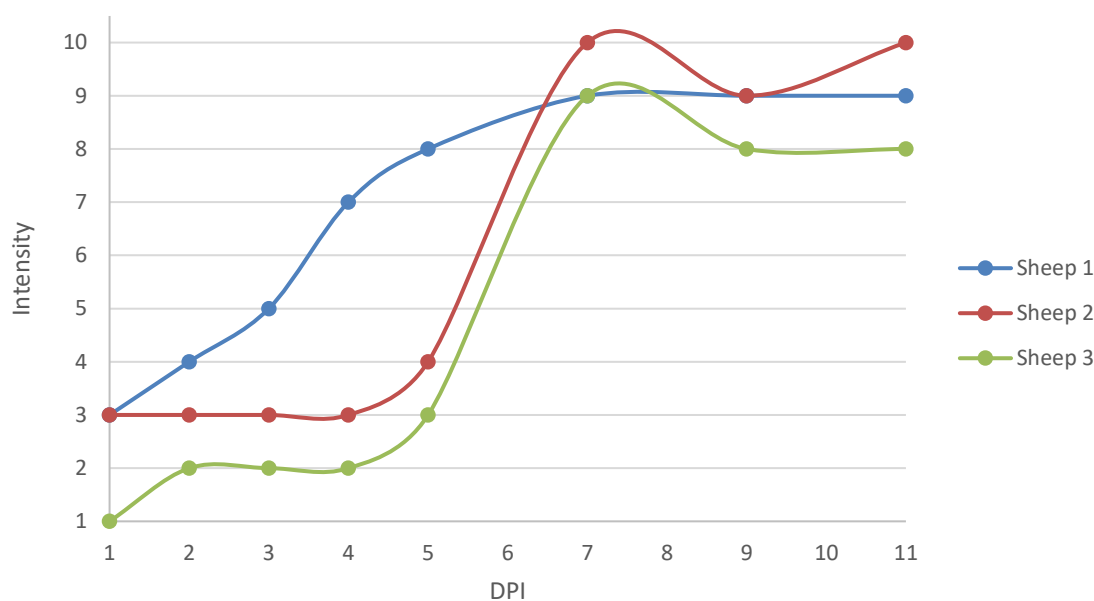
Accordingly, with the results obtained in the double antibody sandwich ELISA, a pool of the experimental sheep sera at 1, 2 and 3 DPI (named negative pool) and a pool at 7, 9 and 11 DPI (named positive pool) were made.

The negative pool was assayed in both tests, which gave a highly positive signal of 7. As the background obtained for the negative pool was high, new buffers were tested to reduce the unspecific binding caused by the negative pool. When using buffer LDB2, the background signal of the negative pool was reduced to 2-3 for Test 1 and to 1 for Test 2. Using this buffer, the positive pool tested in both assays, gave a signal of 9 for Test 1 and of 6 for Test 2. As the difference of signal between the positive and negative pool was higher for the Test 1, this one was selected over Test 2.

To reduce the background of Test 1, Test 3 was made with the same combination as Test 1, but by reducing concentration of 1E9 on the membrane to 0.5 g/mL. After testing Test 3 with the negative and positive pool, signals of 2 and 7 were obtained, respectively. Thus, the final conditions selected were: the mAb 1E9 immobilized on the membrane at 0.5 mg/mL and the mAb 1F8 conjugated to the beads at 1 mg/m<sup>2</sup>.

#### 4.7.2. Validation of the assay with negative sheep sera and RVFV-infected sheep plasma

In order to further validate the double antibody sandwich LFA, six negative sheep sera were tested in Test 3 to determine the potential background. All 6 samples gave a negative signal of 1. Test 3 was then assayed with the plasma of the three RVFV experimentally infected sheep. The results obtained with Test 3 are shown in Figure 4.37.



**Figure 4.37** Double antibody sandwich LFA 1E9/1F8 with the experimental sheep plasma.

The pair 1E9/1F8 was used in the double antibody sandwich LFA Test 3 to test sheep plasma of three animals experimentally infected with RVFV and collected at different time points. All the samples were tested once due to sample volume constraints. The intensity was determined using the intensity scale shown in Figure 2.2. DPI: days post-infection.



For sheep 2 and 3, the same pattern of results was observed, with a low background signal from 1 DPI to 4 DPI (signal between 1 and 3), then the signal increased at 5 DPI to reach a peak at 7 DPI (signal between 9 and 10) and then the signal stayed between 8 and 10 DPI until the final reading at 11 DPI. For sheep 1, the background until 3 DPI was high with a constant increase from a signal of 3 to 5. At 4 DPI, the signal increased to 7, before reaching its peak at 7 DPI (signal of 9) and plateaued until the final reading at 11 DPI.

These results showed that, even if the background signal obtained with the negative plasma (until 5 DPI according to the double antibody sandwich ELISA) was high, an increase in the intensity obtained could be seen for the three sheep at 4-5 DPI, the signal peaked for all sheep at 7 DPI and these signals stayed constant until 11 DPI. These results were comparable to the ones obtained in the double antibody sandwich ELISA, showing that the newly developed double antibody sandwich LFA was able to detect acute RVFV infections in sheep experimentally infected with RVFV.

#### **4.8. Development of a RVFV duplex assay to detect antibodies against two RVFV antigens**

As most RVFV assays are based on the RVFV N protein, to cover a wider antigenic range that could potentially be used as a DIVA assay or for vaccine evaluation, a multiplex assay using the Luminex technology platform was developed. The duplex assay developed was designed to detect antibodies against the RVFV N protein and the G<sub>NE</sub> protein, which were selected as the target viral antigens.

##### **4.8.1. Serum samples**

To evaluate the RVFV duplex assay, a panel of serum samples consisting of 67 positive experimental samples and 186 negative field sera, were included in the test. For detection of antibodies to RVFV, 67 positive experimental samples from sheep were kindly provided by Dr A. Brún from INIA-CISA. These samples were inactivated and tested at Eurofins-Ingenasa.

The collection of 186 negative field sera, included 93 samples from cattle, 45 samples from sheep and 48 from goats. All came from Spanish farms free of RVFV.

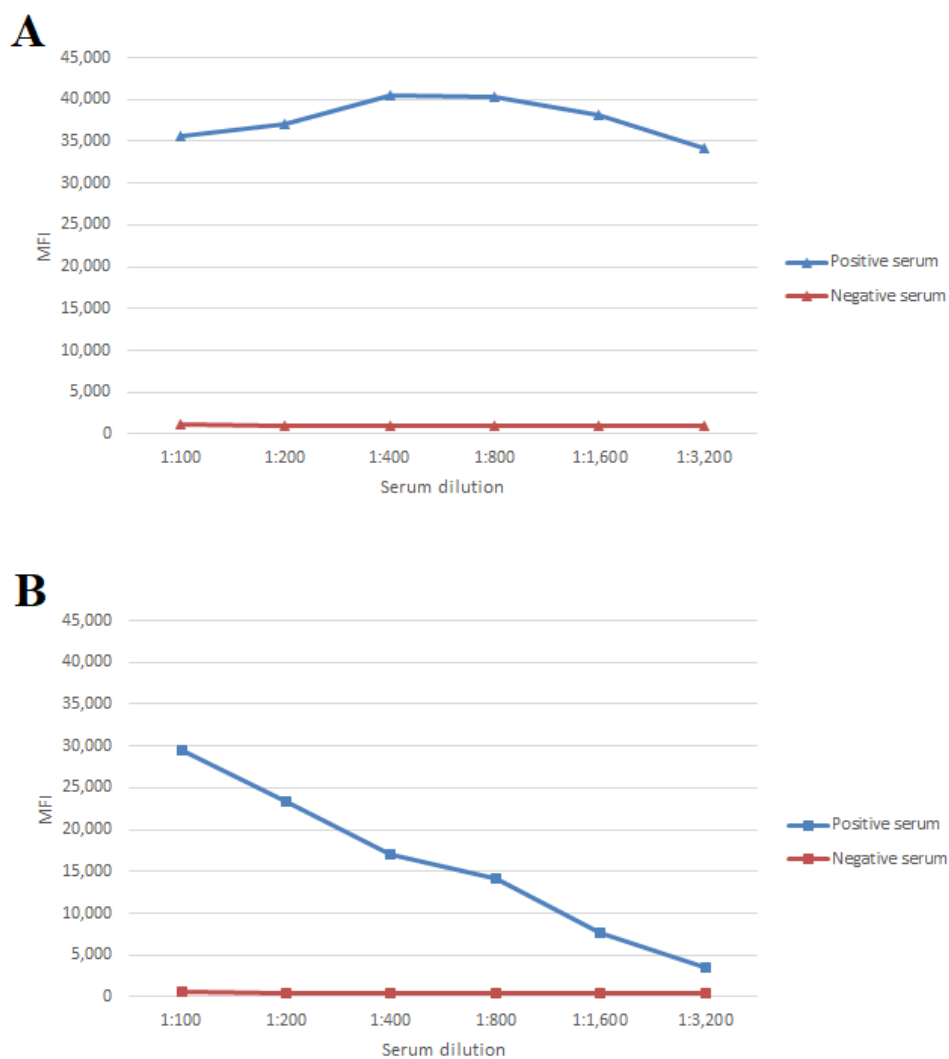
All these samples were assayed in the ID Screen® Rift Valley Fever Competition Multi-species (IDVet) and INgezim FVR Compac (Eurofins-Ingenasa), used as the reference techniques for the development of this assay, and were classified as positive and negative according to the results obtained.

#### **4.8.2. Optimization of the duplex assay**

The RVFV N protein and RVFV G<sub>NE</sub> were used to coat different microsphere regions. Then, the anti-RVFV N protein and anti-GST mAbs were used to confirm the coupling of each individual antigen to its bead region, and then to optimize the coupling concentration of each antigen. The optimal protein coupling concentration was established as the highest MFI obtained with the minimum amount of protein. The following quantities were used to coat  $1 \times 10^6$  beads for each bead region: 25 µg of RVFV N protein (region #12) and 50 µg of RVFV G<sub>NE</sub>-GST (region #30).

Positive and negative serum samples were used to establish the optimal assay conditions for the screening (Figure 4.38). Separately, the two bead regions coupled to the RVFV proteins were incubated with serial dilutions of these positive and negative sera and the assay was performed as described in Materials and Methods.

For the bead #12 RVFV N protein (Figure 4.38A), dilutions of positive sera ranging from 1:100 to 1:3,200 resulted in MFI readings between 34,000 and 40,000, with the maximum MFI reached at 1:400 and 1:800. For the bead #30 RVFV G<sub>NE</sub> (Figure 4.38B) the highest MFI of the positive serum was observed for the 1:100 dilution, with the MFI decreasing with increasing serum dilution. The two beads region gave negligible background signal with the negative serum samples (Figure 4.38A and B). As the bead region #30 seemed to give a lower MFI than the bead region #12, for screening purposes a dilution of the serum at 1:100 was selected (corresponding to a sample volume of 1 µL), since this was the dilution showing the highest positive/negative ratio for bead region #30.



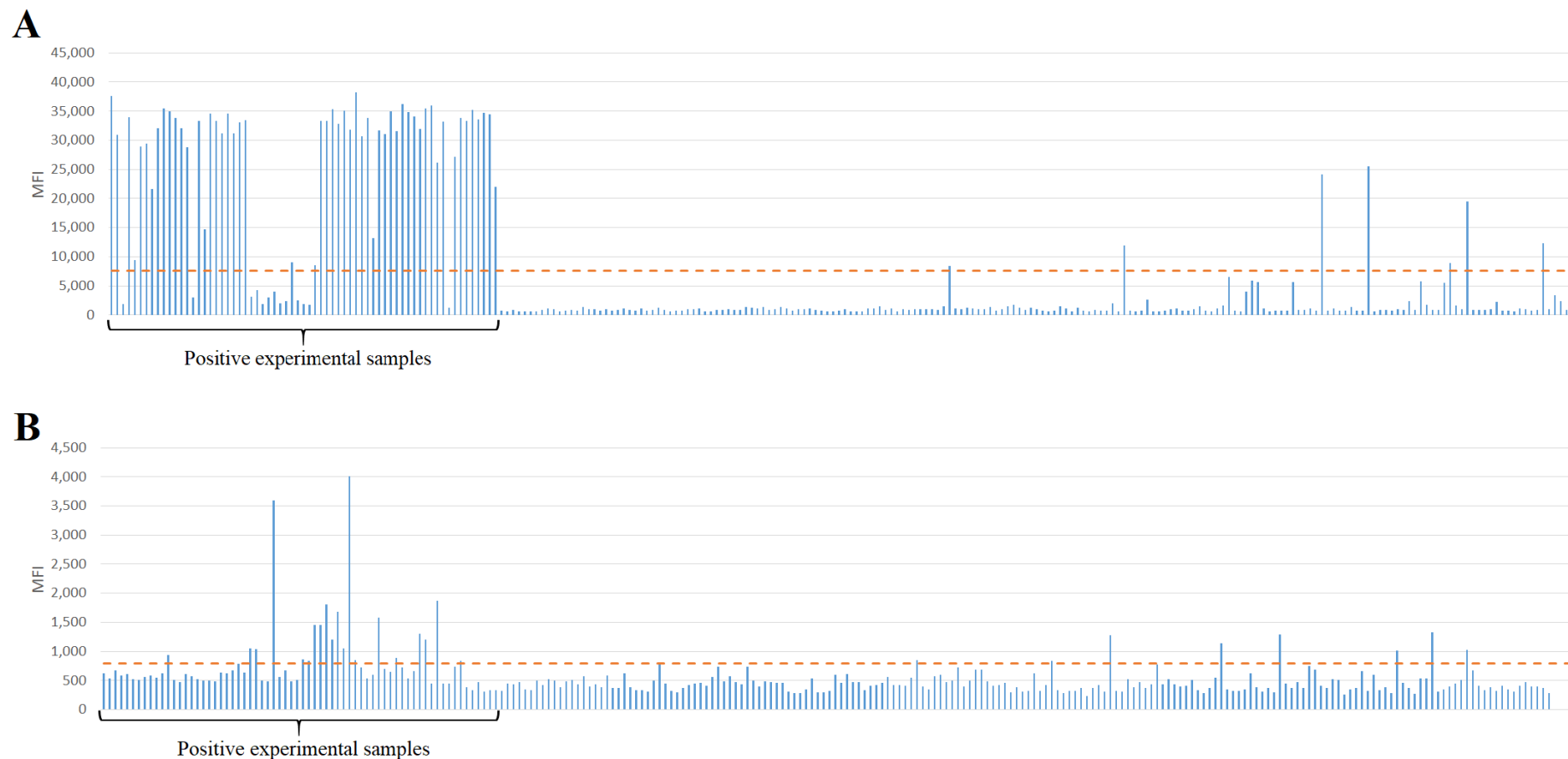
**Figure 4.38** Determination of the screening conditions for the duplex assay.

The MFI for each bead region is given for different serum dilutions (one positive experimental serum sample and one negative field serum sample). A: positive and negative sera with bead #12 RVFV N protein. B: positive and negative sera with bead #30 RVFV G<sub>NE</sub>-GST. The signal was measured as MFI of at least 50 events of each bead region. MFI: median fluorescence intensity.

### 4.8.3. Validation of the duplex assay

Once the conditions of the duplex assay were established, the panel of positive and negative sera was tested in the duplex assay. The 62 experimental serum samples and the 186 negative field serum samples were confirmed to be positive and negative by the ELISA detecting antibodies to RVFV N protein used as a reference.

These samples were tested in the duplex assay to check for the presence of antibodies against these two RVFV proteins (Figure 4.39). A cut-off value was established for each bead region. The cut-off was calculated as the mean obtained for the 186 negative field samples, plus two standard deviations. Thus, cut-off values of 7,529.5 MFI and 791.3 MFI for bead #12 RVFV N protein (Figure 4.39A) and bead #30 RVFV G<sub>NE</sub>-GST (Figure 4.39B) were obtained, respectively. With these cut-off values, out of the 62 positive experimental sera, 54 were considered positive to RVFV N protein (87.1%) and 21 to RVFV G<sub>NE</sub> (33.9%). Out of these positive samples, 17 samples were positive for both the N protein and the G<sub>NE</sub>. On one hand, 36 serum samples were positive to N protein but not to the G<sub>NE</sub> and on the other hand, interestingly, 4 samples were positive to the G<sub>NE</sub>, but not to the N protein. Moreover, with these cut-offs, out of 186 negative field sera tested, 7 were positive for RVFV N protein (3.8%) and 8 were positive for RVFV G<sub>NE</sub> (4.3%), with 1 negative field sample positive for both proteins.



**Figure 4.39** Screening of the positive experimental and negative field sera for antibodies against RVFV N protein (A) and RVFV G<sub>Ne</sub> (B) in the RVFV duplex assay.

The dashed line corresponds to the cut-off values for each bead region and calculated as the mean obtained for the negative field samples plus two standard deviations. The signal was measured as MFI of at least 50 events of each bead region. MFI: median fluorescence intensity.

## 4.9. Chapter summary and discussion

This chapter describes the production of two RVFV proteins: The N protein and the G<sub>NE</sub>. The RVFV N protein was used to produce different detection molecules: monoclonal antibodies by hybridoma technology and affimers by phage display. These reagents were used to develop different serological assays: a double recognition ELISA detecting antibodies to RVFV N protein in different animal species, a double antibody sandwich ELISA and a double antibody sandwich LFA detecting the RVFV N protein in infected animals and a duplex assay detecting antibodies against the two RVFV target proteins.

The RVFV N protein has previously been expressed in *E. coli* using the pET SUMO system and purified under denaturing conditions (with urea 8 M) and with a refolding step before the cleavage of the 6xHis-SUMO tag (321). The RVFV N protein produced in this chapter was expressed as a soluble protein in bacteria and the cells were lysed in the presence of Benzonase<sup>®</sup> Nuclease to degrade DNA and RNA and avoid the binding of bacterial nucleic acid to the N protein. The RVFV N protein was then purified twice by affinity chromatography using a Ni<sup>2+</sup>-NTA column and SEC. The second Ni<sup>2+</sup>-NTA purification was essential as the 6xHis-SUMO protease Ulp1 and the RVFV N protein have similar molecular weight (both around 27 kDa). On the SEC chromatogram, three peaks could be observed, the first one corresponded to the void volume (110 mL) and two other peaks at 130 mL and 180 mL. When observing the samples collected on a SDS-PAGE gel followed by Coomassie staining, a unique band around 25 kDa was observed, with, for the first fractions, an unknown protein contaminant around 17 kDa, likely corresponding to the 6xHis-SUMO tag. The protein around 25 kDa corresponded to the RVFV N protein, which in the SEC column migrated at different speed through the column. In this SEC column, an elution volume of 130 mL corresponds to a MW around 55 kDa as it could be seen in section 3.2.2 for the purification of CCHFV N protein, and an elution volume of 180 mL corresponds to a MW of around 25 kDa. If the protein purified by SEC that migrates around 25 kDa in the SDS-PAGE gel is the RVFV N protein, these MW around 55 and 25 kDa would correspond to dimers and monomers, respectively. It was already shown that the RVFV N protein tends to form dimers, which would explain its elution volume of 130 mL in the SEC (321,322). The small peak at 180 mL in the SEC, could correspond to the MW of monomers of RVFV N protein and/or of

the 6xHis-SUMO protease Ulp1. However, after the addition of the 6xHis-SUMO protease Ulp1 and before the second Ni<sup>2+</sup>-NTA purification, a band above the one of the RVFV N protein can be observed in SDS-PAGE, likely the protease, which was separated from the RVFV N protein during this affinity chromatography purification. Thus, the quantity of protease after this step was probably low and could not be observed after the second Ni<sup>2+</sup>-NTA purification. To confirm the hypothesis that the last peak observed on the chromatogram corresponded to monomers of RVFV N protein, a WB analysis was done with an anti-RVFV N protein mAb that confirmed the presence of RVFV N protein in this fraction. However, this fraction may contain some small quantities of 6xHis-SUMO protease Ulp1. As the RVFV N protein was used to immunize mice to obtain mAbs, its purity was important.

The complete version of the RVFV G<sub>N</sub> has been previously expressed recombinantly in bacteria as an insoluble protein, which after solubilization, was used in an indirect ELISA with high sensitivity and specificity to detect antibodies to RVFV G<sub>N</sub> in field serum samples confirmed to be positive to RVFV by virus neutralization test (323). The same RVFV G<sub>N</sub> was also shown to elicit a high number of mAbs clones after immunizing mice, confirming its strong immunogenicity (324). The ectodomain of RVFV G<sub>N</sub> was also produced as a soluble protein in insect cells and a combination of purified G<sub>NE</sub> and G<sub>C</sub> proteins induced a virus neutralizing antibody response in immunized sheep (325). Finally, in animals, it was shown that natural infections with RVFV correlated with neutralizing antibodies (nAb) that target the viral envelope glycoproteins, which was also confirmed recently in humans and that G<sub>N</sub>-specific antibodies dominate the RVFV nAb response in humans (326). Thus, in this chapter, the RVFV G<sub>N</sub> ectodomain was produced in insect cells using the BES with a fusion tag (GST tag). The GP67 signal peptide present in the vector was supposed to force the secretion of the RVFV G<sub>NE</sub> into the culture medium. However, unlike the CCHFV G<sub>NE</sub> produced in the previous chapter (section 3.3), the RVFV G<sub>NE</sub> could not be detected in the culture medium and had to be purified from the soluble fraction of the cell lysate. After its purification by affinity chromatography, the RVFV G<sub>NE</sub> obtained was not highly pure as two other bands were observed that were not detected by WB analysis with an anti-GST mAb. As mentioned in Chapter 3, the expression of the RVFV G<sub>NE</sub> could be improved by producing that

protein in a mammalian expression system, although at this time the system was not optimized in the laboratory.

In order to produce anti-RVFV N protein mAbs, mice were immunized with the N protein obtained in bacteria. The clones obtained after the fusion were screened with a negative control produced in the same construct with a 6xHis-SUMO tag (6xHis-SUMO-CCHFV N protein was used) as this tag was shown to be highly immunogenic. One of the four clones subcloned at 50 cells per well then gave a negative signal to the RVFV N protein. This positive clone turning negative was due to the instability of the hybridoma at the first stage following the fusion.

Three mAbs obtained were highly specific for the RVFV N protein in non-reducing conditions and could detect up to 100 ng/mL of RVFV N protein. In reducing conditions, the mAb 1E9 slightly cross-reacted with the CCHFV and SBV N proteins. This means that 1E9 recognizes a non-conformational epitope present in RVFV N protein that is probably slightly conserved between the other two bunyavirus N protein tested (from CCHFV and SBV). However, this result is surprising as these three proteins do not have a similar amino acid sequence, nor a similar structure.

These mAbs are important tools as they can be used to develop serological assays to detect the RVFV N protein. In this chapter, anti-RVFV G<sub>NE</sub> mAbs could not be produced as the amount of RVFV G<sub>NE</sub> purified was not enough to immunize mice. The production of anti-RVFV G<sub>NE</sub> mAbs could have been interesting as mAbs targeting the whole G<sub>N</sub> protein have been shown to have a neutralizing activity by binding to G<sub>N</sub> preventing its binding to the cells and preventing the glycoprotein rearrangement (327,328). Such mAbs could have a therapeutic application, especially when no vaccine nor an effective treatment to RVFV has been found yet.

As an alternative to mAbs, anti-RVFV N protein Affimers have been produced to target specifically the RVFV N protein. For the production of these Affimers, the supposedly two forms of RVFV N protein identified (monomeric as F35 and dimeric as F20) were used for the phage display screening. The control proteins used in the screening, the 6xHis-SUMO tag and 6xHis-SUMO protease, allowed the efficient selection of Affimers specific for the target protein and discarded Affimers targeting the tag or the protease potentially present in the RVFV N protein fractions. The screening with the dimeric



RVFV N protein yielded 15 unique binders and 8 unique binders for the monomeric one. A first approximation of the binding capabilities of the specific Affimers was the number of times each Affimer was sequenced, with some of them repeated up to 38 times, meaning an efficient enrichment of the Affimer, and some of them only once. The Affimers were produced in bacteria and purified by affinity chromatography. In SDS-PAGE analysis, all the purified Affimers exhibited a main band corresponding to the MW of the Affimers (13 kDa), however, some of them showed an additional band around 25 kDa suggesting that these Affimers were forming dimers, despite the presence of reducing agents in the SDS-PAGE analysis. The Affimers produced are an alternative to the mAbs produced by hybridoma technology as they can be screened and produced in 7 weeks (when the mAbs require a minimum of 6 months), they do not use animals and can be easily produced once cloned into their expression vector.

A pull-down assay was performed with the anti-RVFV N protein mAbs and Affimers to select the best binders. In this assay, 17 Affimers and the three mAbs successfully bound to the RVFV N protein, with different affinities. The Affimers not binding to the RVFV N protein probably had a weak or unspecific binding to the protein or their binding was due to the presence of biotin.

As described in the introduction of the chapter, there is a limited number of commercial serological assays for the detection of antibodies against RVFV. In this chapter, with the pure RVFV N protein produced, a double recognition ELISA that can detect RVFV N protein antibodies was developed. This assay detected 100% of the positive experimental sera tested, with a specificity of 98.3%. Out of the eight false positive samples detected, seven gave a signal close to the calculated cut-off with only one false positive giving a high signal in the double recognition ELISA. This double recognition ELISA is the first description of a double recognition ELISA detecting antibodies anti-RVFV with the additional advantage over the commercial ELISA available that it is a multi-species assay and that it can detect total antibody response to RVFV. This double recognition ELISA could be a valuable tool in surveillance programs to monitor the spread of RVFV in previously unaffected countries. To confirm the performance characteristic of this assay, well-characterized RVFV positive field sera need to be tested to determine its diagnostic

sensitivity. Furthermore, as this double recognition ELISA is a multi-species assay, positive and negative human sera need to be tested to adapt this assay to detection of human antibodies to RVFV. Finally, due to sample constraints, the negative field samples and positive experimental samples used to develop the double recognition ELISA were only tested once. Although the samples were only used once, a significant number of samples were used to support the results obtained.

In addition, as shown in Table 4.1, no commercial serological assays are currently available for the detection of RVFV antigen. Thus, using the anti-RVFV N protein detection molecules produced (mAbs and Affimers), a double antibody sandwich ELISA was developed. It was shown that a pair of Affimers/mAbs in a double antibody sandwich ELISA could have better performance characteristics than a double antibody sandwich ELISA using a pair of mAbs, when this Affimer was used as the capture molecule (260). Thus, the anti-RVFV N protein Affimers that could bind to the RVFV N protein in the pull-down assay were tested with the anti-RVFV N protein mAbs. All the possible combinations between the Affimers and the mAbs as capture and detection molecule were tested, which resulted in four optimal pairs combining mAbs (1E9 or 1F8) and Affimers (P20 or P28): 1E9/1F8, 1F8/P20, P20/1F8 and P28/1F8. In a spiked serum assay, these pairs could detect the RVFV N protein in sera from 500 ng/mL to 62.5 ng/mL. These pairs were tested with plasma from sheep experimentally infected with RVFV and only the pair of mAbs 1E9/1F8 showed some positive signal with some background signal observed for the first days following the infection, and an increase in the signal obtained at 5 DPI reaching a peak at 7 DPI. As no commercial assay detecting RVFV antigen is available, these results could not be confirmed. However, as these animals were experimentally infected with RVFV, a production of RVFV antigen is expected along with the viral replication. Other in-house double antibody sandwich ELISA assays have been described that could detect  $10^3$  to  $10^6$  pfu/mL in experimentally infected animals (329),  $\log_{10} 10^{3.2}$  to  $10^{4.2}$  TCID<sub>50</sub>/mL in spiked specimens (330) and more recently 78 to 313 pfu/mL in culture supernatant (309), however these studies did not test experimentally infected animals at different times post infection. No data were available regarding the course of RVFV antigen production and detection post-infection, but RVFV viremia usually ranges between 1 to 7 DPI. To optimize the newly developed double antibody sandwich ELISA, its signal background noise should be reduced to maintain or

improve the positive signal-to-noise ratio obtained. Furthermore, this new double antibody sandwich ELISA should be tested with serum samples spiked with RVFV to allow an easier comparison with the double antibody sandwich ELISA described in the literature. Finally, this new double antibody sandwich ELISA should be tested with acute RVFV field samples confirmed to be positive by real-time RT-PCR, to determine the diagnostic sensitivity of the assay compared to a gold standard and with field negative samples to determine its diagnostic specificity.

This new double antibody sandwich ELISA detecting RVFV antigens could be useful to detect acute RVFV infections without the burden of expensive equipment and technical expertise required for the molecular diagnostics. Although the double antibody sandwich ELISA has many advantages, the main diagnostic need regarding RVF, according to the WHO and some experts, is the development of tools detecting RVFV antigens or nucleic acid at the POC (298). Thus, to address this unmet need, the same detection molecules were transferred to LFA to develop an assay that could detect the virus on site. Both detection molecules were tested as the capture and detector and the best combination found was using the mAb 1E9 immobilized on the membrane and the mAb 1F8 conjugated to the beads. This combination was able to detect up to 31.3 µg/mL of RVFV N protein. When tested with the experimental sheep plasma, the double antibody sandwich LFA showed similar results than the ones obtained in the double antibody sandwich ELISA, with some background signal observed at the first DPI and an increase in the signal observed around 5 DPI. The results obtained with this assay looked promising as the double antibody sandwich LFA developed could detect RVFV N protein in the sheep experimental plasma. Recently, a double antibody sandwich LFA was described by Cêtre-Sossah *et al.* (311) with very good performance characteristics with a diagnostic sensitivity of 100% with serum samples spiked with RVFV, a specificity of 98.8% and a LOD between 2,000 and 9,000 pfu per test.

To optimize the double antibody sandwich LFA developed, the background obtained with the negative field samples should be reduced to maintain or improve the positive signal-to-noise ratio obtained. Like the double antibody sandwich ELISA described above, the double antibody sandwich LFA developed in this chapter should be first tested with spiked samples with RVFV to determine the LOD of the assay and compare it to the other available techniques. Finally, the double antibody sandwich LFA should be tested with field confirmed positive samples, to determine the diagnostic sensitivity compared to a

gold standard, and with field negative samples to determine its diagnostic specificity. Finally, due to sample constraints, the positive experimental samples used to develop the double antibody sandwich ELISA and LFA were only tested once. Although the samples were only used once, a significant number of samples were used to support the results obtained.

Lastly, due to the ongoing vaccine development for RVFV and especially the DIVA-compliant vaccines, a need for DIVA accompanying assays using different viral target can be anticipated. For now, most of the serological assays developed for RVF diagnosis use the N protein as their viral target, however the vaccines are most likely going to target the RVFV glycoproteins as these produce nAbs. In this chapter a duplex assay was developed, using the RVFV N protein and the RVFV G<sub>NE</sub> as the target proteins. The duplex assay was able to detect antibodies against both proteins in experimental sheep sera with some of the sera tested being only positive to one protein or to the other. To perform this duplex assay, 1  $\mu$ L of serum was necessary compared to 20  $\mu$ L for the reference ELISA. Compared to the reference assay, 87.1% of the positive experimental sera were positive to the RVFV N protein and 33.9% to the RVFV G<sub>NE</sub>. Most of the sera positive to the RVFV G<sub>NE</sub> were positive to the N protein, however 4 of them were only positive to the G<sub>NE</sub>. These results could be explained by the selection of the reference assay detecting antibodies to the N protein and the lack of commercial ELISA using the G<sub>NE</sub> that could be used as the reference assay for the RVFV G<sub>NE</sub> bead. Moreover, the relatively low rate of positive to the N protein in the duplex assay could be explained by the use of a secondary anti-IgG antibody, when the reference ELISA used is a competition ELISA, detecting both IgG and IgM.

Some DIVA assays have already been published using the same or additional target proteins. The DIVA assay described by van der Wal *et al.* was able to detect IgG to the RVFV N protein and G<sub>NE</sub> in sheep, cattle and humans (318). The same format of assay was used by Ragan *et al.* (319) for detection of IgG and IgM antibodies against the same proteins and the non-structural proteins NS<sub>S</sub> and NS<sub>M</sub>. The non-structural proteins showed weaker immunogenicity than the N and G<sub>N</sub> proteins, confirming the higher immunogenicity of the N and G<sub>N</sub> proteins. Finally, Lindahl *et al.* (320) developed a multiplex bead-based suspension assay with recombinant N, G<sub>N</sub>, NS<sub>S</sub> and NS<sub>M</sub>. NS<sub>M</sub> showed high background but the three other proteins showed a high antibody response.

These kinds of assays could prove to be useful in the eventuality of a vaccine being developed targeting only some of the proteins included in the multiplex assay. For future applications, additional recombinant proteins of RVFV could be included in the multiplex assay developed in this chapter, to make it relevant for vaccines being developed and their different antigenic targets. Finally, for the differential diagnosis of RVF, antigens from other relevant and related pathogens could be included to this multiplex assay.

The results of this chapter respond to the second aim of this project, producing the different tools to allow the development of RVFV diagnostic tests to fill in some of the current gaps in the diagnosis of RVF.

# Chapter 5 Development of a multiplex assay for serological diagnosis of related pathogens affecting ruminants

## 5.1. Chapter introduction

Infectious diseases account for more than 20% of the overall losses in livestock production worldwide, with important consequences for food security and health of both animals and humans. Many of these pathogens are vector-borne diseases, which have a zoonotic character, with serious impact in both animal and public health. Environmental, and socio-economic changes, such as global warming, changes in land use, host migration and globalization have influenced the distribution of those infectious diseases transmitted by vectors, increasing their potential to spread to previously unaffected regions (331–334). This is the case for pathogens such as CCHFV, RVFV, SBV or BTV (9,76,335,336). Moreover, these viruses, with the exception of SBV, as well as the bacteria complex *M. tuberculosis* are listed as notifiable pathogens by the OIE and thus, their identification is crucial to disease management (52). Taken together, these factors are necessary for better preparedness, surveillance and control of pathogens, in order to reduce the social and economic consequences of their diseases.

The panel of pathogens for this chapter include three viruses of the *Bunyavirales* order, namely CCHFV, RVFV and SBV. CCHFV is one of the most widespread tick-borne zoonotic viruses (53) and while causing an asymptomatic infection in infected animals (domestic and wild ruminants), it can cause severe haemorrhagic fever in humans, resulting in high case fatality rates. More recently some human cases have been reported for the first time in South-Eastern Europe (337) and Spain (57). RVFV is a mosquito-borne virus infecting both livestock and humans (338) with infections causing a high rate of abortions in pregnant domestic ruminants, and high mortality rates among newborns, causing devastating socio-economic impacts (77). In addition, numerous outbreaks have been reported in humans especially in Africa and Middle East countries (78–80).

Although not yet detected in Europe, RVFV introduction is a real concern due to the presence of competent arthropod vectors (339).

SBV and BTV, the latter belonging to the *Reoviridae* family of RNA viruses, are among the most important pathogens affecting different species of ruminants such as cattle, goats and sheep (340,341). Biting midges are the main vector involved in the transmission of these two viruses. Clinical signs associated with SBV are typically non-specific in adult cattle (such as fever, reduced milk yield, diarrhoea) and rare in adult sheep and goats, but infection of pregnant females is associated with congenital malformations and stillbirths (342). For BTV, infection in adult cattle and goats is generally subclinical but is more pronounced in adult sheep (such as fever, congestion of nasal and oral mucosa and can cause haemorrhages in the nose, lips, and tongue that can result in death) and infection of pregnant sheep can be associated with congenital malformations and stillbirths (340). Outbreaks of these two diseases have significant economic impact, due to loss of productivity and restrictions of animal movement and trade (343,344).

*M. bovis*, a member of the *Mycobacterium tuberculosis* complex, is a highly pathogenic mycobacterium that causes disease mainly in cattle, but also in other species of ruminants and poses a high zoonotic risk due to possible transmission to humans, which usually occurs after close contact with infected animals or consumption of unpasteurized and contaminated dairy products (345,346). The disease has an impact on productivity of animals and consequently is linked to economic losses (347).

This chapter describes the development of a multiplex serological assay for the simultaneous detection of antibodies in ruminant serum, against CCHFV, RVFV, SBV, BTV and *M. bovis* for surveillance purposes. As target antigens for CCHFV, RVFV and SBV, their respective N proteins were selected (27,29,53). The target antigen chosen for BTV was the viral protein, VP7, one of the two major structural proteins of the BTV core (348), whereas for *M. bovis*, MPB83 was selected, which is one of the two major antigens highly expressed by *M. bovis* (349).

Initially, to set up this multiplex test, several panels of sera from ruminants (cattle, goat and sheep) experimentally infected with the different pathogens, or serum from field animals, were used. To determine the diagnostic specificity of the test, a total of 220 sera from Spanish farms free of these five diseases were included in the studies. All the sera

were previously characterized by individual ELISAs specific for each pathogen, and considered in this study as our reference technique.

This new approach could be used as a high throughput screening tool to assess the presence and prevalence of antibodies against 5 different highly pathogenic agents and identify regions at risk of infection. Moreover, these pathogens are often reported in ruminant populations, which can cause huge economic losses to farmers in developing countries. These infections can routinely be detected using serological or microbiological methods, which can be reinforced or replaced by multiplex assays, where detection of different pathogens is done in a single reaction. In addition, simultaneous testing of these pathogens reduces the volume of sample needed compared to performing the different ELISAs. This information will help to minimize the spread and further transmission of those pathogens within the human population.

## **5.2. Production and purification of the target proteins**

Recombinant viral proteins of the different pathogens were produced in different expression systems, as described in Materials and Methods. The CCHFV N protein and RVFV N protein expression and purification is described in sections 3.2 and 4.2. The SBV N protein was produced and purified following a similar process with its expression in the soluble fraction of *E. coli* lysates, a first Ni<sup>2+</sup>-NTA purification, cleavage of the 6xHis-SUMO tag, a second Ni<sup>2+</sup>-NTA purification and a final SEC purification. The VP7 of BTV was expressed with the BES in the soluble fraction of insect cell lysate and purified by affinity chromatography with an anti-VP7 BTV mAb. The MPB83-GST was already available in the laboratory. A summary of the different target antigens is shown in Table 5.1.

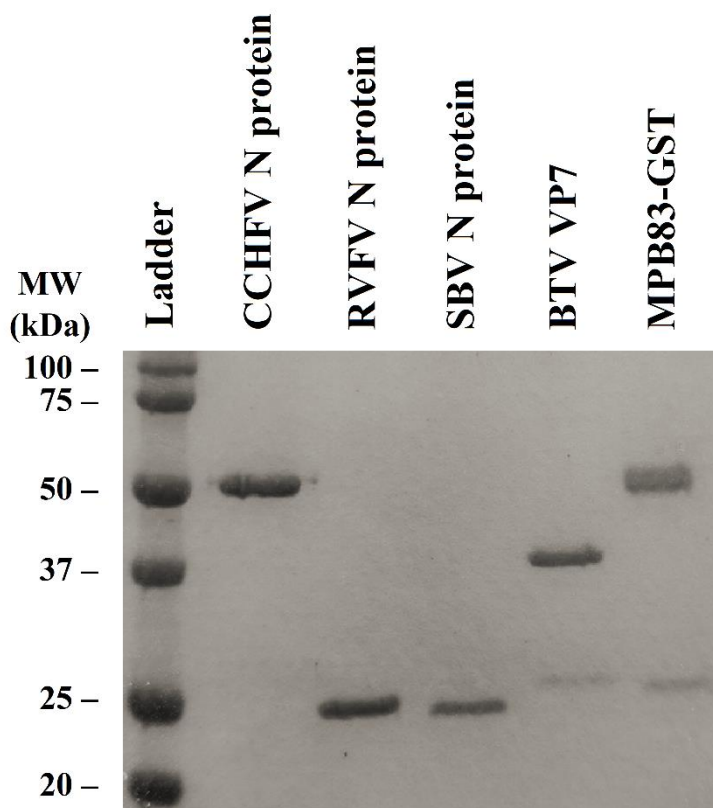
The expression and purification of the proteins was followed by gel electrophoresis and Coomassie blue staining, revealing the recombinant proteins with the expected molecular weights of 54 kDa, 27.4 kDa, 26.2 kDa, 38.5 kDa and 46.3 kDa for CCHFV N protein, RVFV N protein, SBV N protein, VP7 of BTV and the MPB83-GST of *M. bovis*, respectively (Figure 5.1, lane 1 to 5). A faint band probably corresponding to a degradation product of the BTV VP7 (approximately 28 kDa) and a faint band corresponding to the size of the GST (26 kDa) were observed in lanes 4 and 5,



respectively. Western blot analysis using specific mAbs to each of the target proteins was performed to confirm their immunogenicity. A specific band corresponding to each antigenic protein was observed, while neither of the faint bands observed in Figure 5.1 (lanes 4 and 5) were detected in the WB (data not shown).

**Table 5.1 Summary of the antigens used in the multiplex assay.**

<b>Family</b>	<b>Virus/Bacteria</b>	<b>Target antigen</b>	<b>Expected MW (kDa)</b>	<b>Expression system</b>	<b>Vector</b>
<i>Nairoviridae</i>	Crimean-Congo haemorrhagic fever virus	N protein	54	<i>E. coli</i>	pET28a-SUMO
<i>Phenuiviridae</i>	Rift Valley fever virus	N protein	27.2	<i>E. coli</i>	pET28a-SUMO
<i>Peribunyaviridae</i>	Schmallenberg virus	N protein	26	<i>E. coli</i>	pET28a-SUMO
<i>Reoviridae</i>	Bluetongue virus	VP7	38.5	BES	pAcYM1
<i>Mycobacteriaceae</i>	<i>Mycobacterium bovis</i>	MPB83-GST	46.3	BES	pAcSECG2T



*Figure 5.1 SDS-PAGE analysis followed by Coomassie staining of the five purified proteins used in the multiplex assay.*

*From left to right: CCHFV N protein (lane 1, MW: 54 kDa), RVFV N protein (lane 2, MW: 27.2 kDa), SBV N protein (lane 3, MW: 26 kDa), BTV VP7 (lane 4, MW: 38.5 kDa) and MPB83-GST (lane 5, MW: 46.3 kDa).*

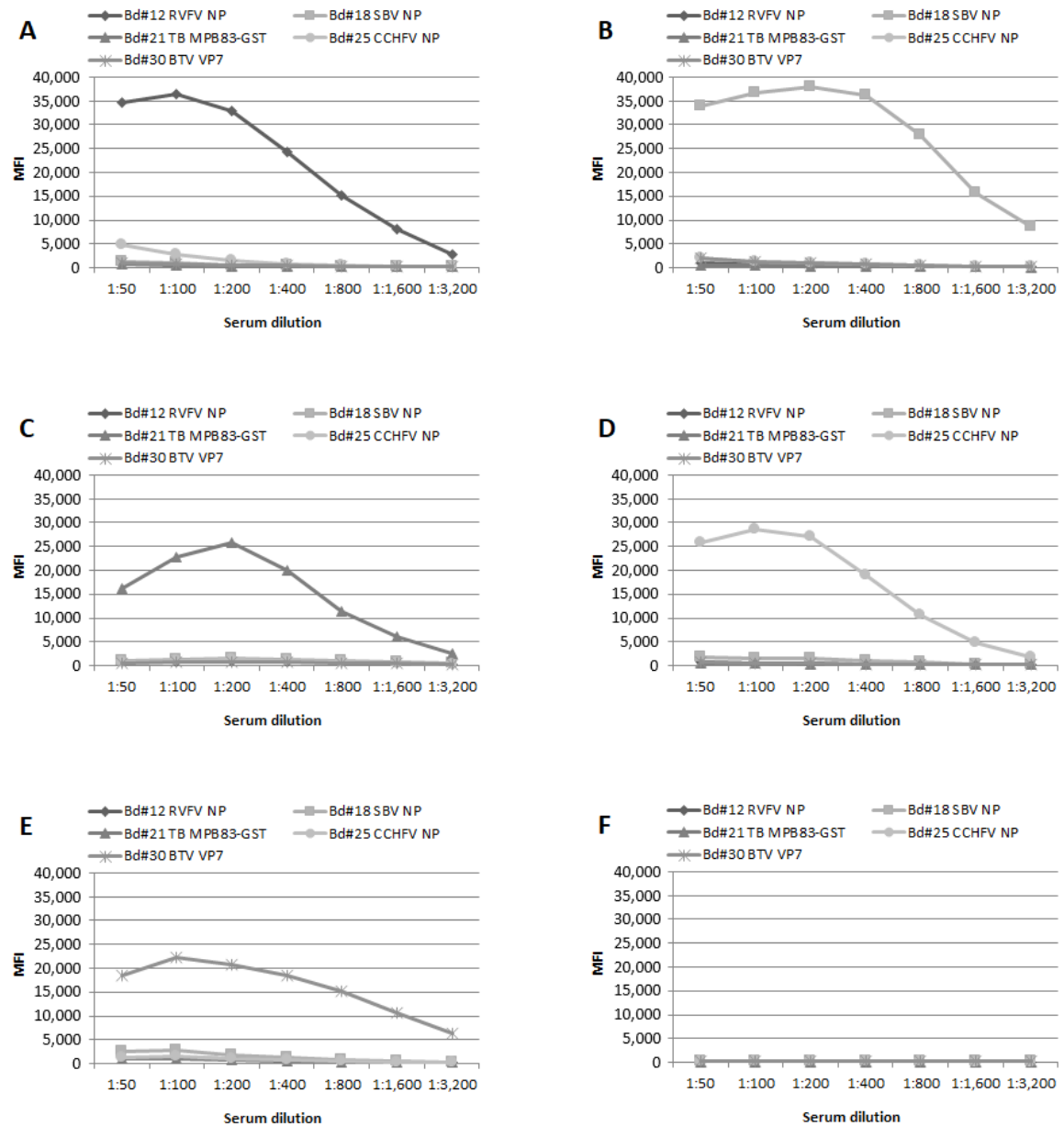
### **5.3. Development of a multiplex assay for antibody detection in serum against pathogens affecting ruminants**

#### **5.3.1. Development and optimization of the multiplex assay**

Firstly, the optimization of the coupling concentration of each antigen to each bead region was determined individually with the specific mAbs produced as described in Materials and Methods (data not shown). The optimal protein coupling concentration was established as the highest MFI obtained with the minimum amount of protein. The following quantities were used to coat  $1 \times 10^6$  beads for each bead region: 25  $\mu\text{g}$  of RVFV N protein (region #12), 25  $\mu\text{g}$  of SBV N protein (region #18), 25  $\mu\text{g}$  of MPB83-GST

(region #21), 25 µg of CCHFV N protein (region #25) and 50 µg of BTV VP7 (region #30).

Well-characterized serum samples for each pathogen were used to establish the optimal assay conditions for the screening. A mix of the 5 bead regions coupled to the target antigens was incubated with serial dilutions of specific reference serum samples against each pathogen and the assay was performed as described in Materials and Methods. The same pattern of results was obtained for each, with an increase in the MFI until a serum dilution of 1:200 or 1:400, and then a decrease in the signal detected, without any signal for the other beads (Figure 5.2A to E). Neither of the specific samples for each disease gave cross-reactivity with any of the other bead regions, corresponding to the other pathogens. Finally, the foetal bovine serum used as background for the different infectious agents did not show any reactivity with any of the five beads (Figure 5.2F). For screening purposes, a dilution of the serum at 1:200 was selected (corresponding to a sample volume of 0.5 µL), since this was the dilution showing the highest signal to most of the five beads regions, with no cross-reactivity with the non-targeted antigens.



**Figure 5.2** Determination of the screening conditions for the bead-based assay.

The median fluorescence intensity (MFI) for each bead region is given for different serum dilutions of one experimental reference serum. The signal was measured as MFI of at least 50 events of each bead region. A: RVFV experimental serum; B: SBV experimental serum; C: tuberculosis (TB) experimental serum; D: CCHFV field positive serum; E: BTV experimental serum; F: foetal bovine serum.

### 5.3.2. Screening of serum samples

After establishing the screening conditions, a collection of 554 ruminants' serum samples from cattle, goats and sheep, previously classified as positive and negative by the ELISAs

used as reference, were tested in the five-plex assay. A total of 56 RVFV experimental serum samples (50 positives and 6 negatives), 88 SBV experimental serum samples (74 positives and 14 negatives), 72 *M. bovis* experimental serum samples (26 positives and 46 negatives), 30 CCHFV field positive serum samples, 88 BTV experimental serum samples (73 positives from experimentally infected cattle and 15 positives from the SBV experimental sera) and 220 field serum samples from ruminants were included in this study. Out of the 220 field sera, all were classified as negative for RVFV and CCHFV. Twelve cattle sera, 1 sheep serum and 23 goat sera were classified as positive for SBV and 13 cow sera were classified as positive for BTV. Finally, out of these 220 field sera, the sheep and goats' sera were assayed in the INGEZIM Tuberculosis double recognition, according to the manufacturer's instructions, and 3 were classified as positive for *M. bovis* (1 sheep and 2 goats). The serum sample volume needed to perform the five ELISAs used as references was 144  $\mu$ L per animal. A summary of this classification is shown in Table 5.2.

**Table 5.2 Serum classification with the ELISAs used as reference techniques for the different antigens.**

		RVFV	SBV	TB	CCHFV	BTV
		ID Screen® RVF Competition Multi-species (IDvet)	INGEZIM Schmallerberg Compac 2.0 (13.SBV.K3)	INGEZIM Tuberculosis double recognition (10.TB*.K0)	ID Screen® CCHF Double Antigen Multi-species (IDVet)	INGEZIM BTV Compac 2.0 (12.BTV.K3)
Experimental samples	Positive in ELISA	50	74	26	0	88
	Negative in ELISA	6	14	46	0	0
Total number of experimental samples		56	88	72	0	88
Field samples	Positive in ELISA	0	36	3	30	13
	Negative in ELISA	220	184	133	220	207
Total number of field samples		220	220	136	250	220

*The numbers refer to the number of animal serum samples available for each group.*

### **5.3.3. Multiplex assay validation using experimental and field serum samples**

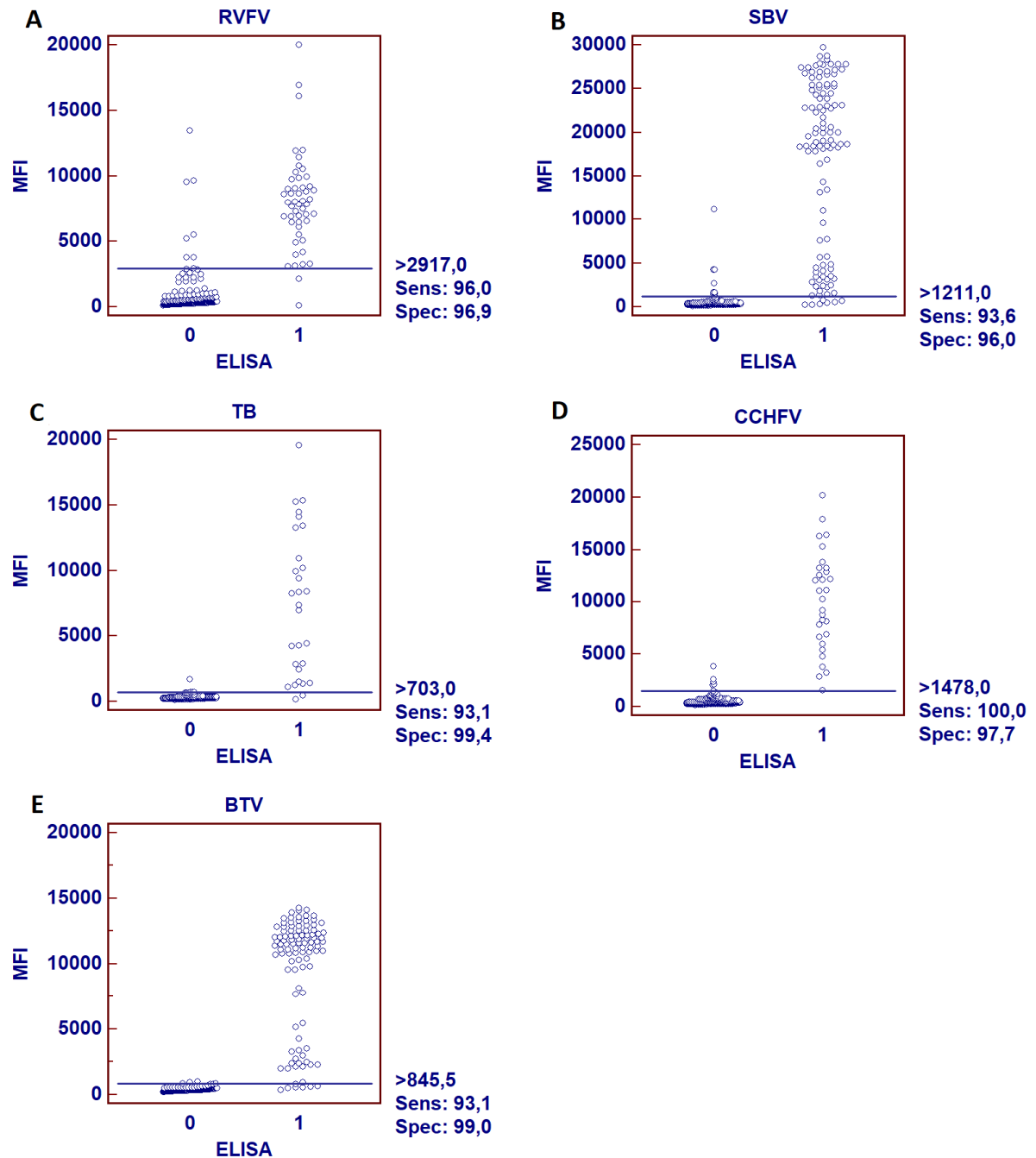
After this classification, the complete panel of 554 ruminant serum samples were assayed in the five-plex assay and the results were statistically analysed by comparison with the results obtained with the reference techniques. Thus, a cut-off value was determined for each antigen using the MedCalc® software. Based on these cut-offs, the performance characteristics of the multiplex assay for each pathogen was determined.

The sensitivity values ranged from 93.1% for tuberculosis (TB) and BTV to 100% for CCHFV, and the specificity ranged from 96% for SBV to 99.4% for TB. For RVFV, most of the positive experimental sera gave a high MFI for its corresponding bead and out of the 220 negative field samples and the 6 negative experimental samples, 96.9% (219/226) were detected as true negatives (Figure 5.3A). Concerning SBV, all the experimental sera were true positive and 96% of the negative field samples (190/198) were classified as true negatives (Figure 5.3B). With regard to TB, the 26 experimental sera were considered true positive with one positive field sample (1/3) considered as true positive (Figure 5.3C). Moreover, 99.4% of the negative field samples (175/176) were classified as true negatives. Regarding CCHFV, all the positive field sera were true positives and 2.3% of the negative field samples (5/220) were considered false positive (Figure 5.3D). Finally, regarding BTV, all the experimental sera were true positive (Figure 5.3E) and 99.0% of the negative field samples were true negatives (205/207). These results are summarized in Table 5.3.

Finally, some of the positive experimental sera tested in the five-plex showed some reactivity with other bead regions than the targeted one: 8 RVFV experimental sera, 39 SBV experimental samples, 24 CCHFV positive field sera and 22 BTV experimental sera (Table 5.4).

Using the MedCalc® software, Cohen's kappa coefficient was calculated to examine the agreement between the results obtained in the ELISAs and in the multiplex assay. For SBV,  $\kappa = 0.894$  with a 95% confidence interval [0.842;0.946]. Cohen's kappa coefficients were ranging from 0.894 for SBV to 0.939 for TB, corresponding to an almost perfect agreement between the ELISAs used as reference and the multiplex assay.

---



**Figure 5.3 Validation of the five-plex bead-based assay.**

Dot plot diagrams where each dot represents an individual sample: results obtained for RVFV N protein coupled to bead #12 (A), SBV N protein coupled to bead #18 (B), MPB83-GST coupled to bead #21 (C), CCHFV N protein coupled to bead #25 (D) and BTV VP7 coupled to bead #30 (E). The horizontal solid line corresponds to the cut-off values in each assay, according to the MedCalc® software. X axis shows the positive (1) or negative (0) classification of samples according to the ELISA used as reference technique in this study and Y axis shows median fluorescence intensity (MFI) obtained in the developed assay. The signal was measured as MFI of at least 50 events of each bead region.

**Table 5.3 Correlation between the bead-based assay and the ELISAs used as reference for the different antigens.**

<b>DIAGNOSIS IN THE FIVE-PLEX</b>	<b>RVFV</b>	<b>SBV</b>	<b>TB</b>	<b>CCHFV</b>	<b>BTB</b>
True positive	50	103	27	30	94
False positive	7	8	1	5	2
True negative	217	190	175	215	205
False negative	2	7	2	0	7
Total	276	308	205	250	308
Cut-off (median fluorescence intensity)	2917	1211	703	1478	845,5
Sensitivity [95% confidence interval]	96% [86.3% - 99.4%]	93.6% [87.3% - 97.4%]	93.1% [77.2% - 99%]	100% [88.3% - 100%]	93.1% [86.2% - 97.2%]
Specificity [95% confidence interval]	96.9% [93.7% - 98.7%]	96.0% [92.2% - 98.2%]	99.4% [96.9% - 99.9%]	97.7% [94.8% - 99.2%]	99.0% [96.5% - 99.9%]

*True positive: samples classified as positive by the reference technique and correctly identified as positive by the multiplex assay. False positive: sample incorrectly identified as positive by the multiplex assay. True negative: samples classified as negative by the reference technique and correctly identified as negative by the multiplex assay. False negative: sample incorrectly identified as negative by the multiplex assay.*

**Table 5.4 Cross-reactivity between the positive experimental and field sera with the four other bead regions.**

		<b>Cross-reactive with other bead regions</b>					<b>Number of positive sera</b>
		<b>Bead #12 RVFV N protein</b>	<b>Bead #18 SBV N protein</b>	<b>Bead #21 TB MPB83- GST</b>	<b>Bead #25 CCHFV N protein</b>	<b>Bead #30 BTB VP7</b>	
<b>Positive serum samples</b>	RVFV experimental sera		0	2	0	6	50
	SBV experimental sera	0		2	16	27	74
	TB experimental sera	0	0		0	0	26
	CCHFV field positive	0	16	11		19	30
	BTB experimental sera	0	1	20	12		88



#### 5.4. Chapter summary and discussion

Multiplex assays, which allow the detection of different pathogens in a single reaction, could replace individual assays routinely carried out for the detection of these pathogens. Moreover, these assays reduce time, labour and sample volume requirements, allowing the testing of many samples for multiple targets simultaneously. This would greatly help in surveillance studies, by allowing the development of one unique plan for a complex infectious disease panel. This could be the case of diseases affecting livestock, especially in cases of zoonoses (such as CCHFV, RVFV and *M. bovis*), to control the distribution of the corresponding pathogens and prevent future outbreaks. This surveillance is also crucial for vector-borne diseases such as CCHFV, RVFV, BTV and SBV, which already have competent vectors in regions or countries where the infectious agents have not yet reached (18,76,335,350). In this chapter, a five-plex assay has been developed and optimized to detect antibodies against the N proteins of RVFV, SBV and CCHFV, and against the VP7 of BTV and MPB83 of *M. bovis* based on the Luminex platform.

The multiplex assay was shown to have an almost perfect agreement with the ELISAs used as reference. Indeed, all Cohen's kappa coefficients had values close to 1. To increase the robustness of the diagnostic sensitivity and specificity of the assay, more positive and negative field sera should be tested.

The ELISAs used as reference techniques were either competition ELISAs (for the detection of antibodies to RVFV, SBV and BTV) or double antigen sandwich ELISAs (for the detection of antibodies to CCHFV and TB), which can detect both IgG and IgM. Our multiplex assay used an anti-ruminant IgG, thus it can only detect IgG. That could explain some of the false negative results, as some of the samples could have been taken at early days post-infection or post-vaccination, giving a high signal in the ELISAs, but being negatives in the multiplex. The confirmation of these results would actually raise the sensitivity of the multiplex assay.

Regarding TB, BTV and CCHFV, the few false positive samples (respectively 1, 2 and 5 serum samples) come from ELISA negative field samples and are clustered close to the cut-off of our multiplex assay. The false positive sample for TB was close to the cut-off ( $A_{450\text{nm}} = 0.32$ ) in the reference ELISA (negative if the  $A_{450\text{nm}} < 0.37$ ). The two false positives for BTV (MFI = 924 and 1,005) are close to the cut-off established by

MedCalc® (negative if MFI < 845.5). Finally, out of the 5 false positives for CCHFV, two are strongly positive to SBV.

This last result raises the question of cross-reactivity of our assay. Due to sample volume constraints, not all the cross-reactive samples were assessed in other reference techniques to check the cross-reactivity. A total of 8 RVFV experimental sera, 39 SBV experimental samples, 24 CCHFV positive field sera and 22 BTV experimental sera gave some positive results with other bead regions than the one it was intended for (see Table 5.4). Out of the 6 RVFV experimental sera positive to BTV, three were infected with BTV-4 (personal communication). The other three sera come from sheep from Spanish farms where the animals could have been vaccinated against BTV, as there was an ongoing BTV vaccination program in Spain, or infected by BTV as it is endemic in certain parts of Spain (351). The 16 SBV experimental sera giving a signal above the cut-off for CCHFV (ranging between 1,488.5 and 4,568) were tested and found to be negative in the reference CCHFV ELISA. For the BTV experimental sera, 20 gave a positive signal to TB, but they were all close to the cut-off with MFI ranging between 735 and 1,469. As all these sera were from cows, they could not be tested in the TB ELISA, designed for all ruminant's species but cows and used as reference technique in order to confirm these results. For the CCHFV field positive sera, 16 sera gave MFI values above the SBV cut-off, between 1,304.5 and 8,863 and 7 of these were positive in the SBV reference ELISA. Some cross-reactivity could be expected between the CCHFV, RVFV and SBV beads, as these three viruses belong to the *Bunyavirales* order, although each is classified within different family taxa, emphasizing their distant genetic relatedness. The N proteins of bunyavirales members are very immunogenic, easy to produce, well conserved within each viral species and the N proteins of CCHFV and RVFV were already used in multiplex assays (318,352). The use of other immunogenic proteins of these viruses such as the glycoproteins could overcome this issue (318).

A multiplex assay has already been developed with the Luminex platform to detect antibodies against RVFV and CCHFV but the proteins used to coat the bead regions were produced from viruses propagated in BSL-3 or BSL-4 laboratories (353). In this chapter, a five-plex assay using recombinant proteins produced in a BSL-2 laboratory was described, thus avoiding the need of high-level containment facilities to develop such an

assay. This approach could also be used to establish similar multiplex assays for other BSL-4 pathogens, as described recently by Surtees *et al.* (354).

Finally, this multiplex assay is advantageous as it allows saving time and sample volume, as 96 samples can be analysed against five diseases in 4 hours, using only 0.5  $\mu\text{L}$  of serum, versus 144  $\mu\text{L}$  of serum that would be required to perform the five independent ELISAs used as references. Moreover, this is a flexible and open system that will allow including target antigens from other pathogens of interest (such as epizootic haemorrhagic disease or peste des petits ruminants), to broaden the range and impact of this assay.

This five-plex assay could be used as a screening tool, to assess the presence and prevalence of antibodies against these five highly pathogenic agents and identify regions at risk of infection. This information will help to minimize the spread and further transmission of those pathogens within the human population.

The results of this chapter respond to the third aim of this project, to develop a multiplex assay for differential diagnosis of CCHFV, RVFV and other relevant related pathogens affecting ruminants. The results presented in this chapter were recently published in a peer-reviewed journal (355).

# Chapter 6 Development of tools for the diagnosis of COVID-19

## 6.1. Chapter introduction

Most of the clinical symptoms caused by SARS-CoV-2 are similar to other respiratory infections and cannot be used to accurately diagnose COVID-19. Thus, testing of suspected cases is the only way to successfully diagnose patients with COVID-19. The pandemic of COVID-19 created a very high demand for *in vitro* tests to perform large screening of the population, thus numerous manufacturers started dedicating their research to the development of diagnostic tools.

The isolation of SARS-CoV-2 in cell culture from patient samples allowed its initial identification (10) but this method of detection is time-consuming and labour-intensive and thus not very useful during a pandemic where time is of the essence. Furthermore, SARS-CoV-2 could not be isolated from patients 8 days after the onset of symptoms, limiting the application of this technique (126).

The first tests developed during the pandemic and which remained the most commonly used for acute COVID-19 diagnosis was identification of viral RNA by real-time RT-PCR on respiratory tract samples. These tests were the first ones developed as soon as the viral sequence was known, allowing design of virus-specific primers. The real-time RT-PCR targets different genes of SARS-CoV-2 depending on the manufacturers, with most tests targeting one or more of the viral genes: envelope, nucleocapsid, spike, RNA-dependent RNA polymerase, and ORF1 genes (356). The real-time RT-PCR can detect SARS-CoV-2 infections as soon as the first day after the onset of symptoms and is most sensitive during the first two weeks of the infection (357,358). By the end of 2020, the FDA issued EUAs for over 160 real-time RT-PCR assays from different manufacturers (companies, universities and institutes) and over 400 molecular assays are commercialized or being developed (359). The nasopharyngeal and oropharyngeal specimens (upper respiratory tract) are the recommended specimens to perform the real-time RT-PCR, and their collection must be performed by a trained healthcare worker. The real-time RT-PCR is highly specific, however some concerns of sensitivity have been raised as the real-time RT-PCR has some vulnerabilities that can lead to false negative

results such as an improper collection of the specimen or a low viral load (360,361). Moreover, inactive virus or viral fragments can lead to some false positive results. In the case of a pandemic, the false negative results are more relevant than false positive results, as a false negative result leads to a delay or lack of supportive treatment and a lack of monitoring of infected individuals, resulting in increased risk of spread of the virus. In addition to these false negative results, the turnaround times of real-time RT-PCR is high and requires expensive equipment and trained technicians. To overcome these issues, POC molecular assays were developed, with most of them based on isothermal amplification (such as RT-LAMP). The POC tests had an overall lower sensitivity than real-time RT-PCR (around 90% sensitivity), but have many advantages over the real-time RT-PCR (362). By the end of 2020, the FDA had granted EUAs for a few POC molecular assays (around 15).

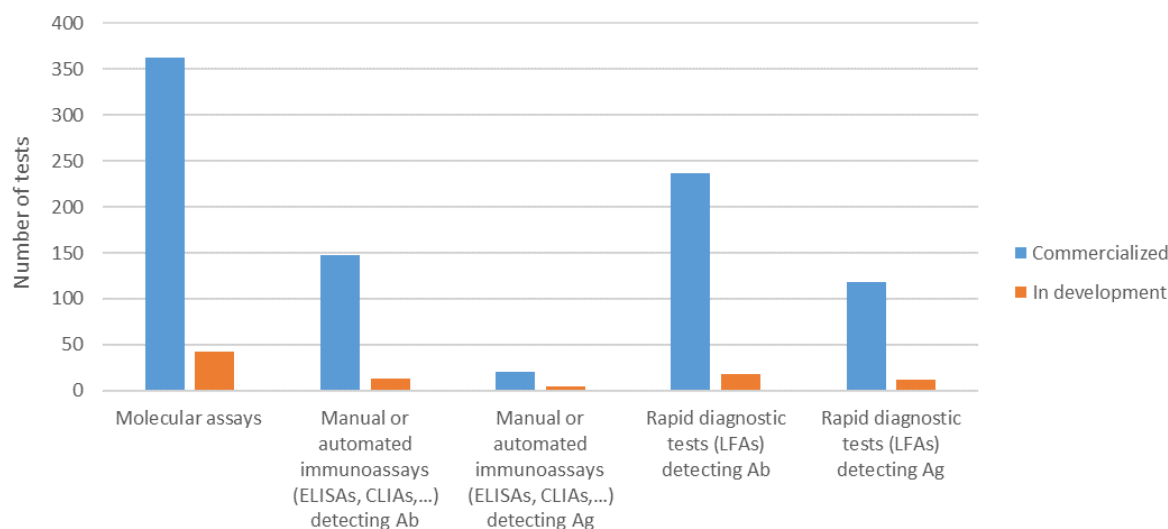
On the other hand, serological assays (mainly ELISAs and CLIAs) were developed to detect antibodies targeting the S or N proteins of SARS-CoV-2, thus needing the production of these proteins. Serological studies can be used to collect epidemiological information on the prevalence of SARS-CoV-2 and information on patients that already have recovered from the disease and more specifically for asymptomatic patients (363). Thus, in cases of COVID-19 not detected by real-time RT-PCR, the serological assays should be considered as a supplementary diagnostic tool, especially from the second week of illness, when the sensitivity of the current molecular tests decreases. Indeed, a combination of molecular and serological assays was shown to have a higher sensitivity than the individual assays taken separately (364). The sample collection and serological assays are easy to perform, however these assays cannot detect an acute infection with SARS-CoV-2, but only past infections and are generally not as accurate as real-time RT-PCR assays. By the end of 2020, over 160 immunoassays targeting SARS-CoV-2 antibodies were commercialized or being developed.

Virus neutralization tests or pseudo virus neutralization tests have been developed to evaluate nAbs to SARS-CoV-2 in convalescent patient sera, most of which are targeting the S protein (365). These assays are very useful for specific cases, such as for vaccine development, to ensure the antibodies induced by the vaccination are nAbs. However, these assays are time-consuming and labour-intensive, thus VNTs are not a high-throughput assay, which limits their impact for the population during a pandemic.

POC serological assays (such as LFAs) were also developed for the rapid and individual detection of antibodies to SARS-CoV-2. Their main advantage is that these assays do not require any infrastructure and provides a rapid solution for the diagnosis (in less than 20 min) at the patient's site. Generally, these assays have a lower diagnostic performance than the ELISAs, due to the low concentration of Abs in the sample leading to false negative results. By the end of 2020, over 250 rapid diagnostic tests targeting SARS-CoV-2 antibodies were commercialized or being developed (366).

Most recently, antigen tests have been developed, which directly detect the presence of SARS-CoV-2 proteins in a sample (usually nasopharyngeal specimens but other specimens are being tested such as saliva). Most of these tests are based on a LFA format. Although these assays are less sensitive than the molecular assays, they offer the possibility of rapid, inexpensive and early detection of COVID-19 cases in appropriate settings (367). These tests were the last being developed as they necessitated the production of Abs detecting the target antigens to start their development. By the end of 2020, 130 rapid diagnostic tests detecting SARS-CoV-2 antigens were commercialized or being developed.

The COVID-19 pandemic created an enormous demand for diagnostic tests, with many now developed (Figure 6.1). However, at the beginning of the pandemic, no diagnostic tools were available and there was an urgent need for the development of molecular and serological diagnostics.



**Figure 6.1** Different diagnostic assays commercialized and in development for COVID-19 diagnosis at the beginning of 2021.

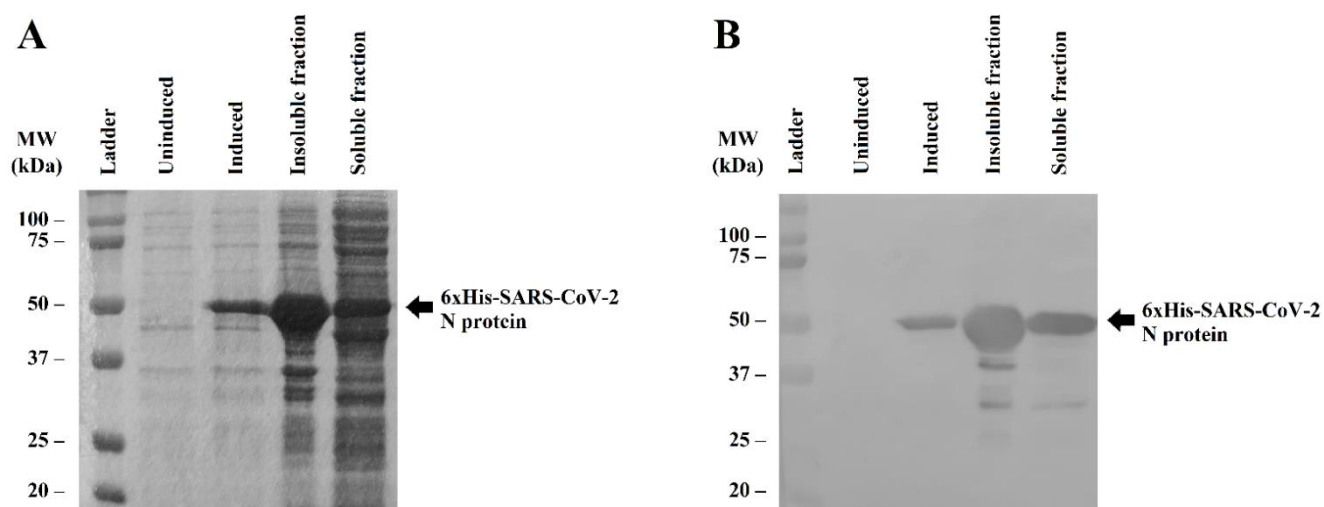
The aim of this thesis was the development of new diagnostic tools for emerging viruses and new viruses that could emerge unexpectedly during the course of this project. This was the case with the discovery of SARS-CoV-2 at the end of 2019. Thus, the aim of experiments described in this chapter was to respond to the gaps in SARS-CoV-2 diagnosis after this virus was discovered, with the development of robust diagnostic tests.

In order to achieve this aim, firstly, the SARS-CoV-2 N protein, one of the most immunogenic proteins of SARS-CoV-2, was recombinantly produced in bacteria and used to develop a double recognition ELISA. Using the same tools, a double recognition LFA was developed to detect human total antibodies at the POC. An indirect ELISA based on the N protein, was developed to discriminate between IgG and IgM antibodies to SARS-CoV-2. Next, using anti-SARS-CoV-2 S protein mAbs, a double antibody sandwich LFA was developed to detect the S protein in clinical samples. Finally, the N protein, the S protein and the RBD were used to develop a triplex assay to detect the immune response of humans infected with SARS-CoV-2 against different viral antigens.

## 6.2. Production of SARS-CoV-2 N protein

### 6.2.1. Expression of SARS-CoV-2 N protein

The ORF of the SARS-CoV-2 N protein was cloned into the pCR<sup>TM</sup>8/GW/TOPO<sup>TM</sup> vector and subsequently in the pDEST17 plasmid, used to transform *E. coli* BL21-AI<sup>TM</sup> One Shot<sup>TM</sup>. The expression of the SARS-CoV-2 N protein was induced by addition of arabinose. After ON incubation, the cells were harvested, lysed and the soluble fraction was separated from the insoluble fraction by centrifugation and analysed by SDS-PAGE followed by Coomassie staining and by WB (Figure 6.2). A band at the expected molecular size of the 6xHis-SARS-CoV-2 N protein (MW= 46.5 kDa) was observed after induction and in the insoluble and soluble fractions on the SDS-PAGE analysis followed by Coomassie staining (Figure 6.2A). These results were confirmed by WB analysis with an anti-6xHis mAb (Figure 6.2B).



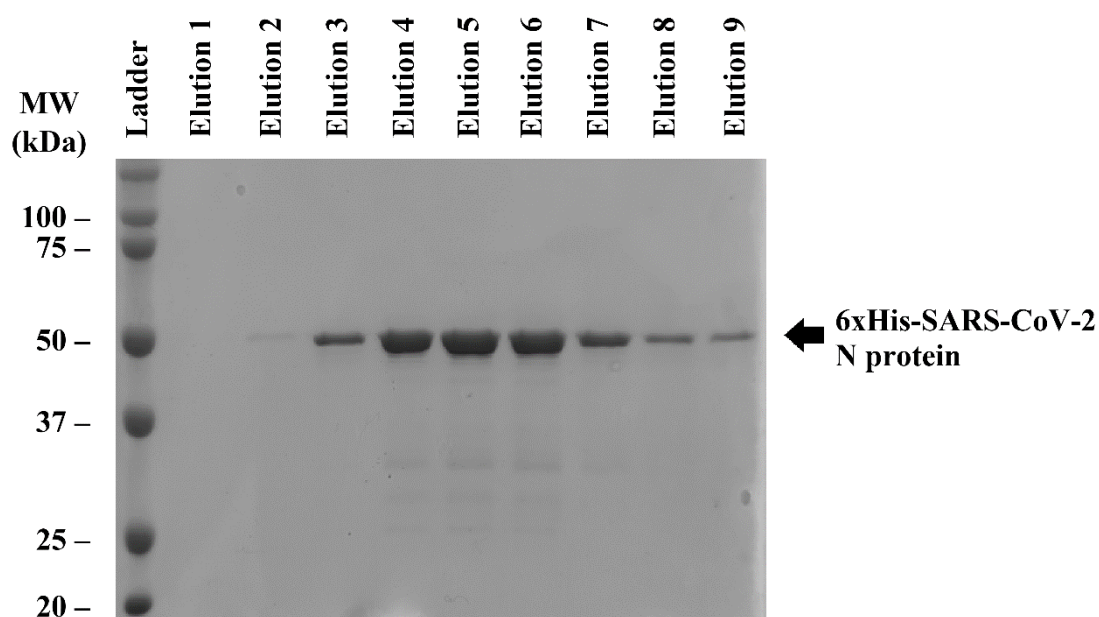
**Figure 6.2** Production of the SARS-CoV-2 N protein.

SDS-PAGE analysis followed by Coomassie staining (A) and Western blot analysis (B) of samples taken at different steps of the expression of the 6xHis-SARS-CoV-2 N protein. An anti-6xHis tag mAb was used as primary antibody in the Western blot analysis. Arrows indicate the bands corresponding to the specified proteins.



### 6.2.2. Purification of SARS-CoV-2 N protein

To separate the 6xHis-SARS-CoV-2 N protein from the other proteins contained in the soluble fraction, a purification step was performed by affinity chromatography using a Ni<sup>2+</sup>-NTA column. The soluble fraction was incubated ON with the Ni<sup>2+</sup>-NTA matrix, the resin was washed and the elution of the 6xHis-SARS-CoV-2 N protein was performed with an elution buffer containing 500 mM imidazole. The elution fractions were observed by SDS-PAGE followed by Coomassie staining (Figure 6.3). A band corresponding to the 6xHis-SARS-CoV-2 N protein was present at a high purity in the elution fractions 3 to 9. The fractions containing the pure 6xHis-SARS-CoV-2 N protein were pooled depending on their concentration, dialyzed and quantified by spectrophotometry and stored at -80°C after addition of glycerol.



**Figure 6.3 Purification of the SARS-CoV-2 N protein by affinity chromatography.** SDS-PAGE analysis followed by Coomassie staining of the different elution fractions of the SARS-CoV-2 N protein purification by Ni<sup>2+</sup>-NTA affinity chromatography. Arrows indicate the bands corresponding to the specified proteins.

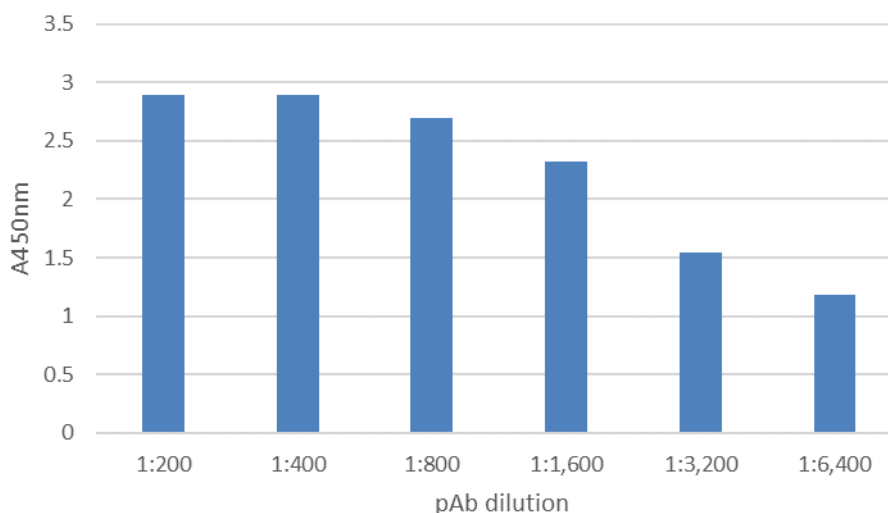
### **6.3. Development of two serological approaches for detection of antibodies to SARS-CoV-2 in different scenarios: a screening tool and a point-of-care test**

To contribute to the production of serological assays to detect antibodies against SARS-CoV-2 in humans and to collect epidemiological information on the prevalence of SARS-CoV-2, two serological assays were developed. Both assays, an ELISA and a LFA, are based on the double recognition of antibodies by the capture and detection antigens.

#### **6.3.1. Development of the double recognition ELISA**

##### **6.3.1.1. Labelling of the SARS-CoV-2 N protein to be used as the detection molecule in the double recognition ELISA**

The SARS-CoV-2 N protein was conjugated to HRP as described in section 2.6.1.1.1, to be used as the capture and detection molecule in the double recognition ELISA. To confirm the labelling of the HRP, a double recognition ELISA was performed with SARS-CoV-2 N protein coated in the 96-well plates and a mouse pAb obtained from the blood of the mice immunized with the SARS-CoV-2 N protein. This pAb was titrated and detected by the newly labelled SARS-CoV-2 N protein at 1:25,000 (Figure 6.4).



**Figure 6.4 Confirmation of the labelling of SARS-CoV-2 N protein with HRP.**

A double recognition ELISA was performed serial dilutions of a mouse pAb obtained from the blood of mice immunized with the SARS-CoV-2 N protein. The newly labelled SARS-CoV-2 N protein-HRP was used at a 1:25,000 dilution. The experiment was performed once.

At a 1:200 and 1:400 dilution of the pAb, the  $A_{450\text{nm}}$  obtained was equal to 2.9. After the 1:400 dilution, the signal obtained with the pAb decreased to reach a signal over 1 at 1:6,400.

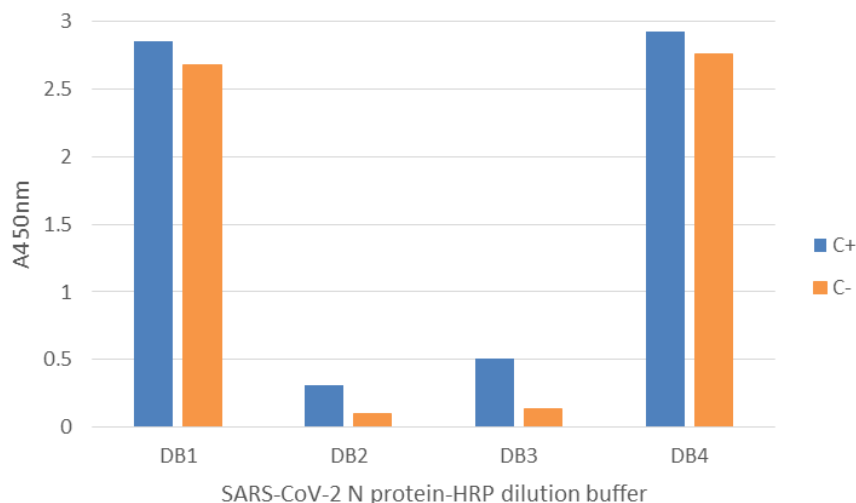
This assay showed the correct labelling of the SARS-CoV-2 N protein with HRP.

### 6.3.1.2. Optimization of the double recognition ELISA

The optimal conditions of the double recognition ELISA were determined. This included coating concentration, serum dilution, the detection molecule dilution, dilution buffers and the times of incubation.

As in a pandemic the turnaround time of an assay is an important factor, to develop an assay that could give results in the shortest period of time, the incubation times with the serum samples and with the conjugate were reduced to 30 min each. For the optimization of the conditions of the assay, the SARS-CoV-2 N protein was coated at 2  $\mu\text{g/mL}$ . In order to determine the dilution buffer for the conjugate and its concentration, the positive control (C+, mouse pAb at 1:1,000) and negative control (C-, FBS) were incubated with

the coated plates and the conjugate was added at 1:10,000 in different dilution buffers (Figure 6.5).

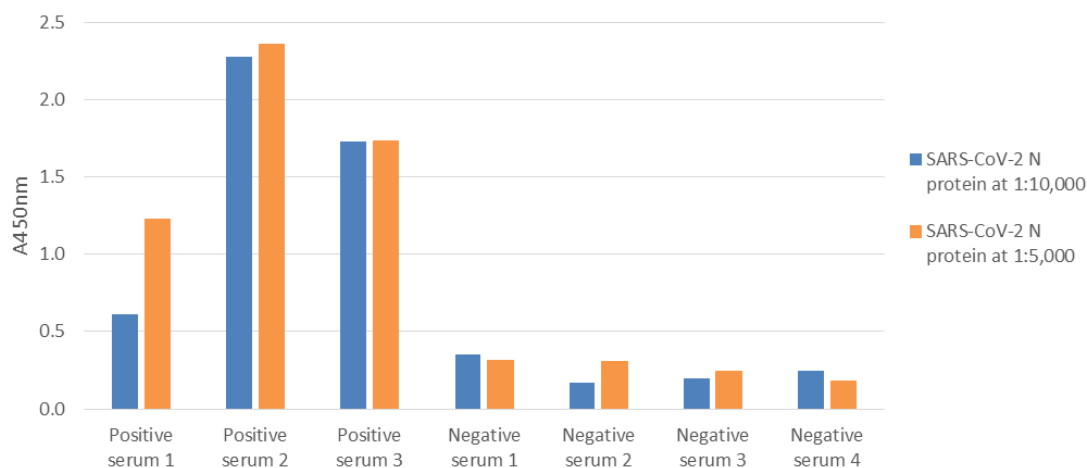


**Figure 6.5 Selection of the best SARS-CoV-2 N protein-HRP dilution buffer.**

A double recognition ELISA was performed with the SARS-CoV-2 N protein-HRP diluted at 1:10,000 in different dilution buffers. C+: mouse pAb obtained from the blood of mice immunized with the SARS-CoV-2 N protein. C-: sera of a mouse immunized with 1X PBS. Dilution buffers (DB) are described in section 2.1.9. The experiment was performed once.

DB1 and DB4 gave high signals with the positive control ( $A_{450\text{nm}}$  close to 3), but the signals obtained were close to that of the negative control. The DB2 and DB3 had a lower  $A_{450\text{nm}}$  with the positive control, but the signal obtained with the negative control corresponded to background noise. The dilution buffer giving the best positive signal to negative signal ratio was the DB3. This dilution buffer was selected as the dilution buffer for the conjugate in the assay.

Then, to optimize the double recognition ELISA with serum samples, some positive and negative human sera at a 1:10 dilution in DB1 were tested in the double recognition ELISA with the SARS-CoV-2 N protein-HRP at a 1:10,000 and 1:5,000 dilution in DB3 (Figure 6.6).



**Figure 6.6 Determination of the optimal SARS-CoV-2 N protein-HRP dilution.**

A double recognition ELISA was performed with three positive and four negative human sera at a 1:10 dilution and with the SARS-CoV-2 N protein-HRP diluted at 1:10,000 and 1:5,000. All the samples were tested once due to sample volume constraints.

At a 1:10,000 dilution of the conjugate, the three positive sera had an  $A_{450\text{nm}} > 0.5$  when the four negative sera had an  $A_{450\text{nm}}$  comprised between 0.17 and 0.35. At a 1:5,000 dilution of the conjugate, the  $A_{450\text{nm}}$  of the positive serum 1 doubled when the  $A_{450\text{nm}}$  of the other two positive sera were equivalent and the  $A_{450\text{nm}}$  of the negative sera stayed constant and was comprised between 0.18 and 0.32. Thus, better positive to negative ratios were obtained when the conjugate was diluted at 1:5,000 compared to 1:10,000.

To increase the simplicity of the assay, it would be desirable to dilute the sera and conjugate in the same dilution buffer. To obtain the same results with the DB3 than with DB1, the sera had to be diluted at a 1:5 dilution in DB3 (data not shown).

After the optimization of the assay, the final conditions of the double recognition ELISA were: SARS-CoV-2 N protein at 2  $\mu\text{g}/\text{mL}$  in carbonate buffer to coat the ELISA plates, a serum dilution of 1:10 in DB3 and, as detection molecule, the SARS-CoV-2 N protein-HRP diluted at 1:5,000 in DB3.

### 6.3.2. Development of the double recognition LFA

For the development of the double recognition LFA, black latex beads were conjugated to different concentrations of SARS-CoV-2 N protein (0.25, 0.5, 0.75 and 1  $\text{mg}/\text{m}^2$ ) and

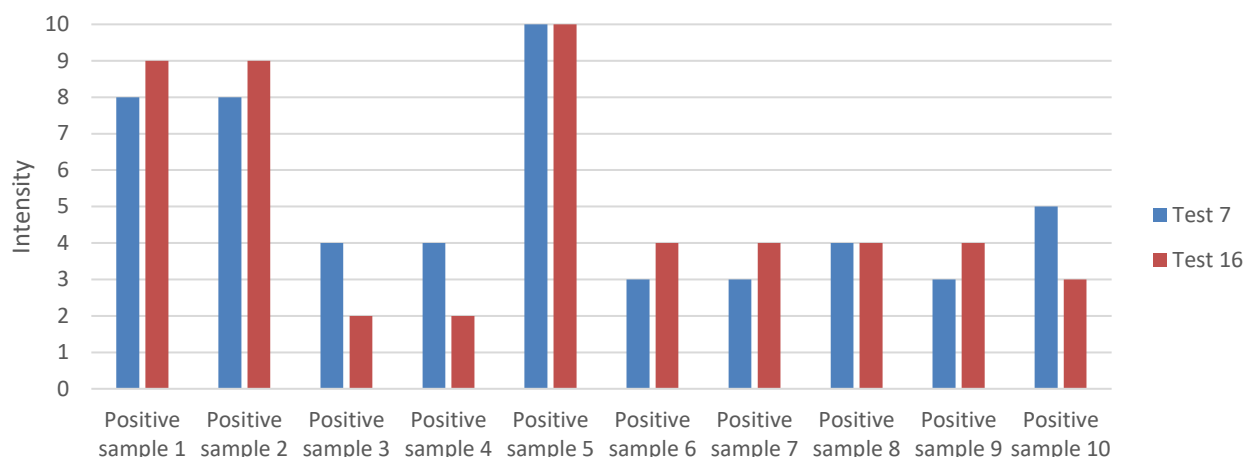
the SARS-CoV-2 N protein was immobilized at different concentrations on the nitrocellulose membrane as the capture molecule (0.075, 0.1, 0.15 and 0.225 mg/mL). A total of 16 different combinations between each conjugate and capture molecule and membrane were tested (Table 6.1).

**Table 6.1 First double recognition LFA prototypes by combination of different concentration of SARS-CoV-2 N protein on the membrane and as conjugate.**

		Membrane with SARS-CoV-2 N protein (mg/mL)			
		0.075	0.1	0.15	0.225
Conjugate with SARS-CoV-2 N protein (mg/m <sup>2</sup> )	0.25	Test 1	Test 2	Test 3	Test 4
	0.5	Test 5	Test 6	Test 7	Test 8
	0.75	Test 9	Test 10	Test 11	Test 12
	1	Test 13	Test 14	Test 15	Test 16

These tests were assayed with different buffers (data not shown) and the buffer selected for the first experiments was LDB4 (LDB1 with 0.75 M NaCl) as it was the only one not giving background signal when added to the strips.

A few tests were selected (Tests 1, 7 and 16) as they had different concentrations of SARS-CoV-2 N protein on membrane and as conjugate. These three tests were tested with negative serum samples, which all gave a negative signal of 1, but the Test 16 gave some background signal, which was reduced to a negative signal of 1 when using LDB5 (LDB1 with 1 M NaCl). Tests 7 and 16 were tested with 10 positive serum samples of patients previously confirmed positive by real-time RT-PCR (Figure 6.7).



**Figure 6.7 Double recognition LFA Test 7 and 16 tested with 10 positive serum samples.**

The 10 positive serum samples were taken from patients previously confirmed positive to COVID-19 by real-time RT-PCR. All the samples were tested once due to sample volume constraints. The intensity was determined using the intensity scale shown in Figure 2.2.

These preliminary results confirmed that the prototypes of double recognition LFA were working properly. Overall, the results obtained were similar between Test 7 and Test 16. Some positive samples (1, 2, 6, 7 and 9) gave a slightly higher signal with Test 16 compared to Test 7, when some weak positive samples in Test 7 (samples 3, 4 and 10) gave a lower signal in Test 16. After these results and to reduce the amount of SARS-CoV-2 N protein used in the assay, Test 7 was selected.

The test was further optimized, and the final conditions selected for the double recognition LFA were: black latex beads conjugated with SARS-CoV-2 N protein at 1 mg/m<sup>2</sup> and SARS-CoV-2 N protein at 0.2 mg/mL on the membrane.

### **6.3.3. Validation of the newly developed tools: double recognition ELISA and double recognition LFA with samples from positive patients to COVID-19 and healthy donors**

The double recognition ELISA and double recognition LFA were validated for the detection of total antibodies against SARS-CoV-2 in sera and blood.

A total of 1,065 samples were tested in the double recognition ELISA, classified as described in section 2.1.8.2. To determine the performance characteristics of the newly developed double recognition ELISA, a ROC analysis was performed. Since there was no serological gold standard when these assays were developed, the samples were considered positive or negative according to the results obtained by real-time RT-PCR (in respiratory material) and a commercial serological assay (in serum). Moreover, the group of serum samples collected before 2019 (before the emergence of SARS-CoV-2) was considered true-negative samples. The correlation between the results obtained in the double recognition ELISA and the classification of the samples as positive (positive in real-time RT-PCR and serological assay) and negative (negative in real-time RT-PCR and serological assay or collected prior 2019) was determined. To calculate the cut-off of the assay, the sample to positive control (S/P) ratio was calculated using:

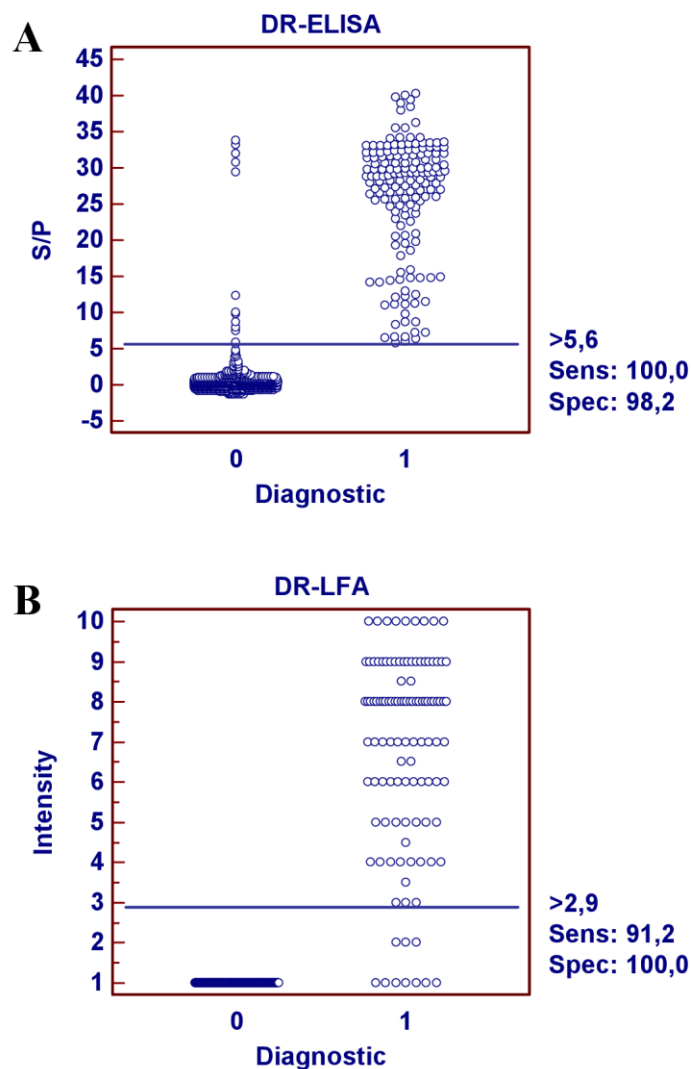
$$S/P = \frac{\text{test sample} - \text{mean negative control}}{\text{mean positive control} - \text{mean negative control}}$$

Based on this S/P value, samples were considered negative when the S/P ratio was under 5.6 and positive when its S/P ratio was equal to or above 5.6. With these values, the diagnostic sensitivity of the double recognition ELISA was 100% with a 95% confidence interval (97.7–100%), and the diagnostic specificity was 98.2% with a 95% confidence interval (97–99.1%) (Figure 6.8A).

A ROC analysis was also performed to determine the performance characteristics of the double recognition LFA and displayed in an interactive dot plot diagram (Figure 6.8B). A lower number of samples were tested in the double recognition LFA: 113 serum samples positive by PCR and a serological assay, 14 negative by real-time RT-PCR and a serological assay, and 120 serum samples collected prior 2019. With the calculated cut-off value, the diagnostic sensitivity of the double recognition LFA was 91.2% with a 95% confidence interval (84.7–95.7%), and the diagnostic specificity was 100% with a 95% confidence interval (97.3–100%). For both assays developed, the null hypothesis was that the area under the ROC curve is equal to 0.5. The P values obtained were 0.0001;



therefore, there is evidence that the 2 assays developed can distinguish between the positive and negative samples tested.



**Figure 6.8 Validation of the double recognition ELISA and double recognition LFA.**

Dot plot diagrams with each dot representing an individual sample: results obtained for double recognition ELISA (A) and double recognition LFA (B). The horizontal solid line corresponds to the cut-off values in each assay, according to the MedCalc® 10 software. X axis shows the positive (1) or negative (0) classification of samples according to the real-time RT-PCR and serological assay and Y axis shows sample to positive control (S/P) ratio and intensity obtained in the double recognition ELISA and double recognition LFA, respectively. All the samples were tested once due to sample volume constraints.

Finally, a comparison was done between the double recognition ELISA and double recognition LFA with the samples tested in both assays. Out of the 114 positive samples in the double recognition ELISA, 92.3% were positive in the double recognition LFA, and out of the 133 negative samples tested in the double recognition ELISA, 100% were also negative in the double recognition LFA. Using the MedCalc® 10 software, Fisher's exact test was performed to examine the relation between the results obtained in the double recognition ELISA and in the double recognition LFA. The null hypothesis being that the variables are independent,  $P < 0.000000001$ , meaning that there is a significant relationship between the 2 assays. The comparison between the 2 techniques is summarized in Table 6.2.

**Table 6.2 Comparison between the samples tested in the double recognition LFA and the double recognition ELISA.**

		Double recognition ELISA		
		Positive	Negative	Total
Double recognition LFA	Positive	106	0	106
	Negative	8	133	141
	Total	114	133	247

#### 6.3.4. Cross-reactivity by antibodies directed to common-cold *Alpha-* and *Betacoronavirus* and other respiratory pathogens

To fully validate the double recognition ELISA and double recognition LFA, the potential cross-reactivity by antibodies induced by infection with seasonal coronaviruses (HCoV-NL63, HCoV-229E, HCoV-HKU1 and HCoV-OC43) were examined by both assays. Moreover, the assays were tested with sera containing antibodies to pathogens that can induce pneumonia in infected patients such as *Chlamydia trachomatis*, *Mycoplasma pneumoniae*, *Legionella pneumophila* and hRSV, the latter only tested in the double recognition ELISA. The results of both assays showed no cross-reactivity with any of the other coronaviruses, neither any other respiratory pathogen, but one of the serum samples containing antibodies to *Mycoplasma pneumoniae* that gave a false positive signal in the double recognition ELISA (see Table 6.3).

**Table 6.3 Cross-reactivity of the double recognition ELISA and LFA with other respiratory pathogens.**

	Double recognition ELISA		Double recognition LFA	
	Positive	Negative	Positive	Negative
<i>Alphacoronavirus</i> (HCoV-NL63/ HCoV-229E) (n=11)	0	11	0	11
<i>Betacoronavirus</i> (HCoV-HKU1/HCoV-OC43) (n=9)	0	9	0	9
<b>Pneumovirus (hRSV) (n=62)</b>	0	62	ND	ND
<i>Chlamydia trachomatis</i> (n=5)	0	5	0	5
<i>Mycoplasma pneumoniae</i> (n=17)	1	16	0	17
<i>Legionella pneumophila</i> (n=21)	0	21	0	21

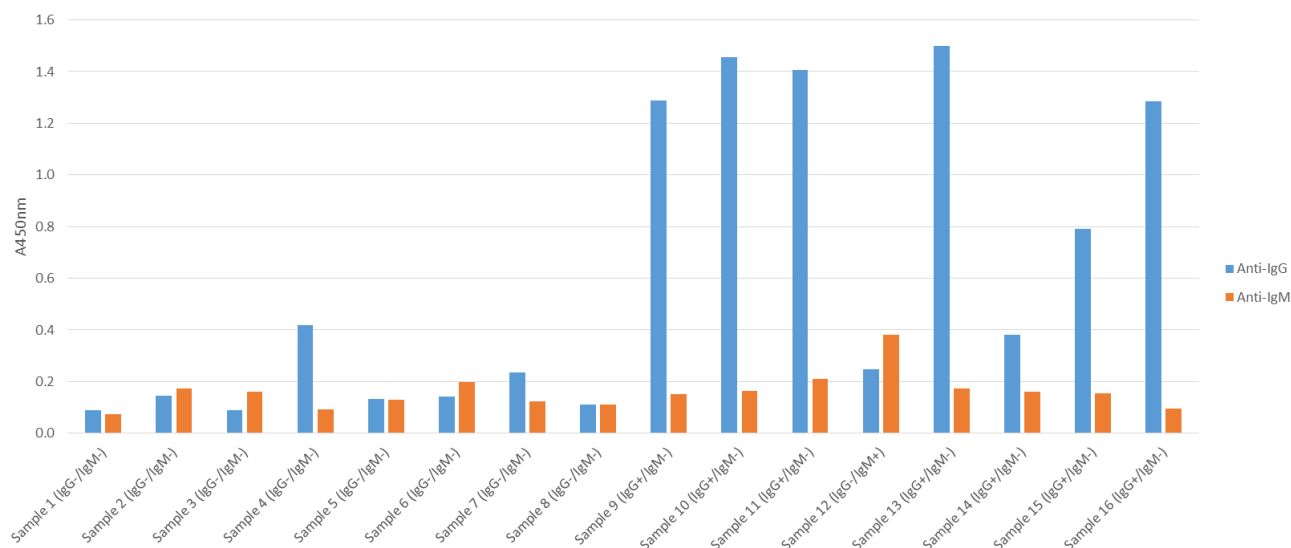
ND: not determined. All the samples were tested once due to sample volume constraints.

## 6.4. Development of an indirect ELISA to detect human IgG and IgM against SARS-CoV-2

The double recognition ELISA described in the previous section detects the presence of total antibodies in human sera. Here the development of two independent assays to detect IgG and IgM antibodies is described.

### 6.4.1. Optimization of the assay

The SARS-CoV-2 N protein was used at 2 µg/mL in carbonate buffer to coat the ELISA plates. For the first assay, a few positive and negative human serum samples to COVID-19, determined by ELISA, were diluted at 1:100 in the same dilution buffer than the double recognition ELISA (DB3). The anti-IgG-HRP and anti-IgM-HRP pAb were both diluted at 1:50,000 in DB1. The results are shown in Figure 6.9.



**Figure 6.9** Detection of IgG and IgM by indirect ELISA, using negative and positive serum samples to COVID-19.

Eight positive and eight negative human serum samples to COVID-19, confirmed by ELISA, were assayed in the new indirect ELISA targeting IgG and IgM. Anti-IgG-HRP and anti-IgM-HRP pAb were used as secondary antibodies. All the samples were tested once due to sample volume constraints.

The ELISA for detection of anti-IgG showed good results, with 7 of the 8 negative sera (IgG-/IgM-) tested having an  $A_{450nm}$  between 0.09 and 0.24 and one negative sample giving an  $A_{450nm}$  of 0.42. The positive samples to IgG gave an  $A_{450nm}$  between 0.38 and 1.5. Overall, the results obtained in the anti-IgM ELISA, exhibited a lower  $A_{450nm}$  (from 0.07 to 0.21), with the only sample positive to IgM giving an  $A_{450nm}$  of 0.38.

These first results showed some potential background issues with the anti-IgG conjugate and some low signal obtained with the anti-IgM conjugate.

Thus, additional assays were performed to reduce the background obtained with the anti-IgG-HRP by changing its dilution buffer to DB4 and using the anti-IgM-HRP at a higher concentration. After optimization of the assay, the final conditions of the indirect ELISA were: SARS-CoV-2 N protein at 2  $\mu\text{g/mL}$  in carbonate buffer to coat the ELISA plates, serum samples diluted at 1:100 in DB3, the anti-human IgG-HRP at 1:50,000 in DB4 or the anti-human IgM-HRP at 1:15,000 in DB4.

### 6.4.2. Validation of the indirect anti-human IgG and IgM ELISA

The assays were then validated with a collection of positive and negative human serum samples. The serum samples were first classified as positive if positive by real-time RT-PCR and by a commercial indirect ELISA anti-human IgG and IgM (NovaLisa® SARS-CoV-2 IgG ELISA and NovaLisa® SARS-CoV-2 IgM ELISA from NovaTec Immundiagnostica GmbH) and as negative otherwise (see Table 6.4).

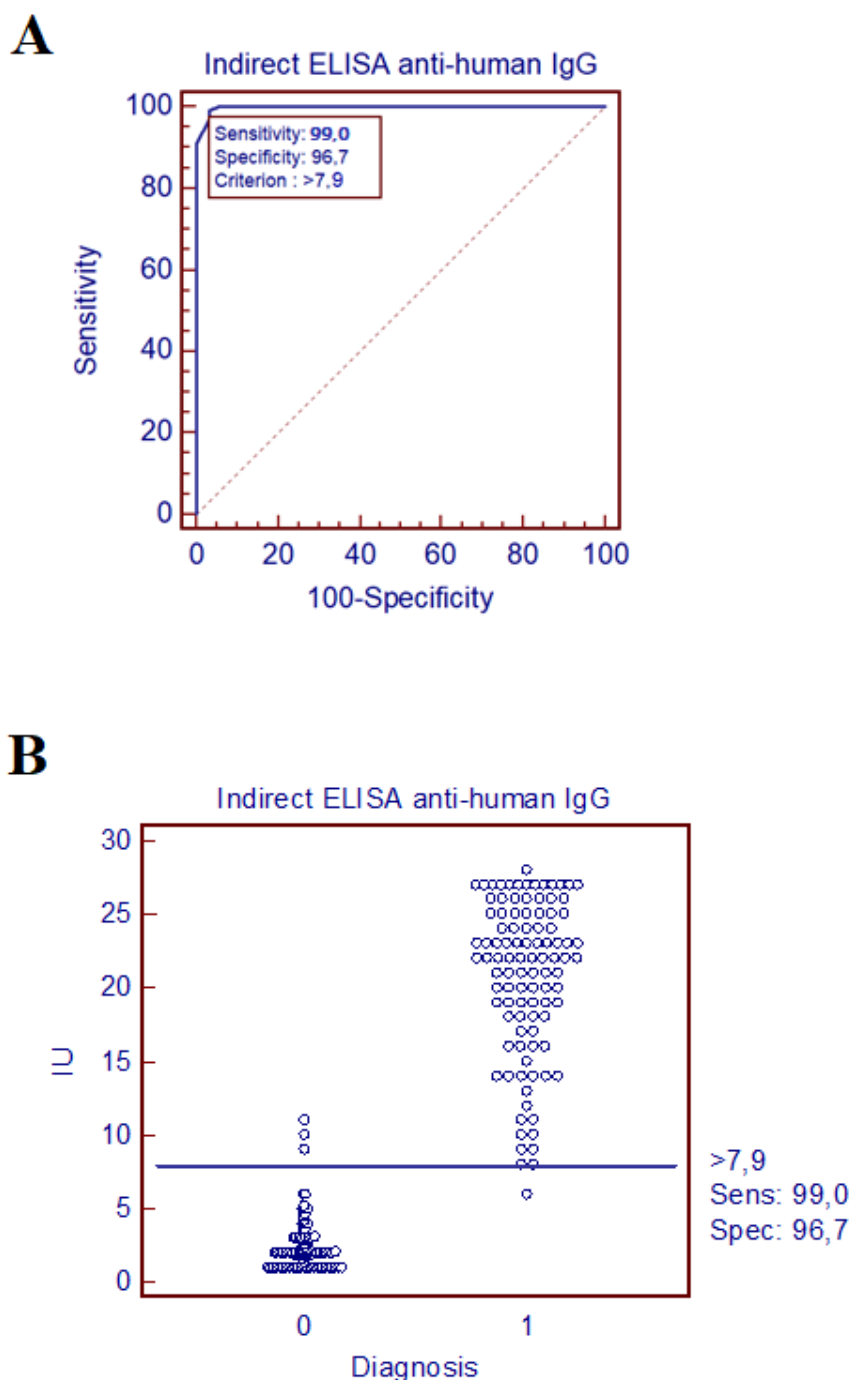
*Table 6.4 Serum samples classification by real-time RT-PCR and serological assay.*

Serum samples	Real-time RT-PCR/ SARS-CoV-2 IgG	Real-time RT-PCR/ SARS-CoV-2 IgM
Positive	100	55
Negative	91	119
Total	191	174

A total of 191 samples were tested in the indirect ELISA anti-human IgG, classified as described in Table 6.4. To determine the performance characteristics of the indirect ELISA developed, a ROC analysis was performed. The correlation between the results obtained in the indirect ELISA anti-human IgG and the classification of the samples as positive (positive in PCR and a commercial indirect ELISA anti-IgG) and negative (negative in PCR and a commercial indirect ELISA anti-IgG or collected prior 2019) was determined. To calculate the cut-off of the assay, a ratio (called Ingenasa Units, IU) was calculated using:

$$IU = \left( \frac{\text{test sample}}{\text{mean cut-off}} \right) \times 10$$

Based on the IU, samples were considered negative when the IU ratio was under 8 and positive when the IU was equal to or above 8. With these values, the diagnostic sensitivity of the indirect ELISA anti-human IgG was 99% with a 95% confidence interval (94.5–99.8%), and the diagnostic specificity was 96.7% with a 95% confidence interval (90.9–99.3%) (Figure 6.10).

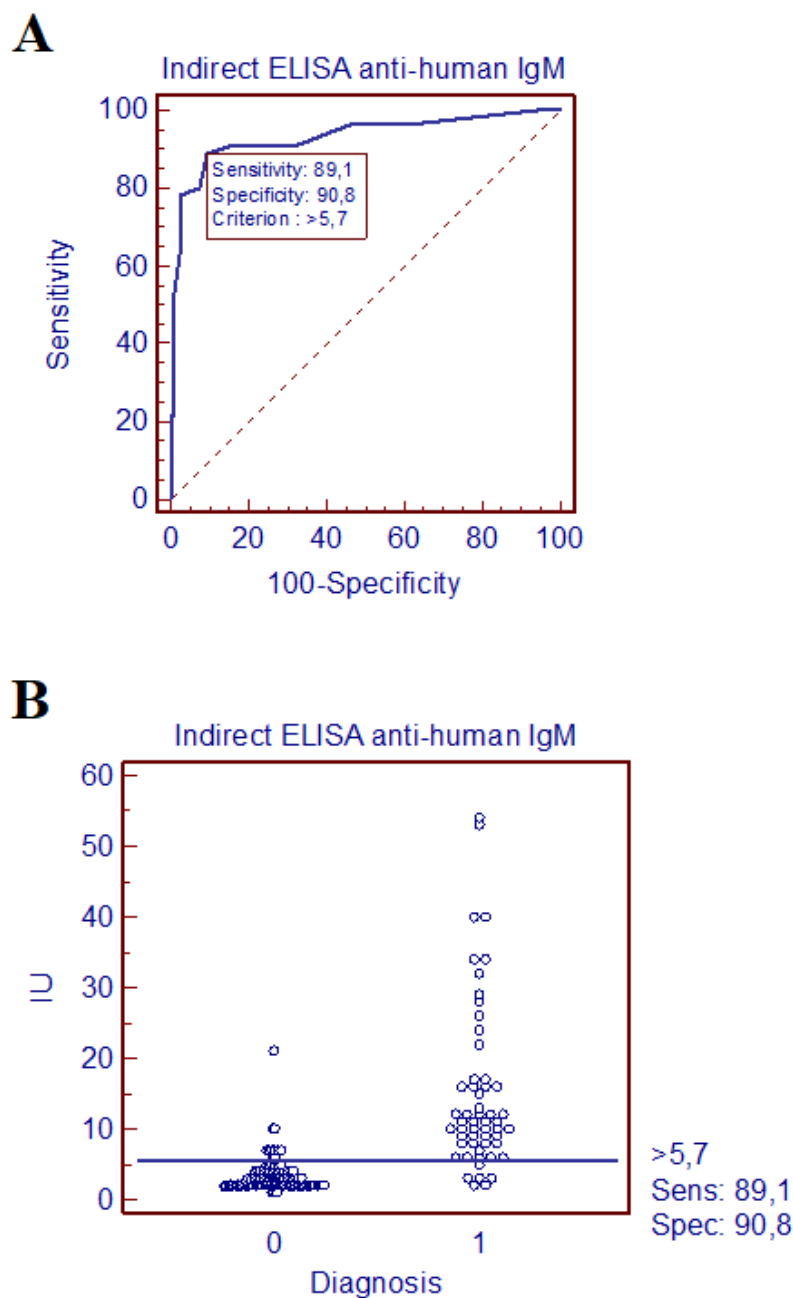


**Figure 6.10** Validation of the indirect anti-human IgG ELISA for the detection of IgG against SARS-CoV-2.

A: ROC curve for the indirect ELISA anti-human IgG. The blue line shows the mean area under the curve (AUC) plot and the red dotted line corresponds to an AUC of 0.5. The sensitivity and specificity values corresponding to the cut-off are represented on the graph. B: dot plot diagram of the indirect ELISA anti-human IgG where each dot represents an individual sample. The horizontal solid line corresponds to the cut-off value according to the MedCalc® 10 software. X axis shows the positive (1) or negative (0) classification of samples according to the real-time RT-PCR and serological assay detecting IgG and Y axis shows Ingenasa Units (IU). All the samples were tested once due to sample volume constraints.

A total of 174 samples were tested in the indirect ELISA anti-human IgM, classified as described in Table 6.4. To determine the performance characteristics of the indirect ELISA developed, a ROC analysis was performed. The correlation between the results obtained in the indirect ELISA anti-human IgM and the classification of the samples as positive (positive in PCR and a commercial indirect ELISA anti-IgM) and negative (negative in PCR and a commercial indirect ELISA anti-IgM or collected prior 2019) was determined.

Based on the IU (described above), samples were considered negative when the IU was under 5.7 and positive when the IU was equal to or above 5.8. With these values, the diagnostic sensitivity of the indirect ELISA anti-human IgM was 89.1% with a 95% confidence interval (77.7–95.9%), and the diagnostic specificity was 90.8% with a 95% confidence interval (84.1– 95.3%) (Figure 6.11). However, with this cut-off value the specificity of the ELISA anti-IgM developed was under 95%, which is not acceptable for a commercial assay. To have an assay that reached at least a 95% specificity, the samples had to be considered positive when the IU were equal or above to 8. With this new cut-off, the diagnostic sensitivity was 78.2% with a 95% confidence interval (65.0–88.2%), and the diagnostic specificity was 97.5% with a 95% confidence interval (92.8– 99.4%).



**Figure 6.11** Validation of the indirect anti-human IgM ELISA for the detection of IgM against SARS-CoV-2.

A: ROC curve for the indirect ELISA anti-human IgM. The blue line shows the mean area under the curve (AUC) plot and the red dotted line corresponds to an AUC of 0.5. The sensitivity and specificity values corresponding to the cut-off are represented on the graph. B: dot plot diagram of the indirect ELISA anti-human IgM where each dot represents an individual sample. The horizontal solid line corresponds to the cut-off value according to the MedCalc® 10 software. X axis shows the positive (1) or negative (0) classification of samples according to the real-time RT-PCR and serological assay detecting IgM and Y axis shows Ingenasa Units (IU). All the samples were tested once due to sample volume constraints.



For both assays developed, the null hypothesis was that the area under the ROC curve is equal to 0.5. The P values obtained were 0.0001; therefore, there is evidence that the 2 assays developed can distinguish between the positive and negative samples tested.

Finally, a comparison was done between the two indirect ELISA developed and the double recognition ELISA with the samples tested in both assays. As the double recognition ELISA detects total antibodies (mostly IgG and IgM), a comparison can be done by adding the results obtained in the indirect ELISA anti-human IgG and IgM. Out of the 104 positive samples in the double recognition ELISA, 97.1% were positive in the indirect ELISAs, and out of the 91 negative samples tested in the double recognition ELISA, 96.7% were also negative in the indirect ELISAs. Moreover, using the MedCalc® 10 software, Fisher's exact test was performed to examine the relation between the results obtained in the double recognition ELISA and in the indirect ELISAs. The null hypothesis being that the variables are independent,  $P < 0.000000001$ , meaning that there is a significant relationship between the 2 assays. The comparison between the 2 techniques is summarized in Table 6.5.

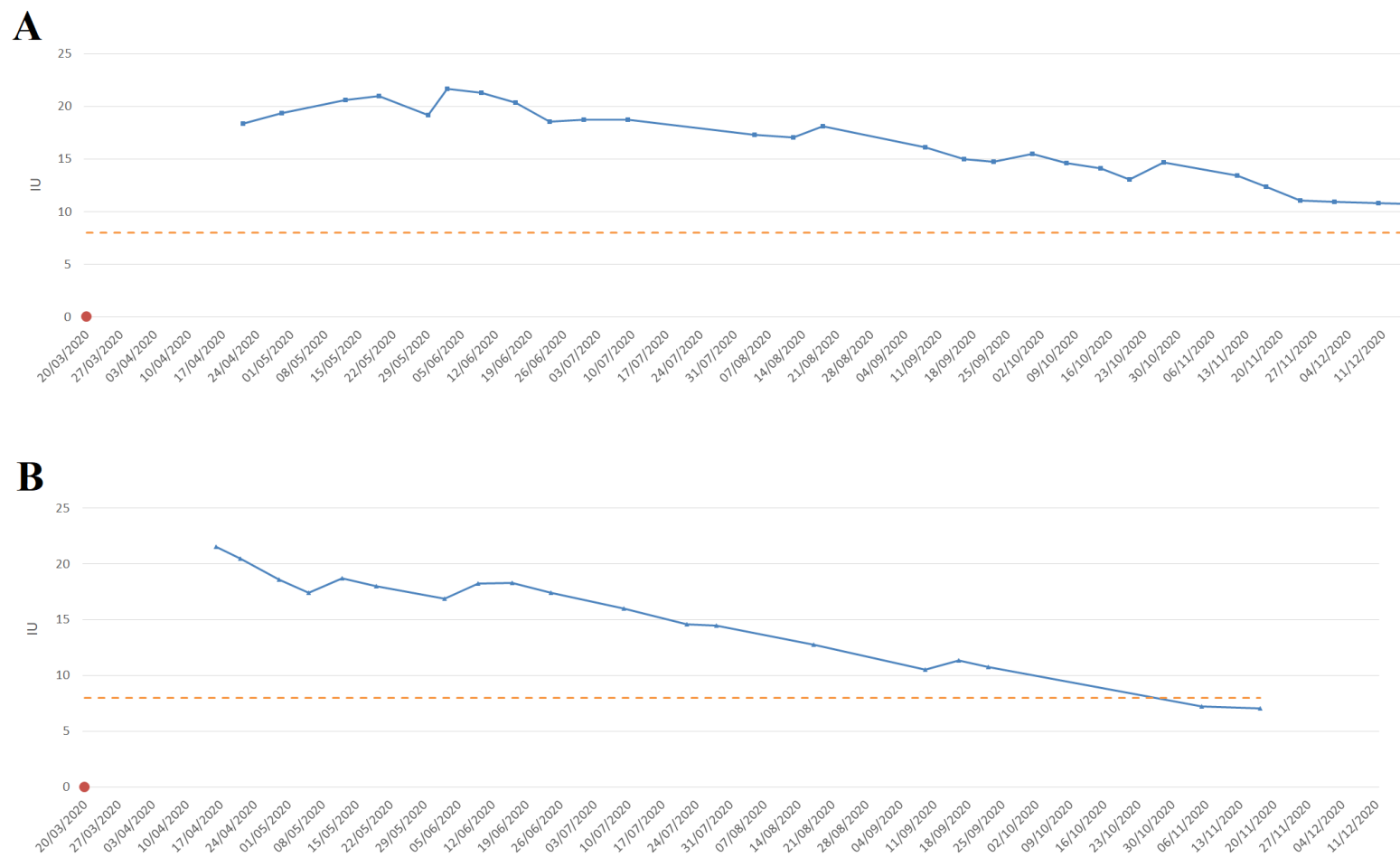
**Table 6.5 Comparison between the indirect ELISAs and the double recognition ELISA.**

		Double recognition ELISA		
		Positive	Negative	Total
Indirect ELISA IgG/IgM	Positive	101	3	104
	Negative	3	88	91
	Total	104	91	195

#### **6.4.3. Indirect ELISA with positive sera at different time points**

A study was done with two positive SARS-CoV-2 patients to evaluate the evolution of their antibodies raised against the SARS-CoV-2 N protein. These two patients were probably infected at the same time as their symptoms, corresponding to an infection with SARS-CoV-2, arose at the same time, but this date of infection was not confirmed by real-time RT-PCR. Patient 1 only had very limited symptoms, such as fatigue and a

slightly sore throat, and patient 2 had some more severe symptoms such as fever (40.5°C), sore throat, fatigue, diarrhoea and rash. A blood sample was taken from patient 1 and 2 every week, the sample was then centrifuged to collect the sera, which was stored at -80°C. Overall, from the 16/04/20 to the 15/12/20, 28 and 19 serum samples were collected from patient 1 and 2, respectively. All these serum samples were tested at once in the indirect ELISA anti-IgG and the results are shown in Figure 6.12.



**Figure 6.12 Indirect ELISA for the detection of IgG against SARS-CoV-2 with the sera of two positive patients collected at different time-points.**  
 A: patient 1. B: patient 2. The patients exhibited some symptoms corresponding to COVID-19 around the 20/03/20, shown by a red dot on the figure. The cut-off value for this assay (IU=8) is represented by an orange dotted line. All the samples were tested once due to sample volume constraints. IU: Ingenasa Units.

For both patients, a decrease tendency can be observed over this large period of time (between 7 and 8 months from the first time-point to the last). Patient 1 (Figure 6.12A) had an increase in the IU, from 18.4 at the first time-point (21/04/20) until 21.8 on the 02/06/20, then the IU started decreasing to reach a value of 10.8 on the 15/12/20. The IU obtained for the last time-point was still above the cut-off of the assay, but this point was half the IU obtained at the peak of IU. Regarding patient 2 (Figure 6.12B), a constant decrease was observed, with the highest IU reached at the first time-point (21.6 on the 16/04/20) and the lowest IU reached at the final time-point (7 on the 17/11/20). Finally, the IU of the last two time-points of patient 2 were lower than the cut-off of the assay.

## **6.5. Development of a double antibody sandwich LFA to detect SARS-CoV-2 S antigens**

To provide a rapid and easy solution for widespread testing of the population, and to reduce the burden on the number of real-time RT-PCR performed daily, a double antibody sandwich LFA to detect the SARS-CoV-2 S protein was developed.

### **6.5.1. Optimization of the double antibody sandwich LFA**

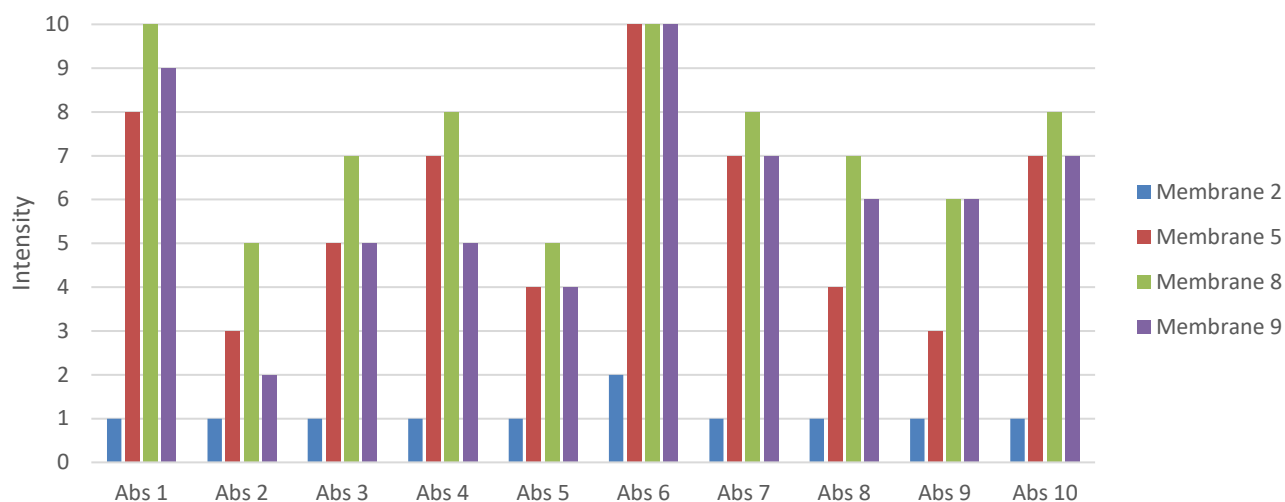
In order to develop the sandwich LFA, ten human recombinant mAbs recognizing the SARS-CoV-2 S protein and the S protein were kindly provided by Dr Marit van Gils (AUMC) to be tested (368). The S protein consisted in stabilized prefusion SARS-CoV-2 S ectodomain, where the furin cleavage site is replaced with a glycine linker (GGGG), two proline mutations are introduced (K986P and V987P), and a trimerization domain preceded by a linker (GSGG) is attached (368). To find the best antibody combination to detect SARS-CoV-2 S protein, all the mAbs were conjugated to red latex beads at 1 mg/m<sup>2</sup> and all the mAbs were dispensed on a membrane at 1 mg/mL. These materials gave a hundred different combinations (Table 6.6).

**Table 6.6** Combinations possible with the 10 monoclonal antibodies used to conjugate red latex beads and immobilized on the membrane.

	Conjugate	1	2	3	4	5	6	7	8	9	10
Membrane	mAb	COV A1-02	COV A1-08	COV A1-19	COV A3-07	COV A3-09	COV A2-03	COV A2-10	COV A2-29	COV A2-31	COV A2-43
1	COVA1-02	1.1	1.2	1.3	1.4	1.5	1.6	1.7	1.8	1.9	1.10
2	COVA1-08	2.1	2.2	2.3	2.4	2.5	2.6	2.7	2.8	2.9	2.10
3	COVA1-19	3.1	3.2	3.3	3.4	3.5	3.6	3.7	3.8	3.9	3.10
4	COVA3-07	4.1	4.2	4.3	4.4	4.5	4.6	4.7	4.8	4.9	4.10
5	COVA3-09	5.1	5.2	5.3	5.4	5.5	5.6	5.7	5.8	5.9	5.10
6	COVA2-03	6.1	6.2	6.3	6.4	6.5	6.6	6.7	6.8	6.9	6.10
7	COVA2-10	7.1	7.2	7.3	7.4	7.5	7.6	7.7	7.8	7.9	7.10
8	COVA2-29	8.1	8.2	8.3	8.4	8.5	8.6	8.7	8.8	8.9	8.10
9	COVA2-31	9.1	9.2	9.3	9.4	9.5	9.6	9.7	9.8	9.9	9.10
10	COVA2-43	10.1	10.2	10.3	10.4	10.5	10.6	10.7	10.8	10.9	10.10

The tests are written as “membrane.conjugate”.

To reduce the number of combinations of mAbs to be tested, the ten mAbs on the conjugate pads were used with four different membranes with mAbs with different affinities for the SARS-CoV-2 S protein (membranes 2, 5, 8 and 9). The forty combinations were tested with LDB1 and with 1 µg/mL of SARS-CoV-2 S protein in LDB1 (Figure 6.13).

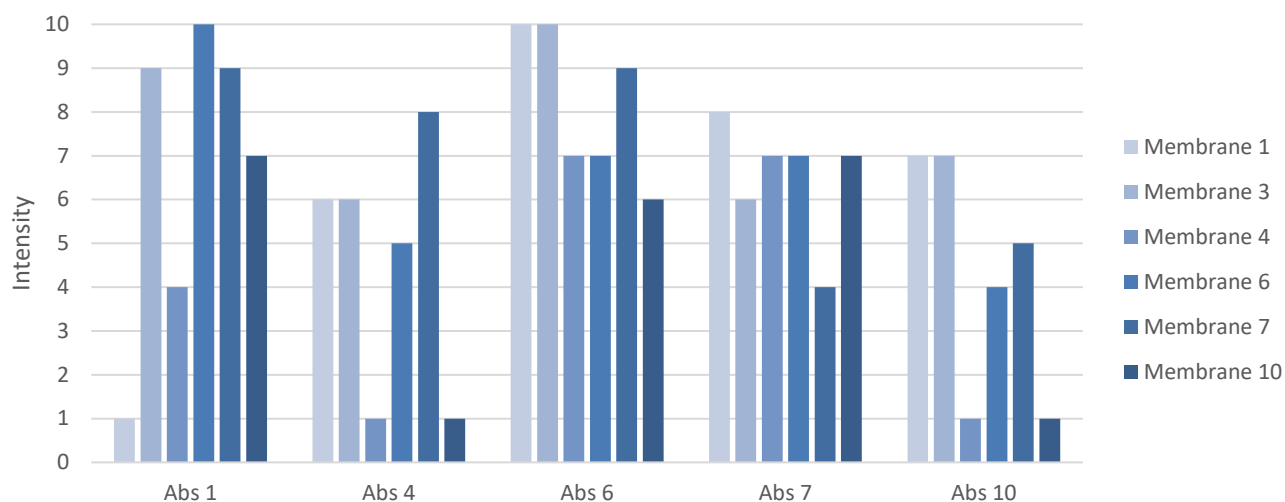


**Figure 6.13 Optimization of the double antibody sandwich LFA for detection of SARS-CoV-2 S protein.**

40 different combinations between the mAb conjugated to red latex beads and mAb dispensed onto the conjugate pad were analysed. A concentration of 1  $\mu\text{g/mL}$  of SARS-CoV-2 S protein diluted in LDB1 was assayed with the forty different combinations. Abs: mAb conjugated to red latex beads and dispensed onto the conjugate pad. The intensity was determined using the intensity scale shown in Figure 2.2. The experiment was performed once.

These preliminary results gave some tendencies in the results obtained with the different mAbs on the membranes and conjugates. The mAb on membrane 2 did not give any signal with the recombinant protein. The mAb on membrane 8 seemed to be the best mAb to be used as capture, as all the detection mAbs (on the conjugates) were giving the highest intensities with this mAb compared to the others. Overall, the detection mAbs (on the conjugates) giving the highest intensities were 1, 4, 6, 7 and 10.

In a second time, the 6 capture mAbs left were tested in combination with the five best detection mAbs identified previously with LDB1 and with 1  $\mu\text{g/mL}$  of SARS-CoV-2 S protein in LDB1 (Figure 6.14).

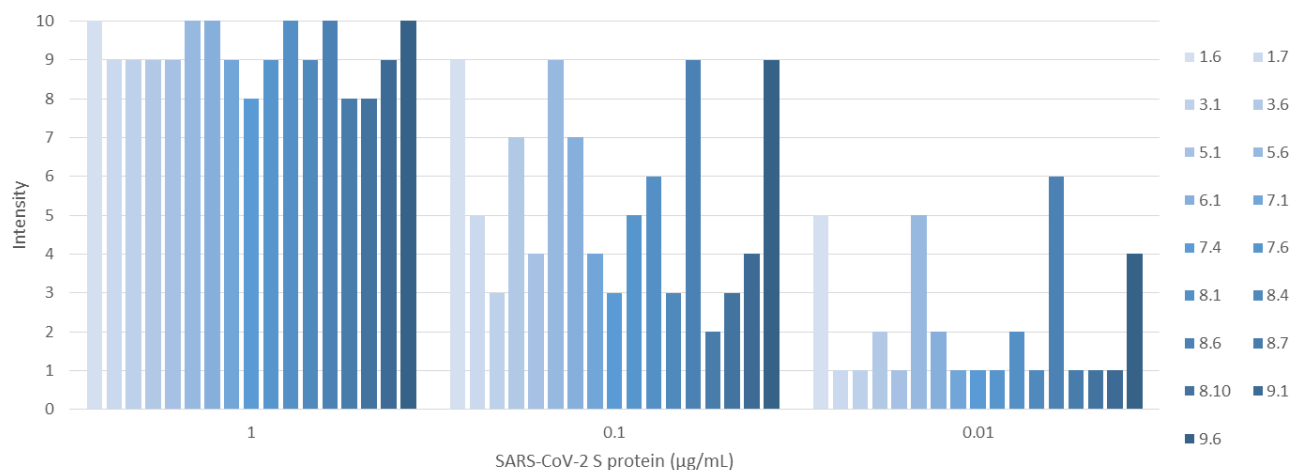


**Figure 6.14** Additional different double antibody sandwich LFA combinations tested with SARS-CoV-2 S.

The rest of the membranes and the absorbent pads previously selected were tested with 1  $\mu\text{g}/\text{mL}$  of SARS-CoV-2 S protein diluted in LDB1. Abs: mAb conjugated to red latex beads and dispensed onto the conjugate pad. The intensity was determined using the intensity scale shown in Figure 2.2. The experiment was performed once.

Out of the 70 combinations tested (Figure 6.13 and Figure 6.14), 17 tests had an intensity over 8 when tested with 1  $\mu\text{g}/\text{mL}$  of SARS-CoV-2 S protein. Out of these 17 combinations, the best capture and detection mAbs could be identified, with the best capture mAbs being (from best to worst): 8, 7, 9 and 3, 5 and 6; and the best detection mAbs (from best to worst): 1 and 6, 7 and 4, 10.

With these 17 test combinations, the SARS-CoV-2 S protein was titrated from 1  $\mu\text{g}/\text{mL}$  to 0.01  $\mu\text{g}/\text{mL}$  in LDB1 (Figure 6.15).



**Figure 6.15 Titration of SARS-CoV-2 S protein with the 17 best combinations of double antibody sandwich LFA.**

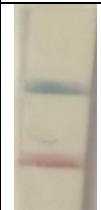
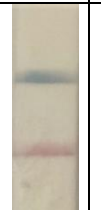
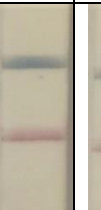


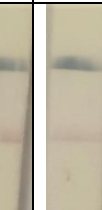
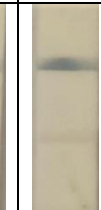

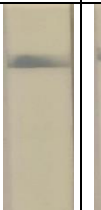

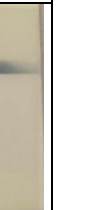
Serial dilutions of SARS-CoV-2 S protein diluted in LDB1 were tested with the best combinations of double antibody sandwich LFA previously selected. The different combinations are described in Table 6.6 and the tests are written as “membrane.conjugate”. The intensity was determined using the intensity scale shown in Figure 2.2. The experiment was performed once.

Four tests gave a positive intensity (between 4 and 6) at 0.01 µg/mL of SARS-CoV-2 S protein: test 1.6, 5.6, 8.6 and 9.6. All the other tests gave a negative signal (intensities between 1 and 2) at 0.01 µg/mL of SARS-CoV-2 S protein.

The limit of detection of the four tests was determined by titration of the SARS-CoV-2 S protein in LDB1 until no signal was observed. The limit of detection of the tests 1.6, 5.6 and 9.6 was 7.8 ng/mL. The limit of detection of test 8.6 was 3.9 ng/mL, which corresponds to 0.47 ng of SARS-CoV-2 S protein per test (Table 6.7).



**Table 6.7 Titration of SARS-CoV-2 S protein with test 8.6.**

Concentration of SARS-CoV-2 S (ng/mL)	1,000	500	250	125	62.5	31.3	15.6	7.8	3.9	1.95	0.98	0.49
Intensity	10	10	9	9	8.5	8	7	7	4.5	3	2	1
Picture												

*Serial dilutions of SARS-CoV-2 S protein diluted in LDB1 were tested with test 8.6 to determine its limit of detection. The intensity was determined using the intensity scale shown in Figure 2.2. The experiment was performed once.*

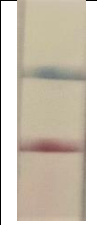
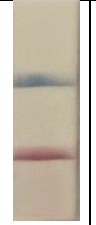
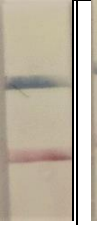

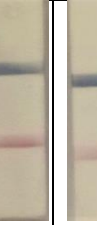


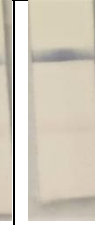




Out of the 100 different mAbs combination, the best combination of mAbs to detect the SARS-CoV-2 S protein in LFA was with mAb 8 (COVA2-29) in the membrane and mAb 6 (COVA2-03) in the conjugate. This test cannot detect the SARS-CoV-2 RBD as only one of the mAbs in the pair detects it, the other detects a different region of the S protein. The test 8.6 was selected as the optimal assay for further studies.

### **6.5.2. Validation of the double antibody sandwich LFA with spiked samples**

To further validate the double antibody sandwich LFA assay (test 8.6), saliva and viral transport medium (VTM, obtained online from <https://www.cdc.gov/coronavirus/2019-ncov/downloads/Viral-Transport-Medium.pdf>) were spiked with the recombinant SARS-CoV-2 S protein. Serial dilutions of the SARS-CoV-2 S protein were done in these two specimens and tested in the double antibody sandwich LFA. Two dilution methods were used: one where 20  $\mu$ L of spiked sample was added to the strip, followed by 100  $\mu$ L of LDB1 and one where 60  $\mu$ L of spiked sample were mixed with 60  $\mu$ L of LDB1 before being added to the strip.

The results of the spiking assay in VTM with the “20  $\mu$ L of sample followed by 100  $\mu$ L of buffer” are shown in Table 6.8.

**Table 6.8 Spiking assay of SARS-CoV-2 S protein in viral transport medium with test 8.6.**

Concentration of SARS-CoV-2 S (ng/mL)	1,000	500	250	125	62.5	31.3	15.6	7.8	3.9	1.95	0.98	0.49
Intensity	10	10	9	9	8.5	8	8	7	6	3	2	1
Picture												

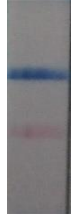



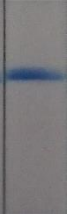

Serial dilutions of SARS-CoV-2 S protein diluted in viral transport medium were tested with test 8.6 to determine its limit of detection. The intensity was determined using the intensity scale shown in Figure 2.2. The experiment was performed once.

At a same concentration, the “20  $\mu$ L plus 100  $\mu$ L” method had a higher intensity than the “60  $\mu$ L plus 60  $\mu$ L” one, thus the first method was selected for the subsequent assays.

The spiking assays done in saliva and in VTM showed similar results than when the SARS-CoV-2 S protein was diluted in LDB1. For the spiking assay in VTM, the limit of detection was the same than for the LDB1 (3.9 ng/mL, which corresponds to 0.47 ng of SARS-CoV-2 S protein per test) although for the spiking assay in saliva, the limit of detection was lower (6 ng/mL, corresponding to 0.72 ng of SARS-CoV-2 S protein per test).

After this first validation of the double antibody sandwich LFA, a second validation was performed with inactivated SARS-CoV-2. Inactivated SARS-CoV-2 (at 56°C for 60 min) was kindly provided by Dr Luis Enjuanes (Centro National de Biotecnología, Spain) with a titre of  $3 \times 10^6$  PFU/mL before inactivation. Serial dilutions of the inactivated virus were performed in LDB1 and tested in the double antibody sandwich LFA following the “20  $\mu$ L plus 100  $\mu$ L” method (Table 6.9).

**Table 6.9 Spiking assay of SARS-CoV-2 virus with double antibody sandwich LFA test 8.6.**

PFU of SARS-CoV-2 per test	7,500	3,750	1,875	938	469	234
Intensity	7	5	4	3	2	1
Picture						

Serial dilutions of SARS-CoV-2 diluted in LDB1 were tested with test 8.6 following the “20  $\mu$ L plus 100  $\mu$ L” method to determine its limit of detection. The intensity was determined using the intensity scale shown in Figure 2.2. All the samples were tested once due to sample volume constraints.

The double antibody sandwich LFA test 8.6 could detect a 1:32 dilution of the inactivated virus, corresponding to 1,875 PFU per test.

### 6.5.3. Validation of the double antibody sandwich LFA with human samples

Oropharyngeal and nasopharyngeal samples, from patients tested positive by real-time RT-PCR, were tested in the double antibody sandwich LFA test 8.6, to determine if this assay could detect the virus in actual samples (Table 6.10). Some negative samples were also included in the analysis.

**Table 6.10 Double antibody sandwich LFA test 8.6 tested with positive and negative oropharyngeal and nasopharyngeal samples.**

Specimen	Oropharyngeal samples						Nasopharyngeal samples				
Ct obtained in real-time RT-PCR	24.5	26	28.5	29.5	/	/	28	/	/	/	/
Intensity	1	1	1	1	1	1	7	1	1	2	2

Blank cells without a cycle threshold (Ct) correspond to the negative samples. The intensity was determined using the intensity scale shown in Figure 2.2. All the samples were tested once due to sample volume constraints.

The double antibody sandwich LFA test 8.6 was not able to detect the SARS-CoV-2 S protein in positive oropharyngeal samples with cycle threshold (Ct) between 24.5 and 29.5 as the test gave intensities of 1 for these samples. The only positive nasopharyngeal sample tested in the double antibody sandwich LFA test 8.6 with a Ct of 28 gave a positive signal with an intensity of 7. The negative nasopharyngeal samples tested gave a negative signal (intensities between 1 and 2).

## **6.6. Development of a SARS-CoV-2 triplex assay to study the immune response to three SARS-CoV-2 proteins**

To assess the immune response to different SARS-CoV-2 antigens, a triplex assay with the SARS-CoV-2 N protein, S protein and RBD was developed. This triplex assay was used to detect the presence of IgG or IgM against these proteins in positive human sera. After optimization of the triplex assay, a collection of positive samples was assayed.

### **6.6.1. Serum samples**

To develop this assay, the panel of serum samples consisted of 104 SARS-CoV-2 positive sera and 55 negative sera. The samples were classified as positive or negative based on a commercial ELISA: INgezim COVID 19 double recognition (Eurofins-Ingenasa) for detection of specific total antibodies against SARS-CoV-2 N protein.

### **6.6.2. Optimal serum dilution**

The three SARS-CoV-2 target proteins were used to coat different microsphere regions. Then, specific mAbs for the SARS-CoV-2 N protein and SARS-CoV-2 RBD were used to confirm the coupling of each individual antigen to its bead region and then to optimize the coupling concentration of each antigen. The optimal protein coupling concentration was established as the highest MFI obtained with the minimum amount of protein. The following quantities were used to coat  $1 \times 10^6$  beads for each bead region: 50  $\mu\text{g}$  of SARS-CoV-2 N protein (region #12), 25  $\mu\text{g}$  of SARS-CoV-2 S protein (region #20) and 25  $\mu\text{g}$  of SARS-CoV-2 RBD (region #25).

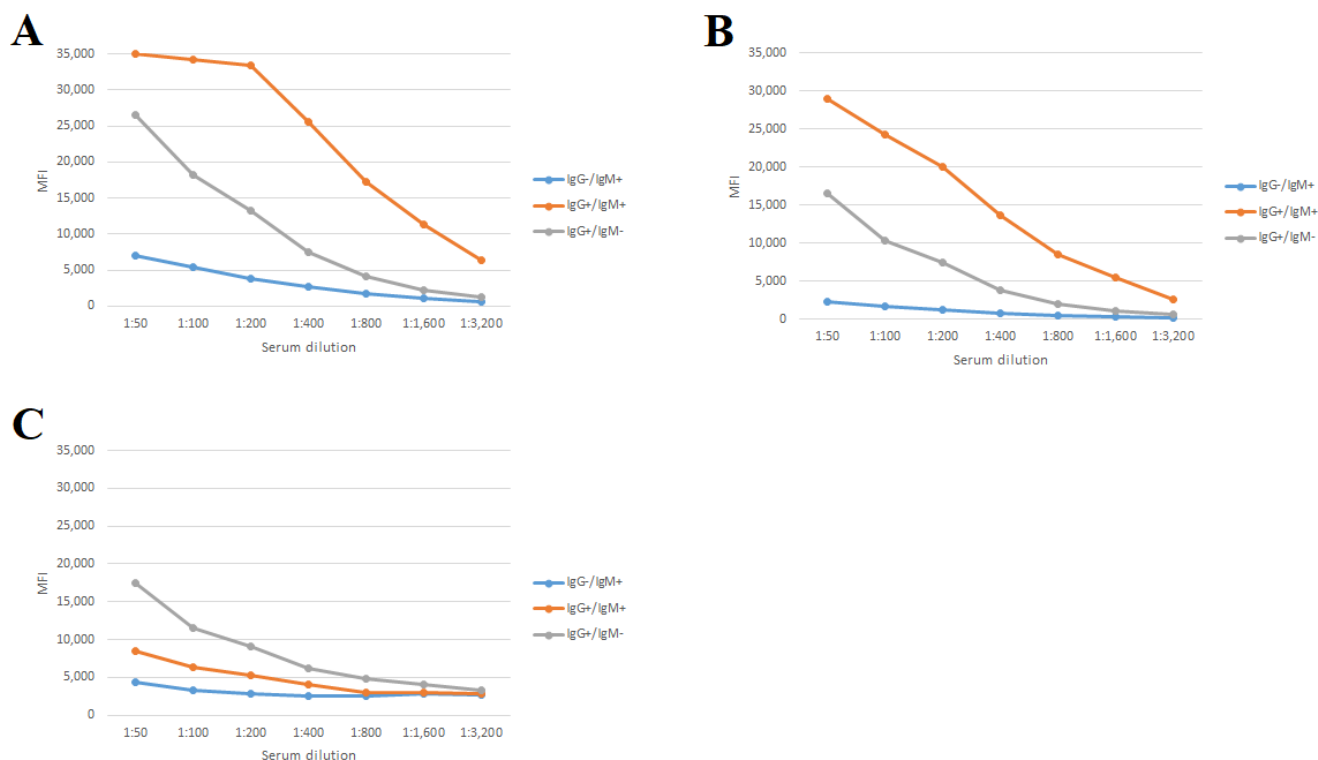
Some serum samples were determined to be positive or negative to IgG and IgM with the indirect ELISA developed in section 6.4. Out of these samples, three sera were selected: one negative to IgG but positive to IgM (IgG-/IgM+), one positive to both IgG and IgM (IgG+/IgM+) and one positive to IgG but negative to IgM (IgG+/IgM-). These three sera were used to establish the optimal assay conditions for the screening. A mix of the 3 bead regions coupled to the SARS-CoV-2 target proteins was incubated with serial dilutions of these sera, and the assay was performed as described in Materials and Methods with either the anti-human IgG or the anti-human IgM.

For the bead #12 SARS-CoV-2 N protein to detect IgG (Figure 6.16A), the two positive IgG sera (IgG+/IgM+ and IgG+/IgM-) showed some high MFI at 1:50 dilution (MFI over 25,000), when the negative IgG serum (IgG-/IgM+) exhibited some background signal (MFI around 7,000). The MFIs decreased for the three sera when the serum dilution increased, although the signal of the serum IgG+/IgM+ was saturated (MFI around 35,000) until the 1:200 dilution. For the bead #20 SARS-CoV-2 S protein to detect IgG (Figure 6.16B), the highest MFI was observed for the three sera at 1:50 dilution: MFI around 29,000, 16,000 and 2,000 for the sera IgG+/IgM+, IgG+/IgM- and IgG-/IgM+, respectively. The MFIs decreased for the three sera when the serum dilution increased. For the bead #25 SARS-CoV-2 RBD to detect IgG (Figure 6.16C), the MFIs for all the sera were lower compared to the other beads, with MFIs around 17,500, 8,500 and 4,500 for the sera IgG+/IgM-, IgG+/IgM+ and IgG-/IgM+, respectively. The MFIs decreased for the three sera when the serum dilution increased, however, for the RBD, the positive to negative ratio was lower than for the two other beads.

Regarding the anti-IgM triplex assay (Figure 6.17), similar results were obtained, with the two positive IgM sera (IgG+/IgM+ and IgG-/IgM+) giving higher MFI than the negative IgM serum (IgG+/IgM-). Overall, the MFIs obtained with the positive sera for the bead #12 SARS-CoV-2 N protein (Figure 6.17A) were higher than for bead #20 SARS-CoV-2 S protein (Figure 6.17B) and bead #25 SARS-CoV-2 RBD (Figure 6.17C). For the three beads, the MFIs decreased for the three sera when the serum dilution increased and the MFIs obtained for these three beads with the negative serum were similar.

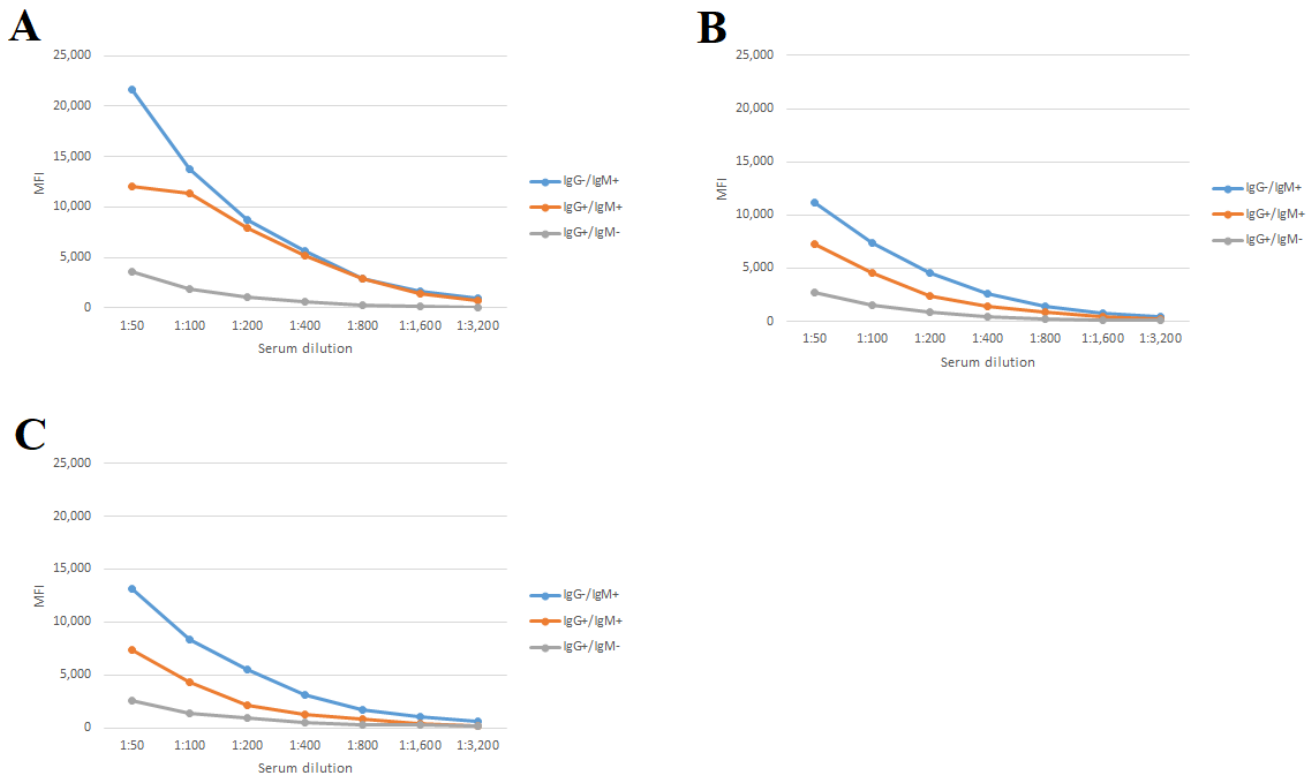
The positive/negative ratios for the three beads coated with the recombinant viral proteins and for the detection of IgG and IgM were determined. A dilution of the serum at 1:100

was selected for screening purposes, since this was the dilution showing the overall highest positive/negative ratios for all the beads and for both IgG and IgM. To simplify the assay, a unique serum dilution was selected for both detection of IgG and IgM.



**Figure 6.16 Determination of the screening conditions for the SARS-CoV-2 triplex assay detecting IgG.**

The MFI for each bead region is given for different serum dilutions (one serum sample negative to IgG and positive to IgM (IgG-/IgM+), one serum sample positive to IgG and to IgM (IgG+/IgM+) and one serum sample positive to IgG and negative to IgM (IgG+/IgM-). A: samples with bead #12 SARS-CoV-2 N protein. B: samples with bead #20 SARS-CoV-2 S protein. C: samples with bead #25 SARS-CoV-2 RBD. The signal was measured as MFI of at least 50 events of each bead region. MFI: median fluorescence intensity.



**Figure 6.17** Determination of the screening conditions for the SARS-CoV-2 triplex assay detecting IgM.

The MFI for each bead region is given for different serum dilutions (one serum sample negative to IgG and positive to IgM (IgG-/IgM+), one serum sample positive to IgG and to IgM (IgG+/IgM+) and one serum sample positive to IgG and negative to IgM (IgG+/IgM-). A: samples with bead #12 SARS-CoV-2 N protein. B: samples with bead #20 SARS-CoV-2 S protein. C: samples with bead #25 SARS-CoV-2 RBD. The signal was measured as MFI of at least 50 events of each bead region. MFI: median fluorescence intensity.

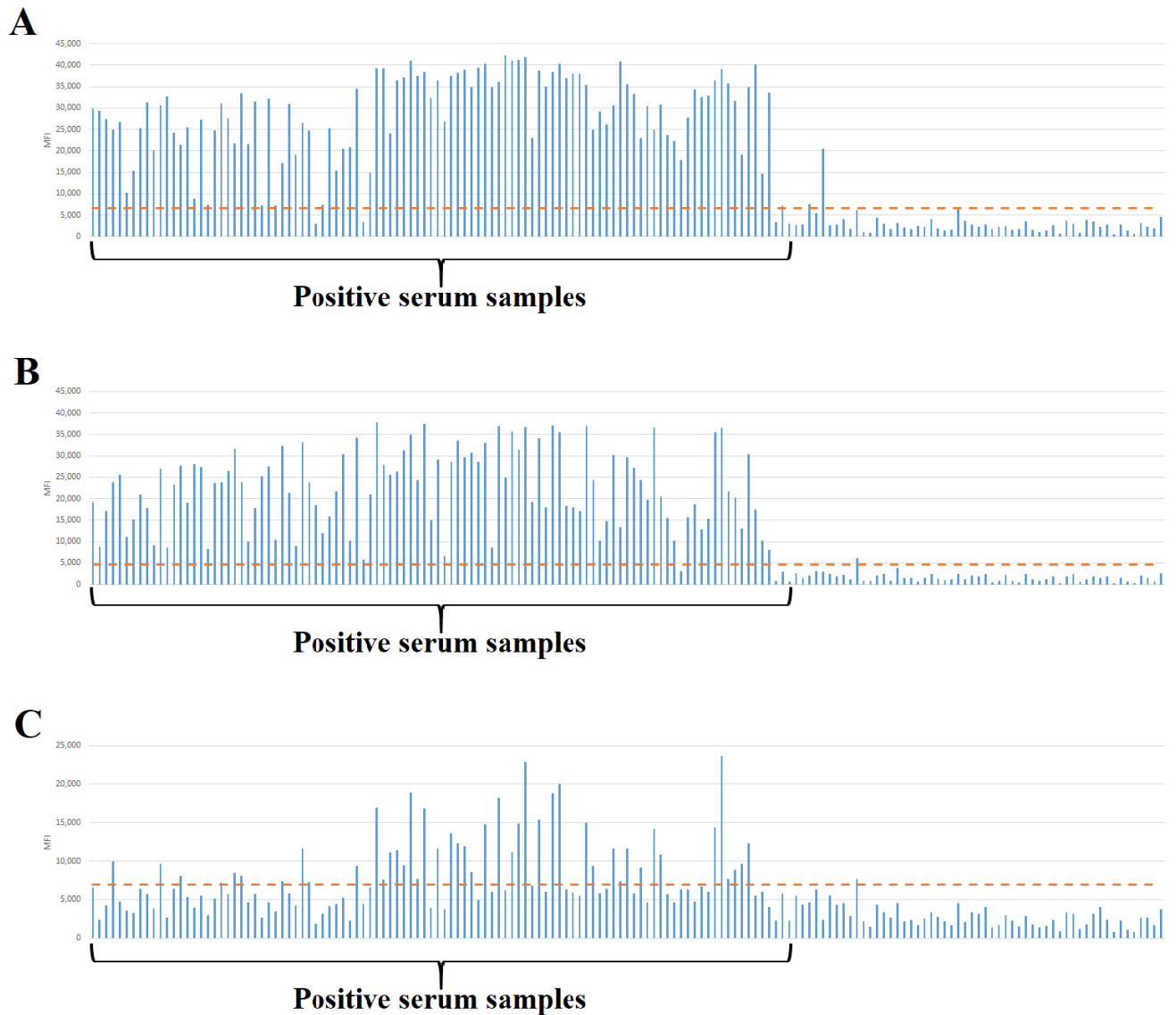
### 6.6.3. SARS-CoV-2 triplex assay

Once the conditions of the triplex assay were established, a panel of positive and negative sera to COVID-19 was tested in the triplex assay. This panel included 104 positive serum samples and 55 negative serum samples, as confirmed by the double recognition ELISA detecting total antibodies to SARS-CoV-2 N protein used as a reference (INgezim COVID double recognition-ELISA). These samples were then tested in the triplex assay to check for the presence of IgG and IgM against these three SARS-CoV-2 proteins (Figure 6.18 and Figure 6.19, respectively). For each bead region, the cut-off value was established as the mean obtained for the 55 negative serum samples plus three standard deviations.

Thus, for the detection of IgG, cut-off values of 6,634 MFI, 4,550 MFI and 6,918 MFI were obtained for bead #12 SARS-CoV-2 N protein, bead #20 SARS-CoV-2 S protein and bead #25 SARS-CoV-2 RBD, respectively. With these cut-off values, out of the 104 positive sera containing total antibodies to SARS-CoV-2 N protein, 100 were considered positive for SARS-CoV-2 N protein and SARS-CoV-2 S protein (96.2%) and 45 to SARS-CoV-2 RBD (43.3%) (see Figure 6.18A, B and C, respectively). Out of the 55 negative serum samples, two gave signals above the cut-off value for the SARS-CoV-2 N protein, one sample gave false positive signal against SARS-CoV-2 S protein and another one to SARS-CoV-2 RBD. The negative sample that gave a false positive result with the S protein, also gave a false positive result for the N protein.

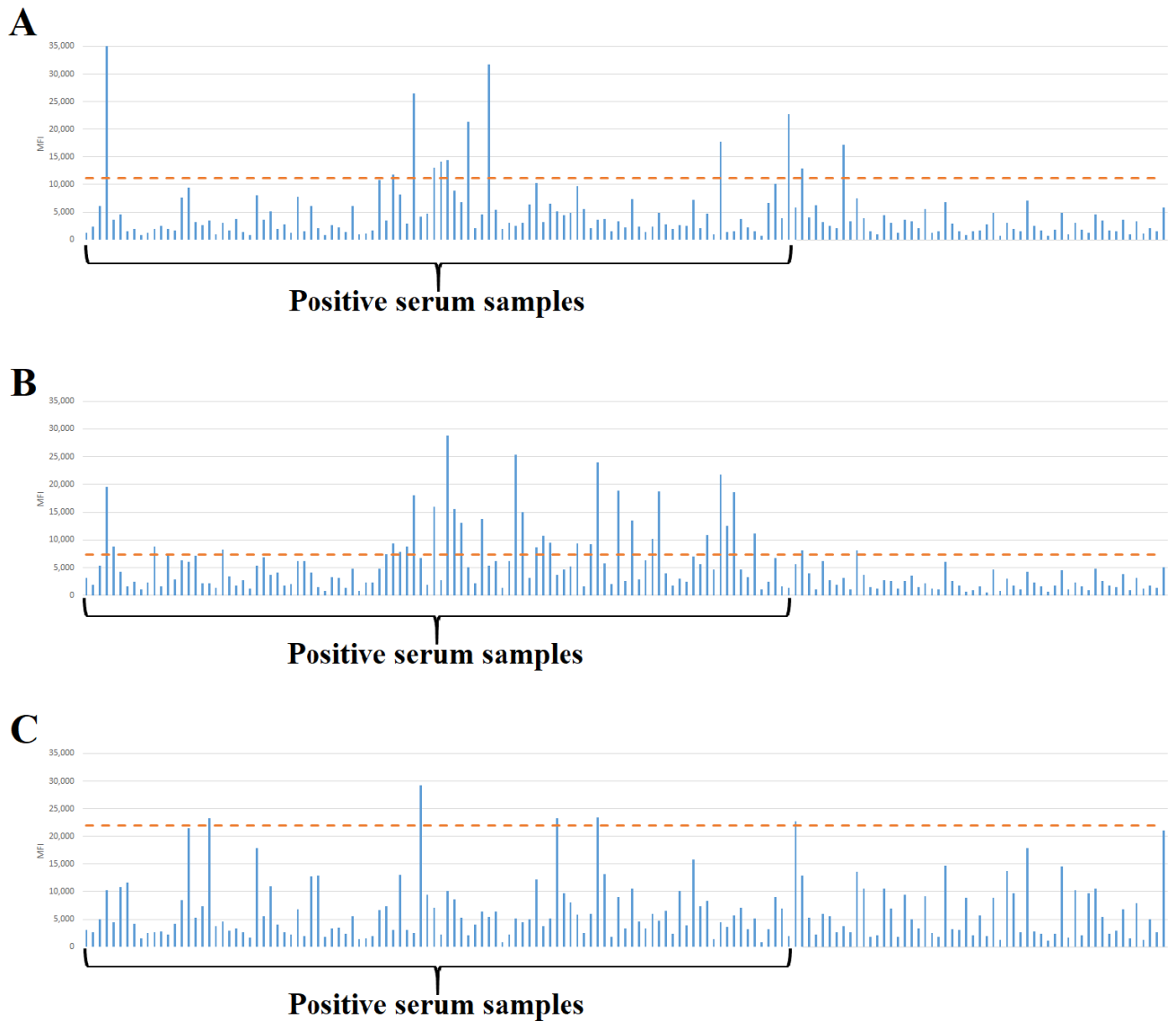
For the detection of IgM, cut-off values of 11,167 MFI, 7,403 MFI and 21,904 MFI were obtained for bead #12 SARS-CoV-2 N protein, bead #20 SARS-CoV-2 S protein and bead #25 SARS-CoV-2 RBD, respectively. Thus, out of the 104 positive sera, 10 were considered positive for SARS-CoV-2 N protein (9.6%), 31 for SARS-CoV-2 S protein (29.8%) and 4 to SARS-CoV-2 RBD (3.8%) (see Figure 6.19A, B and C, respectively). Out of the 55 negative serum samples, two gave signals above the cut-off value for the SARS-CoV-2 N protein, two gave a false positive signal against SARS-CoV-2 S protein and another one to SARS-CoV-2 RBD. One of the negative samples giving a false positive result with bead #20 SARS-CoV-2 S, also gave a false positive result with bead #12 SARS-CoV-2 N protein.





**Figure 6.18** Detection of IgG against SARS-CoV-2 N protein (A), SARS-CoV-2 S protein (B) and SARS-CoV-2 RBD (C) in a triplex assay.

The dashed line corresponds to the cut-off values for each bead region and calculated as the mean obtained for the negative field samples plus three standard deviations. The signal was measured as MFI of at least 50 events of each bead region. MFI: median fluorescence intensity.



**Figure 6.19** Detection of IgM against SARS-CoV-2 N protein (A), SARS-CoV-2 S protein (B) and SARS-CoV-2 RBD (C) in a triplex assay.

The dashed line corresponds to the cut-off values for each bead region and calculated as the mean obtained for the negative field samples plus three standard deviations. The signal was measured as MFI of at least 50 events of each bead region. MFI: median fluorescence intensity.

The results obtained in both triplex assays anti-IgG and anti-IgM were combined to compare the results obtained with the reference assay detecting total antibodies (Table 6.11, Table 6.12 and Table 6.13).

**Table 6.11 Comparison of the results obtained for the bead region #12 SARS-CoV-2 N protein and the reference assay (INgezim COVID 19 double recognition ELISA).**

		INgezim COVID 19 double recognition ELISA		
		Positive	Negative	Total
Bead #12 SARS-CoV-2 N protein	Positive	101	4	105
	Negative	3	51	54
	Total	104	55	159

**Table 6.12 Comparison of the results obtained for the bead region #20 SARS-CoV-2 S protein and the reference assay (INgezim COVID 19 double recognition ELISA).**

		INgezim COVID 19 double recognition ELISA		
		Positive	Negative	Total
Bead #20 SARS-CoV-2 S protein	Positive	100	2	102
	Negative	4	53	57
	Total	104	55	159

**Table 6.13 Comparison of the results obtained for the bead region #25 SARS-CoV-2 RBD and the reference assay (INgezim COVID 19 double recognition ELISA).**

		INgezim COVID 19 double recognition ELISA		
		Positive	Negative	Total
Bead #25 SARS-CoV-2 RBD	Positive	47	2	49
	Negative	57	53	110
	Total	104	55	159

The results obtained with the beads #12 SARS-CoV-2 N protein and #20 SARS-CoV-2 S protein are similar to the reference assay, with most of the positive and negative sera in the INgezim COVID 19 double recognition ELISA being also positive and negative with these beads. However, bead #25 SARS-CoV-2 RBD showed several false negative results. In order to examine the agreement between the results obtained in the reference ELISA and the different beads of the multiplex assay, Cohen's kappa coefficient was calculated using the Medcalc® software. For bead #12 SARS-CoV-2 N protein,  $\kappa = 0.902$  with a 95% confidence interval [0.832; 0.973]. For bead #20 SARS-CoV-2 S protein,  $\kappa = 0.917$  with a 95% confidence interval [0.852; 0.982]. For bead #25 SARS-CoV-2 RBD,  $\kappa = 0.336$  with a 95% confidence interval [0.202; 0.471]. Thus, as Cohen's kappa was over 0.9 for beads #12 and #20, there is an almost perfect agreement between the results obtained with these beads and the reference assay. This agreement is only moderate between bead #25 and the reference assay.

## 6.7. Chapter summary and discussion

Following the emergence of a new virus, SARS-CoV-2, all the efforts were focused on the development of diagnostic tools to detect it. For this purpose, different serological assays were developed: a double recognition ELISA and a double recognition LFA detecting total antibodies to SARS-CoV-2 N protein, an indirect ELISA detecting IgG or IgM to SARS-CoV-2 N protein, a double antibody sandwich LFA detecting the SARS-CoV-2 S protein and a triplex assay detecting antibodies against the three SARS-CoV-2 target proteins (N protein, S protein and RBD).

Among all the structural proteins of SARS-CoV-2, the N protein seemed to be a good target candidate for diagnosis, as this protein was shown to be abundantly produced in infected cells, to be highly immunogenic and easily expressed in bacteria (369–371). Moreover, the N protein of SARS-CoV-1 was successfully used to develop serological assays detecting anti-SARS-CoV-1 antibodies. Additionally, mAbs produced in mice immunized with the N protein of SARS-CoV-1 were used to develop a double antibody sandwich ELISA detecting the N protein in acute serum samples (370,372). All these reasons made the N protein of SARS-CoV-2 a good antigenic target to develop new diagnostic tools against SARS-CoV-2. At the time of the cloning and production of the SARS-CoV-2 N protein (early February 2020), no article describing the recombinant

expression of the SARS-CoV-2 N protein in bacteria was published. Since then, many articles have been published, describing its production, its crystal structure has been resolved and it has been characterized (134,373). The SARS-CoV-2 N protein produced in this chapter has been cloned using the Gateway system. The Gateway system is a powerful tool that, once the gene of interest is cloned in an entry vector, allows the transfer of the gene into different expression vectors. As the N protein of SARS-CoV-2 was a new target protein to be produced, its expression in different expression systems was evaluated (in bacteria and insect cells using the BES). Out of the different systems evaluated, the N protein was better expressed as a soluble protein in bacteria. The N protein was purified by affinity chromatography using a Ni<sup>2+</sup>-NTA column. The N protein obtained was of high purity and was used to develop serological assays and to immunize mice in order to produce mAbs anti-SARS-CoV-2 N protein.

The N protein is well conserved among coronaviruses (see Table 6.14), with high amino acid sequence identity between the different N proteins of coronavirus. Thus, when developing serological assays with this protein, the cross-reactivity with other coronaviruses should be assessed.

**Table 6.14** Sequence identity between the SARS-CoV-2 N protein and the N protein of other human coronaviruses.

	<b>Coronavirus</b>	<b>Identity (%)</b>
<b><i>Alphacoronavirus</i></b>	HCoV-NL63	48.3
	HCoV-229E	28.8
<b><i>Betacoronavirus</i></b>	HCoV-HKU1	36.7
	HCoV-OC43	37.7
	SARS-CoV-1	90.5

For the diagnosis of COVID-19, the routinely used technique is the real-time RT-PCR, which detects the RNA of the virus at early stages of the infection. However, fully validated serological tests were still missing as many of the commercial serological tests available for SARS-CoV-2 early in the pandemic were poorly validated or displayed low sensitivity or specificity (374). In order to determine the prevalence of antibodies in the population and to complement the nucleic acid detection assays, especially at later days after the onset of the symptoms, serological assays are required (375). Detection of

antibodies is the most valuable indicator of the immune status of a person, identifying patients that have had COVID-19 infections, and providing more accurate data related to risk of infection.

Using the recombinant N protein of SARS-CoV-2 as the target antigen, two serological assays were developed in a double recognition format: a double recognition ELISA which is aimed to be used for screening large numbers of samples and could be used in epidemiological studies and a double recognition LFA for POC testing of individual patients, which could be used by physicians without any laboratory setting required. The double recognition method has already been used as a screening tool for detection of antibodies to other infectious diseases, including the ones affecting the swine population (273,376,377).

In order to determine the performance characteristics of the newly developed tests, a panel of standardized samples was included in the study. Positive samples from COVID-19 patients with a range of clinical presentations at multiple time points after onset of symptoms were analysed to determine the sensitivity. Pre-COVID-19 outbreak samples and samples with antibodies to other respiratory pathogens were used to determine the specificity. The diagnostic sensitivity of the assays was 100% and 91.2%, for the double recognition ELISA and double recognition LFA, respectively. The sensitivity of the double recognition LFA was lower than that of the double recognition ELISA, as it has been described in other cases (378). The requirements of each assay are different, as the double recognition LFA can be applied as a point of care test, whereas the double recognition ELISA needs to be done in a laboratory by qualified technicians and is aimed for screening purposes. Moreover, while the double recognition LFA takes 10 minutes to give one result, the double recognition ELISA takes 75 minutes to analyse 92 samples. Out of the PCR+/Antibody- group from Table 2.9, a group of 14 serum samples from early days post infection, positive to COVID-19 by respiratory PCR yet still negative in the commercial serological assay (with seroconversion a few days later) were also tested in our assays. Four of these sera were positive in the double recognition ELISA and three in the double recognition LFA, indicating that the double recognition assays developed are highly sensitive.

Regarding the specificity of the newly developed assays, only one sample positive to *Mycoplasma pneumonia* was found to give a positive signal in the double recognition

ELISA. Interestingly, no cross-reactivity by antibodies directed to seasonal *Alpha*- or *Betacoronavirus* was observed in our double recognition assays, in contrast with regular SARS-CoV-2 antibody tests that do sometimes detect antibodies induced by HCoV-OC43 infection (379).

We tested samples from 452 individuals that were negative for the virus in respiratory material (real-time RT-PCR) and also negative in serological assays, yet they were collected in a high-risk group (personal communications). Eleven serum samples showed a positive signal in the double recognition ELISA. Five had a very high S/P (>30) and the others were found with lower S/P (between 6 and 10). Three of the positives with high S/P were also tested, for confirmation purposes, in the double recognition LFA and in this test the samples showed positive signals. These results could indicate that our tests can give false positives, or that the patients had experienced a previous infection, yet this was not diagnosed by the commercial assays, maybe not fully validated so far. It could also be that the serum samples contained only IgA recognizing SARS-CoV-2, since commercial assays used for classification only detect IgM and IgG (380).

The serological assays could be a great complementary tool to the nucleic acid detection assays, as in this study, out of 626 samples with a negative PCR in respiratory material, 174 serum samples could diagnose a SARS-CoV-2 infection via serology (see Table 2.9). In these 174 patients, 123 were positive only to IgG, 23 were positive only to IgM and 28 were positive to IgG and IgM. An 89% correspondence was found between the double recognition ELISA and the commercial serological assay for the 151 samples positive to IgG or positive to IgG and IgM, but only one of the IgM positive was found positive in the double recognition ELISA. This could demonstrate the higher affinity of IgG compared to IgM (381) which could lead to lower specificity of serological assays specifically targeting IgM. However, due to sample constraints, the positive and negative samples used to develop the double recognition ELISA and LFA were only tested once. Although the samples were only used once, a significant number of samples were used to support the results obtained.

Double recognition assays are sensitive tests, yet they also offer two additional advantages. First, it is a multi-species test, detecting antibodies in human serum, but also in serum samples from other animal species, since it uses the target antigen as the detector molecule, instead of anti-species antibody, and secondly, it detects total antibodies in a

given sample. Unlike the antibody response usually observed in other infectious diseases (first IgM followed by IgG), during COVID-19 infection, IgM and IgG antibody responses appear almost simultaneously (356,382). Moreover, the CDC reports that there are no major advantages between serological assays that detect IgG specific to SARS-CoV-2, IgG and IgM specific to SARS-CoV-2, or total antibody (383). Similar results were described previously for SARS, where the IgM appeared at the same time as the IgA and IgG (375). This shows the importance of having a test that detects total antibodies in serum.

The two double recognition assays developed in this chapter have been fully validated, received the CE marking and are now commercially available: INgezim COVID 19 double recognition and INgezim COVID 19 CROM (Eurofins-Ingenasa). These assays were recently published in a peer-review journal (384).

Using the same target antigen, the N protein, as in the double recognition ELISA, two independent indirect ELISAs, one for detection of IgG and one for detection of IgM, have been developed. These assays are useful tools to have a better understanding of the immune response to SARS-CoV-2 in epidemiological studies. To determine the performance characteristics of these newly developed assays, a commercial anti-IgG ELISA and an anti-IgM ELISA, were used for comparison. This resulted in a diagnostic sensitivity of 97.7% and 78.2% and a diagnostic specificity of 96.7% and 97.5%; for the anti-IgG and anti-IgM ELISA respectively. The indirect anti-IgG ELISA developed, compared well with the commercial anti-IgG ELISA and out of the three false positive results obtained, two of them came from patients that seroconverted and had detectable IgG in the reference assay at the next time-point. Thus, these results could highlight an increased sensitivity of the anti-IgG assay developed that could detect lower amounts of IgG than the reference assay. Regarding the indirect anti-IgM ELISA developed, several serum samples gave a false negative result, which lead to a low diagnostic sensitivity of the assay developed. These results could be explained by a low sensitivity of the anti-IgM assay or that the commercial ELISA anti-IgM gave some false positive results. Indeed, ELISAs targeting IgMs can sometime show high number of false positive results, possibly due to rheumatoid factor, auto-antibodies that recognize epitopes on Fc regions of IgG, or cross-reacting antibodies (385,386). In the case of the two indirect ELISAs



developed, when compared to the double recognition ELISA, the combination of the indirect ELISAs showed a high rate of true positives (97.1%) and true negatives (96.7%). These results confirm the good performance characteristics of the two newly indirect ELISAs developed. The anti-IgM developed likely has a higher diagnostic sensitivity than calculated with the commercial anti-IgM ELISA, otherwise the combination of the two assays developed would not compare well with the double recognition ELISA.

Additionally, the anti-IgG ELISA was used to follow up the presence of antibodies in the sera of two patients infected with SARS-CoV-2. The sera were collected at different time-points, allowing a qualitative follow-up of the antibodies present in the sera of both patients. Using the indirect ELISA, a trend could be observed for both patients, with an overall decrease of the signal obtained due to a probable decrease of the quantity of antibodies in the sera of the patients. For both patients, five months after the highest signal obtained, the signal was only equivalent to half this signal. Although this test is not quantitative and detects non-neutralizing and neutralizing IgG, a clear IgG decreasing trend was observable over time for two patients, one showing very limited symptoms and one with clear symptoms of COVID-19.

As an additional tool for the diagnosis of acute COVID-19, a double antibody sandwich LFA was developed using mAbs anti-SARS-CoV-2 S protein. This double antibody sandwich LFA is a POC test that could help to control the spread of SARS-CoV-2 by providing a rapid and simple test for the population. Ten different mAbs targeting SARS-CoV-2 were screened to be used as the capture and detector molecules and the best combination of mAbs was selected: a mAb that recognizes the RBD as the detector molecule and the other one that detects a different region of the S protein as the capture molecule. These two mAbs were able to detect up to 3.9 ng/mL of SARS-CoV-2 in running buffer and in VTM (corresponding to 0.47 ng per test) corresponding to a limit of detection of 1,875 pfu per test. However, when testing positive samples from nasopharyngeal and oropharyngeal specimens with Ct between 24.5 and 29.5, only one, with a Ct of 28, was positive in the double antibody sandwich LFA. The analytical sensitivity of this double antibody sandwich LFA showed to be lower than that of some POC tests that are now found in the market. The samples tested in the double antibody sandwich LFA were also tested in some commercial LFAs such as PANBIO™ COVID-

19 Ag RAPID TEST DEVICE (Abbott) and SARS-CoV-2 Rapid Antigen Test (Roche). Abbott's and Roche's tests could detect up to 29 and 117 pfu per test, respectively. Moreover, Abbott's test gave positive results with all the positive nasopharyngeal and oropharyngeal specimens tested in the double antibody sandwich LFA. These results highlight the lack of sensitivity of the double antibody sandwich LFA developed for the acute detection of SARS-CoV-2 antigens compared to assays already available in the market. Moreover, with the discovery of new SARS-CoV-2 variants with some of them presenting mutations on the S protein (387), spiking assays should be performed with these variants to analyse the sensitivity of the double antibody sandwich LFA against these new variants.

Finally, to have a better understanding of the immune response to different SARS-CoV-2 antigens, a triplex assay was developed with three SARS-CoV-2 target antigens: the SARS-CoV-2 N protein, SARS-CoV-2 S protein and SARS-CoV-2 RBD. This triplex assay was able to detect antibodies (IgG and IgM) to the three target proteins in positive human sera. After establishing the cut-off values for each bead, out of the 104 positive samples tested in the triplex assay, almost all of them were IgG positive for the N and S proteins (100/104) and a significant lower number of samples were tested positive to IgM (10 and 31, to the N and S proteins, respectively). Moreover, only one sample testing IgM positive to the N protein was not IgG positive. These two beads showed an almost perfect agreement with the reference double recognition ELISA when calculating Cohen's kappa (over 0.9 for both bead regions). The results obtained with the bead region coupled to the SARS-CoV-2 RBD were significantly worse than with the other two target proteins. Indeed, the RBD only detected 45% of the positive sera (most of them IgG positive) and only had a moderate agreement with the reference ELISA. The reference double recognition ELISA, targeting the N protein, does not give any information about the presence of anti-S or anti-RBD antibodies, which could explain the low agreement of the bead region RBD and the reference ELISA. On the other hand, the agreement with the bead region S protein and the reference ELISA is almost perfect and most of the sera presenting some anti-N protein antibodies also had some anti-S protein antibodies according to the triplex assay. Recently, a multiplex assay with different SARS-CoV-2 target antigens has been published by Mariën *et al.* (388). This study showed high specificities and sensitivities to detect IgG for beads coupled to the N protein and the

RBD, which is the case of the N protein in the triplex assay but was not observed for the RBD. In mild cases, over 5 months after infection and at a 99% specificity, their N protein bead had a sensitivity of 85%, the S protein bead one of 95% and the RBD one of 96%. In their cases, the S protein or RBD had a significantly higher sensitivity than the N protein, which is different than the results observed in the triplex assay of this chapter. However, they also observed low sensitivities for their anti-IgM assay, confirming the results obtained in this chapter. Overall, the cut-off values established for the anti-IgM triplex were higher than for the anti-IgG triplex assay, which exhibits the higher background and more sporadic values of MFI obtained for the negative samples in the anti-IgM assay. It should also be noted that the diagnosis results obtained with the combinations of the anti-IgG and anti-IgM assays were not better than the anti-IgG triplex alone. Finally, as shown recently with a magnetic chemiluminescence enzyme immunoassay published by Li *et al.* (389), multiplex assays can help unravel and understand the immune response to this new virus.

The results of this chapter address the final aim of this project to respond to the challenges and the gaps in the diagnosis of COVID-19, by producing the SARS-CoV-2 N protein which allowed the development of diagnostic tests, as soon as SARS-CoV-2 was discovered

## Chapter 7 Concluding remarks

Due to environmental and socio-economic factors, infectious diseases have changed in their distribution and are now threatening regions previously unaffected, and at the same time spread of diseases has never been as fast with globalization. Emerging viruses have recently provoked outbreaks and had disastrous consequences on the health of both humans and animals and on the world's economy, as shown by the emergence of SARS-CoV-2 in 2019.

The aim of this thesis was to develop diagnostic tests for newly emerging viruses, as part of the work package “advanced diagnostics” within the frame of the European project HONOURS, a MSCA-ITN. Several gaps were identified in the diagnosis of two emerging viruses, CCHFV and RVFV, thus new tools were developed to help filling up these gaps. Moreover, the other main objective of this thesis was preparedness to the appearance of a new unknown virus, as it was the case upon the discovery of SARS-CoV-2 at the end of 2019. This unexpected situation led to an urgent need for development of diagnostic assays to detect antibodies against this new virus as well as direct methods for viral detection.

As the result of this research, the following conclusions were drawn:

**Regarding CCHF diagnosis**, different serological assays detecting antibodies against CCHFV were developed to fulfil some of the gaps identified. Future work should focus on the improvement of the double recognition ELISA by characterization of this assay with human sera, to have a unique assay able to detect antibodies to CCHFV in both humans and animals. Moreover, additional CCHFV antigenic targets such as the G<sub>C</sub> could be included in the CCHFV triplex assay. Finally, future work should mainly focus on the development of anti-CCHFV detection molecules for the detection of different CCHFV antigenic targets and their use in a double antibody sandwich ELISA and double antibody sandwich LFA. An evaluation of different antigenic targets should be done to compare the detection of CCHFV N protein and CCHFV glycoproteins. Indeed, the main gap left identified in CCHF diagnosis is the development of a sensitive commercial serological assay that can detect acute CCHFV infection in a laboratory setting and at the POC. One of the main limitations encountered during this thesis was the lack of commercial

serological assays targeting anti-CCHFV glycoproteins antibodies that could be used as a reference assay. The development of such assay and its comparison with available assays targeting anti-CCHFV N protein antibodies could help better understand the immune response to CCHFV.

**Regarding RVF diagnosis,** different serological assays detecting antibodies against RVFV and RVFV antigens were developed to fulfil some of the gaps identified. Future work should focus on the characterization of the double recognition ELISA with human sera, to provide a unique solution for the detection of IgG and IgM against RVFV in both humans and animals. Future development of the duplex RVFV assay should include the addition of other immunogenic proteins of RVFV. The main focus of future work should be the characterization of the double antibody sandwich ELISA and double antibody sandwich LFA developed, as these assays have the potential to address the main gap in RVF diagnosis. As for CCHF diagnosis, no commercial serological assay has been developed using RVFV glycoproteins, which was a drawback for the work regarding RVFV G<sub>NE</sub>.

**To fill the lack of differential diagnosis of CCHFV, RVFV and other relevant pathogens,** a multiplex assay was developed. This new assay could be used as a high throughput screening tool to assess the presence and prevalence of antibodies against 5 different highly pathogenic agents and identify regions at risk of infection. This assay will help to minimize the spread and further transmission of those pathogens within the human population. Future work should focus on the addition of antigens of other relevant pathogens such as peste des petits ruminants.

**Regarding COVID-19 diagnosis,** different serological assays detecting antibodies against SARS-CoV-2 and SARS-CoV-2 antigens were developed to fulfil some of the gaps identified after the discovery of the new virus. Future work should focus on the characterization of the double recognition ELISA and double recognition LFA with other animal species affected by COVID-19. Additional SARS-CoV-2 antigens should be included into the triplex assay, to help having a better understanding of the immune

response to SARS-CoV-2. Different pairs of mAbs should be tested to develop a more sensible double antibody sandwich LFA that could offer a complement to molecular assays. Numerous gaps in COVID-19 were fulfilled in 2020, with the rapid development of molecular and serological assays only a few months after the discovery of this new virus. However, additional serological assays that could be used as surrogates for VNT could be developed, to provide information on the neutralization of patients' antibodies without requiring the labour- and time-intensive VNT.

To conclude, the results presented in this thesis and the different diagnostic tools developed aimed to address some of the gaps in the diagnosis of CCHF, RVF and COVID-19. The tools developed for antibody or antigen detection could help preventing the spread of the corresponding viruses in unaffected countries and be used in surveillance programs and in epidemiological studies to provide a better understanding of the immune response to these viruses. The methods developed could be adapted to newly emerging viruses for the rapid development of serological diagnostic tools in case of an outbreak scenario or the discovery of a new virus, as shown for SARS-CoV-2.

## References

1. Ivanowski, D. 1892. Concerning the mosaic disease of the tobacco plant. *Phytopathological Classics No. 7*. American Phytopathological Society, St. Paul, MN. 1892;(7).
2. Beijerinck MW. Concerning a contagium vivum fluidum as cause of the spot disease of tobacco leaves. *Phytopathological Classics, No. 7*. American Phytopathological Society, St. Paul, MN. *Phytopathol Class*. 1898;(7).
3. Morens DM, Folkers GK, Fauci AS. Erratum: The challenge of emerging and re-emerging infectious diseases (*Nature* (2004) 430 (242-249)). *Nature*. 2010;463(7277):122.
4. Jones KE, Patel NG, Levy MA, Storeygard A, Balk D, Gittleman JL, et al. Global trends in emerging infectious diseases. *Nature*. 2008;451(7181):990–3.
5. Lederberg J, Shope RE, Oaks CJ. *Emerging Infections: Microbial Threats to Health in the United States*. NATIONAL ACADEMY PRESS. Washington, D.C.; 1992.
6. Taylor LH, Latham SM, Woolhouse MEJ. Risk factors for human disease emergence. *Philos Trans R Soc B Biol Sci*. 2001;356(1411):983–9.
7. Woolhouse MEJ, Gowtage-Sequeria S. Host range and emerging and reemerging pathogens. *Emerg Infect Dis*. 2005;11(12):1842–7.
8. Marchi S, Trombetta CM, Montomoli E. Emerging and Re-emerging Arboviral Diseases as a Global Health Problem. *Public Heal - Emerg Re-emerging Issues*. 2018;
9. Maltezou HC, Papa A. Crimean-Congo hemorrhagic fever: Risk for emergence of new endemic foci in Europe? *Travel Med Infect Dis*. 2010;8(3):139–43.
10. Zhu N, Zhang D, Wang W, Li X, Yang B, Song J, et al. A Novel Coronavirus from Patients with Pneumonia in China, 2019. *N Engl J Med*. 2020;382(8):727–33.
11. Neiderud CJ. How urbanization affects the epidemiology of emerging infectious diseases. *African J Disabil*. 2015;5(1):1–9.
12. Kruse H, Kirkemo AM, Handeland K. Wildlife as source of zoonotic infections. *Emerg Infect Dis*. 2004;10(12):2067–72.
13. Mangili A, Vindenes T, Gendreau M. Infectious Risks of Air Travel. *Microbiol Spectr*. 2015;3(5):1–10.
14. Pépin M, Tordo N. Foreword. *Vet Res*. 2010;41(6):7–8.
15. Patz JA, Daszak P, Tabor GM, Aguirre AA, Pearl M, Epstein J, et al. Unhealthy landscapes: Policy recommendations on land use change and infectious disease emergence. *Environ Health Perspect*. 2004;112(10):1092–8.
16. Howard CR, Fletcher NF. Emerging virus diseases: Can we ever expect the unexpected? *Emerg Microbes Infect*. 2012;1.

17. Gould E. Emerging viruses and the significance of climate change. *Clin Microbiol Infect.* 2009;15(6):503.
18. Sanders CJ, Shortall CR, England M, Harrington R, Purse B, Burgin L, et al. Long-term shifts in the seasonal abundance of adult *Culicoides* biting midges and their impact on potential arbovirus outbreaks. *J Appl Ecol.* 2019;56(7):1649–60.
19. Vial L, Stachurski F, Leblond A, Huber K, Vourc'h G, René-Martellet M, et al. Strong evidence for the presence of the tick *Hyalomma marginatum* Koch, 1844 in southern continental France. *Ticks Tick Borne Dis.* 2016;7(6):1162–7.
20. Negredo A, de la Calle-Prieto F, Palencia-Herrejón E, Mora-Rillo M, Astray-Mochales J, Sánchez-Seco MP, et al. Autochthonous Crimean–Congo Hemorrhagic Fever in Spain. *N Engl J Med.* 2017;377(2):154–61.
21. Sanjuán R, Domingo-Calap P. Mechanisms of viral mutation. *Cell Mol Life Sci.* 2016;73(23):4433–48.
22. Graham RL, Baric RS. Recombination, Reservoirs, and the Modular Spike: Mechanisms of Coronavirus Cross-Species Transmission. *J Virol.* 2010;84(7):3134–46.
23. WHO. One Health [Internet]. 2017 [cited 2021 Jan 19]. Available from: <https://www.who.int/news-room/q-a-detail/one-health>
24. WHO. R&D Blueprint [Internet]. 2016 [cited 2021 Jan 17] Available from: [https://www.who.int/blueprint/about/r\\_d\\_blueprint\\_plan\\_of\\_action.pdf?ua=1](https://www.who.int/blueprint/about/r_d_blueprint_plan_of_action.pdf?ua=1)
25. Abudurexiti A, Adkins S, Alioto D, Alkhovsky SV., Avšič-Županc T, Ballinger MJ, et al. Taxonomy of the order Bunyavirales: update 2019. *Arch Virol.* 2019;164(7):1949–65.
26. Elliott RM. Molecular biology of the Bunyaviridae. *J Gen Virol.* 1990;71(3):501–22.
27. Walter CT, Barr JN. Recent advances in the molecular and cellular biology of bunyaviruses. *J Gen Virol.* 2011;92(11):2467–84.
28. Zivcec M, Scholte FEM, Spiropoulou CF, Spengler JR, Bergeron É. Molecular insights into Crimean-Congo hemorrhagic fever virus. *Viruses.* 2016;8(4).
29. Fafetine JM, Tijhaar E, Paweska JT, Neves LCBG, Hendriks J, Swanepoel R, et al. Cloning and expression of Rift Valley fever virus nucleocapsid (N) protein and evaluation of a N-protein based indirect ELISA for the detection of specific IgG and IgM antibodies in domestic ruminants. *Vet Microbiol.* 2007;121(1–2):29–38.
30. Samudzi RR, Leman PA, Paweska JT, Swanepoel R, Burt FJ. Bacterial expression of Crimean-Congo hemorrhagic fever virus nucleoprotein and its evaluation as a diagnostic reagent in an indirect ELISA. *J Virol Methods.* 2012;179(1):70–6.
31. Golden JW, Shoemaker CJ, Lindquist ME, Zeng X, Daye SP, Williams JA, et al. GP38-targeting monoclonal antibodies protect adult mice against lethal Crimean-Congo hemorrhagic fever virus infection. *Sci Adv.* 2019;5(7).



32. Lozach PY, Kühbacher A, Meier R, Mancini R, Bitto D, Bouloy M, et al. DC-SIGN as a receptor for phleboviruses. *Cell Host Microbe*. 2011;10(1):75–88.
33. Xiao X, Feng Y, Zhu Z, Dimitrov DS. Identification of a putative Crimean-Congo hemorrhagic fever virus entry factor. *Biochem Biophys Res Commun*. 2011;411(2):253–8.
34. Jangra RK, Herbert AS, Li R, Jae LT, Lara M, Slough MM, et al. Protocadherin-1 is essential for cell entry by New World hantaviruses. *Nature*. 2018;563(7732):559–63.
35. Harmon B, Schudel BR, Maar D, Kozina C, Ikegami T, Tseng C-TK, et al. Rift Valley Fever Virus Strain MP-12 Enters Mammalian Host Cells via Caveola-Mediated Endocytosis. *J Virol*. 2012;86(23):12954–70.
36. Hackett BA, Yasunaga A, Panda D, Tartell MA, Hopkins KC, Hensley SE, et al. RNASEK is required for internalization of diverse acid-dependent viruses. *Proc Natl Acad Sci U S A*. 2015;112(25):7797–802.
37. Simon M, Johansson C, Mirazimi A. Crimean-Congo hemorrhagic fever virus entry and replication is clathrin-, pH- and cholesterol-dependent. *J Gen Virol*. 2009;90(1):210–5.
38. Fontana J, López-Montero N, Elliott RM, Fernández JJ, Risco C. The unique architecture of Bunyamwera virus factories around the Golgi complex. *Cell Microbiol*. 2008;10(10):2012–28.
39. De Castro IF, Risco C. Imaging RNA virus replication assemblies: Bunyaviruses and reoviruses. *Future Virol*. 2014;9(12):1089–104.
40. Sanchez AJ, Vincent MJ, Erickson BR, Nichol ST. Crimean-Congo Hemorrhagic Fever Virus Glycoprotein Precursor Is Cleaved by Furin-Like and SKI-1 Proteases To Generate a Novel 38-Kilodalton Glycoprotein. *J Virol*. 2006;80(1):514–25.
41. Altamura LA, Bertolotti-Ciarlet A, Teigler J, Paragas J, Schmaljohn CS, Doms RW. Identification of a Novel C-Terminal Cleavage of Crimean-Congo Hemorrhagic Fever Virus PreGN That Leads to Generation of an NSM Protein. *J Virol*. 2007;81(12):6632–42.
42. Sanchez AJ, Vincent MJ, Nichol ST. Characterization of the Glycoproteins of Crimean-Congo Hemorrhagic Fever Virus. *J Virol*. 2002;76(14):7263–75.
43. Vincent MJ, Sanchez AJ, Erickson BR, Basak A, Chretien M, Seidah NG, et al. Crimean-Congo Hemorrhagic Fever Virus Glycoprotein Proteolytic Processing by Subtilase SKI-1. *J Virol*. 2003;77(16):8640–9.
44. Mishra A, Moyer C, Abelson D, Deer D, El Omari K, Duman R, et al. Structure and Characterization of Crimean-Congo Hemorrhagic Fever Virus GP38. 2020;94(8):1–13.
45. Suzich JA, Collett MS. Rift valley fever virus M segment: Cell-free transcription and translation of virus-complementary RNA. *Virology*. 1988;164(2):478–86.
46. Collett MS, Purchio AF, Keegan K, Frazier S, Hays W, Anderson DK, et al.

- Complete nucleotide sequence of the M RNA segment of rift valley fever virus. *Virology*. 1985;144(1):228–45.
47. Kakach LT, Wasmoen TL, Collett MS. Rift Valley fever virus M segment: use of recombinant vaccinia viruses to study Phlebovirus gene expression. *J Virol*. 1988;62(3):826–33.
  48. Suzich JA, Kakach LT, Collett MS. Expression strategy of a phlebovirus: biogenesis of proteins from the Rift Valley fever virus M segment. *J Virol*. 1990;64(4):1549–55.
  49. Gerrard SR, Nichol ST. Synthesis, proteolytic processing and complex formation of N-terminally nested precursor proteins of the Rift Valley fever virus glycoproteins. *Virology*. 2007;357(2):124–33.
  50. Gerrard SR, Nichol ST. Characterization of the Golgi Retention Motif of Rift Valley Fever Virus GN Glycoprotein. *J Virol*. 2002;76(23):12200–10.
  51. Horne KME, Vanlandingham DL. Bunyavirus-vector interactions. *Viruses*. 2014;6(11):4373–97.
  52. OIE. OIE notifiable diseases [Internet]. 2020 [cited 2020 Sep 10]. Available from: <https://www.oie.int/animal-health-in-the-world/oie-listed-diseases-2020>
  53. Bente DA, Forrester NL, Watts DM, McAuley AJ, Whitehouse CA, Bray M. Crimean-Congo hemorrhagic fever: History, epidemiology, pathogenesis, clinical syndrome and genetic diversity. *Antiviral Res*. 2013;100(1):159–89.
  54. Casals J. Antigenic Similarity between the Virus Causing Crimean Hemorrhagic Fever and Congo Virus. *Proc Soc Exp Biol Med*. 1969;131(1):233–6.
  55. Lasecka L, Baron MD. The molecular biology of nairoviruses, an emerging group of tick-borne arboviruses. *Arch Virol*. 2014;159(6):1249–65.
  56. Gargili A, Estrada-Peña A, Spengler JR, Lukashev A, Nuttall PA, Bente DA. The role of ticks in the maintenance and transmission of Crimean-Congo hemorrhagic fever virus: A review of published field and laboratory studies. *Antiviral Res*. 2017;144:93–119.
  57. Negredo A, Habela MÁ, de Arellano ER, Diez F, Lasala F, López P, et al. Survey of crimean-congo hemorrhagic fever enzootic focus, Spain, 2011-2015. *Emerg Infect Dis*. 2019;25(6):1177–84.
  58. Naderi HR, Sarvghad MR, Bojdy A, Hadizadeh MR, Sadeghi R, Sheybani F. Nosocomial outbreak of Crimean-Congo haemorrhagic fever. *Epidemiol Infect*. 2011;139(6):862–6.
  59. WHO. Crimean-Congo haemorrhagic fever [Internet]. 2013 [cited 2020 Sep 12]. Available from: <https://www.who.int/news-room/fact-sheets/detail/crimean-congo-haemorrhagic-fever>
  60. Swanepoel R, Leman PA, Burt FJ, Jardine J, Verwoerd DJ, Capua I, et al. Experimental infection of ostriches with Crimean-Congo haemorrhagic fever virus. *Epidemiol Infect*. 1998;121(2):427–32.

61. Nalca A, Whitehouse CA. Crimean-Congo hemorrhagic fever virus infection among animals. *Crimean-Congo Hemorrhagic Fever A Glob Perspect*. 2007;155–65.
62. Akinci E, Bodur H, Leblebicioglu H. Pathogenesis of Crimean-Congo hemorrhagic fever. *Vector-Borne Zoonotic Dis*. 2013;13(7):429–37.
63. Chumakov MP, Butenko AM, Shalunova NV, Mart'ianova LI, Smirnova SE, Bashkirtsev IN, et al. New data on the viral agent of Crimean hemorrhagic fever. *Vopr Virusol*. 1968;13(3):377.
64. Berezcky S, Lindegren G, Karlberg H, Åkerström S, Klingström J, Mirazimi A. Crimean-Congo hemorrhagic fever virus infection is lethal for adult type I interferon receptor-knockout mice. *J Gen Virol*. 2010;91(6):1473–7.
65. Zivcec M, Safronetz D, Scott D, Robertson S, Ebihara H, Feldmann H. Lethal Crimean-Congo hemorrhagic fever virus infection in interferon  $\alpha/\beta$  receptor knockout mice is associated with high viral loads, proinflammatory responses, and coagulopathy. *J Infect Dis*. 2013;207(12):1909–21.
66. Haddock E, Feldmann F, Hawman DW, Zivcec M, Hanley PW, Saturday G, et al. A cynomolgus macaque model for Crimean-Congo haemorrhagic fever. *Nat Microbiol*. 2018;3(5):556–62.
67. Papa A, Mirazimi A, Köksal I, Estrada-Pena A, Feldmann H. Recent advances in research on Crimean-Congo hemorrhagic fever. *J Clin Virol*. 2015;64:137–43.
68. Oestereich L, Rieger T, Neumann M, Bernreuther C, Lehmann M, Krasemann S, et al. Evaluation of Antiviral Efficacy of Ribavirin, Arbidol, and T-705 (Favipiravir) in a Mouse Model for Crimean-Congo Hemorrhagic Fever. *PLoS Negl Trop Dis*. 2014;8(5).
69. Daubney R, Hudson JR, Garnham PC. Enzootic hepatitis or Rift Valley fever. An undescribed virus disease of sheep cattle and man from East Africa. *J Pathol*. 1931;XXXIV:545–79.
70. Mansfield KL, Banyard AC, McElhinney L, Johnson N, Horton DL, Hernández-Triana LM, et al. Rift Valley fever virus: A review of diagnosis and vaccination, and implications for emergence in Europe. *Vaccine*. 2015;33(42):5520–31.
71. Maluleke MR, Phosiwa M, van Schalkwyk A, Michuki G, Lubisi BA, Kegakilwe PS, et al. A comparative genome analysis of Rift Valley Fever virus isolates from foci of the disease outbreak in South Africa in 2008-2010. *PLoS Negl Trop Dis*. 2019;13(3):1–13.
72. Balkhy HH, Memish ZA. Rift Valley fever: An uninvited zoonosis in the Arabian peninsula. *Int J Antimicrob Agents*. 2003;21(2):153–7.
73. Sissoko D, Giry C, Gabrie P, Tarantola A, Pettinelli F, Collet L, et al. Rift valley fever, mayotte, 2007-2008. *Emerg Infect Dis*. 2009;15(4):568–70.
74. OIE. Rift Valley fever (OIE Technical Disease Cards). 2018;1–7.
75. Chevalier V, Pépin M, Plée L, Lancelot R. Rift valley fever - a threat for Europe?

- Eurosurveillance. 2010;15(10):18–28.
76. Rolin AI, Berrang-Ford L, Kulkarni MA. The risk of Rift Valley fever virus introduction and establishment in the United States and European Union. *Emerg Microbes Infect.* 2013;2(1):1–8.
  77. Sindato C, Karimuribo E, Mboera LEG. The epidemiology and socio-economic impact of Rift Valley Fever in Tanzania: A review. *Tanzan J Health Res.* 2011;13(Suppl 1):1–16.
  78. Aradaib IE, Erickson BR, Elageb RM, Khristova ML, Carroll SA, Elkhidir IM, et al. Rift valley fever, Sudan, 2007 and 2010. *Emerg Infect Dis.* 2013;19(2):246–53.
  79. Hassan OA, Ahlm C, Sang R, Evander M. The 2007 Rift valley fever outbreak in Sudan. *PLoS Negl Trop Dis.* 2011;5(9):1–7.
  80. Himeidan YE, Kweka EJ, Mahgoub MM, El Rayah EA, Ouma JO. Recent outbreaks of Rift Valley fever in East Africa and the Middle East. *Front Public Heal.* 2014;2(169):1–11.
  81. Ikegami T, Makino S. The pathogenesis of rift valley fever. *Viruses.* 2011;3(5):493–519.
  82. SMITHBURN KC, HADDOW AJ, GILLETT JD. Rift Valley fever; isolation of the virus from wild mosquitoes. *Br J Exp Pathol.* 1948;29(2):107–21.
  83. Bouloy M, Flick R. Reverse genetics technology for Rift Valley fever virus: Current and future applications for the development of therapeutics and vaccines. 2009;84(2):101–18.
  84. Ikegami T, Makino S. Rift Valley fever vaccines. *Vaccine.* 2009;27(SUPPL. 4).
  85. Faburay B, LaBeaud AD, McVey DS, Wilson WC, Richt JA. Current status of rift valley fever vaccine development. *Vaccines.* 2017;5(3):1–20.
  86. Muller R, Saluzzo J-F, Lopez N, Dreier T, Turell M, Smith J, et al. Characterization of clone 13, a naturally attenuated avirulent isolate of Rift Valley fever virus, which is altered in the small segment. *Am J Trop Med Hyg.* 1995;53(4):405–11.
  87. Pittman PR, Liu CT, Cannon TL, Makuch RS, Mangiafico JA, Gibbs PH, et al. Immunogenicity of an inactivated Rift Valley fever vaccine in humans: A 12-year experience. *Vaccine.* 1999;18(1–2):181–9.
  88. Kortekaas J, Zingeser J, de Leeuw P, de La Rocque, Stephane Unger, Hermann Moormann RJM. Rift Valley Fever Vaccine Development, Progress and Constraints. *Emerg Infect Dis.* 2011;17(9).
  89. Atkins C, Freiberg AN. Recent advances in the development of antiviral therapeutics for Rift Valley fever virus infection. *Future Virol.* 2017;12(11):651–65.
  90. Wu F, Zhao S, Yu B, Chen YM, Wang W, Song ZG, et al. A new coronavirus associated with human respiratory disease in China. *Nature.* 2020;579(7798):265–9.

91. Hu D, Zhu C, Ai L, He T, Wang Y, Ye F, et al. Genomic characterization and infectivity of a novel SARS-like coronavirus in Chinese bats. *Emerg Microbes Infect.* 2018;7(1).
92. Drosten C, Günther S, Preiser W, van der Werf S, Brodt H-R, Becker S, et al. Identification of a Novel Coronavirus in Patients with Severe Acute Respiratory Syndrome. *N Engl J Med.* 2003;348(20):1967–76.
93. Hamre D, Procknow JJ. A New Virus Isolated from the Human Respiratory Tract. *Proc Soc Exp Biol Med.* 1966;121(1):190–3.
94. Tyrrell DAJ, Bynoe ML. Cultivation of a Novel Type of Common-cold Virus in Organ Cultures. *Br Med J.* 1965;1(5448):1467–70.
95. Van Der Hoek L, Pyrc K, Jebbink MF, Vermeulen-Oost W, Berkhout RJM, Wolthers KC, et al. Identification of a new human coronavirus. *Nat Med.* 2004;10(4):368–73.
96. Woo PCY, Lau SKP, Chu C, Chan K, Tsoi H, Huang Y, et al. Characterization and Complete Genome Sequence of a Novel Coronavirus, Coronavirus HKU1, from Patients with Pneumonia. *J Virol.* 2005;79(2):884–95.
97. Zhou P, Yang X Lou, Wang XG, Hu B, Zhang L, Zhang W, et al. A pneumonia outbreak associated with a new coronavirus of probable bat origin. *Nature.* 2020;579(7798):270–3.
98. Lam TTY, Jia N, Zhang YW, Shum MHH, Jiang JF, Zhu HC, et al. Identifying SARS-CoV-2-related coronaviruses in Malayan pangolins. *Nature.* 2020;583(7815):282–5.
99. Xiao K, Zhai J, Feng Y, Zhou N, Zhang X, Zou JJ, et al. Isolation of SARS-CoV-2-related coronavirus from Malayan pangolins. *Nature.* 2020;583(7815):286–9.
100. Guan Y, Zheng BJ, He YQ, Liu XL, Zhuang ZX, Cheung CL, et al. Isolation and characterization of viruses related to the SARS coronavirus from animals in Southern China. *Science.* 2003;302(5643):276–8.
101. Stalin Raj V, Farag EABA, Reusken CBEM, Lamers MM, Pas SD, Voermans J, et al. Isolation of MERS coronavirus from dromedary camel, Qatar, 2014. *Emerg Infect Dis.* 2014;20(8):1339–42.
102. WHO. COVID-19 Situation Reports [Internet]. 2020 [cited 2021 Jan 21]. Available from: <https://www.who.int/emergencies/diseases/novel-coronavirus-2019/situation-reports>
103. Wang W, Tang J, Wei F. Updated understanding of the outbreak of 2019 novel coronavirus (2019 - nCoV) in Wuhan, China. *J Med Virol.* 2020;92:441–7.
104. Mo P, Xing Y, Xiao Y, Deng L, Zhao Q. Clinical characteristics of refractory COVID-19 pneumonia in Wuhan, China. *Clin Infect Dis.* 2020;ciaa270.
105. Dawson P, Rabold EM, Laws RL, Connors EE, Gharpure R, Yin S, et al. Loss of Taste and Smell as Distinguishing Symptoms of Coronavirus Disease 2019. *Clin Infect Dis.* 2020;48(ciaa799):18–21.

106. Martines RB, Ritter JM, Matkovic E, Gary J, Bollweg BC, Bullock H, et al. Pathology and Pathogenesis of SARS-CoV-2 Associated with Fatal Coronavirus Disease , United States. *Emerg Infect Dis.* 2020;26(9):2005–15.
107. Huang C, Wang Y, Li X, Ren L, Zhao J, Hu Y, et al. Clinical features of patients infected with 2019 novel coronavirus in Wuhan, China. *Lancet.* 2020;395(10223):497–506.
108. Salje H, Kiem CT, Lefrancq N, Courtejoie N, Bosetti P, Paireau J, et al. Estimating the burden of SARS-CoV-2 in France. *Science.* 2020;369(6500):208–11.
109. D’Arienzo M, Coniglio A. Assessment of the SARS-CoV-2 basic reproduction number ,  $R_0$  , based on the early phase of COVID-19 outbreak in Italy. *Biosaf Heal.* 2020;2(2):57–9.
110. Lee S, Meyler P, Mozel M, Tauh T, Merchant R. Asymptomatic carriage and transmission of SARS-CoV-2 : What do we know ? *Can J Anesth Can d’anesthésie.* 2020;67(10):1424–30.
111. Slifka MK, Gao L. Is presymptomatic spread a major contributor to COVID-19 transmission ? *Nat Med.* 2020;26:1531–3.
112. Yuan Z, Xiao Y, Dai Z, Huang J, Zhang Z, Chen Y. Modelling the effects of Wuhan’ s lockdown during COVID-19, China. *Bull World Health Organ.* 2020;98(7):484–94.
113. Altakarli NS. China’ s Response to the COVID-19 Outbreak : A Model for Epidemic Preparedness and Management. *Dubai Med J.* 2020;3:44–9.
114. You J. Lessons From South Korea’ s Covid-19 Policy Response. *Am Rev Public Adm.* 2020;50(6–7):801–8.
115. Barberia LG, Gómez EJ. Political and institutional perils of Brazil’ s COVID-19 crisis. *Lancet.* 2020;396(10248):367–8.
116. FDA. Drug and Biological Products [Internet]. 2021 [cited 2021 Jan 21]. Available from: <https://www.fda.gov/emergency-preparedness-and-response/mcm-legal-regulatory-and-policy-framework/emergency-use-authorization#coviddrugs>
117. WHO Solidarity Trial Consortium. Repurposed Antiviral Drugs for Covid-19 — Interim WHO Solidarity Trial Results. *N Engl J Med.* 2020;1–15.
118. Robinson J. Critically ill COVID-19 patients unlikely to benefit from convalescent plasma, early results from UK trial show. *The Pharmaceutical Journal.* 2021;Vol 306, No 7945.
119. Libster R, Marc GP, Wappner D, Coviello S, Bianchi A, Braem V, et al. Early High-Titer Plasma Therapy to Prevent Severe Covid-19 in Older Adults. *N Engl J Med.* 2021;Epub ahead:1–9.
120. Polack FP, Thomas SJ, Kitchin N, Absalon J, Gurtman A, Lockhart S, et al. Safety and Efficacy of the BNT162b2 mRNA Covid-19 Vaccine. *N Engl J Med.* 2020;383(27):2603–15.

121. Baden LR, El Sahly HM, Essink B, Kotloff K, Frey S, Novak R, et al. Efficacy and Safety of the mRNA-1273 SARS-CoV-2 Vaccine. *N Engl J Med.* 2020;1–14.
122. Voysey M, Clemens SAC, Madhi SA, Weckx LY, Folegatti PM, Aley PK, et al. Safety and efficacy of the ChAdOx1 nCoV-19 vaccine (AZD1222) against SARS-CoV-2: an interim analysis of four randomised controlled trials in Brazil, South Africa, and the UK. *Lancet.* 2020;99–111.
123. Audi A, Allbrahim M, Kaddoura M, Hijazi G, Yassine HM, Zaraket H. Seasonality of Respiratory Viral Infections: Will COVID-19 Follow Suit? *Front Public Heal.* 2020;8(567184):1–8.
124. Watanabe Y, Allen JD, Wrapp D, McLellan JS, Crispin M. Site-specific glycan analysis of the SARS-CoV-2 spike. *Science.* 2020;369(6501):330–3.
125. Walls AC, Park YJ, Tortorici MA, Wall A, McGuire AT, Veesler D. Structure, Function, and Antigenicity of the SARS-CoV-2 Spike Glycoprotein. *Cell.* 2020;181(2):281–92.
126. Wölfel R, Corman VM, Guggemos W, Seilmaier M, Zange S, Müller MA, et al. Virological assessment of hospitalized patients with COVID-2019. *Nature.* 2020;581(7809):465–9.
127. Li W, Moore MJ, Vasilieva N, Sui J, Wong SK, Berne MA, et al. Angiotensin-converting enzyme 2 is a functional receptor for the SARS coronavirus. *Nature.* 2003;426:450–4.
128. Raj VS, Mou H, Smits SL, Dekkers DHW, Müller MA, Dijkman R, et al. Dipeptidyl peptidase 4 is a functional receptor for the emerging human coronavirus-EMC. *Nature.* 2013;495(7440):251–4.
129. Tai W, He L, Zhang X, Pu J, Voronin D, Jiang S, et al. Characterization of the receptor-binding domain (RBD) of 2019 novel coronavirus: implication for development of RBD protein as a viral attachment inhibitor and vaccine. *Cell Mol Immunol.* 2020;17:613–20.
130. Alsaadi EAJ, Jones IM. Membrane binding proteins of coronaviruses. *Future Virol.* 2019;14(4):275–86.
131. Neuman BW, Kiss G, Kunding AH, Bhella D, Baksh MF, Connelly S, et al. A structural analysis of M protein in coronavirus assembly and morphology. *J Struct Biol.* 2011;174(1):11–22.
132. Schoeman D, Fielding BC. Coronavirus envelope protein: Current knowledge. *Virol J.* 2019;16(69).
133. Maier HJ, Bickerton E, Britton P. Coronaviruses: Methods and protocols. In: *Coronaviruses: Methods and Protocols.* 2015. p. 1–23.
134. Zeng W, Liu G, Ma H, Zhao D, Yang Y, Liu M, et al. Biochemical characterization of SARS-CoV-2 nucleocapsid protein. *Biochem Biophys Res Commun.* 2020;527(3):618–23.
135. Hoffmann M, Kleine-Weber H, Schroeder S, Krüger N, Herrler T, Erichsen S, et

- al. SARS-CoV-2 Cell Entry Depends on ACE2 and TMPRSS2 and Is Blocked by a Clinically Proven Protease Inhibitor. *Cell*. 2020;181(2):271-280.e8.
136. V'kovski P, Kratzel A, Steiner S, Stalder H, Thiel V. Coronavirus biology and replication: implications for SARS-CoV-2. *Nat Rev Microbiol*. 2020;
137. Snijder EJ, Limpens RWAL, de Wilde AH, de Jong AWM, Zevenhoven-Dobbe JC, Maier HJ, et al. A unifying structural and functional model of the coronavirus replication organelle: Tracking down RNA synthesis. *PLoS Biol*. 2020;18(6):1–25.
138. Cortese M, Lee JY, Cerikan B, Neufeldt CJ, Oorschot VMJ, Köhler S, et al. Integrative Imaging Reveals SARS-CoV-2-Induced Reshaping of Subcellular Morphologies. *Cell Host Microbe*. 2020;28:853–66.
139. Thoms M, Buschauer R, Ameisemeier M, Koepke L, Denk T, Hirschenberger M, et al. Structural basis for translational shutdown and immune evasion by the Nsp1 protein of SARS-CoV-2. *Science*. 2020;369(6508):1249–56.
140. Schubert K, Karousis ED, Jomaa A, Scaiola A, Echeverria B, Gurzeler LA, et al. SARS-CoV-2 Nsp1 binds the ribosomal mRNA channel to inhibit translation. *Nat Struct Mol Biol*. 2020;27(10):959–66.
141. Gao Y, Yan L, Huang Y, Liu F, Zhao Y, Cao L, et al. Structure of the RNA-dependent RNA polymerase from COVID-19 virus. *Science*. 2020;368(6492):779–82.
142. Ogando NS, Zevenhoven-Dobbe JC, Van Der Meer Y, Bredenbeek PJ, Posthuma CC, Snijder EJ. The Enzymatic Activity of the nsp14 Exoribonuclease Is Critical for Replication of MERS-CoV and SARS-CoV-2. *J Virol*. 2020;94(23):1–24.
143. Ghosh S, Dellibovi-Ragheb TA, Kerviel A, Pak E, Qiu Q, Fisher M, et al.  $\beta$ -Coronaviruses Use Lysosomes for Egress Instead of the Biosynthetic Secretory Pathway. *Cell*. 2020;183(6):1520-1535.e14.
144. Rouse BT, Mueller SN. Host Defenses to Viruses. In: *Clinical Immunology*. Fifth Edition. Elsevier Ltd; 2019. p. 365–74.
145. Rich RR, Chaplin DD. The Human Immune Response. In: *Clinical Immunology*. Fifth Edition. Elsevier Ltd; 2019. p. 3–17.
146. Sarantopoulos S. Antibody Production by the Immune System. In: *Antibodies: A Laboratory Manual*. Greenfield EA, editor. Second Edition. 2014. p. 1–8.
147. Rodgers JR, Rich RR. Antigens and antigen processing. In: *Clinical Immunology*. Third Edition. Elsevier; 2008. p. 91–101.
148. Greenspan NS. Immunoglobulin function. Third Edition. *Clinical Immunology*. Elsevier; 2008. 237–248 p.
149. Hosseini S, Vázquez-Villegas P, Rito-Palomares M, Martínez-Chapa SO. Fundamentals and history of ELISA: The evolution of the immunoassays until invention of ELISA. In: *Enzyme-linked Immunosorbent Assay (ELISA)*. 2018. p. 1–18.



150. Turner M. Antibodies. In: Immunology. Roitt I, Brostoff J, Male D, editors. 6th Edition. Mosby; 2001. p. 65–85.
151. Vidarsson G, Dekkers G, Rispens T. IgG subclasses and allotypes: From structure to effector functions. *Front Immunol.* 2014;5:1–17.
152. Schroeder HW, Cavacini L. Structure and Function of Immunoglobulins. *J Allergy Clin Immunol.* 2010;125(Suppl 2):S41–52.
153. Gutzeit C, Chen K, Cerutti A. The enigmatic function of IgD: some answers at last. *Eur J Immunol.* 2018;48(7):1101–13.
154. Winter WE, Hardt NS, Fuhrman S. Immunoglobulin E: Importance in parasitic infections and hypersensitivity responses. *Arch Pathol Lab Med.* 2000;124(9):1382–5.
155. Stoermer KA, Morrison TE. Complement and viral pathogenesis. *Virology.* 2011;411(2):362–73.
156. Nash AA, Dutia BM. The immune response to viral infection. In: Topley & Wilson's Microbiology and Microbial Infections. 2010. p. 1–22.
157. Palm AKE, Henry C. Remembrance of Things Past: Long-Term B Cell Memory After Infection and Vaccination. *Front Immunol.* 2019;10:1787.
158. Virgin HW, Wherry EJ, Ahmed R. Redefining Chronic Viral Infection. *Cell.* 2009;138(1):30–50.
159. Landry ML, Leland D. Primary Isolation of Viruses. In: Clinical Virology Manual. Fifth Edition. 2016. p. 79–93.
160. Leland DS, Ginocchio CC. Role of cell culture for virus detection in the age of technology. *Clin Microbiol Rev.* 2007;20(1):49–78.
161. Goldsmith CS, Ksiazek TG, Rollin PE, Comer JA, Nicholson WL, Peret TCT, et al. Cell culture and electron microscopy for identifying viruses in diseases of unknown cause. *Emerg Infect Dis.* 2013;19(6):864–9.
162. Mullis KB, Faloona FA. Specific Synthesis of DNA in Vitro via a Polymerase-Catalyzed Chain Reaction. In: Methods in Enzymology. 1987. p. 335–50.
163. White T, Madej R, Persing D. The polymerase chain reaction: clinical applications. In: Advances in Clinical Chemistry. 1992. p. 161–96.
164. Haqqi TM, Sarkar G, David CS, Sommer SS. Specific amplification with PCR of a refractory segment of genomic DNA. *Nucleic Acids Res.* 1988;16(24):11844.
165. Higuchi R, Fockler C, Dollinger G, Watson R. Kinetic PCR analysis: Real-time monitoring of DNA amplification reactions. *Nat Biotechnol.* 1993;11:1026–30.
166. Coffin JM, Hughes SH, Varmus HE, editors. Retroviruses. Cold Spring Harbor Laboratory Press. 1997.
167. De Paz HD, Brotons P, Muñoz-Almagro C. Molecular isothermal techniques for combating infectious diseases: Towards low-cost point-of-care diagnostics. *Expert*

- Rev Mol Diagn. 2014;14(7):827–43.
168. Wittwer CT, Makrigiorgos GM. Nucleic Acid Techniques. In: Principles and Applications of Molecular Diagnostics. Rifai N, Horvath AR, Wittwer CT, editors. Elsevier Inc.; 2018. p. 47–86.
169. Kulski JK. Next-Generation Sequencing — An Overview of the History, Tools, and “Omic” Applications. In: Next Generation Sequencing - Advances, Applications and Challenges. 2016. p. 3–60.
170. Deurenberg RH, Bathoorn E, Chlebowicz MA, Couto N, Ferdous M, García-Cobos S, et al. Application of next generation sequencing in clinical microbiology and infection prevention. *J Biotechnol*. 2017;243:16–24.
171. Koczula KM, Gallotta A. Lateral flow assays. *Essays Biochem*. 2016;60:111–20.
172. Posthuma-Trumpie GA, Korf J, Van Amerongen A. Lateral flow (immuno)assay: Its strengths, weaknesses, opportunities and threats. A literature survey. *Anal Bioanal Chem*. 2009;393(2):569–82.
173. Magi B, Liberatori S. Immunoblotting Techniques. In: Methods in Molecular Biology Immunochemical Protocols. Burns R, editor. Third Edition. 2005. p. 227–53.
174. Corthell JT. Immunohistochemistry. In: Basic Molecular Protocols in Neuroscience: Tips, Tricks, and Pitfalls. 2014. p. 91–103.
175. Ekins R, Chu F, Biggart E. Multispot, multianalyte, immunoassay. *Ann Biol Clin (Paris)*. 1990;48(9):655—666.
176. Silzel JW, Cercek B, Dodson C, Tsay T, Obremski RJ. Mass-sensing, multianalyte microarray immunoassay with imaging detection. *Clin Chem*. 1998;44(9):2036–43.
177. Hsu HY, Joos TO, Koga H. Multiplex microsphere-based flow cytometric platforms for protein analysis and their application in clinical proteomics - From assays to results. *Electrophoresis*. 2009;30:4008–19.
178. Angeloni S, Cordes R, Dunbar S, Garcia C, Gibson G, Martin C, et al. xMAP Cookbook. Third Edition. Luminex Corporation, editor. Luminex Corporation. 2016. p. 1-148.
179. Krishhan VV., Khan IH, Luciw PA. Multiplexed microbead immunoassays by flow cytometry for molecular profiling: Basic concepts and proteomics applications. *Crit Rev Biotechnol*. 2009;29(1):29–43.
180. Dias D, Van Doren J, Schlottmann S, Puchalski D, Ruiz W, Boerckel P, et al. Optimization and Validation of a Multiplexed Luminex Assay To Quantify Antibodies to Neutralizing Epitopes on Optimization and Validation of a Multiplexed Luminex Assay To Quantify Antibodies to Neutralizing Epitopes on Human Papillomaviruses 6,11,16,18. *Clin Diagn Lab Immunol*. 2005;12(8):959–69.
181. Khalifian S, Raimondi G, Brandacher G. The Use of Luminex Assays to Measure

- Cytokines. *J Invest Dermatol.* 2015;135(4):1–5.
182. Cho CY, Nowatzke W, Oliver K, Garber EAE. Multiplex detection of food allergens and gluten. *Anal Bioanal Chem.* 2015;407:4195–4206.
183. Spencer KA, Osorio FA, Hiscox JA. Recombinant viral proteins for use in diagnostic ELISAs to detect virus infection. *Vaccine.* 2007;25(30):5653–9.
184. Hodinka RL, Kaiser L. Is the era of viral culture over in the clinical microbiology laboratory? *J Clin Microbiol.* 2013;51(1):2–8.
185. Cohen SN, Chang ACY, Boyer HW, Helling RB. Construction of biologically functional bacterial plasmids in vitro. *Proc Natl Acad Sci U S A.* 1973;70(11):3240–4.
186. Goeddel D V., Kleid DG, Bolivar F. Expression in *Escherichia coli* of chemically synthesized genes for human insulin. *Proc Natl Acad Sci U S A.* 1979;76(1):106–10.
187. Pham P V. Medical biotechnology: Techniques and applications. In: *Omics Technologies and Bio-Engineering.* Elsevier; 2018. p. 449–69.
188. Brondyk WH. Selecting an Appropriate Method for Expressing a Recombinant Protein. In: *Methods in Enzymology.* Elsevier Inc.; 2009. p. 131–47.
189. Burgess RR. Refolding Solubilized Inclusion Body Proteins. In: *Methods in Enzymology.* Elsevier Inc.; 2009. p. 259–82.
190. Palmer I, Wingfield PT. Preparation and Extraction of Insoluble (Inclusion-Body) Proteins from *Escherichia coli*. In: *Current Protocols in Protein Science.* 2012. p. 1-24.
191. Mergulhão FJM, Summers DK, Monteiro GA. Recombinant protein secretion in *Escherichia coli*. *Biotechnol Adv.* 2005;23(3):177–202.
192. Pelley JW. RNA Transcription and Control of Gene Expression. In: *Elsevier's Integrated Review Biochemistry.* Pelley JW, editor. Mosby; 2007. p. 135–45.
193. Silverstone AE, Arditti RR, Magasanik B. Catabolite-insensitive revertants of lac promoter mutants. *Proc Natl Acad Sci U S A.* 1970;66(3):773–9.
194. Aslanidis C, de Jong PJ. Ligation-independent cloning of PCR products (LIC-PCR). *Nucleic Acids Res.* 1990;18(20):6069–74.
195. Esposito D, Garvey LA, Chakiath CS. Gateway cloning for protein expression. In: *Methods in Molecular Biology: High Throughput Protein Expression and Purification.* Doyle SA, editor. 2009. p. 31–54.
196. Landy A. DYNAMIC, STRUCTURAL, AND REGULATORY ASPECTS OF LAMBDA SITE-SPECIFIC RECOMBINATION. *Annu Rev Biochem.* 1989;58:913–49.
197. Hartley JL, Temple GF, Brasch MA. DNA Cloning Using In Vitro Site-Specific Recombination. *Genome Res.* 2000;10(11):1788–95.

198. Invitrogen. Gateway® Technology A universal technology to clone DNA sequences for functional analysis and expression in multiple systems. 2003. 1–74.
199. Invitrogen. pCR™8/GW/TOPO® TA Cloning® Kit. 2012. 1–34.
200. Weisberg RA, Foeller C, Landy A. Role for DNA Homology in Site-specific Recombination. *J Mol Biol.* 1983;170:319–42.
201. Invitrogen. E. coli Expression System with Gateway® Technology. 2012;1–36.
202. Ogden S, Haggerty D, Stoner CM, Kolodrubetz D, Schleif R. The Escherichia coli L-arabinose operon: Binding sites of the regulatory proteins and a mechanism of positive and negative regulation. *Proc Natl Acad Sci U S A.* 1980;77(6):3346–50.
203. Schleif R. DNA looping. *Annu Rev Biochem.* 1992;61:199–223.
204. Mattanovich D, Branduardi P, Dato L, Gasser B, Sauer M, Porro D. Recombinant protein production in yeasts. In: *Methods in Molecular Biology.* 2012. p. 329–58.
205. Goffeau A, Barrell BG, Bussey H, Davis RW, Dujon B, Feldmann H, et al. Life with 6000 Genes. *Science.* 1996;274(5287):546–67.
206. Demain AL, Vaishnav P. Production of recombinant proteins by microbes and higher organisms. *Biotechnol Adv.* 2009;27(3):297–306.
207. Romanos MA, Scorer CA, Clare JJ. Foreign gene expression in yeast: a review. *Yeast.* 1992;8(6):423–88.
208. Gemmill TR, Trimble RB. Overview of N- and O-linked oligosaccharide structures found in various yeast species. *Biochim Biophys Acta.* 1999;1426(2):227–37.
209. Baghban R, Farajnia S, Rajabibazl M, Ghasemi Y, Mafi AA, Hoseinpoor R, et al. Yeast Expression Systems: Overview and Recent Advances. *Mol Biotechnol.* 2019;61:365–84.
210. Porro D, Sauer M, Branduardi P, Mattanovich D. Recombinant protein production in yeasts. *Methods Mol Biol.* 2005;31:245–59.
211. Cregg JM, Barringer KJ, Hessler AY, Madden KR. *Pichia pastoris* as a host system for transformations. *Mol Cell Biol.* 1985;5(12):3376–85.
212. Jarvis DL. Baculovirus-Insect Cell Expression Systems. In: *Methods in Enzymology.* Elsevier Inc.; 2009. p. 191–222.
213. Smith GE, Fraser MJ, Summers MD. Molecular Engineering of the *Autographa californica* Nuclear Polyhedrosis Virus Genome: Deletion Mutations Within the Polyhedrin Gene. *J Virol.* 1983;46(2):584–93.
214. Smith GE, Summers MD, Fraser MJ. Production of human beta interferon in insect cells infected with a baculovirus expression vector. *Biotechnology.* 1983;3(12):2156–65.
215. Vlak JM, Klinkenberg FA, Zaal KJ, Usmany M, Klinge-Roode EC, Geervliet JBF, et al. Functional studies on the p10 gene of *Autographa californica* nuclear polyhedrosis virus using a recombinant expressing a p10-beta-galactosidase fusion

- gene. *J Gen Virol*. 1988;69(Pt 4):765–76.
216. Passarelli A, Guarino L. Baculovirus Late and Very Late Gene Regulation. *Curr Drug Targets*. 2007;8(10):1103–15.
217. Berretta MF, Leticia Ferrelli M, Salvador R, Sciocco A, Romanowski V. Baculovirus Gene Expression. In: *Current Issues in Molecular Virology - Viral Genetics and Biotechnological Applications*. 2013. p. 57–78.
218. van Oers MM. Opportunities and challenges for the baculovirus expression system. *J Invertebr Pathol*. 2011;107(Suppl):S3–15.
219. Liu F, Wu X, Li L, Liu Z, Wang Z. Use of baculovirus expression system for generation of virus-like particles: Successes and challenges. *Protein Expr Purificatio*. 2013;90(2):104–16.
220. Hitchman RB, Possee RD, King LA. Baculovirus Expression Systems for Recombinant Protein Production in Insect cells. *Recent Pat Biotechnol*. 2009;3(1):46–54.
221. Kitts PA, Ayres MD, Possee RD. Linearization of baculovirus DNA enhances the recovery of recombinant virus expression vectors. *Nucleic Acids Res*. 1990;18(19):5667–72.
222. Kitts PA, Possee RD. A method for producing recombinant baculovirus expression vectors at high frequency. *Biotechniques*. 1993;14(5):810–7.
223. Goley ED, Ohkawa T, Mancuso J, Woodruff JB, D'Alessio JA, Cande WZ, et al. Dynamic nuclear actin assembly by Arp2/3 complex and a baculovirus WASP-like protein. *Science*. 2006;314(5798):464–7.
224. Takara Bio USA Inc. BacPAK™ Baculovirus Expression System User Manual [Internet]. 2013 [cited 2021 Jan 19]. 1–25 p. Available from: [www.clontech.com](http://www.clontech.com)
225. Hartley JL. Why proteins in mammalian cells? In: *Methods in Molecular Biology*. 2012. p. 1–12.
226. Wurm FM. Production of recombinant protein therapeutics in cultivated mammalian cells. *Nat Biotechnol*. 2004;22(11):1393–8.
227. Bandaranayake AD, Almo SC. Recent advances in mammalian protein production. *FEBS Lett*. 2014;588(2):253–60.
228. Geisse S, Fux C. Recombinant Protein Production by Transient Gene Transfer into Mammalian Cells. In: *Methods in Enzymology*. First Edition. Elsevier Inc.; 2009. p. 223–38.
229. Hacker DL, Balasubramanian S. Recombinant protein production from stable mammalian cell lines and pools. *Curr Opin Struct Biol*. 2016;38:129–36.
230. Baldi L, Hacker DL, Adam M, Wurm FM. Recombinant protein production by large-scale transient gene expression in mammalian cells: State of the art and future perspectives. *Biotechnol Lett*. 2007;29(5):677–84.
231. Lee JS, Kallehauge TB, Pedersen LE, Kildegaard HF. Site-specific integration in

- CHO cells mediated by CRISPR/Cas9 and homology-directed DNA repair pathway. *Sci Rep.* 2015;5(8572):1–11.
232. Coskun O. Separation techniques: Chromatography. *North Clin Istanbul.* 2016;3(2):156–60.
233. Bornhorst, J.A., Falke J. Purification of Proteins Using Polyhistidine Affinity Tags. In: *Methods in Enzymology.* 2000. p. 245–54.
234. Moser AC, Hage DS. Immunoaffinity chromatography: an introduction to applications and recent developments. In: *Bioanalysis.* 2010. p. 769–90.
235. Thompson NE, Burgess RR. Immunoaffinity Chromatography: Advantages and Limitations. In: *Analytical Separation Science.* 2015. p. 483–502.
236. Köhler, G., Milstein C. Continuous cultures of fused cells secreting antibody of predefined specificity. *Nature.* 1975;256:495–7.
237. Moldenhauer G. Selection Strategies for Monoclonal Antibodies. In: *Handbook of Therapeutic Antibodies.* 2014. p. 15–42.
238. Greenfield EA. Immunizing Animals. In: *Antibodies: A Laboratory Manual.* Greenfield EA, editor. Second Edition. 2014. p. 107–99.
239. SZYBALSKA EH, SZYBALSKI W. GENETICS OF HUMAN CELL LINES, IV. DNA-MEDIATED HERITABLE TRANSFORMATION OF A BIOCHEMICAL TRAIT. *Proc Natl Acad Sci U S A.* 1962;48(12):2026–34.
240. Littlefield JW. Selection of Hybrids from Matings of Fibroblasts in vitro and Their Presumed Recombinants. *Science.* 1964;145(3633):709–10.
241. McCafferty J, Griffiths AD, Winter G, Chiswell DJ. Phage antibodies: filamentous phage displaying antibody variable domains. Vol. 348, *Nature.* 1990. p. 552–4.
242. Hoogenboom HR, De Brune AP, Hufton SE, Hoet RM, Arends JW, Roovers RC. Antibody phage display technology and its applications. *Immunotechnology.* 1998;4(1):1–20.
243. Antibody fragments as therapeutics. In: *Therapeutic Antibody Engineering.* Woodhead Publishing; 2012. p. 265–97.
244. Holliger P, Hudson PJ. Engineered antibody fragments and the rise of single domains. *Nat Biotechnol.* 2005;23(9):1126–36.
245. Ahmad ZA, Yeap SK, Ali AM, Ho WY, Alitheen NBM, Hamid M. ScFv antibody: Principles and clinical application. *Clin Dev Immunol.* 2012;2012(980250).
246. Harmsen MM, De Haard HJ. Properties, production, and applications of camelid single-domain antibody fragments. *Appl Microbiol Biotechnol.* 2007;77(1):13–22.
247. Škrlec K, Štrukelj B, Berlec A. Non-immunoglobulin scaffolds: A focus on their targets. *Trends Biotechnol.* 2015;33(7):408–18.
248. Vazquez-Lombardi R, Phan TG, Zimmermann C, Lowe D, Jermutus L, Christ D. Challenges and opportunities for non-antibody scaffold drugs. *Drug Discov Today.*
-

- 2015;20(10):1271–83.
249. Simeon R, Chen Z. In vitro-engineered non-antibody protein therapeutics. *Protein Cell*. 2018;9(1):3–14.
250. Ramamurthy V, Krystek SR, Bush A, Wei A, Emanuel SL, Das Gupta R, et al. Structures of adnectin/protein complexes reveal an expanded binding footprint. *Structure*. 2012;20(2):259–69.
251. Löfblom J, Feldwisch J, Tolmachev V, Carlsson J, Ståhl S, Frejd FY. Affibody molecules: Engineered proteins for therapeutic, diagnostic and biotechnological applications. *FEBS Lett*. 2010;584(12):2670–80.
252. Gebauer M, Schiefner A, Matschiner G, Skerra A. Combinatorial design of an anticalin directed against the extra-domain b for the specific targeting of oncofetal fibronectin. *J Mol Biol*. 2013;425(4):780–802.
253. Binz HK, Amstutz P, Kohl A, Stumpp MT, Briand C, Forrer P, et al. High-affinity binders selected from designed ankyrin repeat protein libraries. *Nat Biotechnol*. 2004;22(5):575–82.
254. Dennis MS, Herzka A, Lazarus RA. Potent and selective Kunitz domain inhibitors of plasma kallikrein designed by phage display. *J Biol Chem*. 1995;270(43):25411–7.
255. Tiede C, Bedford R, Heseltine SJ, Smith G, Wijetunga I, Ross R, et al. Affimer proteins are versatile and renewable affinity reagents. *Elife*. 2017;6:e24903.
256. Tiede C, Tang AAS, Deacon SE, Mandal U, Nettleship JE, Owen RL, et al. Adhiron: A stable and versatile peptide display scaffold for molecular recognition applications. *Protein Eng Des Sel*. 2014;27(5):145–55.
257. Smith G. Filamentous fusion phage: novel expression vectors that display cloned antigens on the virion surface. *Science*. 1985;228(4705):1315–1317.
258. De La Cruz VF, Lal AA, McCutchan TF. Immunogenicity and epitope mapping of foreign sequences via genetically engineered filamentous phage. *J Biol Chem*. 1988;263(9):4318–22.
259. Ledsgaard L, Kilstrup M, Karatt-Vellatt A, McCafferty J, Laustsen AH. Basics of antibody phage display technology. *Toxins*. 2018;10(236).
260. Xie C, Tiede C, Zhang X, Wang C, Li Z, Xu X, et al. Development of an Affimer-antibody combined immunological diagnosis kit for glypican-3. *Sci Rep*. 2017;7(9608).
261. Sharma R, Deacon SE, Nowak D, George SE, Szymonik MP, Tang AAS, et al. Label-free electrochemical impedance biosensor to detect human interleukin-8 in serum with sub-pg/ml sensitivity. *Biosens Bioelectron*. 2016;80:607–13.
262. Zhurauski P, Arya SK, Jolly P, Tiede C, Tomlinson DC, Ko Ferrigno P, et al. Sensitive and selective Affimer-functionalised interdigitated electrode-based capacitive biosensor for Her4 protein tumour biomarker detection. *Biosens Bioelectron*. 2018;108:1–8.

263. Robinson JI, Baxter EW, Owen RL, Thomsen M, Tomlinson DC, Waterhouse MP, et al. Affimer proteins inhibit immune complex binding to Fc $\gamma$ RIIIa with high specificity through competitive and allosteric modes of action. *Proc Natl Acad Sci U S A*. 2018;115(1):E72–81.
264. King RJ, Schuett K, Tiede C, Jankowski V, John V, Trehan A, et al. Fibrinogen interaction with complement C3: a potential therapeutic target to reduce thrombosis risk. *Haematologica*. 2020;(SE-Articles).
265. van der Hoek L, Verschoor E, Beer M, Höper D, Wernike K, Van Ranst M, et al. Host switching pathogens, infectious outbreaks and zoonosis: A Marie Skłodowska-Curie innovative training network (HONOURS). *Virus Res*. 2018;257:120–4.
266. Lorenzo G, López-Gil E, Warimwe GM, Brun A. Understanding Rift Valley fever: Contributions of animal models to disease characterization and control. *Mol Immunol*. 2015;66(1):78–88.
267. Lorenzo G, López-Gil E, Ortego J, Brun A. Efficacy of different DNA and MVA prime-boost vaccination regimens against a Rift Valley fever virus (RVFV) challenge in sheep 12 weeks following vaccination. *Vet Res*. 2018;49(1):1–12.
268. Sastre P, Cusi MG, Manoha C, Schildgen O, Ruiz T, Vela C, et al. Serum antibody response to respiratory syncytial virus F and N proteins in two populations at high risk of infection: Children and elderly. *J Virol Methods*. 2010;168(1–2):170–6.
269. Van Bilsen WPH, Boyd A, Van Der Loeff MFS, Davidovich U, Hogewoning A, Van Der Hoek L, et al. Diverging trends in incidence of HIV versus other sexually transmitted infections in HIV-negative MSM in Amsterdam. *Aids*. 2020;34(2):301–9.
270. Sanz A, García-Barreno B, Nogal ML, Viñuela E, Enjuanes L. Monoclonal antibodies specific for African swine fever virus proteins. *J Virol*. 1985;54(1):199–206.
271. Nakane K. Peroxidase-Labeled a New Antibody Method Conjugation. *J Histochem Cytochem*. 1974;22:1084–91.
272. Tang AAS, Tiede C, Hughes DJ, McPherson M, Tomlinson DC. Isolation of isoform-specific binding proteins (Affimers) by phage display using negative selection. *Sci Signal*. 2017;10(505):1–11.
273. Venteo A, Rebollo B, Sarraseca J, Rodriguez MJ, Sanz A. A novel double recognition enzyme-linked immunosorbent assay based on the nucleocapsid protein for early detection of European porcine reproductive and respiratory syndrome virus infection. *J Virol Methods*. 2012;181(1):109–13.
274. Hermanson GT. Zero-Length Crosslinkers. In: *Bioconjugate Techniques*. Third Edition. 2013. p. 259–73.
275. Papa A. Diagnostic approaches for Crimean-Congo hemorrhagic fever virus. *Expert Rev Mol Diagn*. 2019;19(6):531–6.
276. Shepherd AJ, Swanepoel R, Leman PA, Shepherd SP. Comparison of methods for



- isolation and titration of Crimean-Congo hemorrhagic fever virus. *J Clin Microbiol.* 1986;24(4):654–6.
277. Raabe VN. Diagnostic Testing for Crimean-Congo Hemorrhagic Fever. *J Clin Microbiol.* 2020;58(4):1–10.
278. Osman HAM, Eltom KH, Musa NO, Bilal NM, Elbashir MI, Aradaib IE. Development and evaluation of loop-mediated isothermal amplification assay for detection of Crimean Congo hemorrhagic fever virus in Sudan. *J Virol Methods.* 2013;190:4–10.
279. Shepherd AJ, Swanepoel R, Gill DE. Evaluation of enzyme-linked immunosorbent assay and reversed passive hemagglutination for detection of Crimean-Congo hemorrhagic fevers virus antigen. *J Clin Microbiol.* 1988;26(2):347–53.
280. Saijo M, Tang Q, Shimayi B, Han L, Zhang Y, Asiguma M, et al. Antigen-capture enzyme-linked immunosorbent assay for the diagnosis of Crimean-Congo hemorrhagic fever using a novel monoclonal antibody. *J Med Virol.* 2005;77:83–8.
281. Vanhomwegen J, Alves MJ, Avšič Županc T, Bino S, Chinikar S, Karlberg H, et al. Diagnostic assays for Crimean-Congo hemorrhagic fever. *Emerg Infect Dis.* 2012;18(12).
282. Schuster I, Mertens M, Köllner B, Korytář T, Keller M, Hammerschmidt B, et al. A competitive ELISA for species-independent detection of Crimean-Congo hemorrhagic fever virus specific antibodies. *Antiviral Res.* 2016;134:161–6.
283. Sas MA, Comtet L, Donnet F, Mertens M, Vatansever Z, Tordo N, et al. A novel double-antigen sandwich ELISA for the species-independent detection of Crimean-Congo hemorrhagic fever virus-specific antibodies. *Antiviral Res.* 2018;151:24–6.
284. Shrivastava N, Shrivastava A, Ninawe SM, Sharma S, Kumar JS, Alam SI, et al. Development of multispecies recombinant nucleoprotein-based indirect ELISA for high-throughput screening of Crimean-Congo hemorrhagic fever virus-specific antibodies. *Front Microbiol.* 2019;10:1–14.
285. Devignot S, Bergeron E, Nichol S, Mirazimi A, Weber F. A Virus-Like Particle System Identifies the Endonuclease Domain of Crimean-Congo Hemorrhagic Fever Virus. *J Virol.* 2015;89(11):5957–67.
286. DISCONTOOLS. CRIMEAN-CONGO HAEMORRHAGIC FEVER [Internet]. 2016. [cited 2020 Oct 5] Available from: <https://www.discontools.eu/database/81-crimean-congo-haemorrhagic-fever.html>
287. WHO. WHO R&D Blueprint : Priority Diagnostics for CCHF Use Scenarios and Target Product Profiles. 2019.
288. WHO. Roadmap for Research and Product Development against Crimean-Congo Haemorrhagic Fever (CCHF) [Internet]. 2018 [cited 2020 Sep 10]. Available from: <https://www.who.int/blueprint/priority-diseases/key-action/cCHF-draft-r-and-d-roadmap.pdf?ua=1>
-

289. Carter SD, Barr JN, Edwards TA. Expression, purification and crystallization of the Crimean-Congo haemorrhagic fever virus nucleocapsid protein. *Acta Crystallogr Sect F Struct Biol Cryst Commun.* 2012;68:569–73.
290. Rahpeyma M, Samarbaf-Zadeh A, Makvandi M, Ghadiri AA, Dowall SD, Fotouhi F. Expression and characterization of codon-optimized Crimean-Congo hemorrhagic fever virus Gn glycoprotein in insect cells. *Arch Virol.* 2017;162(7):1951–62.
291. Bertolotti-Ciarlet A, Smith J, Strecker K, Paragas J, Altamura LA, McFalls JM, et al. Cellular Localization and Antigenic Characterization of Crimean-Congo Hemorrhagic Fever Virus Glycoproteins. *J Virol.* 2005;79(10):6152–61.
292. Zivcec M, Guerrero LIW, Albariño CG, Bergeron É, Nichol ST, Spiropoulou CF. Identification of broadly neutralizing monoclonal antibodies against Crimean-Congo hemorrhagic fever virus. *Antiviral Res.* 2017;146:112–20.
293. Coetzer JA. The pathology of Rift Valley fever. II. Lesions occurring in field cases in adult cattle, calves and aborted fetuses. *Onderstepoort J Vet Res.* 1982;49(1):11–7.
294. Anderson GW, Saluzzo JF, Ksiazek TG, Smith JF, Ennis W, Thureen D, et al. Comparison of in vitro and in vivo systems for propagation of rift valley fever virus from clinical specimens. *Res Virol.* 1989;140(C):129–38.
295. Drolet BS, Weingartl HM, Jiang J, Neufeld J, Marszal P, Lindsay R, et al. Development and evaluation of one-step rRT-PCR and immunohistochemical methods for detection of Rift Valley fever virus in biosafety level 2 diagnostic laboratories. *J Virol Methods.* 2012;179(2):373–82.
296. Njenga MK, Paweska J, Wanjala R, Rao CY, Weiner M, Omballa V, et al. Using a field quantitative real-time PCR test to rapidly identify highly viremic Rift Valley fever cases. *J Clin Microbiol.* 2009;47(4):1166–71.
297. de St. Maurice A, Harmon J, Nyakarahuka L, Balinandi S, Tumusiime A, Kyondo J, et al. Rift valley fever viral load correlates with the human inflammatory response and coagulation pathway abnormalities in humans with hemorrhagic manifestations. *PLoS Negl Trop Dis.* 2018;12(5):1–15.
298. Petrova V, Kristiansen P, Norheim G, Yimer SA. Rift valley fever: Diagnostic challenges and investment needs for vaccine development. *BMJ Glob Heal.* 2020;5:1–9.
299. Bird BH, Bawiec DA, Ksiazek TG, Shoemaker TR, Nichol ST. Highly sensitive and broadly reactive quantitative reverse transcription-PCR assay for high-throughput detection of Rift Valley fever virus. *J Clin Microbiol.* 2007;45(11):3506–13.
300. Garcia S, Crance JM, Billecocq A, Peinnequin A, Jouan A, Bouloy M, et al. Quantitative real-time PCR detection of Rift Valley fever virus and its application to evaluation of antiviral compounds. *J Clin Microbiol.* 2001;39(12):4456–61.
301. Drosten C, Götting S, Schilling S, Asper M, Panning M, Schmitz H, et al. Rapid detection and quantification of RNA of Ebola and Marburg viruses, Lassa virus,

- Crimean-Congo hemorrhagic fever virus, Rift Valley fever virus, dengue virus, and yellow fever virus by real-time reverse transcription-PCR. *J Clin Microbiol.* 2002;40(7):2323–30.
302. Weidmann M, Sanchez-Seco MP, Sall AA, Ly PO, Thiongane Y, Lô MM, et al. Rapid detection of important human pathogenic Phleboviruses. *J Clin Virol.* 2008;41(2):138–42.
303. Odendaal L, Fosgate GT, Romito M, Coetzer JAW, Clift SJ. Sensitivity and specificity of real-time reverse transcription polymerase chain reaction, histopathology, and immunohistochemical labeling for the detection of Rift Valley fever virus in naturally infected cattle and sheep. *J Vet Diagnostic Investig.* 2014;26(1):49–60.
304. Sall AA, Thonnon J, Sene OK, Fall A, Ndiaye M, Baudez B, et al. Single-tube and nested reverse transcriptase-polymerase chain reaction for detection of Rift Valley fever virus in human and animal sera. *J Virol Methods.* 2001;91(1):85–92.
305. Yeh JY, Lee JH, Seo HJ, Park JY, Moon JS, Cho IS, et al. Simultaneous detection of rift valley fever, bluetongue, rinderpest, and peste des petits ruminants viruses by a single-tube multiplex reverse transcriptase-PCR assay using a dual-priming oligonucleotide system. *J Clin Microbiol.* 2011;49(4):1389–94.
306. Peyrefitte CN, Boubis L, Coudrier D, Bouloy M, Grandadam M, Tolou HJ, et al. Real-time reverse-transcription loop-mediated isothermal amplification for rapid detection of Rift Valley fever virus. *J Clin Microbiol.* 2008;46(11):3653–9.
307. Le Roux CA, Kubo T, Grobbelaar AA, Van Vuren PJ, Weyer J, Nel LH, et al. Development and evaluation of a real-time reverse transcription-loop-mediated isothermal amplification assay for rapid detection of rift valley fever virus in clinical specimens. *J Clin Microbiol.* 2009;47(3):645–51.
308. Euler M, Wang Y, Nentwich O, Piepenburg O, Hufert FT, Weidmann M. Recombinase polymerase amplification assay for rapid detection of Rift Valley fever virus. *J Clin Virol.* 2012;54(4):308–12.
309. Fukushi S, Nakauchi M, Mizutani T, Saijo M, Kurane I, Morikawa S. Antigen-capture ELISA for the detection of Rift Valley fever virus nucleoprotein using new monoclonal antibodies. *J Virol Methods.* 2012;180(1–2):68–74.
310. Mroz C, Schmidt KM, Reiche S, Groschup MH, Eiden M. Development of monoclonal antibodies to Rift Valley Fever Virus and their application in antigen detection and indirect immunofluorescence. *J Immunol Methods.* 2018;460:36–44.
311. Cêtre-Sossah C, Pédarrieu A, Juremalm M, Van Vuren PJ, Brun A, El Mamy ABO, et al. Development and validation of a pen side test for Rift Valley fever. *PLoS Negl Trop Dis.* 2019;13(9):1–16.
312. International Organisation for Animal Health (OIE). Rift Valley fever virus. In: *OIE Terrestrial Manual 2018.* 2018. p. 613–33.
313. Schreur PJW, Paweska JT, Kant J, Kortekaas J. A novel highly sensitive, rapid and safe Rift Valley fever virus neutralization test. *J Virol Methods.* 2017;248:26–30.

314. Faburay B, Wilson W, McVey DS, Drolet BS, Weingartl H, Madden D, et al. Rift Valley fever virus structural and nonstructural proteins: Recombinant protein expression and immunoreactivity against antisera from sheep. *Vector-Borne Zoonotic Dis.* 2013;13(9):619–29.
315. Jansen van Vuren P, Potgieter AC, Paweska JT, van Dijk AA. Preparation and evaluation of a recombinant Rift Valley fever virus N protein for the detection of IgG and IgM antibodies in humans and animals by indirect ELISA. *J Virol Methods.* 2007;140(1–2):106–14.
316. Upreti D, Cernicchiaro N, Richt JA, Wilson WC, Clavijo A, Davis AS. Preliminary evaluation of diagnostic accuracy and precision of a competitive ELISA for detection of antibodies to Rift Valley fever virus in cattle and sheep sera. *J Virol Methods.* 2018;262:6–11.
317. Paweska JT, Burt FJ, Swanepoel R. Validation of IgG-sandwich and IgM-capture ELISA for the detection of antibody to Rift Valley fever virus in humans. *J Virol Methods.* 2005;124:173–81.
318. van der Wal FJ, Achterberg RP, de Boer SM, Boshra H, Brun A, Maassen CBM, et al. Bead-based suspension array for simultaneous detection of antibodies against the Rift Valley fever virus nucleocapsid and Gn glycoprotein. *J Virol Methods.* 2012;183(2):99–105.
319. Ragan IK, Davis AS, McVey DS, Richt JA, Rowland RR, Wilson WC. Evaluation of fluorescence microsphere immunoassay for detection of antibodies to rift valley fever virus nucleocapsid protein and glycoproteins. *J Clin Microbiol.* 2018;56(6):1–13.
320. Lindahl JF, Ragan IK, Rowland RR, Wainaina M, Mbotha D, Wilson W. A multiplex fluorescence microsphere immunoassay for increased understanding of Rift Valley fever immune responses in ruminants in Kenya. *J Virol Methods.* 2019;269:70–6.
321. Raymond DD, Piper ME, Gerrard SR, Smith JL. Structure of the Rift Valley fever virus nucleocapsid protein reveals another architecture for RNA encapsidation. *Proc Natl Acad Sci U S A.* 2010;107(26):11769–74.
322. Le May N, Gaudiard N, Billecocq A, Bouloy M. The N Terminus of Rift Valley Fever Virus Nucleoprotein Is Essential for Dimerization. *J Virol.* 2005;79(18):11974–80.
323. Jäckel S, Eiden M, Balkema-Buschmann A, Ziller M, Jansen van Vuren P, Paweska JT, et al. A novel indirect ELISA based on glycoprotein Gn for the detection of IgG antibodies against Rift Valley fever virus in small ruminants. *Res Vet Sci.* 2013;95(2):725–30.
324. Jäckel S, Eiden M, Dauber M, Balkema-Buschmann A, Brun A, Groschup MH. Generation and application of monoclonal antibodies against Rift Valley fever virus nucleocapsid protein NP and glycoproteins Gn and Gc. *Arch Virol.* 2014;159(3):535–46.
325. Faburay B, Lebedev M, McVey DS, Wilson W, Morozov I, Young A, et al. A

- Glycoprotein subunit vaccine elicits a strong rift valley fever virus neutralizing antibody response in sheep. *Vector-Borne Zoonotic Dis.* 2014;14(10):746–56.
326. Wright D, Allen ER, Clark MHA, Gitonga JN, Karanja HK, Hulswit RJG, et al. Naturally Acquired Rift Valley Fever Virus Neutralizing Antibodies Predominantly Target the Gn Glycoprotein. *iScience.* 2020;23(11):101669.
327. Wang Q, Ma T, Wu Y, Chen Z, Zeng H, Tong Z, et al. Neutralization mechanism of human monoclonal antibodies against Rift Valley fever virus. *Nat Microbiol.* 2019;4:1231–41.
328. Hao M, Zhang G, Zhang S, Chen Z, Chi X, Dong Y, et al. Characterization of two neutralizing antibodies against rift valley fever virus Gn protein. *Viruses.* 2020;12(3):1–15.
329. Niklasson B, Grandien M, Peters CJ, Gargan TP. Detection of Rift Valley fever virus antigen by enzyme-linked immunosorbent assay. *J Clin Microbiol.* 1983;17(6):1026–31.
330. Jansen van Vuren P, Paweska JT. Laboratory safe detection of nucleocapsid protein of Rift Valley fever virus in human and animal specimens by a sandwich ELISA. *J Virol Methods.* 2009;157(1):15–24.
331. Bett B, Kiunga P, Gachohi J, Sindato C, Mbotha D, Robinson T, et al. Effects of climate change on the occurrence and distribution of livestock diseases. Vol. 137, *Preventive Veterinary Medicine.* Elsevier B.V.; 2017. 119–129 p.
332. Brand SPC, Keeling MJ. The impact of temperature changes on vector-borne disease transmission: Culicoides midges and bluetongue virus. *J R Soc Interface.* 2017;14(128).
333. Dash AP, Bhatia R, Sunyoto T, Mourya DT. Emerging and re-emerging arboviral diseases in Southeast Asia. *J Vector Borne Dis.* 2013;50(2):77–84.
334. Weaver SC, Reisen WK. Present and Future Arboviral Threats. *Antiviral Res.* 2010;85(2).
335. Estrada-Peña A, Ruiz-Fons F, Acevedo P, Gortazar C, De la Fuente J. Factors driving the circulation and possible expansion of Crimean-Congo haemorrhagic fever virus in the western Palearctic. *J Appl Microbiol.* 2012;114(1):278–86.
336. Samy AM, Peterson AT. Climate change influences on the global potential distribution of bluetongue virus. *PLoS One.* 2016;11(3):1–12.
337. Mertens M, Schmidt K, Ozkul A, Groschup MH. The impact of Crimean-Congo hemorrhagic fever virus on public health. *Antiviral Res.* 2013;98(2):248–60.
338. Wright D, Kortekaas J, Bowden TA, Warimwe GM. Rift valley fever: Biology and epidemiology. *J Gen Virol.* 2019;100(8):1187–99.
339. Brustolin M, Talavera S, Nuñez A, Santamaria C, Rivas R, Pujol N, et al. Rift Valley fever virus and European mosquitoes: vector competence of *Culex pipiens* and *Stegomyia albopicta* (= *Aedes albopictus*). *Med Vet Entomol.* 2017;31(4):365–72.

340. Rojas JM, Rodríguez-Martín D, Martín V, Sevilla N. Diagnosing bluetongue virus in domestic ruminants: current perspectives. *Vet Med Res Reports*. 2019;10:17–27.
341. Wernike K, Beer M. Schmallenberg Virus: A Novel Virus of Veterinary Importance. In: *Advances in Virus Research*. 1st Edition. Elsevier Inc.; 2017. p. 39–60.
342. Hoffmann B, Scheuch M, Höper D, Jungblut R, Holsteg M, Schirrmeier H, et al. Novel orthobunyavirus in cattle, Europe, 2011. *Emerg Infect Dis*. 2012;18(3):469–72.
343. Häsler B, Alarcon P, Raboisson D, Waret-Szkuta A, Rushton J. Integration of production and financial models to analyse the financial impact of livestock diseases: A case study of Schmallenberg virus disease on British and French dairy farms. *Vet Rec Open*. 2015;2(1).
344. Rushton J, Lyons N. Impatto economico della Bluetongue: Analisi degli effetti sulla produttività. *Vet Ital*. 2015;51(4):401–6.
345. El-Sayed A, El-Shannat S, Kamel M, Castañeda-Vazquez MA, Castañeda-Vazquez H. Molecular Epidemiology of *Mycobacterium bovis* in Humans and Cattle. *Zoonoses Public Health*. 2016;63(4):251–64.
346. Mathema B, Kurepina NE, Bifani PJ, Kreiswirth BN. Molecular epidemiology of tuberculosis: Current insights. *Clin Microbiol Rev*. 2006;19(4):658–85.
347. Ejeh EF, Raji MA, Bello M, Lawan FA, Francis MI, Kudi AC, et al. Prevalence and direct economic losses from bovine tuberculosis in Makurdi, Nigeria. *Vet Med Int*. 2014;2014.
348. Wade-Evans AM, Romero CH, Mellor P, Takamatsu H, Anderson J, Thevasagayam J, et al. Expression of the major core structural protein (VP7) of bluetongue virus, by a recombinant capripox virus, provides partial protection of sheep against a virulent heterotypic bluetongue virus challenge. *Virology*. 1996;220(1):227–31.
349. Wiker HG. MPB70 and MPB83 - Major antigens of *mycobacterium bovis*. *Scand J Immunol*. 2009;69(6):492–9.
350. Medlock JM, Leach SA. Effect of climate change on vector-borne disease risk in the UK. *Lancet Infect Dis*. 2015;15(6):721–30.
351. European Commission. Map showing the location of the restriction zones for different BTV serotypes in Europe as of 9th March 2020 [Internet]. 2020 [cited 2020 Nov 26]. Available from: [https://ec.europa.eu/food/sites/food/files/animals/docs/ad\\_control-measures\\_bt\\_restrictedzones-map.jpg](https://ec.europa.eu/food/sites/food/files/animals/docs/ad_control-measures_bt_restrictedzones-map.jpg)
352. Wu W, Zhang S, Qu J, Zhang Q, Li C, Li J, et al. Simultaneous detection of IgG antibodies associated with viral hemorrhagic fever by a multiplexed Luminex-based immunoassay. *Virus Res*. 2014;187:84–90.
353. O’Hearn AE, Voorhees MA, Fetterer DP, Wauquier N, Coomber MR, Bangura J,

- et al. Serosurveillance of viral pathogens circulating in West Africa. *Virology*. 2016;13(1):1–6.
354. Surtees R, Stern D, Ahrens K, Kromarek N, Lander A, Kreher P, et al. Development of a multiplex microsphere immunoassay for the detection of antibodies against highly pathogenic viruses in human and animal serum samples. *PLoS Negl Trop Dis*. 2020;14(10):1–23.
355. Hoste ACR, Ruiz T, Fernández-Pacheco P, Jiménez-Clavero MÁ, Djadjovski I, Moreno S, et al. Development of a multiplex assay for antibody detection in serum against pathogens affecting ruminants. *Transbound Emerg Dis*. 2020:1–11.
356. Sethuraman N, Jeremiah SS, Ryo A. Interpreting Diagnostic Tests for SARS-CoV-2. *JAMA - J Am Med Assoc*. 2020;323(22):2249–51.
357. Zou L, Ruan F, Huang M, Liang L, Huang H, Hong Z, et al. SARS-CoV-2 Viral Load in Upper Respiratory Specimens of Infected Patients. *N Engl J Med*. 2020;1–3.
358. Pan X, Chen D, Yong X, Wu X, Li T, Ou X, et al. Viral load of SARS-CoV-2 in clinical samples. *Lancet Infect Dis*. 2020;20(4):411–2.
359. Foundation for Innovative New Diagnostics. Molecular assays SARS-CoV-2 diagnostic pipeline [Internet]. 2020 [cited 2021 Jan 8]. Available from: [https://www.finddx.org/covid-19/pipeline/?section=molecular-assays#diag\\_tab](https://www.finddx.org/covid-19/pipeline/?section=molecular-assays#diag_tab)
360. Ravi N, Cortade DL, Ng E, Wang SX. Diagnostics for SARS-CoV-2 detection: A comprehensive review of the FDA-EUA COVID-19 testing landscape. *Biosens Bioelectron*. 2020;165(112454).
361. Lippi G, Simundic AM, Plebani M. Potential preanalytical and analytical vulnerabilities in the laboratory diagnosis of coronavirus disease 2019 (COVID-19). *Clin Chem Lab Med*. 2020;58(7):1070–6.
362. Subsoontorn P, Lohitnavy M, Kongkaew C. The diagnostic accuracy of isothermal nucleic acid point-of-care tests for human coronaviruses: A systematic review and meta-analysis. *Sci Rep*. 2020;10(22349):1–13.
363. Amanat F, Stadlbauer D, Strohmeier S, Nguyen THO, Chromikova V, McMahon M, et al. A serological assay to detect SARS-CoV-2 seroconversion in humans. *Nat Med*. 2020;26(7):1033–6.
364. Wang P. Combination of serological total antibody and RT-PCR test for detection of SARS-COV-2 infections. *J Virol Methods*. 2020;283(113919):1–4.
365. Nie J, Li Q, Wu J, Zhao C, Hao H, Liu H, et al. Establishment and validation of a pseudovirus neutralization assay for SARS-CoV-2. *Emerg Microbes Infect*. 2020;9:680–6.
366. Foundation for Innovative New Diagnostics. Rapid diagnostics SARS-CoV-2 diagnostic pipeline [Internet]. 2020 [cited 2021 Jan 8]. Available from: [https://www.finddx.org/covid-19/pipeline/?avance=all&type=Rapid+diagnostic+tests&test\\_target=Antibody&status=all&section=immunoassays&action=default#diag\\_tab](https://www.finddx.org/covid-19/pipeline/?avance=all&type=Rapid+diagnostic+tests&test_target=Antibody&status=all&section=immunoassays&action=default#diag_tab)
-

367. WHO. Antigen-detection in the diagnosis of SARS-CoV-2 infection using rapid immunoassays [Internet]. 2020 [cited 2021 Jan 8]. Available from: <https://apps.who.int/iris/handle/10665/334253>
368. Brouwer PJM, Caniels TG, van der Straten K, Snitselaar JL, Aldon Y, Bangaru S, et al. Potent neutralizing antibodies from COVID-19 patients define multiple targets of vulnerability. *Science*. 2020;369(6504):643–50.
369. Wu HS, Hsieh YC, Su IJ, Lin TH, Chiu SC, Hsu YF, et al. Early detection of antibodies against various structural proteins of the SARS-associated coronavirus in SARS patients. *J Biomed Sci*. 2004;11(1):117–26.
370. Shang B, Wang XY, Yuan JW, Vabret A, Wu XD, Yang RF, et al. Characterization and application of monoclonal antibodies against N protein of SARS-coronavirus. *Biochem Biophys Res Commun*. 2005;336(1):110–7.
371. Liu SJ, Leng CH, Lien SP, Chi HY, Huang CY, Lin CL, et al. Immunological characterizations of the nucleocapsid protein based SARS vaccine candidates. *Vaccine*. 2006;24(16):3100–8.
372. Shi Y, Yi Y, Li P, Kuang T, Li L, Dong M, et al. Diagnosis of Severe Acute Respiratory Syndrome (SARS) by Detection of SARS Coronavirus Nucleocapsid Antibodies in An Antigen-Capturing Enzyme-Linked Immunosorbent Assay. *J Clin Microbiol*. 2003;41(12):5781–2.
373. Kang S, Yang M, Hong Z, Zhang L, Huang Z, Chen X, et al. Crystal structure of SARS-CoV-2 nucleocapsid protein RNA binding domain reveals potential unique drug targeting sites. *Acta Pharm Sin B*. 2020;10(7):1228–38.
374. Krüttgen A, Cornelissen CG, Dreher M, Hornef M, Imöhl M, Kleines M. Comparison of four new commercial serologic assays for determination of SARS-CoV-2 IgG. *J Clin Virol*. 2020;128(10439).
375. Meyer B, Drosten C, Müller MA. Serological assays for emerging coronaviruses: Challenges and pitfalls. 2014;194:175–83.
376. Sastre P, Pérez T, Costa S, Yang X, Räber A, Blome S, et al. Development of a duplex lateral flow assay for simultaneous detection of antibodies against African and Classical swine fever viruses. *J Vet Diagnostic Investig*. 2016;28(5):543–9.
377. Fresco-Taboada A, Risalde MA, Gortázar C, Tapia I, González I, Venteo Á, et al. A lateral flow assay for the rapid diagnosis of *Mycobacterium bovis* infection in wild boar. *Transbound Emerg Dis*. 2019;66(5):2175–9.
378. Parolo C, de la Escosura-Muñiz A, Merkoçi A. Enhanced lateral flow immunoassay using gold nanoparticles loaded with enzymes. *Biosens Bioelectron*. 2013;40(1):412–6.
379. Okba NMA, Müller MA, Li W, Wang C, Geurtsvankessel CH, Corman VM, et al. Severe Acute Respiratory Syndrome Coronavirus 2-Specific Antibody Responses in Coronavirus Disease Patients. *Emerg Infect Dis*. 2020;26(7):1478–88.
380. Sterlin D, Mathian A, Miyara M, Mohr A, Anna F, Claër L, et al. IgA dominates the early neutralizing antibody response to SARS-CoV-2. *Sci Transl Med*.



- 2021;13(577):1–10.
381. Murphy K, Travers P, Walport M. The Distribution and Functions of Immunoglobulin Classes. In: Janeway's Immunobiology. 7th Edition. New-York: Garland Science; 2008.
382. Long QX, Liu BZ, Deng HJ, Wu GC, Deng K, Chen YK, et al. Antibody responses to SARS-CoV-2 in patients with COVID-19. *Nat Med*. 2020;26(6):845–8.
383. CDC. Frequently Asked Questions about Coronavirus (COVID-19) for Laboratories [Internet]. 2020 [cited 2021 Jan 12]. Available from: <https://www.cdc.gov/coronavirus/2019-ncov/lab/faqs.html>
384. Hoste ACR, Venteo A, Fresco-Taboada A, Tapia I, Monedero A, López L, et al. Two serological approaches for detection of antibodies to SARS-CoV-2 in different scenarios: a screening tool and a point-of-care test. *Diagn Microbiol Infect Dis*. 2020;98(4):115167.
385. Wang Q, Wang Q, Wang Q, Du Q, Du Q, Guo B, et al. A method to prevent SARS-CoV-2 IgM false positives in gold immunochromatography and enzyme-linked immunosorbent assays. *J Clin Microbiol*. 2020;58(6):1–7.
386. Woods CR. False-positive results for immunoglobulin M serologic results: Explanations and examples. *J Pediatric Infect Dis Soc*. 2013;2(1):87–90.
387. CDC. Emerging SARS-CoV-2 Variants [Internet]. 2021 [cited 2021 Jan 18]. Available from: <https://www.cdc.gov/coronavirus/2019-ncov/more/science-and-research/scientific-brief-emerging-variants.html>
388. Mariën J, Ceulemans A, Michiels J, Heyndrickx L, Kerkhof K, Foque N, et al. Evaluating SARS-CoV-2 spike and nucleocapsid proteins as targets for antibody detection in severe and mild COVID-19 cases using a Luminex bead-based assay. *J Virol Methods*. 2021;288(114025).
389. Li K, Huang B, Wu M, Zhong A, Li L, Cai Y, et al. Dynamic changes in anti-SARS-CoV-2 antibodies during SARS-CoV-2 infection and recovery from COVID-19. *Nat Commun*. 2020;11(6044):1–11.